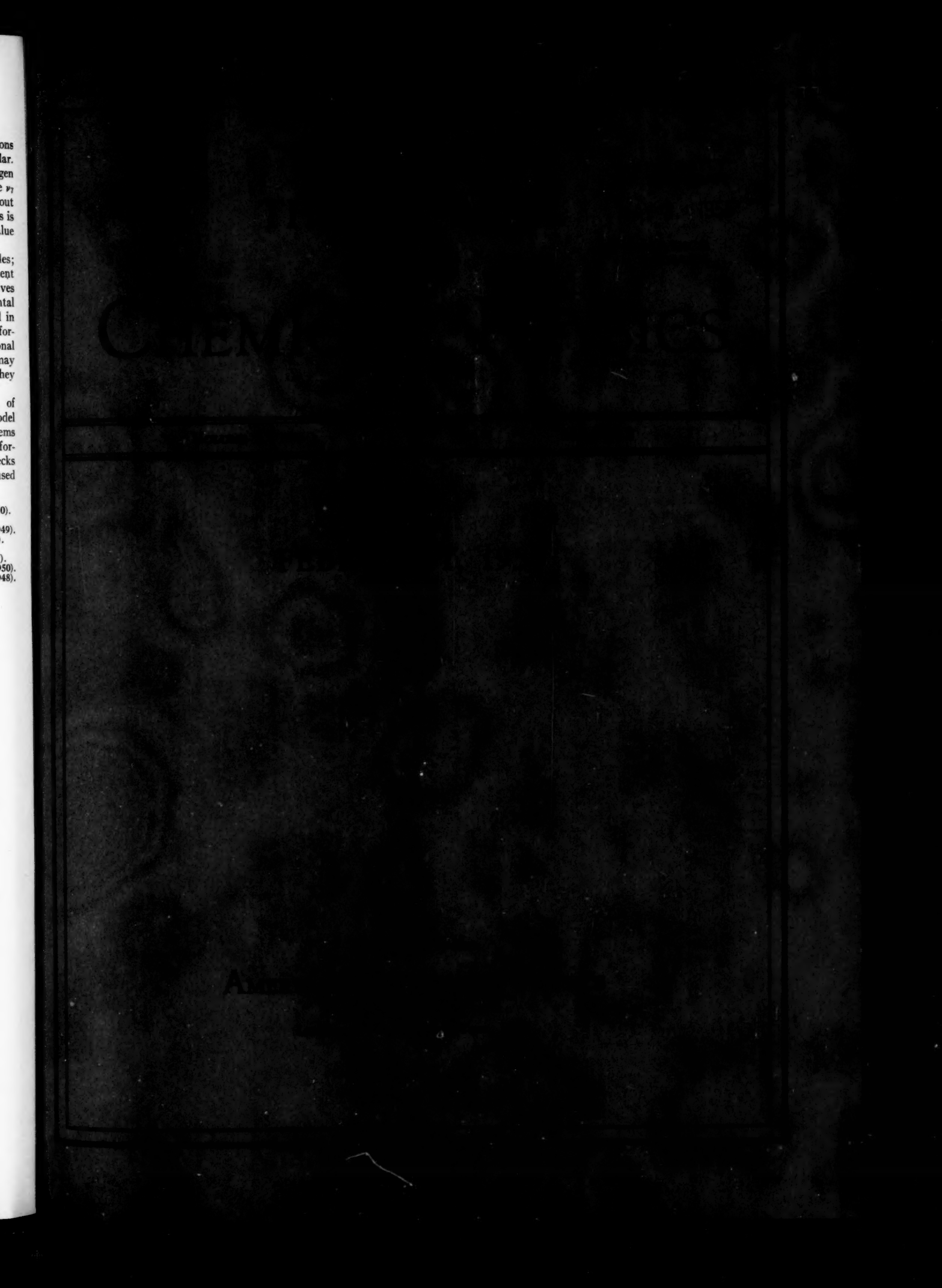

EDITORS

Editor

JAMES B. ARNOLD
JACOB BIGELEISEN
WALLACE CORDES
ALVIN H. NIELSEN
EARLE K. PLYLER
WAVE H. SHAFFER
T. F. YOUNG

erican Institute of Physics and Chemical Abstracts (Chem. Abstracts 45, I-CCLV (1951)).

Tables may be typewritten on sheets separate from the running text. Each table must have a caption which will make the data in the table intelligible without reference to the text. Avoid complicated column headings.

Wherever possible figures should be planned for the width of a column (3 in.). A convenient reduction ratio is about 2:1 or 3:1. Lettering should be large enough on the original that when reduced it shall not be less than about 1/16 in. (~1.5 mm). Line drawings must be in *india ink* on white paper or tracing cloth. Coordinate paper is not desirable but if used must be blue lined and the coordinate lines which are to show must be inked over. Pictures of apparatus, etc., should be glossy prints and should have maximum black and white contrast. Identify each original drawing or photograph on the back with the author's name and the figure number. Figures should be numbered consecutively. Captions should be typed on a separate sheet of paper.

A limited number of alterations in proof are unavoidable, but the cost of making extensive alterations after the article has been set in type will be charged to the author.

Proof and all correspondence concerning papers in the process of publication should be addressed to the Publication Manager, American Institute of Physics, 57 East 55 Street, New York 22, New York.

Subscription Prices

	U. S. and Canada	Elsewhere
To members of the American Institute of Physics and Affiliated Societies	$12.00	$13.00
To all others	15.00	17.00

Back Number Prices

Yearly rate when complete year is available: $18.00.

Single copies: $1.75 each.

Subscriptions, renewals, and orders for single copies should be addressed to the American Institute of Physics, 57 East 55 Street, New York 22, New York.

Changes of address should be sent to the American Institute of Physics.

Printed and Lithoed in the U. S. A. by [illegible], Lancaster, Pennsylvania.

Entered as second class matter at the Post Office at Lancaster, Pa., under the Act of August 24, 1912. Authorized January 21, 1922. Section 34.40, P. L. & R., of [illegible], authorized February 3, 1923.

THE JOURNAL
OF
CHEMICAL PHYSICS

VOLUME 23, NUMBER 2 FEBRUARY, 1955

Stabilization of Energy-Rich Molecules. I. Energy Transfer with Hydrogen

M. BOUDART AND J. T. DUBOIS*
The James Forrestal Research Center, Princeton University, Princeton, New Jersey
(Received June 11, 1954)

The increase in fluorescence yield of β-naphthylamine vapors in the presence of foreign gases provides a new powerful method for studying energy exchange. The effect, discovered by Neporent, is analyzed kinetically and the analog of the Stern-Volmer equation for this effect is derived. Neporent's data are recalculated in the light of this analysis. Fluorescence stabilization by deuterium and sulfur hexafluoride is studied experimentally following the procedure of Neporent. It is concluded, in particular, that the vibrational and rotational modes of the hydrogen molecules are inactive in the excitation or de-excitation of vibrational energy of complex molecules.

INTRODUCTION

VIBRATIONAL excitation is the process by which sufficient energy can be stored in a molecule prior to its unimolecular decomposition. Vibrational de-excitation leads to stabilization of molecules formed by direct association. The number of techniques by which these phenomena may be studied is quite limited. In principle, kinetic investigations of unimolecular reactions in a large partial pressure range of foreign gases might yield the pertinent information but there are many difficulties in that sort of work and only qualitative data have been obtained thus far. Thus, relative efficiencies of various molecules in maintaining the high pressure rate of a given unimolecular reaction have been determined. Similarly, relative efficiencies of third bodies in atom recombinations deal with the stabilization of energy rich diatomic molecules.

From a quantitative standpoint however, the question of interest is the following. Given a polyatomic molecule M with a large excess of vibrational energy ΔE over the thermal mean value, what quantity E of this excess ΔE can be transferred on the average by a collision with a foreign molecule X? This question may be answered by the study of an effect discovered by Neporent[1,2] in Terenin's laboratory. The effect consists in the fluorescence increase of an aromatic molecule as a result of its vibrational deactivation by collision following light absorption.

In this paper, we shall present a kinetic analysis of the phenomenon, a reinterpretation of Neporent's data in the light of this analysis and an account of new measurements concerning the efficiency of hydrogen as a stabilizing agent.

KINETIC ANALYSIS OF FLUORESCENCE STABILIZATION

To Neporent belongs the merit of having discovered the effect of fluorescence stabilization and provided a coherent picture of the phenomenon with a large amount of supporting evidence. Although essentially the same picture will be used in the following considerations, a number of new features will be introduced that indicate clearly the nature of the experiments to be performed with the aim of accumulating data on energy exchange.

The aromatic compound on which Neporent has carried out most of his work is β-naphthylamine, hereafter called M. Both the vapor pressure of M and the location of its absorption and fluorescence spectra are quite convenient for measurements of fluorescence in the gas phase between 120 and 200°C. Some aspects of Neporent's work on this molecule were recently confirmed by Curme and Rollefson.[3]

Upon absorbing a light quantum of sufficiently short wavelength λ_a, a molecule M at a temperature T_1 is excited to a new electronic state M_1. Because of the

* Present address: Aeronautical Research Laboratory, Wright Air Development Center, Dayton, Ohio.
[1] B. S. Neporent, Zhur. Fiz. Khim. **21**, 1111 (1947).
[2] B. S. Neporent, Zhur. Fiz. Khim. **24**, 1219 (1950).
[3] H. G. Curme and G. K. Rollefson, J. Am. Chem. Soc. **74**, 28 (1952).

Franck-Condon principle, M_1 possesses an excess of vibrational energy ΔE. If ΔE is large enough, this energy will be redistributed among all vibrational modes of the molecule in a time short compared to the lifetime τ_1 of M_1. Since we deal with a complex molecule with a very large number of closely spaced vibrational states, M_1 may be said to have a vibrational temperature $T_{1\text{vib}}=T_1+\Delta E/C_{\text{vib}}$ where C_{vib} is the vibrational heat capacity of M.

From the excited state M_1, an isolated molecule may either return to the ground state with emission of the fluorescence spectrum or pass into an unspecified state M^* which may be a triplet from where it eventually returns to the ground state without emission of the fluorescence light. These possibilities are represented in Fig. 1 schematically and only for the purpose of illustration. The rate of the first process can be assumed in first approximation to be independent of $T_{1\text{vib}}$. Its rate constant is k_f. The second process, however, involves accumulation of energy in a critical vibrational degree of freedom. Following the theory of unimolecular reactions, the rate constant k_i for the radiationless transition $M_1 \rightarrow M^*$ will be given by

$$k_i=\nu \exp(-E^*/RT_{1\text{vib}}) \qquad (1)$$

where E^* is an activation energy and ν is the frequency factor. The rate constant for the decay of M_1 is thus equal to k_f+k_i and $\tau_1=1/(k_f+k_i)$. The lifetime of M_1 and also the fluorescence intensity will decrease with increasing $T_{1\text{vib}}$, i.e., for shorter wavelengths λ_a (larger ΔE) or higher temperature T_1.

When M_1 is submitted, during its lifetime, to collisions with foreign molecules X, the fluorescence intensity may either decrease or increase. It decreases if X is a quenching agent which transfers the fluorescing molecule from state M_1 to some other nonfluorescing state. Oxygen, according to Neporent, is such a quenching molecule, probably owing to its paramagnetic triplet ground state. The quenching curves follow the Stern-Volmer law and consequently values of τ_1 can be calculated from the slopes of Stern-Volmer straight lines for various values of λ_a and T_1 provided it is assumed that the quenching cross section is equal to

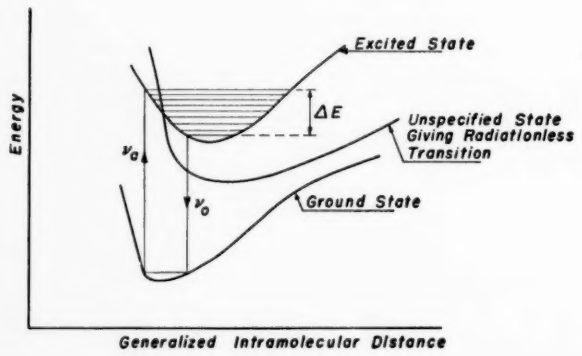

FIG. 1.

TABLE I. Lifetime ($\tau_1\times10^8$ sec) from quenching data.

Temperature °C	Wavelength of exciting light λ_a in A			
	3660	2804	2652	2537
130	1.62	0.815	0.385	0.195
151	1.62	0.685	0.355	0.165
172	1.62	0.600	0.265	0.140
193	1.62	0.495	0.230	0.105

the gas kinetic cross section. The validity of this assumption is shown by the good agreement obtained by Neporent between directly measured values of the relative yield of fluorescence $\gamma=k_f/(k_f+k_i)$ and values of γ calculated from the data of oxygen quenching as shown in Table I. Besides these data, we will also need the values of C_{vib} and of ΔE. Neporent has shown that a 21° increase corresponds to $\Delta E=500$ cm^{-1}. Thus $C_{\text{vib}}=(2.85\times500/21)=67$ cal/mole·degree. The height of the lower vibrational levels of the excited state M_1 above the ground state was determined by Neporent in the following way. As can be seen in Table I, for the $\lambda_a=3660$ A line, $\tau_1=$const at all temperatures so that $k_i=0$. But it is found that the fluorescence yield increases exponentially with temperature and that the activation energy from an Arrhenius plot is 1950 cm^{-1}. Thus, since $\lambda_a=3660$ A corresponds to $\nu_a=27250$ cm^{-1}, the height ν_0 of the lowest vibrational levels of M_1 above the ground state is $\nu_0=27250+1950$ cm^{-1} $=29200$ cm^{-1}. Consequently ΔE (in cm^{-1}) $=\nu_a-29200$, where ν_a is the wave number of the exciting line.

From the data of Table I, it is now possible to calculate $T_{1\text{vib}}$ and k_i. We have done that in order to verify the unimolecular rate in Eq. (1). The obtained values are plotted in an Arrhenius diagram (Fig. 2) and a straight line is obtained giving $E^*=14300$ cal/mole and $\nu=0.254\cdot10^{13}$ sec^{-1}. The value of ν is of the expected order of magnitude while the relatively low activation energy supports the picture of the process $M_1 \rightarrow M^*$ as an internal conversion and not as a predissociation involving rupture of a bond.

Collisions with foreign molecules X may also increase the fluorescence yield of M and the mechanism of this process will now be examined. Upon a collision between M_1 (vibrational temperature $T_{1\text{vib}}$) and X (temperature T_1), a certain amount E of the vibrational energy excess ΔE of M_1 may be transferred to X. After collision, the vibrational temperature of the fluorescing molecule is $T_{2\text{vib}}<T_{1\text{vib}}$ while X has reached a temperature $T_2>T_1$. The state of the fluorescing molecule will now be designated by M_2 with a lifetime $\tau_2>\tau_1$. The longer lifetime of M_2 is responsible for an increase in fluorescence yield. It seems natural to define an accommodation coefficient:

$$\alpha=\frac{T_2-T_1}{T_{2\text{vib}}-T_1} \qquad (2)$$

that gives a measure of the efficiency of the energy transfer process. If no transfer takes place, $T_2=T_1$

and $\alpha=0$. If equilibrium is attained $T_2=T_{2\text{vib}}$ and $\alpha=1$. Since:

$$C_{\text{vib}}(T_{1\text{vib}}-T_{2\text{vib}})=E=C(T_2-T_1)$$

where C is the heat capacity of X at constant volume, Eq. (2) becomes

$$\alpha=\frac{C_{\text{vib}}}{C}\cdot\frac{E}{\Delta E-E}. \tag{3}$$

Thus even in the case of ideal energy transfer ($\alpha=1$), only a fraction $\beta=(E/\Delta E)$ of the total energy excess will be lost by M in a single collision. The optimum value of β is, from Eq. (3),

$$\beta_{(\alpha=1)}=\frac{1}{1+\dfrac{C_{\text{vib}}}{C}}.$$

Thus $\beta=\frac{1}{2}$ if $C_{\text{vib}}=C$ but β would reach unity only for collision with a molecule X of infinite heat capacity. Consequently, in the presence of a foreign gas X at a partial pressure p corresponding to a number Z of times per second that a given fluorescing molecule is collided upon by X molecules, it is necessary to consider a finite series of states M_1, M_2, M_3, $\cdots$, M_{n-1}, M_n. The last state M_n is that of the molecule for which the entire excess ΔE has been dissipated and thus $\tau_n=\tau_f=1/k_f$. Without foreign gas, the fluorescence intensity F_0 is given by:

$$F_0=k_f[M_1].$$

Since $d[M_1]/dt=k_a[M]-k_f[M_1]-k_{t_1}[M_1]=0$, at the steady state, we have:

$$F_0=\frac{k_a[M]\cdot k_f}{k_{t_1}+k_f}=k_a\cdot k_f\tau_1[M]$$

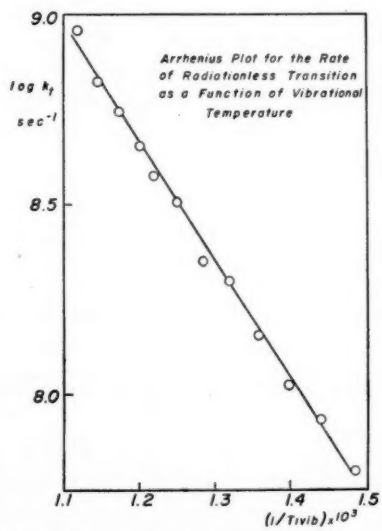

FIG. 2. Arrhenius plot for the rate of radiationless transition as a function of vibrational temperature.

where k_a is the rate of light absorption. With foreign gas, the following processes take place:

$$M+h\nu \xrightarrow{k_a} M_1$$

$$M_1 \xrightarrow{k_f} M+h\nu_1'$$

$$M_1+X \xrightarrow{k} M_2+X$$

$$M_1 \xrightarrow{k_{t_1}} M^*$$

$$M_2 \xrightarrow{k_f} M+h\nu_2'$$

$$M_2+X \xrightarrow{k} M_3+X$$

$$M_2 \xrightarrow{k_{t_2}} M^*$$

$$\cdots\cdots\cdots$$

$$M_{n-1} \xrightarrow{k_f} M+h\nu_{n-1}'$$

$$M_{n-1}+X \xrightarrow{k} M_n+X$$

$$M_{n-1} \xrightarrow{k_{t_{n-1}}} M^*$$

$$M_n \xrightarrow{k_f} M+h\nu_n'.$$

At the steady state:

$$\frac{d[M_1]}{dt}=k_a[M]-(k_f+k_{t_1}+k[X])[M_1]=0$$

$$\frac{d[M_2]}{dt}=k[X][M_1]-(k_f+k_{t_2}+k[X])[M_2]=0$$

$$\cdots\cdots\cdots\cdots\cdots$$

$$\frac{d[M_n]}{dt}=k[X][M_{n-1}]-k_f[M_n]=0.$$

The fluorescence intensity F_z at a concentration of X corresponding to $Z=k[X]$ is equal to

$$F_z=k_f([M_1]+[M_2]+\cdots+[M_n]).$$

From the steady-state equations, we get:

$$F_z=\frac{k_a\cdot k_f\tau_1[M]}{1+\tau_1 Z}\left[1+\frac{\tau_2 Z}{1+\tau_2 Z}+\frac{\tau_2\tau_3 Z^2}{(1+\tau_2 Z)(1+\tau_3 Z)}+\cdots+\frac{\tau_2\tau_3\cdots\tau_n Z^{n-1}}{(1+\tau_2 Z)\cdots(1+\tau_{n-1}Z)}\right].$$

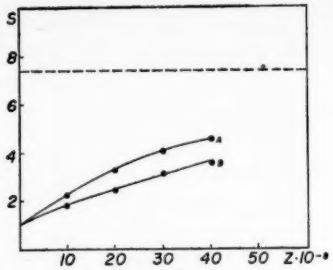

FIG. 3. Relative fluorescence increase at $\lambda=2650$ A, $t=190°C$, as a function of the collision frequency Z for n-pentane (A) and ammonia (B). The dotted line indicates the value of S at infinite pressure.

Thus finally

$$S=\frac{F_z}{F_0}=\frac{1}{1+\tau_1 Z}\left[1+\frac{\tau_2 Z}{1+\tau_2 Z}+\frac{\tau_2\tau_3 Z^2}{(1+\tau_2 Z)(1+\tau_3 Z)}\cdots+\frac{\tau_2\tau_3\cdots\tau_n Z^{n-1}}{(1+\tau_2 Z)\cdots(1+\tau_{n-1}Z)}\right]. \quad (4)$$

Equation (4) corresponds, for the phenomenon of fluorescence stabilization, to the Stern-Volmer expression for the quenching of fluorescence. When S is plotted against Z, curves of the type shown in Figs. 3 and 4 are obtained. The asymptotic value of S for $Z\to\infty$ is (τ_n/τ_1) as can be derived immediately from Eq. (4). The slope of the tangent to the curves at the origin of the abscissas is given by:

$$\left(\frac{dS}{dZ}\right)_{Z=0}=\tau_2-\tau_1.$$

The curvature of the curve at the origin is equal to:

$$\left(\frac{d^2S}{dZ^2}\right)_{Z=0}=2(\tau_1^2-\tau_1\tau_2-\tau_2^2+\tau_2\tau_3).$$

Thus, the curve near $Z=0$ will be concave or convex depending on the sign of this quantity, a condition that can be expressed by the inequalities:

$$\frac{\tau_3-\tau_2}{\tau_2-\tau_1}<\frac{\tau_1}{\tau_2} \quad \text{(Fig. 3)}$$

$$\frac{\tau_3-\tau_2}{\tau_2-\tau_1}>\frac{\tau_1}{\tau_2}. \quad \text{(Fig. 4)}$$

Both cases are found experimentally. In order to determine the energy transfer E between M and a foreign molecule X from a fluorescence stabilization curve, it is thus necessary to obtain data at low pressures of foreign gas so that the slope of the curve at zero pressure may be accurately determined. From the slope, τ_2 is calculated, then $T_{2\text{vib}}$ and finally E by means of the relation:

$$E=C_{\text{vib}}(T_{1\text{vib}}-T_{2\text{vib}}).$$

The theoretical curve giving τ as a function of T_{vib} is represented in Fig. 5 and can be used to speed up the calculations. The experimental points are those of Table I.

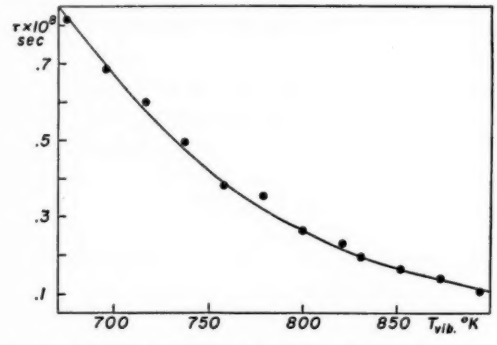

FIG. 5. Lifetime of β-naphthylamine in the excited state as a function of its vibrational temperature.

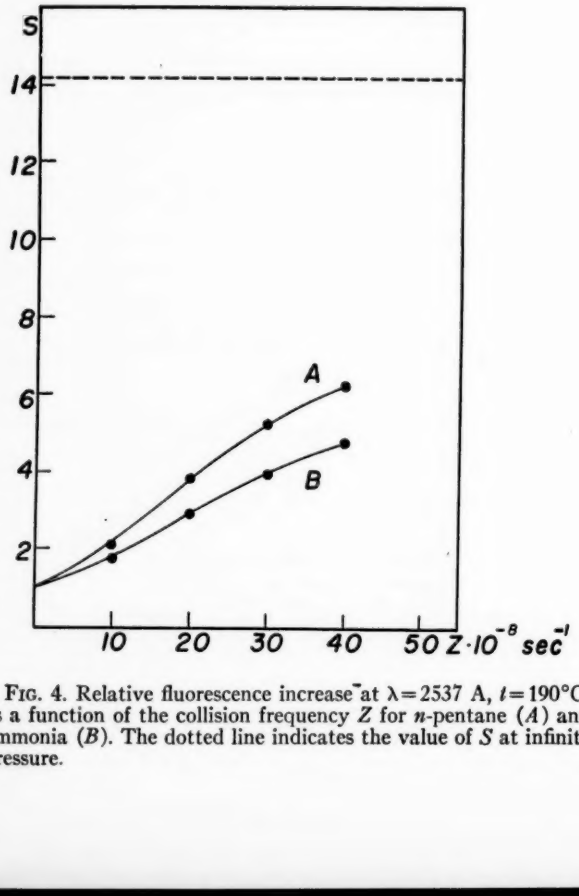

FIG. 4. Relative fluorescence increase at $\lambda=2537$ A, $t=190°C$, as a function of the collision frequency Z for n-pentane (A) and ammonia (B). The dotted line indicates the value of S at infinite pressure.

ENERGY EXCHANGE FROM THE WORK OF NEPORENT

It seems worth while to calculate the amount of energy E transferred on the average by collision with various foreign gases from Neporent's data. Neporent himself computed τ_2 on the assumption that the value of S on the experimental stabilization curve for $Z=1/\tau_1$

is equal to τ_2/τ_1. This is correct only if the curvature of the stabilization curve is zero between $Z=0$ and $Z=1/\tau_1$. Indeed, the equation of the curve, in that range, would be given by $S=1+(\tau_2-\tau_1)Z$, a straight line of slope $(\tau_2-\tau_1)$. Thus for the case of Fig. 3, Neporent found too low values of E (too small values of τ_2) and for the case of Fig. 4, he obtained too high values of E (too large values of τ_2). The gases investigated by Neporent are He, H_2, N_2, CO_2, $CHCl_3$, NH_3, and n-C_5H_{12}. We have determined the slope at $Z=0$ from Neporent's curves (Figs. 6 to 8) and the results of our calculations are summarized in Table II.

The following conclusions are reached:

1. The accommodation coefficient α is large for all gases, with a low value of 0.1 for H_2 and a high value of 0.9 for NH_3. The accommodation coefficient is about the same for He and for n-C_5H_{12}.

2. On the contrary, the amount of energy E removed per collision depends on the complexity of the stabilizing molecule: it is only 70 cm^{-1} for He but may be as high as 1450 cm^{-1} for n-C_5H_{12}.

3. Specific differences between various gases are difficult to account for. Thus, no obvious reason can be provided for the high efficiency of ammonia ($\alpha=0.9$).

4. Neporent's data indicate that the amount of energy removed per collision decreases with increasing temperature. Energy exchange is more favorable when the duration of a collision is longer.

5. The usual assumption that a vibrationally hot complex is deactivated in a single collision does not hold. Thus, with simple molecules (H_2, N_2), several collisions are required to remove excess energy of the order of kT.

The accommodation coefficient α describes energy transfer between vibration of the complex molecule and all degrees of freedom of the stabilizing agent. Thus, for the latter, the value of the total heat capacity at constant volume, at a temperature intermediate between $T_{1\text{vib}}$ and $T_{2\text{vib}}$ was used in the calculations.

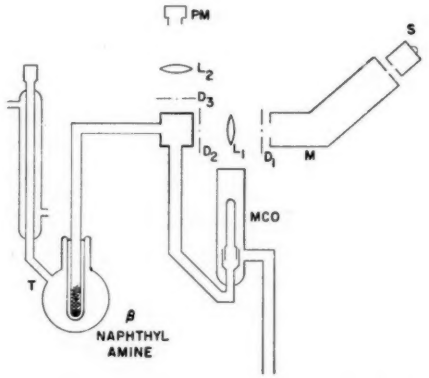

FIG. 6. S—source; M—monochromator; $D_1D_2D_3$—diaphragms; L_1L_2—quartz lenses; PM—photomultiplier; C—quartz cell; MCO—magnetic cut-off; T—temperature bath.

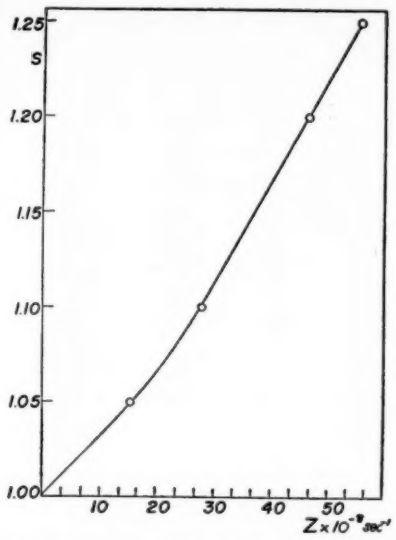

FIG. 7. Fluorescence stabilization by deuterium ($\lambda=2650$ A, $t=186$°C).

This is certainly a poor approximation. For instance, the identical values of E in the case of hydrogen and helium suggest that the internal degrees of freedom of the hydrogen molecule are inactive in the exchange process. The true accommodation coefficient for H_2 would then be equal to that of helium and refer only to a vibrational-translational exchange.

The inefficiency of hydrogen, as determined quantitatively by the fluorescence stabilization method is of interest in connection with several problems of chemical kinetics. Thus the ability of hydrogen to maintain the high pressure rate of unimolecular reactions was attributed[4] to its efficiency in supplying vibrational energy to the dissociating molecule. Zener[5] explained this apparent efficiency by the possibility of a transfer involving the relatively large rotational quanta of the hydrogen molecule. It is now recognized, however, that the unimolecular reactions in question are complex in nature and involve radical chains. More recently, Small

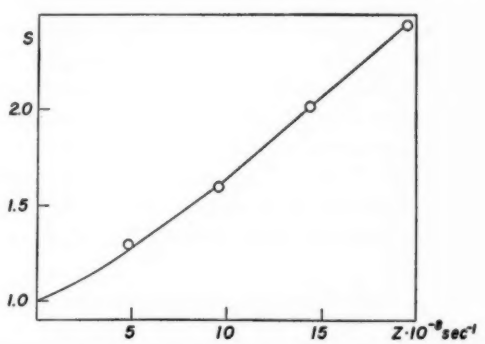

FIG. 8. Fluorescence stabilization by sulfur hexafluoride ($\lambda=2650$ A, $t=186$°C).

[4] C. N. Hinshelwood, *Kinetics of Chemical Change* (Clarendon Press, Oxford, 1940), p. 84.

[5] C. Zener, *Tenth Report of the Committee on Catalysis* (National Research Council, 1935).

TABLE II. Energy exchange from Neporent's data.

Gas	λ_a A	t°C	ΔE cm^{-1}	E cm^{-1}	E Neporent	α
CO_2	2652	150	8460	550	430	0.5
	2537	150	10200	600	630	0.3
NH_3	2652	150	8460	950	750	0.9
	2537	150	10200	1070	1100	0.8
	2652	190	8460	880	630	0.8
	2537	190	10200	1000	1250	0.7
C_5H_{12}	2652	150	8460	1280	1150	0.2
	2537	150	10200	1690	1950	0.2
	2652	190	8460	1240	1350	0.2
	2537	190	10200	1450	1900	0.2
$CHCl_3$	2652	150	8460	1000	950	0.5
	2537	150	10200	1240	1600	0.5
H_2	2652	150	8460	70	30	0.1
	2537	150	10200	70	50	0.1
He	2652	150	8460	70	30	0.2
N_2	2652	150	8460	190	90	0.3

and Ubbelhode[6] have invoked a high stabilizing power of the hydrogen molecule in connection with their study of oxidation processes in the gas phase. There, a complex formed by association of O_2 and a hydrocarbon radical is said to be stabilized with a high efficiency by hydrogen.

In view of the importance of this problem in chemical kinetics, it was decided to extend Neporent's data with the particular aim of elucidating the specificity of individual molecules for energy transfer. Hydrogen was chosen as the first molecule to be investigated: if internal degrees of freedom are inactive and if the vibrational-translational exchange depends only very slightly on relative molecular velocity, hydrogen and deuterium ought to give identical results. The deactivating activity of sulfur hexafluoride was also investigated since this molecule is frequently used in kinetic problems involving energy transfer because of its stability and unreactivity.

EXPERIMENTAL

A. Materials

Deuterium obtained from the Stuart Oxygen Company under U. S. Atomic Energy Commission approval Nos. B-2440, B-2991 was diffused through a heated palladium thimble. Sulfur hexafluoride was supplied 99 percent pure by the Matheson Company, Inc. In addition, this material was further purified by pumping at *ca* −170°C. The J. T. Baker Chemical Company provided β-naphthylamine which was purified by distillation under vacuum until a completely white product was obtained.

B. Apparatus

Other than the usual vacuum manifold and conventional ways of storage for the various substances used in these experiments the apparatus consisted of the components described in Fig. 6. The light source S is a Hanovia S-1 Alpine burner. The monochromator M is a home-made instrument consisting of a condenser lens, a quartz prism, and a quartz focusing lens. The selection of wavelengths on this instrument is made by moving a slit across the beam dispersed by the prism. This means a realignment of the optics for every selection made. The photomultiplier tube is a RCA 1P21. The tube is operated in 90 volts per stage and 45 volts between diode No. 9 and the anode. The power supply for this purpose consists of 20 45-volts B-batteries of the snap-on terminal type (Burgess 30). The cable leading to the multiplier is shielded for its entire length.

The quartz cell has the dimensions 2×2×5 cm. All windows are optically polished. The cell is mounted in a brass block electrically heated.

A magnetic cutoff of the type shown in Fig. 6 is used to separate the reaction cell from the remainder of the system. The temperature bath shown is used to vaporize the naphthylamine. This bath is currently replaced by an electrically heated finger for the same purpose.

Readings of the photomultiplier current are made on a Leeds and Northrup ballistic galvanometer No. 2285H of sensitivity 0.0057 μa/mm. All electrical supply to the apparatus is made through constant voltage Sola transformers.

C. Procedure

The light source was allowed to burn about one hour before any measurements were taken. In the meantime, the naphthylamine would reach the desired pressure by heating the bath surrounding it. The cell temperature was always kept higher than the bath temperature. When the above conditions were reached a reading of the fluorescence was taken, without any foreign gas present, by actuating a shutter between the light source and the cell.

When a pressure of foreign gas was needed, the magnetic cutoff was open to introduce the gas, then closed and a period of 10–15 minutes was allowed before taking a reading of fluorescence. Subsequent readings were at a lower pressure of the foreign gas. This was done by pumping out some of the gas on the system side of the cutoff and then opening the latter for a fraction of a minute to let pressure equilibrate itself on both sides. The final pressure was read on a mercury manometer on the system side of the cutoff. The same procedure was repeated at two different wavelengths: *ca* 2652 A and 3660 A. As shown by Neporent, foreign gases decrease the absorption coefficient of β-naphthylamine. Since at 3660 A the probability for radiationless transition is effectively zero, the relative fluorescence yield at this wavelength: $S_1=(F_z/F_0)_{3660}$ can be used for correcting for the absorption effect at shorter wavelengths. Thus, if $S_2=(F_z/F_0)_{2652}$ is the relative fluorescence yield at 2652 A, the fluorescence increase S, due to stabilization by foreign gases at 2652 A, will be equal to $S=(S_2/S_1)$.

[6] J. H. Small and A. R. Ubbelhode, J. Chem. Soc. **1950**, 723.

RESULTS AND CONCLUSIONS

The results for deuterium and sulfur hexafluoride at 186°C are presented in Figs. 7 and 8 where S, the relative fluorescence increase due to stabilization, is plotted against Z, the collision number. These data fully confirm the reality of the effects reported by Neporent. From the slopes of the curves at $Z=0$, the values of E can be calculated. They are

$E=50$ cm^{-1} for deuterium

$E=570$ cm^{-1} for sulfur hexafluoride.

The data with sulfur hexafluoride illustrate the stabilization effect quite clearly. Gunn[7] has calculated the heat capacity of this molecule and from his values we get an accommodation coefficient for SF_6 equal to 0.5. The favorable capabilities of sulfur hexafluoride strongly recommend its use in kinetic work.

The amount of energy transferred per collision with deuterium (50 cm^{-1}) at 186°C is slightly less than that calculated from Neporent's data with hydrogen at 150°C (70 cm^{-1}). The slight decrease may be due to the higher temperature used in our experiments, the duration of a collision being shorter at the higher temperature. At any rate, the difference does not seem to be significant and the values for both isotopic molecules permit one to conclude without any doubt that rotational degrees of freedom of light and heavy hydrogen do not take part in the vibrational deexcitation. If this were so, the amount of energy transferred by collision should be *at least* equal to twice the size of a rotational quantum *viz.* 120 and 60 cm^{-1} for H_2 and D_2, respectively. A stronger argument in favor of this conclusion is the value of $E=70$ cm^{-1} obtained by Neporent for helium at 150°, which coincides with the value for hydrogen at the same temperature. Thus hydrogen is no better than helium as a stabilizing agent because no internal degrees of freedom of the diatomic molecule take part in the exchange. In point of fact, the argument of Zener[4] concerning the relatively large size of the rotational quanta of hydrogen may be used to show that a vibrational-rotational transfer is unlikely in the case of hydrogen: it is because the rotational quanta are too large that the transfer does not take place easily. Indeed, with nitrogen, the value of E calculated from Neporent's data is considerably higher (190 cm^{-1}), showing that rotational degrees of freedom now participate in the exchange, the lack of restriction being presumably due to the small size of the rotational quanta for this molecule.

[7] J. C. Gunn, Gt. Brit. Aeronautical Research Council. Reports and Memoranda, No. 2338 (1952).

ACKNOWLEDGMENT

It is a pleasure to thank Dean Hugh Taylor for his encouragement and advice during the course of this investigation. Support of this work by the Air Materiel Command Contract No. AF 33(038)-23976 is gratefully acknowledged. Thanks are also due Dr. David Garvin, of this laboratory, for suggesting the use of sulfur hexafluoride.

APPENDIX

The number of collisions Z suffered per second by a naphthylamine molecule M with a foreign gas X at a pressure p (mm Hg) and absolute temperature T. From the kinetic theory formula:

$$Z_t=n_M n_X \sigma_{MX}^2\left[8\pi kT\frac{m_M+m_X}{m_M\cdot m_X}\right]^{\frac{1}{2}}$$

it follows that

$$Z=\frac{Z_t}{n_M}=\frac{pN_0}{RT}\cdot\sigma_{MX}^2(8\pi k)^{\frac{1}{2}}T^{\frac{1}{2}}\mu^{-\frac{1}{2}}$$

or

$$Z=0.44p\cdot\sigma_{MX}^2(1/\mu T)^{\frac{1}{2}},$$

where

σ_{MX} is the collision diameter of M and X, in A

μ is the reduced mass of M and X, in g mole.

The gas kinetic diameters used in these calculations are: 7 A (β-naphthylamine), 2.46 A (deuterium), and 5.5 A (sulfur hexafluoride).

Infrared Studies of Naphthalene and Naphthalene-d_8

WILLIS B. PERSON,* GEORGE C. PIMENTEL, AND OTTO SCHNEPP †
Department of Chemistry and Chemical Engineering, University of California, Berkeley, California
(Received June 2, 1954)

Infrared spectroscopic studies of naphthalene and naphthalene-d_8 are reported as follows: (a) far infrared studies of solid $C_{10}H_8$ in the region 450 to 130 cm^{-1}, (b) studies of single crystals of $C_{10}H_8$ with polarized light in the spectral region 3500–450 cm^{-1} for the *ab* and *bc* planes at normal incidence, (c) study of gaseous $C_{10}H_8$ in the spectral region 1350–440 cm^{-1}, (d) studies of single crystals of $C_{10}D_8$ with polarized light in the spectral region 3400–500 cm^{-1} for the *ab* plane at normal incidence, (e) study of a gaseous $C_{10}D_8$ in the spectral region 1000–700 cm^{-1}. Most likely symmetry assignments for the absorptions of $C_{10}H_8$ and $C_{10}D_8$ are given and some of the bands of $C_{10}D_8$ are correlated with those of $C_{10}H_8$.

A CONSIDERABLE amount of effort has been devoted to the infrared study of naphthalene in this laboratory. Infrared spectra of $C_{10}H_8$ in the gas phase, in solution, and in the solid state, have been reported.[1] The solid state studies included polarized spectra using single crystals of naphthalene and the observed dichroic effects were interpreted using a simple model, the "oriented gas" model. To test the correctness of the interpretation of dichroic frequency shifts, further studies of mixed crystals of naphthalene in anthracene[2] and of $C_{10}D_8$ in $C_{10}H_8$[3] were made.

Important contributions to the understanding of the vibrational assignment of naphthalene have been made recently by Goubeau, Luther, Feldmann, and Brandes,[4] and by Lippincott and O'Reilly.[5] Goubeau, *et al.*, studied the Raman spectra of naphthalene-d_8, 1-naphthalene-*d* and 2-naphthalene-*d*. Lippincott and O'Reilly present both Raman and infrared studies of napthalene-d_8 and offer a tentative vibrational assignment.

Additional infrared studies of naphthalene which have been made in this laboratory will be reported here. Interpretation of these spectral results will be made in a companion report. In summary, the new work presented here includes: (a) far infrared studies of solid naphthalene in the spectral range 450–130 cm^{-1}; (b) polarized infrared spectra of single crystals of $C_{10}H_8$ studied at normal incidence to the *bc* plane; (c) gas phase spectra of $C_{10}D_8$ in the spectral range 1000–700 cm^{-1}; (d) polarized infrared spectra of single crystals of $C_{10}D_8$ studied at normal incidence to the *ab* plane. In addition, the normal incidence single crystal and gas phase spectra reported in reference 1 have been completely repeated, using more perfect single crystals and improved resolution. These spectra are included when significant new information is apparent.

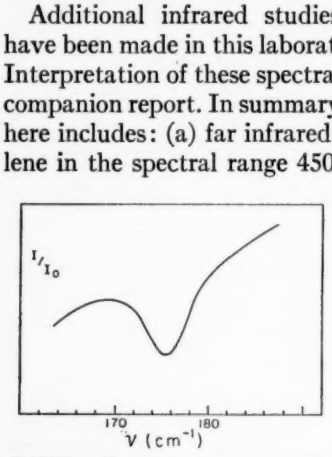

FIG. 1. Infrared spectrum of naphthalene near 175 cm^{-1}: solid $C_{10}H_8$ suspended in paraffin.

EXPERIMENTAL

The far infrared studies were obtained on a grating spectrometer described elsewhere.[6,7] Frequency accuracy is ±1 cm^{-1} at 175 cm^{-1}. Naphthalene was melted with paraffin and a thin sheet of the paraffin-naphthalene melt poured onto a flat surface. Upon solidification, a small piece of this mixture was supported immediately in front of the thermocouple detector. The background spectrum of the paraffin alone was obtained in a similar manner.

The crystals used for the studies of the *bc* plane were grown, using the technique described in reference (1). The *bc* plane was located relative to the cleavage plane (the *ab* plane) by using the optical properties of the naphthalene crystal as given by Sundararajan.[8] A crystal section cut parallel to the *bc* plane was prepared and polished to a thickness of 0.1±0.02 mm. The spectra were taken of this sample using a Perkin-Elmer Model 12C infrared spectrometer with NaCl and KBr prisms. A conventional transmission polarizer with ten AgCl plates was used. Slit widths are shown on the spectra. The crystal was mounted with the *b* axis parallel to the entrance slit and the plane of polarization of the incident light was altered by rotating the polarizer.

Completely deuterated naphthalene was prepared[9] by a procedure similar to that used in the deuteration of

* Present address: School of Chemistry, University of Minnesota, Minneapolis, Minnesota.

† Present address: Hebrew Institute of Technology, Haifa, Israel.

[1] G. C. Pimentel and A. L. McClellan, J. Chem. Phys. **20**, 270 (1952); earlier infrared studies are summarized in this reference.

[2] G. C. Pimentel, J. Chem. Phys. **19**, 1536 (1951).

[3] W. B. Person and G. C. Pimentel, J. Chem. Phys. **20**, 1913 (1952).

[4] Gaubeau, Luther, Feldmann, and Brandes, Chem. Ber. **86**, (2) 214–226 (1953).

[5] E. R. Lippincott and E. J. O'Reilly, Jr., J. Chem. Phys. **23**, 238 (1955).

[6] Bohn, Freeman, Gwinn, Hollenberg, and Pitzer, J. Chem. Phys. **21**, 719 (1953).

[7] The authors wish to express appreciation to Dr. Conrad Bohn and Mr. J. L. Hollenberg for taking the far infrared spectra. Dr. Bohn devised the sample suspension technique.

[8] K. S. Sundararajan, Z. Krist. **93**, 238 (1936).

[9] We wish to thank Mr. Nelson Alley and Mr. Henry Rodeen for preparing the $C_{10}D_8$.

benzene.[10] Resublimed Baker's naphthalene was shaken with 50 percent D_2SO_4 (made by mixing SO_3 with D_2O) at a temperature near 120°C. for 50 to 100 hours. After four such exchanges, the amount of hydrogen remaining in the sample was estimated spectroscopically from the intensity of the absorption near 3000 cm^{-1} to be about two atom percent. This corresponds to about fifteen mole percent of $C_{10}D_7H$.

The spectra of gas and solid phase $C_{10}D_8$ were obtained on the same spectrometer used for the *bc* plane studies of $C_{10}H_8$. The vapor phase was studied using a heated cell 7 cm long with AgCl windows. The crystals were grown by sublimation, and perfect single crystals were selected on the basis of completeness of extinction when observed between crossed polarizers in a petrographic microscope. Carefully selected single crystals grown by sublimation displayed more complete extinction than was ever observed using the melt-solidification technique described in reference 1.

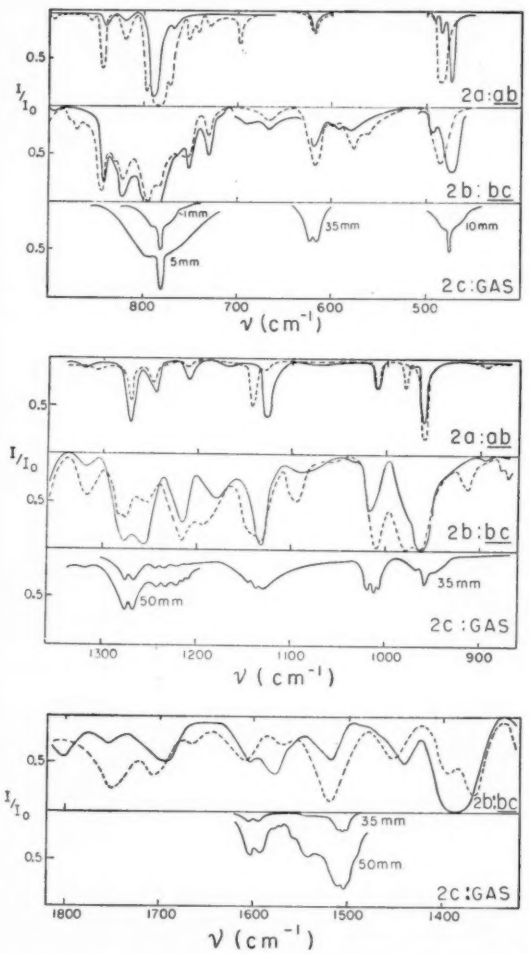

FIG. 2(a). Infrared spectra of a single crystal of naphthalene using polarized light, *ab* Plane at normal incidence. ——— Polarization parallel to *b* axis. - - - - Polarization perpendicular to *b* axis. (b). Infrared spectra of a single crystal of naphthalene using polarized light. *bc* Plane at normal incidence. ——— Polarization parallel to *b* axis. - - - - Polarization perpendicular to *b* axis. (c). Infrared spectrum of gaseous naphthalene. Pressures are shown on the spectrum.

[10] Ingold, Raisin, and Wilson, J. Chem. Soc. **1936**, 915.

TABLE I. Polarized infrared spectra of solid naphthalene: *bc* plane.

Frequency (cm^{-1}) and relative intensity Plane of polarization oriented: Parallel to *b* axis	Perpendicular to *b* axis
473 (4)	485 (3)
491 (1)	...
580 (1)	577 (2)
618 (2)	617 (3)
730 (2)	730 (1)
750 (2)	752 (1)
790 (10)	794 (10)
821 (4)	822 (4)
841 (4)	846 (5)
...	914 (2)
964 (9)	962 (9)
...	980 (9)
1015 (5)	1009 (8)
1088 (1)	1093 (4)
1131 (8)	1132 (7)
...	1143 (6)
1178 (4)	...
...	1193 (6)
1217 (6)	1217 (7)
1255 (8)	1252 (4)
1276 (7)	1276 (5)
1316 (1)	1316 (4)
...	1368 (6)
1387 (9)	1392 (5)
1442 (4)	1454 (4)
1519 (4)	1519 (7)
1578 (5)	1572 (1)
1604 (4)	1610 (4)
...	1667 (1)
1694 (4)	1706 (5)
1754 (1)	1750 (6)
1803 (2)	...
...	1836 (3)
1865 (3)	1870 (3)

The repetition of the $C_{10}H_8$ spectral studies was considerably more informative than the earlier studies. More perfect single crystals were obtained by sublimation as just described and the dichroic intensity variations observed earlier were accentuated. Improvements in spectral resolution resulted from modifications to the spectrometer including addition of a glass disk for "chopping" the light in the KBr prism region to eliminate stray light.

RESULTS

A portion of the far infrared spectrum near 175 cm^{-1} of randomly oriented solid $C_{10}H_8$ suspended in paraffin is shown in Fig. 1. Three bands were observed in these far infrared studies—475, 362, and 176 cm^{-1}. The first band was reported in reference 1 and the second mentioned briefly by Sponer and Nordheim.[11] The last band, 176 cm^{-1}, which has not been observed previously,

[11] H. Sponer and G. P. Nordheim, Discussions Faraday Soc. **9**, 19 (1950).

TABLE II. Infrared spectra of naphthalene-d_8 in the vapor and solid phases.

Gas	Solid: *ab* plane, plane of polarization oriented parallel to *b* axis	Solid: *ab* plane, plane of polarization oriented perpendicular to *b* axis	Solution[5]	Symmetry class
	...	546 (2)	408 *s*	?
			541 *mw*	1*u*, 3*u*
	...	572 (2)	...	*H*
	595 (2)	595 (2)	593 *s*	2*u*?
	634 (8)	624 (8) 632 (9)	628 *vs*	1*u*, 3*u*
	653 (5)	653 (6)	...	*H*
	680 (5)	680 (7)	...	1*u*, 3*u*
	...	...	721 *w*	?
	739 (3)	739 (2)	738 *m*	2*u*
	...	...	756 *w*	?
	773 (2)	773 (2)	...	*H*
785 (5)	785 (2)	786 (5)	791 *vs*	(1*u*)
791 (10)	791 (8)	791 (8)		
800 (5)				
	803 (½)	804 (1)	819 *s*	1*u*, 3*u*
825 (6)	831 (3)	828 (3)	831 *vs*	(3*u*)
830 (7)	838 (1)	836 (3)	837 *vs*	
835 (6)				
880 (5)	879 (7)	880 (3)	879 *vs*	(2*u*)
889 (4)	886 (2)	889 (1)	886 *vs*	
905 (1)	905 (2)	905 (3)	905 *vw*	*H*
	920 (3)	920 (4)	...	*H*
	...	...	946 *w*	?
	963 (2)	963 (1)	...	2*u*
	1046 (1)	1053 (1)	1039 *w*	1*u*, 3*u*
	...	...	1087 *w*	?
	...	...	1172 *m*	?
	1192 (1)	...	1193 *m*	2*u*
	1203 (3)	1205 (2)	1214 *vw*	2*u*
	1227 (5)	1227 (3)	1228 *m*	2*u*
	1243 (6)	1240 (4)	...	2*u*
1258 (4)	1258 (8)	1259 (7)	1260 *vs*	2*u*
	...	...	1292 *w*	?
1316 (1)	1312 (4)	1312 (3)	1311 *w*	2*u*
	1391 (2)	1391 (2)	1403 *m*	?
	1418 (4)	1416 (3)	1418 *vw*	2*u*
	1440 (4)	1440 (3)	...	2*u*
	...	...	1540 *m*	?
	1568 (1)	1570 (2)	1562 *m*	1*u*, 3*u*
	1630 (3)	1630 (2)	1626 *m*	2*u*
	1675 (½)	1675 (½)	...	1*u*, 3*u*?
	...	...	2101 *vw*	?
	...	...	2149 *vw*	?
	2260 (10)	2253 (6)	2259 *s*	2*u*
	...	2271 (9)	2278 *vs*	1*u*, 3*u*
	2285 (7)	2285 (3)	2299 *vs*	2*u*
	2323 (1)	2323 (2)	...	1*u*, 3*u*
	...	...	2431 *vw*	?
	2866 (1)	2866 (1)	2861 *w*	?
	3042 (1)	3040 (½)	...	*H*
	3091 (1)	...	...	*H*
	3132 (1)	3121 (2)	...	*H*
	...	...	3152 *w*	?

is important in a vibrational assignment based upon calorimetric measurements.[12]

The spectra of single crystals of $C_{10}H_8$ using polarized light are shown in Fig. 2a (*ab* plane at normal incidence) and Fig. 2b (*bc* plane at normal incidence). Table I lists the bands observed in the *bc* plane studies together with relative intensities. Figure 2c shows the spectrum of $C_{10}H_8$ in the gas phase where improved band contour resolution was obtained.

[12] G. M. Barrow and A. L. McClellan, J. Am. Chem. Soc. **73**, 573 (1951).

The spectra of single crystals of $C_{10}D_8$ using polarized light are shown in Fig. 3a (*ab* plane at normal incidence). The spectrum of $C_{10}D_8$ in the gas phase is shown in Fig. 3b in the region 1000–700 cm^{-1}, where band contours were observed. Table II lists the bands of $C_{10}D_8$ observed, together with relative intensities. Several of the bands shown in Fig. 3a and listed in Table II are caused by the impurity $C_{10}D_7H$. These were identified by comparing the solution spectra of this sample to the spectra presented by Lippincott and O'Reilly.[5] The frequencies observed by Lippincott and O'Reilly for their purer sample of $C_{10}D_8$ are listed for comparison in Table II.

It is possible to deduce the symmetry class of the vibrations on the basis of gas phase band contour and also on the basis of the dichroic effects assuming the "oriented gas" model.[13] The dichroic ratios predicted

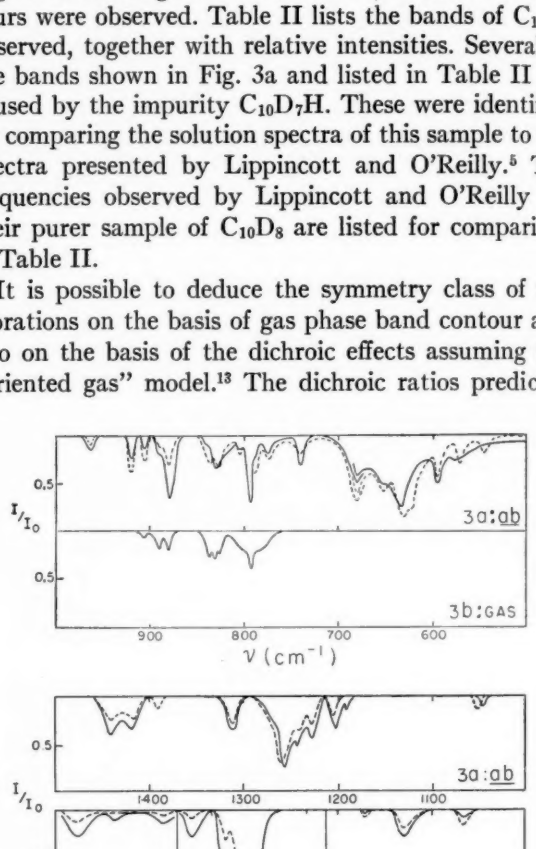

FIG. 3(a). Infrared spectra of a single crystal of naphtahlene-d_8 using polarized light. *ab* Plane at normal incidence. ——— Polarization parallel to *b* axis. – – – – Polarization perpendicular to *b* axis. (b). Infrared spectrum of gaseous naphtahlene-d_8 pressure, about 30 mm.

TABLE III. Predicted dichroic ratios for naphthalene.

Symmetry class	$I_\perp/I_\parallel$ *ab* plane	$I_\perp/I_\parallel$ *bc* plane
B_{1u}	3.6	0.20
B_{2u}	0.14	0.025
B_{3u}	4.2	23.2

[13] Before interpreting a polarized spectrum of an absorbing crystal, it is necessary to examine the optical properties of the crystal. The planes of naphtalene examined here, the *ab* and *bc* planes, each contain the monoclinic *b* axis, a unique symmetry axis. Therefore, one of the principal axes of each of the dielectric and conductivity tensors coincides with this crystal axis. Since the other principal axes of these tensors must then be perpendicular to the *b* axis, their projections on the *ab* and *bc* planes will coincide, respectively, with the *a* and *c* axes. Therefore, if light polarized in a plane containing the *b* axis or perpendicular to the *b* axis strikes at normal incidence either of the *ab* or *bc* planes, no elliptic polarization can result.

TABLE IV. Symmetry assignments for infrared active vibrations of $C_{10}H_8$.

Gas frequency (cm^{-1})	Gas Contour	Symmetry *ab* Plane	Symmetry *bc* Plane	Symmetry Best
176[a]	...	...	...	?
362[a]	...	...	...	?
475	1*u*	1*u*, 3*u*	1*u*, 2*u*	B_{1u}
581[a]	...	?	3*u*	B_{3u}
620	2*u*	?	3*u*	B_{2u}, B_{3u}
698	?	1*u*, 3*u*	1*u*, 2*u*	B_{1u}
730[a]	...	1*u*, 3*u*	1*u*, 2*u*	B_{1u}
742[a]	...	1*u*, 3*u*	...	B_{1u}, B_{3u}
747	?	1*u*, 3*u*	1*u*, 2*u*	B_{1u}
780	1*u*	1*u*, 3*u*	1*u*, 2*u*	B_{1u}
821	?	1*u*, 3*u*	1*u*, 2*u*	B_{1u}
842[a]	...	1*u*, 3*u*	3*u*	B_{3u}
868	?	?	3*u*	B_{3u}
878	?	1*u*, 3*u*	3*u*	B_{3u}
891	?	1*u*, 3*u*	1*u*, 2*u*	B_{1u}
915[a]	...	1*u*, 3*u*	3*u*	B_{3u}
956	1*u*	1*u*, 3*u*	1*u*, 2*u*	B_{1u}
978[a]	...	1*u*, 3*u*	3*u*	B_{3u}
1012	3*u*	?	3*u*	B_{3u}
1094[a]	...	1*u*, 3*u*	3*u*	B_{3u}
1125	?	2*u*	1*u*, 2*u*	B_{2u}
1143[a]	?	1*u*, 3*u*	3*u*	B_{3u}
1178[a]	...	2*u*	2*u* ?	B_{2u}
1193[a]	...	1*u*, 3*u*	3*u*	B_{3u}
1210	3*u* ?	2*u*	3*u*	B_{3u}
1234	2*u*	2*u*	1*u*, 2*u*	B_{2u}
1268	2*u*	2*u*	1*u*, 2*u*	B_{2u}
1310[a]	...	1*u*, 3*u*	3*u*	B_{3u}
1366	...	?	3*u*	B_{3u}
1389	?	2*u*?	1*u*, 2*u*	B_{2u}
1440[a]	...	2*u*	?	B_{2u}
1508	3*u*	1*u*, 3*u*	3*u*	B_{3u}
1565[a]	...	2*u*	2*u*	B_{2u}
1601	2*u*	2*u*	2*u* ?	B_{2u}
1662	?	2*u*	3*u*	?
1723	3*u* ?	1*u*, 3*u*	3*u*	B_{3u}
1767	2*u* ?	2*u*	3*u*	?
1804	3*u* ?	1*u*, 3*u*	1*u*, 2*u*	?
1840	3*u* ?	2*u*	3*u*	?
1919	?	2*u*	...	?
1944	?	2*u*	...	?

[a] Average solid phase frequency.

TABLE V. Correlation of infrared bands of $C_{10}H_8$ and $C_{10}D_8$.

ν_H $C_{10}H_8$	ν_D $C_{10}D_8$	$R=\nu_H/\nu_D$	Symmetry class	Vibration type
475	408	1.16	B_{1u}	o.p. skeletal bend
780	628	1.24	B_{1u}	o.p. hydrogen bend
956	790	1.21	B_{1u}	o.p. hydrogen bend
1125	885	1.27	B_{2u}	i.p. hydrogen bend
1268	1203–1258	1.05–1.01	B_{2u}	i.p. skeletal bend?
1601	1440	1.11	B_{2u}	i.p. skeletal bend
1012	830	1.22	B_{3u}	i.p. hydrogen bend
361	328	1.10	?	skeletal mode
620	595	1.04	B_{2u}?	i.p. skeletal distortion

o.p. =out-of-plane.
i.p. =in-plane.

for the *bc* plane differ from those predicted for the *ab* plane as shown in Table III.[14]

Table IV summarizes the information available relating to the symmetry class of the vibrations of $C_{10}H_8$ and an estimate of the most likely symmetry assignment. The last column of Table II includes this information for $C_{10}D_8$. For simplicity, the symmetry notations B_{1u}, B_{2u}, and B_{3u}, have been abbreviated 1*u*, 2*u*, and 3*u*. The symmetries derived from gas phase band contours are listed parenthetically in Table II.

Using all of the information in Figs. 2 and 3, and in Tables II and IV, several of the bands of $C_{10}D_8$ may be correlated to those of $C_{10}H_8$. These correlations are listed in Table V, together with the conclusions which can be drawn concerning the nature of some of the vibrations.

CONCLUSION

The experimental work presented here, together with the recent Raman studies of $C_{10}D_8$ [4,5] offer a favorable opportunity to examine the assignment of the fundamental vibrations of naphthalene.

[14] Calculated from the crystal structure of naphthalene given by Abrahams, Robertson, and White, Acta Cryst. **2**, 233 (1949). Regrettably, erroneous values of the calculated dichroic ratios for the *ab* plane of naphthalene were reported in reference (2). The values in Table III should be used.

Interpretation of the Infrared Spectrum of a Molecular Crystal: Naphthalene

GEORGE C. PIMENTEL, A. L. MCCLELLAN,* WILLIS B. PERSON,† AND OTTO SCHNEPP ‡
Department of Chemistry and Chemical Engineering, University of California, Berkeley, California
(Received June 2, 1954)

A critical examination of the oriented gas model is made on the basis of several suggested criteria applied to the infrared studies of solid $C_{10}H_8$ and $C_{10}D_8$. The frequency difference between gas and solid spectra is as high as 1 percent ν for only a few naphthalene bands. The dichroic band splittings which can be assigned to intermolecular interactions are small, averaging less than 3 cm^{-1}, but with a few well defined exceptions. A comparison between the observed and predicted dichroic behaviors for those bands whose symmetry classes are known indicates that the dichroism is dominated by the gas phase symmetries of the vibrational modes. The general applicability of the oriented gas model for naphthalene indicates its usefulness in interpreting those solid spectra. On the other hand, the occasional, distinct deviations from the model warn that it is not likely to be useful in studying crystals involving stronger crystal forces (such as hydrogen bonds or ionic forces).

THE general theory of the vibrational spectrum of a molecular crystal has been well discussed by several authors. The spectrum differs from that of the same substance in the gas phase because crystalline forces with the lattice symmetry have been superimposed on the forces and symmetry of the free molecule. The magnitude and nature of the spectral differences will be related to the magnitude and nature of the intermolecular interactions in the crystal. In molecular crystals it is likely that these intermolecular forces will be small compared with the intramolecular forces within the free molecule. In the limiting case of negligibly small intermolecular forces, the spectrum of the crystal should be the same as that of isolated molecules, except that the molecules are oriented in fixed positions. Such considerations have led to the use of an "oriented gas" model to interpret the spectrum of the crystal.[1,2] This model and its inherent assumption that intermolecular forces are negligible have been tacitly assumed by a number of workers in interpreting the spectra of molecular crystals. Although there has been some support of the assumption, systematic investigations of the importance of lattice perturbations in determining the spectra of molecular crystals are needed. This paper reports such a systematic study based on the spectra of naphthalene.

Naphthalene has been studied intensively in this laboratory[1,3–5] and the spectra provide an opportunity to investigate in some detail the spectral behavior of this molecular crystal. There are several spectral characteristics which can be used as tests to determine the importance of crystal effects and the area of applicability of the oriented gas model.

1. *Frequency shift on solidification:*—If lattice perturbations are small, there should be no frequency differences between gas phase and solid phase spectra.

2. *Dichroic splitting of bands:*—Depending upon the lattice symmetry and number of molecules per unit cell, molecular vibrations may split into several components with, in general, different intensity dependence on crystal orientation. When the splitting is small, these components are evidenced by a variation of the band frequency as the crystal orientation is changed. This frequency shift, or band splitting, should be absent for an oriented gas.

3. *Correlation of dichroic intensity effect and vibrational symmetry class:*—The oriented gas model offers a qualitative prediction of the relative intensity of a band observed with polarized infrared light at various crystal orientations. This prediction is based on the assumption that the orientation of the molecules and the direction of dipole moment change on exciting the vibration in an isolated molecule are the dominant factors determining the dichroism.

4. *Gas phase selection rules:*—A vibrational mode which is inactive in the infrared or the Raman spectrum in the molecular symmetry should remain inactive in an oriented gas, even though the crystal symmetry selection rules indicate the motion to be active.

5. *Quantitative prediction of the dichroic intensity effect:*—The relative intensity of a band observed with polarized infrared light at various crystal orientations should correlate quantitatively with the square of the appropriate projection of a unit vector parallel to the direction of dipole change.[1,2]

If weak crystal coupling could be applied to a perfect oriented gas, it is probable that the spectral characteristic No. 5 would be influenced before the others. As the coupling is increased, the other spectral characteristics would reflect the coupling roughly in turn in inverse numerical order. It seems unlikely that, for any given band, any characteristic will show oriented gas behavior if preceding characteristics do not. On the other hand, it is quite possible that the oriented gas predictions of a given spectral characteristic could be reliable

* California Research Corporation, Richmond, California.
† University of Minnesota, Minneapolis, Minnesota.
‡ Hebrew Institute of Technology, Haifa, Israel.
[1] G. C. Pimentel and A. L. McClellan, J. Chem. Phys. **20**, 270–277 (1952).
[2] Ambrose, Elliott, and Temple, Proc. Roy. Soc. (London) **A206**, 192 (1951).
[3] G. C. Pimentel, J. Chem. Phys. **19**, 1536 (1951).
[4] W. B. Person and G. C. Pimentel, J. Chem. Phys. **20**, 1913 (1952).
[5] Person, Pimentel, and Schnepp, J. Chem. Phys. **23**, 230 (1955).

and useful even though a later characteristic deviates from oriented gas behavior.

The data available allow critical examination of these tests as applied to solid naphthalene, with the exception of the fourth.

1. FREQUENCY SHIFT ON SOLIDIFICATION

The frequency shift on solidification has been examined for the *ab* plane of $C_{10}H_8$ using 18 bands of gaseous $C_{10}H_8$.[1] The average absolute difference in frequency between the gas phase absorption and the nearest band in the solid spectrum was found to be 2.6 cm^{-1}. Six bands of $C_{10}D_8$ show a corresponding average shift of 2.0 cm^{-1}. It is of particular interest, however, to investigate the examples of bands which definitely shift by a larger amount. Three bands of gaseous $C_{10}H_8$, 780, 1234, and 1268 cm^{-1}, show shifts of $+7\pm3$, $+16\pm6$, and $+8\pm5$ cm^{-1}, respectively (ν solid-ν gas; ν solid is taken to be the average frequency of the band when splitting is observed). The first band, 780 cm^{-1}, displays significant dichroic splitting, indicative of large intermolecular coupling for this vibrational mode. The other two bands, 1234 and 1268 cm^{-1}, do not exhibit this large splitting, yet the band shifts are distinctly outside the probable uncertainties and the gas-to-solid correlations relatively unambiguous. Since these two bands have similar band contours in the gas phase spectrum, there must be intramolecular, resonance interaction between the two vibrational modes whether the molecule is in the gas or solid phase. It is possible that this interaction is important in these unusually large band shifts.

If a band shows a frequency change, on solidification, of only a few reciprocal centimeters, it seems reasonable to conclude that the normal modes of vibration are not substantially altered in character when the molecule is placed in the crystal lattice. For naphthalene only a small number of modes are altered in energy by as much as 1 percent.

2. DICHROIC SPLITTING

The magnitude of the dichroic splitting has been investigated for one band of naphthalene, $C_{10}H_8$,[3] and for one band of deuterated naphthalene, $C_{10}D_8$,[4] by use of mixed crystals. In the first instance, the $C_{10}H_8$ band at 780 cm^{-1} displays a splitting of 8 cm^{-1} and the $C_{10}D_8$ band at 632 cm^{-1} displays a splitting of 3.5 cm^{-1}. Each splitting is fairly unambiguously associated with intermolecular effects.

Determining the splitting without such mixed crystal studies requires the correlation of bands in the polarized spectra of a single crystal in two distinct orientations. Since the large splittings are of most interest and these are the most difficult to identify, we shall consider in turn each suggested large splitting. The splittings will uniformly be expressed as $(\nu_{\parallel}-\nu_{\perp})$ where the subscript indicates the relation between the *b* axis and the plane of polarization of the light.

Because of the comparative isolation of the $C_{10}H_8$ band at 475 cm^{-1} the dichroic splitting is easily observed. In both *ab* and *bc* plane $\Delta\nu=-12$ cm^{-1}.

The $C_{10}H_8$ features at 1129 and 1142 cm^{-1} provide an interesting example of possible splitting of a single fundamental mode. However, the alternate possibility that there are two fundamental frequencies visible in this region of the solid spectrum is more likely. The indistinct contour of the gas phase band at 1125 cm^{-1} is strong evidence of two bands here. The absence of a similar pair of bands with about the same splitting in the spectrum of solid $C_{10}D_8$ also supports the alternate suggestion. Finally, the spectrum of naphthalene in CCl_4 solution displays more than one absorption in this region. It is probable that the $C_{10}H_8$ bands at 1129 and 1142 cm^{-1} are independent features.

Two regions of the spectrum of the *ab* plane of $C_{10}H_8$ show pairs of bands which suggest doublets with large splittings, 1250–1279 and 1362–1385 cm^{-1}; but it is unlikely that either of these pairs arises from a single molecular mode. Each of these bands has a counterpart in both gas and solution spectra. In the gas spectra, however, there is significant contrast in intensity between the members of each of the pairs. This contrast is less marked in the solid phase, as well as in the solution spectra. It seems definite that neither of the pairs is derived from a split molecular mode, but rather each band arises from a distinct molecular mode which experiences significant intensity alteration in the condensed phase spectra.

There is one other pair of $C_{10}H_8$ bands which suggests doublet splitting, 1563–1594 cm^{-1}. This pair can be discussed together with the pair of bands 1417–1440 cm^{-1} in the spectrum of solid $C_{10}D_8$. In the spectra of the *ab* plane, all four of these bands display the same dichroic behavior. For the $C_{10}H_8$ pair there is only one band visible in this region of the gas phase spectrum (1596 cm^{-1}) and, similarly, only one in the CCl_4 solution spectrum (1595 cm^{-1}). The only evidence that neither the 1563–1594 cm^{-1} nor the 1417–1440 cm^{-1} pair arises from a split band is the dichroic intensity behavior. The factor group analysis leads to the prediction that the maximum of intensity of one of the components of a split band should occur at a crystal orientation perpendicular to the orientation at which the other is maximized. This is not the case for these bands.

One final pair of bands in the solid $C_{10}D_8$ spectrum suggests doublet splitting, 828–836 cm^{-1}. The gas phase band contour in this region indicates only one naphthalene fundamental absorbs here.

There are many bands for which there is no evidence for large dichroic splitting. Table I compiles the bands for which dichroic splitting can be evaluated.

Of the 23 bands listed in Table I, 11 show no discernible dichroic splitting in the *ab* plane. The average of the absolute value of all of the dichroic splittings is 2.6 cm^{-1}, but a few bands display well-defined splittings consid-

TABLE I. Dichroic splitting in naphthalene.

	Gas frequency cm^{-1}	Splitting ($\nu_{\parallel}-\nu_{\perp}$) *ab* plane	*bc* plane
$C_{10}H_8$	475	−12	−12
	620	0	+1
	747	0	+2
	780	+8	−4
	821	0	−1
	956	−1.5	+2
	1012	0	+6
	1210	−1	0
	1234	−3	+3
	1268	−2	0
	1506	−2	0
$C_{10}D_8$	595	0	
	632	+3.5	
	680	0	
	738	0	
	791	0	
	832	−8	
	880	−1	
	963	0	
	1050	−7	
	1258	−1	
	1312	0	
	1391	0	

erably above this average, 7 to 12 cm^{-1}. Even so, the lattice perturbations are generally small, indicating little intermolecular coupling.

3. DICHROISM AND VIBRATIONAL SYMMETRY CLASS

To make a significant test of the correlation between the vibrational symmetry class (using the molecular symmetry in the free molecule) and the dichroism of a band as predicted by the oriented gas model, it is necessary to restrict consideration to bands for which the symmetry assignment is unambiguously known. The gas phase spectra of $C_{10}H_8$ and $C_{10}D_8$[5] permit the definite assignment of nine bands of $C_{10}H_8$ and three bands of $C_{10}D_8$. In addition, the symmetry of one band of $C_{10}D_8$ (632 cm^{-1}) can be assigned quite definitely on the basis of correlation with the corresponding band of $C_{10}H_8$ (780 cm^{-1}). These thirteen bands provide 22 definitive tests of the dichroism prediction because the polarized spectra of $C_{10}H_8$ are known for both *ab* and *bc* planes. The results are compiled in Table II, where the symbols $\perp$ and $\parallel$ refer to the orientation of the plane of polarization relative to the *b* axis when maximum absorption is predicted (or is observed) to occur.

We may conclude that the dichroism of a band in the solid spectrum is dominated by the gas phase symmetry of that band. Roughly 70 percent (16/22) of the bands studied display the dichroism appropriate to the gas phase symmetry. Only one example of direct contradiction (as opposed to the absence of dichroism) was observed (620 cm^{-1}). The dichroism of this band could not be distinguished in the *ab* plane but it is quite distinct in the *bc* plane. The band contour appropriate to the B_{3u} class (the class indicated by the dichroism) is characterized by the presence of a weak *Q* branch. No evidence for the presence of a *Q* branch could be found after study of this band at a number of pressures and varied optical conditions. The minimum spectral slit width used was 2 cm^{-1}.

4. GAS PHASE SELECTION RULES

Naphthalene does not offer a favorable opportunity to study change of selection rules because the site and factor group symmetries retain the molecular center of symmetry and hence the rule of mutual exclusion. As a result, the only expected change in selection rules concerns the motions of the A_u class of the free molecule. These A_u vibrations are Raman- and infrared-inactive in the free molecule whereas they are predicted to become infrared-active, both in the site and factor group symmetries (for further discussion see reference 1). Thus only four fundamental motions become active by a change of selection rules and their frequencies are unknown.

There are a few bands of $C_{10}H_8$ which are absent in the gas phase spectrum but appear with significant intensity in the solid phase spectra. These include, in order of decreasing intensity, bands detected at 841, 970, 726, 1180, 1307, 1094, and 581 cm^{-1}. Presumably some of these are combinations but it is also possible that some of them correspond to A_u fundamental modes. It is interesting that every one of the bands mentioned displays significant dichroic intensity changes. As mentioned earlier, however, naphthalene has a crystal structure which does not facilitate a critical test of the model.

5. QUANTITATIVE PREDICTION OF THE DICHROIC INTENSITY EFFECT

In view of the imperfect agreement in the qualitative correlation of test No. 3, it is unlikely that quantitative predictions of intensities will be accurate for many of the bands. This does not preclude usefulness of the quantitative intensity predictions, as will be seen below.

As a practical matter, it is exceedingly difficult to obtain meaningful intensity measurements for solids. The natural widths of bands in the spectra of solids may be extremely narrow, comparable in size with the slit width of the spectrometer under the best possible operating conditions. In such a case, the observed shape of the band and the apparent intensity are primarily determined by the slit width. Other sources of difficulty are inherent in studies of solids using polarized light. When the solid scatters light, resolution must be sacrificed. Frequency- and orientation-dependent reflection losses provide some uncertainty in band position and intensity. Imperfect polarization and instrumental polarization can cause incorrect dichroic effects. Most serious in some instances is the difficulty of obtaining a sufficiently thin sample of uniform, known thickness and perfect orientation. As a result of these problems, it is

more reasonable to search for predictions regarding the relative intensities of bands obtained with a fixed crystal orientation rather than to compare intensities of a single band viewed in different crystal orientations.

The spectra of reference 5 provide studies extending from 1300 to 700 cm^{-1} of the *ab* plane of a single sample. The spectral features at lower frequencies are not considered because of stray light interference. In the useful region there are five bands whose gas phase band contours identify their symmetry types, 1268, 1234, 1012, 956, and 780 cm^{-1}. The last of these is so much more intense than the others that it does not provide a useful comparison. Of the other four bands, the B_{3u} band at 1012 cm^{-1} is the most intense in the gas phase spectra. Using the oriented gas model, the intensity of this band should be very much reduced relative to the B_{1u} band at 956 cm^{-1} when viewed at normal incidence to the *ab* plane whatever the angle of the *b* axis. Furthermore, the 956 cm^{-1} band should be significantly more intense than the B_{2u} bands at 1234 and 1268 cm^{-1} when the plane of polarization is perpendicular to the *b* axis. These intensity relations are observed in the solid spectra and reassure the correlation of the weak band at 1012 cm^{-1} in the solid spectrum (*ab* plane) with the intense gas phase absorption at this frequency. Among this small number of bands, the relative intensities predicted in the *ab* plane are sufficiently close to the observed intensities to be useful as a self-consistency check on the assignments. It is unfortunate that the spectra of the *bc* plane shown in reference 5 are not useful for intensity comparisons because of the crystal thickness. It would be helpful to have more examples, particularly comparisons between the spectra of the gas phase and more than one crystal plane.

CONCLUSIONS

The detailed examination of the vibrational spectrum of naphthalene indicates only small spectral effects that can be attributed to intermolecular forces in the crystal.

TABLE II. Dichroism observed and predicted from correlation of gas phase band contours.

	Frequency cm^{-1}	Gas phase assignment	*ab* plane Predicted	*ab* plane Observed	*bc* plane Predicted	*bc* plane Observed
$C_{10}H_8$	475	B_{1u}	⊥	⊥	∥	∥
	620	B_{2u}	∥	?	∥	⊥
	780	B_{1u}	⊥	⊥	∥	∥
	955	B_{1u}	⊥	⊥	∥	∥
	1010	B_{3u}	⊥	∥≈⊥	⊥	⊥
	1238	B_{2u}	∥	∥	∥	∥
	1268	B_{2u}	∥	∥	∥	∥
	1508	B_{3u}	⊥	⊥	⊥	⊥
	1601	B_{2u}	∥	∥	∥	∥?
$C_{10}D_8$	632	B_{1u}	⊥	⊥		
	790	B_{1u}	⊥	∥≈⊥		
	830	B_{3u}	⊥	∥≈⊥		
	880	B_{2u}	∥	∥		

Several properties of the oriented gas model have been tested for naphthalene and deuterated naphthalene, restricting consideration to those bands for which distinct gas phase band contours have been resolved. For these bands occasional, distinct deviations from oriented gas behavior are observed, indicating that even for a molecular crystal involving relatively weak intermolecular forces the model is not completely applicable. On the other hand, it is evident that the dichroic intensity properties of solid naphthalene are most often consistent with the predictions of the model. The occasional failures warn that the spectra of crystals involving stronger intermolecular interactions (hydrogen bonds or ionic forces) might not correlate well enough to provide helpful information. However, the extremely simple nature of the model and its general qualitative agreement with the spectral data of naphthalene suggest that the model provides a valuable guide in the interpretation of the spectra of crystals involving only van der Waals intermolecular forces.

Vibrational Spectra and Assignment of Naphthalene and Naphthalene-*d*-8

ELLIS R. LIPPINCOTT, *Department of Chemistry, Kansas State College, Manhattan, Kansas*

AND

EDWARD J. O'REILLY, JR.,* *Department of Chemistry, University of Connecticut, Storrs, Connecticut*

(Received February 9, 1954)

Infrared and Raman spectra taken of samples of naphthalene-*d*-8 of high deuterium content are reported. These spectra along with spectral data on naphthalene have been used to make an assignment of frequencies to the normal modes of vibration for this molecule. Although this assignment represents a significant contribution towards a correct one and provides good agreement with the experimental thermodynamic data, it still contains a number of tenuous points.

INTRODUCTION

THE vibrational spectra of naphthalene have been studied by many investigators.[1–7] Mannebach[8] has given a theoretical discussion of the planar skeletal vibrations of the molecule. Pimentel and McClellan have made infrared dichroic studies of naphthalene and naphthalene-*d*-8, and published some band contour data for naphthalene peaks observed in the vapor state.[2] Nedungadi[4] has studied the polarization spectrum of a naphthalene single crystal in the Raman effect. Goubeau[9] has published the Raman spectra of naphthalene-*d*-8 and other substituted deuteronaphthalenes. L. Corsin has studied the infrared spectrum of naphthalene-*d*-8, (private communication).

Pimentel and McClellan have recently offered a vibrational assignment of naphthelene and naphthalene-*d*-8, and recalculated the thermodynamic functions of naphthalene,[10] improving upon previous data.[11]†

Sponer and Cooper[12] have recently given a vibrational analysis of the vapor absorption spectra of light and heavy naphthalenes in the region 2900–2500 A.

The complexity of the infrared and Raman spectra of naphthalene has as yet precluded a satisfactory complete vibrational assignment, much less a determination of the force constants of the molecule. Difficulties associated with the problem arise from the fact that many of the fundamental active vibrations are weak, often much less intense than some combination tones and overtones. In addition the interpretation of the spectra has been hampered by conditions of accidental resonance, strong shadows of the Raman exciting line, poor agreement of data among various investigators, and the large number of active fundamentals, attended by the associated mathematical difficulties.

We have investigated the infrared and Raman spectra of naphthalene and naphthalene-*d*-8. The recent data of Pimentel and McClellan[10] has necessitated changes in our original assignment.[13] Our results lead to values of the heat capacity and entropy which agree with the experimental results of Barrow and McClellan.[11]

While we believe that we have made a significant contribution toward a correct assignment there are still many tenuous points.

EXPERIMENTAL

The naphthalene, Eimer and Amend cp product, was sublimed and recrystallized from alcohol. Naphthalene-*d*-8 was prepared by an exchange reaction based upon an observation of Weldon and Wilson.[14] Sixteen g of naphthalene, 56 g of calcium oxide dried at 1100°C for 3 hours, and 20 ml of 99.8 percent deuterium oxide were added under a nitrogen atmosphere to a 125 ml capacity steel bomb. The sealed bomb was heated for 24 hours in a furnace at 400°C. At the end of a run, the naphthalene was vacuum distilled from the heavy calcium hydroxide, dried, and the reaction rerun with fresh samples of calcium oxide and deuterium oxide. This procedure was repeated seven times, the final pass being made with double the quantities of inorganic constituents. The product naphthalene-*d*-8 was purified from a yellow contaminent by repeated distillation. Yield 25 percent, mp 82.6–83.0°C. There was no CH absorption in the infrared spectrum of the product, and mass spectroscopic analysis showed it to have a deuterium content of 101±3 percent of theoretical. We believe this method to be general for hydrocarbon materials. The mass spectroscopic analysis of the heavy naphthalenes were made by Dr. Graff at the Yale Medical School, Department of

* Based on a Ph.D. thesis presented by Edward J. O'Reilly, Jr., to the Graduate School of the University of Connecticut, Storrs, Connecticut, 1953.

[1] G. B. Bonino, Gazz. chim. ital. **66**, 827–843 (1936).

[2] G. C. Pimentel and A. L. McClellan, J. Chem. Phys. **20**, 270–277 (1952); (1913).

[3] R. Norris, Proc. Indian. Acad. Sci. **16A**, 250–255 (1942).

[4] Nedungadi, Proc. Indian. Acad. Sci. **15A**, 376 (1942).

[5] H. Luther, Z. Elektrochem. **52**, 210–219 (1948).

[6] Braun, Spooner, and Fenske, Anal. Chem. **22**, 1074 (1950).

[7] H. Luther and B. Hampel, Z. Physik. Chem. **202**, 390 (1954).

[8] C. Mannebach, J. Chim. Phys. **46**, 49–57 (1949).

[9] Goubeau, Luther, Feldmann, and Brandes, Chem. Ber. **86**, 214–226 (1953).

[10] A. L. McClellan and G. C. Pimentel, J. Chem. Phys. **23**, 245 (1954).

[11] G. M. Barrow and A. L. McClellan, J. Am. Chem. Soc. **23**, 573–575 (1951).

† Their reference 1, generally corresponds to our reference 13.

[12] H. Sponer and C. D. Cooper, J. Chem. Phys. (to be published).

[13] E. J. O'Reilly, Jr., thesis submitted to the Graduate School, University of Connecticut, 1953.

[14] L. H. P. Weldon and C. L. Wilson, J. Chem. Soc. **1946**, 235–239.

Physiological Chemistry. The samples were diluted by a factor of 50 with $C_{10}H_8$ so that the deuterium content would be in the range covered by his instrument.

A heavy naphthalene was also prepared by refluxing under reduced pressure a solution of 12.8 g of naphthalene in 225 ml of carbon tetrachloride with 8 ml of 65 mole-percent sulfuric acid-*d*-2 for 197 hours, with magnetic stirring. The acid was replaced every 24 hours.

TABLE I. Raman and infrared frequencies of naphthalene and naphthalene-*d*-8 in cm^{-1}.

Naphthalene		Naphthalene-*d*-8	
Raman[a]	Infrared[a]	Raman[a]	Infrared[a]
3190 w	3223 w		3152 w
3129 m	3192 w	2780 mw	2861 w
3063[b] s	3107 s	2302 m	2431 vw
3051[b] s	3072 vs	2268[c] s	2299 vs
3028 mw	3014 s	2257 mw	2278 vs
3011 mw	2994 m	1573 w	2259 s
2975 mw	2976 s	1548[c] m	2149 vw
2945 mw		1437 w	2101 vw
2914 mw	2947 m	1408 w	1626 m
2873 m	2859 w	1380[c] vs	1562 m
2822 mw	2611 w	1295 mw	1540 m
2785 m	2539 w	1219 w	1418 vw
2712 w	2512 w	1170 w	1403 m
2676 w	2439 w	1120 w	1330 w
2496 mw	2430 m	1006 w	1311 w
1682 w	2310 w	929 w	1292 w
1628 mw	2298 w	875 w	1260 vs
1586 mw	2289 w	862[c] s	1228 m
1578[b] s	2258 w	829 mw	1214 vw
1460[b] s	2154 w	777 vw	1193 m
1440 m	2081 w	752 mw	1172 m
1376[b] vs	1952 s	694[c] m	1087 w
1337 mw	1942 m	671 w	1039 w
1240 m	1919 m	569 vw	946 w
1168 mw	1907 m	541 mw	905 vw
1144 m	1857 m	491[c] s	886 vs
1099 vw	1842 m		879 vs
1025[b] s	1818 m	339 w	837 vs
941[b] mw	1779 m	270 mw	831 vs
878[b] w	1747 m	180 w	819 s
774[b] mw	1733 m		791 vs
760[b] vs	1716 m		756 w
715 w	1680 m		738 m
611 vw	1595 s		721 w
585 w	1510 m		628 vs
511[b] s	1387 vs		593 s
385 mw	1360 m		541 mw
285 mw	1339 w		408 s
191 w	1268 vs		328[d] m
	1237 m		
	1211 s		
	1156 m		
	1139 s		
	1129 vw		
	1012 s		
	957 s		
	942 m		
	876 m		
	825 s		
	782 vs		
	752 s		
	740 m		
	717 m		
	618 s		
	475 s		
	361[d] m		

[a] vs very strong, s strong, m medium, mw medium weak, w weak, vw very weak.
[b] Considered as Ag because of intensity.
[c] Polarized 4, 5, 6, 7.
[d] Data of Corrsin (private communication).

TABLE II. Selection rules for D_{2h} structure.

Species	Number of vibrations	Activity	a[a]
A_g	9	R	(∥)
A_u	4	Inactive	(⊥)
B_{1g}	8	R	(∥)
B_{1u}	4	IR	(⊥)
B_{2g}	3	R	(⊥)
B_{2u}	8	IR	(∥)
B_{3g}	4	R	(⊥)
B_{3u}	8	IR	(∥)

[a] a refers to modes of vibration which involve displacements parallel to or perpendicular to the plane of the molecule respectively.

The resulting heavy naphthalene solution was separated from the attending sulfonic acids by shaking with alkali, dried, and distilled to give a heavy naphthalene in 25 percent yield. The deuterium content from mass spectroscopic analysis was 95.3 percent of theoretical, calculated on the basis of naphthalene-*d*-8, indicating the presence of approximately 35 percent naphthalene-*d*-7. The influence of hydrogen on the frequencies of naphthalene-*d*-8 is illustrated by the spectrum of this sample (Fig. 3), especially in the regions 565–687 cm^{-1} and 3000 cm^{-1}.

An attempt to prepare 1-, 4-, 5-, and 8-naphthalene-*d*-4, which has the same D_{2h} symmetry as the parent molecule, was unsuccessful. O'Reilly[13] has shown that all the usual preparative procedures would probably fail and that a successful preparation must await more extensive knowledge of the chemistry of polysubstituted naphthalenes.

The infrared spectra of all three compounds were run ln carbon disulfide and carbon tetrachloride solutions in the region 667–4000 cm^{-1} on a Beckman IR-2 spectrometer using NaCl and LiF optics. The region 400–667 cm^{-1} was run using Nujol as a solvent with a Perkin Elmer model 12 C spectrometer with KBr optics by one of us (ERL) at Kansas State College. The infrared spectra of these compounds are shown in Figs. 1, 2, and 3 and are tabulated in Table I.

The Raman spectra of the three naphthalenes were taken with a Hilger E 612 glass Raman spectrograph. The camera aperture was F 5.7, slit width 0.15 mm and the time of exposure was 3–10 min. Mercury 4358 A excitation and Kodak 103J plates were utilized. A saturated sodium nitrite solution was used to filter out the mercury radiation below the exciting line, and a dilute Rhodamine solution was used to reduce the radiation above this wavelength. Spectra were obtained in the liquid state by passing water at 98°C through a jacket of the filter cell surrounding the Raman tube. A six-inch column of naphthalene, a four-inch and two and one-half inch column of naphthalene-*d*-8 were used in 6-mm o.d. Raman tubes. The weakness of the naphthalene-*d*-8 lines in the observed spectra is attributed in part to the small quantity used. The ob-

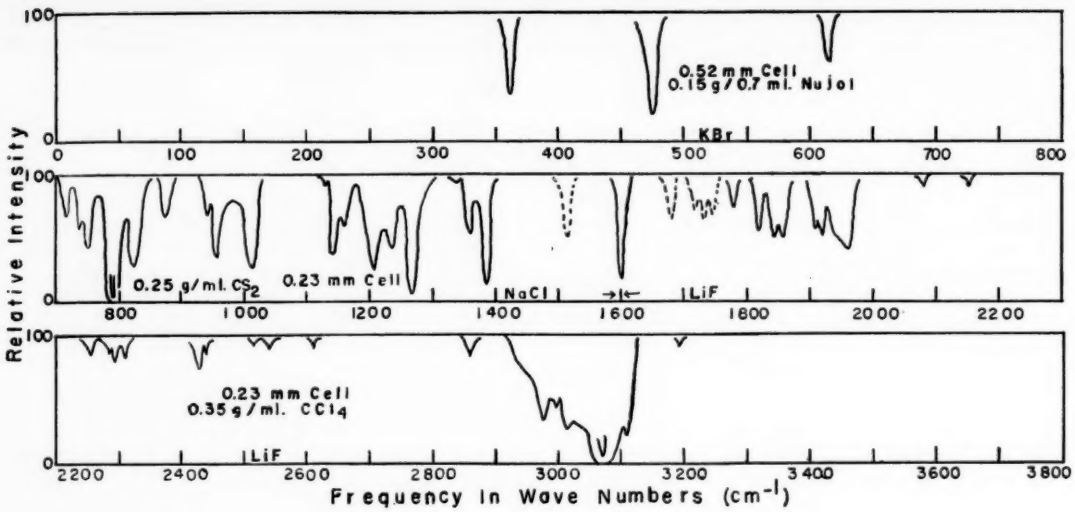

FIG. 1. Infrared spectrum of naphthalene.

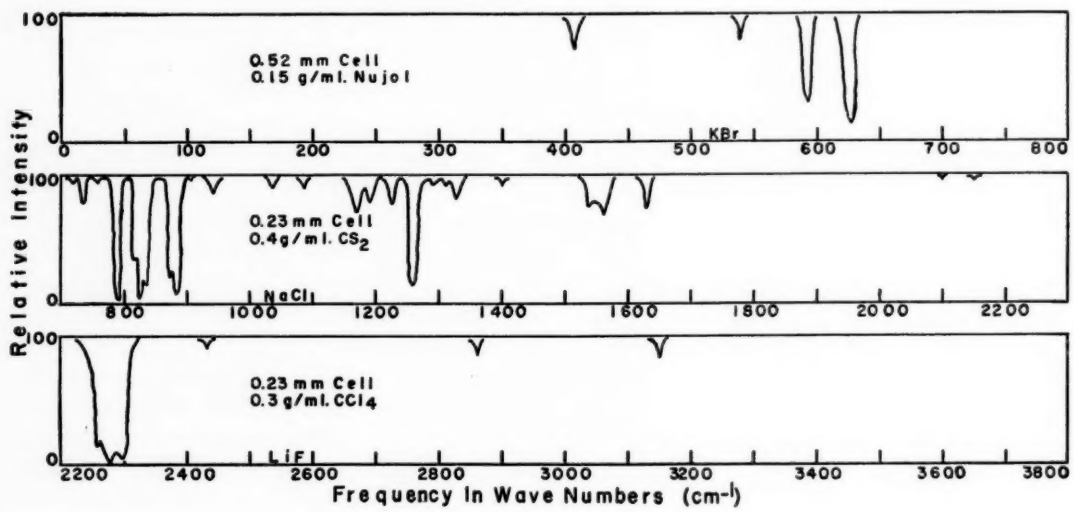

FIG. 2. Infrared spectrum of naphthalene-*d*-8.

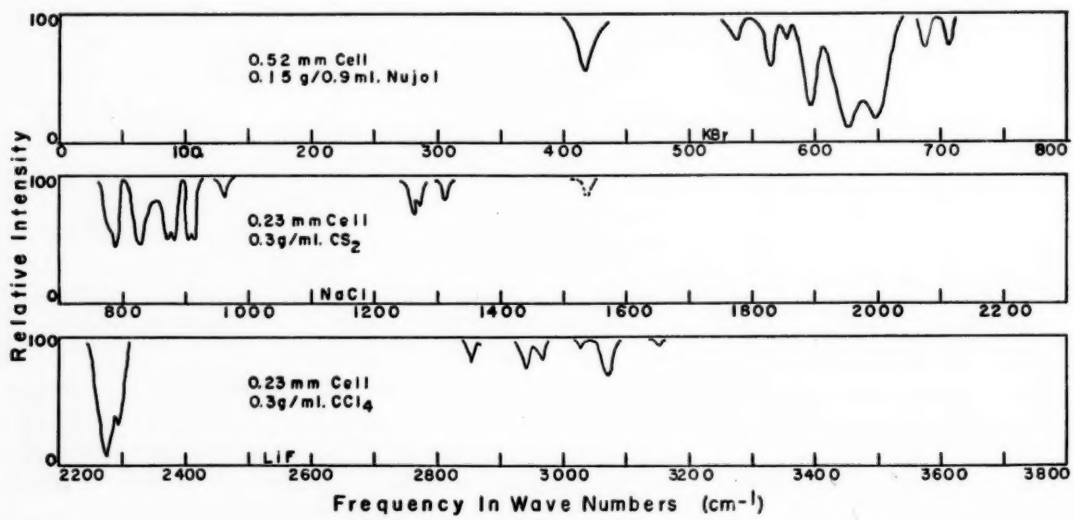

FIG. 3. Infrared spectrum of naphthalene-*d*-8 showing the effects of small amounts of hydrogen.

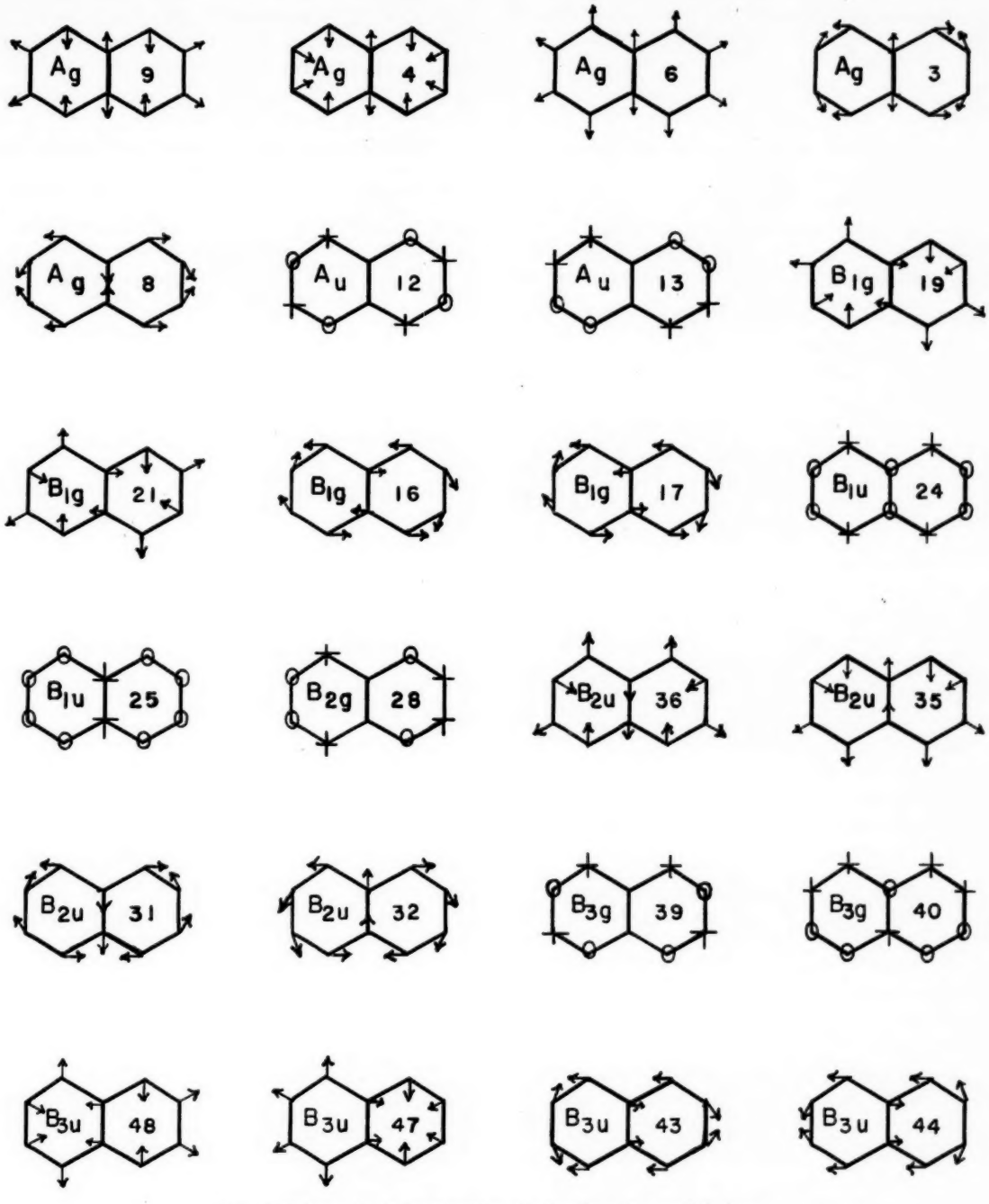

FIG. 4. Schematic skeletal modes of vibrations for naphthalene.

served Raman spectra of naphthalene and naphthalene-*d*-8 are given in Table I.

The 4358.35 A mercury exciting line is actually a quartet. Its secondary components, 4347.59 A, 4343.64 A, and 4339.235 A, lie 57, 84, and 101 cm^{-1} lower than the main exciting line. The first and last of these three secondary components are strong enough to give rise to shadows of the strong or medium Raman lines arising from 4358.35 A excitation. These shadows were eliminated from the tabulation of Raman frequencies.

GENERAL DISCUSSION

The naphthalene molecule is considered to have the conventional planar, bihexagonal, catacondensed structure of D_{2h} symmetry. There are 48 fundamental vibrations. Because of the presence of a symmetry center the rule of mutual exclusion should hold, and, except for accidental cases of degeneracy, there should be no coincidences between Raman and infrared frequencies. The selection rules and distribution of frequencies among the various symmetry species are given in

TABLE III. Spectral regions associated with different type of vibrations, and values of R.

Type vibration	Region cm^{-1}	Guide value of R
CH stretching	2900–3100	1.30–1.35
CD stretching	*ca* 2200	
CC stretching	1300–1650	1.05
Ring breathing	900–1000	
H(||) bending	1000–1500	1.20–1.28
H($\perp$) bending	700–1200	1.20–1.28
C(||) bending	<1000	1.05
C($\perp$) bending	<700	1.1

Table II. Figure 4 gives a schematic representation of the skeletal normal modes of vibration.

In the analysis, besides using the empirical position and intensity rules, there was also employed an empirical quantity, R, which measures the magnitude of the isotopic shift. R is defined as the ratio of the frequency of a vibration in the normal molecule, to the corresponding frequency in the isotopically substituted molecule. This quantity was determined from the data for benzene-benzene-*d*-6, and used as a rough guide to associate similar vibrations in naphthalene and naphthalene-*d*-8.[15] These quantities are presented in Table III.

The Teller-Redlich product rule, evaluated with the aid of Robertson's data for bond distances and angles,[16] was utilized as a measure of the correctness of the choice of frequencies in a given species, reasonable allowance being made for anharmonicity. The calculated and observed values for this rule are given in Table IV. Undetected accidental resonance, which can well occur in such a complex molecule, diminishes the value of this last criterion.

ASSIGNMENT OF RAMAN FREQUENCIES

There are nine totally symmetric vibrations corresponding to species A_g. The frequencies which immediately bear consideration as A_g type because of their intensity or the fact that they have been reported polarized are indicated by refs. b and a respectively in Table I. The systems 1025–862, 760–694, and 511–491 cm^{-1} of naphthalene and naphthalene-*d*-8 are readily connected because of their intensity. With the use of R, they are designated ν_6 skeletal breathing ν_8C(||), and ν_9C(||), respectively.

An anomally now exists. There are no lines in the naphthalene-*d*-8 spectrum which can be related on an intensity basis to the strong 1460 cm^{-1} naphthalene line. Further the 1376 cm^{-1} line of naphthalene, the strongest line in the spectra, is obviously related to the naphthalene-*d*-8 1380 cm^{-1} line, which is of comparable intensity. However, the direction of the shift 1376–1380, which has been verified by accurate measurement, is wrong for an explanation on the basis of simple isotopic substitution.‡ A reasonable interpretation is that the 1376-cm^{-1} line has been displaced from its natural position, about 1393 cm^{-1}, by Fermi resonance with the 1460-cm^{-1} line which is assigned as an overtone of an A_u

TABLE IV. Assignment of frequencies for naphthalene and naphthalene-*d*-8.

Species	Frequency No.	Type of vibration[a]	$C_{10}H_8$	$C_{10}D_8$	T_c	T_{obs}
A_g(||)	1	CH stretching	3063	2268	0.250	0.252
	2	CH stretching	3028	2257		
	3	CC stretching	1578	1548		
	4	Gamma C stretching	1393[b]	1380		
	5	CH bending (||)	1240	929		
	6	Skeletal breathing	1025	862		
	7	CH bending (||)	878	752		
	8	Skeletal distortion (||)	760	694		
	9	Skeletal distortion (||)	511	491		
A_u($\perp$)	10	CH bending	1000		0.500	
	11	CH bending	875			
	12	Skeletal distortion ($\perp$)	700			
	13	Skeletal distortion ($\perp$)	400			
B_{1g}(||)	14	CH stretching	3051	2302	0.268	0.270
	15	CH stretching	3011	2280		
	16	CC stretching	1628	1573		
	17	CC stretching	1586	1437		
	18	CH bending (||)	1440	1295		
	19	CC distortion (||)	1337	1219		
	20	CH bending (||)	1144	829		
	21	Skeletal distortion (||)	585	541		
B_{1u}($\perp$)	22	CH bending ($\perp$)	957	791	0.515	0.518
	23	CH bending ($\perp$)	782	628		
	24	CC distortion ($\perp$)	475	408		
	25	Ring wagging	176	160		
B_{2g}($\perp$)	26	CH bending ($\perp$)	1168	875	0.531	0.544
	27	CH bending ($\perp$)	941	777		
	28	Skeletal distortion ($\perp$)	385	339		
B_{2u}(||)	29	CH stretching	3014	2278	0.258	0.277
	30	CH stretching	2947	2215		
	31	CC stretching	1595	1540		
	32	CC stretching	1387	1260		
	33	CH bending (||)	1268	1039		
	34	CH bending (||)	1139	886		
	35	Skeletal distortion (||)	752	721		
	36	Skeletal distortion (||)	361	328		
B_{3g}($\perp$)	37	CH bending ($\perp$)	1440	1120	0.546	0.553
	38	CH bending ($\perp$)	715	569		
	39	Skeletal distortion ($\perp$)	285	270		
	40	Skeletal distortion ($\perp$)	191	180		
B_{3u}(||)	41	CH stretching	3072	2299	0.258	0.272
	42	CH stretching	2976	2259		
	43	CC stretching	1680	1626		
	44	CC stretching	1510	1403		
	45	CH bending (||)	1211	946		
	46	CH bending (||)	1012	831		
	47	Skeletal breathing	876	756		
	48	Skeletal distortion (||)	618	593		

[a] Since in some instances there is considerable mixing between CC stretching and CC(||) distortion modes, the distinction between these types is not always justified. The distinction in this case has been made arbitrarily on the basis of the spectral regions in which the frequencies are observed.
[b] Denotes the estimated unperturbed position of a fundamental that is affected by Fermi resonance.

[15] G. Herzberg, *Molecular Spectra and Molecular Structure. II. Infrared and Raman Spectra of Polyatomic Molecules* (D. Van Nostrand Company, Inc., New York, 1947), pp. 364–365.
[16] Abrahams, Robertson, and White, Acta Cryst. **2**, 233–238 (1949).

‡ Luther (see ref. 5) gives a value of 1374 cm^{-1} for this naphthalene line, and Goubeau (see ref. 9) cites 1381 cm^{-1} for the corresponding line in naphthalene-*d*-8.

fundamental at about 700 cm^{-1}. The system 1376–1380 cm^{-1} has been designated $A_g\nu_4$, a frequency which is essentially a symmetric gamma carbon stretching vibration.

The naphthalene 1578 cm^{-1} frequency was chosen as an $A_g\nu_3$CC stretching vibration. It is strong and sharp; it falls in the region where such a vibration is expected. The naphthalene-*d*-8, 1548-cm^{-1} line is apparently its isotopic counterpart. The fact that the 1578-cm^{-1} frequency is not reported polarized in the melt by Kohlraush[5] and Nedungadi[4] is not critical. While all polarized lines are of necessity A_g type, not all A_g lines need be polarized.§

In the CH region the strong naphthalene system, 3063–3051 cm^{-1} has been generally reported as a single polarized line about 3058 cm^{-1}. Norris[3] reports vibrations at 3057 and 3046 cm^{-1}, which may have also been a resolution of this 3058-cm^{-1} line. The upper (3063 cm^{-1}) component has been taken as $A_g\nu_1$, and associated with the 2268-cm^{-1} naphthalene-*d*-8 line. The 3028 cm^{-1} naphthalene frequency was chosen as the $A_g\nu_2$ vibration, and associated with the 2257-cm^{-1} naphthalene-*d*-8 line.

There remain two vibrations ν_5H(||) bending and ν_7H(||) bending to assign in the A_g species. The A_g 774-cm^{-1} vibration is too low for either of these. Further it is so close to the strong A_g 760-cm^{-1} line that it is more sensibly interpreted as a second harmonic of the 385-cm^{-1}, its intensity being strengthened by Fermi resonance with the 760-cm^{-1} fundamental.

The 1240-cm^{-1} naphthalene line is a good choice for the H(||) vibration. The 941-cm^{-1} vibration is not observed by Kohlraush[5] but he classifies the 878 cm^{-1} line as polarized. Braun, Spooner, and Fenske[6] observe both and give values of ρ equal to 0.63 and 0.8 for the 941 and 878-cm^{-1} lines respectively. An attempt to secure a reasonable source for the naphthalene-*d*-8, 752-cm^{-1} frequency, considering all the Raman data, has it arising from the 878-cm^{-1} naphthalene line. Then still considering the best fit for all the data in the Raman spectra the system 1240–929 cm^{-1} is designated $A_g\nu_5$H(||) and the system 878–752-cm^{-1} is assigned as the $A_g\nu_7$H(||) bending frequency.

We consider now the assignment of the B_{1g}, B_{2g}, and B_{3g} species. In the CH region, the 3051 and 3011-cm^{-1} naphthalene vibrations are selected as $B_{1g}\nu_{14}$ and ν_{15}. The naphthalene-*d*-8, 2302-cm^{-1} frequency is selected as the CD ν_{14} stretching vibration. There is no other line observed in the spectrum of naphthalene-*d*-8 which could be chosen as ν_{15}, so its value was calculated to be 2280 cm^{-1}, by assuming R has the same value for ν_{15} as in the ν_{14} system. The line 3011 cm^{-1}, which has been generally reported to be between 3001 and 3004 cm^{-1} by various authors, has had its value accurately rechecked.

The naphthalene 1628-cm^{-1} and 1586-cm^{-1} lines were taken to be the $B_{1g}\nu_{16}$ and ν_{17} CC stretching vibrations. The 1573 cm^{-1} and 1437 cm^{-1} naphthalene-*d*-8 lines were sensible choices as their isotopic counterparts.

There are three C(⊥) vibrations, one B_{2g} and two B_{3g}. These were assigned as 385 cm^{-1} $B_{2g}\nu_{28}$; 285 cm^{-1} $B_{3g}\nu_{39}$; and 191 cm^{-1} $B_{3g}\nu_{40}$. Their partners in the naphthalene-*d*-8 spectrum were obviously 339, 270, and 180 cm^{-1}. The distribution of the three frequencies between the two species was made so that there was a good over-all fit of data in the Raman spectra.

The naphthalene 1440-cm^{-1} line appears to be double, and was chosen to be both H(||) and H(⊥) bending vibrations, although this value is high for H(⊥) bending vibration.

The lines 1168 and 1144 cm^{-1} were both diffuse and appeared logically to drop to the 875- and 829-cm^{-1} lines in the naphthalene-*d*-8 spectrum. They were also classified as H(||) and H(⊥) bending type vibrations, respectively. The remaining assignments to the B_{1g}, B_{2g} and B_{3g} are shown in Table IV. These were made so that the data on intensities, frequency positions, value of R, the Teller-Redlich product rule, and the rule of "no-crossovers" were best obeyed.

The 611-cm^{-1} frequency was very faint and did not fit in with the assignment. The 671-cm^{-1} naphthalene-*d*-8 line did not fit either, but was readily interpreted as an overtone of the 339-cm^{-1} fundamental, intensified by resonance with the 694-cm^{-1} A_g fundamental.

The naphthalene 2873-cm^{-1} line appears to be a second harmonic of the 1440 cm^{-1} fundamental. The naphthalene 2785-cm^{-1} and naphthalene-*d*-8 2780-cm^{-1} lines are probably second harmonics of the (1393)–1380 ν_4 system.

INFRARED ASSIGNMENT

In the infrared spectrum of naphthalene there are twenty active fundamentals, sixteen located below about 1600 cm^{-1}. There probably are conditions of accidental resonance, because of the high concentration of absorption peaks; however, none could be definitely ascertained.

The $B_{2u}-B_{3u}$CH−CD region is assigned in a fashion similar to that of Pimentel and McClellan, using their dichroism data.[2] There is no CD band observed to associate with the lowest B_{2u}CH vibration, ν_{30}, so its value is calculated to be 2215 cm^{-1} by giving R the same value as with the $B_{2u}\nu_{29}$ system.

Using the band contour data of Pimentel and McClellan,[2] the peaks at 1595 and 1387 cm^{-1} are assigned to the B_{2u} species. They are readily associated with the naphthalene-*d*-8, 1540- and 1260-cm^{-1} peaks, and are designated as CC stretching vibrations. The systems 1680–1626 cm^{-1} and 1510–1403 cm^{-1} properly fit the conditions and data for the vibrational types B_{3u}CCν_{43} and ν_{44}, respectively.

Some characteristics of the spectra should now be indicated. The strongest naphthalene vibration by far is 782 cm^{-1}. The naphthalene-*d*-8, 791-cm^{-1}, absorption peak is of lesser, but still comparable intensity. No

§ Luther (see reference 7) reports a depolarization factor of 0.56.

satisfactory explanation unites these as skeletal vibrations under the influence of Fermi resonance as with the Raman 1376–1380 cm^{-1} system. That they are similarly related as H-bending vibrations is more improbable. The 800–900 cm^{-1} region of naphthalene-*d*-8 contains six intense bands in the solution spectra, at 791, 819, 831, 837, 879, and 886 cm^{-1}. Since these six strong bands are located within a 100-cm^{-1} region, it does not appear reasonable that they can all be assigned as B_{1u}, B_{2u}, or B_{3u} fundamentals.

There are four B_{1u} fundamentals. Pimentel[10] indicates that the naphthalene peaks at 957, 782, and 475 cm^{-1} and the naphthalene-*d*-8, 791-cm^{-1} peak have B_{1u} character. The system 957–791 cm^{-1} is necessarily designated as $B_{1u}H(\perp)\nu_{22}$. There are no other bands which could act as sinks and sources for the 957- and 791-cm^{-1} peaks, respectively. The 782–628-cm^{-1} system is designated as $B_{1u}H(\perp)\nu_{23}$. This choice is a result of the following facts. On the basis of intensities and *R*-values the 752- and 825-cm^{-1} naphthalene bands are ruled out for association with the naphthalene-*d*-8 peak at 628 cm^{-1}. Furthermore, there is no other strong peak for the 782-cm^{-1} naphthalene peak to drop to in the isotopic compound except the one at 593 cm^{-1}. This latter transition is not allowed, however, because the *R*-value (1.33) is too high for a hydrogen-bending vibration. The 475–408-cm^{-1} system is classified as $B_{1u}C(\perp)\nu_{24}$.

The region below 400 cm^{-1} should contain a B_{1u} fundamental, the so-called wing-wagging vibration.

Pimentel and McClellan[10] report a naphthalene frequency at 176 cm^{-1} which is taken as the lowest $B_{1u}C(\perp)$ type vibration ν_{25}. They calculated its isotopic counterpart to be at 160 cm^{-1}.

In the region of H-planar-bending frequencies the naphthalene 1268 and 1012 cm^{-1} peaks are B_{2u} and B_{3u} band contour respectively.[10] The strong naphthalene bands at 1211 and 1139 cm^{-1} in addition are chosen as fundamental vibrations. Since there are only four fundamentals in this region, the other bands are classified as combination tones. The series 1156, 1139, 1129 cm^{-1} appear to be one fundamental and two combination tones, even though Pimentel's band contour data indicate two frequencies in the vapor phase in this region.[10] The naphthalene-*d*-8 peaks at 886 and 831 cm^{-1} are of B_{2u} and B_{3u} character respectively.[10]

A disposition of these frequencies is as follows. The system 1012–831 cm^{-1} is chosen as $B_{3u}H(\|)\nu_{46}$. The 1268-cm^{-1} naphthalene frequency is associated with a naphthalene-*d*-8 peak at 1039 cm^{-1} as the $B_{2u}H(\|)\nu_{33}$. This choice, which is dictated by the value of *R* for a planar hydrogen-bending type vibration and the product rule, is not best on an intensity basis because of the low absorption of the 1039 cm^{-1} band. Similar considerations apply to the characterization of the systems 1139–886 cm^{-1} and 1211–946 cm^{-1} as $B_{2u}H(\|)\nu_{34}$, and $B_{3u}H(\|)\nu_{45}$, respectively.

Before discussing the four B_{2u} and B_{3u} skeletal deformation fundamentals, it is well to point out that the naphthalene-*d*-8 grouping 593, 541 cm^{-1} can, on the basis of *R*-values, only arise from the 618-cm^{-1} naphthalene peak. On the same basis, the naphthalene groupings 752, 740, 717 cm^{-1} and 825 cm^{-1} can go over only in the isotopic molecule to the grouping 756, 738, 721 cm^{-1}; the naphthalene 876-cm^{-1} line can go over to the naphthalene-*d*-8 grouping 819, 756 cm^{-1}. In each of these groups there is one band strong enough to demand explanation as a fundamental.

The naphthalene 618 and 876-cm^{-1} lines have $B_{1u}B_{3u}$ band contour,[2] and are associated with the naphthalene-*d*-8 peaks at 593 and 756 cm^{-1} as $B_{3u}C(\|)\nu_{48}$ and ν_{47}, respectively. These systems satisfy the B_{3u} product rule best, while still maintaining a proper balance between intensity relations and *R*-values.

The B_{2u} skeletal deformation assignment is 752–721 cm^{-1} ν_{35} and 361–328 cm^{-1} ν_{36}. This choice of 752 cm^{-1} as a B_{2u} fundamental is at variance with Pimentel and McClellan's dichroism data.[2] The choice of 361 cm^{-1} as B_{2u} is in agreement with Mannebach.[8]

The four inactive A_u frequencies ν_{10}, ν_{11}, ν_{12}, and ν_{13}, were assigned the values of 1000, 875, 700, and 400 cm^{-1} respectively. The assignment of all fundamental frequencies are tabulated in Table IV.

No serious attempt has been made to interpret the unused frequencies as combination tones or overtones.

We wish to acknowledge a grant-in-aid supporting this work by the Research Corporation. We wish to express our appreciation to G. C. Pimentel and H. Sponer for several helpful discussions.

Vibrational Assignment and Thermodynamic Properties of Naphthalene

A. L. McCLELLAN * AND GEORGE C. PIMENTEL
Department of Chemistry and Chemical Engineering, University of California, Berkeley, California
(Received June 2, 1954)

A complete vibrational assignment of naphthalene and naphthalene-d_8 is presented. This assignment is in substantial agreement with the experimental thermodynamic properties, the product rule and the spectroscopic data. The assigned frequencies are used to calculate the thermodynamic properties of naphthalene, S^0, C_p^0, $(H^0-E_0^0)/T$, and $-(F^0-E_0^0)/T$ from 273.16° to 1500°K.

RECENTLY, several studies of the infrared and Raman spectra of naphthalene and naphthalene-d_8 have appeared.[1–4] These data, combined with the measured thermodynamic properties of naphthalene,[5] permit a more reliable vibrational assignment than that proposed earlier by the present authors.[5]

Lippincott and O'Reilly[1] give a complete assignment for naphthalene without an attempt to fit the thermodynamic properties exactly. Partial assignments of the Raman-active fundamentals were given by Kohlrausch and Seka,[6] Nedungadi,[7] and Luther.[8] Mannebach[9] considered the planar skeletal vibrations.

VIBRATIONAL ASSIGNMENT

The symmetry of a number of vibrations can be assigned on the basis of the band contours in the spectra of gaseous naphthalene.[2] Coupled with the infrared[1,2,10] and Raman[1,3] spectra of naphthalene-d_8, these assignments provide a firm basis for determining approximate spectral locations of the characteristic vibrational modes of naphthalene. Table I lists the bands for which symmetry assignment and frequency shift on deuteration are definitely known. The deuteration frequency shift is expressed as R, the ratio $\nu(C_{10}H_8)/\nu(C_{10}D_8)$.

From the data presented in Table I, the vibrational assignment of benzene and a simple normal coordinate analysis of the out-of-plane skeletal vibrations, we have determined probable spectral ranges for each characteristic vibration type of naphthalene. The results are quite similar to the spectral regions and guide values of R derived independently by Lippincott and O'Reilly.[1] Only the estimates of the lower bounds for the skeletal distortions are significantly different from their Table III. We estimate that the lowest out-of-plane skeletal bend has a frequency between 100 and 200 cm^{-1}, and the lowest in-plane distortion has a frequency around 400 cm^{-1}.

The selection rules for naphthalene (molecular symmetry D_{2h}) have been given earlier.[1,10] The classes are taken up in the order of certainty of the assignment. The Raman frequencies listed here are average values based on twenty-one investigations.

A_g (9 FUNDAMENTALS)

The choice of the fundamental frequencies of this class is greatly simplified by the use of the polarization data.[6,11–13] The Raman shifts observed at 512, 762, 778, 880, 943, 1024, 1324, 1379, 1460, and 3058 cm^{-1} have been reported as polarized. In agreement with I, frequencies at 512, 762, 1024, 1379, and 3058 cm^{-1} are chosen as fundamentals. Furthermore, the argument presented in I, attributing a totally symmetric mode to the unpolarized line at 1576 cm^{-1} in preference to the polarized line at 1460 cm^{-1}, is accepted. The second hydrogen stretching motion of this class is assigned at 3001 cm^{-1}. Because it is more intense and has a lower

TABLE I. Naphthalene bands of known symmetry and deuteration shift.

Frequency		Class	R	Vibrational mode
$C_{10}H_8$	$C_{10}D_8$			
475 cm^{-1}	408 cm^{-1}	B_{1u}	1.16	op† skeletal bend
512	491	A_g	1.04	ip‡ skeletal distortion
620	595	B_{2u}?	1.04	ip skeletal distortion
762	694	A_g	1.10	ip skeletal distortion
1379	1379	A_g	1.00	ip skeletal stretch
1601	1440	B_{2u}	1.11	ip skeletal stretch
780	628	B_{1u}	1.24	op hydrogen bend
956	790	B_{1u}	1.21	op hydrogen bend
1012	830	B_{3u}	1.22	ip hydrogen bend
1024	862	A_g	1.19	ip hydrogen bend
1125	885	B_{2u}	1.27	ip hydrogen bend

† op = out-of-plane.
‡ ip = in-plane.

* Present address: California Research Corporation, Richmond, California.

[1] E. R. Lippincott and E. J. O'Reilly, Jr., J. Chem. Phys. **23**, 238 (1955). Hereafter this paper will be called I.

[2] Person, Pimentel, and Schnepp, J. Chem. Phys. **23**, 230 (1955). Hereafter this paper will be called II.

[3] Goubeau, Luther, Feldman, and Brandes, Chem. Ber. **86**, (2), 214–26 (1953).

[4] Pimentel, McClellan, Person, and Schnepp, J. Chem. Phys. **23**, 234 (1955).

[5] G. M. Barrow and A. L. McClellan, J. Am. Chem. Soc., **73**, 573 (1951).

[6] K. W. F. Kohlrausch and R. Seka, Deut. Chem. Gel. Ber. **71**, 1551 (1938).

[7] T. M. K. Nedungadi, Proc. Indian Acad. Sci. **15A**, 387 (1942).

[8] H. Luther, Z. Elektrochem. **52**, 210 (1948).

[9] C. Mannebach, J. chim. phys. **46**, 49–57 (1949).

[10] G. C. Pimentel and A. L. McClellan, J. Chem. Phys. **20**, 270 (1952).

[11] B. D. Saksena, Proc. Indian Acad. Sci. **8A**, 73 (1938).

[12] Benel, Kastler, and Rousset, Compt. rend. **211**, 595 (1940).

[13] Braun, Spooner, and Fenske, Anal. Chem. **22**, 1074 (1950).

value of ρ[13], the line at 943 cm^{-1} was selected instead of the line at 880 cm^{-1}. The line at 778 cm^{-1} is not considered because of its proximity to the more intense line at 762 cm^{-1}.

On the basis of intensities, the assignment of the corresponding $C_{10}D_8$ lines is fairly definite; 491, 694, 862, 1380, 2268, 1548, 2257, and 752 cm^{-1}. The $C_{10}D_8$ line at 829 cm^{-1} is omitted from this class because of proximity to the stronger line at 862 cm^{-1}.

The one A_g vibrational mode remaining, a hydrogen bending motion, is assigned to 1240 cm^{-1} ($C_{10}H_8$) and 1006 cm^{-1} ($C_{10}D_8$). The polarized $C_{10}H_8$ line at 1324 cm^{-1} is rather close to the intense polarized absorption at 1379 cm^{-1} and it can be associated with the combination between the two B_{3u} frequencies 742 and 581 cm^{-1}.

The values of R associated with this complete assignment of the A_g class suggest that the skeletal breathing mode absorbs at 1024 cm^{-1} but involves considerable interaction with the symmetric hydrogen bending motions. The high intensities of the 1024–862 cm^{-1} pair are consistent with the high intensities of the breathing motions of benzene and benzene-d_6, which provide the most intense lines observed in the respective Raman spectra.

B_{1u} (4 FUNDAMENTALS)

Three prominent bands in the infrared spectrum of gaseous $C_{10}H_8$ have the band contour appropriate to the B_{1u} class; 475, 780, and 956 cm^{-1}. The correlation of counterparts in the spectrum of $C_{10}D_8$ is straightforward; 403, 628, and 790 cm^{-1}, respectively. The remaining fundamental mode is ν_{25}, the motion identified in I as the "wing-wagging" motion. The simple normal coordinate analysis of the out-of-plane skeletal vibrations indicated that this motion should have the lowest frequency of the out-of-plane modes, and it was estimated to be between 100 and 200 cm^{-1}. The far infrared studies reported in II extend to 130 cm^{-1} and the band observed at 176 cm^{-1} is the only absorption detected below 362 cm^{-1}. This band is assigned as ν_{25} and from the product rule the $C_{10}D_8$ counterpart is calculated to be near 160 cm^{-1}.

B_{2u} (8 FUNDAMENTALS)

The gas phase spectra identify three B_{2u} fundamentals; 1268 and 1601 cm^{-1} for $C_{10}H_8$ and 885 cm^{-1} for $C_{10}D_8$. Correlation of the spectra of the solids allows choice with confidence of two $C_{10}H_8$–$C_{10}D_8$ pairs: 1601–1440 and 1125–885 cm^{-1}. The values of R, 1.11 and 1.27 show that the 1601 cm^{-1} band is associated with a skeletal stretching motion and the 1125 cm^{-1} band with a hydrogen bending motion.

Although the gas phase contour of the $C_{10}H_8$ band at 1385 cm^{-1} was not successfully resolved,[2] the investigations of the spectra of the solid phases indicate that this band has B_{2u} symmetry. The $C_{10}D_8$ counterpart could be the band observed at 1316 cm^{-1} or one of the features in the region near 1258 cm^{-1}. In either case, the isotopic shift identifies this fundamental as a skeletal stretching mode. Since only two skeletal stretching modes are expected, the intense B_{2u} band of $C_{10}H_8$ at 1268 cm^{-1} must be the unassigned hydrogen bending motion. This argument raises the dilemma that no band of suitable intensity is observed in the infrared spectrum of $C_{10}D_8$. The band at 1050 cm^{-1} is chosen despite a slight dichroism suggesting B_{1u} or B_{3u} symmetry. The selection of the band at 963 cm^{-1} as the $C_{10}D_8$ counterpart of the 1268 cm^{-1} fundamental frequency leads to product rule difficulties. With the pairing of 1268 cm^{-1} ($C_{10}H_8$)—1050 cm^{-1} ($C_{10}D_8$), however, the selection of the remaining fundamentals is not difficult. The $C_{10}H_8$ band at 620 cm^{-1} seems to be associated with a vibration of B_{2u} symmetry, although the polarized spectra of the solid phase do not corroborate the gas phase band contour. There is a band at 595 cm^{-1} with the dichroic properities of the B_{2u} class in the spectrum of solid $C_{10}D_8$. One of the skeletal distortion modes of the B_{2u} class is assigned to this 620–595 cm^{-1} pair. The other skeletal distortion motion is assigned to the $C_{10}H_8$ band at 362 cm^{-1} and the $C_{10}D_8$ band at 339 cm^{-1}.

The present assignment gives a satisfactory fit of the product rule and differs from I in the selection of skeletal distortion frequencies which are in better accord with the data of II.

B_{3u} (8 FUNDAMENTALS)

The spectra of gaseous naphthalene indicate three B_{3u} fundamentals: 1508 and 1012 cm^{-1} for $C_{10}H_8$ and 830 cm^{-1} for $C_{10}D_8$. The correlation of the 1012 and 830 cm^{-1} bands identifies one of the hydrogen bending motions. The band at 1508 cm^{-1}, associated with the $C_{10}D_8$ band at 1391 cm^{-1}, is considered to be caused by one of the two skeletal stretching motions. The other stretching motion is assigned to the 1723–1569 cm^{-1} pair. Just as in the B_{2u} class, the assignment of the second hydrogen bending motion is difficult. The pair 1144–905 cm^{-1} is selected, although the data of I indicate that much of the intensity of the $C_{10}D_8$ absorption near 905 cm^{-1} must be attributed to $C_{10}D_7H$ impurity. The remaining two skeletal motions are assigned to the $C_{10}H_8$–$C_{10}D_8$ pairs 742–680 and 581–546 cm^{-1}. With reasonable choices of the two hydrogen stretching motions, the complete assignment is in accord with the data of II and the product rule.

B_{1g} (8 FUNDAMENTALS)

The investigations of Nedungadi[7] using polarized light incident upon a single crystal of naphthalene segregate the in-plane vibrational modes from the nonplanar modes. After selection of the fundamental frequencies of the A_g class, the remaining in-plane modes can be attributed to B_{1g} motions. In agreement with Nedungadi, and Lippincott and O'Reilly,[1] we include the Raman shifts 1145, 1439, and 1586 cm^{-1} among the B_{1g} fundamental frequencies of $C_{10}H_8$. The

absorption observed at 1625 cm^{-1} is also designated as a B_{1g} fundamental. Presumably the two frequencies, 1625 and 1586 cm^{-1}, correspond to the two skeletal stretching motions of this symmetry. These can be associated with the two $C_{10}D_8$ bands at 1573 and 1473 cm^{-1}. Therefore, the $C_{10}H_8$ bands at 1439 and 1145 cm^{-1} must be associated with hydrogen bending motions The correlations given in I give values of R which are implausible. More acceptable selections for the $C_{10}D_8$ fundamentals are the Raman shifts observed at 1120 and 929 cm^{-1}.

Two B_{1g} hydrogen stretching motions and two skeletal distortion motions must be assigned on the basis of the frequency range expected and the product rule. The skeletal frequencies selected are 879 and 611 cm^{-1} for $C_{10}H_8$ and 777 and 569 cm^{-1} for $C_{10}D_8$.

B_{2g} AND B_{3g} (3 AND 4 FUNDAMENTALS)

Little basis exists for segregation of the Raman-active out-of-plane fundamentals. The skeletal normal coordinate analysis indicates that the frequencies of the lowest nonplanar motions have the order $B_{1u}<B_{2g}<B_{3g}$. The product rule provides the only other evidence in support of any distribution of frequencies between the B_{2g} and B_{3g} classes.

Each of the $C_{10}H_8$ bands at 191 and 285 cm^{-1} has a counterpart in the Raman spectrum of $C_{10}D_8$ (at 180 and 270 cm^{-1}). Since the lowest vibrational frequency for $C_{10}H_8$ is thought to be the B_{1u} frequency at 176 cm^{-1}, no explanation of 191 or 285 cm^{-1} involving sum combinations is possible. In the low temperature (20°K) fluorescence spectra of solid $C_{10}H_8$ and $C_{10}D_8$, McClure[14] has observed spectral features which can be associated with the vibrational frequencies 191–180 and 285–270 cm^{-1}, thus eliminating the explanation of any of these lines as a difference combination or as an impurity absorption. It seems necessary to include both 191 and 285 cm^{-1} as fundamentals of $C_{10}H_8$, and hence, the 191–180 cm^{-1} pair is assigned to the B_{2g} class and the 285–270 cm^{-1} pair to the B_{3g} class.

The second out-of-plane skeletal motion of the B_{3g} class is expected to absorb near 500 cm^{-1} (by comparison to the frequencies of the B_{1u} class) and the 588–541 cm^{-1} pair is selected. The $C_{10}H_8$–$C_{10}D_8$ pair 385–339 cm^{-1} was not used since the thermodynamic properties are consistent with an assignment containing only two Raman-active frequencies at or below 400 cm^{-1} if infrared-active frequencies at 176 and 362 cm^{-1} are included. The 385–339 cm^{-1} pair can be explained as harmonics of the lines at 191 and 180 cm^{-1}, respectively. If a frequency of 385 cm^{-1} is included in the assignment, the experimental thermodynamic properties seem to necessitate the elimination of one of the low frequencies: 176, 191, 285, 362, or 400 cm^{-1}. It seems necessary to retain the assignments of 176, 191, and 285 cm^{-1}. The infrared band at 362 cm^{-1} could be eliminated by assigning it to the combination of 176 cm^{-1} and 191 cm^{-1}. A final alternative is to raise the A_u frequency estimated at 400 cm^{-1} to a frequency above 500 cm^{-1}.

The hydrogen bending motions of the B_{3g} class were assigned to the Raman shifts at 774 and 1099 cm^{-1} for $C_{10}H_8$, and 671 and 829 for $C_{10}D_8$ on the basis of intensities and the product rule.

TABLE II. The fundamental vibrational frequencies for naphthalene and naphthalene-d_8.

Species	Freq. no.	Type of vibration	$C_{10}H_8$ cm^{-1}	$C_{10}D_8$ cm^{-1}	R
A_g	1	CH stretching	3058	2268	1.35
	2	CH stretching	3001	2257	1.33
	3	CC stretching	1576	1548	1.02
	4	CC stretching	1379	1379	1.00
	5	§ip CH bending and	1240	1006	1.23
	6	skeletal	1024	862	1.19
	7	breathing	943	752	1.25
	8	ip skeletal distortion	762	694	1.10
	9	ip skeletal distortion	512	491	1.04
			$\pi(R)=3.83$		(4.00)
A_u	10	‖op CH bending	1307		
	11	op CH bending	1094		
	12	op skeletal distortion	842		
	13	op skeletal distortion	(400)		
B_{1g}	14	CH stretching	3025	2302	1.31
	15	CH stretching	2980	2257	1.32
	16	CC stretching	1625	1573	1.03
	17	CC stretching	1586	1437	1.10
	18	ip CH bending	1439	1170	1.23
	19	ip CH bending	1145	929	1.23
	20	ip skeletal distortion	879	777	1.13
	21	ip skeletal distortion	611	569	1.07
			$\pi(R)=3.58$		(3.75)
B_{1u}	22	op CH bending	956	790	1.21
	23	op CH bending	780	628	1.24
	24	op skeletal bending	475	408	1.16
	25	op wing-wagging	176	(160)	1.10
			$\pi(R)=1.91$		(1.93)
B_{2g}	26	op CH bending	1167	875	1.33
	27	op CH bending	715	541	1.32
	28	op skeletal bending	191	180	1.06
			$\pi(R)=1.86$		(1.89)
B_{2u}	29	CH stretching	3034	2285	1.33
	30	CH stretching	2942	2256	1.30
	31	CC stretching	1601	1440	1.11
	32	CC stretching	1385	1258	1.10
	33	ip CH bending	1268	1050	1.21
	34	ip CH bending	1125	885	1.27
	35	ip skeletal distortion	620	595	1.04
	36	ip skeletal distortion	362	328	1.10
			$\pi(R)=3.71$		(3.85)
B_{3g}	37	op CH bending	1099	829	1.33
	38	op CH bending	774	671	1.15
	39	op skeletal bending	588	541	1.09
	40	op skeletal bending	285	270	1.06
			$\pi(R)=1.77$		(1.84)
B_{3u}	41	CH stretching	3070	2323	1.32
	42	CH stretching	2984	2271	1.31
	43	CC stretching	1723	1569	1.10
	44	CC stretching	1508	1391	1.08
	45	ip CH bending	1143	905	1.26
	46	ip CH bending	1012	830	1.22
	47	ip skeletal distortion	742	680	1.09
	48	ip skeletal distortion	581	546	1.06
			$\pi(R)=3.65$		(3.85)

§ ip = in-plane.
‖ op = out-of-plane.

[14] D. C. McClure (private communication).

TABLE III. Comparison of the experimental and calculated values of the heat capacity and entropy of naphthalene.

T °K	$C_p°$ cal/deg-mole Expt.	Calc'd	$S°$ cal/deg-mole Expt.	Calc'd
451.0	48.18±0.48	48.13	96.85±0.44	96.92
522.7	54.17±0.54	54.28	104.41±0.44	104.48

The two unassigned B_{2g} hydrogen motions were selected at 725 and 1167 cm^{-1} for $C_{10}H_8$ and at 541 and 875 cm^{-1} for $C_{10}D_8$. This choice places two $C_{10}D_8$ fundamentals at 541 cm^{-1}, a proposal which is consistent with the high intensity of this band.

A_u (4 FUNDAMENTALS)

Bands which could be associated with A_u motions are those observed in the infrared spectrum of solid naphthalene but absent in the spectrum of the gas. Seven bands which show this behavior are listed in reference 4. The normal coordinate analysis permits an estimate that the lowest A_u vibration is in the range 300–500 cm^{-1}. This frequency was guessed to be 400 cm^{-1}. The remaining three frequencies were selected from the seven bands listed in reference 4 with consideration of the expected spectral location and the thermodynamic properties. The final selections are 842, 1094, and 1307 cm^{-1}.

DISCUSSION

Table II summarizes the present assignment for $C_{10}H_8$ and $C_{10}D_8$. The table includes the value of R and the presumed vibration mode. For each symmetry species, agreement with the product rule can be seen by comparing $\pi(R)$, the product of the assigned R's, with the product calculated from the appropriate molecular parameters (given parenthetically after $\pi(R)$ in Table II).

The calculated entropy depends heavily upon the selections of the fundamental frequencies below 500 cm^{-1}. The present work utilizes two important data in the choice of these low frequency fundamentals; the observed infrared absorption at 176 cm^{-1}, and the argument in favor of assigning both 191 and 285 cm^{-1} as fundamentals.[14] To establish the sensitivity of the calculated thermodynamic properties toward changes of these low frequency motions, two alternative assignments were made, omitting the Raman line at 285 cm^{-1} or the Raman line at 191 cm^{-1}. In each case, the compensating changes required to restore agreement with the experimental thermodynamic properties were such that the calculated thermodynamic properties were unchanged within 0.3 cal/deg-mole over the temperature range 300–1500°K. These assignments suggest that alternate interpretations of the low frequency fundamentals will not radically alter the calculated thermodynamic properties.

TABLE IV. Calculated values of the thermodynamic properties of naphthalene in the ideal gas state.

T, °K	$C_p°$ cal/deg-mole	$\frac{H°-E_0°}{T}$ cal/deg-mole	$\frac{-(F°-E_0°)}{T}$ cal/deg-mole	$S°$ cal/deg-mole
273.16	29.18	15.83	61.92	77.75
298.16	32.08	17.07	63.36	80.43
300	32.28	17.16	63.46	80.63
400	43.20	22.34	69.11	91.44
500	52.44	27.47	74.65	102.11
600	59.94	32.28	80.08	112.36
700	66.01	36.68	85.40	122.07
800	71.00	40.67	90.56	131.22
900	75.13	44.27	95.56	139.83
1000	78.59	47.54	100.40	147.93
1100	81.52	50.50	105.07	155.56
1200	84.00	53.19	109.58	162.77
1300	86.11	55.64	113.93	169.57
1400	87.93	57.89	118.14	176.03
1500	89.49	59.94	122.20	182.14

THERMODYNAMIC PROPERTIES

Table III shows a comparison of the experimental and calculated values of the heat capacity and entropy. The calculated values are identical to those given by Barrow and McClellan[5] except for the thermodynamic contributions by the vibrational degrees of freedom. The agreement is within the experimental error.

Table IV lists the calculated values of the thermodynamic properties of naphthalene in the ideal gas state from 273.16° to 1500°K. The calculated values are probably accurate to ±0.5 cal/deg-mole but they are listed with more significant figures for uses where internal consistency is desired.

ACKNOWLEDGMENT

We wish to express our appreciation to the American Petroleum Institute Research Projects 44 and 50 for support of this investigation, and to Dr. E. R. Lippincott, Dr. D. S. McClure, and Dr. H. Sponer for extremely helpful discussions.

Nuclear Quadrupole Interaction in HCN and DCN in the Bending Vibrational Mode*

ROBERT L. WHITE†
Physics Department, Columbia University, New York, New York
(Received June 21, 1954)

The $\Delta J=0$, $\Delta F=0$ transition in HCN and DCN in an excited bending mode of vibration was observed to possess structure due to an asymmetry in the electric field gradient at the nitrogen nucleus coupling to the quadrupole moment of that nucleus. A selective breaking of the π bond perpendicular to the plane of bending when the molecule assumes its ionic structure is suggested as the source of the asymmetry.

INTRODUCTION

THE microwave spectra of HCN and DCN contain a number of lines characterized by the transition $\Delta J=0$,[1,2] where J is the molecular angular momentum exclusive of spins. The transitions occur between upper and lower l-type doublet levels belonging to the first excited state of the bending vibrational mode ν_2.[3] The $J=10$ line of HCN at 24 660.40 Mc and the $J=11$ line of DCN at 24 539.96 Mc have recently been observed with a high resolution spectrometer in the laboratory. It was discovered that the $\Delta F=0$ components previously reported as single were indeed multiple. Although the splitting is not due in the usual way to quadrupole coupling its explanation involves the quadrupole coupling of the N^{14} nucleus to an asymmetric electric field, and hence yields information on the bonding electrons contributing to the field.

APPARATUS AND EXPERIMENTAL PROCEDURE

The spectrometer used for the present investigation is a heterodyning balanced-bridge spectrometer of the type used by Geschwind.[4] Several important modifications of the prototype have been made, including the introduction of low frequency Stark modulation to eliminate the effects of frequency sensitive reflections in the bridge.[5] With such a spectrometer line widths of approximately 60 kc/sec at dry ice temperature have been attained repeatedly. However the attaining of such small line widths accentuates the problem of signal klystron wander, especially at low sweep rates. In particular, when a recording galvanometer was used with a sweep rate of about 100 kc per minute, it became obvious that some method of frequency stabilization was imperative if line shape were to be meaningful. Such slow sweep rates are desirable to permit the use of long time-constant filters, with the resulting improvement of signal-to-noise ratio and increase of spectrometer sensitivity.

Frequency stabilization was accomplished by a method similar to that used by C. A. Lee *et al.*,[6] and was instrumented as follows. There is in this laboratory a frequency standard with outputs at 30 270 and 3240 Mc. These frequencies, mixed in a crystal, produce markers every 30 Mc across the microwave region. Accordingly, a fraction of the signal klystron power was mixed with the frequency standard outputs, and the resulting sum and difference frequencies were fed to the antennas of two receivers: one a Hallicrafter SX-28 communications receiver (AM) operating in the range 0–15 Mc; the other a Hallicrafter S-36 FM receiver operating in the range 30 to 45 Mc. The FM receiver is tuned to the approximate difference frequency, and its discriminator output amplified and fed as an error voltage to the klystron repeller, thus locking the klystron to the difference frequency. Klystron tuning is accomplished by receiver tuning. For recorder applications a constant speed motor drives the receiver dial.

The AM receiver is used to measure the frequency of the klystron, which is in general not the same as the discriminator cross-over frequency. Different ranges of the two receiver and decoupling filters at their antennas were found necessary to prevent cross-tuning and other interactions.

In the present measurement, line shape was much more important than absolute frequency of the absorption maxima. Therefore extreme care was exercised to make certain that the group was traced out linearly, whereas little attention was paid to causing any one frequency marker to coincide with a line peak. Frequency markers were placed at 50 kc/sec intervals on the recorder trace by listening on the AM receiver for the zero beat as the klystron passed through the receiver frequency. The 50 kc increments in receiver setting were in turn measured on a BC-221 frequency meter. A number of traces of each compound were made, and the traces compared. The linearity of the sweep was in all cases confirmed to a few kilocycles per hundred.

CALCULATION OF THE SPECTRA

As was stated in the introduction, the K band lines of both HCN and DCN are $\Delta J=0$ transitions between l-type doublet levels. Upper and lower doublet levels

* Work supported jointly by the Signal Corps, Office of Naval Research, and Air Force.
† Present address: Hughes Research and Development Laboratories, Culver City, California.
[1] R. G. Shulman and C. H. Townes, Phys. Rev. **77**, 421 (1950).
[2] T. L. Weatherly and D. Williams, Phys. Rev. **87**, 517 (1952).
[3] Gerhard Herzberg, *Infrared and Raman Spectra* (D. Van Nostrand Company, Inc., New York, 1945).
[4] S. Geschwind, Ann. N. Y. Acad. Sci. **55**, 751 (1952).
[5] Gunther-Mohr, White, Schawlow, Coles, and Good, Phys. Rev. **94**, 1184 (1954).
[6] Lee, Fabricand, Carlson, and Rabi, Phys. Rev. **91**, 1395 (1953).

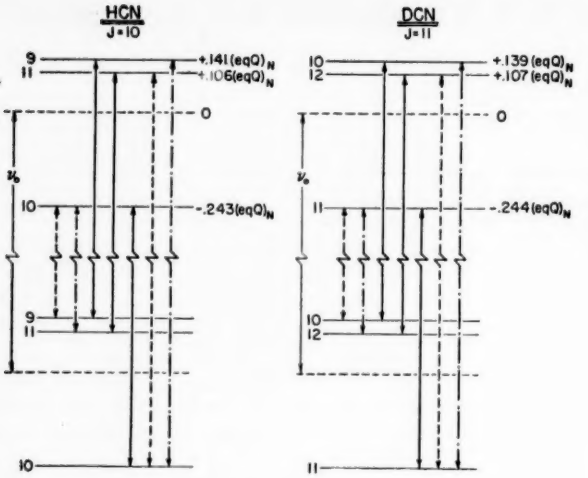

FIG. 1. Energy levels and expected spectra, neglecting asymmetries, of hydrogen cyanide.

are further split by the coupling of the nitrogen nuclear quadrupole moment to its surrounding field. The energy levels and expected spectra are given in Fig. 1. The $\Delta F=0$ transition is seen to be threefold degenerate, while the $\Delta F=\pm 1$ lines are weaker than those for which $\Delta F=0$ by a factor of greater than 100 and were not observed.

In the present investigation it was observed that the threefold degeneracy was removed by some interaction which might reasonably be expected to be either a coupling of the nuclear magnetic moment to the surrounding magnetic field, or a coupling of the nitrogen electric quadrupole moment to an asymmetry in the electric field gradient.

Consider the first possibility. To lift the degeneracy a difference in the magnetic interaction in upper and lower doublet levels would be required. For J of 10 or 11 and K of 1 the change in interaction energy with doublet level would be expected to be at most one percent of the magnetic coupling constant. The constants for the nitrogen nucleus in HCN and DCN are known

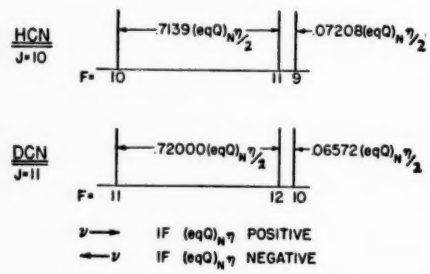

FIG. 2. Structure of $\Delta F_1=0$ transition arising from an asymmetry in electric field at the nitrogen.

to be 10 kc/sec and 8 kc/sec, respectively,[7] and the hydrogenic magnetic interaction might be expected to be of the same order of magnitude. Thus any splitting of magnetic origin would not be larger than a few hundred cycles.

To test the second hypothesis a fairly accurate calculation of the spectra can be made by treating the vibrating molecule as a slightly asymmetric rotor.[8] We introduce the asymmetry parameter η,[9] defined as

$$\eta=\frac{\dfrac{\partial^2 V}{\partial y_m^2}-\dfrac{\partial^2 V}{\partial x_m^2}}{\dfrac{\partial^2 V}{\partial z_m^2}},$$

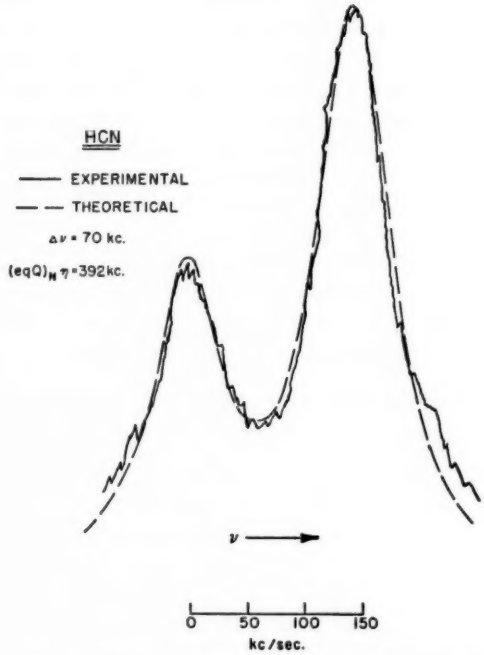

FIG. 3. Comparison of recorder trace of line with theoretical construct for HCN.

where V is the potential due to all charges outside a small sphere surrounding the nucleus, and x_m, y_m, and z_m are the molecular principal axes of greatest, intermediate, and least moment of inertia, respectively. For an asymmetric rotor the quadrupole energy of any level is given by

$$W_q=\frac{2J+3}{J}eq_J Q\left[\begin{array}{l}\text{Casimir's function as tabulated in}\\ \text{Appendix I, Kisliuk and Townes}^{10}\end{array}\right],$$

[7] J. A. Klein and A. H. Nethercott, Columbia Radiation Laboratory Quarterly Report, October 30, 1953.

[8] The treatment follows the arguments developed in C. H. Townes and A. L. Schawlow, *Microwave Spectroscopy of Gases* (McGraw-Hill Book Company, Inc., New York, to be published). Since this work is not yet available, source references are also included at certain points.

[9] J. K. Bragg, Phys. Rev. **74**, 533 (1948).

[10] P. Kisliuk and C. H. Townes, Molecular Microwave Spectra Tables, National Bureau of Standards Circular 518 (1952).

where for $K=1$[11]

$$q_J=q_m\left[\frac{3-J(J+1)}{(J+1)(2J+3)}\pm\eta\frac{J}{2(2J+3)}\right].$$

The upper sign refers to the upper asymmetric top level, and the lower sign to the lower, and

$$q_m=\frac{\partial^2 V}{\partial z_m{}^2}.$$

The fact that the quadrupole splitting is different for upper and lower levels removes the threefold degeneracy of the $\Delta F=0$ transition and gives the pattern shown in Fig. 2.

EXPERIMENTAL RESULTS

In Fig. 3 is presented a typical trace ot the $\Delta F=0$ transition for HCN superimposed upon a theoretical plot of the line, with $(eqQ)\eta$ and $\Delta\nu$, the line width parameter, adjusted for best fit. Figure 4 presents the same information for the DCN line. From the best fit of the theoretical plot one obtains for HCN $(eq_mQ)\eta=+392\pm8$ kc, for DCN $(eq_mQ)\eta=+372\pm12$ kc. The quadrupole coupling of nitrogen in HCN and DCN is known to be[12] $(eq_mQ)_N=-4.58$ Mc. Values of the asymmetry parameter of $\eta=-0.084$ for HCN and $\eta=-0.080$ for DCN are thus obtained.

It is also significant that the line width for best fit is greater in DCN than in HCN. The additional line width may be attributed to deuteron quadrupole coupling, but discussion of this point will be deferred to the paper immediately following.

DISCUSSION

The measured asymmetry parameter may be compared to that expected from the calculable molecular bending, assuming that the bond remains symmetric about the inter-nuclear axis. Let the molecule be bending in the YZ plane (Fig. 5), a specification consistent with our selection of x, y, and z in the definition of η. Consider now the coordinate system x', y', z', with x' parallel to x, z' along the carbon nitrogen bond, and y' perpendicular to these two. Assume, as before mentioned, that the fields at the nitrogen nucleus are symmetric about z'. Then if

$$\frac{\partial^2 V}{\partial z'^2}=q_0,\quad \frac{\partial^2 V}{\partial x'^2}=\frac{\partial^2 V}{\partial z'^2}=-\frac{q_0}{2}.$$

These quantities are components of a tensor, so can easily be transformed into the xyz coordinate system of the unbent molecule. The asymmetry parameter, defined in terms of derivatives with respect to the unprimed axes, becomes a simple function of ϕ, the angle between z and z'. Making the approximation that $\sin^2\phi=\phi^2$, one obtains

$$\eta=\frac{3\phi^2}{2-3\phi^2}.$$

This is inconsistent with the experimental result on two counts. First of all it is necessarily positive, while the experimental η is negative. Secondly, to obtain an η as large as 0.08 requires a ϕ of 13°, whereas the most probable ϕ for $v_2=1$ is less than 1°. Even with the hydrogen bent at right angles to the C–N bond, the CN axis makes an angle of only 6.5° with the principal axis of the inertial ellipsoid. One is led therefore to question the assumption that the electric field remains symmetric about the CN axis during vibration.

The C–N bond in HCN is discussed explicitly in reference 13. The bonding in the ground vibrational state may be considered to resonate between the

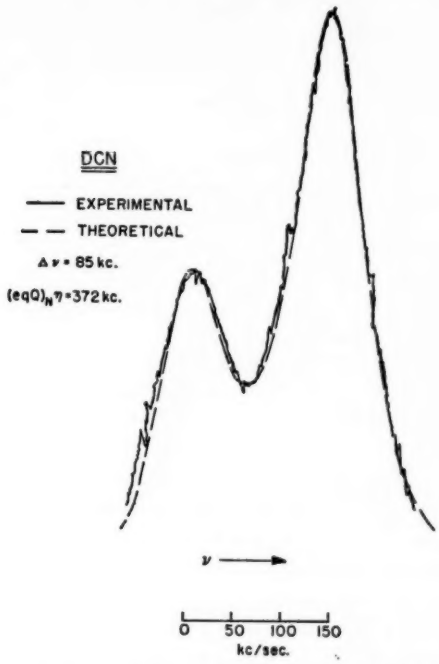

FIG. 4. Comparison of recorder trace of line with theoretical construct for DCN.

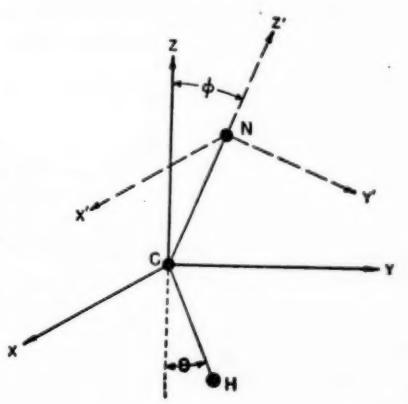

FIG. 5. Diagram of coordinate frames used in calculating η from molecular bending.

[11] G. Knight and B. T. Feld, Report No. 123, MIT Research Laboratory of Electronics (1949).
[12] Simmons, Anderson, and Gordy, Phys. Rev. **77**, 77 (1950).

TABLE I.

	Electron orbital assignment	Orbital contribution to field gradient V_{xx}	V_{yy}	V_{zz}
H−C≡N	ψ_{Pz}	q_0	$-q_0/2$	$-q_0/2$
	ψ_{Py}	$-q_0/2$	q_0	$-q_0/2$
	$\frac{1}{2}\psi_s+\frac{\sqrt{3}}{2}\psi_z$	$-\frac{1}{4}q_0$	$-\frac{1}{4}q_0$	$\frac{1}{2}q_0$
	$2\times\left[\frac{\sqrt{3}}{2}\psi_s+\frac{1}{2}\psi_z\right]$	$-q_0/4$	$-q_0/4$	$+q_0/2$
	Total A	$-q_0/8$	$-q_0/8$	$q_0/4$
H−C≡N	$P_{x\pi}$ bond broken Total B	$\frac{1}{4}q_0$	$-\frac{1}{4}q_0$	$-\frac{1}{4}q_0$
H−C≡N	$P_{y\pi}$ bond broken Total C	$-\frac{1}{4}q_0$	$\frac{1}{4}q_0$	$-\frac{1}{4}q_0$
	Weighted average of A, B, and C allowing for nonequivalence of P_x and P_y orbitals. (See text)	$-q_0(0.10-0.00075)$	$-q_0(0.10+0.00075)$	$0.20q_0$

two forms

$$\mathrm{H-\overset{+}{C}=\overset{-}{N}} \quad \text{and} \quad \mathrm{H-C\equiv N}$$

with the relative importance of approximately 10 percent and 90 percent, respectively. In the more important structure the σ bond between the carbon and nitrogen is formed by a $1/\sqrt{2}(\psi_S+\psi_{Pz})$ orbital from the carbon and $\frac{1}{2}(\psi_S+\sqrt{3}\psi_{Pz})$ orbital from the nitrogen, where the z axis is taken as the internuclear axis. The two π bonds are assumed to be formed by pure p orbitals. The nonbonding s orbitals of the nitrogen are 25 percent p character due to the p_z hybridization. In the less important structure one of the π bonds is broken and the nitrogen is negatively ionic. Details of the gradient calculation proceeding from these bond and ionic character assumptions are given by Townes and Dailey.[13]

Consider now the effect of a molecular bending, again in the YZ plane as in Fig. 5. In HCN and DCN the bending is quite large, even for $v_2=1$. For HCN $\bar{\theta}=18.7°$; for DCN $\bar{\theta}=16.7°$ (see Fig. 5). This bending removes the equivalence of the bonds in the XZ and YZ planes, and hence the equivalence of $\partial^2V/\partial x^2$ and $\partial^2V/\partial y^2$ which depend in part on the electrons occupying these orbits. The nonequivalence would probably be manifested as (1) a partial hybridizing of one of the nitrogen $p\pi$ orbitals in the fully covalent structure, or (2) a preferential breaking of one of the π bonds when the ionic structure is formed.

Possibility (1) was investigated in detail on the assumption that only the p orbital forming a π bond in the plane of bending would be affected by the bending. Hybridization of this orbital was found to produce an asymmetry parameter of the opposite sign from that measured experimentally, so cannot be the dominant effect.

Possibility (2), the preferential breaking of one of the π bonds can yield an η of either sign, depending on which bond is broken preferentially. It is difficult to state *a priori* which bond is the more likely to be broken. Let us calculate the asymmetry parameter consequent upon the preferential breaking of the π bond perpendicular to the plane of bending. In Table I are tabulated the field gradients at the nitrogen nucleus, resolved into rectangular components, which the various assumed resonant structures would produce. The contribution V_{ZZ} of a pure p_Z orbital is taken to be q_0. The fully covalent structure is treated in some detail, the contribution of each orbital being listed separately to indicate how a typical total gradient is obtained. The effective gradient will be obtained by taking a weighted average of A, B, and C. Suppose the perpendicular π bond breaks a percent of the time more often than the p_y bond. The total average gradient will then consist of 90 percent A, $(5+0.05a)$ percent B and $(5-0.05a)$ percent C. This weighted average is given on the last line of Table I. The asymmetry parameter is then calculated to be

$$\eta=-7.5\times10^{-3}a.$$

It is seen that a preference of the direction assumed gives the sign of η measured experimentally, and that a value a of only 11 percent is required to give the asymmetry observed. It is therefore suggested that this effect is the source of the asymmetry observed.

ACKNOWLEDGMENT

The author wishes to express his gratitude to Professor Charles H. Townes for the guidance given and suggestions offered in the course of this investigation. He is also indebted to Dr. Ali Javan for important criticism and suggestions, to Dr. Gene A. Silvey for preparation of the compounds used, and to Mr. Paul Fletcher and Mr. George Dousmanis for aid in the computation.

[13] C. H. Townes and B. P. Dailey, J. Chem. Phys. **17**, 782 (1949).

Quadrupole Coupling of the Deuteron in DCCCl and DCN*

ROBERT L. WHITE†
Physics Department, Columbia University, New York, New York
(Received June 21, 1954)

The quadrupole coupling of the deuteron $(eqQ)_D$ was measured in DCCCl where it was found to be $+175\pm20$ kc/sec. A less accurate determination of the absolute value $(eqQ)_D$ in DCN yielded approximately 290 kc/sec. The field gradient, q, at the deuterium nucleus in DCCCl is $+8.85\pm10$ percent$\times10^{14}$ esu. A calculation of q based on a Hund-Mulliken molecular model yields a q of the same sign as that observed but approximately twice as large, indicating the insufficiency of the model for such detailed calculations.

I. INTRODUCTION

THE quadrupole moment of the deuteron is known from the work which has been done on the hydrogen molecule. The coupling of the nuclear moment to the field gradient was measured by molecular beam methods,[1,2] and the field gradient then calculated to approximately one percent from a James-Coolidge wave function.[3] For more complicated molecules the field calculation to such accuracy is not generally feasible, so the deuteron is unique in having its quadrupole moment rather accurately known.

In the present investigation the quadrupole coupling of the deuteron in D−C≡C−Cl and D−C≡N was measured. The former compound gives a more accurate determination for reasons which will become apparent. The motivation for the investigation was the desire to compare the field actually occurring at the deuteron to that calculated from the electronic orbitals assigned in a simple valence bonding model. The calculations are described in considerable detail in the latter parts of this paper.

Fine structure, probably arising from deuteron quadrupole coupling, has also been observed in HDO in another laboratory.[4] This information is also discussed in connection with the gradient calculation.

II. THE CHLOROACETYLENE MEASUREMENT

The apparatus and techniques used to measure the DCCCl spectrum[5] were very similar to those used for the DCN and HCN investigation described in the preceding paper. A frequency stabilized klystron was driven slowly over the lines and frequency markers placed every measured 50 kc/sec on a recorder tracing. Traces thus obtained are compared with theoretical plots and a best fit for the value of $(eqQ)_D$ is obtained. The theoretical pattern expected is as follows.[6] The molecule DCCCl contains two nuclei with electric quadrupole moments, with one quadrupole coupling energy, that of the chlorine, much larger than the other. Let us denote the chlorine spin by I_1, the deuteron spin by I_2, a partial angular momentum $\mathbf{F}_1=\mathbf{J}+\mathbf{I}_1$, and the total angular momentum $\mathbf{F}=\mathbf{F}_1+\mathbf{I}_2$. Each transition will bear, in addition to the J transition specification, a designation $F_1{}^f$, $F^f\leftarrow F_1{}^i$, F^i, where the superscript i refers to the initial state and f to the final. The $J=2\leftarrow1$ transition will be split by the chlorine quadrupole moment into several groups about 5–10 Mc apart, each involving a particular transition of F_1. Spacings within a group, arising from energy variation with deuteron orientation, are on the order of tens of kilocycles. The $F=\frac{1}{2}\leftarrow\frac{1}{2}$ transition can show no quadrupole broadening, so affords an unwidened line from which the half-width parameter $\Delta\nu$ may be determined. Several traces of the $\frac{1}{2}\leftarrow\frac{1}{2}$ transition gave $\Delta\nu=55$ kc/sec at -78°C, pressure less than 10^{-3} mm Hg and microwave power a few microwatts. The $F_1=\frac{3}{2}\leftarrow\frac{3}{2}$ transition shows best the deuteron quadrupole splitting, and was accordingly selected for the determination. In Fig. 1 a theoretical plot of the $F_1=\frac{3}{2}\leftarrow\frac{3}{2}$ transition, using $\Delta\nu=55$ kc, is presented superimposed on two experimental traces of the group. One obtains for best fit:

$$(eqQ)_D=+175\pm20 \text{ kc.}$$

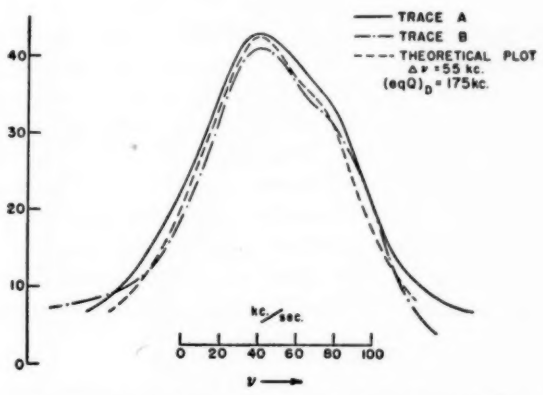

FIG. 1. Comparison of theoretical plot with recorder traces of $J=2\leftarrow1$, $F_1=\frac{3}{2}\leftarrow\frac{3}{2}$ transition of DCCCl.

* Work supported by the U. S. Atomic Energy Commission; and jointly by the Signal Corps, Office of Naval Research, and Air Force Research and Development Command.
† Present address, Hughes Research and Development Laboratories, Culver City, California.
[1] Kellogg, Rabi, Ramsey, and Zacharias, Phys. Rev. **57**, 677 (1940).
[2] Kolsky, Phipps, Ramsey, and Silsbee, Phys. Rev. **80**, 483 (1950); **81**, 1061 (1951); **87**, 395 (1952).
[3] A. Nordsieck, Phys. Rev. **57**, 556 (A) (1940).
[4] Y. Beers and S. Weisbaum, Phys. Rev. **91**, 1014 (1953).
[5] Westenberg, Goldstein, and Wilson, J. Chem. Phys. **17**, 1319 (1949).
[6] J. Bardeen and C. H. Townes, Phys. Rev. **73**, 97 (1948).

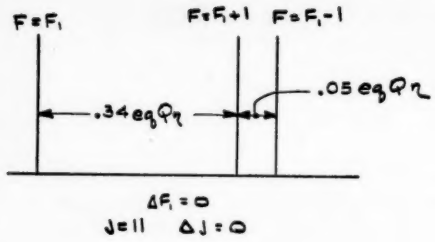

FIG. 2.

Since the pattern is asymmetric the sign of the quadrupole coupling is unambiguously determined.

III. THE HCN MEASUREMENT

In the preceding paper the experimental procedures for obtaining traces of the HCN and DCN transitions at 24 660.40 and 24 539.96 Mc/sec, respectively, are discussed at considerable length. In Fig. 3 of that paper a typical trace of the HCN line is plotted superimposed on a theoretical construct of the same group. Figure 4 is a similar presentation of the DCN information. It is to be noted that, although the traces were made under identical conditions of temperature, pressure, and microwave power, a half-width of 70 kc/sec is needed to give a best fit of theoretical to experimental curve for HCN, whereas a half width of 85 kc/sec is best for DCN. Magnetic interactions could not be the source of broadening since the deuteron gyromagnetic ratio is one sixth that of the proton, and less broadening in DCN would therefore be expected. On the other hand, a small quadrupole coupling of the deuteron would produce an unresolved pattern appearing as additional line width.

We treat DCN, then, by the methods appropriate to a molecule containing two quadrupole moments. Denoting the nitrogen spin by I_1 and the deuteron spin by I_2, we have a partial angular momentum F_1 with values 9 through 11 and a total angular momentum F with values 8 through 12 inclusive. Only the $\Delta F=0$, $\Delta F_1=0$ transitions were observed and will be discussed here. A calculation for the case of two nuclei with hyperfine structure was carried out following Bardeen and Townes.[6] This showed that for such high J and F_1, the hyperfine energy due to the deuteron was very nearly the same as if no other quadrupole were present. The $\Delta F_1=0$ transitions all have therefore essentially the same structure, that given in Fig. 2. As was detailed in the foregoing paper only asymmetries in the quadrupole coupling appear. The increase of 15 ± 6 kc/sec in line width represents a component spacing totaling approximately 0.37 $(eqQ)_D\eta$, yielding

$$|(eqQ)_D\eta| = 40\pm16 \text{ kc.}$$

To extract a value of $(eqQ)_D$ it is necessary to calculate η, the field asymmetry parameter at the deuteron. The average angle which the D—C axis makes with the principal axis of the inertial ellipsoid is large (16.7°) compared to that made by the C—N axis (less than 1°). Consequently the asymmetry introduced by a simple rotation of the gradient tensor through the deviation angle—assuming fields symmetric about the bond axis—would produce a much larger effect at the deuteron than at the nitrogen, the effect being in fact proportional to the sine squared for small angles. Furthermore, since the deuteron participates in no π bonds the effects dominant at the nitrogen should be absent here. Hence we take η to be, as a first approximation, simply that calculated from the rotation of the axes through the angle

$$\eta=\frac{3\sin^2\theta}{3\cos^2\theta-1}.$$

Using the molecular parameters for DCN given in Herzberg[7] one obtains θ, the expectation half-angle of the deuteron vibration, as 16.7°, giving

$$\eta=0.14.$$

Combining this with the experimental value of $(eqQ)_D\eta$, one obtains

$$(eqQ)_D=\pm290\pm120 \text{ kc.}$$

The error quoted is the statistical error of the measurement, and does not reflect the uncertainty of the assumptions made in calculating η. Since only moderate agreement is obtained here with the more accurately measured value of $(eqQ)_D$ in DCCCl, this section of the experiment might be regarded more profitably as a test of our assumptions concerning η than as an independent measurement of the quadrupole coupling. However it should be noted that the confirmation is still incomplete insofar as ambiguities of sign have not been removed.

The Field Gradient

The quadrupole moment of the deuteron is known to be $+2.73\times10^{-27}$ cm^2 from the work which has been done on the hydrogen molecule, outlined in the introduction. From the coupling constant of $+175\pm20$ kc/sec we can calculate $q=\partial^2V/\partial z^2=8.85\pm0.9\times10^{14}$ esu at the deuteron in a D—C bond. Ordinarily the q

TABLE I. Electron orbital assignments in D—C≡.

No. of electrons occupying wave function	Wave function
2 (bonding)	$\frac{0.82}{\sqrt{2}}\psi_{1s}^{(H)}+\frac{0.82}{\sqrt{4}}(\psi_{2s}^{(C)}+\psi_{2P_Z}^{(C)})$
1	$\frac{1}{\sqrt{2}}(\psi_{2s}^{(C)}-\psi_{2P_Z}^{(C)})$
2	$\psi_{1s}^{(C)}$
1	$\psi_{2P_X}^{(C)}$
1	$\psi_{2P_X}^{(C)}$

[7] Gerhard Herzberg, *Infrared and Raman Spectra* (D. Van Nostrand Company, Inc., New York, 1945).

TABLE II. Contributions to field gradient at deuteron by various parts of the charge distribution.

Charge specification	q contribution esu $\times 10^{14}$
$-0.67(\psi_{1s}^{(H)})^2$	0
$-\frac{1.34}{\sqrt{2}}(\psi_{1s}^{(H)})(\psi_{2s}^{(C)}+\psi_{2P_Z}^{(C)})$	−2.01
$-0.33(\psi_{2s}^{(C)}+\psi_{2P_Z}^{(C)})^2$	−3.58
$-\frac{1}{2}(\psi_{2s}^{(C)}-\psi_{2P_Z}^{(C)})^2$	−3.98
$-(\psi_{2P_X}^{(C)})^2-(\psi_{2P_Y}^{(C)})^2$	−4.56
$-2(\psi_{1s}^{(C)})^2$	−16.22
+6 Carbon nuclear charge	+48.66
Total	+18.31

at the nucleus is due almost entirely to "unbalanced" p electrons belonging to that nucleus.[8] In the case of the deuteron no such unbalanced p exists, or more accurately, very little exists because of the rather large energy required to promote an electron from the ground $1s$ state to the lowest available p state, the $2p$. Furthermore the average radius of a hydrogen $2p$ orbital is so large that the q it contributes, being proportional to $\langle 1/r^3\rangle$ is small, even if the state were populated. Consequently the field at the deuteron is due primarily to charges resident on the carbon and to overlap effects. A calculation was made of the effect of these charges using the customary Hund-Mulliken assignments of the valence electrons. In Table I this assignment is given. For the carbon $2s$ and $2p$ orbitals, a Z_{eff} of 3.20 was used,[9] for carbon $1s$ orbitals a Z_{eff} of 5.65; for the hydrogen orbitals $Z_{\text{eff}}=1$. The bonding orbitals were normalized using the overlap integrals of Mulliken *et al.*[10] The small percentage of ionic character conceivably present affects the gradient calculation but little and consequently was omitted from this calculation. A tabulation of the contributions to q of the various charge segments is given in Table II, separated in a manner suggested by the way in which the integrals were handled. All integrals were evaluated in closed form except the hydrogen-carbon overlap integral, which was done numerically.

The calculated q, $+18.31\times10^{14}$ esu, is of the same sign as the experimentally obtained q, but too large by a factor of over two. The model used fails to place sufficient electronic charge between the two nuclei and close to the internuclear axes. Similar conclusions were reached by Harris and Melkanoff[11] for the Li_2 molecule. Since, however, the calculated q is given by the difference of two fairly large numbers, representing the contributions to the field gradient by the positive carbon nucleus and the negative carbon electrons, respectively, it is not surprising that the discrepancy between calculated and measured q should be so large. One may conclude that in such a detailed calculation the Hund-Mulliken model will yield the proper order of magnitude of gradient but cannot be relied on for more exact information.

Evidence of a q of similar magnitude has been obtained by Yardley Beers of New York University in the low-frequency microwave spectrum of the asymmetric rotor HDO. He has observed structure to the $3_{31;2}\leftarrow3_{30;3}$ transition at 824.6 Mc which suggests a quadrupole coupling for the deuteron of about 260 kc/sec.[12] Though the bonding is somewhat different, and the estimation of q complicated by the presence of an additional hydrogen, one would nonetheless expect a similar order of magnitude for the coupling, as proves to be the case.

SUMMARY

The quadrupole coupling of the deuteron in the D−C≡ bond is $+175\pm20$ kc/sec, yielding a value of q of $+8.85\pm0.9\times10^{14}$ esu as the field gradient at the deuteron. The theoretical value of q obtained from a calculation based on a simple Heitler-London valence model of the bond is of the same sign and about twice as large as the experimental value.

ACKNOWLEDGMENTS

The author wishes to thank Professor Charles H. Townes for the guidance he has given and suggestions he has made during the foregoing investigation. The author wishes also to thank Dr. Gene A. Silvey for preparing the compounds used and Mr. Paul Fletcher and Mr. George Dousmanis for aiding in the calculations.

[8] C. H. Townes and B. P. Dailey, J. Chem. Phys. **17**, 782 (1949).
[9] J. C. Slater, Phys. Rev. **36**, 57 (1930).
[10] Mulliken, Rieke, Orloff, and Orloff, J. Chem. Phys. **17**, 1248 (1949).
[11] E. G. Harris and M. A. Melkanoff, Phys. Rev. **90**, 585 (1953).
[12] Yardley Beers, New York University Physics Department (private communication).

Theoretical Evaluation of Atomic Polarizations of Diatomic Molecules

A. P. ALTSHULLER
2715 E. 116th Street, Cleveland 20, Ohio
(Received June 28, 1954)

The atomic polarizations, P_A (theor.), of five diatomic molecules, HCl, DCl, HBr, NO, and CO, have been calculated from an equation derived from dispersion theory (Van Vleck, 1927), using recent data obtained from infrared dispersion and absorption intensity measurements. These P_A (theor.) values are compared with the P_A (exp.) values obtained from dielectric constant and optical refractive index measurements. The greater accuracy of the P_A (theor.) values is emphasized. The P_A (theor.) values have been used to recalculate the dipole moments, μ, of the diatomic molecules considered. A qualitative relationship is discussed between the series of $d\mu/dr$ and μ values for some of the diatomic molecules. The P_A (theor.) are calculated approximately for the gaseous alkali halides.

THE atomic polarization, P_A, of a molecule results from bond stretching and bending vibrations.[1,2] For diatomic molecules only stretching vibrations are involved. If diatomic molecules are treated as one-dimensional harmonic oscillators, both classical and quantum mechanics[1,2] give the following equation for P_A (theor.),

$$P_A\,(\text{theor.})=\frac{4\pi N}{9}\frac{1}{k_s}\left(\frac{d\mu}{dr}\right)^2=8.41\times10^{23}\frac{1}{k_s}\left(\frac{d\mu}{dr}\right)^2, \quad (1)$$

where $d\mu/dr$ is the rate of change of the dipole moment with internuclear distance, the so-called effective charge, and k_s is the stretching force constant.

From Eq. (1) it is evident that for monatomic molecules such as the inert gases and Hg and for homonuclear diatomic molecules ($d\mu/dr=0$), P_A equals zero. The experimental results substantiate the fact that these molecules have no atomic polarizations.[3]

The quantities $d\mu/dr$ have been obtained fairly accurately in recent years for a number of heteronuclear diatomic molecules from infrared dispersion and infrared absorption intensity measurements.[4–9] The stretching force constants are readily obtainable from the stretching frequencies, ω_e.[10] Consequently, the atomic polarizations, P_A (theor.), may be calculated fairly accurately from these molecular quantities. These P_A (theor.) values may be compared with the atomic polarizations, P_A (exp.), calculated from polarization (dielectric constant) and refraction (optical refractive index) measurements ($P_A=P_T-P_E-P_O$, where P_T, P_E and P_O are the total, electronic (molar refraction at $\lambda=\infty$) and orientation polarizations, respectively). The quantities $d\mu/dr$, P_A (theor.) and P_A (exp.) are given for five diatomic molecules in Table I.

TABLE I. Atomic polarizations of diatomic molecules.

Gas	$d\mu/dr\times10^{-10}$, esu[a]	P_A (theor.), cm³	P_A (exp.),[b] cm³
HCl	0.954±0.015,[c] 0.95±0.1[d]	0.015, 0.015	0.12, 0.47, 1.12
DCl	1.001±0.007[c]	0.017	0.66
HBr	0.58±0.08[d]	0.007	0.23
NO	1.69±0.08,[d] 2.24±0.11,[e] 2.45[f]	0.015, 0.026, 0.032	0.01, 0.44
CO	3.15±0.08,[g] 3.18±0.06,[e] 4.18[f]	0.044, 0.045, 0.077	0.09, 0.12, (−0.24)

[a] The uncertainties in the $d\mu/dr$ values are taken from the investigator's estimates of errors for $d\mu/dr$ in the case of the dispersion measurements or are estimated from the uncertainties given for the integrated infrared intensities, α_F.
[b] Reference 3.
[c] Reference 5.
[d] Reference 9.
[e] Reference 4.
[f] Reference 6.
[g] References 7 and 8.

The atomic polarizations, P_A (theor.), calculated from Eq. (1) are generally considerably smaller than the P_A (exp.) values. Where several P_A (exp.) values are available for a given molecule, it may be seen that the differences among values are large. Many of the $d\mu/dr$ values which would result from using the P_A (exp.) data in Eq. (1) are impossibly large. For example, if P_A (exp.) for HCl were 0.47 cm³, $d\mu/dr$ would equal 5.37×10^{-10} esu. This value, which is greater than the electronic charge (4.803×10^{-10} esu), is obviously much too large a value of $d\mu/dr$ for a partially covalent diatomic molecule such as HCl. Since P_A (exp.) is usually a small difference between two fairly large quantities, $A=P_E+P_A$ and P_E, both of which are quite sensitive to errors arising from impurities in the substance being studied and from instrumental imperfections, the P_A (exp.) data are often considerably in error. On the other hand, the P_A (theor.) data are probably uncertain to only ±5 to ±30 percent. The very careful work of Watson *et al.*[11] on NO and CO resulted in the P_A (exp.) values of 0.01 cm³ and 0.09

[1] J. H. Van Vleck, Phys. Rev. **30**, 31 (1927).
[2] I. E. Coop and L. E. Sutton, J. Chem. Soc. 1269 (1938).
[3] A. A. Maryott and F. Buckley, "Table of Dielectric Constants and Electric Dipole Moments of Substances in the Gaseous State," NBS Circular 537, 1953.
[4] R. J. Havens, University of Wisconsin, Ph.D. thesis, 1938.
[5] C. F. Hammer, Jr., University of Wisconsin, Ph.D. thesis, 1948.
[6] H. L. Dinsmore and B. F. Crawford, Jr., Report NR-019-104, University of Minnesota (1949).
[7] S. S. Penner and D. Weber, J. Chem. Phys. **19**, 807 (1951).
[8] D. Weber and S. S. Penner, J. Chem. Phys. **19**, 974 (1951).
[9] S. S. Penner and D. Weber, J. Chem. Phys. **21**, 649 (1953).
[10] G. Herzberg, "Molecular Spectra and Molecular Structure," I. Diatomic Molecules (Prentice Hall, Inc., New York, 1939).
[11] Watson, Rao, and Ramaswamy, Proc. Roy. Soc. (London) **A143**, 558 (1934); H. E. Watson and K. L. Ramaswamy, Proc. Roy. Soc. (London) **A156**, 144 (1936).

cm³, respectively, listed in Table I. Considering the experimental difficulties mentioned above, these particular P_A (exp.) values are in fairly good agreement with the P_A (theor.) values.

There are some small differences among the various P_A (theor.) values (and $d\mu/dr$ values) calculated for NO and CO. The values of $d\mu/dr$ for HCl and CO calculated from the infrared absorption intensities of Penner and Weber[7–9] are in agreement with the values from infrared dispersion measurements;[4,5] however, their $d\mu/dr$ value for NO[9] is somewhat smaller than the value of $d\mu/dr$ obtained from the dispersion data.[4] Since Penner and Weber's $d\mu/dr$ data for NO were obtained by two independent methods—pressure broadening with inert gases and self-broadening, the correct value of P_A (theor.) for NO very likely lies between 0.015 and 0.026 cm³. The $d\mu/dr$ values of Dinsmore and Crawford[6] for NO and CO thus appear to be somewhat higher than the correct values.

The P_A (theor.) values may be added to the P_E values available[3] to obtain corrected A data, when the P_A (exp.) data probably are in error. These A values may be combined with the P_T data[3] to obtain revised dipole moments, μ_r, by employing the Debye equation in the form

$$\mu_r = 0.01281\times10^{-18}[(P_T-A)T]^{\frac{1}{2}} \qquad (2)$$

at each experimental temperature.[12]

For the hydrogen halides, especially HF and HCl, the correction term in the Debye equation arising from the quantum mechanical treatment[1] is appreciable. With this correction the Debye equation assumes the form

$$\mu_r' = 0.01281\times10^{-18}[(P_T-A)]^{\frac{1}{2}}[1-f(T)]^{-\frac{1}{2}}, \qquad (3)$$

where $f(T)=h^2/24\pi^2kIT$, I is the moment of inertia, h is Planck's constant and k is the Boltzmann constant.

The values of P_A (theor.), P_E,[3] A, the literature values for the dipole moments as calculated in the NBS Circular,[3] μ_r and μ_r' are given in Table II.

The revised μ_r' for HCl of 1.09–1.10D are to be compared with the value of 1.120±0.012D calculated directly from the infrared dispersion data,[5] while for DCl, the μ_r' of 1.10D should be compared with the value of 1.145±0.012D obtained from the infrared dispersion data.[5] For HCl, the quantum-mechanical correction amounts to about 0.01D, while for DCl, HBr, HI, NO, and CO, the quantum correction amounts to 0.005D or less. The recalculation of the polarization data of Smyth for NO brings the dipole moment obtained from these data up from 0.07D to 0.17D in good agreement with the value of Watson, *et al.*[11] which is 0.16D.

It is interesting to note that the order of the values of $d\mu/dr$ for DCl, HCl, and HBr is the same as that of their dipole moments, that is, $d\mu/dr_{DCl}>d\mu/dr_{HCl}>d\mu/dr_{HBr}$ and $\mu_{DCl}>\mu_{HCl}>\mu_{HBr}$. No infrared data are available from which $d\mu/dr$ values for HF or HI may be calculated. It would seem reasonable to expect $d\mu/dr$ for HF ($\mu=1.91$D) to be in the range from $2-3\times10^{-10}$ esu and $d\mu/dr$ for HI to be less than 0.5×10^{-10} esu. It would be valuable to have infrared dispersion and/or absorption intensity data for HF and HI and also for the interhalogens.

TABLE II. Revised dipole moments.

Gas	P_A (theor.), cm³	P_E[b], cm³	A, cm³	μ (lit.),[b] D	μ_r,[g] D	μ_r',[g] D
HCl	0.02	6.51	6.53	1.050[c]	1.091	1.100
				1.081[d]	1.088	1.095
				1.077[e]	1.080	1.089
DCl	0.02	6.50	6.52	1.085[d]	1.097	1.101
HBr	0.01	8.87	8.88	0.80[e]	0.816	0.821
HI	0.00[a]	13.2	13.2	0.42[e]	0.449	0.451
NO	0.02	4.30	4.32	0.07[f]	0.17	0.17

[a] Here $d\mu/dr$ for HI is assumed to be appreciably less than the value of 0.58×10^{-10} esu for HBr; thus, P_A for HI is probably less than 0.005 cm³.
[b] Reference 3. The μ (lit.) values are given as recalculated in reference 3.
[c] C. T. Zahn, Phys. Rev. **24**, 400 (1924).
[d] R. P. Bell and I. E. Coop, Trans. Faraday Soc. **34**, 1209 (1938).
[e] H. Braune and T. Asche, Z. physik. Chem. **B14**, 18 (1931).
[f] C. P. Smyth and K. B. McAlpine, J. Am. Chem. Soc. **55**, 453 (1933).
[g] In some instances, the third decimal place is not experimentally significant but is given to indicate the magnitude of the corrections.

The large values of $d\mu/dr$ for NO and CO compared with their quite small dipole moments would seem in contradiction to the relationship given above. However, a quantum mechanical calculation of the dipole moment of CO,[13] gives a contribution from hybridization of the σ electrons to the dipole moment of −2.1D. This value is counterbalanced by ionic and homopolar contributions to the dipole moment from the π electrons of +1.9D giving a resultant moment of about 0.2D. The magnitude of $d\mu/dr$ is associated with the rate of change of the hybridization with internuclear distance and with the resulting variation in the σ-electron charge distribution. Since $\mu(\sigma)=-2.1$D, the value of $d\mu/dr=3.1-3.2\times10^{-10}$ esu falls in line with the order given above. A similar situation probably exists for NO.[14]

Diatomic molecules with appreciable covalent character may be expected from the previous discussion to have very small atomic polarizations of below 0.1 cm³. In contrast, polyatomic molecules have atomic polarizations[3] of the order of magnitude of 100 times larger than the diatomic molecules previously considered. However, extremely ionic diatomic molecules may have large $d\mu/dr$ values and consequently may have P_A values of the same magnitude as many polyatomic molecules. The gaseous alkali halides provide the best example. If

[12] Where the dielectric constant value for the calibrating gas, usually air, differs from the recommended value given by the NBS (reference 3), the values of P_T were recalculated using the recommended value.

[13] W. Moffitt, Proc. Roy. Soc. (London) **A196**, 524 (1949).
[14] C. A. Coulson, *Valence* (Oxford University Press, London, 1952), p. 212.

the very crude assumption is made that $d\mu/dr = e = 4.80 \times 10^{-10}$ esu ($\mu = er_e$), then the P_A (theor.) values may be calculated for the alkali halides. The stretching force constants may be calculated from Rittner's values for ω_e.[15] The P_A (theor.) values calculated range from 1.08 cm³ for LiF to 2.55 cm³ for CsI. Admittedly, the neglect of polarization effects is a very severe approximation, especially for more polarizable ions. However, Benson and Van der Hoff[16] have made quantum mechanical calculations on the LiF molecule and they found a $d\mu/dr$ of 5.2×10^{-10} esu. This value for $d\mu/dr$ would give a P_A (theor.) of 1.27 cm³. Thus, although the exact numerical values may be somewhat in error, it may be seen that highly polar diatomic molecules may have P_A values about 100 times greater than diatomic molecules having large covalent contributions to their bonding.

[15] E. S. Rittner, J. Chem. Phys. **19**, 1030 (1951).

[16] G. C. Benson and M. E. Van der Hoff, J. Chem. Phys. **22**, 469 (1954).

THE JOURNAL OF CHEMICAL PHYSICS VOLUME 23, NUMBER 2 FEBRUARY, 1955

Absorption of Bicycloheptane and Bicycloheptene in the Vacuum Ultraviolet*

SUZANNE STOKES AND LUCY W. PICKETT
Department of Chemistry, Mount Holyoke College, South Hadley, Massachusetts

(Received July 2, 1954)

The vacuum ultraviolet absorption spectra of bicycloheptane and bicycloheptene have been investigated in the region from 45 000 to 65 000 cm^{-1}. Two distinct band systems with maxima at 51 125 and 59 715 cm^{-1} were noted in the case of bicycloheptene, each with an oscillator strength of 0.15. The first observed absorption of bicycloheptane was near 55 000 cm^{-1} while that of the unsaturated hydrocarbon was displaced more than 8000 cm^{-1} toward lower frequencies. In both compounds, sharp narrow bands were superimposed on the continuous absorption. In a study of the photodecomposition, it was shown that cyclopentadiene and ethylene were formed as photodecomposition products of bicycloheptane and also of bicycloheptene.

INTRODUCTION

BRIDGED ring compounds such as bicyclo(2.2.1)-heptane and bicyclo(2.2.1)-2-heptene have become of recent interest in studies of reaction mechanisms and carbonium ions. No record of the ultraviolet absorption spectra of the two bicyclic compounds was found in the literature; however, the light scattering of bicycloheptane[1] and the infrared spectra of the chloride[2] and bromide[3] derivatives have been measured.

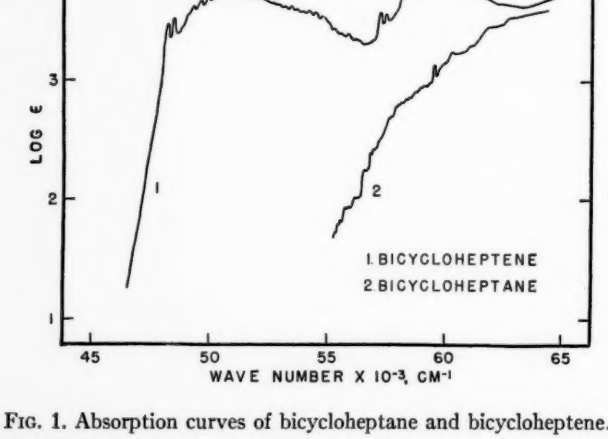

FIG. 1. Absorption curves of bicycloheptane and bicycloheptene.

* This work has been supported by a grant from the National Science Foundation (NSF-G226) and one from the Standard Oil Development Company.

EXPERIMENTAL

Samples of these compounds were prepared in the laboratory of Dr. J. D. Roberts and obtained through the courtesy of the latter. The physical constants supplied with the compounds were: bicycloheptane, bp 105.6° (758 mm), bicycloheptene, bp 95–96° (760 mm). The samples, which were solids at room temperature, were further purified for spectral measurements by fractional sublimation in an evacuated system.

The method of measurement has been described previously.[4] A Hilger fluorite prism spectrograph was used with a hydrogen discharge tube as light source. The absorption cell, 32.4 cm in length, and the hydrogen lamp were equipped with calcium fluoride windows which transmitted light to 1400 A. Photographs of the flowing vapor were taken over a pressure range of 0.062 to 1.73 mm on Ilford Q-1 plates using three minute exposure times. A modified McLeod gauge was used with care that the mercury height difference not exceed one-third the vapor pressure of the compound.

[1] Kazanskiĭ, Koperina, and Batuev, Doklady Akad. Nauk S.S.S.R. **62**, 337 (1948).

[2] Roberts, Urbanek, and Armstrong, J. Am. Chem. Soc. **71**, 3049 (1949).

[3] Roberts, Trumbull, Bennett, and Armstrong, J. Am. Chem. Soc. **72**, 3116 (1950).

[4] Harrison, Gaddis, and Coffin, J. Chem. Phys. **18**, 221 (1950).

Band intensities were calculated from microphotometer records bearing exposures of the compound and four calibration exposures of the hydrogen lamp. The molar extinction coefficient was computed, $\epsilon = 1/cl \log I_0/I$ where c is the molar concentration of the vapor, assuming ideal gas behavior. No correction was made for deviation from the perfect gas law or for the Schwartzschild constant[4] as each correction is believed to be less than 5 percent and is not definitely known.

The wavelength standards used were the copper spark spectrum, the absorption bands of oxygen,[5] the nitrogen emission lines at 1745.2 and 1742.7 A and the emission lines of molecular hydrogen. Positions of the bands were measured directly from microphotometer records on which the spectrum of the compound and that of the standard were partially overlapping. In most cases the band positions could be duplicated to ± 10 cm^{-1}.

Table I lists the positions of band maxima of bicycloheptene (not including the shallow bands which appeared only as stepouts) and the average value of $\log\epsilon$, together with number of values, standard deviations and 95 percent confidence limits. The absorption curves are shown in Fig. 1.

In the photodecomposition studies of the compounds, the vapor was retained in the absorption cell and was irradiated for varying periods while three minute exposures were successively made. The maximum irradiation period was twelve minutes.

TABLE I. Position and intensity of bicycloheptene band maxima.

Wave number in cm^{-1}	Number of values	Average $\log\epsilon$	Standard deviation	95 percent confidence limits
48 150	13	3.468	0.042	±0.025
48 445	13	3.507	0.044	±0.027
49 290	10	3.628	0.042	±0.030
49 615	10	3.675	0.041	±0.029
49 895	10	3.701	0.036	±0.026
50 460	10	3.723	0.035	±0.025
50 780	10	3.732	0.033	±0.024
51 125	10	3.733	0.032	±0.023
51 410	10	3.730	0.035	±0.025
52 135	8	3.690	0.037	±0.031
53 155	10	3.637	0.042	±0.030
53 440	10	3.635	0.045	±0.032
53 660	8	3.617	0.039	±0.033
53 930	7	3.590	0.039	±0.036
54 200	8	3.580	0.044	±0.037
54 485	9	3.571	0.041	±0.032
54 820	9	3.551	0.047	±0.036
55 260	4	3.432	0.021	±0.033
55 555	3	3.404	0.010	±0.025
55 875	3	3.391	0.017	±0.042
56 210	3	3.348	0.010	±0.025
57 240	9	3.569	0.037	±0.029
57 500	10	3.548	0.037	±0.027
58 280	10	3.741	0.029	±0.021
58 500	10	3.753	0.032	±0.023
59 715	8	3.793	0.033	±0.028

DISCUSSION OF RESULTS

The absorption band of bicycloheptane, as shown in Fig. 1, begins near 55 000 cm^{-1} and rapidly increases in intensity; the band maximum does not fall within the limits of the reliable measurements but seems to lie beyond 64 000 cm^{-1}. The slope of the curve is similar to that of cyclohexane[6] but is displaced to lower frequencies by about 1500 cm^{-1}. Superimposed on the long wavelength side of the band in both compounds are narrow shallow bands. In the case of the bridged compound these appear as triplets between 55 430 and 55 645 cm^{-1}, then as doublets between 56 930 and 58 450 cm^{-1}. Separations between the successive triplets or doublets range from 350 to 500 cm^{-1}, and the individual narrow bands which compose the doublets or triplets are separated by frequencies of 40 to 70 cm^{-1}. A sharp narrow band appears at 59 530 cm^{-1} and this is followed by a less intense band at 60 300 cm^{-1} and a series of stepouts which, although measurement in this region of the hydrogen line spectrum is uncertain, seem to indicate a series with a separation of about 770 cm^{-1}.

This band system must be due to the excitation of a σ electron. Its position at lower energies than either cyclohexane or cyclopentane may be a result of the strained conditions of the bridged ring.

The first observed absorption of bicycloheptene occurs near 46 500 cm^{-1}, a shift toward the visible of about 8500 cm^{-1} in comparison with the saturated compound. Unlike other hydrocarbons containing one double bond, two clearly marked bands are evident in this region with maxima at 51 125 and 59 715 cm^{-1} respectively. A series of sharp bands are superimposed on each. While the second band is slightly higher, the oscillator strengths, calculated from the formula, $f = 4.32 \times 10^{-9} \int \epsilon dr$, are each 0.15.

The double bond in bicycloheptene is simultaneously located in a five and a six membered ring and, for this reason, comparison of its spectrum with those of cyclohexene and cyclopentene[6,7] is of interest. All three compounds have absorption bands beginning at nearly the same wavelength though that of the cyclopentene is somewhat shorter. However cyclohexene and cyclopentene each have a low band with marked vibrational structure, overlapped by a more intense band of less distinct structure at slightly higher frequencies, which gives the appearance of two overlapping bands in the case of the six-membered ring. Bicycloheptene gives the appearance of two distinct bands. The combined oscillator strengths in the region between 47 000 and 65 000 cm^{-1} (bicycloheptene 0.30, cyclohexene 0.40, and cyclopentene 0.32) are comparable to each other and to other monoolefins in this region. The band pattern is distinctive in each case and would be useful for analytical purposes.

[5] H. P. Knauss and S. S. Ballard, Phys. Rev. **48**, 796 (1935).
[6] Pickett, Muntz, and McPherson, J. Am. Chem. Soc. **73**, 4862 (1951).
[7] E. P. Carr and H. Stücklen, J. Chem. Phys. **6**, 55 (1938).

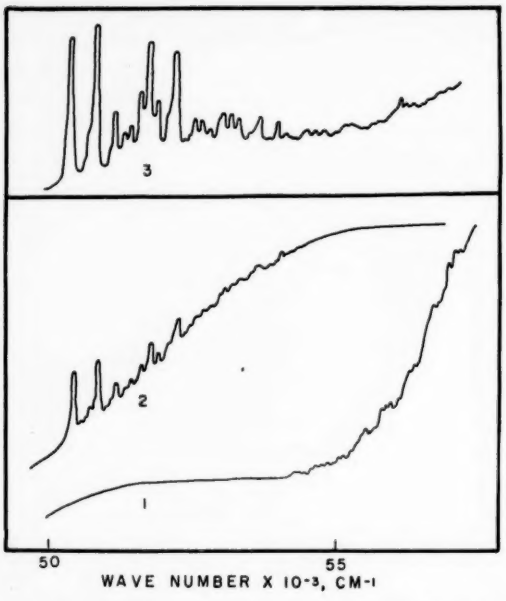

FIG. 2. Microphotometer tracings of (1) bicycloheptane vapor spectrum, (2) irradiated bicycloheptane showing bands of cyclopentadiene formed by photodecomposition, and (3) (top) cyclopentadiene vapor spectrum.

The vibrational patterns of the two bands of bicycloheptene are similar as may be seen in Table II. In this the prominent bands of each system are listed, together with separations from the band selected as the 0—0 band. Especially prominent in each case is the separation of low frequency which is thought to be a ring twisting vibration. If the four vibrational frequencies listed are taken as fundamentals, 17 of the remaining 22 bands or stepouts in the first band system may be ascribed to overtones or combinations; in the second band system the hydrogen line spectrum made analysis uncertain. Comparable frequencies of 1485 and 2670 cm^{-1} in cyclohexene have been ascribed to double bond stretching and carbon-hydrogen stretching.[7]

PHOTODECOMPOSITION OF BICYCLOHEPTANE AND BICYCLOHEPTENE

During the investigation of the ultraviolet absorption spectra of these compounds several photographs were taken of the stationary vapor in order to test for the presence of photodecomposition. The resulting microphotometer records of the photographic plates revealed bands which had developed after the first three minute period of irradiation. These bands were unmistakably identified as the characteristic bands of the cyclopentadiene spectrum.

Figure 2 represents the microphotometer records; the lower tracings are of exposures of the flowing bicycloheptane vapor and of the stationary vapor. Both measurements were made at a pressure of 1.73 mm. The tracing of the stationary vapor is of a photograph in which the vapor had been irradiated for three minutes preceding the three minute exposure. For comparison the top record shows a tracing of the pure cyclopentadiene spectrum which had been previously measured in this laboratory.[8]

TABLE II. Bicycloheptene.

First band system		Second band system	
Wave No.	$\Delta\nu$	Wave No.	$\Delta\nu$
48 150	0	57 240	0
48 445	295	57 500	260
49 290	1140	58 280	1040
49 615	1465	58 500	1260
50 780	2630	59 715	2475

When photodecomposition plates of bicycloheptene were studied, the cyclopentadiene spectrum was present but did not appear as prominently as in the case of the saturated compound. However the bicycloheptene absorbs in the same region as cyclopentadiene and thus covers up evidence of the latter.

Several decomposition photographs were taken at lower pressures and the records were studied for evidence of ethylene. Since both compounds have high absorption in the region where the sharp ethylene bands would appear, these characteristic bands were not as easily detected as those of cyclopentadiene. In view of this only three ethylene bands were found and these were identified with the reported wavelengths of 1744 A, 1730 A, and 1703 A.[9]

In Fig. 2 the microphotometer tracing of bicycloheptane flowing vapor illustrates that cyclopentadiene and ethylene were not present as impurities in the compound; similarly the flowing vapor photographs of bicycloheptene showed no evidence of these impurities. Therefore, it is clear that cyclopentadiene and ethylene are formed as the result of photodecomposition of bicycloheptane and of bicycloheptene.

This phenomenon may be comparable to the thermal dissociation of certain higher boiling homologs of bicycloheptene.[10] In the process of distillation these derivatives have been reported to dissociate into cyclopentadiene and the dienophile. This reaction is a reversal of the Diels-Alder synthesis and when suitable conditions were used, the dissociated products again combined to form the original derivative.

[8] Pickett, Paddock, and Sackter, J. Am. Chem. Soc. **63**, 1073 (1941).
[9] M. Zelikoff and K. Watanabe, J. Opt. Soc. Am. **43**, 756 (1953).
[10] K. Alder and H. F. Rickert, Ann. **524**, 180 (1936).

Relative Diameter of Oxygen and Hydrogen Molecules, using Negative Pressure as an Indicator

LYMAN J. BRIGGS
National Bureau of Standards, Washington 25, D. C.
(Received June 25, 1954)

A vertical glass tube (1 cm bore and about 100 cm long) carries at its closed upper end two opposed spherical platinum electrodes, approximately 1 and 2 mm in diameter. The lower end of the tube is bent upward in the form of a *J*, to which is attached a cylindrical reservoir. After introducing sufficient electrolyte ($1NH_2SO_4$) to more than fill the long tube, the system is evacuated and sealed off.

On rotating the long tube from an inverted to a vertical position, the column of liquid remains hanging from the top of the tube, under a negative pressure (at the top), equal to the length of the column down to the meniscus, times its density, less the vapor pressure in the reservoir. The *minimum* electric charge required to drop the column is determined by successive trials, using a mica capacitor (adjustable in steps of 0.001 μf), which is first charged to a known potential and then connected to the electrodes through a quick-acting switch. After each drop of the column, the polarity is reversed. Hydrogen is deposited as an incomplete monomolecular film when the smaller test electrode is the cathode; oxygen, when it is the anode.

The critical anodic charge was divided by 2, oxygen being bivalent. The ratio of the critical charges gives the relative number of molecules involved; and its reciprocal, the ratio of the projected areas. The mean of 9 series of measurements gave 1.022 ± 0.006 as the ratio of the diameter of the oxygen to the hydrogen molecule. Measurements by other methods range from 1.54 to 0.89.

IN an earlier paper[1] on the limiting thickness of an electrolyzed gas film capable of sustaining a given negative pressure, the writer found that the thickness of the film increased in a definite and reprodicible manner as the negative pressure was decreased. The gas film was generated electrolytically on the surface of a spherical platinum electrode by the sudden discharge of a mica capacitor. The "thickness" of the gas film approached that of a complete monolayer as the negative pressure approached zero. This conclusion was based on (1) the measured negative pressure, (2) the measured area of the spherical electrode, (3) the number of gas molecules in the incomplete monolayer (computed from the critical charge), and (4) the diameter of the gas molecules as derived by other investigators, using van der Waals equation.

The present paper deals with the *relative* diameter of the oxygen and hydrogen molecules, or more specifically their relative projected areas. The molecules of each gas are alternately generated on the surface of the test electrode in numbers just sufficient to release a column of electrolyte which is under negative pressure. The release of the column shows that the gas population on the electrode (the fractional "thickness" of the monolayer) now equals the critical value.

The experimental tube was similar to that used in the earlier experiments[1] and is shown diagrammatically in Fig. 1. An important modification was made in the spherical platinum electrodes. The diameter (1 mm) of the test electrode was one-half of that of its companion, so that the ratio of their areas was 1 to 4. Consequently, the test electrode always controlled the release of the column of electrolyte, even when the quantity of gas generated on its companion was relatively twice as great. The test electrode was made either anode or cathode, as desired, by means of a reversing switch. Another switch kept the electrodes short-circuited up to the moment preceding the discharge of the capacitor. The system was permanently grounded.

Each electrode was made by fusing the end of a 0.42-mm Pt wire, held vertically in an oxygen-gas flame, until it formed a sphere. The inner shank of each electrode was coated with a very thin layer of glass, fused in place.

The electrolyte used was normal sulfuric acid. After filling the apparatus to a suitable level (Fig. 1), it was evacuated until the residual gas pressure was less than 1 cm of water and then sealed off. It is helpful to leave a small amount of gas in the system to provide a bubble for sweeping out the multitude of microscopic bubbles which are formed in the tumultuous fall of the column

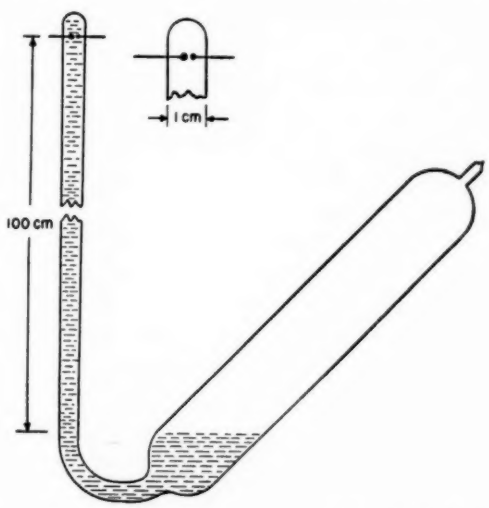

FIG. 1. Negative pressure apparatus with spherical platinum electrodes. The surface area of the test electrode is one-fourth that of its companion.

[1] Lyman J. Briggs, J. Chem. Phys. **21**, 779 (1953).

TABLE I. Ratio of diameters O_2/H_2, using negative pressure as an indicator.

Ratio of critical charge, anode/cathode	Relative number of molecules, O_2/H_2	Relative cross section, O_2/H_2	Relative diameter, O_2/H_2
1.945	0.972	1.028	1.014
1.95	0.975	1.025	1.012
1.936	0.968	1.032	1.016
1.87	0.935	1.065	1.032
1.93	0.965	1.035	1.017
1.89	0.945	1.055	1.027
1.91	0.955	1.045	1.022
1.91	0.955	1.045	1.022
1.86	0.93	1.07	1.035
			1.022±0.006

when released. Finally, an ac potential was applied to generate hydrogen and oxygen gas sufficient to saturate the electrolyte, and thus prevent the immediate dissolving of gas from the electrode during discharge.

The experimental procedure was as follows: With the column of electrolyte suspended under negative pressure from the top of the vertical tube, a known quantity of electricity in the mica capacitor was discharged between the electrodes through a quick-acting switch, with the test electrode forming the anode. On the fall of the column, the tube was inverted, filled and again erected, but with the test electrode now forming the cathode. The process was repeated with gradually reduced charges, the test electrode being alternately first anode, then cathode, until a critical charge just sufficient to release the column was reached in each case. The applied potential was 46 volts. The system was as a rule sensitive to a change of 0.001 μf, the smallest division of the capacitor. This corresponded to a change of 1 percent for H_2 and 0.5 percent for O_2. There was at times a small change in the critical charge required to drop the column, but this did not appear to influence the *ratio* of the critical charges. It does however emphasize the desirability of reversing the electrodes after each drop of the liquid column. The temperature ranged from 20° to 24°C. The corresponding negative pressure in cm of electrolyte was equal to the height of the column less the vapor pressure in the reservoir (in the same units), i.e., 103 less 23 or 30 cm.

The results from 9 series of measurements are given in Table I. The mean value found for the ratio of the diameter of O_2 to H_2 is 1.022±0.006, where 0.006 is the average deviation. The first column gives the ratio of the observed critical charges; the second, the ratio of the number of molecules involved, oxygen being bivalent; the third, (reciprocal of column 2) the ratio of the projected areas; the fourth, (square root of column 3) the ratio of the diameters.

Earlier measurements[2] in which the polarity was not reversed after each drop, but a critical charge was first established for oxygen and later for hydrogen, gave 1.008±0.004. I believe, however, that the procedure described in this paper is preferable, since it tends to annul any change in the test electrode.

A comparison with the results of measurements by other methods,[3] involving separate determinations of the diameters of the two molecules, is given in Table II.

TABLE II. Ratio of diameters O_2/H_2 molecules.

From viscosity measurements	1.31
	1.19
From van der Waals equation	1.06
From density measurements	0.89
From electron collision	1.54
From negative pressure meas.	1.022±0.006

I thought at first that the measurements might be extended to include the relative diameter of the chlorine molecule, since chlorine is given off when an aqueous HCl is electrolyzed. In this case, since chlorine is monovalent, one would expect the critical charge on anode and cathode to be nearly the same. But I found, as before, that the critical anodic charge was nearly twice that required on the cathode. The result was the same as that found with an aqueous solution of H_2SO_4. In other words, oxygen and hydrogen *first* appear on the electrodes in the *initial* stages of the electrolysis of an aqueous solution. Chlorine is set free only through an overvoltage.

[2] See abstract, Lyman J. Briggs, Science **119**, 577 (1954).
[3] Saul Dushman, *Vacuum Technique* (John Wiley and Sons, Inc., New York, 1949), p. 43.

THE JOURNAL OF CHEMICAL PHYSICS VOLUME 23, NUMBER 2 FEBRUARY, 1955

Mixtures of Rigid Spherical Molecules

BERNI J. ALDER
Department of Chemistry and Chemical Engineering, University of California, Berkeley, California
(Received June 25, 1954)

The radial distribution functions for binary mixtures of rigid spheres with a size ratio of 3 to 1 have been calculated at several mole fractions and at several densities by numerical solution of a set of integral equations obtained with the use of the superposition approximation. The distribution functions have then been used to evaluate the relevant thermodynamic properties of the system.

I.

THE quantitative treatments of mixtures at relatively high densities have so far been confined to the quasi-crystalline model[1] and the free volume theory.[2] Both of these methods have the well-known inherent difficulty of evaluating the communal entropy. The quasi-crystalline model furthermore is necessarily restricted to a lattice in which each molecule in a mixture occupies an integral number of sites. The free volume theory, on the other hand, involves an additional approximation in that the relative probability density in configuration space is written as a product function. As has been shown[3] this approximation is equivalent to evaluating the potential of average force acting on a pair of molecules by the sum of the potentials of average force acting on the individual molecules. When the latter approximation is improved by superposing the mean force between pairs of molecules to yield the potential of average force for a set of three molecules, a system of integral equations is obtained for the radial distribution functions in pair space.[4–7] Even though the error introduced by the superposition approximation in the configuration space of triplets is as yet unknown, the theory eliminates the communal entropy problem.

The radial distribution function and the thermodynamic functions derived from it have previously been evaluated for pure fluids with several forms of the intermolecular force.[8,9] The fluid consisting of a single type of rigid spheres proved to be a first approximation to fluids with more complicated types of interaction between the molecules, and so for mixtures this same system is investigated first. It represents the high-temperature behavior of any real system. Besides the greater ease of handling the numerical work, the rigid sphere mixture has the further advantage of a well defined potential of intermolecular force between the different species. It is a truly athermal mixture with a rigorously determined volume occupied by the molecules. A binary mixture of rigid spheres having diameters in the ratio of 3 to 1 was chosen to exaggerate the effects of having two different sized species present. This ratio is somewhat larger than usually encountered in ordinary mixtures. A size ratio of 100 to 1 being more representative of macromolecular systems would be desirable to work out also. It is planned to present for the 100 to 1 mixture as well as the 3 to 1 mixture the exact virial coefficients in a subsequent publication together with the virial coefficients obtained by the use of the superposition approximation for comparison.

II.

The statistical mechanical theory for liquids developed by Born and Green[4] and others [5,6] can easily be extended to mixtures.[7] For a binary mixture composed of N_α molecules of type α (always taken to be the smaller one) and N_β molecules of type β, the potential of intermolecular force is taken to be of the form

$$V_N=\sum_{i<k=1}^{N_\alpha} V_{\alpha\alpha}(R_{ik})+\sum_{i<k=1}^{N_\beta} V_{\beta\beta}(R_{ik})+\sum_{i,k=1}^{N_\alpha,N_\beta} V_{\alpha\beta}(R_{ik}). \quad (1)$$

Under the restriction of uniform average number densities in singlet space for each species, a system of integrodifferential equations is obtained which relates the distribution function of the set of n molecules to the distribution function of the set of $n+1$ molecules. In order to close this cycle the distribution function for a set of 3 molecules is related to the one for 2 molecules by the superposition approximation. In the case of a binary mixture three types of pair distribution functions exist corresponding to the correlation found between the position of a molecule α and another molecule α, a molecule β and another molecule β, and finally between a molecule α and a molecule β, designated by $g_{\alpha\alpha}^{(2)}(R)$, $g_{\beta\beta}^{(2)}(R)$, and $g_{\alpha\beta}^{(2)}(R)$, respectively. All three can at least in principle be determined by x-ray scattering techniques. The four possible distribution functions in triplet space are then related to the

[1] E. A. Guggenheim, *Mixtures* (Oxford University Press, London, 1952).
[2] Z. W. Salsburg and J. G. Kirkwood, J. Chem. Phys. **21**, 2169 (1953).
[3] J. G. Kirkwood, J. Chem. Phys. **3**, 300 (1935).
[4] M. Born and H. S. Green, Proc. Roy. Soc. (London) **A188**, 10 (1946).
[5] J. Yvon, *Actualités Scientifiques et Industrielles* (Hermann & Cie, Paris, 1935).
[6] J. E. Mayer, J. Chem. Phys. **15**, 187 (1947).
[7] G. Fournet, J. phys. radium **592**, 12 (1951).
[8] Kirkwood, Maun, and Alder, J. Chem. Phys. **18**, 1040 (1950).
[9] Kirkwood, Lewinson, and Alder, J. Chem. Phys. **20**, 929 (1952).

pair distribution function as follows:

$$
\begin{aligned}
&g_{\alpha\alpha\alpha}{}^{(3)}(\mathbf{R}_1,\mathbf{R}_2,\mathbf{R}_3)\\
&\qquad=g_{\alpha\alpha}{}^{(2)}(\mathbf{R}_1,\mathbf{R}_2)g_{\alpha\alpha}{}^{(2)}(\mathbf{R}_1,\mathbf{R}_3)g_{\alpha\alpha}{}^{(2)}(\mathbf{R}_2,\mathbf{R}_3),\\
&g_{\alpha\alpha\beta}{}^{(3)}(\mathbf{R}_1,\mathbf{R}_2,\mathbf{R}_3)\\
&\qquad=g_{\alpha\alpha}{}^{(2)}(\mathbf{R}_1,\mathbf{R}_2)g_{\alpha\beta}{}^{(2)}(\mathbf{R}_1,\mathbf{R}_3)g_{\alpha\beta}{}^{(2)}(\mathbf{R}_2,\mathbf{R}_3),\\
&g_{\alpha\beta\beta}{}^{(3)}(\mathbf{R}_1,\mathbf{R}_2,\mathbf{R}_3)\\
&\qquad=g_{\alpha\beta}{}^{(2)}(\mathbf{R}_1,\mathbf{R}_2)g_{\alpha\beta}{}^{(2)}(\mathbf{R}_1,\mathbf{R}_3)g_{\beta\beta}{}^{(2)}(\mathbf{R}_2,\mathbf{R}_3),\\
&g_{\beta\beta\beta}{}^{(3)}(\mathbf{R}_1,\mathbf{R}_2,\mathbf{R}_3)\\
&\qquad=g_{\beta\beta}{}^{(2)}(\mathbf{R}_1,\mathbf{R}_2)g_{\beta\beta}{}^{(2)}(\mathbf{R}_1,\mathbf{R}_3)g_{\beta\beta}{}^{(2)}(\mathbf{R}_2,\mathbf{R}_3).
\end{aligned}
\tag{2}
$$

With these superposition approximations and some further mathematical operations, the following set of four coupled integral equations for the pair distribution functions results:

$$
\begin{aligned}
&\log g_{\alpha\alpha}{}^{(2)}(R)+\beta V_{\alpha\alpha}(R)\\
&\qquad=\frac{\pi\beta}{R}\frac{N_\alpha}{v}\int_{-\infty}^{\infty}K_{\alpha\alpha}(R-r)\varphi_{\alpha\alpha}(r)dr\\
&\qquad\quad+\frac{\pi\beta}{R}\frac{N_\beta}{v}\int_{-\infty}^{\infty}K_{\alpha\beta}(R-r)\varphi_{\alpha\beta}(r)dr, \quad \text{I}\\
&\log g_{\beta\beta}{}^{(2)}(R)+\beta V_{\beta\beta}(R)\\
&\qquad=\frac{\pi\beta}{R}\frac{N_\beta}{v}\int_{-\infty}^{\infty}K_{\beta\beta}(R-r)\varphi_{\beta\beta}(r)dr\\
&\qquad\quad+\frac{\pi\beta}{R}\frac{N_\alpha}{v}\int_{-\infty}^{\infty}K_{\alpha\beta}(R-r)\varphi_{\alpha\beta}(r)dr, \quad \text{II}\\
&\log g_{\alpha\beta}{}^{(2)}(R)+\beta V_{\alpha\beta}(R)\\
&\qquad=\frac{\pi\beta}{R}\frac{N_\alpha}{v}\int_{-\infty}^{\infty}K_{\alpha\alpha}(R-r)\varphi_{\alpha\beta}(r)dr\\
&\qquad\quad+\frac{\pi\beta}{R}\frac{N_\beta}{v}\int_{-\infty}^{\infty}K_{\alpha\beta}(R-r)\varphi_{\beta\beta}(r)dr, \quad \text{III}\\
&\log g_{\alpha\beta}{}^{(2)}(R)+\beta V_{\alpha\beta}(R)\\
&\qquad=\frac{\pi\beta}{R}\frac{N_\beta}{v}\int_{-\infty}^{\infty}K_{\beta\beta}(R-r)\varphi_{\alpha\beta}(r)dr\\
&\qquad\quad+\frac{\pi\beta}{R}\frac{N_\alpha}{v}\int_{-\infty}^{\infty}K_{\alpha\beta}(R-r)\varphi_{\alpha\alpha}(r)dr, \quad \text{IV}
\end{aligned}
$$

where

$$
\varphi_{ij}(r)=r[g_{ij}{}^{(2)}(r)-1],
$$

$$
K_{ij}(R-r)=\int_{|R-r|}^{\infty}[y^2-(R-r)^2]\frac{dV_{ij}(y)}{dy}g_{ij}{}^{(2)}(y)dy, \tag{3}
$$

$$
\beta=1/kT,
$$

v is the total volume of the system, and R is the scalar distance between the representative molecular pair.

By this procedure two integral equations for $g_{\alpha\beta}(R)$ result which are not identical unless $V_{\alpha\alpha}$ is equal to $V_{\beta\beta}$. Such a situation would arise for example for symmetric salts interacting with Coulomb's potential. In such cases $g_{\alpha\alpha}(R)$ is equal to $g_{\beta\beta}(R)$ and then there are only two distinct distribution functions in triplet space. In the more general situation the potentials are different and then, due to the fact that the superposition approximation is introduced in an unsymmetrical way in $g_{\alpha\alpha\beta}$ and $g_{\alpha\beta\beta}$, two different equations for $g_{\alpha\beta}(R)$ are obtained. Rather than force these two equations to become identical or taking the mean of these two to be the equation from which to determine $g_{\alpha\beta}$, it was thought worth while to solve the set of integral equations [Eq. (3)] with each of the Eqs. (III) and (IV) separately. The difference in the radial distribution functions obtained in this way is a reflection of the error introduced by the superposition approximation.

For rigid spheres of diameters $a_{\alpha\alpha}$ and $a_{\beta\beta}$, respectively, Eq. (3) becomes

$$
\begin{aligned}
\psi_{\alpha\alpha}(x)&=\frac{\lambda_0{}^{(\alpha)}}{4}g_{\alpha\alpha}(1)\int_{-\infty}^{\infty}K_{\alpha\alpha}(x-r)\varphi_{\alpha\alpha}(x)dr\\
&\quad+\frac{\lambda_0{}^{(\beta)}}{4}g_{\alpha\beta}\left(\frac{a_{\alpha\beta}}{a_{\alpha\alpha}}\right)\int_{-\infty}^{\infty}K_{\alpha\beta}(x-r)\varphi_{\alpha\beta}(r)dr, \quad \text{I}\\
\psi_{\beta\beta}(x)&=\frac{\lambda_0{}^{(\beta)}}{4}g_{\alpha\beta}\left(\frac{a_{\alpha\beta}}{a_{\alpha\alpha}}\right)\int_{-\infty}^{\infty}K_{\beta\beta}(x-r)\varphi_{\beta\beta}(r)dr\\
&\quad+\frac{\lambda_0{}^{(\alpha)}}{4}g_{\beta\beta}\left(\frac{a_{\beta\beta}}{a_{\alpha\alpha}}\right)\int_{-\infty}^{\infty}K_{\alpha\beta}(x-r)\varphi_{\alpha\beta}(r)dr, \quad \text{II}\\
\psi_{\alpha\beta}(x)&=\frac{\lambda_0{}^{(\alpha)}}{4}g_{\alpha\alpha}(1)\int_{-\infty}^{\infty}K_{\alpha\alpha}(x-r)\varphi_{\alpha\beta}(r)dr\\
&\quad+\frac{\lambda_0{}^{(\beta)}}{4}g_{\alpha\beta}\left(\frac{a_{\alpha\beta}}{a_{\alpha\alpha}}\right)\int_{-\infty}^{\infty}K_{\alpha\beta}(x-r)\varphi_{\beta\beta}(r)dr, \quad \text{III}\\
\psi_{\alpha\beta}(x)&=\frac{\lambda_0{}^{(\beta)}}{4}g_{\beta\beta}\left(\frac{a_{\beta\beta}}{a_{\alpha\alpha}}\right)\int_{-\infty}^{\infty}K_{\beta\beta}(x-r)\varphi_{\alpha\beta}(r)dr\\
&\quad+\frac{\lambda_0{}^{(\alpha)}}{4}g_{\alpha\beta}\left(\frac{a_{\alpha\beta}}{a_{\alpha\alpha}}\right)\int_{-\infty}^{\infty}K_{\alpha\beta}(x-r)\varphi_{\alpha\alpha}(r)dr, \quad \text{IV}
\end{aligned}
\tag{4}
$$

where

$$
a_{\alpha\beta}=\frac{a_{\alpha\alpha}+a_{\beta\beta}}{2},
$$

$$
\begin{aligned}
g_{ij}(x)&=e^{\psi_{ij}(x)/x} && |x|>a_{ij}/a_{\alpha\alpha}\\
&=0 && |x|<a_{ij}/a_{\alpha\alpha},\\
K_{ij}(\epsilon)&=\epsilon^2-\left(\frac{a_{ij}}{a_{\alpha\alpha}}\right)^2 && |\epsilon|<a_{ij}/a_{\alpha\alpha}\\
&=0 && |\epsilon|>a_{ij}/a_{\alpha\alpha},
\end{aligned}
$$

and

$$\lambda_0^{(\alpha)}=\frac{4\pi N_\alpha a_{\alpha\alpha}^3}{v}, \quad \lambda_0^{(\beta)}=\frac{4\pi N_\beta a_{\alpha\alpha}^3}{v}.$$

In Eq. (4) all distances have been expressed in terms of units in $a_{\alpha\alpha}$ and the definitions of $g_{ij}(x)$ and $V_{ij}(x)$ have been extended to the negative real axis as they also had been in Eq. (3),

$$g_{ij}(-x)=g_{ij}(x); \quad V_{ij}(-x)=V_{ij}(x). \tag{5}$$

The hard sphere potential has the property that

$$\begin{aligned} e^{-\beta V_{ij}(x)}&=0 \quad 0\leqslant x\leqslant\frac{a_{ij}}{a_{\alpha\alpha}} \\ &=1 \quad x>\frac{a_{ij}}{a_{\alpha\alpha}}, \end{aligned} \tag{6}$$

which allows the integral in the kernel to be carried out explicitly. The kernel is thus greatly simplified and depends only on the value of the distribution function at the point of discontinuity in the potential, $g_{ij}(a_{ij}/a_{\alpha\alpha})$, by which is meant $g_{ij}(a_{ij}/a_{\alpha\alpha}+\delta)$ as $\delta\to 0$.

III.

The distribution functions obtained from the solution of the coupled set of integral equations [Eq. (4)] permit the calculation of the thermodynamic functions for the system. The theory for pure fluids can easily be extended to mixtures to yield the equation of state

$$\frac{pv}{NkT}=1-\frac{2\pi}{3NkTv}\int_0^\infty \sum_{i,j} N_iN_jg_{ij}(R)\frac{dV_{ij}}{dR}R^3dR, \tag{7}$$

where N is the total number of molecules in the system. For a binary mixture of rigid spheres Eq. (7) reduces to

$$\begin{aligned} \frac{pv}{NkT}=1+\frac{2\pi N}{3v}\Big[&x_\alpha^2a_{\alpha\alpha}^3g_{\alpha\alpha}(1)+2x_\alpha x_\beta a_{\alpha\beta}^3g_{\alpha\beta}\left(\frac{a_{\alpha\beta}}{a_{\alpha\alpha}}\right) \\ &+x_\beta^2a_{\beta\beta}^3g_{\beta\beta}\left(\frac{a_{\beta\beta}}{a_{\alpha\alpha}}\right)\Big], \end{aligned} \tag{8}$$

where

$$x_\alpha=\frac{N_\alpha}{N}, \quad x_\beta=\frac{N_\beta}{N}.$$

Since the excess internal energy of this fluid is zero, the other thermodynamic functions can be derived from the equation state alone by the use of thermodynamic relations. Thus the total excess entropy, S^E,

$$\begin{aligned} S&=-R\log p+S_p^*(T)+S_p^E, \\ S_p^E&=\int_0^p\left[\frac{R}{p}-\left(\frac{\partial v}{\partial T}\right)_p\right]dp, \\ S_p^*&=\lim_{p\to 0}[S+R\log p], \end{aligned} \tag{9}$$

when changed over to volume rather than pressure integrations

$$\begin{aligned} S_p^E/R&=S_v^E/R+\log pv/RT, \\ S_v^E/R&=\int_\infty^v\left[\frac{1}{R}\left(\frac{\partial p}{\partial T}\right)_v-\frac{1}{v}\right]dv, \end{aligned} \tag{10}$$

becomes for rigid spheres

$$\begin{aligned} S_v^E/R=\frac{2\pi N}{3}\int_\infty^v\Big[&x_\alpha^2a_{\alpha\alpha}^3g_{\alpha\alpha}(1)+2x_\alpha x_\beta a_{\alpha\beta}^3g_{\alpha\beta}\left(\frac{a_{\alpha\beta}}{a_{\alpha\alpha}}\right) \\ &+x_\beta^2a_{\beta\beta}^3g_{\beta\beta}\left(\frac{a_{\beta\beta}}{a_{\alpha\alpha}}\right)\Big]\frac{dv}{v^2}. \end{aligned} \tag{11}$$

The excess chemical potential and Helmholtz free energy are then obtained from

$$S_p^E/R=A_p^E/RT=-\mu_p^E/RT+pv/RT-1. \tag{12}$$

The partial molal volume $\bar{v}_\alpha$ is evaluated from the expression

$$\begin{aligned} \frac{N\bar{v}_\alpha}{v}\Big\{&\frac{2pv}{RT}-1-\frac{2\pi}{3N}\Big[N_\alpha^2a_{\alpha\alpha}^3\left(\frac{\partial g_{\alpha\alpha}(1)}{\partial v}\right)_{N_\alpha,N_\beta} \\ &+2N_\alpha N_\beta a_{\alpha\beta}^3\left(\frac{\partial g_{\alpha\beta}(a_{\alpha\beta}/a_{\alpha\alpha})}{\partial v}\right)_{N_\alpha,N_\beta} \\ &+N_\beta^2a_{\beta\beta}^3\left(\frac{\partial g_{\beta\beta}(a_{\beta\beta}/a_{\alpha\alpha})}{\partial v}\right)_{N_\alpha,N_\beta}\Big]\Big\} \\ =1+\frac{2\pi}{3v}\Big[&N_\alpha^2a_{\alpha\alpha}^3\left(\frac{\partial g_{\alpha\alpha}(1)}{\partial N_\alpha}\right)_{v,N_\beta} \\ &+2N_\alpha N_\beta a_{\alpha\beta}^3\left(\frac{\partial g_{\alpha\beta}(a_{\alpha\beta}/a_{\alpha\alpha})}{\partial N_\alpha}\right)_{v,N_\beta} \\ &+N_\beta^2a_{\beta\beta}^3\left(\frac{\partial g_{\beta\beta}(a_{\beta\beta}/a_{\alpha\alpha})}{\partial N_\alpha}\right)_{v,N_\beta}+2N_\alpha a_{\alpha\alpha}^3g_{\alpha\alpha}(1) \\ &+2N_\beta a_{\alpha\beta}^3g_{\alpha\beta}\left(\frac{a_{\alpha\beta}}{a_{\alpha\alpha}}\right)\Big]. \end{aligned} \tag{13}$$

The partial molal free energy μ_α and the fugacity p_α are related by

$$\begin{aligned} &\mu_\alpha=RT\log p_\alpha+\mu_\alpha^*(T), \quad p_\alpha=px_\alpha\exp(\mu_\alpha^E/RT) \\ &\mu_\alpha^E=\int_0^p\left[\bar{v}_\alpha-\frac{RT}{p}\right]dp=-RT\log pv/RT \\ &\qquad+\int_\infty^v\left[\frac{RT}{v}-N\left(\frac{\partial p}{\partial N_\alpha}\right)_{v,N_\beta}\right]dv \\ &\mu_\alpha^*(T)=\lim_{p\to 0}[\mu_\alpha-RT\log p_\alpha]. \end{aligned} \tag{14}$$

TABLE I. Radial distribution function at several mole fractions at a density where the spheres occupy 7/180 v. $\psi(x)$ as a function of x for $a_{\beta\beta}/a_{\alpha\alpha}=3$.

	$N_\alpha=N_\beta$			$N_\alpha=3N_\beta$			$N_\alpha=27N_\beta$		
x	$\psi_{\alpha\alpha}$	$\psi_{\alpha\beta}$	$\psi_{\beta\beta}$	$\psi_{\alpha\alpha}$	$\psi_{\alpha\beta}$	$\psi_{\beta\beta}$	$\psi_{\alpha\alpha}$	$\psi_{\alpha\beta}$	$\psi_{\beta\beta}$
1.0	0.062			0.064			0.079		
1.1	0.063			0.063			0.074		
1.2	0.064			0.063			0.069		
1.3	0.065			0.063			0.063		
1.4	0.065			0.063			0.056		
1.5	0.064			0.062			0.048		
1.6	0.062			0.060			0.040		
1.7	0.061			0.057			0.034		
1.8	0.059			0.054			0.030		
1.9	0.056			0.052			0.028		
2.0	0.054	0.145		0.049	0.153		0.026	0.199	
2.1	0.051	0.143		0.047	0.148		0.024	0.180	
2.2	0.048	0.140		0.044	0.142		0.022	0.161	
2.3	0.044	0.136		0.041	0.136		0.020	0.141	
2.4	0.041	0.132		0.038	0.129		0.019	0.120	
2.5	0.037	0.127		0.035	0.122		0.017	0.099	
2.6	0.034	0.121		0.031	0.115		0.016	0.080	
2.7	0.030	0.116		0.028	0.108		0.014	0.066	
2.8	0.026	0.109		0.024	0.101		0.012	0.056	
2.9	0.022	0.103		0.019	0.094		0.010	0.049	
3.0	0.018	0.097	0.303	0.017	0.088	0.320	0.009	0.044	0.447
3.1	0.015	0.090	0.290	0.015	0.082	0.298	0.007	0.041	0.388
3.2	0.011	0.083	0.277	0.011	0.076	0.282	0.005	0.038	0.332
3.3	0.008	0.076	0.264	0.008	0.070	0.261	0.004	0.035	0.279
3.4	0.005	0.069	0.250	0.005	0.064	0.243	0.003	0.032	0.229
3.5	0.002	0.062	0.235	0.002	0.058	0.225	0.002	0.029	0.183
3.6	0.000	0.055	0.220	0.000	0.051	0.208	0.001	0.026	0.143
3.7	−0.002	0.048	0.206	−0.002	0.044	0.192	0.000	0.023	0.110
3.8	−0.003	0.041	0.192	−0.003	0.038	0.176	−0.001	0.020	0.086
3.9	−0.004	0.035	0.178	−0.003	0.032	0.162	−0.001	0.017	0.072
4.0	−0.004	0.028	0.165	−0.003	0.026	0.150	−0.001	0.014	0.062
4.1	−0.003	0.022	0.153	−0.003	0.020	0.139	−0.001	0.011	0.057
4.2	−0.003	0.016	0.141	−0.003	0.015	0.128	−0.001	0.008	0.054
4.3	−0.003	0.011	0.127	−0.002	0.010	0.115	0.000	0.006	0.052
4.4	−0.002	0.006	0.113	−0.002	0.016	0.103		0.004	0.049
4.5	−0.002	0.002	0.100	−0.002	0.002	0.091		0.002	0.045
4.6	−0.002	−0.002	0.088	−0.002	−0.001	0.078		0.000	0.040
4.7	−0.001	−0.004	0.076	−0.001	−0.003	0.067		−0.001	0.035
4.8	−0.001	−0.006	0.064	−0.001	−0.004	0.056		−0.002	0.030
4.9	−0.001	−0.007	0.054	−0.001	−0.005	0.045		−0.003	0.025
5.0	−0.001	−0.007	0.043	−0.001	−0.006	0.039		−0.002	0.020
5.1	−0.001	−0.006	0.032	−0.001	−0.007	0.029		−0.002	0.016
5.2	0.000	−0.005	0.022	0.000	−0.006	0.022		−0.001	0.012
5.3		−0.005	0.013		−0.005	0.012		−0.001	0.009
5.4		−0.004	0.007		−0.004	0.006		−0.001	0.006
5.5		−0.003	0.002		−0.004	0.002		−0.001	0.003
5.6		−0.003	−0.003		−0.003	−0.003		−0.001	0.000
5.7		−0.002	−0.007		−0.003	−0.005		0.000	−0.001
5.8		−0.002	−0.011		−0.002	−0.007			−0.002
5.9		−0.002	−0.012		−0.002	−0.010			−0.002
6.0		−0.001	−0.011		−0.002	−0.010			−0.003
6.1		−0.001	−0.010		−0.001	−0.008			−0.003
6.2		−0.001	−0.008		−0.001	−0.008			−0.003
6.3		0.000	−0.006		−0.001	−0.006			−0.002
6.4			−0.005		−0.001	−0.005			−0.002
6.5			−0.004		0.000	−0.004			−0.002
6.6			−0.004			−0.003			−0.002
6.7			−0.003			−0.003			−0.001
6.8			−0.003			−0.003			−0.001

For rigid spheres the excess partial molal free energy is then related to the entropy by

$$S_\alpha^E/R=\frac{p\bar{v}_\alpha}{RT}-1-\mu_\alpha^E/RT. \tag{15}$$

IV.

The procedure for the numerical solution of Eq. (4) employed the methods of iteration previously developed.[8,9] The ratio of diameters $a_{\beta\beta}/a_{\alpha\alpha}$ was chosen as 3 so that $a_{\alpha\beta}/a_{\alpha\alpha}$ was 2. A choice of $\lambda_0^{(\alpha)}$ and $\lambda_0^{(\beta)}$ determined the mole fraction of each species present and the volume of the system. With this choice of parameters, a trial function $g_{\alpha\beta}(x)$ was assumed and Eq. (4), (II) was solved by iteration for $g_{\beta\beta}(x)$. The assumed trial function $g_{\alpha\beta}(x)$ was then improved by using the solution for $g_{\beta\beta}(x)$ from Eq. (4), (II) in Eq. (4), (III) to solve for a new $g_{\alpha\beta}(x)$. A trial value for $g_{\alpha\alpha}(1)$ also

TABLE II. Radial distribution functions at several mole fractions at a density when the spheres occupy 7/60 v. $\psi(x)$ as a function of x for $a_{\beta\beta}/a_{\alpha\alpha}=3$.

	$N_\alpha=N_\beta$			$N_\alpha=3N_\beta$			$N_\alpha=27N_\beta$					
x	$\psi_{\alpha\alpha}$	$\psi_{\alpha\beta}$	$\psi_{\beta\beta}$	$\psi_{\alpha\alpha}$	$\psi_{\alpha\beta}$	$\psi_{\beta\beta}$	$\psi_{\alpha\alpha}$	$\psi_{\alpha\beta}$	$\psi_{\beta\beta}$	$\psi_{\alpha\alpha'}$	$\psi_{\alpha\beta'}$	$\psi_{\beta\beta'}$
1.0	0.198			0.204			0.242			0.238		
1.1	0.198			0.203			0.225			0.219		
1.2	0.197			0.201			0.205			0.198		
1.3	0.197			0.196			0.181			0.175		
1.4	0.197			0.189			0.153			0.149		
1.5	0.194			0.180			0.122			0.121		
1.6	0.187			0.170			0.094			0.094		
1.7	0.177			0.160			0.074			0.073		
1.8	0.166			0.150			0.063			0.062		
1.9	0.156			0.141			0.058			0.057		
2.0	0.146	0.482		0.131	0.501		0.055	0.622		0.054	0.466	
2.1	0.135	0.468		0.121	0.479		0.052	0.549		0.051	0.410	
2.2	0.124	0.452		0.111	0.455		0.048	0.475		0.048	0.353	
2.3	0.112	0.434		0.100	0.429		0.045	0.400		0.045	0.295	
2.4	0.099	0.413		0.090	0.401		0.042	0.329		0.042	0.238	
2.5	0.086	0.290		0.078	0.373		0.039	0.262		0.039	0.185	
2.6	0.072	0.367		0.066	0.344		0.035	0.202		0.036	0.137	
2.7	0.057	0.343		0.054	0.315		0.030	0.152		0.032	0.094	
2.8	0.041	0.318		0.042	0.288		0.025	0.114		0.028	0.069	
2.9	0.036	0.293		0.031	0.264		0.020	0.093		0.023	0.059	
3.0	0.021	0.268	0.892	0.020	0.242	0.908	0.016	0.085	$1.23\bar{3}$	0.018	0.055	1.331
3.1	−0.008	0.244	0.845	0.010	0.229	0.842	0.011	0.083	$1.03\bar{3}$	0.013	0.055	1.136
3.2	−0.003	0.219	0.798	0.001	0.205	0.776	0.006	0.082	$0.83\bar{9}$	0.008	0.059	0.948
3.3	−0.012	0.194	0.750	−0.009	0.181	0.710	0.002	0.080	0.657	0.004	0.064	0.771
3.4	−0.020	0.169	0.701	−0.016	0.157	0.648	−0.001	0.076	$0.49\bar{5}$	0.001	0.066	0.610
3.5	−0.026	0.145	0.652	−0.022	0.133	0.589	−0.003	0.068	$0.35\bar{3}$	−0.001	0.063	0.466
3.6	−0.030	0.119	0.604	−0.026	0.111	0.533	−0.005	0.059	$0.23\bar{2}$	−0.003	0.057	0.340
3.7	−0.033	0.095	0.557	−0.029	0.090	0.480	−0.007	0.050	$0.13\bar{5}$	−0.005	0.050	0.235
3.8	−0.034	0.072	0.510	−0.031	0.071	0.434	−0.008	0.042	$0.07\bar{3}$	−0.006	0.043	0.165
3.9	−0.032	0.051	0.465	−0.029	0.053	0.394	−0.007	0.035	0.055	−0.006	0.037	0.128
4.0	−0.029	0.032	0.423	−0.026	0.035	0.360	−0.006	0.027	0.051	−0.005	0.030	0.112
4.1	−0.026	0.013	0.382	−0.022	0.018	0.329	−0.004	0.019	0.061	−0.004	0.022	0.108
4.2	−0.022	−0.005	0.341	−0.019	0.001	0.297	−0.003	0.011	0.076	−0.003	0.014	0.107
4.3	−0.018	−0.022	0.300	−0.016	−0.015	0.265	−0.002	0.003	0.087	−0.002	0.006	0.106
4.4	−0.015	−0.036	0.259	−0.013	−0.028	0.233	−0.002	−0.003	0.093	−0.002	0.000	0.103
4.5	−0.012	−0.046	0.218	−0.010	−0.037	0.201	−0.001	−0.007	0.088	−0.002	−0.005	0.095
4.6	−0.009	−0.053	0.177	−0.008	−0.042	0.169	−0.001	−0.010	0.081	−0.002	−0.008	0.081
4.7	−0.006	−0.056	0.139	−0.006	−0.044	0.137	−0.001	−0.011	0.072	−0.001	−0.009	0.063
4.8	−0.004	−0.056	0.104	−0.004	−0.045	0.105	0.000	−0.011	0.061	−0.001	−0.010	0.049
4.9	−0.002	−0.054	0.071	−0.002	−0.044	0.075		−0.010	0.050	−0.001	−0.011	0.037
5.0	0.000	−0.049	0.040	−0.001	−0.041	0.048		−0.009	0.039	0.000	−0.011	0.025
5.1	0.001	−0.041	0.010	0.000	−0.036	0.022		−0.007	0.028		−0.009	0.013
5.2	0.002	−0.033	−0.019	0.001	−0.030	−0.002		−0.005	0.017		−0.007	0.001
5.3	0.003	−0.025	−0.046	0.001	−0.023	−0.024		−0.003	0.006		−0.005	−0.010
5.4	0.004	−0.018	−0.066	0.002	−0.018	−0.043		−0.002	−0.002		−0.003	−0.018
5.5	0.004	−0.012	−0.080	0.002	−0.014	−0.057		−0.002	−0.008		−0.002	−0.023
5.6	0.004	−0.008	−0.088	0.002	−0.010	−0.066		−0.002	−0.011		−0.002	−0.026
5.7	0.004	−0.004	−0.091	0.002	−0.007	−0.070		−0.002	−0.012		−0.002	−0.026
5.8	0.004	−0.001	−0.091	0.003	−0.004	−0.071		−0.002	−0.013		−0.001	−0.025
5.9	0.004	0.001	−0.086	0.003	−0.002	−0.068		−0.001	−0.012		−0.001	−0.022
6.0	0.004	0.003	−0.078	0.003	0.000	−0.061		−0.001	−0.011		−0.001	−0.018
6.1	0.003	0.005	−0.067	0.003	0.002	−0.051		−0.001	−0.009		−0.001	−0.013
6.2	0.003	0.006	−0.055	0.002	0.003	−0.040		−0.001	−0.006		0.000	−0.009
6.3	0.003	0.006	−0.043	0.002	0.003	−0.031		−0.001	−0.004			−0.005
6.4	0.002	0.006	−0.032	0.002	0.004	−0.024		−0.001	−0.002			−0.003
6.5	0.002	0.007	−0.023	0.002	0.004	−0.018		0.000	−0.002			−0.002
6.6	0.001	0.007	−0.016	0.001	0.005	−0.013		0.000	−0.001			−0.001
6.7	0.001	0.007	−0.010	0.001	0.005	−0.008		0.001	−0.001			−0.001
6.8	0.001	0.007	−0.005	0.000	0.005	−0.004		0.001	−0.001			0.000

had to be assumed in the last step. By working in this manner back and forth between Eq. (4), (II) and (III), a solution of these two coupled integral equations was obtained consistent with the assumed value of $g_{\alpha\alpha}(1)$. The value of $g_{\alpha\alpha}(1)$ was finally improved by obtaining a solution for $g_{\alpha\alpha}(x)$ from Eq. (4), (I). The new $g_{\alpha\alpha}(1)$ was then substituted in Eq. (4), (III) and the procedure repeated. For the relatively low densities used this method converged within a few iterations. Equation (4), (IV) could have been used equally well instead of Eq. (4), (III), and a similar procedure was developed in that case.

The choice of parameters of $\lambda_0^{(\alpha)}$ and $\lambda_0^{(\beta)}$ was determined so that the volume occupied by the spheres was kept constant at several different mole fractions. This was done to study the equation of state under these conditions. The fraction of the volume occupied by the spheres was taken to be 7/180 v, 7/60 v, and 7/30 v.

TABLE III. Radial distribution function at 50 mole percent at a density where the spheres occupy 7/30 v. Nodes and peaks of $\psi(x)$ for $a_{\beta\beta}/a_{\alpha\alpha}=3$.

x	$\psi_{\alpha\alpha}$	x	$\psi_{\alpha\beta}$	x	$\psi_{\beta\beta}$
1.00	0.439	2.00	1.238	3.00	1.610
2.50	0.000	3.80	0.000	4.85	0.000
3.50	−0.205	4.60	−0.240	5.60	−0.312
4.50	0.000	5.50	0.000	6.55	0.000
5.20	0.048	6.20	0.064	7.30	0.079
6.30	0.000	7.35	0.000	8.35	0.000
6.90	−0.016	8.00	−0.020	9.00	−0.026
8.10	0.000	9.20	0.000	10.00	0.000
9.00	0.005	9.80	0.006	10.80	0.009
10.00	0.000	10.80	0.000	11.70	0.000
				12.30	−0.004
				12.80	0.000

The mole fractions chosen at these densities were $x_\alpha=1/2$, 3/4, and 27/28. The latter value corresponds to equal volume fractions occupied by the two kinds of spheres.

In Tables I, II, and III the numerical solutions to the integral equations are given under the various conditions. In all cases integral equations (I), (II), and (III) have been used except for one representative case in Table II where integral equations (I), (II), and (IV) were solved to get a comparison in the radial distribution functions. Iteration was continued in every case for a given mixture until input and output agreed within ± 0.003 in ψ for each of the 3 distribution functions. In Table IV, the value of $\psi_{\alpha\beta}$ at $x=1$ obtained from Eqs. (I), (II), and (III) is compared with the value of $\psi_{\alpha\beta}(1)$ calculated from Eq. (IV) substituting in the latter equation the solutions obtained from the first three equations. The difference in these two values of $\psi_{\alpha\beta}$ is an indication of the error introduced by the superposition approximation. The value of $\psi_{\alpha\beta}(1)$ obtained in this way from Eq. (IV) is not very different from the value one would obtain by solving Eqs. (I), (II), and (IV) simultaneously, as can be seen for the mixture where $x_\alpha=27/28$ and the spheres occupy 7/60 of the total volume. The value of $\psi_{\alpha\beta}(1)$ of 0.453 is to be compared with 0.466 obtained by solving the set of integral equations involving Eq. (IV). At the highest density studied where the spheres occupy 7/30 v, the superposition approximation as used in Eq. (2) becomes very poor. Thus, it was not deemed worth while to get further solutions at this or higher densities without improving the superposition approximation. This density corresponds roughly to the critical condition for real molecules with van der Waals forces. At lower densities the approximation becomes better using the criteria of comparing the two $\psi_{\alpha\beta}$'s. As will be seen later, the thermodynamic functions are not as sensitive to which integral equation is used as the individual distribution functions.

TABLE IV. Comparison of $\psi_{\alpha\beta}(1)$ and $\psi_{\alpha\beta}^*(1)$.[a]

Mixture	$\psi_{\alpha\beta}$	$\psi_{\alpha\beta}^*$
$N_\alpha=N_\beta$; 7/180 v	0.145	0.137
$N_\alpha=27N_\beta$; 7/180 v	0.199	0.181
$N_\alpha=N_\beta$; 7/60 v	0.482	0.374
$N_\alpha=3N_\beta$; 7/60 v	0.501	0.367
$N_\alpha=27N_\beta$; 7/60 v	0.622	0.453
$N_\alpha=N_\beta$; 7/30 v	1.238	0.436

[a] $\psi_{\alpha\beta}^*(1)$ is the value of $\psi_{\alpha\beta}$ from the fourth integral equation at x equal one, when the solutions of the first three integral equations are substituted therein.

The radial distribution functions for a characteristic mixture are plotted in graph I, where $x_\alpha=27/28$ and the spheres occupy 7/60 v. The peaks for the three distribution functions occur at the points of contact between the spheres. This behavior was previously also found for a fluid of single spheres up to relatively high densities. Each distribution function then goes through periods of damped oscillations about $g=1$, the normalized uniform density. At the low density represented by this mixture these oscillations are too small to be represented on this graph. The period of these oscillations for each distribution function is different and for each of these less uniform than the periods found for pure fluids. This reflects the complicated geometric arrangements of little and big spheres in a given mixture. A striking indication of this geometric stacking can be seen in the curve for $g_{\beta\beta}(x)$. The dip at about $x=4$ for $g_{\beta\beta}(x)$ shows that there is a decreased probability of finding another big sphere at that position relative to a central big sphere due to the fact that quite a few little spheres are in immediate contact with the central big sphere. Thus, two big spheres separated by a little sphere is a reasonably probable configuration which gives rise to the structure found in $g_{\beta\beta}(x)$ near $x=4$. This arrangement is also reflected in $g_{\alpha\beta}(x)$ and $g_{\alpha\alpha}(x)$. As the number of small spheres relative to big spheres is decreased at

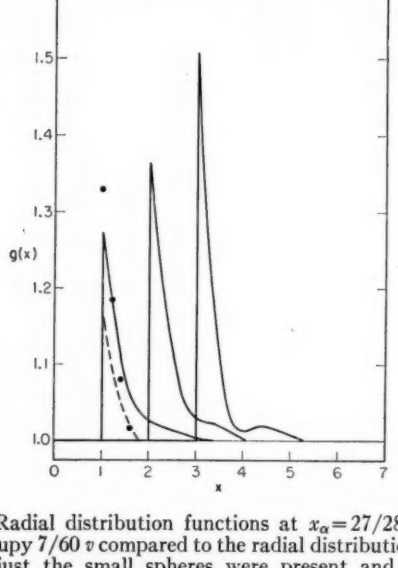

FIG. 1. Radial distribution functions at $x_\alpha=27/28$ when the spheres occupy 7/60 v compared to the radial distribution function (– – –) if just the small spheres were present and the radial distribution function (●) if the small spheres along occupied 7/60 v.

constant density this dip in $g_{\beta\beta}(x)$ becomes less pronounced. The effect of the big spheres on the distribution of little spheres is illustrated by the comparison of the dashed curve in Fig. 1 with the solid curve for $g_{\alpha\alpha}(x)$. The dashed curve representing the distribution function for the little spheres if all the big spheres were removed from the system shows that the big spheres crowd the little spheres together so that there is a higher probability of finding them at close distances to each other. The circles represent for comparison the distribution function for the system where also only little spheres are present but they occupy the same volume fraction as the little and big spheres did previously. The probability of finding another little sphere nearby is higher than for the mixture, but the correlation does not extend as far out.

In Fig. 2 the radial distribution function, $g_{\beta\beta}(x)$, is

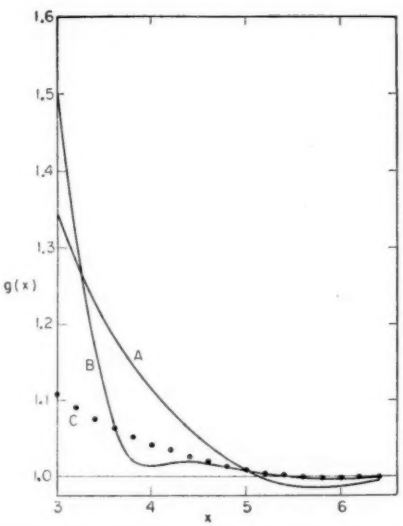

FIG. 2. Comparison of the radial distribution function, $g_{\beta\beta}$, at two mole fractions (A, $x_\alpha=1/2$; B, $x_\alpha=27/28$) keeping the volume occupied by the spheres constant at $7/60\,v$, and a comparison at two different volumes occupied by the spheres (A at $7/60\,v$; C at $7/180\,v$) keeping the mole fraction fixed at 1/2.

compared at two different mole fractions and the same fraction of the volume occupied by the spheres, $7/60\,v$. At the lower mole fraction, $x_\alpha=1/2$ (curve A), the number of little spheres are too few to cause the structure near $x=4$ seen in curve B where $x_\alpha=27/28$. In spite of the fact that there are fewer big spheres on the average in unit volume in the system represented by curve B, the geometric arrangement is such that the relative probability of finding two big spheres very close together is higher than in the mixture represented by curve A. Curves A and C demonstrate that as the volume is increased for a given mixture the correlation between molecules decreases, eventually approaching unity as the volume becomes very large. Figure 3 shows the difference in $g_{\alpha\beta}(x)$ obtained at $x_\alpha=27/28$ and $7/60\,v$ when the alternative Eqs. (4), (III) and (4), (IV) are used. The difference, a reflection of the

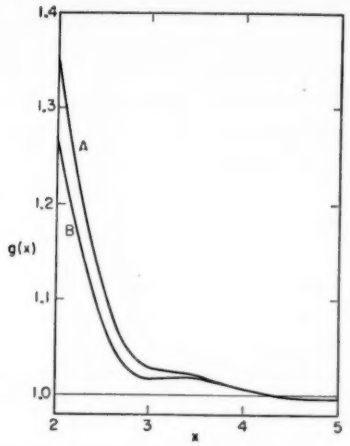

FIG. 3. Comparison of the radial distribution function, $g_{\alpha\beta}$, obtained by the use of Eq. (4), (III) (Curve A) and Eq. (4), (IV) (Curve B).

error introduced by the superposition approximation, is noticeable at small values of x and diminishes at larger distances.

V.

The integral equations have been solved under the condition that the volume fraction occupied by the spheres remain constant at several mole fractions in order to test the behavior of the equation of state under these circumstances. Simpler theories would predict that pv/RT is dependent only on the volume available to the spheres and thus would not change with mole fraction under these conditions. Table V and Fig. 4 show the deviation from constancy of $pv/RT-1$ at two different volumes as evaluated from Eq. (8). For pure fluids consisting of either just little or big spheres the thermodynamic functions depend only on the volume fraction occupied by the spheres, hence at $x_\alpha=0$ and 1, $pv/RT-1$ has the same value.[8] For any mixture, however, Fig. 4 shows that $pv/RT-1$ is smaller. The lower

TABLE V. Equation of state of the fluid mixture of rigid spheres.

Fraction of volume occupied by spheres	x_α	$\frac{pv}{RT}-1$
7/180	0	0.171
	1/2	0.134
	3/4	0.119
	27/28	0.133
	1	0.171
7/60	0	0.625
	1/2	0.483
	3/4	0.425
	27/28	0.481
	27/28[a]	0.467
	1	0.625
7/30	0	1.602
	1/2	1.295
	1	1.602

[a] Obtained from the solution of the fourth integral equation rather than the third.

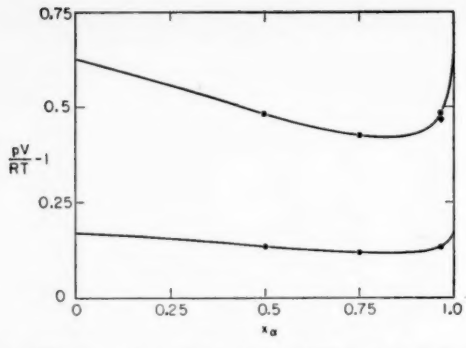

FIG. 4. The equation of state: $(pv/RT)-1$ as a function of mole fraction keeping the fraction of the volume occupied by the spheres constant in each of the two curves. ■ spheres occupy $7/60\,v$; ● spheres occupy $7/180\,v$; ◆ at $7/60\,v$ using Eq. (4), (IV).

the density, the more constant $pv/RT-1$ becomes, approaching as a limit the ideal behavior, where $pv/RT-1=0$ for all mole fractions. The dip in the equation of state is way beyond any error that could have been introduced by the superposition approximation as can be seen by comparing the diamond and square points in Fig. 4. The equation of state, at least, seems to be relatively insensitive at this density to which equation is used to solve for $g_{\alpha\beta}$. The behavior of pv/RT under the conditions of constant volume occupied by the spheres indicates that in a mixture greater net attractive forces exist than in the corresponding pure fluids just due to the particular geometric arrangement. As has been pointed out,[10] this net attractive force between two rigid spheres separated by a small fixed distance arises from an unsymmetrical bombardment of the other spheres in the system because the two spheres protect each other from bombardment in directions which would force them apart. At x_α approximately 0.9 this mutual protection of little and big spheres must be largest so that a minimum in $pv/RT-1$ occurs.

TABLE VI. The total excess entropy and free energy of the mixture of spheres and the excess entropy of mixing.

Fraction of volume occupied by sphere	x_α	S_p^E/R	μ_p^E/RT	$\Delta S^E/R$
7/180	1/2	−0.0025	0.136	
	3/4	−0.0022	0.120	
	27/28	−0.0025	0.136	
7/60	0	−0.075		
	1/2	−0.028	0.510	0.047
	3/4	−0.015	0.440	0.060
	27/28	−0.018	0.499	0.057
	1	−0.075		
7/30	0	−0.27		
	1/2	−0.13	1.420	0.14
	1	−0.27		

[10] J. de Boer, Repts. Progr. Phys. XII, 305 (1949).

The total excess entropy and free energy are obtained from the equation of state by Eqs. (10), (11), and (12). Table VI shows that these functions and the excess entropy of mixing, $\Delta S^E/R$, also have an extremal point. In Table VII the partial molal quantities are given as calculated from Eqs. (13), (14), and (15). The appropriate derivatives of the distribution functions have been evaluated by interpolation of the distribution function to the proper condition followed by numerical differentiation.

Although the densities studied in this investigation are relatively low, it is interesting to speculate as to the behavior of the system at much higher densities. It is quite conceivable that two transitions occur as the system is compressed. The first one would be similar to the one found for the system consisting of single spheres.[8] A further compression beyond this point can result in a separation of the spheres. Whether such a separation occurs depends very critically on the relative sizes of the spheres, that is, whether no close packed arrangement of the mixture can be found whose volume

TABLE VII. Partial molal quantities for the mixture of spheres.

x_α	$\lambda_0^{(\alpha)}$	$\lambda_0^{(\beta)}$	$\frac{pv}{RT}-1$	$\frac{N\bar{v}_\alpha}{v}$	μ_α^E/RT	S_α^E/R	p_α/px_α
1/2	1/30	1/30	0.134	0.867	−0.021	0.004	0.979
	7/135	7/135	0.219	0.802	−0.032	0.009	0.969
	1/10	1/10	0.483	0.663	−0.051	0.034	0.951
3/4	1/10	1/30	0.127	0.896	0.010	0.000	1.010
	7/45	7/135	0.208	0.844	0.015	0.005	1.015
	3/10	1/10	0.451	0.738	0.050	0.021	1.051
27/28	9/10	1/30	0.280	0.922	0.189	−0.009	1.208
	7/5	7/135	0.481	0.900	0.337	−0.005	1.401

is less than the combined volumes of the separate close packed arrangements of the spheres or less than a mixture of spheres and part of the spheres of one component close packed.

The physical nature of the first transition mentioned above remains unclear. A suggestive analogy would be to liken this transition to one from random close packing to one of more order. By random close packing is meant the arrangement resulting when the spheres are randomly introduced to fill a container. The introduction of an additional sphere in the container would necessitate an extensive rearrangement of the spheres in the box to make room for the additional one. This new arrangement contains more order since the spheres are more efficiently packed. The random close packed volume has been experimentally determined as being $v/v_0=1.28$, where v_0 is the close packed volume. Glass beads of relatively uniform size were dropped into various liquid media having the approximate density of glass. The density of the liquid as well as the choice of the size of the beads has little effect on the value of v/v_0. This value of v/v_0 is to be compared with the value

of 1.24 and 1.48 obtained by the criterion of the non-integrability of the radial distribution function for the transition from the Kirkwood and Born-Green theories, respectively.[8] The value of v/v_0 of 1.28 corresponds to 58 percent of the volume occupied by the spheres themselves. For a 50 percent mixture of spheres of size ratio 1.7 to 1 the experimental random close packing volume was also such that 58 percent of the volume was occupied by the spheres.

The continued interest of Professor J. H. Hildebrand in this research is gratefully acknowledged, as well as the calculational help of Mr. C. Cedarholm and Mr. J. Little. This work was supported in part by the U. S. Atomic Energy Commission.

THE JOURNAL OF CHEMICAL PHYSICS VOLUME 23, NUMBER 2 FEBRUARY, 1955

Gaseous Detonations. VI. The Rarefaction Wave*

G. B. KISTIAKOWSKY AND P. H. KYDD†
Gibbs Chemical Laboratory, Harvard University, Cambridge 38, Massachusetts

(Received June 18, 1954)

The density profile of the rarefaction wave which follows a detonation has been determined using the technique of x-ray absorption measurements to follow rapid gas density changes. The observed density-time dependence was found to agree, within experimental errors, with the predictions of the hydrodynamic theory developed by Taylor, Doering, and others. As the theory predicts, the density in the rarefaction wave decreases for approximately one-half of the distance traveled by the detonation wave; behind this is the region of quiescent gas at constant density.

WHILE studying the detailed density profile of the detonation front,[1] it was decided to use the same apparatus to check the hydrodynamic predictions for the density profile of the nonsteady rarefaction wave following the steady detonation front. The theoretical distributions of pressure and mass velocity have been described by Taylor[2] and others[3,4] and were approximately verified with respect to the distribution of mass velocity by Patterson[5] and with respect to pressure by Gordon.[6] Langweiler's[7] earlier treatment has been shown to be incorrect,[2] in that he neglected the fact that a rarefaction wave cannot remain abrupt but must spread out in time.

The density distribution behind a detonation wave in a closed tube may be worked out readily from the equations in reference 3, p. 192, on the assumption that the detonation is initiated instantaneously as a plane wave at the end plate of the tube, that there are no wall effects, that the gases are ideal, and that no chemical reactions take place in the rarefaction wave:

$$\frac{x}{t}=D-c_1\frac{\gamma+1}{\gamma-1}\left[1-\left(\frac{\rho_x}{\rho_1}\right)^{(\gamma-1)/2}\right]. \tag{1}$$

Here x is a distance from the initiation end of the tube, t the time from the instant of initiation, D the detonation velocity, c_1 the acoustic velocity in the reacted gas at the Chapman-Jouguet state, γ the (constant) ratio of specific heats, ρ_1 the density of the C-J state, and ρ_x density at the distance x. To derive the variation of the density ρ_x with time at a fixed distance x, one utilizes the familiar approximation

$$c_1=\frac{\gamma}{\gamma+1}D. \tag{2}$$

Then

$$\frac{\rho_x}{\rho_1}=\left(\frac{\gamma-1}{\gamma}\frac{x}{tD}+\frac{1}{\gamma}\right)^{2/(\gamma-1)} \tag{3}$$

and

$$\frac{\rho_1}{\rho_0}=\frac{\gamma+1}{\gamma}. \tag{4}$$

Behind the detonation in a closed tube the gas expands until its mass velocity drops to zero; it then remains at rest (reference 2) behind the point

$$x_f=\frac{Dt}{2} \tag{5}$$

and has a density:

$$\rho_f=\rho_1\left(\frac{\gamma+1}{2\gamma}\right)^{2/(\gamma+1)}. \tag{6}$$

The explosive mixtures chosen for the experiments described below contained argon and equal mole fractions of acetylene and oxygen. The result of their reaction in the detonation front is an almost quanti-

* Work supported under contract N5ori-76, T. O. XIX, NR-053-094, Office of Naval Research.
† National Science Foundation Predoctoral Fellow.
[1] J. Chem. Phys. (to be published).
[2] G. I. Taylor, Proc. Roy. Soc. (London) **A200**, 234 (1950).
[3] W. Doering and G. Burkhardt, Tech. Rept. No. F. T. S.-1227-1A (GDAM A9-T-46).
[4] H. Pfriem, Forsch. auf dem Geb. d. Ing. W. **12**, 143 (1941).
[5] S. Patterson, Research (London) **3**, 99 (1950).
[6] W. E. Gordon, *Third Symposium on Combustion, Flame and Explosion Phenomena* (Williams and Wilkins, Baltimore, 1949).
[7] H. Langweiler, Z. Tech. Phys. **19**, 271 (1938).

tative formation of carbon monoxide and hydrogen.[8] Since the heat capacity of the burned gases is a function of temperature and, moreover, a significant fraction of hydrogen is dissociated into atoms in the C-J state, an approximate calculation allowing for these effects was carried out for the experimental mixture of 20 percent argon, 40 percent acetylene, and 40 percent oxygen. The Chapman-Jouguet conditions were calculated using the observed detonation velocity of 2663 m/sec, the usual equations of the steady detonation wave:

$$\sigma=\frac{\rho_1}{\rho_0}=\tfrac{1}{2}\left(1+\frac{1}{\gamma_1}\right)+\left[\left(1+\frac{1}{\gamma_1}\right)^2-\frac{4n_0T_0}{n_1T_1\gamma_1}\right]^{\frac{1}{2}}, \quad (7)$$

$$T_1=\frac{D^2}{\sigma^2\gamma_1 n_1 R} \quad (8)$$

and the equilibrium equation for the only reaction assumed to occur in the rarefaction, $\frac{1}{2}H_2 \leftrightarrows H$:

$$K=\frac{XP^{\frac{1}{2}}}{\left(M-\frac{X}{2}\right)^{\frac{1}{2}}\left(N+\frac{X}{2}\right)^{\frac{1}{2}}}, \quad (9)$$

where X denotes the number of moles of hydrogen atoms per gram of products, M the total number of moles of hydrogen, as H_2, per gram, N the total number of moles of all constituents per gram, not allowing for hydrogen dissociation, and n the total number of moles per gram including dissociation ($=N+X/2$). Best guesses for σ, γ_1, n_1, and the observed D were substituted in Eq. (8) to give T_1. This in turn gave values for K and P from which X and thus a new value of n_1 were obtained. n_1 and T_1 were used in Eq. (7) and in the specific heat equation to give better values for σ and γ_1. The values so obtained were substituted into Eq. (8) and the calculation continued until adequate convergence was obtained. The self consistent values obtained are as follows:

$T_0=300°\text{K}$; $P_0=1$ atmos; $\rho_0=1.26$ g/l; $T_1=4350°$; $P_1=38.2$ atmos; $\rho_1=2.17$ g/l; $c_1=1540$ m/sec; $\gamma_1=1.34$; $A=0.0064$ moles/g; CO = 0.0256 m/g; $H_2=0.0084$ m/g; H = 0.00906 m/g.

Since the rarefaction wave is an isentropic expansion, $dS=0$; $dE=Pd\rho/\rho^2$ and, therefore,

$$C_v dT+\Delta E dX=P\frac{d\rho}{\rho^2}, \quad (10)$$

where ΔE is the energy absorbed by the reaction $\frac{1}{2}H_2=H$. For a small finite change in ρ one may then write

$$\bar{C}_v \ln\frac{T_2}{T_1}+\frac{\Delta E\Delta X}{\bar{T}}=\bar{n}R\ln\frac{\rho_2}{\rho_1}, \quad (11)$$

since T, n, and C_v do not change as rapidly as ρ. Using Eq. (11) the adiabat was calculated in the density range of interest by iteration. Taking a value ρ_2, smaller than ρ_1, and reasonable values for C_{v2}, T_2, and n_2 (hence for $\bar{C}_v$, $\bar{T}$, $\bar{n}$), ΔX was obtained, from which followed new values for X_2 and n_2. From Eq. (9) and the known dependence of K on T a value for T_2 was then obtained which corresponded to X_2. This resulted in improved values for $\bar{C}_v$ and $\bar{T}$ which were inserted again in Eq. (11) to yield an improved value for ΔX. The calculation was thus repeated until ΔX converged to 0.5 percent, giving T_2 to within 5°. The same calculation was then performed for the next density interval and so on to ρ_f. The equation of state data obtained for each value of ρ allowed one to calculate the acoustic velocity $c(\rho)$ and hence to construct a graph of $c(\rho)/\rho$ against ρ. The mass velocity $U(\rho)$ was obtained by a graphical integration of the equation

$$U(\rho)=U_1-\int_{\rho}^{\rho_1} c(\rho)\frac{d\rho}{\rho}, \quad (12)$$

as discussed in reference 3, and the experimentally observable density-time profile at the observational distance x_{obs} was derived by the substitution of $U(\rho)$ into

$$t(\rho)=\frac{x_{\text{obs}}}{U(\rho)+c(\rho)}, \quad (13)$$

where $U(\rho)+c(\rho)$ represents the "velocity" of a given density value as it travels forward behind the Chapman-Jouguet state. It was found that the simplified approach, not allowing for hydrogen dissociation, gave results quite close to those of the above calculation.

EXPERIMENTAL

Experiments were carried out using improved equipment of the x-ray absorption type.[9] The explosive mixture was confined in a closed steel tube, 10 cm i.d., 133 cm long, and was ignited at one end by a spark. At a point 69 cm from the ignition end there were two opposing beryllium windows which defined a 1.5 mm wide beam of x-rays perpendicular to the pipe axis. The x-ray tube was a General Electric Type CA-7 with a copper target,[10] operated at 22 kv and 26 mA. The scintillation detector on the opposite side of the tube was a terphenyl crystal backed by a 1P21 photomultiplier tube. The output was amplified and photographed as a density *vs* time trace on a CRO with an accurately timed sweep. By static calibrations with mixtures of argon, carbon monoxide, and hydrogen in proper ratio at room temperature, the output of the photomultiplier was related to gas density. An appropriate auxiliary circuit permitted feeding into the amplifier square

[8] Kistiakowsky, Knight, and Malin, J. Chem. Phys. **20**, 884 (1952).

[9] G. B. Kistiakowsky, J. Chem. Phys. **19**, 1611 (1951).

[10] We are indebted to the General Electric X-Ray Corporation and particularly to Dr. H. W. Pickett for the gift of this tube.

waves of chosen amplitude to obtain calibration marks on the film following each run. Thus the vertical deflections of the experimental trace were quantitatively related to gas density changes.

As used for the other experiments, the time constant of the electronic equipment was about 0.3 μsec, but the statistical fluctuations of the x-ray intensity produced rather irregular oscilloscope traces. Since the present experiments required less rapid time resolution but called for more accurately measurable density changes, a by-pass condenser was placed across the output of the photomultiplier, theoretically lengthening the time constant to 2 μsec, which was verified with a square wave generator. This permitted using higher amplification and more accurate reading of the records.

The explosion tube was also equipped with ionization gauges[11] to determine the velocity and the degree of stability of the detonation waves. The gauges were spaced at 10-cm intervals, starting 10 cm from the spark end, along the entire tube; there were also three gauges coincident with the x-ray windows, at 120° to each other, to detect possible tilting of the wave front. An additional gauge could be inserted axially into the tube to determine the degree of curvature of the wave front.

THE RESULTS

A comparison of the outlined theory with experiment presents considerable practical difficulties because the immediate result of ignition of a detonable gas mixture is a localized deflagration, even when a condensed spark discharge is used, while the theory calls for an immediate detonation at the entire end plate. A gaseous mixture which changes rapidly from deflagration to detonation is equimolar acetylene and oxygen. Unfortunately this combination does not give adequate x-ray absorption and hence argon had to be added. As a compromise between inadequate absorption and too slow initiation, a mixture of 20 percent argon and 80 percent $C_2H_2+O_2$ was chosen for all subsequent experiments. Even this gave rather unsteady waves after initiation with a single spark in the center of the end plate. The tube was therefore fitted with a conical end, expanding from *ca* 2 cm diameter at the spark to the full tube diameter over a distance of 10 cm. This arrangement gave steady waves of satisfactory planarity but, presumably because of reflections on the conical surface, a density hump, not anticipated by the theory, was observed near the end of the rarefaction wave, as shown in Fig. 1. Best results were obtained with seven sparks distributed evenly over the flat end plate of the tube and fired simultaneously. This resulted in detonation waves which had reached a steady velocity within 10 cm from the end plate. The detonation, however, did not start immediately at the end plate, as shown by the time interval between the sparks and the signal from the first gauge. While the detonation wave should travel this distance in about 40 μsec, the intervals actually observed were 207 μsec with a single spark, 184 μsec with the conical end and 171 μsec with the multiple initiation. In the latter case, at any rate, the volume of the gas involved in the nonsteady processes is quite small, since the wave reaches steady velocity so soon and the disturbances in the density-time profile should be limited to the very tail end of the wave. Figure 2 shows the combined results of the three experiments with multiple initiations, each point on the graph being the product of a comparator reading of the record, converted to density values as mentioned earlier. In taking these readings no attempt was made to smooth the statistical fluctuations of the CRO trace and therefore the individual points of each run do not fall on a smooth line. Two of the traces obtained are shown in Fig. 3 to demonstrate the magnitude of these statistical fluctuations. The theoretical density-time curve is shown by a solid line in Figs. 1 and 2. The experimental points, particularly in

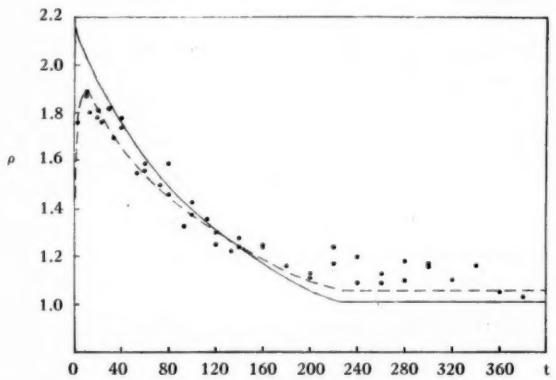

FIG. 1. A comparison of calculated density-time profile in the rarefaction wave with experimental density measurements. Points taken from three runs made with single spark-conical insert initiation. Solid line, exact theoretical curve; dashed line, corrected curve. Time in microseconds from the instant of passage of the detonation wave by the x-ray beam. Density in grams per liter.

[11] H. T. Knight and R. E. Duff, Rev. Sci. Instr. (to be published).

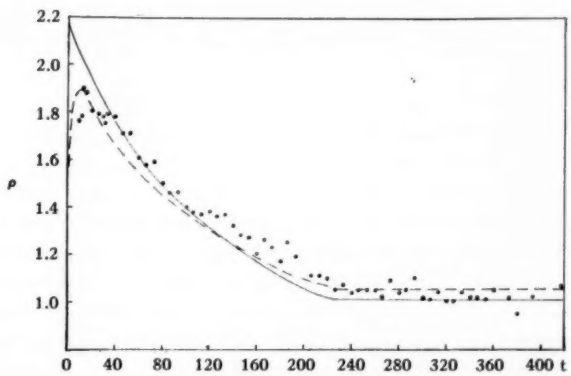

FIG. 2. A comparison of calculated density-time profile in the rarefaction wave with experimental density measurements. Points taken from three runs made with multiple spark initiation. Solid line, exact theoretical curve; dashed line, corrected curve. Time in microseconds from the instant of passage of the detonation wave by the x-ray beam. Density in grams per liter.

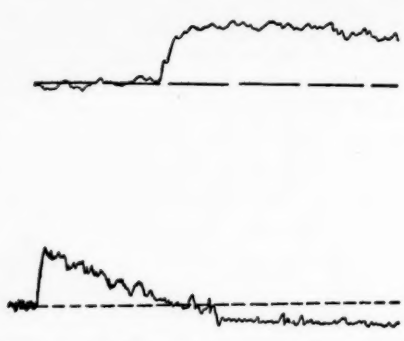

FIG. 3. Upper trace showing a run in the 240 cm long tube; lower trace showing a run in the short tube. Vertical deflections indicate density changes. Each horizontal dash equals 20 microseconds.

Fig. 2, are seen to reproduce in general the theoretical predictions, except near the front of the wave. This discrepancy, however, we believe to be due to experimental imperfections. To explore the response of the modified equipment to the wave front, experiments were made with a long tube, measuring 240 cm from the initiation end to the x-ray windows. As the first CRO tracing in Fig. 3 shows, the rarefaction wave in this long tube is so flat that the Chapman-Jouguet density should be well established on the record. Three experiments of this type were performed, two with the by-pass condenser installed and one without it. The experiment without the condenser showed a square profile with a total rise time of 1.4 μsec compared to the sum of the transit time across the slit (0.6 μsec) and the nonplanarity of the wave (0.3 μsec). The average C-J density by extrapolation of the records to the initial rise was 1.99 ± 0.10 g/l and on this basis the two runs with the condenser gave a time constant of 3.1 ± 0.5 μsec agreeing with that previously determined with the square wave generator when the nonideality of the wave front and slit system are considered. The records can also be fitted reasonably well by assuming the correct C-J density and a time constant of 10 μsec, but because of the internal consistency of the above approach it is considered preferable. Thus it is concluded that the calibrational procedure has introduced a systematic error of some 20 percent into the ratios of observed densities to the initial density. Therefore a dashed theoretical curve allowing for this error, coupled with a time constant of 3 μsec, has been drawn in Figs. 1 and 2 for comparison with the data. An additional modification of the theoretical curves is required by the imperfect planarity of wave fronts in the short tube, which amounted to 2–3 μsec and should have similar effect on the trace as a lengthened time constant of the recording equipment. The introduction of this correction should further flatten the initial peak and thus bring observation and theory into closer agreement.

As regards the rest of the experimental points, it is believed that they also fall as near the theoretical curve as could be expected. Two separate gas mixtures were used for static calibrations and the results agreed to 0.05 g/l. Four measurements of the oscilloscope traces are required to convert a point on a trace into a density value; the error inherent in these measurements is estimated as 0.1 g/l. Finally the calculations may be in error by as much as 0.02 g/l. Thus, the deviations of experimental points from the theoretical curve in Fig. 2 are seen to be well within the experimental errors. This good agreement is believed not to be an accidental result of the effects of tube walls on the density profile in the rarefaction wave. While a calculation of such effect is not possible at present, it is surely too small to compare with the other sources of error inherent in the present measurements. Early work on pressures resulting from gas explosions in closed vessels[12] has shown that the cooling effect of the walls amounted to an initial rate of pressure drop of the order of 1 percent per millisecond. In those experiments the ratio of surface to the energy content of the gases was comparable to the present work but here the recording of the wave was terminated less than a millisecond after the ignition of the gas. It is believed, therefore, that the present experiments constitute a definitive proof of the Taylor-Doering rarefaction wave.

In conclusion we wish to express our thanks to Mr. Roger Humberger who constructed much of the equipment used in these experiments.

[12] B. Lewis and G. von Elbe, *Combustion, Flames and Explosions of Gases* (Academic Press, Inc., New York, New York, 1951).

THE JOURNAL OF CHEMICAL PHYSICS VOLUME 23, NUMBER 2 FEBRUARY, 1955

Capacitance and Conductance Effects in Photoconducting Alkali Halide Crystals

JAMES ROSS MACDONALD*
Chemistry Division, Argonne National Laboratory, Lemont, Illinois
(Received March 29, 1954)

Measurements of the ac and dc response of illuminated F-centered potassium bromide single crystals have been carried out. The dependence of crystal capacitance and conductance on frequency, light intensity, electrode character and separation, F-center concentration, applied voltage, temperature, and optical bleaching time have been investigated. Most of the measurements were made on crystals containing both U and F centers, but a few were also made on additively colored and plain untreated crystals for comparison.

It was found that F centers in U-centered crystals bleached much slower under strong illumination than did those in additively F-centered crystals. The frequency response of the crystals depended significantly upon whether the electrodes were blocking or rectifying, but in both cases it was characterized by a single relaxation time given by the quotient of a series capacitance C_0 and G_∞, the normal conductance of the crystal. C_0 was found to be independent of all variable parameters except dark storage and bleaching time and is thought to arise from a charge-free layer located at one or both electrodes. Space-charge capacitance effects were apparently largely hidden by C_0 but did probably produce a small voltage-dependent nonlinearity observed at low frequencies with high applied voltages. G_∞, and thus the conduction-band electron concentration, depended linearly on light intensity over a wide range but underwent a transition from linear dependence on F-center concentration to independence thereof at high concentrations. Partly bleached crystals in total darkness exhibited appreciable conductivity, probably electronic in character. Most of the results on U-centered crystals can be tentatively explained in terms of electron trapping by negative-ion vacancies, F centers, interstitial hydrogen atoms, and hydrogen atoms in negative-ion vacancies.

I. INTRODUCTION

POLARIZATION effects arising from the buildup near electrodes of space charge under the influence of an electric field may be expected to appear in any material containing charge carriers which cannot pass freely from material to electrodes and/or from electrodes into the material. Such effects are therefore widespread and have, indeed, been observed in all materials except metals.

Polarization in liquid ionic conductors, including both strong electrolytes[1–3] and dielectric liquids containing impurities,[4] has been extensively investigated in the past for dc applied fields and, to a lesser extent, for ac fields. This work has led to the picture of a polarization, or double layer, capacitance localized near the electrodes and in series with the normal ionic conductivity of the material. The equivalent circuit is considerably more complicated when electrode reactions occur[5] or when two or more ions of different but comparable mobility are present. Space-charge effects attributed to ionic motion in solids have also been observed at high temperatures for glass[6] and various single crystals such as quartz[7] and at room temperature for selenium rectifiers.[8]

Electronic or hole conduction in semiconductors arising from either thermal or optical excitation may also give rise to polarization effects. Thus, Kolomoĭtsev[9] has recently observed polarization effects in calcite ascribed to electrons thermally ionized from impurities, and Kallman, Kramer, and Perlmutter[10] have reported polarization effects arising from optically released electrons in luminescent powders. Earlier work of Joffé[7] and others showed that electronic polarization effects were also apparently of importance in single crystals of F-centered alkali halides exposed to light in the F-absorption band.

In ionic conductors, space-charge polarization arises from the inability of the metallic electrodes to supply ions to the material or to accept ions. Such electrodes are termed blocking or polarized for the ionic carriers considered. There are two other possibilities which often appear in electronic conductors. If charge carriers can pass freely from material to electrode or from electrode into the material but cannot travel freely in both of these directions, the contact is said to be rectifying. In the ohmic case, carriers can move across the contact freely in either direction. Smith and Rose[11] have recently shown how either rectifying or ohmic contacts can be produced between n-type cadmium sulfide single crystals and indium or gallium electrodes. Earlier, Bube[12] found that the potential barriers rendering silver paste contacts rectifying on zinc sulfide single crystals could be largely removed by heating several minutes at 650°C.

There has been very little experimental work on polarization effects for ac applied fields in spite of the

* Then on leave from Armour Research Foundation. Now at Texas Instruments Incorporated, 6000 Lemmon Avenue, Dallas 9, Texas.

[1] D. C. Grahame, J. Am. Chem. Soc. **68**, 301 (1946).
[2] H. Chang and G. Jaffé, J. Chem. Phys. **20**, 1071 (1952). References to older literature are given in this paper.
[3] G. Jaffé and J. A. Rider, J. Chem. Phys. **20**, 1077 (1952).
[4] G. Jaffé and C. Z. LeMay, J. Chem. Phys. **21**, 920 (1953).
[5] D. C. Grahame, J. Electrochem. Soc. **99**, 370C (1952).
[6] D. M. Robinson, Physics **2**, 52 (1932).
[7] A. F. Joffé, *The Physics of Crystals* (McGraw-Hill Book Company, Inc., New York, 1928).
[8] G. Jaffé, Phys. Rev. **85**, 354 (1952).
[9] F. I. Kolomoĭtsev, Doklady Akad. Nauk SSSR **75**, 185 (1950).
[10] Kallman, Kramer, and Perlmutter, Phys. Rev. **89**, 700 (1953).
[11] R. W. Smith and A. Rose, Phys. Rev. **92**, 857 (1953).
[12] R. H. Bube, Phys. Rev. **83**, 393 (1951).

fact that they allow capacitative and conductive effects to be separated uniquely. The present investigation was undertaken to explore some of the possibilities of this measuring technique applied to photoconducting alkali-halide crystals, and to use the results to gain a better understanding of photoconduction, space charge, and trapping processes within such crystals. A few of the experimental results have been reported previously.[13] It should be emphasized that the capacitative effects arising from free electrons described in the present paper are completely different from the low-frequency dispersion results obtained by Breckenridge[14] on specially treated alkali-halide crystals. Breckenridge's results arise from bound ionic-vacancy pairs which can reverse their direction of polarity in an electric field. The most characteristic feature of the present results, on the other hand, is that with the crystals in the dark one measures at low frequencies only the normal geometric capacitance of the crystal arising from the polarization of bound charges. When the crystal is illuminated with F-band light, however, the apparent capacitance at low frequencies increases by a factor of as much as 100 times. This "photocapacitative" effect is thus obviously closely connected with the free electrons produced by the absorption of light and is an entirely different phenomenon than that investigated by Breckenridge.

II. DISCUSSION OF SPACE-CHARGE THEORY

Before discussing the experimental results in detail, it will be useful to compare briefly some of the space-charge theories which may possibly apply to the experimental situation. Space-charge formation occurs whenever charge carriers cannot pass freely across the junction between the charge-containing material and one or both of its electrodes. In the present case, electrons can leave a photoconducting alkali halide crystal at a metallic anode in intimate contact with the crystal but cannot re-enter at a metallic cathode.[15] The crystal thus acts like two rectifiers connected back-to-back. In addition, we shall need to consider the behavior of these crystals with blocking electrodes such that electrons can neither leave nor enter at electrodes of either polarity.[16]

When a dc voltage is applied across a photoconducting alkali halide crystal, electrons will move toward the anode where they will either be discharged or, if blocked, will establish a negative space charge. At the same time, a positive space charge of ionized F centers, or negative-ion vacancies, will form near the cathode. The total static capacitance C_0 of the crystal will be the series combination of the two capacitances represented by the space charge at the electrodes. When space charge forms at both electrodes, the total capacitance will thus be half of that obtained with a single space-charge layer. As the applied voltage is increased, the concentration p of negative ion vacancies at the cathode will increase until the original F-center concentration N_F, assumed initially uniform throughout the crystal, is reached. An applied voltage of only the order of 0.5 volt is required to produce this condition for $N_F=5\times10^{15}$ cm^{-3}, and c_0, the initial free electron concentration, of 10^{10} cm^{-3}. Since larger voltages cannot increase p beyond N_F, all they can accomplish is to increase the width of the cathode exhaustion layer composed of negative-ion vacancies of concentration N_F.

When an ac voltage of sufficiently low frequency is applied, a space-charge distribution essentially equal to that which would be caused by a dc voltage equal to the peak ac voltage will be produced at the peak of each half cycle. If an exhaustion layer is established, it will move from one electrode to the other through the medium of F-center ionization and electron:negative-ion-vacancy recombination. The maximum ac capacitance at sufficiently low frequencies will therefore be of the same order of magnitude as that produced by a corresponding dc voltage although voltage-dependent nonlinearity may cause extensive harmonic generation. It should be pointed out that at sufficiently high frequencies, on the other hand, no appreciable space charge will have time to build up during a half cycle, and the admittance of the crystal will be entirely determined by its geometrical capacitance $C_g=\epsilon/4\pi L$, and its photoconductance $G_\infty=\mu e c_0/L$.[17] Here ϵ is the dielectric constant of the material in the absence of free charges; L, the separation of electrodes; and μ the microscopic electron mobility.

Unfortunately, there are available no exact ac or dc theories of space-charge formation which cover the voltage range from zero up to hundreds of volts. For the purposes of comparison with experiment, we can, however, make use of the predictions of several theories which cover different parts of the voltage range. For applied dc voltages less than about $2kT/e$ or 50 mv at room temperature, the author's linearized ac theory may be applicable.[18] When the space-charge capacitance C_0 is at least several times larger than C_g, which is usually the case, it predicts a frequency- and voltage-independent series capacitance of

$$C_0=\epsilon/4\pi L_{D(\mathrm{rms})}, \tag{1}$$

$$L_{D(\mathrm{rms})}=[\epsilon kT/2\pi e^2 c_0]^{\frac{1}{2}}, \tag{2}$$

and a charging time constant of $\tau=C_0/G_\infty$. In Eq. (2), $L_{D(\mathrm{rms})}$ is the rms Debye length.

For larger voltages, an exact, nonlinear dc theory may be employed.[19] It is first necessary to distinguish

[13] J. R. Macdonald, Phys. Rev. **85**, 381 (1952); **90**, 364 (1953).
[14] R. G. Breckenridge, *Imperfections in Nearly Perfect Crystals* (John Wiley and Sons, Inc., New York, 1952), p. 219. See also Y. Haven, J. Chem. Phys. **21**, 171 (1953).
[15] N. F. Mott and R. W. Gurney, *Electronic Processes in Ionic Crystals* (Clarendon Press, Oxford, 1948), second edition, p. 169.
[16] Sample preparation and dimensions are discussed in Appendix I; experimental details in Appendix II.
[17] Theoretical expressions for capacitance and conductance will apply throughout to unit electrode area.
[18] J. R. Macdonald, Phys. Rev. **92**, 4 (1953).
[19] J. R. Macdonald, J. Chem. Phys. **22**, 1317 (1954).

TABLE I.

Theory	Monomolecular C_0	Monomolecular τ	Bimolecular C_0	Bimolecular τ	F-center capture C_0	F-center capture τ
Linearized	$[IN_F/N_T]^{\frac{1}{2}}$	$L[N_T/IN_F]^{\frac{1}{2}}$	$[IN_F]^{\frac{1}{2}}$	$L[IN_F]^{-\frac{1}{2}}$	$I^{\frac{1}{2}}$	$LI^{-\frac{1}{2}}$
Exhaustion layer	$[N_F/(\phi+V_{dc})]^{\frac{1}{2}}$	$\frac{L}{I}\left[\frac{N_T^2}{N_F(\phi+V_{dc})}\right]^{\frac{1}{2}}$	$[N_F/(\phi+V_{dc})]^{\frac{1}{2}}$	$L[I(\phi+V_{dc})]^{-\frac{1}{2}}$	$[N_F/(\phi+V_{dc})]^{\frac{1}{2}}$	$\frac{L}{I}[N_F/(\phi+V_{dc})]^{\frac{1}{2}}$
Constant capacitance	...	LN_T/IN_F	...	$L[IN_F]^{-\frac{1}{2}}$	...	L/I

between static and differential capacitance. Static capacitance is defined by Q_{dc}/V_{dc} and differential capacitance by dQ_{dc}/dV_{dc}. Measurements with dc yield the static capacitance C_0, as do measurements with sufficiently low frequency ac alone, at least approximately. On the other hand, when a dc bias is applied and capacitance is measured with a much smaller ac voltage, the differential capacitance is obtained. Whenever there is dependence of capacitance on voltage, the differential and static capacitances differ, except at zero voltage where their limiting values are equal. The nonlinear theory predicts an expression similar to (1) but with the added voltage-dependent terms $\cosh\alpha V_{dc}$ for the differential capacitance and $\sinh\alpha V_{dc}/\alpha V_{dc}$ for the static capacitance. The constant α is $e/2kT$ for only one space-charge layer, $e/4kT$ for a layer at each electrode. The charge density at the cathode is given by $p=c_0\exp(2\alpha V_{dc})$. As we have seen above, this quantity cannot exceed N_F; this restriction thus limits the voltage range of applicability of the theory.

When an exhaustion layer has formed at the cathode, the usual exhaustion layer formula for its differential series capacitance is[20]

$$C_0=\epsilon/4\pi L_e, \tag{3}$$

$$L_e=[\epsilon(\phi+V_{dc})/2\pi eN_F]^{\frac{1}{2}}, \tag{4}$$

where ϕ is the difference between the work function of the metallic electrode and the electron affinity of the crystal.[15] The corresponding expression for the static capacitance arising from V_{dc} is

$$C_0=\frac{1}{V_{dc}}\left(\frac{\epsilon N_F e}{2\pi}\right)^{\frac{1}{2}}[(\phi+V_{dc})^{\frac{1}{2}}-(\phi)^{\frac{1}{2}}]. \tag{5}$$

This expression will not differ appreciably from that of Eqs. (3) and (4) until V_{dc} is considerably greater than ϕ. The expressions (1) through (5) show that if $\phi=0$ the static capacitance will start independent of V_{dc} as this quantity increases from zero, undergo a transition to an essentially exponential rise with V_{dc}, reach a maximum, then finally fall off proportional to $V_{dc}^{-\frac{1}{2}}$. If ϕ is not zero but is sufficiently large to cause an exhaustion layer to be formed, the capacitance will remain constant until V_{dc} is comparable to ϕ, then will decrease.

[20] H. C. Torrey and C. A. Whitmer, *Crystal Rectifiers* (McGraw-Hill Book Company, Inc., New York, 1948), p. 76.

Now, for future comparison with experiment, it is of interest to tabulate the dependence of C_0, and τ (defined as usual as C_0/G_∞) on N_F, L, and I, where I is the intensity of F-band illumination. For this purpose, it is necessary to distinguish between the various types of electron:electron-trap recombination which may possibly occur. The rate at which F centers are ionized by light in the F band is proportional to N_FI. The recombination rate is proportional to the product of c_0 and (a) c_0, in the bimolecular case of capture by ionized F centers whose electrons are in the conduction band; (b) N_F, in the case of capture by F centers themselves to form F' centers so long as c_0 and the concentration of F' centers are both much less than N_F; (c) N_T, the concentration of traps not arising from F centers or negative-ion vacancies, in the monomolecular case of all recombination with foreign traps. On setting ionization and recombination rates equal, one obtains the dependence of c_0 on I, N_F, and N_T and can form Table I. We have also included the dependence of τ obtained when C_0 is independent of all preceding quantities, including frequency.

Next, we shall use some typical experimental results to eliminate some of the above theories from further consideration. From the data of Fig. 3, we obtain for a strongly illuminated KBr crystal with $N_F\simeq 5\times10^{15}$ cm^{-3}, $C_0=31.2$ $\mu\mu$f/cm^2 and $G_\infty=1.25\times10^{-7}$ mhos/cm^2. Using the room-temperature value of 12.5 cm^2/volt-sec for the Hall mobility of photoelectrons in similar crystals obtained by Macdonald and Robinson[21] and neglecting any small difference between Hall and microscopic mobilities, one obtains $c_0=1.25\times10^{10}$ cm^{-3} from the above value of G_∞. This value of c_0 corresponds to an rms Debye length of 3.31×10^{-3} cm and a space-charge capacitance of 131 $\mu\mu$f/cm^2, more than four times larger than the observed value of C_0. A value of $\epsilon=4.9$ was used in this calculation.[22] Lack of agreement between measured and calculated values of C_0 is not surprising, since the above data were obtained with an ac voltage of the order of 5 volts rms. The nonlinear as well as the linearized theory should thus be inapplicable here.

A stringent test of the exhaustion layer theory is

[21] J. R. Macdonald and J. E. Robinson, Phys. Rev. **95**, 44 (1954).

[22] A. von Hippel, Tables of Dielectric Materials, Vol. 4, Technical Report No. 57, Laboratory for Insulation Research, M.I.T., January, 1953.

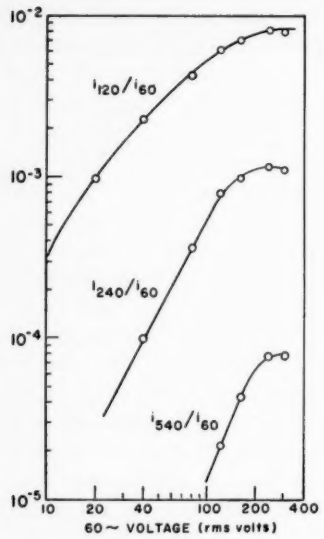

FIG. 1. Harmonic generation by photoconducting KBr Crystal U-1.

afforded by the calculation of ϕ from Eq. (3) or (5) with V_{dc} taken equal to zero. From the measured value of C_0 and the above value of N_F, we obtain $\phi \simeq 1.8\times10^5$ volts. Since this value is many orders of magnitude too large, it is clear that exhaustion layer formation cannot account for the results. Finally, if we arbitrarily write C_0 as $\epsilon/4\pi L_x$, where L_x is a charge-free region between either electrode and the bulk of the crystal, we obtain $L_x=1.39\times10^{-2}$ cm assuming that the charge-free region has the normal dielectric constant of the material. If equal charge-free regions abut each electrode, then $L_x=7.0\times10^{-3}$ cm.

A charge-free region producing a constant capacitance such as that discussed above and in Table I might possibly arise from the influence of surface states on the internal charge distribution.[23] More probably, it could arise in the present crystals from an absence of F centers or negative-ion vacancies in a region of thickness L_x (or $L_x/2$) at each surface of the crystal. How such a region could arise and experimental evidence for its existence will be discussed later.

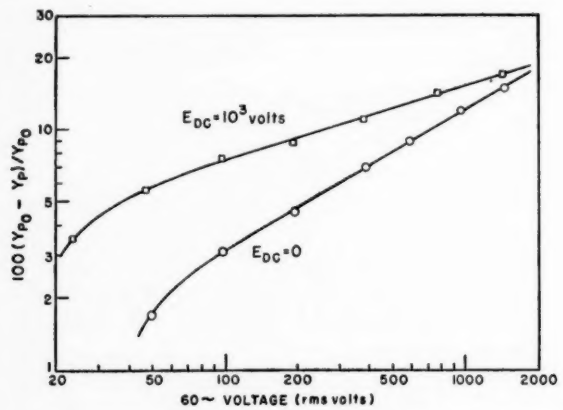

FIG. 2. Dependence of percentage relative change in admittance of photoconducting crystal U-1 on 60-cps voltage.

[23] J. Bardeen, Phys. Rev. **71**, 717 (1947).

III. EXPERIMENTAL RESULTS

(a) Voltage-Dependent Nonlinearity

Most space-charge theories predict some voltage-dependent nonlinearity of space-charge capacitance, especially with high voltages applied. An attempt was made to observe any such nonlinearity with an illuminated crystal and only a surprisingly small amount observed. It was found that no appreciable ac voltage dependence of capacitance could be measured with a sensitive capacitance bridge in the range of 0.5 to 15 volts rms. Measurements were carried out at sufficiently low frequencies that the admittance of the crystal was almost entirely capacitative so that C_0, the low-frequency limiting value of the capacitance, was obtained.

Next, the series method for harmonic and total admittance measurements was employed.[24] Crystal U-1 containing an F-center concentration of about 5×10^{15} cm^{-3} was used. It had evaporated aluminum electrodes (rectifying) and was strongly illuminated with white light. At the measuring frequency of 60 cps, the admittance was still almost entirely capacitative. Figure 1 shows the voltage dependence of several harmonics, normalized with respect to the fundamental. All harmonics up to the 14th could be detected, but no harmonic generation by a high-grade mica capacitor of the same capacitance as the illuminated crystal was observed with the same apparatus. At 300 volts rms and above, where the harmonics seem to saturate relative to the fundamental, the total harmonic generation is still less than two percent of the fundamental.

Figure 2 shows how the percentage change in relative admittance varies with applied ac voltage up to 2000 volts rms for zero dc bias and for 10^3 volts bias. The capacitative decrease which may be inferred from Fig. 2 is very small and its dependence on voltage much less rapid than $V_{ac}^{-\frac{1}{2}}$, in keeping with the small amount of harmonic generation observed. These results are therefore inconsistent with simple exhaustion-layer formation. If, however, most of the applied voltage drop occurred across a voltage- and frequency-independent capacitance in series with one or both electrodes, the total capacitance would be largely determined by this constant capacitance. Larger nonlinear capacitative effects of the exponential or exhaustion-layer type occurring within the crystal would hardly affect the total capacitance but might quite possibly lead to the small nonlinearity observed.

(b) Frequency Dependence

We shall initially assume that a photoconductive crystal can be represented electrically by a frequency-independent capacitance C_0 localized near one or both

[24] See Appendix II.

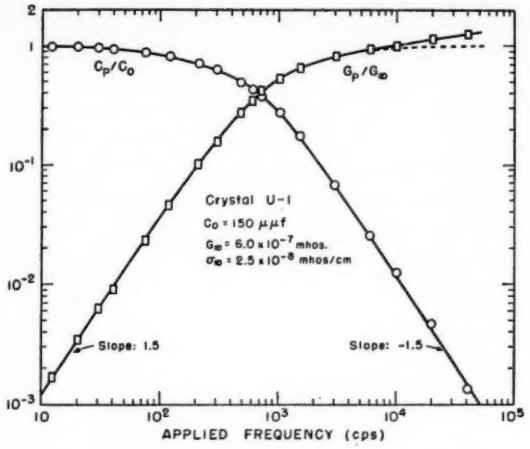

FIG. 3. Dependence of normalized parallel capacitance and conductance on frequency.

electrodes and in series with the bulk conductivity G_∞. This series combination is then in parallel with C_g, the geometrical capacitance of the crystal (measured, e.g., with the crystal in darkness or at a very high frequency). For ac, the frequency-independent series quantities C_0 and G_∞ can be replaced by their parallel equivalents C_P and G_P, whose frequency dependence will be of the form

$$C_P/C_0=[1+(\omega\tau)^2]^{-1}, \tag{6}$$

$$G_P/G_\infty=(\omega\tau)^2[1+(\omega\tau)^2]^{-1}, \tag{7}$$

where $\tau=C_0/G_\infty$. These are simply Debye dispersion formulas. A bridge measurement of parallel capacitance and conductance will therefore yield G_P and the sum of C_P and C_g. Thus, C_P may be obtained very easily from such a measurement.

Figure 3 shows the dependence of C_P/C_0 and G_P/G_∞ on frequency for crystal U-1 strongly illuminated and held at room temperature. It is found that τ, as calculated from the frequency at which $C_P/C_0=G_P/G_\infty$, is equal to that calculated from C_0/G_∞ to within five percent. There is thus no doubt that the G_P and C_P curves arise from the same dispersion mechanism. On the other hand, they differ from Debye curves in that the limiting slopes are $\pm\frac{3}{2}$ instead of ± 2.[25] It is probable, as we shall see later, that this deviation from the above simple theory arises from the fact that the electrodes used were only rectifying so electrons could discharge at the anode.

The dependence of C_P and G_P on the wavelength of the incident light was investigated for a number of newly F-centered samples using interference filters and various combinations of gelatin filters. It was found that only light in the F-absorption band produced capacitance and conductance additional to that of a specimen in the dark. Since M and R bands and colloidal aggregates[26] probably form in these crystals after considerable F-band illumination or long-term dark storage, white light illumination, such as that used in most of the present work, will release electrons from these centers, if they are present, as well as from F centers.

The same data shown in Fig. 3 are replotted in a different fashion in Fig. 4 and lead to the larger circular curve. This figure is essentially the circle diagram common in electrical circuit analysis, but we have chosen to plot G_P/ω *vs* C_P rather than the more usual but equivalent G_P *vs* ωC. In the form given in Fig. 4, the ordinate is proportional to the apparent dielectric loss ϵ'' and the abscissa to the dielectric constant. We shall not use these terms in this paper, however, because the dielectric constant and loss of a material are usually considered as intensive quantities, the same at each point in the material. In the present situation, the dispersion contribution to the capacitance and conductance of the specimen is localized in layers near the electrodes and is therefore by no means intensive. It may be noted that Debye-type frequency dependence, involving a single relaxation time, should yield a semicircle with

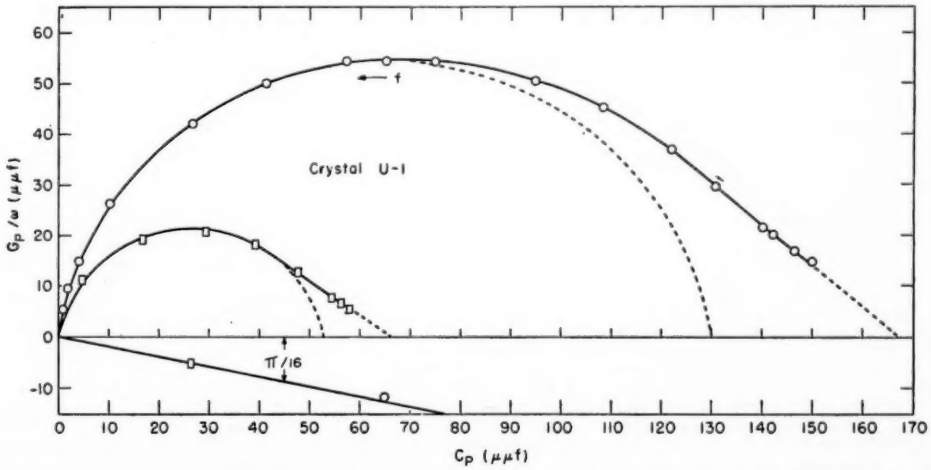

FIG. 4. Circle diagram plot of G_P/ω *vs* C_P for Crystal U-1. Small curve measured six months after large curve.

[25] The small increase of the G_P/G_∞ curve above its limiting value, shown dotted, may be explained as arising from the series resistance of the evaporated electrodes of this crystal as will be discussed later.

[26] F. Seitz, Revs. Modern Phys. **18**, 384 (1946); **26**, 7 (1954).

center on the abscissa in a plot of this type. The smaller curve in Fig. 4 also refers to crystal U-1 but was taken for the same light intensity about six months after the larger curve. During the intervening time, the crystal was bleached quite strongly with F light and given several gamma-ray exposures to bring the F-center concentration back to approximately its original value. It is evident that bleaching and redosing have reduced C_0 considerably.

These curves are similar in form to Cole-Cole plots[27] in that they yield circular arcs over part of their lengths. The centers of these arcs are shown in the figure and fall approximately on the same line. In spite of the similarity to Cole-Cole plots, the curves are, in fact, very different. The difference arises chiefly from the frequency dependence of the capacitance and conductance curves. If this dependence is computed from Fig. 4 treating it as a Cole-Cole plot, which implies a certain distribution of relaxation times, the dependence is very different from the experimental results shown in Fig. 3. Therefore, these data do not arise from a material having a distribution of relaxation times of the form demanded by the Cole-Cole equations. It is also worth noting that the curves of Fig. 3 cannot be fitted well by the Fuoss-Kirkwood theory[28] which involves a different relaxation time distribution function than that of the Cole-Cole theory.

Figure 5 shows the frequency dependence of C_P and G_P obtained for additively F-centered crystal AF-1 containing about 1.5×10^{16} F centers per cm^3. This measurement was made with the same light intensity as that employed for the U-centered crystal of Fig. 3. The areas of the two crystals were approximately the same, and the respective values of C_0 are obviously of at least the same order of magnitude. On the other hand, the conductivity σ_∞ is about 70 times smaller for the additively colored than for the U-centered crystal, in spite of the former's having had about three times as

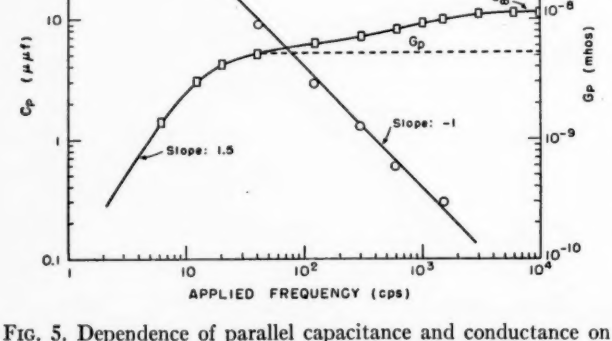

FIG. 5. Dependence of parallel capacitance and conductance on frequency for additively F-centered Crystal AF-1.

[27] K. S. Cole and R. H. Cole, J. Chem. Phys. **9**, 341 (1941)
[28] J. R. Macdonald, J. Chem. Phys. **20**, 1107 (1952).

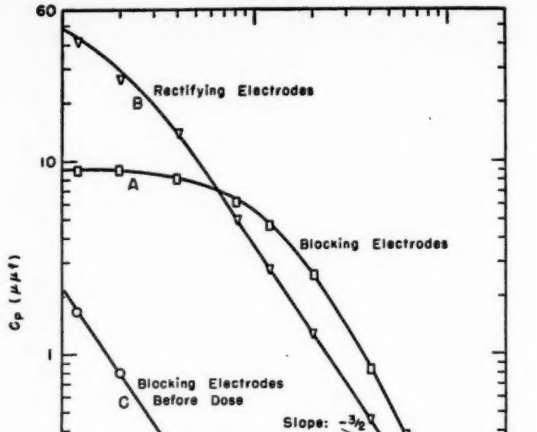

FIG. 6. Comparison of frequency dependence of parallel capacitance of a Type II specimen with blocking electrodes to that with rectifying electrodes.

many F centers. This result clearly indicates that there is a much higher conduction-band electron density for the U-centered crystal than for the additively-colored one. The shape of the curves for the additively-colored crystal is somewhat different from those presented in Fig. 3. Although the G_P curve may involve a $\frac{3}{2}$ slope at low frequencies in agreement with the result of Fig. 3, the C_P limiting slope is approximately -1 instead of $-\frac{3}{2}$. Because of their rapid bleaching under strong illumination and their low conductivity, which leads to large values of τ, we shall not consider capacitative results for additively-colored crystals further in this paper. Qualitatively, the same effects are obviously present in additively-colored as in U-centered crystals, although there may be quantitative differences in behavior.

The previous results have pertained to Type I crystals[16] with aluminum electrodes evaporated directly on the crystal surface. The frequency dependence of such crystals type involves limiting slopes of $\pm\frac{3}{2}$ instead of ±2. In order to determine if this difference arose from the rectifying electrodes employed, a number of Type II crystals were made up in such a way that for a given crystal the electrode conditions could be changed from rectifying to blocking. First, frequency dependence measurements were carried out for such crystals with silver paint electrodes directly on the ends of the crystals. Exactly the same results were obtained as with the aluminum-electrode Type I crystals previously considered, indicating that it is immaterial whether light enters the crystal through an electrode or between two electrodes. Since no appreciable difference in the rectifying character of aluminum or silver con-

tacts was observed, it seems possible that such character may be at least partly controlled by gas adsorbed on or near the crystal surface or by surface states.[23]

Figure 6 shows the dependence of C_P on frequency for a single crystal with rectifying and with blocking electrodes. The bottom curve C was taken before the crystal had been exposed to gamma radiation, whereas the top two curves were obtained after sufficient exposure to produce about 5×10^{15} F centers per cm^3. Curve B for rectifying electrodes is of the same form as previously discussed and clearly shows the $-\frac{3}{2}$ slope at high frequencies. On the other hand, Curve A for blocking electrodes is considerably different. The only difference in the crystal for Curves A and B was that for B silver electrodes were directly on the crystal while for A they were separated from it by a thin sheet of mica. The line drawn in Curve A is a theoretical Debye curve fitted to the experimental points. The agreement is excellent and indicates that Debye-type frequency dependence is indeed obtained for blocking electrodes and that therefore a frequency-independent series capacitance C_0 is involved. The difference in limiting slopes of A and B is thus obviously due to the difference in the electrodes.

The difference in the low-frequency limiting values of C_P arises, however, partly from the mica sheets between crystal and metal electrode not being sufficiently thin that their capacitative reactance was negligible compared to that of the crystal itself. Thus, with blocking electrodes, the observed capacitance at low frequencies was smaller than that of the crystal itself, since the crystal capacitance and that of the mica sheets were in series. This effect cannot account for a reduction in the value of C_0 by more than a factor of two at most. The observed ratio between the values obtained with blocking and with rectifying electrodes is, however, greater than six as indicated by Fig. 6. It thus appears that the character of the electrode-crystal contact may affect C_0 directly.

Curve C in Fig. 6 shows that there are considerable photocapacitative effects present for a U-centered crystal even before gamma-ray dosage. These effects probably arise from a residual concentration of F centers of the order of 10^{13} to 10^{14} cm^{-3} not removed during the U-centering process. Since the crystal had blocking electrodes when Curve C was obtained, the limiting slope might have been expected to be -2; it is, however, about -1.4. This discrepancy was often noted for very low concentrations of F centers and/or very low light intensities. It probably arises from a number of causes. It is possible that the reduced slopes apparent with low carrier concentrations arise from the presence of another dispersion mechanism present in addition to the motional dispersion which we have been considering. Lawson, Miller, Schiff, and Stephens[29] have developed a dispersion theory in which dispersion arises from a finite ionization time for the ionization of charge carriers from neutral centers. This theory yields a limiting slope for parallel capacitance of -1 and for parallel conductance of 2. The theory is not directly adaptable in its present form to the present experimental situation, but it is possible that long average ionization time becomes of importance here for very low F-center concentrations or low light intensities and reduces the limiting C_P slopes. For either very low light intensities or very low F-center concentrations, the probability of excitation of any given F center will be very small, and its average ionization time will be long. It is interesting to note that residual capacitance greater than C_g could often be measured in the dark for crystals with F-center concentrations of the order of 10^{16} cm^{-3} and such measurements yielded limiting slopes again of the order of -1. Unfortunately, the influence of thermal ionization of electrons from any shallow traps which may be present becomes of greater importance as the light intensity is reduced. The combination of the two types of ionization make it impractical at present to apply the combination of motional and finite-ionization-time dispersions to the present experimental case in a quantitative fashion.

Figure 7 presents the results of frequency dependence measurements of G_P corresponding to the measurements of C_P shown in Fig. 6. The measurements of these two graphs were made at the same time, on the same crystal, and with the same light intensity. Curve A is again for blocking electrodes and the experimental points are well fitted by a Debye curve of the same time constant as that required to fit the corresponding C_P curve of Fig. 6. Curve B of Fig. 7 for rectifying electrodes shows that there is no appreciable dependence of

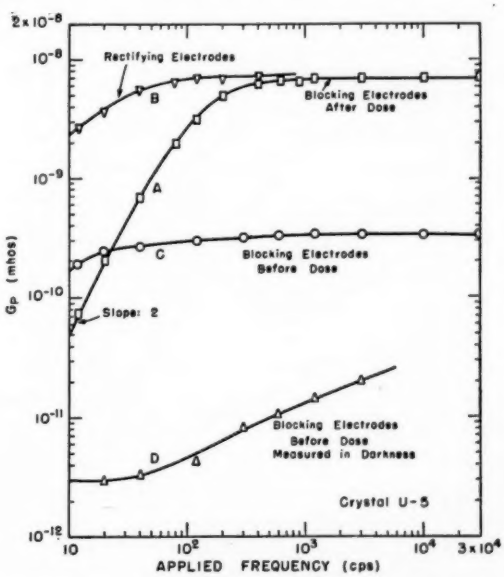

FIG. 7. Comparison of frequency dependence of parallel conductance of Crystal U-5 with blocking electrodes to that with rectifying electrodes.

[29] Lawson, Miller, Schiff, and Stephens, National Defense Research Council Report WDRC-14-153, July 1, 1943 (unpublished). See also reference 20, p. 103.

G_∞ on electrode character. The time constant of Curve B is considerably longer than that of Curve A, however, and this result is in quantitative agreement with the relation $\tau=C_0/G_\infty$ and the evidence of Fig. 6 that C_0 is six or seven times greater for this crystal with rectifying than with blocking electrodes. The time constant of Curve C taken before gamma-ray dosage is even longer than that of Curve B but for a different reason from that accounting for the increase observed between Curves A and B. The value of C_0 for Curves A and C is substantially identical but G_∞ is some 20 times less for C than for A, as one might expect from the smaller concentration of F centers present in the former case. Within experimental error, this same factor of 20 is the ratio of the time constants of Curves C and A. Finally, Curve D was taken on the same crystal in the dark before dosage. The cause of the observed rise of Curve D at high frequencies with a slope of approximately $\frac{1}{2}$ is unknown.

Figure 8 presents results similar to those of Fig. 6 but for another crystal. This crystal was of approximately the same dimensions as that of Fig. 6 but it had a cleavage plane transversely across its entire cross section nearly midway between the electrodes. If charge carriers cannot cross this cleavage plane, the crystal should behave as two crystals in series, with the cleavage plane acting as a blocking electrode. If, on the other hand, carriers can discharge slowly across the midplane, as the frequency is decreased a frequency should be found below which the influence of this cleavage plane should be negligible. Below this frequency, C_0 would be that for the entire crystal, whereas at high frequencies the pertinent C_0 which would determine τ would be approximately half as large, reducing τ by a factor of two since G_∞ would be unchanged by

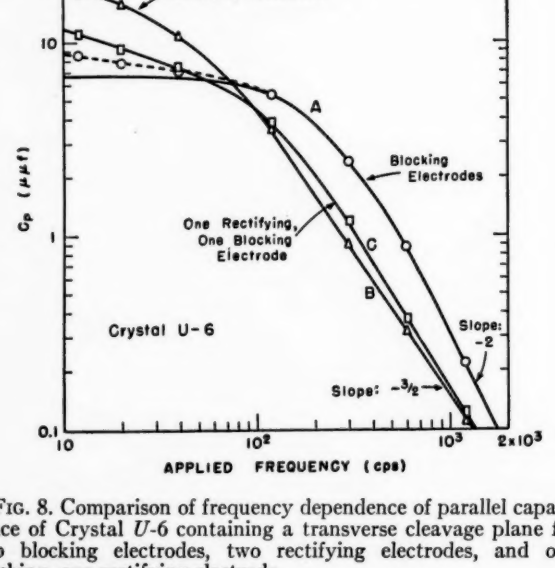

FIG. 8. Comparison of frequency dependence of parallel capacitance of Crystal U-6 containing a transverse cleavage plane for two blocking electrodes, two rectifying electrodes, and one blocking, one rectifying electrode.

the cleavage plane. Curve A shows that the latter hypothesis is apparently in better agreement with experiment. The solid line of Curve A is a Debye curve fitted to the high-frequency experimental points. At low frequencies, the dotted line shows how these points progressively deviate from the theoretical Debye curve. The result of a dc measurement of capacitance gave a value of 13 $\mu\mu$f, which is probably then the value towards which the dotted line is tending. The limiting value C_0 for the Debye curve is 6.7 $\mu\mu$f, however, and this is approximately half of the low frequency or dc value of 13 $\mu\mu$f. Figure 15 also shows the frequency dependence for this crystal with two rectifying electrodes and with one rectifying, one blocking electrode. As expected, the latter curve C falls between the rectifying-rectifying and blocking-blocking curves over most of its range and its limiting slope is between $-\frac{3}{2}$ and -2. Note that here the difference between the blocking and rectifying values of C_0 is smaller than that apparent in

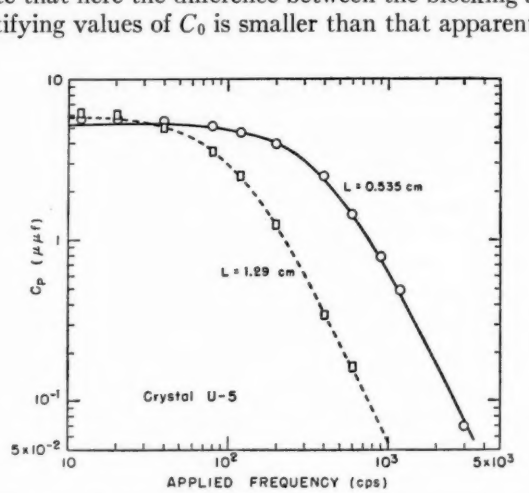

FIG. 9. Dependence of parallel capacitance on frequency for two values of electrode separation. The lines are Debye curves.

Fig. 6 and may be almost entirely ascribed to the effect of the mica layers used to produce blocking electrodes.

The Debye-type frequency dependence observed with blocking electrodes is a necessary but insufficient condition that the observed effects arise from a localized, frequency-independent capacitance. For example, such frequency dependence might also arise from the polarization of electrons localized in very shallow traps as postulated by Garlick[30] to explain a small photocapacitative effect in illuminated powder phosphors. However, because of the electrode influence on frequency dependence, Garlick's hypothesis cannot explain the present results.

Figures 9 and 10 show the frequency dependence of parallel capacitance and conductance of crystal U-5 with blocking electrodes for two different values of L, the electrode separation. The same electrodes were employed for both values of L. The lines in these graphs

[30] G. F. J. Garlick, *Luminescent Materials* (Clarendon Press, Oxford, 1949), p. 123.

are theoretical Debye curves and fit the experimental points well. The time constants for the C_P and G_P curves corresponding to a given L are, of course, the same. Since the Debye curves are completely specified by the series quantities C_0 and G_∞, we need consider only the experimental dependence of these quantities upon L.

Figure 9 shows that a reduction in L by a factor of 2.41 makes less than a five percent difference in the value of C_0. If the observed values of C_0 arose from an intensive process in the crystal, C_0 would be inversely proportional to L and would be biggest for smallest L. The small observed variation is, however, in the opposite direction and since it is so small, the photocapacitative effect must arise from processes localized near the electrodes and may be considered to involve a frequency-independent series capacitance. It should be noted here that if the capacitance of the mica spacers used to produce blocking electrodes were much smaller than that of the crystal itself, the former capacitance would dominate the measured capacitance and one would expect little dependence of measured capacitance on electrode separation. In the above measurement, however, the series mica capacitance was of the order of two to three times as large as the crystal capacitance so that the latter dominated the series combination.

The high-frequency conductance should be inversely proportional to L. In the present case, the value of G_∞ corresponding to the smaller length should therefore be larger than the value corresponding to the larger length by a factor of 2.41. The observed ratio is, however, 3.2. This result implies that the electrical length of the crystal after shortening is smaller than the mechanical length by about 1.9 mm. Somewhat similar behavior is obtained for space-charge effects in electrolytes.[3] Time was not available unfortunately for a more complete investigation of the dependence of G_∞ on L for these crystals. The difference L_x between the electrical and mechanical length of the crystal is in agreement with the idea that a charge-free region at one or both of the electrodes is responsible for C_0. The value 1.9 mm for this layer leads to a value of C_0 about five times smaller than the observed value. It is probable, however, that a more accurate determination of L_x from measurements of G_∞ with a wide range of electrode separations would yield better agreement with that derived from the experimental C_0.

If there is no charge in the region L_x, there can be no F centers or negative-ion vacancies there. If we assume a region $L_x/2$ thick at each electrode, then during each half cycle the cathode region will be electrically neutral while the anode region will contain an approximately normal concentration of electrons c_0 for rectifying electrodes or perhaps an excess of electrons for blocking electrodes. At sufficiently high frequencies, however, electrons will not have time during a half-cycle to move into the L_x region. Thus, it appears plausible that $L_x/2$ may determine C_0 and L_x determine G_∞. If this

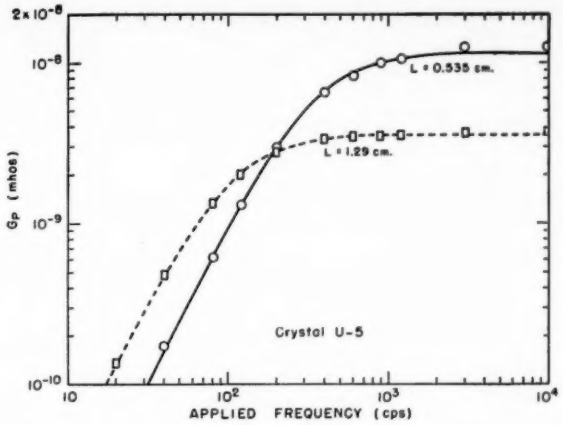

FIG. 10. Dependence of parallel conductance on frequency for two values of electrode separation. The lines are Debye curves.

is the case, the above discrepancy is reduced by a factor of two.

A charge-free region near the surface may occur by the diffusion to the surface of negative-ion vacancies in a layer of thickness L_x (or $L_x/2$). If the crystal initially contained a uniform distribution of negative-ion vacancies stabilized as either U or F centers, any nonzero ionization rate of these centers would produce negative-ion vacancies which could slowly diffuse to the surface and disappear. Thus, one might expect that long dark-storage of U- or F-centered crystals could increase L_x. In addition, continued optical ionization of an F-centered crystal would tend to destroy F centers and negative-ion vacancies initially near the surface. In agreement with this hypothesis, U-centered crystals stored in the dark for a year or more were found to produce no F centers under subsequent gamma-ray irradiation in a region as large as 1 mm in from each surface. The line of demarcation in the crystal where the F centers began was visible with the eye and was surprisingly sharp. In addition, the reduction in C_0 (and increase in L_x) shown by the two curves of Fig. 4, which was caused by considerable F-center bleaching and redosing, further confirms the above hypothesis.

Although all the results of the present work combine to indicate that there is a charge-free layer at one or both electrodes, the above explanation of its genesis does not, apparently, agree completely with all the data. In spite of the fact that many of the crystals used in this work were U centered a year or more before F centering, their surfaces were usually cleaved off before using them for measurements. Further, additively-colored crystals which showed the same photocapacitative effects were measured within a week or two of their coloration. In the length-dependence study, if there were a charge-free region initially at each electrode, the reduction of the electrode separation by a factor of more than two should have eliminated one of these regions and caused a much larger change in C_0 than observed. It is therefore evident that further work

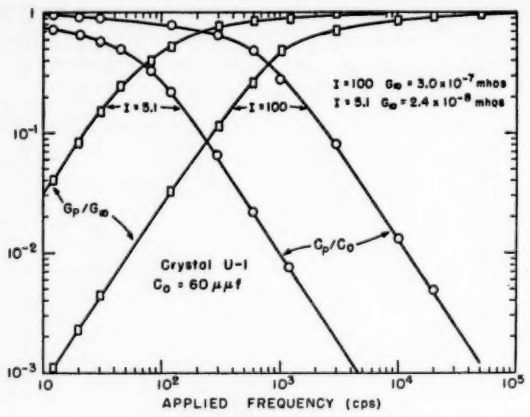

FIG. 11. Dependence of normalized parallel capacitance and conductance on frequency for two fixed light intensities.

will be required to yield a better understanding of the production and character of the charge-free layer.

(c) Light Dependence

The light dependence of C_0 and τ predicted by various space-charge theories for different types of recombination is summarized in Table I. It will be noted that the last two rows predict, for monomolecular or F-center type recombination, a light-independent C_0 and a τ proportional to I^{-1}. These results are in approximate agreement with experiment. Both ac and dc measurements extending over almost four decades of light intensity showed no dependence of C_0 on I. Since the exhaustion layer theory has been shown to be inapplicable, we are again forced to the conclusion that C_0 arises from a charge-free layer near the electrodes.

If we consider the expressions for C_P/C_0 and G_P/G_∞ given by Eqs. (6) and (7) in the light of these results, we see that these quantities should be functions of the ratio $(f/I)^2$, since τ is proportional to I^{-1}. On the other hand, for crystals with rectifying rather than blocking contacts, we should instead expect, as shown by the results of Fig. 3, that C_P/C_0 and G_P/G_∞ would be

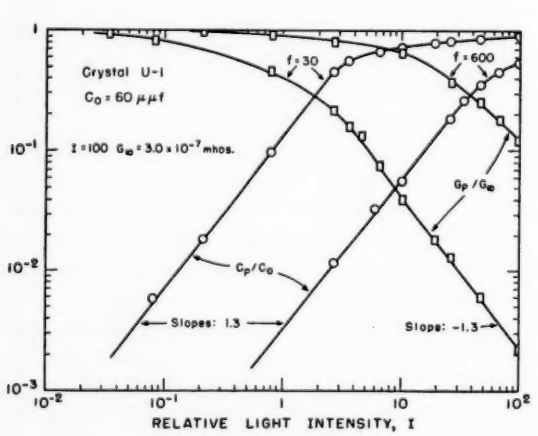

FIG. 12. Dependence of normalized parallel capacitance and conductance on light intensity for two fixed frequencies.

functions of $(f/I)^{\frac{1}{2}}$ instead of $(f/I)^2$. These expectations are largely realized.

Figure 11 shows the normalized frequency dependence of C_P and G_P for two different relative light intensities. The usual limiting slopes of $\pm\frac{3}{2}$ are present: C_0 is independent of light intensity, G_∞ is approximately proportional thereto, and the curves for the two different light intensities differ principally in a frequency translation arising from the difference in τ occasioned by the light-intensity dependence of G_∞. For comparison with Fig. 11, we have plotted in Fig. 12 the dependence of C_P/C_0 and G_P/G_∞ on light intensity for two constant frequencies of approximately the same ratio as the two light intensities of Fig. 11. The values of C_0 and G_∞ are the same for Figs. 11 and 12.[31] The curves of Fig. 12 are approximately mirror images of those of Fig. 11. Thus, the dependence on I^{-1} is nearly the same as that on f as indicated by the above considerations. Instead, however, of being functions of $(f/I)^{\frac{1}{2}}$, these curves are more nearly functions of $f^{\frac{1}{2}}/I^{1.3}$ as is shown by the limiting slopes of Fig. 12. The reason for this small discrepancy is unknown.

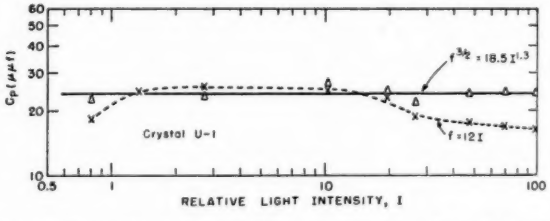

FIG. 13. Dependence of parallel capacitance on light intensity for $f/I = 12$ and $f^{\frac{1}{2}} = 18.5I^{1.3}$.

The dependence of C_P and G_P on $f^{\frac{1}{2}}/I^{1.3}$ is shown more graphically in Figs. 13 and 14. If f and I are varied together so that $f^{\frac{1}{2}}/I^{1.3}$ remains constant, there should be no change in C_P. Figure 13 shows that this is indeed the case over a wide range of light intensities and frequencies. Also shown on this graph are the results of keeping (f/I) constant while varying I. The variation of C_P is obvious in this case, proving that the exponents of f and I are indeed somewhat different. Figure 14 shows how G_P depends on light intensity for two constant values of f/I. The variation in G_P is linear over most of the range of light intensities and thus proves the linear dependence of G_∞ on light intensity. The deviations from linearity at high light intensities are not so much due to a failure of the linear relation between G_∞ and I as due to variation in G_P arising from keeping f/I rather than $f^{\frac{1}{2}}/I^{1.3}$ constant. This conclusion is confirmed by Fig. 15 which shows the results of a direct measurement of the dependence of G_P on I at a sufficiently high frequency that the terms involving $f^{\frac{1}{2}}/I^{1.3}$ completely cancel out and $G_P = G_\infty$.

[31] For convenience, the actual quantity plotted for normalized conductance in Fig. 12 was $(G_P/I)/(G_P/I)_{I=0}$. From Eq. (7), together with the linear dependence of G_∞ on I, this ratio may be shown to equal G_P/G_∞.

Note that the linear dependence of G_∞ on I is in agreement with the constant-capacitance assumption provided recombination is monomolecular or takes place by F-center type electron capture.

We have been previously concerned with the effect of fairly strong light intensities on these photoconducting crystals. Their electrical behavior in the dark is also of interest for comparison with results under illumination. Figure 16 shows the frequency dependence of conductivity for three Type I crystals measured in the dark. All these crystals had about the same electrode areas but their separations ranged from 1.46 to 5.42 mm. Curves A and B refer to the same crystal which was of untreated KBr. Curve A was taken when the crystal had evaporated aluminum electrodes, one of which was very thin and of relatively high resistivity. This curve shows a fairly constant value of conductivity

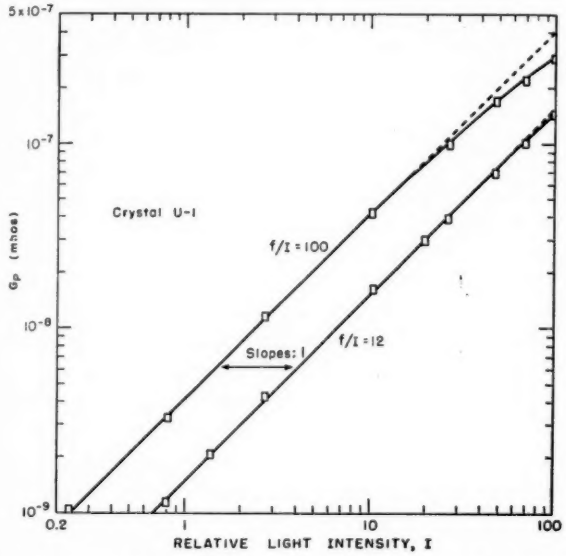

FIG. 14. Dependence of parallel conductance on light intensity for $f/I=12$ and 100.

at low frequencies and a transition region which leads to a final ω^2 dependence on frequency. If this latter portion of the curve were considered as corresponding to a series rather than a parallel resistance, one would obtain a frequency-independent value of series resistance of the order of 10^3 ohms. This resistance value is in qualitative agreement with dc measurements of the resistance of the thin semitransparent aluminum electrode, and it thus seems clear that this portion of the conductivity curve arises from electrode resistance. In order to test this hypothesis, both aluminum electrodes were covered over with silver paint, reducing the electrode resistance to one ohm or less. Curve B was then obtained. Instead of removing the frequency dependence entirely as was expected, it was reduced to a ω-type dependence. The reason for this dependence is unknown, but it seems clear that electrode resistance is important in producing the ω^2 rise in Curve A.

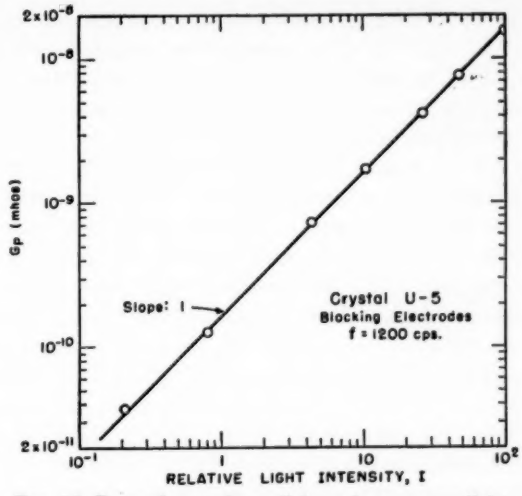

FIG. 15. Dependence of parallel conductance on light intensity for $f=1200$ cps.

The low-frequency portions of Curves A and B are interesting. This more-or-less frequency-independent conductivity in a plain KBr crystal must arise from ionic motion, ionic vacancy motion, or from surface leakage. Since great care was exercised to eliminate the latter effect, it is likely that the measured conductivity arises from one or both of the other two conduction processes. However, it can be shown that the ionic mobility at room temperature is several orders of magnitude too small to yield the observed values. On the other hand, if we use Etzel and Maurer's results[32] for

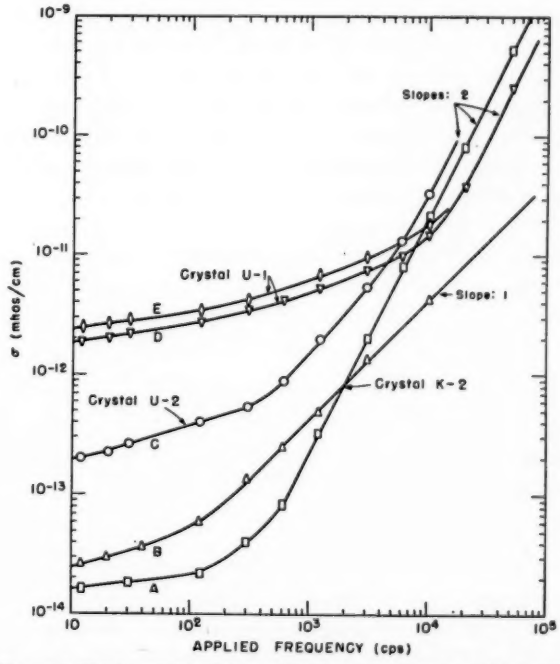

FIG. 16. Dark conductivity of 3 Type I crystals *vs* frequency. Crystal K-2 is plain untreated KBr; U-1 and U-2 are U-centered crystals. U-1 has been exposed to gamma radiation; U-2 has not.

[32] H. W. Etzel and R. J. Maurer, J. Chem. Phys. **18**, 1003 (1950).

the concentration of positive-ion vacancies present in KCl,[33] 10^{17} cm^{-3}, and extrapolate their vacancy-mobility data to room temperature, a conductivity value only three times smaller than the limiting value of Curve *A* is obtained. Since we are here dealing with KBr rather than KCl, it is reasonable to conclude that the observed low-frequency conductivity arises from the motion of positive-ion vacancies. This view is strengthened by the fact that Curve *B* was measured during warmer weather than was Curve *A* and the laboratory temperature was somewhat higher. A temperature differential of only 5°C is required to explain the difference in the low-frequency conductivity values of the two curves on the basis of vacancy motion. Since the quasi-static current observed for these crystals an hour or more after a high dc field is applied is in approximate agreement with their low-frequency dark conductivity values, it may be postulated that this current also arises from vacancy motion. Neither the ac nor dc conductivities observed on plain KBr crystals showed any light dependence whatsoever. The dark conductivity of both plain KBr crystals and those containing *F* centers was ohmic, thus reducing the possibility that field-emission is responsible for the observed results.

Curve *C* was measured on a *U*-centered crystal which had never been exposed to radiation. As expected, it also shows the electrode-resistance characteristic at high frequencies. Since the conductivity is a factor of about ten times greater than that of crystal *K*-2, there are either 10 times more positive-ion vacancies in *U*-2 than in *K*-2 or the conduction arises from thermal ionization of electrons from shallow traps. Both *K*-2 and *U*-2 came from the same batch of crystals. It is easy to calculate from the known electron mobility[21] that the low-frequency conductivity of crystal *U*-2 could be produced by only about 10^5 conduction-band electrons per cm^3. At the completion of the *U*-centering process not all *F* centers have been destroyed; of the order of 10^{13} to 10^{14} cm^{-3} still usually remain in the crystal. It is possible that exposure to *F*-band light bleaches some of these remaining *F* centers and that most of the resulting electrons are captured by shallow traps rather than by negative-ion vacancies. If these traps are sufficiently shallow, it is possible that as many as 10^5 electrons per cm^3 could be maintained in the conduction band in the dark by thermal excitation alone. It can easily be shown[34] that the equilibrium concentration of conduction-band electrons produced from 10^{14} *F* centers per cm^3 by thermal ionization is negligibly small at room temperature.

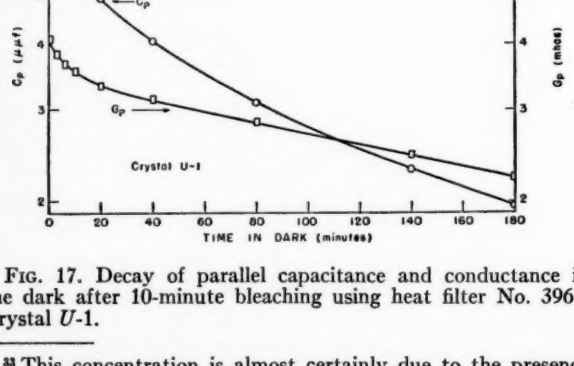

FIG. 17. Decay of parallel capacitance and conductance in the dark after 10-minute bleaching using heat filter No. 3961. Crystal *U*-1.

The argument that the main contribution to the dark conductivity of crystal *U*-2 arises from free electrons is strengthened by consideration of Curves *D* and *E* in Fig. 16. When Curve *D* was obtained, crystal *U*-1 had been exposed to about 10^3 roentgens of Co^{60} radiation, producing about 5×10^{15} *F* centers per cm^3. It had also been exposed to strong *F*-band light and a fraction of the *F* centers destroyed. We may suppose that its dark conductivity is another factor of 10 times larger than that of *U*-2 because of the possible production of more shallow traps by the gamma rays and their population by electrons from bleached *F* centers and other sources. Curve *E* was taken sometime later after the crystal had been re-exposed to gamma rays and partly bleached out once more, again increasing the dark conductivity. Table II summarizes conduction-band electron concentration for various conditions. It will be noted that all these Type I crystals with evaporated aluminum electrodes show the electrode-resistance rise in dark conductivity at high frequencies. We may now refer back to the conductance curves of Figs. 3 and 5 and explain the continued rise in G_P above the dotted saturation value as being due to electrode resistance.

In Fig. 17, some measurements of the secondary photoeffect in crystal *U*-1 are presented. This crystal, then containing about 5×10^{15} *F* centers per cm^3, was left in total darkness for several days. It was then strongly illuminated for 10 minutes; the light extinguished; and the decay of capacitance and conductance in the dark measured at 20 cps. A number of rough measurements have been carried out to establish that C_P and G_P reach their final values within a time of 10^{-2} second or less after an *F*-centered crystal is exposed to light. Usually, these quantities also drop essentially to zero within the same time interval after illumination is removed. In some instances, however, such as that shown in Fig. 17, C_P and G_P dropped in the dark to many times less than their illuminated values but still to values which were appreciably above final dark values. Each of the dark decay curves shown in Fig. 17 can be quite accurately represented as the sum of two exponentials. If we assume that the added capacitance and conductance represented by these curves is due to the presence of conduction-band

[33] This concentration is almost certainly due to the presence of an equal concentration of divalent impurity atoms present in the "pure" crystal; it is unrelated to the thermal equilibrium concentration of positive- and negative-ion vacancies.

[34] Reference 15, p. 143, Eq. (15).

electrons in the crystal in the dark, these curves indicate how the concentration of electrons decays. The decay is monomolecular and, since the curves are made up of two exponentials, it seems likely that the electrons are trapped by two (or more) types of traps located at different depths below the conduction band. We may postulate that with the crystal illuminated and a fairly high concentration of electrons in the conduction band, a much larger number of shallow traps contain electrons than would be the case in the dark. When the light is extinguished, these traps give up their electrons by thermal ionization until a new equilibrium between electrons in traps and electrons in the conduction band is established. It is probably the effect of these thermally ionized electrons which we observe in Fig. 17, and the decay in electron concentration occurs as electrons leave shallow traps and become permanently trapped at deeper levels. We shall discuss the nature of some of these traps later.

The experimental values of the decay constants for the exponential decay of C_P and G_P are very nearly in the ratio 3:2 for the latter portion of the curves of Fig. 7 after the initial rapid decay has died out. This result is made very plausible by consideration of the Debye-curve expressions of Eqs. (6) and (7) with τ given by C_0/G_∞. In the present case G_∞ is so small that $G_P=G_\infty$ at 20 cps, and C_P becomes $C_0/(\omega\tau)^2=G_\infty^2/\omega^2C_0$. Thus, changes in G_∞ and in C_0 may cause changes in C_P. Let us suppose that the only physical change which occurs during the decay is the reduction in G_∞ produced by the trapping process discussed above. Thus C_0 remains constant during the decay; such stability is consistent with all other measurements of C_0. Then if G_∞ decays exponentially, C_P will also decay exponentially, but with twice the decay constant of G_∞. For this crystal with rectifying electrodes, the frequency-response curves show that $(\omega\tau)^{\frac{1}{2}}$ is involved rather than $(\omega\tau)^2$ as for Debye curves. When the above treatment is modified by the change of exponent from 2 to $\frac{3}{2}$, one finds that C_P is proportional to $G_\infty^{\frac{1}{2}}$; thus, the decay constants of C_P and G_P will be in the observed ratio of 3:2. This treatment also applies, at least approximately, to the initial rapid-decay portion of the curves. Therefore, the C_P curve yields further independent evidence that C_0 does not change when G_∞ does so.

(d) Temperature Dependence

The majority of the work reported in this paper has been carried out at room temperature. Measurements of the frequency dependence of C_P and G_P for one crystal at 25°C and at 125°C showed, however, that C_0 was independent of temperature in this range as expected and that G_∞ increased by a factor of 2.2 on raising the temperature to 125°C. The increase in G_∞ indicates that the product μc_0 increased by the same factor. Unlike the mobility of ionic vacancies, which increases with increasing temperature, electronic mobility in polar crystals decreases with temperature. Thus, the average concentration of electrons in the conduction band, c_0, must have increased by a factor greater than 2.2. As Glaser and Lehfeldt[35] have shown, this increase cannot, at these temperatures, arise from an increase in the quantum yield associated with the optical ionization of F centers. The most reasonable explanation of the increase is that there is present a large number of shallow traps some of which contain electrons originally from F centers. If the electron concentration in these traps is determined by thermal equilibrium between conduction-band electrons and electrons in the shallow traps, an increase in temperature will increase the conduction-band concentration.

TABLE II. Conduction-band electron concentration for various conditions. The light source was a 500-watt slide projector whose output was focused on the crystal.

c_0 (cm^{-3})	No dose $N_F \approx 10^{12}-10^{14}$ cm^{-3}	Saturation dose $N_F \gtrsim 5\times10^{15}$ cm^{-3}
Crystal dark	10^5 to 10^7	10^6 to 10^8
Crystal illuminated	10^7 to 10^9	10^{10}

Since the conduction-band concentration increases linearly with light intensity, we must assume that the concentration of empty shallow traps is much greater, for any light intensity employed, than the concentration of shallow traps containing electrons. If we temporarily neglect the decrease in μ with increasing temperature, we can compute a very rough average thermal activation energy of the shallow traps of 0.04 ev.[36] The temperature dependence of μ will make the actual activation energy larger than 0.04 ev but will probably not increase this figure by a factor of more than two or three. This small a trap activation energy indicates that the shallow traps, when empty, are almost certainly electrically neutral. Note that the above calculation of activation energy is based on a trap concentration independent of temperature, which is probably not the case here [see Part (f) of this section.] The possible nature of these traps will be discussed later. Temperature dependence of the optical bleaching of F centers will be discussed later in connection with Fig. 19.

(e) Gamma-Ray Dose Dependence

When a U-centered crystal is exposed to penetrating gamma-rays, the quanta absorbed in the crystal produce a conversion of U centers to F centers. The number of F centers produced by a given dose of radiation will be proportional to dose so long as this number is small compared to the number of U centers available for conversion. There were between 5×10^{17} and 10^{18} U centers per cm^3 in the crystals used in the present investigation; therefore, one would expect to find a

[35] G. Glaser and W. Lehfeldt, Nachr. Ges. Wiss. Göttingen **2**, 91 (1936).

[36] Reference 15, p. 159, Eq. (12).

linear relationship between dose and F-center concentration up to concentrations of 10^{16} cm^{-3} or greater. Optical measurements of the absorption coefficient at the peak of the F band, in conjunction with the factor of Hilsch and Pohl[37] relating absorption coefficient to F-center concentration, showed that this expectation was justified. It was found that $(N_F-N_0)=5.8\times10^{12}r$ cm^{-3} up to almost 10^4 roentgens, where r is the dose of Co^{60} gamma radiation in roentgens and N_0 is the initial concentration of F centers before dosing. The coefficient in this equation varied by a few percent from crystal to crystal.

The theories of Table I predict various dependencies of C_0 and G_∞ (or c_0) on N_F. It was actually found from both ac and dc measurements that there was little or no dependence of C_0 on N_F over a range of at least 10^3 in N_F. This result is thus in agreement with the charge-free layer hypothesis. For monomolecular or F-center capture type recombination, the last row of Table I shows that c_0 should be proportional to N_F (or r) or be independent of N_F, respectively. In Fig. 18 the high-frequency conductivity of two different crystals is plotted *versus* r and neither dependence is obtained. Because of the presence of the residual concentration of F centers in these crystals before any dose, we have actually used as ordinate in this figure the conductivity at a dose r, $\sigma(r)$ minus that at zero dose, $\sigma(0)$. The initial values of $\sigma(0)$ are shown on the graph by the two horizontal dotted lines. To avoid appreciable bleaching of F centers during a measurement of $\sigma(r)$, relatively low light intensity was used.

Figure 18 shows that the experimental points can be well fitted by a relation of the form $[\sigma(r)-\sigma(0)]=[\sigma(\infty)-\sigma(0)][\beta r/(1+\beta r)]$ up to 10^3 roentgens. Further, $\sigma(\infty)$ is almost reached by a dose of 10^3r. For very low doses less than $10r$, the increase in σ produced by gamma-ray absorption is proportional to N_F as expected for monomolecular recombination; however, for the range between 10^3 and 10^4 roentgens where N_F is still increasing linearly with dose, σ does not increase appreciably. The concentration c_0 is determined, for any light intensity, by the equations of detailed balance governing the flow of electrons from F centers to shallow and deep traps. The most reasonable explanation for the above dependence of c_0 on r (and on N_F) is that additional traps such as F centers themselves are produced proportional to r in the range of r here considered. This hypothesis, and its consequences, will be discussed in more detail later.

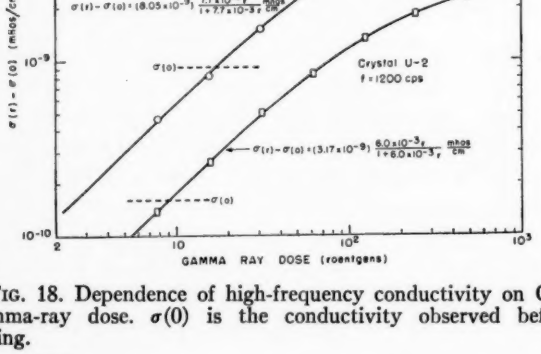

FIG. 18. Dependence of high-frequency conductivity on Co^{60} gamma-ray dose. $\sigma(0)$ is the conductivity observed before dosing.

[37] R. Hilsch and R. W. Pohl, Z. Physik **64**, 606 (1930).

(f) Optical Bleaching Results

If all electrons ionized to the conduction band from F centers were eventually trapped by single negative-ion vacancies, there would be no bleaching of F centers. On the other hand, if all such electrons were trapped elsewhere than at negative-ion vacancies, there would be a monomolecular, exponential decay of F-center concentration with time of the form $N_F=N_0\exp(-k_1t)$, where k_1 is the probability per unit time of F-center ionization. For photoionization, k_1 is proportional to the F-band light intensity.

Figure 19 shows the results of optical measurements of the bleaching of an F-centered crystal under strong illumination at two different temperatures. After four hours of bleaching, the temperature was abruptly increased from 25°C to 125°C. At 125°C the bleaching is definitely exponential since the points fall on a good straight line on the semilogarithmic graph. The decay constant for this portion of the curve is 1.28 hr^{-1}. At room temperature, the decay is somewhat more complex but can be quite accurately represented by the sum of two exponentials of different decay constants. For the longer-lived component, the value of the decay constant is 1.78×10^{-2} hr^{-1}. This increase in temperature thus increases the decay constant by a factor of 72.

It is worth noting that the initial rapid decay observed at room temperature can be produced once more when it has disappeared after several hours of bleaching by leaving the crystal in darkness for 10 or more hours. No change in N_F is produced by such dark storage, however. The rapid decay apparently arises from the slow formation in the dark of trapping centers which have a considerably larger capture cross section for electrons than the traps which lead to ordinary bleaching.

If we neglect the rapid initial decay present at room temperature, it is still probable that the succeeding decay is only approximately of a monomolecular type. Since F centers in U-centered crystals bleach considerably slower on exposure to F light than do F centers in additively-colored crystals even though there is a higher conduction-band electron concentration in the former, it seems likely that more re-formation of F centers occurs in U-centered than in additively-colored crystals. If the flow of electrons back to negative-ion vacancies is much smaller than the flow from F centers to the conduction band, however, the observed decay

of F-center concentration will still be at least approximately exponential, as observed.

The temperature increase from 25 to 125°C apparently increases k_1 by a factor of 72. A similar increase in k_1 produced by an increase in light intensity by a factor of 72 would cause an increase in c_0 by this same factor. The results of Part (d) of this section show, however, that the same temperature increase enlarges c_0 by no more than a factor of about four. It is, therefore, obvious that the temperature increase differs from the light-intensity increase in enlarging the concentration of traps other than negative-ion vacancies and thereby reducing the flow of conduction electrons back to negative-ion vacancies. This contention is borne out by the observation that a 72-fold increase in light intensity at room temperatures produces a very much smaller increase in bleaching rate than the temperature increase which increases the decay constant by 72 times. Evidently the receiving end of the process is the determining factor.

In addition to observing optically the build-up on exposure to gamma radiation of the F band and the decay of the U band using a U-centered crystal less than 1 mm thick, optical bleaching at room temperature was carried out on the same crystal after a total gamma-ray exposure of 1.5×10^5 roentgens. At this exposure, the U band was greatly reduced and more than 10^{17} F centers per cm^3 had been formed. There were no absorption bands observable in the range from 200 to 800 mμ other than the U and F bands. Bleaching was carried out with a 750-watt tungsten bulb in the slide projector without a heat filter so that some heating occurred. Glass lenses served to keep any U-band light from reaching the crystal. As F-band bleaching progressed, the U band was re-formed.[38] On the basis of equal oscillator strengths, fewer U centers were reformed than F centers destroyed, although the reverse process indicated that an F center was produced for each U center destroyed by gamma radiation. In fact, additional absorption in the long-wavelength tail of the F band became apparent after considerable bleaching. Such absorption probably arises from M and R centers or colloidal metal aggregates.[26] Since the spectrum of the bleaching light employed extended to the wavelengths of this absorption, further bleaching eventually reduced this long-wavelength absorption as well as the F band. These results indicate that the efficiency of the F-to-U conversion is less than 80 percent a few degrees above room temperature, and that M or R centers, or both, may be formed. The absorption coefficients for the various bands were in good agreement with the hypothesis that those F centers which, on bleaching, did not re-form U centers formed M or R centers instead. The F-to-U conversion during bleaching probably occurs in the following sequence. Since it is reasonable to expect a small attachment force to exist between a negative-ion vacancy and a hydrogen atom, a negative-ion vacancy produced from an F center by photoionization first captures a hydrogen atom, then a conduction-band electron is captured by the vacancy-atom complex, and thus a U center is re-formed. The first part of the process should require a much greater time than the latter part and should be quite temperature-dependent. Alternatively, it may be possible that an interstitial hydrogen atom might capture an electron to form a hydrogen negative ion. This ion might then wander until captured by a halogen negative-ion vacancy to re-form a U center.

At room temperature even in the dark, there is considerable probability that a hydrogen-atom:negative-ion-vacancy complex will eventually capture a conduction-band electron and re-form a U center. This process probably accounts for the growth of the U band during dark storage observed by Alger[38] in a U-centered crystal containing F centers after partial F-center bleaching. At very low temperatures, this probability will be negligible because of the virtual absence of free electrons in the dark. If a number of such complexes have been formed at room temperature and the crystal is then cooled with liquid nitrogen or helium, another mechanism may be envisioned whereby U centers can be re-formed. This mechanism involves the absorption of a light quantum by the valence-band electron of a negative ion situated close to a given complex. If radiation of about 1030 mμ is absorbed by KBr, just sufficient energy will be given a valence electron to raise it to a U-center energy state, and a U center and a hole will be formed. This absorption band is likely to be exceedingly weak because of the limited concentration of complexes which can be formed at room tem-

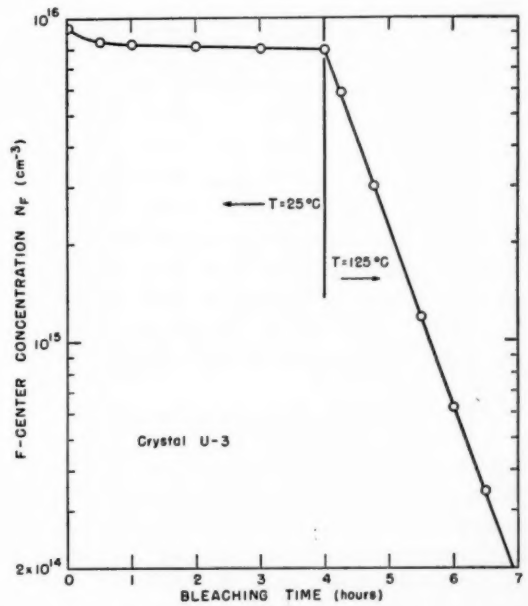

FIG. 19. Optical bleaching of F centers at two temperatures.

[38] In agreement with unpublished observations of R. S. Alger (private communication).

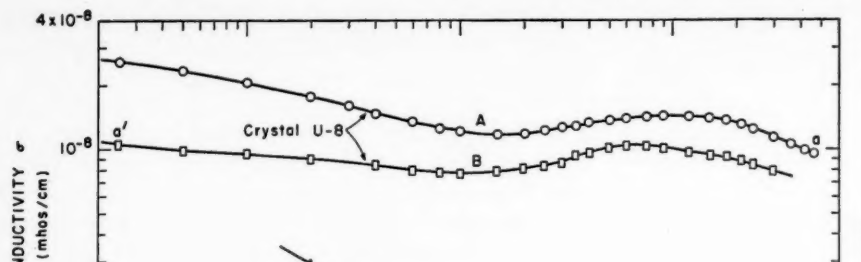

FIG. 20. Dependence of high-frequency conductivity on optical bleaching time.

perature even in the dark, and it may be below the range of detection with present techniques.

Finally, Fig. 20 presents measurements of the conductivity at 10^4 cps of two F-centered crystals *vs* bleaching time using the 500-watt bulb, slide projector, and heat filter 3962. These curves are, therefore, a measure of the variation of conduction-band electron concentration with bleaching time. The curve shape is surprising in that it shows both a minimum and a maximum, and these points occur at approximately the same times for all three curves. Curve A is the initial bleaching curve for crystal U-8. After a day of bleaching, the crystal was left in the dark overnight and bleaching resumed the next day. Curve B shows the results obtained during the second day. Note that c_0 is slightly increased after a night in the dark, possibly indicating the presence of fewer traps at time a' than at time a.

The bottom curve C was measured under the same conditions as the top curves for a crystal which was first exposed to gamma radiation until about 5×10^{15} cm^{-3} F centers were produced, then bleached until most of these centers were destroyed, and finally re-exposed to radiation to produce about the same F-center concentration. In spite of this complicated history and the probable formation of some M and R centers during the first bleaching, the curve shape is of the same character as that of the upper two curves. Note that the vertical separation between the curves for crystals U-8 and U-2 is about doubled over that for the same crystals in Fig. 18. The relative decrease in c_0 for U-8 is almost certainly due to the formation of additional electron traps in this crystal by bleaching and re-dosing.

(g) Direct Current Measurements

Direct current measurements of capacitative effects connected with electron motion must be carried out in a time short compared to that necessary for appreciable positive-ion vacancy polarization to be established. All such measurements on a wide variety of crystals confirmed the lack of dependence of C_0 on light intensity, temperature, applied voltage up to 1000 volts dc, and F-center concentration. Measurements on crystals with rectifying electrodes consistently gave larger values of C_0 than when blocking electrodes were employed; in addition, it is worth noting that no dependence of C_0 on polarity was observed for a crystal with one blocking, one rectifying electrode.

Figure 21 shows the dependence of charging current on time for an F-centered crystal with relatively low illumination, about 10^{-3} of the maximum used in this work. One thousand volts was applied to this crystal at $t=0$. The initial drop, extending over the first minute or two is probably due to polarization set up by electronic motion, since variation in light intensity changed the current during this time. The drop apparent after 10 minutes may be due to vacancy motion; light caused little change in current for this region of the curve.

Discharge currents have also been measured for a few crystals. One crystal containing about 10^{16} cm^{-3} F centers and no more than 10^{18} cm^{-3} U centers which was charged with 500 volts applied for 20 hours in low ambient room light showed a particularly interesting dark discharge curve. The discharge current started near zero, reached a maximum of more than 10^{-6} amperes in 20 minutes, and thereafter decayed approximately as t^{-1} for several weeks with a decay rate very sensitive to temperature. Such behavior is quite analogous to that of electrets. An integration of the discharge-current curve yielded a total charge of about 10^{-1} coulomb! Since the geometrical capacitance of the crystal was less than one $\mu\mu$f, the effective dc dielectric constant was therefore of the order of 10^7. The above charge storage in a space-charge layer would require a normal concentration of mobile charges of almost 10^{22} cm^{-3}. This large a concentration is difficult to explain. This crystal was not well moisture-proofed and had been kept in a moist atmosphere for four months prior to measurement. Further, heating at 125°C for 30 minutes destroyed its ability to store such large charges. It is therefore likely that the effects observed arose from a reversible electrode reaction at

the interface between crystal and silver electrode analogous to that of a storage battery. All other crystals showed more normal charge storage consistent with a concentration of about 10^{17} cm^{-3} positive-ion vacancies.

A number of experiments were carried out in which a crystal was charged while strongly illuminated, the light extinguished, and the crystal then discharged in total darkness. In order to obtain the total charge stored in the crystal, discharge into the polystyrene sink capacitor for more than an hour was usually required. No difficulties from vacancy motion were thought to arise in such measurements because the charging time could be made sufficiently short that negligible vacancy polarization could occur. This experiment showed that if the discharge time were made sufficiently long, the same value of C_0 would be obtained for dark discharge as for discharge with the crystal illuminated. Such dark discharge is very slow since it must occur through the motion of the very few conduction-band electrons present in the dark.

When a dc voltage is applied to a well insulated, illuminated crystal containing F centers, electrons will leave the crystal at a rectifying anode and cannot reenter except by leakage or breakdown after the charging voltage is removed. During the time the electrons leak back in, the crystal is positively charged and should attract negative charges. Macroscopic indication of such behavior was observed with several crystals by charging an illuminated crystal with 10^3 volts, removing the applied voltage, and then using the crystal to attract small bits of paper. Such attraction lasted for as long as an hour. Since the sign of the crystal charge was not determined in these experiments, it is not conclusively established that the observed behavior arose from missing electrons; it is possible that positive-ion vacancy polarization was also of importance here.

IV. DISCUSSION OF RESULTS

Space is unavailable for a complete discussion of the present results, nor is such a discussion warranted by the limited data presented herein. We shall, however, summarize certain tentative conclusions suggested by the data. First, it seems clear that the capacitative effects observed are only indirectly, if at all, connected with space-charge formation. They most probably arise from a charge-free layer containing no F centers located between one or both electrodes and the bulk of the crystal. Such layers may arise from diffusion of negative-ion vacancies to the surface of the crystal. Although it was found that there was a significant difference in frequency dependence of parallel capacitance and conductance depending on whether electrodes were blocking or rectifying, for most purposes the electrical properties of a photoconducting crystal can be represented by a frequency-independent capacitance C_0 in series with the normal conductance G_∞ of the crystal appropriate to the light level employed. Even though

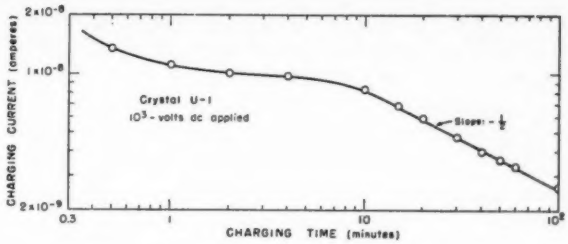

FIG. 21. Decay with time of dc charging current of an illuminated crystal.

the capacitance C_0 does not arise from space-charge formation, the small voltage-dependent nonlinearity observed almost certainly does. Space-charge capacitative effects were probably not observed because the space-charge capacitance was in series with the much smaller charge-free layer capacitance C_0.

The observed linear dependence of G_∞ on light intensity can arise either from monomolecular recombination of electrons with traps whose concentration N_T is independent of F-center concentration N_F or from recombination with traps whose concentration is proportional to N_F, such as F-centers themselves. In the first case, G_∞ should be proportional to N_F; in the second, independent of it. As shown by Fig. 18, monomolecular recombination seems to be dominant at low values of N_F; however, for F-center concentrations greater than about 5×10^{14} cm^{-3}, the type of recombination goes through a transition region until the second type is dominant for $N_F=5\times10^{15}$ cm^{-3} or greater. Since the linear dependence on light held up to the highest intensities available, it is clear that for both types of recombination, the empty trap concentration must always be considerably greater than that of filled traps.

In the U-centered crystals with which we are here concerned, there will be a high concentration of U centers before any gamma-ray dosing and a low concentration of F centers. In addition, there will be some hydrogen atoms at interstitial positions in the lattice left from the original U-centering process. The initial, monomolecular traps mentioned above must be relatively independent of F-center concentration below $N_F\simeq5\times10^{14}$ cm^{-3} and might possibly be either U centers themselves or interstitial hydrogen atoms. It is unlikely, however, that U centers play such a rôle because their concentration is essentially independent of N_F until N_F reaches 5×10^{16} cm^{-3} or more. It is therefore likely that the initial shallow traps are interstitial hydrogen atoms which can capture an electron to form hydrogen negative ions. As N_F increases from its low initial value, the conversion of U centers to F centers will produce new interstitial hydrogen atoms proportional to N_F. When the concentration of hydrogen atoms thus produced becomes comparable to those initially present, recombination will cease being monomolecular and G_∞ will tend towards independence

of N_F. Since electron binding in hydrogen-atom traps will be small, a large fraction of them may be expected to be empty on the average because of thermal ionization. They may thus play the role of the shallow traps envisioned in Section III-c to explain dark conduction and dark conductivity decay and in Section III-d to explain temperature dependence results.

Although hydrogen-atom traps can apparently explain many of the experimental results in U-centered crystals, it must be mentioned that F'-center formation may also be of importance, especially when N_F is of the order of 10^{15} cm^{-3} or greater. At -100°C Pohl found that the mean range of electrons in additively colored KCl crystals was inversely proportional to N_F above N_F values of about 10^{15} cm^{-3} and attributed this result to F'-center formation.[39] At room temperature or above in KBr, F' centers will be considerably less stable, but it is still possible that some of our effects arise from F'-center formation or from a combination of trapping by F centers and interstitial hydrogen atoms.

The optical bleaching behavior of Fig. 19 requires the existence of at least two different types of traps. If there is present a large concentration of shallow traps with small recombination cross section and a much smaller concentration of traps of large cross section, then the initial rapid decay of Fig. 19 will arise from the latter. Since this rapid decay region can be regenerated by dark storage, during which we know the U band increases somewhat, it is reasonable to suppose that the traps responsible for this decay are U-center precursors. During dark storage, interstitial hydrogen atoms perhaps move about until they become attached to negative-ion vacancies or to negative- and positive-ion vacancy pairs. These U-center precursors will have a large electron recombination cross section, and those which were formed during dark storage but did not capture electrons to form U centers will rapidly do so when the conduction-band electron concentration is increased by illumination. As we have seen in Section III (f), although a temperature increase to 125°C does not increase c_0 very much, it does increase the bleaching rate greatly. The temperature rise must therefore much increase the formation rate of empty deep traps which can hold electrons more or less permanently at this temperature. Since the hydrogen-atom diffusion rate will increase strongly with temperature, it is probable that at 125°C the rapid monomolecular bleaching of F centers observed is again due to electron capture by U-center precursors formed at a greatly increased rate at this temperature in an illuminated crystal. The increase in the deep trap concentration will tend to reduce c_0; the relatively small increase observed probably arises from the over-riding effect of increased thermal ionization of the shallow traps.

Data are insufficient to make it worthwhile to attempt a detailed explanation of the conductivity decay curves of Fig. 20. It is probable that they can be largely explained in terms of trapping by the two above kinds of traps, although the maxima reached after about 100 minutes of bleaching are difficult to interpret. Although much of the previous data were explained in terms of only two principal types of traps, it is quite possible that trapping by M and R centers, colloidal metal aggregates, dislocations, etc., may also be of importance. Unfortunately, many of the explanations of the results presented in this work were reached after the experiments were completed. It is obvious that many further experiments could be carried out to check and extend the present results and explanations, and it is hoped that this study will stimulate others to do so.

[39] Reference 15, p. 126.

ACKNOWLEDGMENTS

I wish to thank Dr. P. Pringsheim, Dr. P. H. Yuster, and Dr. C. Delbecq of the Argonne National Laboratory and Professor F. Seitz and Professor R. J. Maurer of the University of Illinois for many valuable discussions. I welcome this opportunity to express my appreciation to the Argonne National Laboratory and especially to Dr. O. C. Simpson for a visiting appointment.

APPENDIX I. CRYSTAL PREPARATION

The alkali-halide crystals employed in this investigation were all potassium bromide obtained from the Harshaw Chemical Company. These crystals were treated in various ways. Several were additively F centered[15] by prolonged heating at 500°C in sodium vapor to produce approximately 1.5×10^{16} F centers per cm^3 homogeneously distributed within the crystals. The F-center concentration was determined from the optical absorption coefficient at the F-band maximum. As shown by Hilsch and Pohl,[37] the F-center concentration N_F is proportional to this coefficient.

In addition, a large number of crystals were U centered. A U center is thought to be a hydrogen negative ion trapped at the site of a missing halogen ion in the crystal lattice.[40] Thus, an F center, which is an electron trapped in a negative-ion vacancy, can be converted into a U center by the addition of a hydrogen atom. The F-absorption band maximum for potassium bromide at room temperature occurs in the visible at 620 mμ, whereas the wavelength of maximum absorption by U centers is located in the ultraviolet at about 228 mμ. Crystals were U centered by first being additively F centered with potassium vapor for 15 hours at 600°C. This treatment produces a maximum concentration of F centers approaching 10^{18} cm^{-3} and renders the crystals opaque. Without cooling, the potassium vapor is then trapped out and hydrogen admitted to the Pyrex reaction chamber. A slow flow of hydrogen is maintained for 40 to 50 hours and then the crystals are rapidly cooled to room temperature. Almost all of

[40] Reference 15, p. 147.

the F centers are converted to U centers by this process and the crystals are transparent in the visible once more. The above procedure is essentially a single-stage process since the crystals are not cooled to room temperature after being additively F centered. A two-stage process where such cooling does occur has been described by Friedman and Glover.[41]

The photoconductivity with which we are concerned in the present paper arises principally from the optical excitation of electrons from F centers to the conduction band. It is thus desirable to have available a method of easily producing a given concentration of F centers homogeneously distributed in a crystal. The gamma-ray conversion of U centers to F centers furnishes us with such a method. When a U-centered crystal containing about 10^{18} U centers per cm^3 is exposed to penetrating gamma rays such as the radiation of Co^{60}, some U centers are converted to F centers. The dependence of F-center concentration on dosage is linear until the number of F centers produced approaches the number of U centers originally available, and this does not occur for our crystals until about 10^4 roentgens have been received. Since the absorption coefficient of the crystal for gamma rays of the 1-Mev energy range is very low, the F-center distribution formed in this way is essentially as uniform as the original U-center distribution.

In addition to allowing F-center concentrations to be conveniently controlled, the U- to F-center conversion yields another important advantage which makes U-centered crystals more suitable for the present work than additively-colored ones. This advantage is that F centers produced in U-centered crystals by the U to F conversion bleach out on exposure to F-band light much less rapidly than do F centers produced by additive coloring. Thermal bleaching of F centers is also exceedingly slow in U-centered crystals. This slower bleaching is probably connected with the presence of fewer deep electron traps in U-centered crystals than in additively colored ones. An added advantage of the presence of fewer traps in U-centered crystals is that for a given light intensity and given concentration of F centers the equilibrium concentration of electrons in the conduction band will be higher in the U-centered than in the additively-colored crystal; the former will thus be more photoconducting.

Two general types of specimens have been prepared from plain potassium bromide single crystals, from additively colored, and from U-centered crystals. These two types of specimens will be referred to as Types I and II. In the first type, a square crystal was cleaved to a thickness of between one and six mm. The area of the sheet was about 5 cm^2. On one side of this sheet a heavy mirror coating of aluminum was evaporated, and on the other side a thin aluminum coating of about 70 percent light transmission in the visible was evaporated. After evaporation, the edges of the crystal were carefully ground to remove any aluminum which might have shorted the coatings together. These metallic coatings served as electrodes with incident light passing into the crystal through the front electrode and being reflected at the back electrode. This arrangement helped to make the light intensity within the crystal more uniform. It was largely unnecessary, however, since the F-center concentrations used were always sufficiently low that there was little decrease in F-band light intensity for light passing through the crystal. In the other general type of specimen, the crystals were parallelopipeds as long as 2 cm with air-drying silver paint electrodes applied to square end faces of about 0.5 cm^2 area. For these samples, light passed transversely into the crystal between the electrodes. In all cases contacts were made to the metallic electrodes by attaching fine wires to them with silver paint.

Since metallic electrodes directly on the crystal gave rectifying contacts, a number of crystals of the second type were made up to have blocking electrodes. This was accomplished by gluing 0.01 to 0.05 mm thick clear mica sheets to the ends of the crystals with polystyrene coil dope. The mica projected well beyond the edges of the crystals. Then silver-paint electrodes were painted on the outside of the mica. The series capacitance/cm^2 of two such mica layers between crystal and metal is of the order of 40 to 200 $\mu\mu$f/cm^2.

The final stage in specimen preparation involved heating the samples for an hour at 120°C in the dark and then dipping them in molten ceresin wax. This procedure was necessary to eliminate surface conductivity in these hygroscopic crystals. The wax coating was very thin over the semitransparent aluminum electrode or, in some cases, was removed entirely from this electrode without deleterious effects. Finally, the samples were mounted on flat polystyrene holders attached to General Radio double banana polystyrene plugs. The electrode wires were then connected to the plugs, and the sample thus made a compact, rigid unit which could be directly plugged into a capacitance bridge. A summary of some of the pertinent characteristics of the principal samples used in the present work is presented in Table III.

TABLE III. Summary of sample treatment, type, dimensions, and measured dark capacitance.

Sample	Treatment	Type	Electrode area (cm^2)	Electrode separation (mm)	C_θ (including fringing) ($\mu\mu$f)
U-1	U centered	I	4.81	2.02	11.3
U-2	U centered	I	4.81	5.42	3.9
U-3	U centered	...	...	...	...
U-5	U centered	II	0.443	12.9	0.4_0
U-6	U centered	II	0.540	14.4	0.4_0
U-8	U centered	II	2.00	10.0	1.3
AF-1	Additively F centered	I	4.83	1.57	14.5
K-2	Untreated	I	4.84	1.46	15.8

[41] H. Friedman and C. P. Glover, Nucleonics **10**, 24 (1952).

APPENDIX II. EXPERIMENTAL DETAILS

The principal light source used to produce photoconductivity in F-centered crystals was a slide projector employing a tungsten filament bulb of either 500 or 750 watts. Such a source has a high light output at 620 mμ. The entire output of the slide projector was sometimes focused on the crystals by means of lenses of 12- or 20-cm focal length. To avoid heating during such exposure, glass heat filters[42] were usually employed. In order to investigate the effect of light intensity, it was desirable to have some means of controlling the intensity precisely. Only light in the F-absorption band is effective in producing photoconductivity in these crystals, but the F band is so wide that gelatin neutral-density filters could not be employed for this purpose because of their wide density variations over the F band. To overcome this difficulty, perforated metal sheet filters which were truly neutral were employed. Their transmittance was calibrated with both a Beckman Model B spectrophotometer and a Cary Recording spectrophotometer, Model 11. These same instruments were also employed for transmittance measurements on the alkali halide crystals used in the investigation. It may be pointed out that although the gelatin neutral-density filters could have been used in conjunction with an interference filter transmitting in the F band, the use of such an interference filter was found to reduce the maximum available light intensity below a desirable level.

Most of the measurements reported in this paper were of sample capacitance and conductance at frequencies between 6 and 5×10^4 cps. Such measurements were carried out by the substitution method using a General Radio Type 716-C capacitance bridge in conjunction with a Type 722-D variable air capacitor for initial balance. To eliminate the capacitance of the sample holder and leads, the initial balance was made using a dummy holder containing leads but no crystal. The ac source employed was a Hewlett-Packard Model 202-B oscillator. The ac voltage applied to the crystals seldom exceeded five volts. The output of the bridge was amplified by a battery-operated Tektronix preamplifier having a gain of 1000 and was displayed on a Dumont Type 304-A oscillograph. To reduce residual 60-cycle pickup from the unshielded sample, a parallel-T rejection filter tuned to this frequency was also employed. For accurate frequency setting, either a 60-cycle line-voltage signal or the output of an electrically-driven 1000-cycle tuning fork was connected to the horizontal oscillograph input and the appropriate Lissajous figure produced by varying the oscillator frequency. Individual measurements were made in a period of a few seconds and the light extinguished between measurements to avoid heating of the specimen. Whenever sufficiently high light intensities were employed that appreciable bleaching was apparent during the course of a series of measurements, the measurements were repeated in reverse order. Since bleaching was always small enough during a set of frequency response measurements that it could be considered linear with time, an average of ascending and descending results substantially removed the effects of such variation.

In order to measure any harmonics produced by nonlinearity of these crystals and to measure the total admittance for large applied ac voltages, 60-cycle line voltages as high as several thousand volts were passed through a three-section RC filter to reduce harmonic content and then applied to the crystals. The voltage developed across a resistance of 4×10^4 to 10^5 ohms in series with the crystal was amplified by a preamplifier of gain 100 or 1000 and the harmonic content of this voltage measured with a Hewlett-Packard wave analyzer. To avoid overloading the preamplifier, the 60-cycle component of the voltage applied to it was greatly reduced using the parallel-T 60-cycle rejection filter. The ratio of the voltage of any given harmonic across the series resistance to the fundamental 60-cycle component is then the ratio of harmonic and fundamental currents in the photoconducting crystal.

In addition to ac measurements, some measurements were also made of the dc capacitance of the specimens. Such measurements were carried out by charging the specimen with 1000 volts, then discharging it into a 30-second-period Leeds and Northrup ballistic galvanometer calibrated in terms of capacitance. An Aryton shunt slightly under-damping the galvanometer was used in such measurements. In some cases, the specimens required more than five seconds to discharge. To allow measurements of capacitance to be obtained for longer discharge times, the specimens were first discharged as long as necessary into a 0.1 μf polystyrene-dielectric capacitor. This capacitor had negligible charge absorption and leakage and would hold a charge for a week or more with little or no decay. After the specimens were completely discharged into the polystyrene capacitor, it in turn was discharged into the galvanometer and the total dc capacitance thus determined.

The ballistic galvanometer was sometimes used as a current-indicating instrument to observe charging or discharging currents and to determine leakage or residual sample resistance. This latter quantity was also measured more accurately by using the sample whose resistance was to be determined as a resistance in series with the polystyrene capacitor and the voltage source. After a given period of time, the charge which had leaked into this capacitor was measured by the galvanometer used ballistically, and, from this result the series resistance could be computed. In such measurements, it was necessary to apply the charging voltage for about an hour to allow initial polarization currents to decay to a quasi-equilibrium value before beginning charge integration in the polystyrene capacitor.

In all these dc measurements, involving as they did a

[42] Corning, numbers 3961 or 3962.

1000-volt source of voltage and an extremely sensitive galvanometer, special care had to be exercised to reduce leakage currents in the apparatus to negligible values. The crystal specimen to be measured was plugged into contacts on a polystyrene strip mounted on porcelain stand-off insulators. These contacts were connected to the movable center contacts of a D.P.D.T. relay all of whose contacts had been remounted on polystyrene. In the unenergized condition, the crystal was connected to the 1000-volt supply voltage; in the energized condition it was connected to the galvanometer or to the polystyrene capacitor. Relay switching was necessary so that the sample could be completely enclosed within a light-tight box for measurements of capacitance *versus* light intensity while charging and discharging. In addition to being able to control the charging and discharging of the specimen from outside the box, the polarity of the voltage applied to the crystal could be similarly controlled by means of a D.P.D.T. impulse relay. This polarity was reversed after each charge-discharge cycle to reduce ionic and ionic-vacancy polarization effects as much as possible.

THE JOURNAL OF CHEMICAL PHYSICS VOLUME 23, NUMBER 2 FEBRUARY, 1955

A Theory of Thermal Diffusion in Liquids*

E. L. Dougherty, Jr., and H. G. Drickamer
Department of Chemistry and Chemical Engineering, University of Illinois, Urbana, Illinois
(Received July 14, 1954)

A theory of thermal diffusion in liquids has been developed based on Denbigh's interpretation of the "net heat of transport" which arises in the thermodynamics of irreversible processes. The thermal diffusion ratio α is expressed in terms of the energies of vaporization of the pure components, the excess energy, entropy and volume of mixing, and the concentration dependence of ΔU_e. The efficiency with which the two species pack together is also introduced. The Hildebrand-Scatchard solution theory is applied to these results and α is expressed in terms of solubility parameters, molal volumes and packing efficiencies.

The equations are compared with previously published experimental results, and reasonably explainable packing efficiencies are obtained.

In the appendices the effects of nonrandomness of mixing are considered and the theory is extended to ternary mixtures.

In a recent paper by Rutherford and Drickamer,[1] a theory of thermal diffusion in liquids was presented. This theory is based on a molecular interpretation of the "net heat of transport" due to Denbigh[2] and is an attempt to give a quantitative measure of the average intermolecular potentials defined in regular solution theory in terms of known thermodynamic properties of the pure liquids. The theory of Denbigh was extended by introducing a correction for differences in size and shape of the molecules. In reference 1 and succeeding papers[3–6] the theory is compared to experimentally determined thermal diffusion ratios for a wide variety of systems both at atmospheric pressure and under pressure to 10 000 atmospheres.

In this paper Denbigh's interpretation of the "net heat of transport" is reconsidered. Expressions for the energy quantities which appear in the theory are obtained in terms of partial molal "cohesive" energies of the components in the solution. In this manner a general expression for the thermal diffusion ratio α is obtained which involves only the heats of vaporization of the pure components, the excess energy, entropy and volume of mixing, and the slope of the excess energy-composition curve.

The Hildebrand-Scatchard[7,8] expressions for the heat of mixing and chemical potential are then introduced to give an expression for α in terms of properties of the pure components and the composition of the solution. This theory has a much firmer foundation than the previous one[1] since no assumptions concerning energy relationships in the solution are involved which have not been accepted as reasonable approximations in solution theory for 25 years. In the light of the revised theory, the data included in the above papers[1,3–6] have been reinterpreted.

* This work was supported in part by the U. S. Atomic Energy Commission.
[1] W. M. Rutherford and H. G. Drickamer, J. Chem. Phys. **22**, 1157 (1954).
[2] K. G. Denbigh, Trans. Faraday Soc. **48**, 1 (1952).
[3] Saxton, Dougherty, and Drickamer, J. Chem. Phys. **22**, 1166 (1954).
[4] R. L. Saxton and H. G. Drickamer, J. Chem. Phys. **22**, 1287 (1954).
[5] W. M. Rutherford and H. G. Drickamer, J. Chem. Phys. **22**, 1284 (1954).
[6] Rutherford, Dougherty, and Drickamer, J. Chem. Phys. **22**, 1289 (1954).
[7] G. Scatchard, Chem. Revs. **8**, 321 (1931).
[8] J. H. Hildebrand and R. L. Scott, *The Solubility of Nonelectrolytes* (Reinhold Publishing Company, 1950), third edition.

THEORY

Thermodynamics of Irreversible Processes

In the thermodynamics of irreversible processes,[9–11] two energy quantities, the "heat of transport,"[12] Q_i, and the "net heat of transport," Q_i^*, appear which were not previously defined in equilibrium thermodynamics. It can readily be shown that Q_i is the amount of energy transported across a given reference plane per mole of the ith component in the absence of a temperature gradient. The net heat of transport is defined by the equation

$$Q_i^*=Q_i-\bar{H}_i, \tag{1}$$

where $\bar{H}_i$ is the partial molal enthalpy of the ith component in the solution. The significance of Q^* is discussed below.

In terms of the heat of transport the flux equation for the ith component in a multicomponent constant pressure system is

$$\mathbf{J}_i=-\sum_{k=1}^{n} L_{ik}\left[(Q_k-\bar{H}_k)\frac{\text{grad}\mathbf{T}}{T}+\sum_{j=1}^{n-1}\frac{\partial\mu_k}{\partial x_j}\text{grad}\mathbf{x}_j\right], \tag{2}$$

where $\mathbf{J}$ = flux of component i, moles/cm^{2}hr, μ_k = chemical potential of component k, T = absolute temperature, °K, x_i = mole fraction component i, and L_{ik} = phenomenological coefficients. This gives the following relationship for the steady-state concentration gradient resulting from a temperature gradient ($\mathbf{J}_i=0$, $i=1, 2\cdots$) in a binary system:

$$\frac{1}{x_1}\text{grad}\mathbf{x}_1=-\frac{Q_1-\bar{H}_1}{x_1(\partial\mu_1/\partial x_1)}\frac{\text{grad}\mathbf{T}}{T}=\frac{-Q_1^*}{x_1(\partial\mu_1/\partial x_1)}\frac{\text{grad}\mathbf{T}}{T}, \tag{3}$$

where Eq. (1) has been used. Similarly, for the second component,

$$\frac{1}{x_2}\text{grad}\mathbf{x}_1=\frac{-Q_2^*}{x_2(\partial\mu_2/\partial x_1)}\frac{\text{grad}\mathbf{T}}{T}. \tag{4}$$

Combining Eqs. (3) and (4) and making use of the Gibbs-Duhem relation in the form

$$x_1\frac{\partial\mu_1}{\partial x_1}+x_2\frac{\partial\mu_2}{\partial x_1}=0 \tag{5}$$

gives for the steady state concentration gradient

$$\frac{1}{x_1x_2}\text{grad}\mathbf{x}_1=\frac{Q_2^*-Q_1^*}{x_1(\partial\mu_1/\partial x_1)}\frac{\text{grad}\mathbf{T}}{T}. \tag{6}$$

The conventional flux equation for a binary system is

$$\mathbf{J}_1=-\rho D\left[\text{grad}\mathbf{x}_1-\frac{\alpha x_1x_2}{T}\text{grad}\mathbf{T}\right], \tag{7}$$

where ρ = density, D = diffusion coefficient, and α = thermal diffusion ratio sT (s = Soret coefficient). For the steady-state separation, Eq. (7) gives

$$\frac{1}{x_1x_2}\text{grad}\mathbf{x}_1=\alpha\frac{\text{grad}\mathbf{T}}{T}. \tag{8}$$

Comparison of Eq. (8) with Eq. (6) gives the desired expression for α:

$$\alpha=\frac{Q_2^*-Q_1^*}{x_1(\partial\mu_1/\partial x_1)}. \tag{9}$$

This is the basic expression for our thermal diffusion theory.

When Eq. (8) is integrated for a two-chamber cell, the following expression for α in terms of the steady-state separation is obtained:

$$\ln\left(\frac{x_1}{x_2}\right)_H\left(\frac{x_2}{x_1}\right)_C=\alpha\ln\frac{T_H}{T_C}, \tag{10}$$

where the obvious notation for the hot and cold chambers has been used. It can be seen from this equation that sign assigned to α is arbitrary. The convention adopted will be discussed below.

The Gibbs-Duhem relation [Eq. (5)] yields the following relationship which the net heats of transport must satisfy:

$$x_1Q_1^*+x_2Q_2^*=0.[13] \tag{11}$$

Kinetic Theories

Other expressions for the thermal diffusion ratio, similar in form to Eq. (9), have been developed by Hiby and Wirtz and by Prigogine *et al.*[14,15] by considering thermal diffusion to be a stepwise activated process. Prigogine extended the derivation by interpreting the activation energies (free energies) to be potential energies necessary for breaking cohesive bonds. In this way he obtains an expression involving the cohesive energy density (defined as $(\Delta U^V/V)$,

[9] S. R. de Groot, *The Thermodynamics of Irreversible Processes* (Interscience Publishers, New York, 1951).

[10] K. G. Denbigh, *The Thermodynamics of the Steady State* (John Wiley and Sons, Inc., New York, 1951).

[11] S. R. de Groot, *L'Effet Soret* (Amsterdam, 1945).

[12] It should be noted that in the past it has been the custom to call Q_i^* "the heat of transport" and to give no name to Q_i. In this paper Q_i and Q_i^* will be referred to as above since this nomenclature seems to define the issue logically.

[13] This equation, as well as Eqs. (3) and (4), from which it is derived, although frequently used, is actually more restrictive than necessary (see de Groot, reference 9). In any case, it does not effect the further derivation except possibly in the physical interpretation of the ψ's.

[14] K. Wirtz and J. W. Hiby, Physik. Z. 44, 369 (1943).

[15] Prigogine, de Broukere, and Amand, Physica 16, 577, 851 (1950).

where ΔU^V equals the energy of vaporization per mole and V equals the molar volume) of the pure components and from this predicts that the compound with the higher cohesive energy density should be enriched at the cold wall. When the free energies of activation are considered to be functions of temperature, it has been shown[1] that α is given by the difference between activation enthalpies rather than free energies.

The disadvantage of this type of expression is that the energy quantities appearing therein, being activation quantities, cannot be readily and clearly interpreted in terms of other physical properties. The assumption that the activation energies are some fraction of the energy of vaporization is supported by the work of Eyring *et al.*,[16] who found that they could obtain qualitative agreement between their activated complex theory of viscosity in liquids and experiment by assuming the energy of activation to be about $\frac{1}{3}$ to $\frac{1}{4}$ the energy of vaporization. However, at present, one cannot quantitatively predict the effect of pressure upon such quantities.

On the other hand Denbigh[2] has given a very clear and concise physical interpretation of the net heat of transport and has shown that theoretically it is susceptible to measurement. For this reason the treatment of Denbigh was adopted in the previous theory[1] and is retained as the basis of the revised theory.

The Net Heat of Transport

First consider a region in a fluid. Suppose that dn_1 moles diffuse outward from this region across the boundary surface. From the definition of Q_1 given above, it follows that the diffusional flow will be accompanied by a flow of energy across the boundary surface in the amount $Q_1 dn_1$. Presume further that the region is maintained at constant temperature and pressure by means of a thermostat. Thus a quantity of heat, dq, will be absorbed, and in the process an amount of work, dw, will be performed, *quasi* statically, by the fluid remaining in the region. Then the change in internal energy of the region is given by

$$dU = -Q_1 dn_1 + dq - dw. \tag{12}$$

However, since the region remains at constant temperature and pressure, the change in internal energy can also be written $-\bar{U}_1 dn_1$ and its change in volume $-\bar{V}_1 dn_1$, where $\bar{V}_1$ = partial molal volume of component 1, $\bar{U}_1$ = partial molal energy of component 1. Thus the work done is $-p\bar{V}_1 dn_1$. Substituting in Eq. (12), the change in internal energy becomes

$$-U_1 dn_1 = -Q_1 dn_1 + dq + p\bar{V}_1 dn_1. \tag{13}$$

[16] Glasstone, Laidler, and Eyring, *Theory of Rate Processes* (McGraw-Hill Book Company, Inc., New York, 1941).

Hence dq, the heat absorbed from the reservoir, is given by

$$\begin{aligned} dq &= (Q_1 - \bar{U}_1 - p\bar{V}_1)dn_1 = (Q_1 - \bar{H}_1)dn_1 \\ &= Q_1^* dn_1. \end{aligned} \tag{14}$$

Therefore, $Q_1^* = dq/dn_1$, is the *net* amount of energy which must be absorbed by the region per mole of component 1 diffusing out in order to maintain constancy of temperature and pressure.

The net heat of transport for the two components of a binary solution can be expressed in terms of two energy quantities, (a) the energy of detaching a molecule from its neighbors, designated W_H and (b) the energy given up when one molecule fills a hole, W_L. (Denbigh calls this the energy of filling a hole, which he can do since he assumes all the holes are the same size.) Once again consider a region in a fluid. It is assumed that there is not net change in kinetic energy when a molecule is removed from this region. Thus, W_H is some fraction of the potential energy required to detach completely a molecule from the solution. Let W_{H_1} designate the energy required to remove a molecule of type 1 from the region, and similarly W_{H_2} for a type 2 molecule. Assume for the time being that for each molecule which is removed from the region on the average one molecule returns to the region (this assumes the holes to be of the same size). Assuming the distribution to be completely random, the relative probability of the hole being filled by a molecule of type 1 or 2 is in the ratio x_1/x_2. The probable energy supplied is

$$W_L = x_1 W_{H_1} + x_2 W_{H_2}. \tag{15}$$

Under the assumption of equal size holes, the net heat of transport is

$$Q_1^* = W_{H_1} - W_L, \tag{16}$$

with a similar expression for Q_2^*. It is readily seen that these quantities satisfy the Gibbs-Duhem relation (Eq. (11)). Substitution into Eq. (9) gives

$$\alpha = \frac{W_{H_2} - W_{H_1}}{x_1(\partial\mu_1/\partial x_1)}. \tag{17}$$

For molecules of different size and shape, the volume and the shape of the holes occupied by the two types of molecules must be different. It seems reasonable to assume that for mixtures of large and small molecules, on the average more than one molecule will move into the hole left by the larger molecule and conversely for the smaller molecule. Assuming that ψ_1 molecules move into a hole left by a type 1 molecule, and similarly for ψ_2, the following expressions for the net heats of transport are obtained:

$$Q_1^* = W_{H_1} - \psi_1 W_L, \tag{18}$$

$$Q_2^* = W_{H_2} - \psi_2 W_L. \tag{19}$$

Applying the Gibbs-Duhem relation to the Q^*'s gives the following expression:

$$x_1\psi_1+x_2\psi_2=1. \tag{20}$$

This equation states that on the average one molecule moves into the region for each molecule which moves out. Further, as $x_1\rightarrow 1$, $\psi_1\rightarrow 1$, and as $x_2\rightarrow 1, \psi_2\rightarrow 1$, as is physically necessary.

In his paper Denbigh[2] derives an expression for Q^* for the components of a binary regular solution in terms of the average intermolecular potentials introduced in the theory of regular solutions. His treatment was extended in the manner outlined above in Eqs. (18) and (19) to include molecules of different size and shape.[1] In order to compare the theory with the experimental results, it was necessary to obtain a macroscopic measure of the average intermolecular potentials in terms of known thermodynamic properties of the pure liquids. This was done by defining a molar interaction potential, H_i, *viz.*,

$$H_i=-NZw_{ii}=\left[T\frac{\partial p}{\partial T}\right)_V\left(V-T\frac{\partial V}{\partial T}\right)_p\Bigg)\Bigg]_i,$$

where w_{ii}=average intermolecular potential between two molecules of type i, Z=number of nearest neighbors, N=Avogadro's number, and V=molar volume. The justification for this expression was mainly empirical.

Aside from its rather equivocal background, two other objections to this expression are (a) it has no obvious direct physical significance, and (b) when the H's are substituted into the expression given for the heat of mixing by regular solution theory, the values obtained are not always even in qualitative agreement with the values predicted by the Hildebrand-Scatchard theory, which is known to be at least qualitatively correct.

Derivation of W_H and a General Expression for the Thermal Diffusion Ratio

In an attempt to alleviate these difficulties, a considerably different approach is adopted in interpreting W_H. This approach is as follows:

The internal energy of a solution of n_1 moles of component one and n_2 moles of component two may be written

$$U_m=n_1\bar{U}_1^0+n_2\bar{U}_2^0+(n_1+n_2)U_e, \tag{21}$$

where $\bar{U}_1^0$=molar energy of pure i, and $U_e=\Delta U_m$ =excess energy of mixing per mole of solution.

Differentiating with respect to n_1 gives for the partial molal energy of component 1

$$\bar{U}_1=\left(\frac{\partial U_m}{\partial n_1}\right)_{n_2,T,p}=\bar{U}_1^0+U_e+(n_1+n_2)\frac{\partial U_e}{\partial n_1}. \tag{22}$$

The internal energy of a mole of pure 1 can be written

$$\bar{U}_1^0=\bar{U}_{1g}^0+u_1, \tag{23}$$

where $\bar{U}_{1g}^0$ is the energy of the ideal gas at zero pressure and at the same temperature as the liquid and u_1 is the cohesive energy of the liquid. It is essentially equal to the potential energy in the liquid. Substituting in Eq. (22) and rearranging slightly,

$$\bar{U}-\bar{U}_{1g}^0=u_1+(n_1+n_2)(\partial U_e/\partial n_1)+U_e. \tag{24}$$

This might be called the partial molal potential energy of the component 1 in the solution. From the definition of a partial molal quantity, it follows that this is the change in potential energy when one mole of component 1 is removed from a large volume of solution and expanded to zero pressure. Therefore, the W_H can be defined as

$$W_H=-\frac{1}{\tau}(\bar{U}_1-U_{1g}^0)$$
$$=-\frac{1}{\tau}[u_1+U_e+(n_1+n_2)(\partial U_e/\partial n_1)], \tag{25}$$

where $\tau>1$ and the negative sign is included to make W_{H1} positive. In terms of mole fractions, the energies of detachment for the two components are

$$W_{H1}=-\frac{1}{\tau}\left[u_1+x_2\frac{\partial U_e}{\partial x_1}+U_e\right], \tag{26}$$

$$W_{H2}=-\frac{1}{\tau}\left[u_2-x_1\frac{\partial U_e}{\partial x_1}+U_e\right]. \tag{27}$$

By Eq. (15) the energy of filling a hole becomes

$$W_L=-\frac{1}{\tau}[x_1u_1+x_2u_2+U_e]. \tag{28}$$

Combining these three expressions with Eqs. (9), (18), and (19),

$$\alpha=(W_{H2}-W_{H1})+(\psi_1-\psi_2)W_L$$
$$=\frac{\{[u_2-u_1-(\partial U_e/\partial x_1)]+(\psi_1-\psi_2)[x_1u_1+x_2u_2+U_e]\}}{\tau x_1(\partial\mu_1/\partial x_1)}. \tag{29}$$

The cohesive energy of a pure liquid is essentially the molal energy of vaporization, ΔU^V, taken with a negative sign. The chemical potential may be expressed as

$$\mu_1=\mu_{01}+RT\ln x_1-T\bar{S}_{e1}+\bar{U}_{e1}+p\bar{V}_{e1}, \tag{30}$$

where $\bar{S}_{e1}$=partial molal excess entropy of mixing, $\bar{V}_{e1}$=partial molal volume change on mixing, and $\bar{U}_{e1}$=partial molal excess energy of mixing, whence

$$x_1\frac{\partial\mu_1}{\partial x_1}=RT-Tx_1\frac{\partial\bar{S}_{e1}}{\partial x_1}+x_1\frac{\partial\bar{U}_{e1}}{\partial x_1}+x_1p\frac{\partial\bar{V}_{e1}}{\partial x_1}. \tag{31}$$

Substituting in Eqs. (29) it follows that

$$\alpha=\frac{\left(\Delta U_2^V-\Delta U_1^V+\frac{\partial U_e}{\partial x_1}\right)+(\psi_1-\psi_2)[x_1\Delta U_1^V+x_2\Delta U_2^V-U_e]}{\tau\left[RT-Tx_1\frac{\partial \bar{S}_{e1}}{\partial x_1}+x_1\frac{\partial \bar{U}_{e1}}{\partial x_1}+x_1 p\frac{\partial \bar{V}_{e1}}{\partial x_1}\right]}. \tag{32}$$

Except for the parameters ψ_1, ψ_2, and τ, this expression involves only the heats of vaporization of the two pure components and the excess thermodynamic quantities on mixing, all of which are physically measurable quantities. In particular no assumption as to the type of interaction between unlike molecules is involved, and it is shown in Appendix A that to the first approximation the effect of nonrandomness is of minor importance for most liquids. Thus this expression can be expected to apply to solutions of polar molecules as well as to solutions of molecules of different size.

Before calculations can be made, a value must be inserted for τ and an approximation as to the magnitude of ψ must be introduced. These are discussed in a later section.

A strong test of the theory would be to apply it to mixtures for which careful measurements of the excess thermodynamic quantities on mixing have been made. It is planned to make such a project the object of a future study.

Application of the Hildebrand-Scatchard Equation for the Energy of Mixing

In order to apply Eq. (29) to experimental thermal diffusion data for systems for which accurate measurements of the excess quantities are not available, it is necessary to substitute an expression which predicts the excess energy of mixing from the properties of the pure components. The Hildebrand-Scatchard equation[7,8] which is known to give at least qualitative agreement for a large number of binary solutions was utilized. This expression gives for the excess energy of mixing

$$U_e=(x_1V_1+x_2V_2)(\delta_1-\delta_2)^2\varphi_1\varphi_2, \tag{33}$$

where V_i = molar volume of pure i, φ_i = volume fraction of i in the solution, and

$$\delta_i=[\Delta U_i^V/V_i]^{\frac{1}{2}}$$
$$=\text{solubility parameter of component } i. \tag{34}$$

After differentiating in Eq. (33) with respect to x, and introducing this result and V_e from Eq. (33) into Eq. (29), the expression for α is

$$\alpha=\frac{V_2\delta_2^2-V_1\delta_1^2+(\delta_1-\delta_2)^2(\varphi_2^2V_1-\varphi_1^2V_2)+(\psi_1-\psi_2)[x_1V_1\delta_1^2+x_2V_2\delta_2^2-\varphi_1\varphi_2\bar{V}(\delta_1-\delta_2)^2]}{\tau x_1(\partial\mu_1/\partial x_1)}, \tag{35}$$

where Eq. (34) has been used. After a little manipulation this may be written

$$\alpha=\frac{\bar{\delta}[2(\delta_2V_2-\delta_1V_1)+\bar{\delta}(V_1-V_2)+(\psi_1-\psi_2)\bar{\delta}\bar{V}]}{\tau x_1(\partial\mu_1/\partial x_1)}, \tag{36}$$

where

$$\bar{\delta}=\varphi_1\delta_1+\varphi_2\delta_2, \quad \bar{V}=x_1V_1+x_2V_2.$$

Introduction of a Value for τ

From Eq. (25) it can be seen that introduction of the factor $1/\tau$ is equivalent to assuming that the energy which must be supplied for molecular motion is $1/\tau$ times the cohesive energy of the liquid. Since the latter is approximated very closely by the energy of vaporization, in light of the previous discussion concerning the consideration of thermal diffusion as an activated process, it follows that the value of $1/\tau$ should be about $\frac{1}{3}$ to $\frac{1}{4}$. (This is the value Eyring obtains for $\Delta U^{visc}/\Delta U^V$.) The value of $\frac{1}{4}$ was used in all calculations made in comparing the experimental results with the theory in this paper. This particular value was chosen because it seemed to give somewhat better agreement between experiment and theory, especially for the system CCl_4-CBr_4 for which the theory should be most likely to hold.

Rather than assign the same value of τ to each molecular species it might be desirable to define τ for each species as the ratio of the energy of vaporization to the activation energy for viscous flow for that species. Then Eq. (26) becomes

$$W_{H1}=-\frac{1}{\tau_1}\left[u_1+x_2\frac{\partial U_e}{\partial x_1}+U_e\right] \tag{26'}$$

with an analogous modification of Eq. (27). Equation (28), for W_L, becomes

$$W_L=-\frac{x_1u_1}{\tau_1}-\frac{x_2u_2}{\tau_2}-x_1x_2\left(\frac{1}{\tau_1}-\frac{1}{\tau_2}\right)\frac{\partial U_e}{\partial x_1}$$
$$-U_e\left(\frac{x_1}{\tau_1}+\frac{x_2}{\tau_2}\right). \tag{28'}$$

Finally, letting $-u_i/\tau_i=(\Delta U_i^{\text{visc}})$, Eq. (32) for α can be written

$$\alpha=\frac{\Delta U_2^{\text{visc}}-\Delta U_1^{\text{visc}}+U_e\left(\frac{1}{\tau_1}-\frac{1}{\tau_2}\right)+\left(\frac{x_1}{\tau_1}+\frac{x_2}{\tau_2}\right)\frac{\partial U_e}{\partial x_1}}{RT+x_1\frac{\partial \bar{U}_{e1}}{\partial x_1}-x_1T\frac{\partial \bar{S}_{e1}}{\partial x_1}+x_1p\frac{\partial \bar{V}_{e1}}{\partial x_1}}$$

$$+\frac{(\psi_1-\psi_2)\left[x_1\Delta U_1^{\text{visc}}+x_2\Delta U_2^{\text{visc}}-x_1x_2\left(\frac{1}{\tau_1}-\frac{1}{\tau_2}\right)\frac{\partial U_e}{\partial x_1}-U_e\left(\frac{x_1}{\tau_1}+\frac{x_2}{\tau_2}\right)\right]}{RT+x_1\frac{\partial \bar{U}_{e1}}{\partial x_1}-x_1T\frac{\partial \bar{S}_{e1}}{\partial x_1}+x_1p\frac{\partial \bar{V}_{e1}}{\partial x_1}}. \quad (32')$$

Interpretation of ψ_1 and ψ_2

From Eq. (20) it follows that the number of molecules in the region considered in interpreting the net heat of transport is constant. It can also be readily shown that the volume of this region also remains constant. For suppose that N molecules are removed randomly from the region. Of these x_1N will be type 1 and x_2N, type 2. The volume of 1 and 2 removed will be $x_1N\bar{V}_1$ and $x_2N\bar{V}_2$ where the bar refers to the partial molal quantity. The number of molecules of type 1 returning will be $x_1^2N\psi_1+x_1x_2N\psi_2$ and of type 2, $x_1x_2N\psi_1+x_2^2N\psi_2$; the sum of these is N. The total volume of the returning molecules will be $(x_1^2N\psi_1+x_1x_2N\psi_2)\bar{V}_1+(x_1x_2N\psi_1+x_2^2N\psi_2)\bar{V}_2$ and by utilizing Eq. (20), it can be seen that the volume of the molecules returning to the region equals the volume of the molecules leaving the region.

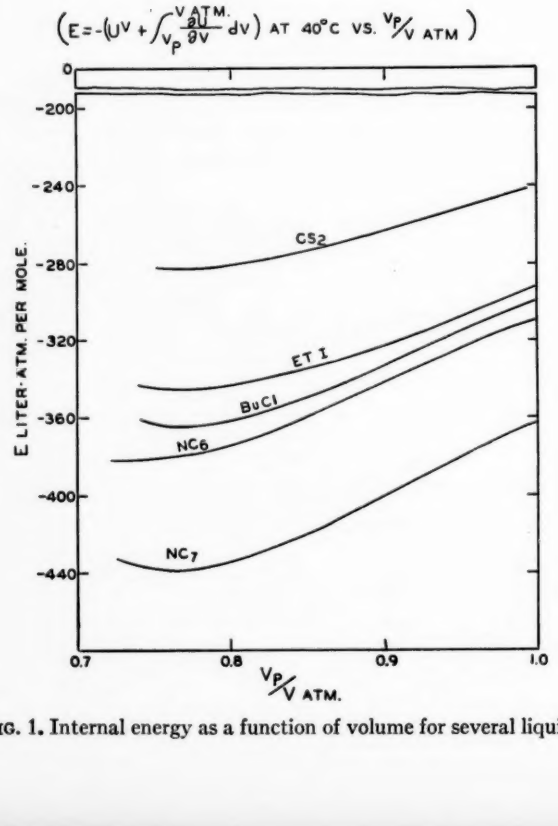

FIG. 1. Internal energy as a function of volume for several liquids.

Consider only the molecules of type 1. The volume of the molecules removed is $x_1N\bar{V}_1$ while the volume of the molecules returning to fill this volume is $x_1^2N\psi_1\bar{V}_1+x_1x_2N\psi_1\bar{V}_2$. Equating these two volumes gives

$$\psi_1=\frac{\bar{V}_1}{x_1\bar{V}_1+x_2\bar{V}_2} \quad (37)$$

and similarly for ψ_2. If it is assumed that the volume change on mixing is zero (this is one of the assumptions implicit in the use of Scatchard's equation for the energy of mixing), the partial molal quantities are replaced by the molar volumes of the pure components, i.e.,

$$\psi_i=\frac{V_i}{\sum_i x_iV_i}=\frac{V_i}{\bar{V}}. \quad (38)$$

In general ψ will differ from the value given by Eq. (38) for two reasons. First the change in volume on mixing may not be zero and second the volume of the molecules returning to fill a type 1 hole may not equal the volume of the hole itself. The first of these will generally introduce only a small correction. The second should be closely related to differences in the shapes of the molecules, and conceivably could become fairly large for solutions of molecules with considerably different packing. Thus, a correction for these factors is necessary, *viz.*,

$$\psi_i=\frac{V_i+\eta_i}{\bar{V}}. \quad (39)$$

Application of Eq. (20) gives the following relationship which the η's must satisfy:

$$x_1\eta_1+x_2\eta_2=0. \quad (40)$$

Equation (39) shows η to be the excess (or deficiency) of volume resulting in the region when a mole of type 1 is replaced with $x_1\psi_1$ moles of 1 and $x_2\psi_1$ moles of 2. Equation (40) states that the excess (or deficiency) in volume due to one species is exactly counterbalanced by the deficiency (or excess) of volume of the second species, in keeping with the fact that the total volume

of the region remains constant. Further as $x_1 \rightarrow 1$, $\eta_1 \rightarrow 0$ and as $x_2 \rightarrow 1$, $\eta_2 \rightarrow 0$ as is physically necessary.

If Eq. (39) is written in the form

$$\psi_i = \frac{V_i}{\bar{V}}(1+\eta_i/V_i), \tag{41}$$

the physical meaning of η_i becomes clearer. The volume decrease of the region when a mole of component i is removed is V_1 and $\psi_i V_i$ is the volume returned. Thus η_i/V_i represents the apparent fractional excess (or deficiency) of the molal volume which is removed from the region. Therefore η_i/V_i must be closely related to differences in packing of the two molecules. This is illustrated by the extreme sensitivity of η_i/V_i to differences in molecular structure for isomers. (See the discussion of experimental results below.)

From the Hildebrand-Scatchard theory using the Flory-Huggins entropy one obtains for the chemical potential

$$\mu_i = \mu_0 + RT \ln \varphi_1 + \varphi_2(1 - V_1/V_2) + V_1 \varphi_2^2 (\delta_1 - \delta_2)^2, \tag{42}$$

then

$$x_1 \frac{\partial \mu_1}{\partial x_1} = RT\left[1 + x_1 x_2 \left(\frac{V_2 - V_1}{\bar{V}}\right)^2\right] - \frac{2\varphi_1 \varphi_2 V_1 V_2 (\delta_1 - \delta_2)^2}{\bar{V}}. \tag{43}$$

Introducing Eqs. (39) and (43) into Eq. (36), and taking the value to be $\frac{1}{4}$, gives the following expression for the thermal diffusion ratio:

$$\alpha = \frac{\bar{\delta}\left[(\delta_2 - \delta_1)\dfrac{V_1 V_2}{\bar{V}} + \dfrac{(\eta_1 - \eta_2)\bar{\delta}}{2}\right]}{2\left[RT\left\{1 + x_1 x_2 \left(\dfrac{V_2 - V_1}{\bar{V}}\right)^2\right\} - 2\varphi_1 \varphi_2 \dfrac{V_1 V_2}{\bar{V}}(\delta_2 - \delta_1)^2\right]}, \tag{44}$$

$$\alpha = \alpha' + \frac{\bar{\delta}^2(\eta_1 - \eta_2)}{4\left[RT\left\{1 + x_1 x_2 \left(\dfrac{V_2 - V_1}{\bar{V}}\right)^2\right\} - 2\varphi_1 \varphi_2 \dfrac{V_1 V_2}{\bar{V}}(\delta_2 - \delta_1)^2\right]}, \tag{45}$$

where

$$\alpha' = \frac{\bar{\delta}(\delta_2 - \delta_1)\dfrac{V_1 V_2}{\bar{V}}}{2\left[RT\left\{1 + x_1 x_2 \left(\dfrac{V_2 - V_1}{\bar{V}}\right)^2\right\} - 2\varphi_1 \varphi_2 \dfrac{V_1 V_2}{\bar{V}}(\delta_2 - \delta_1)^2\right]}. \tag{46}$$

Equation (44) indicates that the magnitude of α is determined by two factors. The first term (designated α') is the most important for molecules similar in shape. Although it is directly dependent upon the difference in the solubility parameters (the square root of the cohesive energy density) of the two components, it should be noted that this is not purely an energetic term since it includes differences in molar volume (Eq. (38)). The second term, which is related essentially to molecular shape, becomes of major importance for systems in which the components differ considerably in structure or where they differ very little in cohesive energy density. This is illustrated by the data for binary mixtures of CS_2–hexane isomers shown in Fig. 8.

Experimentally it is found, in agreement with the conclusion of Prigogine[15] noted earlier, that in most cases the component with the higher cohesive energy density becomes enriched at the cold wall. Equation (44) predicts this would be true in all cases for molecules very similar in shape. Thus if α is designated positive when the component with the higher solubility parameter is enriched at the cold wall, the subscript 2 refers to this component. This convention has been adopted throughout this paper.

The thermal diffusion ratio will always be positive (since the denominator is always positive) when $\eta_1 \geq 0$; it is only when component one leaves such a hole as to admit less type two molecules than the volume ratio would predict that α becomes negative. Near the critical solution temperature the numerator will become very small, indicating that α should become large in this region.

The Cohesive Energy at High Pressure

In applying the theory to high-pressure data it is necessary to calculate the solubility parameters at the elevated pressure. This was done by adding to the cohesive energy value (the energy of vaporization) at atmospheric pressure the change in cohesive energy

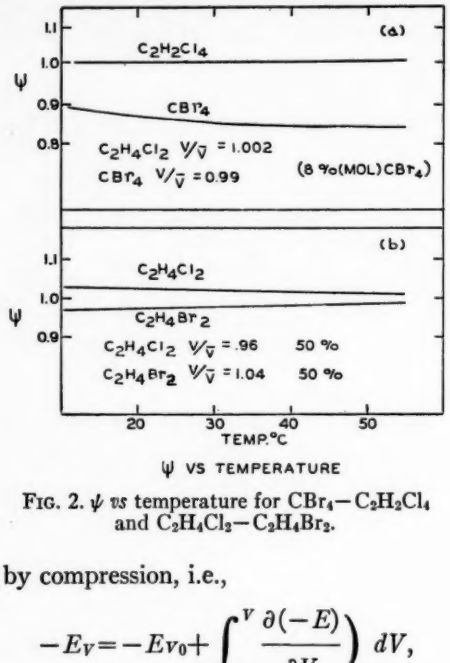

FIG. 2. ψ *vs* temperature for $CBr_4-C_2H_2Cl_4$ and $C_2H_4Cl_2-C_2H_4Br_2$.

caused by compression, i.e.,

$$-E_V=-E_{V_0}+\int_{V_0}^{V}\frac{\partial(-E)}{\partial V}\Big)_T dV, \qquad (47)$$

where $-E_{V_0}=\Delta U^V$ is the cohesive energy of the liquid at atmospheric pressure and volume V_0 and $-E_V$ is the cohesive energy at volume V, pressure p. (The minus sign is included to make all terms positive.) At constant temperature the change in cohesive energy is approximately equal to the change in internal energy, i.e.,

$$-\frac{\partial E}{\partial V}\Big)_T=-\frac{\partial U}{\partial V}\Big)_T.$$

Therefore, making use of the thermodynamic equation

$$\frac{\partial U}{\partial V}\Big)_T=T\frac{\partial p}{\partial T}-p, \qquad (48)$$

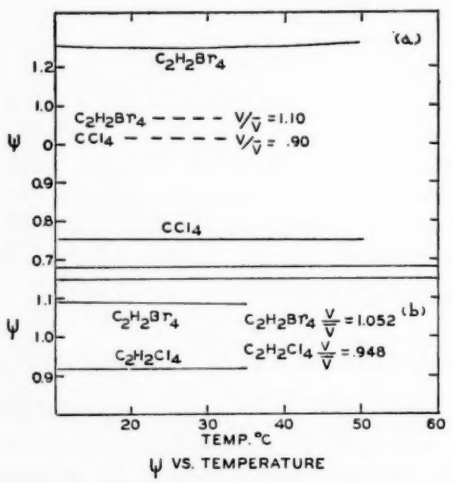

FIG. 3. ψ *vs* temperature for $C_2H_2Br_4-CCl_4$ and $C_2H_2Br_4-C_2H_2Cl_4$.

Eq. (46), for the cohesive energy, becomes

$$-E_V=\Delta U^{V_0}+\int_V^{V_0}\left[T\left(\frac{\partial p}{\partial T}\right)_V-p\right]dV. \qquad (49)$$

The solubility parameter is then obtained by dividing by the molar volume at the given pressure and extracting the square root, i.e.,

$$\delta_V=\left[\frac{\Delta U^{V_0}+\int_V^{V_0}\left[T\left(\frac{\partial p}{\partial T}\right)_V-p\right]dV}{V}\right]^{\frac{1}{2}}. \qquad (50)$$

Values of $(\partial p/\partial T)_V$ for the liquids for which high-pressure data are included in this paper were calculated by Rutherford[17] from the compressibility data of Bridgman. The integration in Eq. (49) was performed graphically. The results for several typical systems are shown in Fig. 1.

It can be seen that the measurements over the range to 10 000 atmospheres cover average intermolecular distances over the whole bottom of the potential energy well, a region most important in the modern theory of liquids.

TABLE I. Comparison of experimental and predicted thermal diffusion data for the system CBr_4, 9 percent (mole)$-CCl_4$, 91 percent.

Temp., °C	α_{exp}	α'[a]	(η_1/V_1)[b]	η_2/V_2	ψ_1	$V_1/\bar{V}$	ψ_2	$V_2/\bar{V}$
10	1.76	1.81	−0.001	0.011	0.982	0.994	1.087	1.078
25	1.58	1.52	+0.001	−0.014	0.995	0.994	1.052	1.068
40	1.50	1.33	+0.005	−0.044	0.998	0.993	1.022	1.068
55	1.42	1.21	+0.006	−0.061	0.999	0.992	1.010	1.070

[a] Calculated from Eq. (43).
[b] The subscript 1 refers to CCl_4.

In applying the theory to high pressures, it is assumed that the Hildebrand-Scatchard expressions for the excess energy of mixing, Eq. (33), and the chemical potential, Eq. (42), apply over the pressure range included in the study (1–10 000 atmos). Although at first it may seem that these equations cannot be expected to apply at high pressure, a little reflection convinces one that the assumptions underlying these expressions are as justifiable at high pressures as at atmospheric. The basic assumptions are (excluding the entropy of mixing term in Eq. (42) which is merely accepted) essentially[7,8]: (1) additivity of molecular pairs, (2) complete randomness, (3) zero volume change on mixing, and (4) geometric mean for 1–2 interactions.

In Fig. 1 values of $-E$, the potential energy of the liquid, calculated for several pure liquids, are plotted *versus* V_p/V_{atm}, the ratio of the molar volume at the pressure p to that at atmospheric pressure. The minima of these curves correspond to a pressure of about

[17] W. M. Rutherfore, Ph.D. thesis, University of Illinois (1954).

7000–9000 atmos; thus most of the pressure range studied was to the right of these minima. Since the intermolecular forces are similar in nature everywhere in this range, there is no obvious reason why the expressions should not be expected to apply equally well throughout this region.

In the region of the minimum and beyond repulsive forces are becoming of importance, and the assumption of the geometric mean may be less correct. However, since the distance through the minimum was so small there is no reason to expect the expressions to be much poorer. This is supported by the fact that agreement between the theory and experiment is as consistent at the highest pressures as at intermediate and lower pressures.

COMPARISON WITH EXPERIMENT

Our previously published experimental results[1,3,4] can be classified under six headings:

(A) Binary mixtures of molecules of simple symmetry at atmospheric pressure over the temperature range 0–55°C.

(B) Binary mixtures of normal paraffin hydrocarbons with 1, 1, 2, 2 tetrachloroethane at atmospheric pressure and over the same temperature range as above.

(C) Binary mixtures of normal alkyl halides with carbon disulfide at 40°C and from 300–10 000 atmospheres.

(D) Binary mixtures of CS_2 and benzene and its monosubstituted halogenic derivatives at 40° to 6000 atmospheres pressure.

(E) Binary mixtures of normal paraffin hydrocarbons with CS_2 at 40°C and 78°C and from 300–10 000 atmospheres pressure.

(F) Binary mixtures of CS_2 with the five isomers of hexane at atmospheric pressure and 60°C, and at 40°C to 10 000 atmospheres.

The results of calculations based on the theory of this paper are shown in Table I and Figs. 2–9. The important features for each of these groups will be discussed below, but first some general conclusions can be enumerated. Our discussion of results will center around ψ_i, the number of molecules entering a hole left by a type i molecule, and η_i/V_i, the measure of the packing efficiency. It will be important to note whether $\psi_i \cong V_i/\bar{V}$, which indicates identical packing efficiencies for the two species ($\eta_i/V_i=0$). Where this does not obtain the magnitude and sign of η_i/V_i and particularly any regular variation of this quantity with temperature and pressure, or from system to system, is significant. A large negative value of η_i/V_i corresponds to inefficient packing in a hole left by species i. The following conclusions can reasonably be drawn:

(1) ψ_i-1 and $V_i/\bar{V}-1$ almost always have the same sign. They are usually of about the same magnitude and the variation from system to system in an homologous series is in the expected direction and frequently in very nearly quantitatively the expected amount.

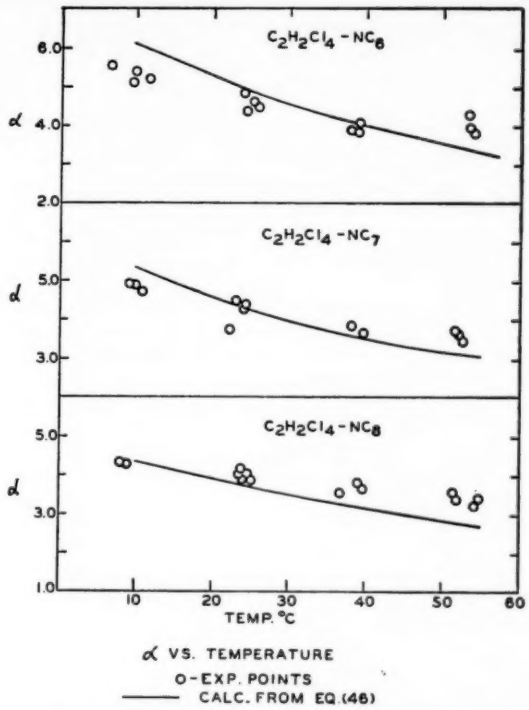

FIG. 4. Comparison of measured and calculated values of α for $C_2H_2Cl_4$–hydrocarbon mixtures. The symbol 0 indicates experimental and — indicates calculations from Eq. (46).

(2) For the larger molecule the largest values of ψ are almost always obtained at low pressure and at high temperature. At high pressure and low temperature, ψ for the larger molecule tends to approach one. That is to say the packing is less efficient at high pressure and

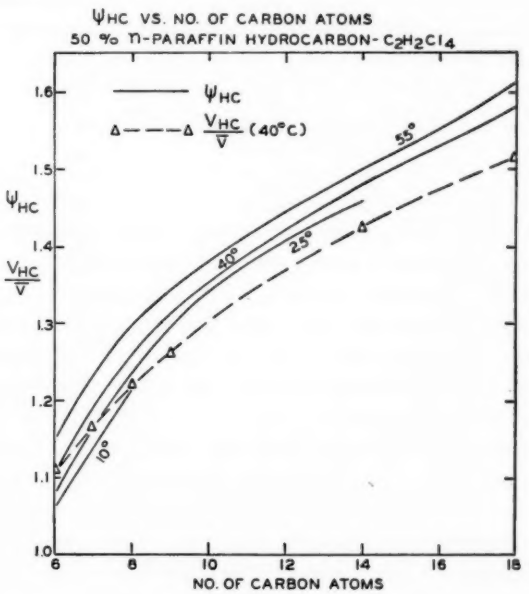

FIG. 5. ψ_{HC} and $V_{HC}/\bar{V}$ *vs* number of carbon atoms for $C_2H_2Cl_4$–hydrocarbon mixtures.

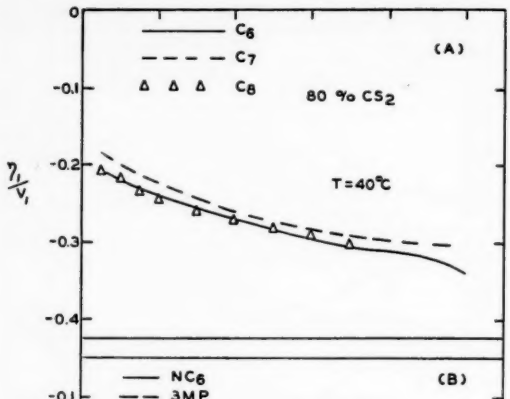

FIG. 6. Packing efficiency η/V for hydrocarbons *vs* pressure for CS_2—hydrocarbon mixtures to 10 000 atmospheres pressure.

low temperature. In a rigid lattice the exchange would be strictly one for one, so at high pressure and low temperature the system acts more like a lattice. This is rather an obvious picture but is interesting to note that our theory is consistent with the picture.

(3) For the one set of geometrical isomers studied to date, the packing becomes less efficient the greater the degree of branching of the chain.

Molecules of Simple Symmetry

The systems discussed here include CBr_4-CCl_4, $C_2H_4Cl_2-C_2H_4Br_2$, $C_2H_2Cl_4-CBr_4$, $CCl_4-C_2H_2Br_4$, and $C_2H_2Cl_4-C_2H_2Br_4$. These molecules should provide a good test for the theory, but the data are less accurate than the average because of the tendency for the bromides to decompose, and the calculations are in doubt because of lack of reliable energy of vaporization data, or inadequate means for evaluation of the solubility parameter.

The system CBr_4-CCl_4 is in a class by itself because the molecules are spherically symmetrical with nearly the same molar volume. The results (shown in Table I) are gratifying, although the predicted temperature coefficient for α is a little larger than the measured one.

The solubility parameter for CBr_4 was calculated from solubility measurements. The molar volume for liquid CBr_4 was estimated by comparison with other solid and liquid carbon tetrahalides.

The results for the other systems are shown in Figs. 2 and 3.

For the system $CBr_4-C_2H_2Cl_4$ the ψ's are in the expected direction and reasonable in magnitude.

For $C_2H_4Cl_2-C_2H_4Br_2$ the ψ's are in the opposite direction from the $V/\bar{V}$'s, but the magnitude of both quantities is very close to one. A 30-percent change in α or in the difference of solubility parameters would make ψ identical with $V/\bar{V}$. This is probably larger than the possible error, but the difference in solubility parameters could be varied by 10–20 percent by various interpretations of available data, and such a change would be sufficient to give the same direction to ψ and $V/\bar{V}$.

The systems $C_2H_2Cl_4-C_2H_2Br_4$ and $CCl_4-C_2H_2Brr$ (Fig. 3) show the expected directions for ψ but rathe, too large a magnitude for ψ $C_2H_2Br_4$, especially with CCl_4. This may be due to unusually efficient packing of unlike species but is much more likely to be based on inadequacy of the data. No vapor pressure data were available for $C_2H_2Br_4$, so the solubility parameters were estimated from surface tension measurements. It was assumed that the relative values of δ for $C_2H_2Br_4$, $C_2H_2Cl_4$, and CCl_4 are the same when obtained from

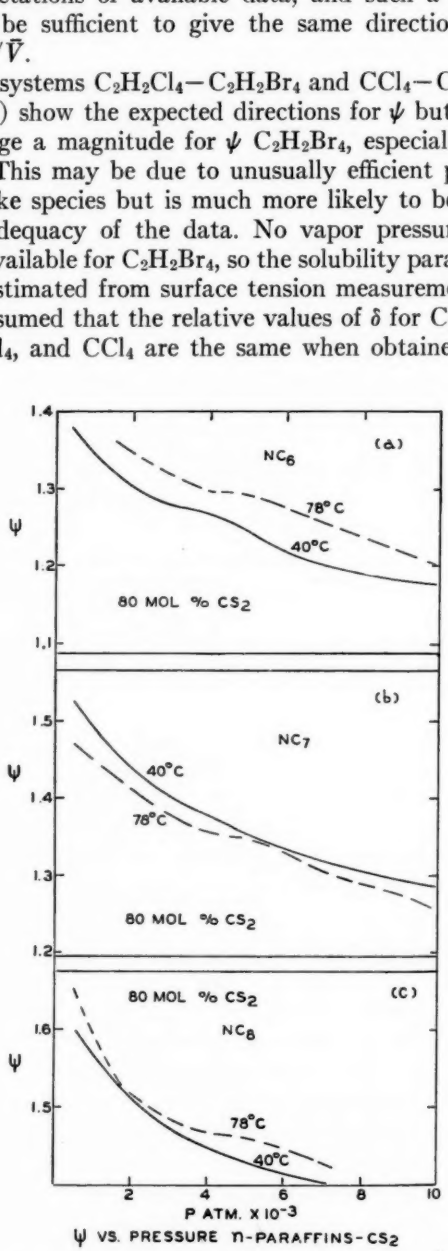

FIG. 7. ψ_{HC} *vs* pressure at 40° and 78°C for mixtures of *n*-paraffin hydrocarbons with CS_2.

surface tension measurements as they are from vapor pressure measurements.

50 Mole Percent Mixtures of Normal Paraffin Hydrocarbons with 1,1,2,2 Tetrachloroethane

The systems studied include nC_6, nC_7, nC_8, nC_9, nC_{14}, and nC_{18} with $C_2H_2Cl_4$. The first three systems were studied over a range from 10–55°C, the others over a smaller range. In Fig. 4 the experimental points for α are compared with the values obtained from Eq. (46) assuming $\psi_i = V_i/\bar{V}$. The agreement is surprisingly good considering the difference in shape of the molecules. Apparently the structure of the solution is sufficiently "loose" that the molecules or segments thereof are interchangeable with no loss in packing efficiency. The predicted temperature coefficient is again slightly larger than that obtained experimentally.

In Fig. 5 is plotted ψ_{HC} and $V_{HC}/\bar{V}$ *versus* number of carbon atoms. There is good qualitative agreement between ψ and $V/\bar{V}$ over the whole range studied, but for the longer chains ψ is larger than $V/\bar{V}$. This would indicate that a hole left by a long chain hydrocarbon is filled more efficiently from the 50–50 mixture of hydrocarbon and $C_2H_2Cl_4$, than by the pure hydrocarbon. More extensive evidence is necessary before one could lean too heavily on this conclusion.

These data show consistently the decrease in ψ with decreasing temperature discussed earlier in the general conclusions.

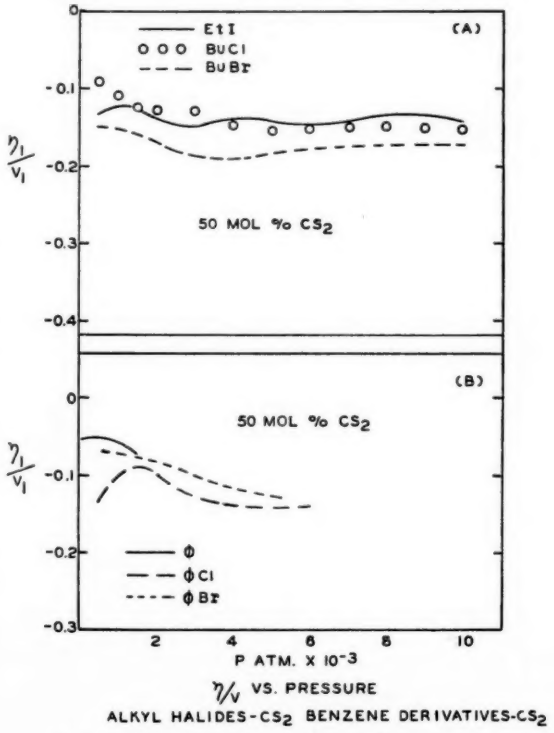

FIG. 8. η/V *vs* pressure. (A) alkyl halides—CS_2. (B) benzene derivatives—CS_2.

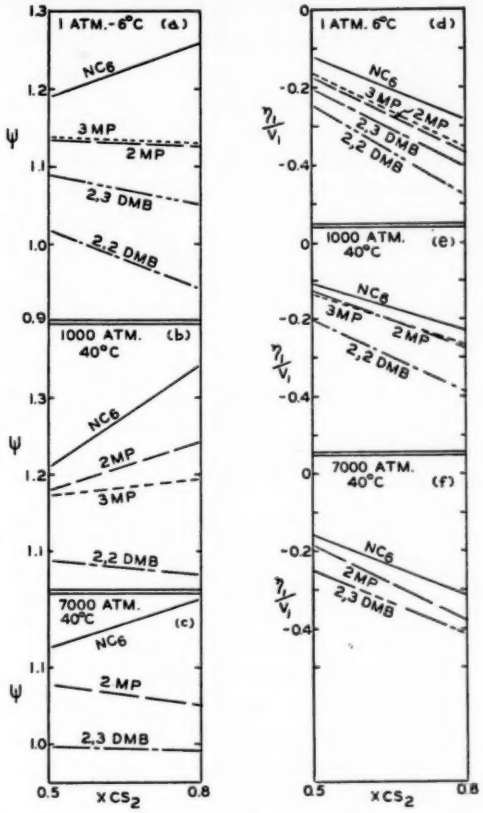

FIG. 9. ψ and η/V *vs* composition at various pressures for isomers of hexane in CS_2.

Binary Solutions of CS_2 and Alkyl Halides Under Pressure

The results obtained for 50–50 binary solutions of C_2H_5I, C_4H_9Cl, and C_4H_9Br in CS_2 are shown in Fig. 6(a). In this figure values of η_1/V_1 (the subscript 1 referring to the halogenated compound as it has the lower solubility parameter) are plotted as a function of pressure over the range 300–10 000 atmos. The internal consistency between these three compounds is good, indicating the structure of the solution to be similar for the three compounds. Apparently, the C_2H_5I and C_4H_9Cl form CS_2 solutions nearly identical in structure, while the C_4H_9Br has somewhat more of a lattice structure. The effect of pressure is small, but the trend is for a more negative value of η_1/V_1 as the pressure is increased. Since the molar volumes of the hydrocarbon derivatives are larger than that of CS_2 this means [Eq. (41)] that ψ tends towards 1 as the pressure is increased, as discussed in the foregoing.

CS_2–Benzene Derivatives

Figure 6(b) is a plot of similar data for 50–50 binary solutions of benzene, chlorobenzene, and bromobenzene in CS_2. The consistency between the three compounds and decrease in η_1/V_1 with increasing pressure should be noted.

Binary Solutions of CS_2-n Paraffin Hydrocarbons

In Fig. 7 the values of ψ_{HC} obtained for 50–50 binary solutions of *n*-hexane, *n*-heptane, and *n*-octane in CS_2 are plotted as a function of pressure (300–10 000 atmos) at average temperatures 40°C and 78°C. The effect of pressure is similar on all three solutions, ψ_{HC} decreasing as the pressure is increased. For nC_6 and nC_8 the effect of temperature is as expected, ψ_{HC} decreasing with the temperature, but with nC_7 a slight increase was noted at the lower temperature. With the accuracy of the data one cannot at present be sure whether this is significant.

In Fig. 8(a) the values of η_1/V_1 for these three hydrocarbons are compared as a function of pressure at 40°C. The similarity between C_6 and C_8 is striking, indicating nearly identical packing in these solutions. The C_7 data indicate a less efficient packing. These differences between even and odd hydrocarbons are reflected in the shape of the energy wells (Fig. 1) and in atmospheric freezing point data.

CS_2–Hexane Isomers

In Fig. 8(b) the values of η_1/V_1 for 50–50 binary solutions of the five isomers of hexane (*n*-hexane, 3-methylpentane, 2-methylpentane, 2,3 dimethylbutane, 2,2 dimethylbutane) in CS_2 are compared as a function of pressure. The consistency of the effect of pressure on all five isomers is apparent.

The differences in the packing in CS_2 solutions indicated by the curves are also striking. Volumetrically it would be predicted that the ψ's of all isomers would be essentially identical. Thus the data indicate that the greater the degree of branching the less efficient becomes the packing.

In Fig. 9(a–c) are plotted the values of ψ for the hydrocarbon at 50 and 80 mole percent CS_2 at atmospheric pressure and 6°C and under 1000 and 7000 atmospheres at 40°C.

The results are quite consistent with pressure, but two rather surprising phenomena are present. In the first place the ratio of molar volumes between the hexanes and CS_2 is over 2 to 1, yet the values of ψ for the more highly branched isomers is nearly equal to or even slightly less than one. This can be accounted for by the picture of very inefficient packing for a hole left by a highly branched isomer. Moreover, the ψ's for the more highly branched isomers do not seem to be approaching one with increasing hydrocarbon concentration. These deviations in slope are not large, however, and it is possible that data over a wider range of concentration (these do not go above 50 percent hydrocarbon) or better cohesive energy data would eliminate the discrepancy.

In Fig. 9(d–f) are plotted the packing efficiencies η_i/V_i for the hexanes. These are very consistent among themselves at each pressure, and over the whole range of pressures. Their variation with concentration is as one would expect. A study of these packing efficiencies for other isomeric sets is most desirable and is being undertaken.

Using the theory presented in this paper, it is possible to predict thermal diffusion measurements from solubility theory or from measurements of energies of vaporization excess quantities of solutions plus a knowledge of the packing efficiency η/V. This latter quantity contributes significantly to the result. At present it is possible to establish fairly well the value of η/V for an homologous series of pairs from measurements on one or two members of the series. Otherwise the packing must be estimated by analogy to whatever data are available or by intuition. It is hoped that some more general theory of the packing efficiency can be developed.

E. L. Dougherty would like to acknowledge financial assistance from the Pan American Refining Corporation.

APPENDIX A

Effect of Nonrandomness

In the definition of W_L in Eq. (15), it was assumed that the relative probability of a hole being filled by a type one or type two molecule was in the ratio x_1/x_2. This is equivalent to the assumption of a completely random solution. Guggenheim[18] has shown that this assumption is not justifiable where the heat of mixing is nonzero.

In order to calculate the effect that nonrandomness will have upon the thermal diffusion ratio it is first necessary to adopt a model for the solution. The model adopted is the strictly regular solution ($\psi\equiv 1$) and the effect of the first approximation of Guggenheim[18] will be determined.

For this approximation, let n_1 and n_2 be the number of molecules of type one and type two, respectively, in the solution. The *quasi*-chemical equation states

$$\frac{\bar{x}^2}{(n_1-\bar{x})(n_2-\bar{x})}=\exp\left(-\frac{2W}{ZKT}\right), \tag{51}$$

where $Z\bar{x}$=No. of 1–2 pairs in the liquid, Z=coordination number, and W=interchange energy. Solving for $\bar{x}$ gives

$$\bar{x}=\frac{n_1n_2}{n_1+n_2}\frac{2}{\beta+1} \tag{52}$$

where the function β has been defined as

$$\beta=\left\{1+4x_1x_2\left(\exp\frac{2W}{ZKT}-1\right)\right\}^{\frac{1}{2}}. \tag{53}$$

Since $Z\bar{x}$ is the number of 1–2 pairs, this is also the number of bonds between molecules of type one and

[18] E. A. Guggenheim, *Mixtures* (Oxford University Press, London, 1952).

two. The total number of type one bonds in the solution is Zn_1. Hence the probability of finding a type two molecule bonded to a type one molecule is $\bar{x}/n_1$. The following definitions may then be given.

Probability of a type 2 molecule bonded to a type 1 molecule:

$$x_1''=\frac{\bar{x}}{n_1}=\frac{2x_2}{\beta+1}. \tag{54}$$

Probability of a type 1 molecule "bonded" to a type 1 molecule:

$$x_1'=1-\frac{\bar{x}}{n_1}=1-\frac{2x_2}{\beta+1}. \tag{55}$$

Probability of a type 1 molecule bonded to a type 2 molecule:

$$x_2'=\frac{\bar{x}}{n_2}=\frac{2x_1}{\beta+1}. \tag{56}$$

Probability of a type 2 molecule "bonded" to a type 2 molecule:

$$x_2''=1-\frac{\bar{x}}{n_2}=1-\frac{2x_1}{\beta+1}. \tag{57}$$

In place of Eq. (15) one will now have:

$$W_{L1}=x_1'W_{H1}+x_1''W_{H2} \tag{58a}$$

$$W_{L2}=x_2'W_{H1}+x_2''W_{H2} \tag{58b}$$

and in place of Eq. (16) and its counterpart for component two:

$$Q_1^*=W_{H1}-W_{L1} \tag{59a}$$

$$Q_2^*=W_{H2}-W_{L2}. \tag{59b}$$

Substituting Eqs. (54), (55), (56), and (57) into Eqs. (58a) and (58b), one obtains

$$W_{L1}=\left(1-\frac{2x_2}{\beta+1}\right)W_{H1}+\frac{2x_2}{\beta+1}W_{H2}$$

$$=W_{H1}+\frac{2x_2}{\beta+1}(W_{H2}-W_{H1}) \tag{60a}$$

$$W_{L2}=\frac{2x_1}{\beta+1}W_{H1}+\left(1-\frac{2x_1}{\beta+1}\right)W_{H2}$$

$$=W_{H2}-\frac{2x_1}{\beta+1}(W_{H2}-W_{H1}) \tag{60b}$$

and Eqs. (59a) and (59b) become:

$$Q_1^*=-\frac{2x_2}{\beta+1}(W_{H2}-W_{H1}) \tag{61a}$$

$$Q_2^*=\frac{2x_1}{\beta+1}(W_{H2}-W_{H1}). \tag{61b}$$

It is readily seen that these satisfy the relationship

$$x_1Q_1^*+x_2Q_2^*=0.$$

Substituting Eqs. (61a) and (61b) into Eq. (17) one obtains

$$\alpha=\frac{Q_2^*-Q_1^*}{x_1\dfrac{\partial\mu_1}{\partial x_1}}=\frac{2x_1}{\beta+1}\frac{(W_{H2}-W_{H1})}{x_1\dfrac{\partial\mu_1}{\partial x_1}}=\frac{2x_1}{\beta+1}\alpha_0 \tag{62}$$

where α_0 is the thermal diffusion ratio for a completely random strictly regular solution. See Eq. (17).

The effect of nonrandomness can now be readily seen. In regular solution theory $W/KT\cong 2$ corresponds to critical mixing, hence $(W/KT)<2$ (above T_C). Further $W=\epsilon_{11}+\epsilon_{22}-2\epsilon_{12}$ where ϵ_{ij} is the interaction potential between molecules taken with a negative sign. Hence for dispersion forces, $\epsilon_{12}=(\epsilon_{11}\epsilon_{22})^{\frac{1}{2}}$, and $W\geqslant 0$. Assuming $Z=8$, this gives $0\leqslant(W/ZKT)\leqslant\frac{1}{4}$ for all positive values of W. The maximum value of β for a given W will occur when $x_1=x_2=\frac{1}{2}$. Thus,

$$\beta_{\max}=1+4(0.25)(e^{\frac{1}{2}}-1)=1.28.$$

Substituting in Eq. (62), this gives $\alpha=\alpha_0/1.14$ a maximum correction of about 15 percent for $W>0$. If $W=0$, $\alpha=\alpha_0$.

For associated solutions ($W<0$) the effect can be estimated from the following figures. (a) If $W/ZKT=-\frac{1}{4}$ (i.e., the same magnitude as the positive W/ZKT at the critical solution temperature) then $\alpha=1.125\alpha_0$. (b) If $W/ZKT=-1$ then $\alpha=1.24\alpha_0$. (c) If $W/ZKT=-\infty$, then $\alpha=2.0\alpha_0$.

It can be seen that for nonassociated solutions the effect of nonrandomness is almost always negligible. For associated solutions it might, in some circumstances, be significant. However, for ethyl alcohol–water mixtures the maximum value of Hm is (−180) calories per mole at 25°C.[19] For $Z=4$ this gives $W/ZKT=-0.150$, and a negligible correction for nonrandomness.

APPENDIX B

Application of Theory to Ternary Mixtures

For the general case the equations become quite complicated and this treatment will be deferred until a later paper. For the case of ideal solutions, however, the equations are very simple and this case will be treated.

[19] A. G. Mitchell and W. F. K. Wynne-Jones, Disc. Faraday Soc. **15**, 161 (1953).

The general flux equation, as seen in Eq. (2), gives, for the steady state,

$$\frac{\partial\mu_1}{\partial x_1}\text{grad}\mathbf{x}_1+\frac{\partial\mu_1}{\partial x_2}\text{grad}\mathbf{x}_2=-Q_1^*\frac{\text{grad}\mathbf{T}}{T} \quad (63a)$$

$$\frac{\partial\mu_2}{\partial x_1}\text{grad}\mathbf{x}_1+\frac{\partial\mu_2}{\partial x_2}\text{grad}\mathbf{x}_2=-Q_2^*\frac{\text{grad}\mathbf{T}}{T} \quad (63b)$$

$$\frac{\partial\mu_3}{\partial x_1}\text{grad}\mathbf{x}_1+\frac{\partial\mu_3}{\partial x_2}\text{grad}x_2=-Q_3^*\frac{\text{grad}\mathbf{T}}{T}. \quad (63c)$$

The multiplication of Eqs. (63a), (63b), and (63c) by x_1, x_2, and x_3, respectively, summing the result and taking into account the Gibbs-Duhem equation gives a relationship which the net heats of transport must satisfy. Therefore,

$$x_1Q_1^*+x_2Q_2^*+x_3Q_3^*=0. \quad (64)$$

This is the analog of Eq. (11) for binary mixtures.

For an ideal solution the chemical potential may be written as

$$\mu_i=\mu_{0i}+RT\ln x_i, \quad (65)$$

where μ_{0i} is the chemical potential of pure i and is a function of temperature and pressure only. Performing the differentiations indicated in Eq. (65) and introducing the result into Eqs. (63a, b, c) gives the following steady-state separation:

$$\frac{RT}{x_i}\text{grad}\mathbf{x}_i=-Q_i^*\frac{\text{grad}\mathbf{T}}{T} \quad (66)$$

or

$$\frac{\text{grad}x_i}{x_i}=-\frac{Q_i^*}{RT}\frac{\text{grad}\mathbf{T}}{T}. \quad (67)$$

For an ideal solution Eqs. (3) and (4) reduce to these same equations for a binary system. When Eq. (8) was integrated to give Eq. (10), α was assumed constant. A comparison of Eqs. (6) and (8) reveals that this is equivalent to assuming $(Q_i^*/x_i)(\partial\mu_i/\partial x_i)$ to be constant, which for an ideal solution becomes (Q_i^*/RT). If this assumption is again made, Eq. (67) gives

$$\ln\frac{x_{iH}}{x_{iC}}=-\frac{Q_i^*}{RT}\ln\frac{T_H}{T_C}. \quad (68)$$

For an ideal solution, U_e, the excess energy of mixing is zero and Eq. (25), for the energy of detachment, becomes

$$W_{Hi}=-\frac{1}{\tau}u_i=\frac{\Delta U_i^V}{\tau} \quad (i=1, 2, 3), \quad (69)$$

where ΔU_i^V is the energy of vaporization of pure component i. Equation (28) for the energy of filling a hole becomes

$$W_L=-\frac{1}{\tau}(\sum_{i=1}^{3}x_iu_i)=\frac{1}{\tau}(\sum_{i=1}^{3}\Delta U_i^V). \quad (70)$$

The net heat of transport by Eq. (18) is

$$Q_i^*=\frac{1}{\tau}[\Delta U_i^V-\psi_i(\sum_{j=1}^{3}x_j\Delta U_j^V)]. \quad (71)$$

Application of Eq. (64) reveals the following relationship which the ψ's must satisfy:

$$x_1\psi_1+x_2\psi_2+x_3\psi_3=1. \quad (72)$$

The separation factors in Eq. (68) become

$$\ln\frac{x_{iH}}{x_{iC}}=-\frac{1}{\tau RT}[\Delta U_i^V-\psi_i\sum_{j=1}^{3}x_j\Delta U_j^V]\ln\frac{T_H}{T_C}$$

$$(i=1, 2, 3). \quad (73)$$

From Eqs. (3) and (4) it can be seen that for a binary ideal mixture analogous separation factors are obtained, *viz.*,

$$\ln\frac{x_{iH}}{x_{iC}}=-\frac{1}{\tau RT}[\Delta U_i^V-\psi_i(x_1\Delta U_1^V+x_2\Delta U_2^V)]\ln\frac{T_H}{T_C}$$

$$(i=1, 2). \quad (74)$$

In the following discussion we shall designate the separation factor by

$$\nu_i=\ln\frac{x_{iH}}{x_{iC}}\Big/\ln\frac{T_H}{T_C}. \quad (75)$$

We shall consider three cases.

Case I. Molecules of the Same Size and Shape

For this case $\psi_i=1$ $(i=1, 2, 3)$ and from Eq. (73) we obtain, for component 1,

$$\nu_1=\frac{1}{\tau RT}[\Delta\bar{U}^V-\Delta U_1^V]. \quad (76)$$

The corresponding separation factor for a binary mixture of 1 and 2 is

$$\nu_1=\frac{1}{\tau RT}[\Delta\bar{U}^V-\Delta U_1^V] \quad (77)$$

$$=\frac{1}{\tau RT}[x_2(\Delta U_2^V-\Delta U_1^V)]. \quad (77')$$

Consider a binary mixture of composition x_1, x_2, the separation factor for component 1 given by Eq. (77). If $\Delta U_2^V>\Delta U_1^V$, component 1 will concentrate at the hot wall. Now, in a mixture at the same concentration of component 1, but with some of component 2 replaced

by component 3, the separation will be enhanced if the average energy of vaporization of the ternary mixture is greater than that of the binary. If $\langle \Delta U^V \rangle$(ternary) $< \langle \Delta U^V \rangle$(binary) then the separation will be decreased. If $\Delta U_3{}^V \ll \Delta U_1{}^V$ the direction of the separation may be reversed.

It can readily be seen that the separation factor is a linear function of concentration and that no extremum in α with concentration will be obtained.

Case II. Molecules of Different Size but with the Same Packing Efficiency

For this case the ψ_i's are given by Eq. (38), *viz.*,

$$\psi_i = V_i/\bar{V} \quad \text{and} \quad \sum x_i \psi_i = 1. \tag{38}$$

From Eqs. (73) and (74) one obtains, for the separation factor ν_1 in the ternary and binary cases in Eqs. (78) and (79),

$$\nu_1 = \frac{1}{\tau RT}\left[\frac{V_1}{\bar{V}}(x_1 \Delta U_1{}^V + x_2 \Delta U_2{}^V + x_3 \Delta U_3{}^V) - \Delta U_1{}^V\right] \tag{78}$$

$$\nu_1 = \frac{1}{\tau RT}\left[\frac{V_1}{\bar{V}}\langle \Delta U_{\text{tern}}{}^V \rangle - \Delta U_1{}^V\right] \tag{78'}$$

$$\nu_1 = \frac{1}{\tau RT}\left[\frac{V_1}{\bar{V}}(x_1 \Delta U_1{}^V + x_2 \Delta U_2{}^V) - \Delta U_1{}^V\right] \tag{79}$$

$$\nu_1 = \frac{1}{\tau RT}\left[\frac{V_1}{\bar{V}}\langle \Delta U_{\text{bin}}{}^V \rangle - \Delta U_1{}^V\right]. \tag{79'}$$

Now, for the binary mixture, the separation depends on ΔU^V and on the molal volume. Consider the case $\Delta U_2{}^V > \Delta U_1{}^V$. If $V_2 < V_1$ the concentration of component 1 at the hot wall will be enhanced over the value given by Eq. (77) by the volumetric term, and *vice versa* if $V_2 > V_1$. A large enough difference in molal volumes could reverse the direction of separation. The arguments for the case $\Delta U_2{}^V < \Delta U_1{}^V$ easily follow from the equations and above discussion.

The addition of a third component will change $\langle \Delta U^V \rangle$ and $\bar{V}$. Consider again the case $\Delta U_2{}^V > \Delta U_1{}^V$. An increase in $\langle \Delta U^V \rangle$ by adding a third component of high latent heat will enhance the separation. An increase in $\bar{V}$ will work in the opposite direction. If $\Delta U_2{}^V < \Delta U_1{}^V$ the addition of a third component with large latent heat will decrease the separation while an increase in $\bar{V}$ will increase the separation. Again, the possibility exists of reversing the direction of separation by adding a third component.

Case III. Molecules Different in Size and Packing

For this case $\psi_i = (V_i + \eta_i)/V$ and $\sum \eta_i x_i = 0$. The equations for the separation factors in ternary and binary mixtures can be written as

$$\nu_1 = \frac{1}{\tau RT}\left[\frac{V_1}{\bar{V}}\langle \Delta U^V \rangle + \frac{\eta_1}{\bar{V}}\langle \Delta U^V \rangle - \Delta U_1{}^V\right] \tag{80}$$

where

$$\langle \Delta U^V \rangle = x_1 \Delta U_1{}^V + x_2 \Delta U_2{}^V + x_3 \Delta U_3{}^V \quad \text{(ternary)} \tag{81}$$

$$\langle \Delta U^V \rangle = x_1 \Delta U_1{}^V + x_2 \Delta U_2{}^V \quad \text{(binary)} \tag{82}$$

$$\bar{V} = x_1 V_1 + x_2 V_2 + x_3 V_3 \quad \text{(ternary)} \tag{83}$$

$$\bar{V} = x_1 V_1 + x_2 V_2. \quad \text{(binary)} \tag{84}$$

We shall mention here only the effect of packing efficiency on the separations discussed in Case II above.

Consider again the case $\Delta U_2{}^V > \Delta U_1{}^V$. For the binary mixture, if $\eta > 0$ (i.e., if it is possible to pack more molecules into a hole left by a type 1 molecule than is indicated by the ratio $V_1/\bar{V}$) the separation will be enhanced over that predicted by Eq. (78'). If $\eta_i < 0$ the opposite effect obtains. The arguments for the case $\Delta U_2{}^V < \Delta U_1{}^V$ follow readily.

The addition of a third component can effect η_1 in addition to changing $\langle \Delta U^V \rangle$ and $\bar{V}$. The effects of changing η_1 can be obtained from the above paragraph. At present it is not possible to estimate what molecular properties are necessary in a third component to affect η_1.

Free Electron Theory, Finite Differences, and LCAO Molecular Orbitals*

ARTHUR A. FROST
Department of Chemistry, Northwestern University, Evanston, Illinois
(Received July 2, 1954)

Simpson first called attention to the analogy between the free electron method in finite difference form and the simple LCAO molecular orbital method for electronic energy calculation. This analogy is extended to branched molecules using both the one- and two-dimensional viewpoints and also applied to a case of two electrons in interaction. It appears that the success of the free electron method is due to this similarity to the LCAO method.

SIMPSON[1] has shown the formal resemblance between the LCAO molecular orbital method for π electrons in linear conjugated systems and the free electron method (FEM) in finite difference form. Coulson[2] has recently extended this analogy using the finite difference concept to include applications to branched chains and condensed rings. A set of linear equations (and corresponding matrix equation) of a form similar to that of LCAO-MO theory has also been deduced from free electron theory by Ruedenberg and Scherr[3] and by Griffith[4] but without the use of the finite difference approximation.

The purpose of this paper is to extend the use of the finite difference concept. This leads to slightly different results than obtained by FE and LCAO-MO methods. It also makes possible a practical extension of the FE method to include electron repulsion. Perhaps most important is the conclusion that the free electron method is as successful as it is because of its analogy in finite difference form to the simple LCAO method.

ONE-DIMENSIONAL NONBRANCHED CHAINS AND RINGS

The one-dimensional free electron Schrödinger equation may be written as

$$-\frac{\hbar^2}{2m}\frac{d^2\psi}{dx^2}=E\psi \tag{1}$$

where $\hbar$ is Planck's constant divided by 2π, m the mass of the electron, x the coordinate, and E and ψ the desired one-electron energy and wave function respectively. The potential energy is taken as zero.

Consider first an open chain conjugated system such as a polyene with N π orbitals, the coordinate following zigzag along the chain. Let the nuclei be at points $x_1, x_2, \cdots, x_N$, assumed to be at a constant interval D. These points form a natural network for a finite difference approximation to the differential equation. Let the free electron wave function at these points be $\psi_1, \psi_2, \cdots, \psi_N$. For any point between the first and last the finite difference approximation for the second derivative is

$$\left(\frac{d^2\psi}{dx^2}\right)_{x=x_i}=\frac{\psi_{i-1}+\psi_{i+1}-2\psi_i}{D^2}, \tag{2}$$

and the Schrödinger equation becomes approximately

$$\psi_{i-1}+\left(\frac{2mD^2E}{\hbar^2}-2\right)\psi_i+\psi_{i+1}=0. \tag{3}$$

For the first and last orbital positions Eqs. (2) and (3) may still be used if two additional points x_0 and x_{N+1} are added at the same interval D beyond x_1 and x_N respectively and then requiring the boundary condition $\psi_0=\psi_{N+1}=0$. This situation that Eqs. (2) and (3) apply at the ends only if the additional intervals are of length D, is the most convincing argument for the usual custom of taking this particular added distance in the free electron model.

For simple ring conjugation without branching Eqs. (1)–(3) also apply. Here of course point x_N will be a neighbor to x_1 so no extra points need be introduced.

The set of N linear equations of Eq. (3) in N ψ_i requires the solution of a secular equation of the form (for chain with $N=4$)

$$\begin{vmatrix} -F & 1 & 0 & 0 \\ 1 & -F & 1 & 0 \\ 0 & 1 & -F & 1 \\ 0 & 0 & 1 & -F \end{vmatrix}=0 \tag{4}$$

where

$$F=2\left(1-\frac{mD^2E}{\hbar^2}\right). \tag{5}$$

This is of the same form as obtained with the simple LCAO theory (with overlap neglected and only nearest neighbor interaction considered) as pointed out by Simpson. The energy levels agree in spacing if the exchange integral β is set equal to

$$\beta=-\frac{\hbar^2}{2mD^2}. \tag{6}$$

* Presented at the Symposium on Molecular Structure and Spectroscopy, Columbus, Ohio, June, 1954.

[1] W. T. Simpson, J. Chem. Phys. **17**, 1218 (1949); W. T. Simpson, J. Am. Chem. Soc. **73**, 5361 (1951).

[2] C. A. Coulson, Proc. Phys. Soc. (London) **66A**, 652 (1953).

[3] K. Ruedenberg and C. W. Scherr, J. Chem. Phys. **21**, 1565 (1953).

[4] J. S. Griffith, J. Chem. Phys. **21**, 174 (1953); Proc. Cambridge Phil. Soc. **49**, 650 (1953).

The finite difference expression in Eq. (2) is only an approximation and therefore Eqs. (3) and (4) are not expected to be exact. A more accurate expression of Eq. (2) would either bring in contributions from nonneighboring points on the right side or contributions from higher derivatives[2] on the left. In either case Eq. (2), as it stands, becomes more and more accurate as the free electron wavelength becomes greater, i.e., for the lower energy levels.

Nevertheless, for the one-dimensional problems under consideration the secular Eq. (4) is exact for the free electron calculation if the parameter F is redefined. Using the notation of Ruedenberg and Scherr[3] let the free electron wave function be

$$\psi(x)=a\cos\left(\frac{\kappa x}{D}+\delta\right) \tag{7}$$

corresponding to the free electron energy

$$E=\frac{\hbar^2\kappa^2}{2mD^2} \tag{8}$$

where κ is a kind of wave number—waves per distance $2\pi D$. The phase angle is δ, and κ and δ are adjusted to satisfy boundary conditions. Now if the value of ψ of Eq. (7) at three successive points with interval D are calculated for arbitrary κ and δ, it follows from simple trigonometry that the approximation in Eq. (2) can be replaced by the exact equation

$$\left(\frac{d^2\psi}{dx^2}\right)_{x=x_i}=\frac{\kappa^2}{2-2\cos\kappa}\left[\frac{\psi_{i-1}+\psi_{i+1}-2\psi_i}{D^2}\right]. \tag{9}$$

When substituted in the Schrödinger equation, it is easily seen that the secular Eq. (4) accurately follows but with

$$F=2\cos\kappa=2\cos\left[\frac{D}{\hbar}(2mE)^{\frac{1}{2}}\right], \tag{10}$$

a result already obtained by Ruedenberg and Scherr[3] but without explicitly using the relation in Eq. (9).

Because the same form of secular equation is obtained there is an accurate correspondence between free electron wave function and LCAO coefficients as emphasized by Jaffé.[5] However the energy levels are different in the two methods because of the different relation between F and E as in Eqs. (5) and (10). In fact the ratio of the FE energy to the LCAO energy using Eq. (6) is just $\kappa^2/(2-2\cos\kappa)$, the same factor appearing in Eq. (9). This ratio approaches unity as $\kappa\to 0$ just as Eq. (9) becomes Eq. (2) in the same limit.

ONE-DIMENSIONAL TREATMENT OF BRANCHED CHAINS AND CONDENSED RINGS

The one-dimensional free electron theory for conjugated systems of π electrons with branching points was first given by Kuhn.[6] Griffith,[7] Nakajima and Kon,[8] and Perkampus[9] made similar applications. It was further developed by Griffith[4] and by Ruedenberg and Scherr[3] who also showed the analogy with the LCAO-MO method. The analogy here is not as complete as in the nonbranched systems inasmuch as the branch points require special treatment where the corresponding diagonal elements in the secular equation have an extra factor of 3/2 as compared with ordinary points.

Jaffé[5] also discussed this analogy by working back from the LCAO-MO equations to get free electron wave functions. Certain low energy states turn out to involve hyperbolic function waves. This corresponds to an imaginary wave number and a total energy lower than the potential energy everywhere except at the branching points. Thus this is not a strictly free electron solution in the ordinary sense of zero potential energy everywhere inside the box but with negative δ-function potentials implicitly added at the branching points.

The finite difference approximation of the free electron method can be carried out as in the preceding section, but the branching point must be given special treatment as follows. Consider a branching point or joint J with three neighbors K, L, and M each at distance D. A finite difference expression is needed for the one-dimensional second derivative at point J. Apply Eq. (2) to each of the three possible paths through J: KJL, KJM, and LJM. Then take the average. The result is the approximation

$$\left(\frac{d^2\psi}{dx^2}\right)_J=\frac{2(\psi_K+\psi_L+\psi_M-3\psi_J)}{3D^2}. \tag{11}$$

Another way of obtaining this result is to take one-half of the two-dimensional finite difference expression for the Laplacian of ψ at a point in a hexagonal network.[10]

Substituting Eq. (11) in Eq. (1) results in

$$\psi_K+\psi_L+\psi_M+3\left(\frac{mD^2E}{\hbar^2}-1\right)\psi_J=0. \tag{12}$$

Simultaneous solution of equations of the type of Eq. (12) for branch points and equations of the type of Eq. (3) for ordinary points leads to a secular equation identical with that of Ruedenberg and Scherr,[3] but again with the parameter F defined as in Eq. (5).

FINITE DIFFERENCE METHOD FOR A TWO-DIMENSIONAL HEXAGONAL NETWORK

Schmidt[11] and Platt[12] have both used the free electron method in two dimensions. The most obvious applica-

[5] H. H. Jaffé, J. Chem. Phys. **20**, 1646 (1952); **21**, 1287 (1953).

[6] H. Kuhn, Helv. Chim. Acta **32**, 2247 (1949).

[7] J. S. Griffith, Trans. Faraday Soc. **49**, 345 (1953).

[8] T. Nakajima and H. Kon, J. Chem. Phys. **20**, 751 (1952).

[9] H. Perkampus, Z. Naturforsch. **7a**, 594 (1952).

[10] R. V. Southwell, *Relaxation Methods in Theoretical Physics* (Oxford University Press, London, 1946).

[11] O. Schmidt, Chem. Ber. **73A**, 97 (1940).

[12] J. R. Platt, J. Chem. Phys. **22**, 1033 (1954).

tion is to condensed aromatic hydrocarbons where the π-orbitals have their centers on a hexagonal network. Coulson[2] has shown how to apply finite differences to this case.

The finite difference approximation for the Laplacian of ψ as given by Southwell[10] is

$$(\nabla^2\psi)_J=\frac{4(\psi_K+\psi_L+\psi_M-3\psi_J)}{3D^2}. \tag{13}$$

When substituted in the two-dimensional Schrödinger equation for a free-electron difference, equations of the following form result

$$\psi_K+\psi_L+\psi_M+3\left(\frac{mD^2E}{2\hbar^2}-1\right)\psi_J=0 \tag{14}$$

with J any point in the π-electron network and K, L, and M its three neighbors. The network is considered extended with fictitious orbitals so as to provide every actual orbital with three neighbors. The fictitious orbitals are taken with zero coefficient, corresponding to a boundary for the free electron box one bond length away from the last actual π-orbital in each direction.

The result of this finite difference approximation for a molecule with N π-orbitals is a set of N linear equations as seen in Eq. (14) and an Nth degree determinantal secular equation like Eq. (4). The off-diagonal elements in the latter are zero except for elements connecting neighbors, which are unity. The diagonal elements are all equal. If each of these is designated as $-F$, F now has the value

$$F=3\left(1-\frac{mD^2E}{2\hbar^2}\right). \tag{15}$$

This differs from the one-dimensional result for branched chains or condensed rings not only in the expression for F, Eq. (5), but also in that branching points have the same coefficient in the diagonal element as do ordinary points. This two-dimensional finite difference treatment shows exact agreement with the simple LCAO-MO calculation in the form of the wave function, in the sense that the coefficients of the atomic orbitals in the LCAO method are in the same ratio as the values of the free electron wave function at the particular nuclei or orbital centers. There is also exact agreement in energy level spacing if the LCAO exchange integral is

$$\beta=-2\hbar^2/3mD^2. \tag{16}$$

However, this differs from the one-dimensional result Eq. (6).

Unbranched chains or rings can also be included in this two-dimensional treatment, a zigzag chain fitting naturally in the hexagonal network.

Therefore, in all cases of conjugated hydrocarbons that fit onto a hexagonal network there is accurate correspondence between the two-dimensional free electron theory in finite difference approximation and the simple LCAO-MO method with β given by Eq. (16). On the other hand, there appears to be no simple exact relation of the type of Eq. (9) for two dimensions to take the place of the approximation given by Eq. (13), so that an exact free electron wave function (in contrast with its finite difference approximation) does not in general correlate quantitatively with the simple LCAO-MO coefficients. Furthermore, the energy levels not only differ in spacing but can also differ in order.

CALCULATIONS

Two examples will now be given to illustrate how the one- and two-dimensional finite difference approximations compare with free electron and LCAO methods for one-electron energy levels and also to show a possible extension of free electron methods to electronic interaction.

Example 1. Benzene

With six π-orbitals there is the familiar sixth degree secular equation which in terms of the energy parameter F is the same for all methods. The solutions are

$$F=2,\ 1,\ 1,\ -1,\ -1,\ -2$$

with corresponding one-electron energies calculated from Eqs. (5) and (15).

$$\text{One dimension:}\quad E=\frac{\hbar^2}{2mD^2}(0,\ 1,\ 1,\ 3,\ 3,\ 4).$$

$$\text{Two dimensions:}\quad E=\frac{2\hbar^2}{3mD^2}(1,\ 2,\ 2,\ 4,\ 4,\ 5).$$

Besides a shift of the lowest level due to a zero point energy in the two-dimensional theory not present in the one-dimensional ring, the level spacing is 4/3 times as great in the two-dimensional case.

To compare with experiment and with predictions of other methods consider the excitation of an electron from $F=1$ to $F=-1$. The various calculations result as follows (using $D=1.40$ A):

One-dimensional finite difference

$$\Delta E=\hbar^2/mD^2=31\,600\ \text{cm}^{-1}.$$

Two-dimensional finite difference

$$\Delta E=4\hbar^2/3mD^2=42\,200\ \text{cm}^{-1}.$$

One-dimensional free electron

$$\Delta E=52\,300\ \text{cm}^{-1}.$$

LCAO-MO with overlap

$$\Delta E=49\,100\ \text{cm}^{-1}.$$

Experimental, using singlet-triplet center of gravity

$$\Delta E=43\,400\ \text{cm}^{-1}.$$

The last three values are quoted from Scherr.[13] It is interesting to note that the experimental value agrees best with the value calculated by the two-dimensional finite difference approximation. Although considerations of the last section lead one to expect this to be preferred over the one-dimensional theory, all of these methods are sufficiently crude so that any accurate agreement with experiment probably is coincidental.

Example 2. The Hydrogen Molecule

Although the free electron method is usually applied only to π-electrons, it is of interest to see what it can do with a molecule such as H_2 inasmuch as this is the simplest molecule in which interelectronic repulsion appears. Each of the two electrons can be considered to move one-dimensionally along the internuclear axis. The two-electron problem is then equivalent to a single particle in two dimensions with a square array of points representing possible positions of the two electrons at the two nuclei *a* and *b*. Figure 1 shows such a square network with a free electron boundary drawn one bond length away in each direction. The interior points can be designated as *aa*, *ab*, *ba*, and *bb*, using the first and second symbol to represent the positions of the first and second electron respectively. The first and last of these points, *aa* and *bb*, correspond to ionic states while the second and third, *ab* and *ba*, represent covalent states in analogy to the valence-bond method.

The four points provide a natural network for a finite difference approximation. For such a network with four nearest neighbors the two-dimensional Laplacian of the wave function is approximated by[10]

$$(\nabla^2\psi)_P=(\psi_A+\psi_B+\psi_C+\psi_D-4\psi_P)/D^2 \qquad (17)$$

where A, B, C, and D are the four neighbors of point P. In the present application two of the neighboring points are on the boundary, and the corresponding values of ψ are taken to be zero.[14] A fourth degree secular equation

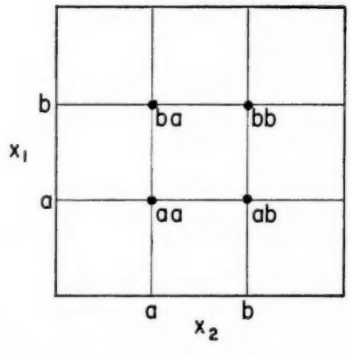

FIG. 1.

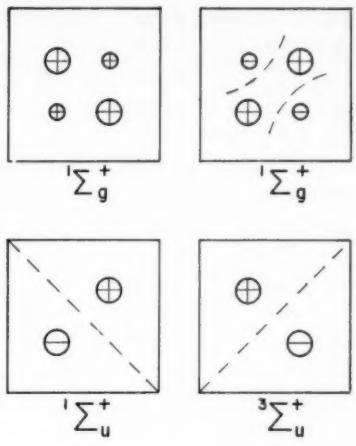

FIG. 2.

results such that

$$\begin{vmatrix} E'+\Delta & 1 & 0 & 1 \\ 1 & E' & 1 & 0 \\ 0 & 1 & E'+\Delta & 1 \\ 1 & 0 & 1 & E' \end{vmatrix}=0 \qquad (18)$$

where

$$E'=\frac{2mD^2}{\hbar^2}(E-V_C)-4$$

and

$$E'+\Delta=\frac{2mD^2}{\hbar^2}(E-V_I)-4.$$

The potential energies at covalent and ionic points are V_C and V_I, respectively, and Δ is V_I-V_C in units of $\hbar^2/2mD^2$. For a strictly free electron calculation the potential energy inside the box would be constant and Δ would be zero. There would be three equally spaced energy levels with the middle one double.[15]

To take account of the electron repulsion accurately on the free electron model would be difficult as there would be an infinite potential ridge on the box diagonal where $x_1=x_2$, the repulsive potential increasing like $1/|x_1-x_2|$. The finite difference method can handle this much more easily by choosing an appropriate value for Δ. Since the points such as *aa* and *ab* are analogous to ionic terms and covalent terms respectively, a sensible choice of V_I-V_C would appear to be the difference between the ionization potential and electron affinity of the hydrogen atom. Taking this to be 13.6−0.8=12.8 ev and D=0.74 A (equilibrium distance for ground state of H_2) Δ=1.88 (dimensionless). Solution of Eq. (18) yields E' values of −3.16, −1.88, 0, and 1.28. The corresponding energy values, when the lowest state is arbitrarily taken as the zero of energy, are E=0, 8.7, 21.5, 30.2 ev, and the wave functions are easily seen to correspond to the states $^1\Sigma_g^+$, $^3\Sigma_u^+$, $^1\Sigma_u^+$, and $^1\Sigma_g^+$ respectively.

[13] C. W. Scherr, J. Chem. Phys. **21**, 1582 (1953).

[14] This same network and Eq. (17) can be used for a one-electron four-membered ring such as in the cyclobutadiene problem. The energy-level spacing turns out to be the same as in the one-dimensional treatment in this case in contrast to the benzene problem.

[15] This is equivalent to a ring of four orbitals and follows easily using the mnemonic device published by A. A. Frost and B. Musulin, J. Chem. Phys. **21**, 572 (1953). This author wishes to acknowledge that he has heard since publication that a similar scheme had previously been used, without publication, by H. C. Longuet-Higgins.

Figure 2 includes diagrams of these four wave functions which show the relative signs at the four points and qualitatively indicating relative magnitudes of covalent and ionic terms by the size of the circles. Perhaps the greatest value of this example is the simple way in which one can, with its aid, visualize the relation of valence bond and molecular orbital methods and the fact that resonance between covalent and ionic terms leads to the same set of states as the use of products of molecular orbitals with configuration interaction, as shown generally by Longuet-Higgins.[16] Unfortunately, for systems of more than two electrons the spin functions do not factor out so that this geometric scheme is not easily generalized.

The states are in the expected energy order, and the excitation energies are probably of the right order of magnitude considering that these are for vertical excitations with D constant. Although the appropriate value of D for each stable state could be inserted in calculating its energy, this would not appear to be significant since the free electron theory in its usual form gives no sensible result for electronic energy as a function of internuclear distance, the energy decreasing with increasing distance instead of increasing.

DISCUSSION

In this paper the finite difference approximation has been used only in its crudest form with such a course network of points that there is only one for each atomic orbital in the one electron model. Although finer networks have been used[17,18] in order to get more exact solutions to the Schrödinger equation in cases of variable potential energy, the purpose of this article has been to show the relation to the LCAO-MO method which purpose requires just this course network. The result is that with the two-dimensional finite difference approximation there is complete agreement between the values of the wave function at these network points and the coefficients of atomic orbitals in the LCAO-MO method. Furthermore, the energy levels agree if the exchange integral is chosen appropriately in the *simple* LCAO-MO. The free electron method without finite difference approximation gives somewhat different energy levels which however can be made to agree closely with those obtained by LCAO-MO *with overlap*. There seems to be no way to relate the finite difference approximation directly to the latter method.

The free electron method has been phenomenally successful in predicting various spectroscopic results with hardly any necessity for using an arbitrary parameter. On the other hand, it has serious defects. One defect is that on the usual basis of an infinite potential well there is no finite ionization potential predicted. To be sure a more refined model with a finite potential well can give a sensible result[17,19] but only at the expense of a more difficult calculation.

A more serious defect is the inability of the simplest model to give electronic energy as a suitable function of internuclear distance. This has been alluded to in Example 2 above on H_2. Even if one uses a finite potential well, it would be necessary to decrease its depth in some fashion as its width increases with increasing internuclear distance. It appears to be accidental that the excitation energy calculations are as good as they are for the normal internuclear distance of π-orbitals in conjugated hydrocarbons, unless it is really true that for just this situation the electronic potential energy is nearly constant through the conjugated system and that interelectronic repulsions can be neglected.

The general conclusion from the finite difference considerations of this paper is that the free electron method is successful primarily because of its close relationship to the simple LCAO-MO method.

ACKNOWLEDGMENT

The author takes pleasure in acknowledging helpful discussion with J. R. Platt, K. Ruedenberg, C. W. Scherr, and W. T. Simpson, but points out that his conclusions are not necessarily shared by them.

This research was supported by a grant from the National Science Foundation.

[16] H. C. Longuet-Higgins, Proc. Phys. Soc. (London) **60**, 270 (1948).
[17] N. S. Bayliss and J. C. Riviere, Australian J. Sci. Research **4A**, 344 (1951).
[18] W. T. Simpson, private communication.
[19] S. Nikitine and S. G. Komoss, J. phys. et radium **12**, 635 (1951).

Kinetics of the Thermal *Cis-Trans* Isomerization of Dideuteroethylene*

JOHN E. DOUGLAS,† B. S. RABINOVITCH, AND F. S. LOONEY
Department of Chemistry, University of Washington, Seattle, Washington
(Received July 12, 1954)

The thermal *cis-trans* isomerization of *trans*-ethylene, d_2 has been studied from 450° to 550°C over a pressure range of 0.9 cm to 31 cm Hg in two quartz reactors. The rate is pressure dependent over the entire pressure range. It is concluded that at 0.9 cm the reaction is a homogeneous, unimolecular reaction. A high pressure activation energy of 65 kcal and frequency factor of 10^{13} sec^{-1} are deduced. At higher pressures the reaction is sensitized by processes attendant on polymerization, which occurs as a side reaction with propylene as the principal product. The relation of this study to other work on substituted ethylenes is discussed briefly, as well as a few other topics pertinent to the results obtained.

THE gas phase thermal *cis-trans* isomerization reactions of substituted ethylenes, studied extensively by Kistiakowsky and co-workers,[1] are believed to constitute examples of homogeneous, unimolecular reactions. The reactions fall into two categories; those reactions which possess an essentially normal frequency factor and a high activation energy, approximately 43 kcal, and those characterized by a low frequency factor, 10^5 or less, and low activation energy, around 20 kcal.[2] Magee, Shand, and Eyring (MSE)[3–5] have interpreted these reactions quantitatively, on the basis of absolute rate theory, in terms of the electronic potential energy surfaces for ethylene; a general analysis of the electronic states of ethylene has been given by Mulliken[6] whose notation is employed here. MSE proposed their well-known "singlet" and "triplet" mechanisms according to whether the reaction proceeds entirely *via* the singlet electronic state N or involves a switch to the triplet state T at $\phi<\pi/2$, where ϕ is the torsion angle.

In the present paper are presented the details of a study of the gas phase, thermal isomerization of *trans*-ethylene, d_2, together with a few results for the reverse isomerization of *cis*-ethylene, d_2. The kinetics of *cis-trans* isomerization of ethylene, d_2, are of interest since this molecule is the simplest prototype of a disubstituted ethylene. Also, information may be obtained concerning the electronic energy levels of ethylene. The isomerization of ethylene, d_2 should proceed by the singlet mechanism in the absence of effective collisional perturbations, since the spin-orbit interaction connecting the singlet and the triplet states is very small.[3] The nature of the binding, bond distances, etc. are essentially unaltered in dideuteroethylene relative to light ethylene. Applying the Born-Oppenheimer approximation, the activation energy for isomerization of ethylene, d_2 is related to the height of the lowest singlet state in perpendicular light ethylene (N'). The energies of the electronic states of ethylene have been the subject of a considerable number of calculations.[6,7] Isomerization studies made with substituted ethylenes such as stilbene or butene cannot reliably be employed to assist in the calibration of these calculations inasmuch as the energy of a particular state of a substituted ethylene may vary appreciably from that in ethylene itself.[6,8]

A preliminary account of some of this work has already been given.[9]

EXPERIMENTAL

Materials

Cis-ethylene, d_2 was prepared by reduction of acetylene, d_2 with a zinc-HCl couple.[10] Mass spectrographic

* This work was supported by the Office of Naval Research under Contract No. N8-52009 with the University of Washington. Presented to the Division of Inorganic and Physical Chemistry, American Chemical Society, Sept., 1953.

† Present address: Department of Chemistry, University of Wyoming, Laramie, Wyoming.

[1] (a) G. B. Kistiakowsky and M. Nelles, Z. Physik. Chem., Bodenstein Festband, 369 (1931); J. Am. Chem. Soc. **54**, 2208 (1932); (b) G. B. Kistiakowsky and W. R. Smith, *ibid.* **56**, 638 (1934); **57**, 269 (1935); **58**, 766, 2428 (1936).

[2] See also M. Calvin and H. W. Alter, J. Chem. Phys. **19**, 768 (1951).

[3] Magee, Shand, and Eyring, J. Am. Chem. Soc. **63**, 677 (1941).

[4] Hulburt, Harman, Tobolsky, and Eyring, Ann. N. Y. Acad. Sci. **44**, 371 (1943).

[5] Glasstone, Laidler, and Eyring, *The Theory of Rate Processes* (McGraw-Hill Book Company, Inc., New York, 1941), p. 323; see also H. McConnell, J. Chem. Phys. **20**, 1043 (1952).

[6] (a) R. S. Mulliken, Phys. Rev. **41**, 751 (1932); **43**, 297 (1933); (b) R. S. Mulliken and C. C. J. Roothaan, Chem. Revs. **41**, 219 (1947).

[7] Some of these are (a) R. G. Parr and B. L. Crawford, Jr., J. Chem. Phys. **16**, 526 (1948); (b) D. P. Craig, Proc. Roy. Soc. London **A200**, 272 (1950); (c) S. L. Altmann, Proc. Roy. Soc. London **A210**, 343 (1952); (d) R. Pariser and R. G. Parr, J. Chem. Phys. **21**, 767 (1953); (e) M. Wolfsberger, *ibid.* **21**, 943 (1953); (f) W. Moffitt and J. Scanlan, Proc. Roy. Soc. (London) **A218**, 464 (1953).

[8] In this connection an interesting question arises which could affect the interpretation of *cis-trans* isomerization given by MSE and others (see references 3–5). These authors identified the high range of isomerization activation energies (40–45 kcal) found for substituted ethylenes with the height of the singlet barrier for ethylene. At the time of their work, the accepted value for the ethylene torsional frequency, $\omega_4=825$ cm^{-1}, as they pointed out, would correspond on the basis of a parabolic potential function for torsion to a not unreasonable value of 20 kcal "resonance" stabilization at $\phi=\pi/2$. Subsequently, however, Arnett and Crawford [R. L. Arnett and B. L. Crawford, Jr., J. Chem. Phys. **18**, 118 (1950); Crawford, Lancaster, and Inskeep, *ibid*, **21**, 678 (1953)] showed that $\omega_4=1027$ cm^{-1}, a value which on the same basis seems incompatible with a barrier height in ethylene ~43 kcal. The resolution of this problem might conceivably involve the validity of the Eyring mechanism; for example, interaction of N and V states, for $\phi<\pi/2$, *could* be the singlet mechanism; such a possibility animated some of our early interest in this problem.

[9] Rabinovitch, Douglas, and Looney, J. Chem. Phys. **20**, 1807 (1952).

[10] B. S. Rabinovitch and F. S. Looney, J. Am. Chem. Soc. **75**, 2652 (1953).

and infrared analysis showed the products to be 98.8 percent *cis*-ethylene, d_2 with ethylene, d_1 as the major impurity, together with a trace of higher weight material.

Trans-ethylene, d_2 was prepared in 99 percent purity by reduction of acetylene, d_2 in chromous chloride solution.[10] The sole impurity was ethylene d_1.

Methane, helium, and nitrogen were obtained commercially. They were passed through cold traps and over heated copper to remove oxygen. Mass spectrographic analysis showed no detectable impurities (<0.01 percent oxygen).

All other materials were prepared or obtained commercially in the purest grade available and were purified further by various distillation procedures.

Analysis

Analyses for *cis*- and *trans*-ethylene d_2 were made from their infrared spectrum by means of a Beckman IR-2 spectrophotometer, equipped with a Brown recorder. Empirical calibration curves for the 842 cm^{-1} *cis* band and the 987 cm^{-1} *trans* band were established with known *cis-trans* mixtures at two standard total pressures. The accuracy obtainable from the *cis* line appreciably exceeded that of the other. Analytical error is estimated at around 5 percent, but varied somewhat with the percentage of *cis* in the sample.

Analysis of ethylene exchange products was made with a Consolidated 21-103 mass spectrograph. Pure ethylenes, d_0, d_2 (*cis* and *trans*), and d_4 were available. The patterns for ethylenes, d_1 and d_3 were estimated from the others by applying statistical considerations.

Higher products were also estimated mass spectrographically. Propylene was the principal one formed; its breakdown pattern was modified for the various possible deutero-derivatives by applying simple statistical considerations.

Apparatus and Procedure

A conventional Pyrex vacuum system was used. The reaction bulbs were of fused quartz. Three reactors were used. Two were spherical and had volumes of 35 cc and 175 cc; the smaller reactor was used for runs at 8.6 cm and higher; the larger reactor was used at 8.6 cm and lower; shortage of materials at the time forced the use of relatively small vessels. The third reactor was filled with quartz chips and had a volume, after packing, of 103 cc. The surface to volume ratio was nominally seven times that for the 175 cc reactor; the ratio was actually greater, since the packing was in part translucent fused quartz which contained many capillaries.

The reaction furnace was a lagged copper tube 16 in. long and 6 in. in diameter, wound in sections and stirred by a fan. A gradient of less than one degree existed over the reactor and the temperature was volume averaged. Temperature fluctuation during a run was less than $\pm 0.5°$.

Rate runs were made as follows. The apparatus was evacuated to approximately 10^{-4} mm or better. The desired pressure of ethylene was admitted to the reactor. After a given reaction time, the sample was quickly pumped into a liquid nitrogen trap. Following infrared analysis, the sample was frozen into the reactor section, volatilized rapidly and allowed to react further. In general, analyses were obtained at four reaction times from one ethylene sample, and two or more samples were run under each experimental condition. Runs were usually not carried beyond 45 percent reaction.

Runs with addends were handled similarly; if removal of the addend was necessary for pumping or analytical purposes, a fresh sample was employed for each point in a run. Higher products were removed from certain high pressure runs by fractionating the ethylene from the less volatile products at $\sim -160°C$.

Standardization of the Reactor; Seasoning

It was necessary to poison the reactor with ethylene before the rate slowed down to a reproducible value. After the larger bulb was seasoned, only small fluctuations in activity occurred; however, the activity eventually would increase, perhaps due to a leak, necessitating reseasoning. The activity of the bulb was checked periodically against defined standard conditions. A standard rate was the lowest rate attainable under certain given conditions; this rate was reproducible. Admission of air to the bulb for any reason made reseasoning necessary. It was much more difficult to season the smaller reactor and, under the same reaction conditions, the lowest rate attainable was higher than in the large bulb.

RESULTS

Handling of the Data

The analytical and rate data were corrected for (a) dead space, a correction which varied from 2 percent to 5 percent depending upon the reactor; (b) a small loss of sample on transfer for analysis; (c) the existence of by-products from side reactions; and (d) small variations in the reactor activity from the standard value.[11] Velocity constants were calculated under the assumption that the opposing first order reactions were equal. This assumption of equality was based upon the following evidence. Equilibration of *trans*-ethylene d_2 catalysed by iodine gave mixtures in the region 250–350°C which averaged 51.5 percent *trans*.[12a] Debromination of a 50–50 mixture of *meso*- and *d,l*-dibromodideuteroethylene by sodium (ammonia) gave a product averaging 49.7 percent *trans*.[12b] Results with mercaptan at

[11] Details of the corrections and of typical runs may be found in J. E. Douglas, Ph.D. thesis, University of Washington (1952).

[12] (a) B. S. Rabinovitch and N. R. Larson, unpublished results; (b) Schubert, Rabinovitch, Larson, and Sims, J. Am. Chem. Soc. **74**, 4590 (1952).

520°C, cited later, show no temperature coefficient of the equilibrium constant.

Variation of Rate with Pressure

The rate of isomerization was determined at 520.7°C from 0.9 cm to 31.2 cm, and in less detail at other temperatures (Table I). The dependence of rate on pressure varies somewhat with pressure but is less than second order. The discontinuity at 8.6 cm results from the change over in reactors in this pressure.

The rate of reaction was also measured in the presence of inert gases (Table I). In this connection it may be mentioned that it has been found that our nitrogen sample gave no acceleration of the rate of the nitric oxide catalysed isomerization of ethylene, d_2, a reaction which is appreciably more sensitive to traces of oxygen than is the present one.

Dependence of Rate on Temperature

The dependence of the rate on temperature at constant concentration, for several concentrations, is presented in Table II. All the data in the present study refer to the *trans* compound aside from the results in Table II labelled *cis*. Frequency factors and activation energies were calculated using the Arrhenius equation. The parameters of the plot of $\log k - 1/T$ were calculated by least squares. The error in the observed activation energy has been estimated to be ± 1.2 kcal. The probable error of an individual measurement within a given run was usually less than 3 percent of average rate constant; (this was true even at higher pressures where the reaction is shown to be complex). A larger systematic error has been assumed, however, due to the small variation in condition of the reactor between runs mentioned earlier.

TABLE I. Variation of observed rate of isomerization of *trans*-ethylene, d_2 with pressure (520.7°C).

Run	Pressure cm	Addend	$k \times 10^5$ sec^{-1}
175 cc reactor			
112	0.90		3.96
127	2.48		5.50
42, 48	3.76		6.30
7 A		60 cm nitrogen	9.9
8 A		52 cm nitrogen	9.7
3 A		35 cm nitrogen	9.1
4 A		34 cm nitrogen	8.9
5 A		19 cm nitrogen	8.2
6 A		7.4 cm nitrogen	7.4
52		27 cm methane	12.1
128	6.69		8.8
9 A	7.44		9.3
108	8.6		10.1
35 cc reactor			
58	8.6		12.4
59	12.1		14.4
64	15.7		16.2
60	18.6		17.1
74	25.1		20.6
75	31.2		25.3

TABLE II. Rate data and Arrhenius parameters for the isomerization of *trans*-ethylene, d_2.

Run	Pressure cm	Temperature °C	$k \times 10^5$ sec^{-1}	E kcal	A sec^{-1}
large reactor					
121	0.93	550.5	14.3		
114	0.93	544.0	10.4		
119	0.91	532.5	6.4	61.3	3.2×10^{12}
112	0.90	520.7	3.96		
117	0.88	504.4	1.47		
125	3.90(*cis*)	544.0	16.2		
47	3.89	543.6	18.6		
42, 48	3.76	520.7	6.30		
124	3.76(*cis*)	520.2	6.66		
46	3.74	504.4	2.98		
126	3.74(*cis*)	504.4	2.79	60.8	3.3
54	3.60	483.5	0.95		
44	3.47	458.1	0.230		
105	8.7	532.5	17.4		
108	8.6	520.7	10.1	59	2
109	8.4	504.4	4.55		
small reactor					
58	8.6	520.7	12.4		
81	8.4	504.4	6.08		
80	8.2	483.5	2.76	49.4	4.5×10^9
82	7.9	459.3	0.850		
60	18.6	520.7	17.1		
69	18.2	504.4	10.2		
62, 65	17.7	483.5	4.29	46.5	1.0
70	17.2	459.3	1.45		
75	31.2	520.7	25.3		
85	30.3	494.9	10.0		0.30
84	29.2	471.0	3.74	44.0	
86	28.4	450.0	1.72		

Tests of Elementary Nature of the Isomerization

A number of experiments were performed in an effort to assess the elementary nature of the isomerization and the importance of heterogeneity.

Heterogeneous Reaction

The packed reactor was used to evaluate the extent of heterogeneous reaction. After three poisoning periods k came down to 7.25×10^{-5} sec^{-1} at a pressure of 3.8 cm at 520.7°C, compared to a standard value of 6.30×10^{-5} sec^{-1} in the 175 cc reactor. This acceleration corresponds to less than 2 percent heterogeneous reaction in the 175 cc vessel. This work was done during our earliest experience with seasoning and probably more effective poisoning would have reduced the rate in the packed bulb further. Other evidence is discussed later for the negligible role of heterogeneous reaction in the large seasoned vessel.

Oxygen

Storch,[13] in the study of ethylene polymerization, found an acceleration by traces of oxygen. The isomerization of ethylene might possibly be catalyzed by oxygen and some runs were made to gauge the magni-

[13] H. H. Storch, J. Am. Chem. Soc. **57**, 2598 (1935).

TABLE III. Effects of addends on isomerization and side reactions of *trans*-ethylene, d_2.

Run	Addend mm	Pressure cm	Temperature °C	$k \times 10^5$ sec^{-1}	t min	reaction percent	polym. percent	exchange percent
42, 48	...	3.8	520.7	6.3	75	48	0.1	<1.0
58	...	8.6	520.7	12.4				
86	...	28.4	450.0	1.7	275	38	4.7	3.4
	oxygen							
23	1.0	3.8	520.7		2	26	0.3	2.0
		3.8	520.7		24	50	0.6	5.0
		3.8	520.7		30	63	0.6	6.3
26	0.2	3.8	520.7	8.4	55	53	0.1	2.2
22	0.02	3.8	520.7		56	38	0.1	0.6
19, 20	0.01	3.8	520.7	6.3				
	azomethane							
28	1.0	3.8	520.7	17.5	14	36	0.5	3.0
		3.8	520.7		20	42	0.5	2.0
29	0.1	3.8	520.7	11.5	30	40	0.3	3.2
	nitric oxide							
33	0.2	3.8	520.7	8.9	54	46	0.1	0.2
77	0.5	8.6	520.7	18.5				
14	5.0	28.4	450.0	8.6	70	51	0.6	0.2
	butene-2							
72	0.2	8.6	520.7	13.6				
	propylene							
76	0.2	8.6	520.7	15.0				
	packing							
34, 35	unseasoned	3.8	450.0		70	61	0.25	2.7
36	seasoned	3.8	450.0	7.25	70	48	0.1	1.2

tude of this factor. With 1 mm oxygen (see Table III for conditions) there was fast initial isomerization, the rate being roughly ten times normal; later in the run the rate became slower. With 0.2 mm oxygen the rate was 35 percent greater than normal. Runs made with 10^{-2} -10^{-4} mm oxygen gave deviations from the normal rate within experimental error. At these lower pressures oxygen was also without effect on side reactions of exchange and polymerization. It is concluded that oxygen traces in the ethylene, on the walls of the apparatus, or occluded in stopcock grease, had negligible effect on the rate.

After each run with oxygen in the higher pressure range (above 10^{-2} mm) the reactor activity increased, necessitating reseasoning between runs.

Ethyl Mercaptan

Storch[13] showed in his work on the effect of oxygen impurity that small quantities of ethyl mercaptan brought the rate of polymerization of ethylene into agreement with the lowest rates reported for the most highly purified ethylene. In our work, runs were also made with 0.2 mm of ethyl mercaptan at 3.8 cm ethylene and 520.7°C. Reaction for ten minutes, which normally produced less than 4 percent *cis*, gave a *cis-trans* mixture of 50–50 proportions. Since hydrogen sulfide is a decomposition product of ethyl mercaptan, this substance was also investigated and a similar catalysis was obtained. No polymerization or exchange occurred. 0.2 mm water had no effect.

Free Radicals

The effect of free radicals on isomerization was investigated by adding azomethane (Table III). Very rapid initial reaction occurred, after which the reaction slowed and proceeded at a rate only somewhat faster than normal. For example, with 1 mm of azomethane present, extrapolation to zero time gave an intercept of 5.6 percent *cis* formed "instantaneously"; the same procedure applied to a run with 0.1 mm azomethane present gave an intercept of less than 3 percent *cis* at zero time. Hence free methyl radicals accelerate the rate of isomerization, probably are destroyed during the course of reaction, and are somewhat more efficient in lower concentrations.

Stopcock grease vapor was shown to be without effect on the reaction.

Nitric Oxide

The effect of small amounts of nitric oxide alone was explored (Table III). Interestingly enough, an acceleration of the rate was found showing that nitric oxide catalyzes reaction. At the same time, side reactions of polymerization and exchange, which therefore presumably arise largely from free radical processes, were greatly reduced.

Polymer

Since higher olefins were produced during isomerization, the effect of this material was investigated by removing most of the polymer by periodic fractionation during some runs. At a high pressure of 28.2 cm ethylene and 450.0°C, conditions which normally produced 4.7 percent polymer in 275 min, a fractionated run showed only 0.5 percent polymer present after 240 minutes; at 240 min, 15 percent *cis* was formed, compared to the normal amount of 19.5 percent.

At a rather lower pressure of 7.4 cm ethylene and

521°C in a run which went to 22 percent reaction, fractionation reduced the average velocity constant in the second half of the run from 9.3 to 9.0×10^{-5} sec^{-1}.

The effect of added propylene and butene-2 was also examined by adding 0.2 mm (2.4 percent) of either substance to 8.5 cm, 520.7°C runs (Table III). The overall rate constants obtained were 10–20 percent larger than the normal rate, with a somewhat more rapid initial rate. Hence higher olefins accelerate the rate of isomerization.

Side Reactions

As mentioned above, exchange and polymerization occurred simultaneously with isomerization. The exchange products were ethylene, d_1 and d_3. The principal polymerization products (>85 percent) were propylene d_2, d_3, and d_4, the remainder being essentially butene.

Both polymerization and exchange products increased approximately linearly with time in a given run. These products became relatively more important at higher ethylene pressure and lower reaction temperature. Percentage polymerization, when measured at a fixed amount of isomerization, increased linearly with pressure of the run. Only 0.1 percent polymer was formed at 3.8 cm ethylene pressure, 520°C (the amount of polymerization at 0.9 cm, 520°C, is estimated at 0.025 percent); this increased to nearly 5 percent at 28.2 cm, 450°C. These figures refer to 20 percent *cis* formation. Exchange under these conditions increased from <1 percent to 5 percent (illustrative data given in Tables III and IV).

No increase over the normal amount of exchange was found with a mixture of two cm each of ethylene, d_0 and d_2 at 520°C in a time such that 42 percent isomerization occurred. Similar results were obtained in a number of runs in which a complex mixture of deuteroethylenes at 10 cm and 500° was employed.

Oxygen and azomethane addends increased the amount of polymerization and exchange. Nitric oxide greatly reduced the extent of these reactions.[14] Side reactions in the seasoned packed reactor were similar in magnitude to those in the 175 cc reactor (Table III).

There is a significant difference between the polymer products found here and those reported in the literature for homogeneous studies in glass. Although the reported products vary considerably, four-carbon materials have usually been found in the largest amounts. Even in the (homogeneous) study of Frey and Smith[15] done in a silica reactor, an instance of relatively high propylene formation, only 29 percent of the product was propylene. It has been suggested[4] that Frey's result was due to the silica vessel employed.

[14] See (a) E. W. R. Steacie, *Atomic and Free Radical Reactions* (Reinhold Publishing Corporation, New York, 1946), Ch. IV; (b) K. J. Laidler, Chemical Kinetics (McGraw-Hill Book Company, Inc., New York, 1950), Ch. 12, for discussion and references on polymerization of ethylene.

[15] F. E. Frey and D. F. Smith, Ind. Eng. Chem. **20**, 948 (1928).

TABLE IV. Some data on rates and activation energies for polymerization of *trans*-ethylene, d_2.

Run	p(520.7°C) cm	Temperature °C	Rate: percent min$^{-1}\times10^3$	E kcal
175 cc reactor				
19, 24	3.8	520.7	0.18	50
45, 102		483.5	0.040	
40	8.6	520.7	0.66	40
104		459.3	0.10	
35 cc reactor				
...	8.6	520.7	0.68[a]	25
82		459.3	0.18	
60	18.7	520.7	1.9	20
		520.7	2.1	
69		504.4	2.1	
65		483.5	1.1	
70		459.3	0.84	
75	31.2	520.7	5.6	20
84		471.0	2.1	
86		450.0	1.7	

[a] Obtained by extrapolation from results at higher pressures.

Other information on polymerization from the present work is as follows. On the one hand, the amounts of polymer and exchange were not affected by the increased surface of the seasoned packed vessel, showing presumably that adequate seasoning eliminates heterogeneity (the same reactor with little seasoning gave higher amounts of side reactions); on the other hand, higher rates of polymerization were found in the small reactor (Table IV, 8.6 cm). Over the pressure range of this study no significant difference was noted in the polymer composition. The activation energies for the polymerization reaction were calculated; in the 175 cc reactor E_p was 40–50 kcal and in the 35 cc reactor E_p was 20–25 kcal (Table IV). These values are order of magnitude only, because the number of data was relatively small, and because the measurement of the smaller quantities of polymer may involve considerable error. The decrease in E_p coupled with the increase in rate of polymerization on going from the large to small bulb at a given pressure shows the influence of heterogeneity; the apparent decline in E with increase of pressure and the results with nitric oxide reveal the effect of chain or radical processes. If the reaction in a well seasoned vessel is truly homogeneous as indicated by the results in the packed reactor, the reason for the predominance of propylene product rather than butene as in glass vessel studies is not clear; intervention of the wall may not therefore be ruled out. Further study of ethylene polymerization seems desirable.

ELEMENTARY NATURE OF ISOMERIZATION

Early in the work with the small reactor it became apparent that the data were complex; the studies in this bulb were continued to assist in recognition of the features of the reaction under conditions where heterogeneity and free radical processes are believed to be of

importance. Comparison of these features with the behavior in the large reactor at lower pressure is of assistance in assessing the extent of heterogeneity and free radical sensitization under the latter conditions. The results in the 175-cc reactor at lower pressures are the ones of principal value in connection with the original purposes of this research. In the present section an attempt is made to evaluate these results; whether they represent a homogeneous, elementary process. The conclusion arrived at below on the basis of the data is believed to be a reasonable, although not indisputable, one.

Heterogeneity

Evidence for heterogeneous processes in the small bulb was furnished by the difficulty experienced in seasoning this bulb in contrast to the relative ease with which the large reactor and the packed bulb were poisoned. The rate constant for isomerization, at a given pressure (8.6 cm), was approximately 25 percent higher in the small reactor, while the activation energy is 10 kcal lower than that for the large vessel (Table II). Polymerization in the small vessel was also faster than in the large, under comparable conditions, while again the activation energy is lower (Table IV). Results with the packed vessel gave <2 percent as the maximum effect of heterogeneity on the rate in the large vessel at a pressure of 3.8 cm. The activation energy for isomerization in the large reactor shows no decline on reduction of pressure from 3.8 to 0.9 cm (Table II) as might occur if wall reaction was important (admittedly, such an effect could be masked by relatively decreased sensitization of isomerization at the lower pressure). It is suggested that for purposes of the present study heterogeneous reaction is not significant at lower pressures in the large reactor.

Sensitized Isomerization

The susceptibility of isomerization to catalysis by free radicals, the existence of free radical intermediates in formation of polymer and exchange, and the influence of higher hydrocarbons on isomerization have been shown in the results. The effect of pressure on rate shows the increasing importance of sensitization at higher pressures; it may be seen from Table I that the increase in rate with pressure is greater at higher pressures, despite the fact that the effect of unimolecular fall-off (below) is in the opposite direction. The magnitude of these effects will now be discussed.

It is necessary to consider the sensitization of isomerization attendant on processes such as (1) decomposition of ethylene; (2) decomposition of polymer; (3) formation of polymer; (4) formation and decomposition of C_4 compounds and other possible reactions. For those processes involving radical production, estimation of the effect was made by computing radical production rates from available information and by assuming that in promoting isomerization all radicals are as effective as methyl radicals, as measured in the run with 0.1 mm of azomethane added.

For the estimation of the rate of decomposition of ethylene the excellent data of Molera and Stubbs[16] were employed. With the arbitrary assumption that each decomposing ethylene produces two radicals, calculation shows that this process makes no contribution under any of our conditions.

The method employed to estimate the effect of polymer decomposition was empirical. Using the data on polymer formation, the known rate of propylene decomposition,[17] the effect of fractionation of polymer on reduction of rate found in some experiments, and a correlation factor between the theoretical computation and the experimental finding, calculation of the percentage catalysis due to the polymer decomposition was made for a variety of conditions. It is found that while catalysis is significant at higher pressure it is negligible at lower pressure (e.g. <1.5 percent of the total amount of isomerization at 0.9 cm; <4.5 percent at 8.6 cm; and <8.5 percent at 31 cm (520.7°C) increasing to 30 percent at 28 cm (450°C). The effect on E_{isom} is to give a lowering of not more than 0.2 kcal at 0.9 cm pressure, 1.5 kcal at 8.6 cm, rising to 9 kcal at 31 cm. These figures appear to be of correct order of magnitude. The negligible effect at the lowest pressure is readily understandable from the fact that whereas 2.4 percent propylene or butene addend or 4.7 percent (final amount) propylene polymer under certain conditions increased the constant for isomerization, k_{isom}, from 10–60 percent as described earlier, the percentage polymer at 0.9 cm is less than one two-hundredth of the above figures. The rates corrected for polymer decomposition at 0.9, 3.8, and 8.6 cm at 520°C in the large reactor are respectively $k_{\text{isom}}=3.91$, 6.0, and 9.3×10^{-5} sec^{-1}.

Decomposition[16] of the relatively small amount of butene polymer can also be shown to make a negligible contribution to isomerization at low pressure.

The mechanism of formation of propylene from ethylene is not known. If it be assumed that each propylene product arose by a process involving two radicals, the associated induced isomerization may be found. There again results a possible effect of approximately 0.1 kcal on the observed activation energy at low pressures with a very appreciable effect at high pressures. The correction to the velocity constants would again be small at the lower pressures, becoming significant at intermediate and higher pressures.

The decline in activation energy and acceleration in rate at higher pressures (Tables I and II) are attributed therefore to complexities associated with polymer. This is consistent with the observation that in the higher pressure range there was a tendency for the rate to show an upward trend with time during a run.

Possible isomerization consequent on intermediate

[16] M. J. Molera and F. J. Stubbs, J. Chem. Soc. 381 (1952).
[17] M. Szwarc, J. Chem. Phys. 17, 284 (1949); K. V. Ingold and F. J. Stubbs, J. Chem. Soc. 1749 (1951).

reversible formation from ethylene of a C_4 molecule or diradical is not believed of importance and, for a butene or cyclobutane intermediate, could only be at most of the order of the (negligible) amount of exchange found. Various reaction schemes that may be constructed do not appear to lead to the proper kinetics or to the correct magnitude for the frequency factor and activation energy.

Finally, the relative constancy of E values found for the reaction studied in the large bulb at lower pressures and the reasonable magnitude of the frequency factor support the conclusion that the isomerization at 0.9 cm is an elementary, homogeneous process essentially free of heterogeneity or free radical sensitization. In any case the observed activation energy for isomerization at 0.9 cm, concluded here to be the true value, is at the least a lower limit to the true value. It is intended in the future to extend the study to lower presures and, at the same time, to make a detailed investigation of inert gas effect.

DISCUSSION

Unimolecular Fall-Off

The dependence on pressure of the first order rate constants for the reaction studied in the large reactor, coupled with the positive effect of inert gases, shows that at the pressures employed (0.9–8.6 cm) the reaction was studied in the unimolecular fall-off region.

It is desirable to find a value for k_0', the low concentration second order constant, and s, the effective number of oscillators. Some brief speculation will be admitted as follows. The constant k_∞ may be estimated by extrapolation with use of the nitrogen data. The derived value varies with the assumed nitrogen efficiency (taken here to be 0.25) and shape of the extrapolation curve but reasonable values would appear to lie in the range $12-30\times10^{-5}$ sec^{-1}. Johnston[18] has shown that $k_0'=Fk_\infty^2/m_j$, where $m_j=(dk/d(1/p))_{p=\infty}$ and F is a dimensionless parameter. If the more conventional plot of $1/k$ against $1/p$ is employed as advocated by Kassel,[19] then it follows that $k_0'=F/m_k$, where $m_k=(d(1/k)/d(1/p))_{p=\infty}$. Setting $F=10$ as an arbitrary intermediate value, we have $k_0'\simeq15\times10^{-5}$ cm^{-1} sec^{-1}. The midpoint of the fall-off region[19] is $R=k_\infty/k_0'$ and equals one cm, within a factor of perhaps ten. To obtain s, it suffices to use the classical relation

$$k_0'=b(T)\sum_{r=0}^{s-1}1/r!(E^*/RT)^re^{-E^*/RT}.$$

Also $E_{obs}=E^*-(s-3/2)RT$ at low pressures; $E^*\gg sRT$. Now $E_{obs}=61.3$ kcal at 0.9 cm and $R\simeq1$ cm whence $s=6$; $E^*=65{,}000$ cal and the frequency factor at high pressure is of the order of 10^{13}.

Of compounds which proceed by the singlet mechanism, Kistiakowsky and Smith[1b] have found that there is no fall-off down to 0.5 cm for stilbene and methyl cinnamate and they estimate $s>12$ and >6 respectively Evidently s is lower and fall-off occurs at higher pressures for ethylene, d_2 and this appears reasonable. The relevant number of vibrational degrees of freedom is higher in the complex substituted ethylenes.[20] Also the interaction of non-planar vibrations with in-plane modes is less for ethylene, d_2 than for the complex compounds; the degree of mixing of "torsional" with other modes presumably increases in general with the increasing anharmonicity of the torsional potential function and reduction of symmetry consequent on replacing H in C_2H_4 by complex substituents.[21] Complex noncoplanar substituents will destroy the symmetry distinction in ethylene between in-plane and out-of-plane modes, even for the ground state.

Tunneling

The effect of tunneling in *cis-trans* isomerizations has been considered by MSE who concluded that although the effect is negligible for ethylenes with heavy substitutents, it might be of importance for light ethylene itself. Calculations have been made for ethylene, d_2 following the same treatment as MSE. A parabolic potential constructed from the torsional force constant for light ethylene[8] was employed. An idealized torsion frequency, ν_0, of 838 cm^{-1} derived from the force constant for ethylene and the reduced moment of inertia for twisting in ethylene, d_2 was used.[22] Tunneling calculations for various assumed barriers was made. In particular, for a barrier of 70 kcal, the rate of tunneling at 65 kcal is

$$k_{tun}=5\times10^{10}e^{-65\,000/RT}\ \text{sec}^{-1}.$$

Within the approximations of the calculation gross tunneling thus appears negligible.

---

[18] H. S. Johnston, J. Chem. Phys. **20**, 1103 (1952).

[19] L. S. Kassel, J. Chem. Phys. **21**, 1093 (1953).

[20] For example, J. E. Kilpatrick and K. S. Pitzer, J. Research Natl. Bur. Standards **38**, 191 (1947), found in a normal coordinate analysis of ethylene and butenes that, for the latter, coupling of methyl rocking with the skeletal motion had to be considered.

[21] The possible physical origin of the coupling of torsional motion in ethylene with in-plane vibrations may be seen from the considerations which have been advanced in several papers by Coulson, Duchesne, and Manneback, V. Henri Mem. Vol., Desoer, Liege, 1948. The C=C bond lengthens with twist while at the same time the C hybridization may *tend* to sp^3 [J. Duchesne, Bull. Class. Sci. **37**, 197 (1952)]. See also reference 6 and Linnett, Heath, and Wheatley, Trans. Faraday Soc. **45**, 832 (1949), for discussion of hyperconjugation and distortion of C–H bond orbitals with twisting.

[22] The results of the calculation are, for present purposes, insensitive to the exact frequency chosen. "Twisting" in *cis* and *trans* substituted ethylenes, particularly at large angles of twist where interactions are prominent, is a complex motion. *Trans*-ethylene d_2 belongs to the point group C_{2h}, and the coordinates corresponding to torsion and inversion are both of species A_u. A value of $\nu_0=890$ cm^{-1} is calculated from the F and G matrices of Arnett and Crawford, upon an arbitrary setting of the interactions between these motions equal to zero; this corresponds formally to N. B. Slater's "particular case" [Proc. Roy. Soc. (London) **194A**, 112 (1948)]. The calculated rate of tunneling is little affected, and variation in the moment of inertia with twist and probable anharmonicities in the potential function at large angles suggest that it may not be worth while refining this point.

TABLE V. Some estimates and calculations of the energy to open the ethylenic double bond.

Basis	Energy kcal	Remarks
Thermochemical	58.5[a,b]	Based on $D(CH_3CH_2-H) = D(CH_2CH_2-H)$; no specification of final state.
	57.5[c]	Specified as the energy of the second valence in a double bond.
	65[d], $\gtrsim$48[e]	Based on $D(C=C) - D(C-C)$; unspecified.
Semiempirical AO method	41.5[f]	$E_{N'}$
Semiempirical LCAO MO method	57.5(41.5−76)[g]	$E_{N'}$; range corresponding to various values of the parameters of the calculation.
Approximate LCAO MO theoretical method	50.5(21−62)[h]	$E_{N'}$; see references (7d) and (7f) for discussion; range corresponds to various values of screening constant.
"Atoms in molecules" MO method	69[i]	$E_{N'}$ for r_{c-c}=1.50 A.

[a] E. P. Carr, Chem. Revs. **41**, 293 (1947).
[b] D. H. R. Barton and K. E. Howlett, J. Chem. Soc. 155 (1949).
[c] E. C. Baughan and M. Polanyi, Nature **146**, 685 (1940), as modified slightly in later papers.
[d] D. D. Eley, Discussions Faraday Soc. No. **8**, 34 (1950).
[e] F. H. Field, J. Chem. Phys. **20**, 1734 (1952).
[f] J. Duchesne, reference (21); based on the calculations of Penney but with the π electron exchange integral, J =27.6 kcal.
[g] Reference 6b.
[h] Reference 7a.
[i] Reference 7f.

Estimation of Some Electronic Energy Levels of Ethylene

In this section, the present results are applied to an estimation or approximation of some electronic energy levels of ethylene.

State N′; The Singlet Barrier

The value of the high-pressure activation energy obtained here (65 kcal) is evidently compatible with the mechanism of MSE (see reference 8) and is identified with the energy of the lowest singlet state, N', of perpendicular ethylene. A number of factors which might make the two quantities differ, such as the difference in zero-point energy levels between ethylene, d_2 and ethylene, and tunneling at the top of the barrier, are negligible; the value of $E_{N'}$ is approximately 65 kcal (2.8 ev). Comparison with a number of thermochemical and theoretical calculations and estimates of this quantity is given in Table V.

State Z′

From a knowledge of $E_{N'}$, the value of $E_{Z'}$ may be estimated. As shown by Parr and Crawford[7a] using a two-electron approximation for ethylene by the LCAO MO method,

$$\Psi_N = a_1\Psi_1 - a_2\Psi_2$$
$$\Psi_z = b_1\Psi_1 + b_2\Psi_2,$$

where, neglecting spin functions and normalization constants,

$$\Psi_1 = \varphi_+(1)\varphi_+(2)$$
$$\Psi_2 = \varphi_-(1)\varphi_-(2),$$

and φ_+ and φ_- are molecular orbitals formed from the sum and difference respectively of the $2p\pi$ atomic orbitals for each carbon. For perpendicular ethylene ($\phi=\pi/2$), $a_1=a_2$ and $b_1=b_2$; also $E_{1'}=E_{2'}$, and the interaction of the "states" represented by Ψ_1 and Ψ_2 is a maximum. Then

$$E_{N'} = E_{1'} - \delta_\pm,$$
$$E_{Z'} = E_{1'} + \delta_\pm,$$

where $\delta_\pm = \int \Psi_1 \mathbf{H} \Psi_2 d\tau$.

The value of $E_{1'}$ may be approximated by taking $E_N \simeq E_1(\phi=0)$[7d,e] and identifying a harmonic torsional potential function,[6] corresponding to a frequency of 1027 cm^{-1} in ethylene, with the potential energy for states 1 and 2 as a function of angle of twist. This puts their crossing point at 95.5 kcal; whence $\delta_\pm \simeq 30$ kcal and $E_{Z'} \simeq 126$ kcal (5.5 ev).

The theoretical calculations by Moffitt and Scanlan[7f] of $E_{N'}$ and $E_{Z'}$, by the method of "atoms in molecules," correspond reasonably closely to the values cited above for the case r_{cc}=1.50A.

States T′ and V′

Reid[23] has found ultraviolet absorption by ethylene above 2600A which has a band structure with an average spacing of about 965 cm^{-1} and no noticeable convergence.‡ He interprets this as a TN transition, where 965 cm^{-1} is the twisting frequency of the triplet state. The absorption, Reid suggests, takes place from the ground state with an angle of twist of between 20° and 30°.

A value for $E_{T'}$ may be calculated from this data on the following somewhat arbitrary basis: (1) the potential function for the T state is harmonic corresponding to the frequency 965 cm^{-1}; (2) the center band (33,698 cm^{-1}) arises from an angle of twist of 25°; and (3) the moment of inertia for torsion in the triplet state is the same as in the ground state. This places $E_{T'}$ at 52 kcal so that $E_{N'} - E_{T'} \simeq 13$ kcal (0.6 ev). This value is consistent with the many calculations that indicate that the $N'-T'$ separation is relatively small.[6,7] In the treatment given by Parr and Crawford[7a] $E_{Z'} - E_{N'} = 2\delta_\pm = E_{V'} - E_{T'}$; so $E_{V'} \simeq 112$ kcal (4.9 ev).

Double Bond Opening; Some Thermochemical Quantities

The double bond is not entirely destroyed[6] upon twisting ethylene to the perpendicular configuration, but it is convenient and conventional to speak of double bond "opening" as synonomous with twisting. There are

[23] C. Reid, J. Chem. Phys. **18**, 1299 (1950).
‡ Reid gives the figure of 995 cm^{-1} in his text, but inspection of his data shows that this is evidently a typographical error.

three opening processes of interest for thermal reactions which may conveniently be specified. Two of these are the transitions from the ground state to the singlet diradical, N', and to the triplet diradical, T'; both possibilities have been invoked to explain the mechanism and steric course of certain olefin reactions;[14b,24] energy values have been cited earlier above. The third opening process involves the energy change accompanying reduction of π electron interaction across the bond to zero, without any concomitant change in σ electron energy; this hypothetical process has been discussed in some detail recently by Gold,[25] with reference to rotation about unsaturated linkages, and by simple molecular orbital approximation corresponds to an energy intermediate between $E_{T'}$ and $E_{N'}$.

As shown in Table V, a number of estimates of the energy required to open the double bond in ethylene have been made, based on various assumptions. In a number of cases in Table V and in more numerous instances in the literature no specification is made of the nature of the opening process being discussed. In some of these cases it seems intuitively reasonable to identify the π bond dissociation energy referred to with process three above.

We now apply our results to the calculation of some thermochemical quantities but restrict ourselves to derivatives of the quantity, $E_{N'}$. The magnitude of the C−H bond dissociation energy in ethyl radical has been inferred in a number of thermochemical calculations in the literature. By an appropriate cycle[26] we have $D[\dot{C}H_2CH_2-H\rightarrow C_2H_4(N')+H]=104$ kcal as the value for one formal process.

By specification of a value of $D(\dot{C}H_2-H)$ (CH_2 produced in the ground, presumably singlet, state), and thus of ΔH_f for CH_2, some related C−C bond dissociation energies may be obtained.[26] Values of $D(\dot{C}H_2-H)$ in the literature fall into two groups both of which will be employed and which will be designated as $\leqslant 87$ kcal and $\leqslant 80$ kcal.[27] Mulliken[6a] has pointed out that although ethylene in its ground state may be thought of as derived from two excited triplet methylene radicals, dissociation of ethylene would probably occur adiabatically into two ground-state radicals. The values for $D(\dot{C}H_2-H)$ cited above correspond respectively to $D[C_2H_4\rightarrow 2CH_2]\leqslant 122$ or $\leqslant 108$ kcal. There can be calculated also $D[CH_3-\dot{C}H_2]\leqslant 74$ or $\leqslant 67$ kcal and $D[\dot{C}H_2-\dot{C}H_2(N')]\leqslant 57$ or $\leqslant 43$ kcal. The latter quantity, coupled with $E_{N'}=65$ kcal, corresponds to one possible, formal mode of resolution of $D(C=C)$ into components. Mulliken[28] has recently discussed the resolution of multiple bond energies into π and σ components and has pointed out that, contrary to the conventional idea, the π contribution may indeed be larger than the σ contribution.

A Remark on Polymerization Reactions of Olefins

It has been suggested[4,24] that polymerization reactions of olefins, including ethylene, fall into two categories, analogous to isomerization, depending upon whether reaction goes by a singlet or triplet mechanism i.e. passage to the N' or T' states; the activation energies and frequency factors fall into two groups possessing magnitudes similar to those for isomerization; the N' state has been designated as ionic[4] and singlet polymerization therefore as ionic,[29] in contrast to homopolar triplet radical polymerization.[4]

It appears that ethylene does not conform to the above classification inasmuch as E_{isom} is appreciably different from E_{polym} (40 kcal[13,14]). A similar discrepancy exists for butene since, from the data of Kistiakowsky and Smith,[1] the value of the singlet barrier must be in excess of 60 kcal for any reasonable value of a singlet frequency factor for isomerization while E_{polym} is approximately 40 kcal.[30]

It is a pleasure to thank Professor D. F. Eggers, Jr. and W. T. Simpson for many valuable discussions, and Professor A. L. Crittenden for his cooperation in the use of the mass spectrometer.

[24] R. Harman and H. Eyring, J. Chem. Phys. **10**, 557 (1942).

[25] V. Gold, Trans. Faraday Soc. **45**, 191 (1949).

[26] Relevant thermochemical data taken from J. S. Roberts and H. A. Skinner, Trans. Faraday Soc. **45**, 339 (1949); no corrections have been applied, and since these may largely cancel, the calculated quantities may be taken as referred to 25°C, the reference temperature for heats of formation of molecules.

[27] (a) K. J. Laidler and E. J. Casey, J. Chem. Phys. **17**, 1087 (1949), $\leqslant 87$ kcal by thermochemical cycle; D. P. Stevenson, J. Chem. Phys. **18**, 1347 (1950), 89.4 kcal (for $D(CH_3-H)$ taken as 102 kcal) by electron impact; H. Branson and C. Smith, J. Am. Chem. Soc. **75**, 4133 (1953), $\leqslant 87.4$ kcal by electron impact; (b) L. S. Kassel, J. Am. Chem. Soc. **54**, 3949 (1932), 79 kcal from E_{act} for $CH_4\rightarrow CH_2+H_2$ (but see L. H. Long, Proc. Roy. Soc. A**198**, 62 (1949)); G. B. Kistiakowsky and N. W. Rosenberg, J. Am. Chem. Soc. **72**, 321 (1950), ~80 kcal by thermochemical cycle; C. A. McDowell and J. W. Warren, Discussions Faraday Soc. No. **10**, 53 (1951), $\leqslant 79.5$ by electron impact.

[28] R. S. Mulliken, J. Phys. Chem. **56**, 295 (1952).

[29] The N′ state of ethylene is actually not ionic but is homopolar as has been pointed out by Mulliken (reference (6a) and private communication) and later by Moffitt (reference (7f)); however, the polarizability of state N is evidently (in π electron approximation) greater than that of T, inasmuch as the $N-V$ transition (to mention one interaction of N with other singlet states) is allowed and intense, and the energy separation much less than that between T and other excited triplet states.

[30] It has been shown that low frequency factors for polymerization can be explained in terms of entropy considerations (J. H. Baxendale and M. G. Evans, Trans Faraday Soc. **43**, 210 (1947)). Some further discussion of the mechanism of polymerization is given in reference (14b). It may be remarked that some of the data in this field bearing on the above classification is conflicting or of dubious validity.

Vibrational Spectra of Cyclobutforene (Hexafluorocyclobutene)*

J. RUD NIELSEN AND M. Z. EL-SABBAN, *Department of Physics, University of Oklahoma, Norman, Oklahoma*

AND

MORRIS ALPERT,† *Naval Research Laboratory, Washington, D. C.*

(Received July 2, 1954)

The infrared spectrum of gaseous cyclobutforene has been obtained in the region from 2 to 38μ with the aid of LiF, NaCl, KBr, and KRS-5 prisms. The Raman spectrum of the liquid phase has been photographed with a three-prism glass spectrograph of linear dispersion 15 A/mm at 4358 A. With some uncertainties, especially as to symmetry species, all of the twenty-four fundamental vibration frequencies have been assigned, and the spectra have been interpreted in detail.

INTRODUCTION

A NUMBER of olefinic fluorocarbons have been prepared in recent years.[1] Among the cyclic compounds of this kind, the simplest known is cyclobutforene,

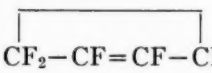

$CF_2-CF=CF-CF_2$.

Its vibrational spectra, which do not seem to have been studied previously, will be described in the present paper. All of the normal vibration frequencies will be assigned, and a detailed interpretation of the spectra will be given.

EXPERIMENTAL RESULTS

The sample of cyclobutforene, bp 1.0°C, was prepared and purified by Professor W. T. Miller of Cornell University. No information was available about its purity. The infrared absorption spectrum of gaseous cyclobutforene was observed in the region from 2 to 38μ with a prism spectrometer of high resolution.[2] The infrared spectrum is shown in Fig. 1. The wave numbers of the observed absorption maxima are listed in the first column of Table I. The Raman spectrum of the compound in the liquid state, in a sealed Raman tube at room temperature, was photographed with a 3-prism glass instrument of linear dispersion 15 A/mm at 4358A.[3] Polarization measurements were made with an apparatus similar to that described by Crawford and Horwitz.[4] The observed Raman shifts are listed in the first column of Table II. In other columns of this table are given the relative intensities of the Raman bands, the measured depolarization ratios, and the Kohlrausch symbols for the exciting mercury lines.[5]

INTERPRETATION

The

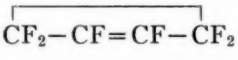

$CF_2-CF=CF-CF_2$

molecule probably has the symmetry C_{2v}, the carbon ring forming a plane that contains two of the fluorine atoms, while the other fluorine atoms lie symmetrically with respect to this plane and to a plane perpendicular to and through the midpoint of the C=C bond. If this is correct, the twenty-four normal vibrations divide themselves into symmetry species in the following manner: $8a_1+5a_2+4b_1+7b_2$, where b_1 denotes symmetry with respect to the plane perpendicular to the carbon ring, and antisymmetry with respect to the plane of the latter as well as to the twofold axis; while b_2 denotes symmetry with respect to the plane of the carbon ring, and antisymmetry with respect to the other symmetry elements.

All fundamentals, and all overtones and combinations, are active in the Raman effect, those of species A_1 yielding polarized and all others depolarized bands. In infrared absorption all vibrations except those of species A_2 (such as the binary combinations $a_1 \cdot a_2$ and $b_1 \cdot b_2$) are allowed.

Assuming the following values for the atomic distances and angles: C−C 1.54, C=C 1.33, C−F 1.36A, F−C−F 109°, and C=C−F 120°, we find the principal moments of inertia of the molecule to be 539.0, 649.5, and 877.3×10^{-40} g cm^2. The smallest moment is about the twofold symmetry axis, and the largest moment is about an axis perpendicular to the plane of the carbon ring. Thus, infrared bands of species a_1, b_1, and b_2 should have contour types A, C, and B, respectively. From Badger and Zumwalt's curves[6] the PR separations for types A and C contours are found to be 11 and 14 cm^{-1}, respectively, and the Q branch doubling for type B bands 3 cm^{-1}.

* A part of this work has been supported by the U. S. Atomic Energy Commission under Contract AT-(40-1)-1074.

† Present address: Naval Ordnance Laboratory, Silver Spring, Maryland.

[1] See *Fluorine Chemistry* edited by J. H. Simons (Academic Press, Inc., New York, 1950), Vol. I.

[2] Nielsen, Crawford, and Smith, J. Opt. Soc. Am. **37**, 296 (1947).

[3] Smith, Nielsen, and Claassen, J. Chem. Phys. **18**, 326 (1950).

[4] B. L. Crawford, Jr., and W. Horwitz, J. Chem. Phys. **15**, 882 (1947).

[5] K. W. F. Kohlrausch, *Der Smekal-Raman-Effect* (Julius Springer, Leipzig, 1931), p. 19.

[6] R. M. Badger and L. R. Zumwalt, J. Chem. Phys. **6**, 711 (1938).

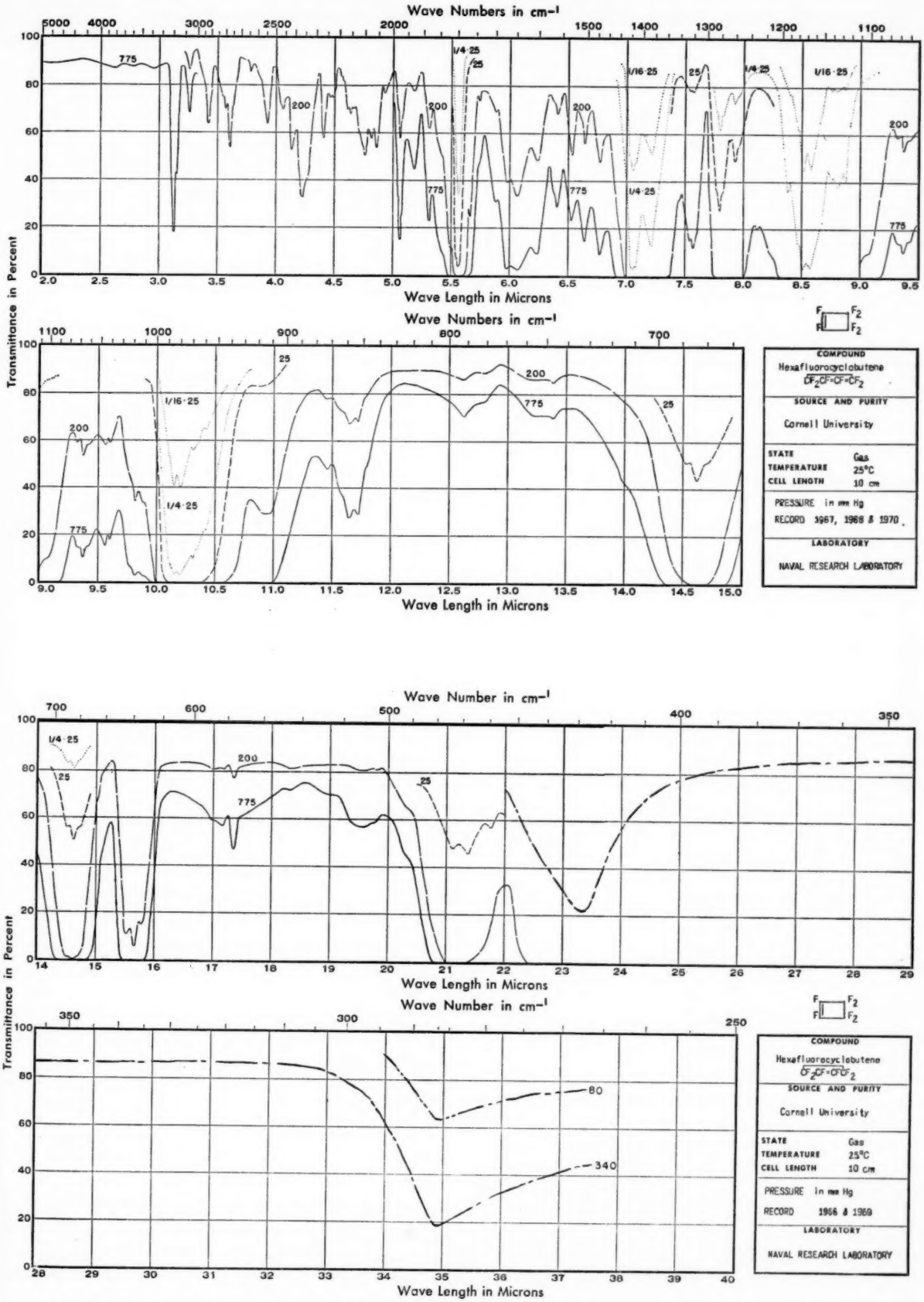

FIG. 1. Infrared absorption spectrum of liquid cyclobutforene (hexafluorocyclobutene). KRS-5 data are not included.

TABLE I. Infrared absorption spectrum of gaseous cyclobutforene.

Wave number	Description[a]	Interpretation
286	m	a_1 fundamental
429	vs	b_2 fundamental
459		
469	vs	a_1 fundamental
473		
494	vvw	$684-187=497\ B_1$
~506	vw	$217+286=503\ B_2$
513	w	$174+337=511\ A_1$
~531	vvw	$98+429=527\ B_1$
545	vvw	$217+337=554\ B_1$
576	w	b_2 fundamental
582	w	
588	vvw	$98+493=591\ A_1$
634		
638	vs	b_1 fundamental
644		
~662		$174+493=667\ A_1$
~678		
684	vs	a_1 fundamental
689		
714	vvw	$286+429=715\ B_2$
747	vw	$174+579=753\ B_1$
~758	vw	$286+469=755\ A_1$
~781	vvw	$146+638=784\ A_1$
792	vw	$217+579=796\ A_1$
~845	vvw	
853	m	$2\times429=858\ A_1$
858	m	
864	vvw	$286+579=865\ B_2$
873	vw	$187+684=871\ B_1$
~917	s	$429+493=922\ B_1$; $238+684=922\ B_2$; $286+638=924\ B_1$
960		
~966	vs	a_1 fundamental
970		
980	vvs	b_2 fundamental
985	vvs	
~990	vw	$2\times493=986\ A_1$
~1010		
1019	s	$429+579=1008\ A_1$
~1026		
1042	m	$469+579=1048\ B_2$
1046	m	
~1062		
1067	w	$493+579=1072\ B_1$
~1073		
~1101	vvw	$469+638=1107\ B_1$
1127		
1136	vs	a_1 fundamental
1143		
~1157	w	$174+983=1157\ B_1$
1167	vvs	b_2 fundamental
1175	vvs	
~1183	w	$217+966=1183\ B_2$
1193	w	$217+983=1200\ A_1$; $238+966=1204\ B_2$
~1215	vvw	$238+983=1221\ A_1$
1232	vw	$1418-187=1231\ B_1$
~1257	s	b_2 fundamental
1261	s	
~1267	w	$98+1171=1269\ B_1$
~1277		
1282	vs	b_1 fundamental
~1290		
~1314	w	$337+983=1320\ B_1$
1321	m	$187+1136=1323\ B_1$; $638+684=1322\ B_1$
1326	w	$146+1182=1328\ B_2$
1387	vvs	a_1 fundamental
~1410		
1418	vvs	a_1 fundamental
~1423		
1477	m	$217+1259=1476\ A_1$; $493+983=1476\ B_1$
1506	m	$337+1171=1508\ B_1$
1531	m	$146+1387=1533\ B_1$
1560	m	$579+983=1562\ A_1$; $146+1418=1564\ B_1$; $429+1136=1565\ B_2$; $286+1282=1568\ B_1$
~1572	vw	$187+1387=1574\ B_1$
1603	m	$638+966=1604\ B_1$; $217+1387=1604\ B_2$; $187+1418=1605\ B_1$
1647	m	$684+966=1650\ A_1$
1672	m	$286+1387=1673\ A_1$; $493+1182=1675\ A_1$
1701	m	$286+1418=1704\ A_1$
1742	w	$579+1171=1750\ A_1$; $469+1282=1751\ B_1$
1767	vw	$638+1136=1774\ B_1$; $493+1282=1775\ B_2$
1799	vs	a_1 fundamental
~1804		
~1818	vw	$429+1387=1816\ B_2$; $684+1136=1820\ A_1$; $638+1182=1820\ B_2$
~1852	vw	$684+1171=1855\ B_2$; $469+1387=1856\ A_1$
1883	w	$469+1418=1887\ A_1$
1931	w	$2\times966=1932\ A_1$
1976	m	$187+1799=1986\ B_1$
~1983	vvvw	$579+1418=1997\ B_2$
2028	vw	$638+1387=2025\ B_1$; $238+1799=2037\ B_2$
2058	w	$638+1418=2056\ B_1$
2075	w	$684+1387=2071\ A_1$; $286+1799=2085\ A_1$
2101	w	$684+1418=2102\ A_1$; $966+1136=2102\ A_1$
~2146	w	$983+1171=2154\ A_1$
2155	w	$983+1182=2165\ B_1$
~2169	w	
2227	vw	$429+1799=2228\ B_2$; $966+1259=2225\ B_2$
2237	vw	$983+1259=2242\ A_1$; $966+1282=2248\ B_1$
2268	w	$469+1799=2268\ A_1$; $2\times1136=2272\ A_1$
~2333	w	$2\times1171=2342\ A_1$
2364	m	$2\times1182=2364\ A_1$; $983+1387=2370\ B_2$
2415	w	$1136+1282=2418\ B_1$
2463	vw	$1182+1282=2464\ B_2$
~2481	vw	$684+1799=2483\ A_1$
2506	vvvw	$2\times1259=2518\ A_1$
2545	w	$1136+1418=2554\ A_1$; $1171+1387=2558\ B_1$
~2593	vvw	$1171+1418=2589\ B_2$
2646	vw	$1259+1387=2646\ B_2$
2770	w	$2\times1387=2774\ A_1$
2801	vw	$1387+1418=2805\ A_1$
~2828	vvvw	$2\times1418=2836\ A_1$
2924	w	$1136+1799=2935\ A_1$
3067	w	$1282+1799=3081\ B_1$
~3175	w	$1387+1799=3186\ A_1$
3195	s	$1418+1799=3217\ A_1$
3379	vvw	
3597	vw	$2\times1799=3598\ A_1$

[a] The following abbreviations are used: vs very strong, s strong, m medium, w weak, vw very weak, etc.

Unfortunately, the measured depolarization ratios for several of the Raman bands are not accurate enough to permit one to conclude whether they are polarized or depolarized, and the contours of many of the infrared bands are not well resolved. Nevertheless, the following assignments of fundamentals can be made with a high degree of plausibility.

Species a_1

The strong infrared band at 1799, and the strong polarized Raman band at 1794 in liquid cyclobutforene, certainly represent an a_1 fundamental associated largely with a stretching of the C=C bond. The strong bands at 1419, 1387, and 966 cm^{-1}, which are all definitely polarized in the Raman spectrum, are undoubtedly a_1

fundamentals, as is probably also the band at 1136 cm^{-1}. Its fairly high depolarization ratio may be caused by overlapping with 493+638=1131 B_2. These fundamentals involve C−F and C−C stretching. The strong bands at 684 and 469 cm^{-1} have rather well resolved *PQR* contours and are polarized in the Raman spectrum. They are interpreted as a_1 fundamentals involving symmetrical CF_2 deformation and C−F bending. The unresolved infrared band at 286 cm^{-1}, and the depolarized Raman band at 285 cm^{-1}, are assigned as the lowest a_1 fundamental, which involves largely CF_2 wagging.

Species a_2, b_1, and b_2

For convenience, these three species will be discussed together. The assignment of the highest fundamentals of these species, involving C−F and C−C stretching, presents little difficulty. The band at 1282 cm^{-1} has type *C* contour in the infrared and is apparently depolarized in the Raman spectrum. It is assigned as the highest b_1 fundamental. The band at 1259 cm^{-1}, assigned as the highest b_2 fundamental, appears to be depolarized and may have type *B* contour, although this cannot be stated with certainty because of its proximity to the more intense band at 1282 cm^{-1}. The highest a_2 fundamental is identified with the strong Raman band at 1182 cm^{-1}, which may be depolarized although its measured depolarization ratio is rather low. This assignment is made uncertain by the presence of a weak infrared band at 1183 cm^{-1}. However, this band may be interpreted as an active binary combination 217+966=1183 B_2. The intense infrared bands at 1171 and 983 cm^{-1} have type *B* contours. The former is definitely depolarized in the Raman spectrum, while the latter is so weak that its depolarization ratio could not be estimated. These two bands are undoubtedly b_2 fundamentals.

The very strong infrared band at 638 cm^{-1} has a contour rather similar to that of the stronger band at 684 cm^{-1} which was assigned as an a_1 fundamental. It could be interpreted as the combination 146+493 =639 which would be of species A_1 if both 146 and 493 belonged to a_2. However, since its depolarization ratio is high enough to make it likely that it is depolarized, since the second highest b_1 fundamental may be expected to lie in this region, and since 146 is best assigned as a b_1 fundamental, the band at 638 cm^{-1} has been interpreted as a b_1 fundamental. It is probably associated largely with C−F bending perpendicular to the plane of the ring. The infrared band at 579 cm^{-1} has abnormal contour. It is assumed to be a b_2 fundamental, involving largely CF_2 deformation, overlapped by the combination 238+337=575 B_1. The strong depolarized Raman band at 493 cm^{-1} seems to have an extremely weak counterpart in the infrared spectrum, which, however, can readily be interpreted as a combination band. It is therefore assigned as an a_2 fundamental.

TABLE II. Raman spectrum of liquid cyclobutforene.

Wave number	Relative intensity[a]	Depolarization	Exciting Hg lines	Interpretation
98	18	0.6	*e*	a_2 fundamental
146	vvw	...	*e*	b_1 fundamental
174	vw	...	*e*	a_2 fundamental
187	5	0.8	*e*	b_1 fundamental
217	3	0.7	*e*	b_2 fundamental
238	34	0.8	±*e,k*	b_2 fundamental
285	6	0.3	*e,k*	a_1 fundamental
337	vvw	...	*e*	a_2 fundamental
432	13	0.7	±*e,k,i*	b_2 fundamental
470.2	31	0.2	±*e,k,i*	a_1 fundamental
493	16	0.9	*e,k*	a_2 fundamental
577	6	0.8	*e,k,i*	b_2 fundamental
638	5	0.8	*e,k*	b_1 fundamental
685	100	0.1	±*e,k,i,l*	a_1 fundamental
763	1	0.1	*e*	285+470=755 A_1
917	vvw	...	*e*	238+685=923 B_2; 285+638=923 B_1; 432+493=925 B_1
958	2	0.2	*e,k*	a_1 fundamental
973	1	...	*e*	b_2 fundamental
1134	6	0.6	*e,k,i*	a_1 fundamental
1161	5	0.9	*e,k*	b_2 fundamental
1182	5	0.7	*e,k*	a_2 fundamental
1260	5	0.8	*e,k*	b_2 fundamental
1281	11	0.8	*e,k*	b_1 fundamental
1323	vw	...	*e*	146+1182=1328 B_2; 638+685=1323 B_1; 187+1134=1321 B_1
1374	9	0.1	*e,k*	2×685=1370 A_1
1385	9	0.1	*e,k*	a_1 fundamental
1419	2	0.3	*e*	a_1 fundamental
1794.2	18	0.1	*e*	a_1 fundamental

[a] For abbreviations used see footnote to Table I.

The corresponding motion must be largely out-of-phase C−F bending at right angles to the planar ring. The band at 429 cm^{-1} of unresolved contour and doubtful polarization has been assumed to be a b_2 fundamental, probably involving CF_2 wagging.

The strong Raman bands at 238 and 98 cm^{-1} undoubtedly represent fundamentals. They are assigned to species b_2 and a_2, respectively, and are believed, because of their high intensities, to involve ring deformations. The somewhat weaker Raman bands at 217 and 187 cm^{-1} are also taken to be fundamentals. In order to provide satisfactory interpretations of the weak infrared bands at 792 and 1183 cm^{-1}, the fundamental at 217 cm^{-1} is assumed to belong to species b_2. It probably involves mostly CF_2 wagging. Similarly, the presence of the weak infrared band at 1232 cm^{-1} suggests that the fundamental at 187 cm^{-1} does not belong to a_2. It has been assigned to b_1 and probably involves largely CF_2 twisting.

There remain two a_2 and one b_1 fundamentals. The only direct evidence for the assignment of these is the observation of three very faint, and possibly spurious, Raman bands at 337, 174, and 146 cm^{-1}. The first of these which lies within the infrared region explored but which was not observed, is tentatively assigned as an a_2 fundamental, and the second and third are assigned as a_2 and b_1 fundamentals, respectively. The choice of species has been based mainly on the usefulness for

TABLE III. Fundamental vibrational frequencies of cyclobutforene.

Symmetry species	Infrared (gas) Wave number	Infrared (gas) Description[a]	Raman (liquid) Wave number	Raman (liquid) Relative intensity[a]	Raman (liquid) Depolarization
a_1	1799	vs	1794.2	18	0.1
a_1	1418	vvs	1419	2	0.3
a_1	1387	vvs	1385	9	0.1
a_1	1136	vs	1134	6	0.6
a_1	966	vs	958	2	0.2
a_1	684	vs	685	100	0.1
a_1	469	vs	470.2	31	0.2
a_1	286	m	285	6	0.3
a_2	...	...	1182	5	0.7
a_2	...	...	493	16	0.9
a_2	...	...	337	vvw	...
a_2	...	...	174	vw	...
a_2	...	...	98	18	0.6
b_1	1282	vs	1281	11	0.8
b_1	638	vs	638	5	0.8
b_1	...	...	187	5	0.8
b_1	...	...	146	vvw	...
b_2	1259	s	1260	5	0.8
b_2	1171	vvs	1161	5	0.9
b_2	983	vvs	973	1	...
b_2	579	w	577	6	0.8
b_2	429	vs	432	13	0.7
b_2	...	...	238	34	0.8
b_2	...	...	217	3	0.7

[a] For abbreviations used see footnote to Table I.

interpreting infrared combination bands. Thus, the infrared bands at 781 and 1531 cm^{-1} can be interpreted most satisfactorily if 146 is assumed to belong to b_1. These fundamentals involve CF_2 twisting and rocking.

The assigned fundamentals are listed in Table III. On the basis of these fundamentals it has been possible to interpret all but a couple of the observed infrared bands and all of the Raman bands. The interpretations are given in the last columns of Tables I and II.

DISCUSSION

The interpretation of the spectra, given in the last columns of Tables I and II, is quite satisfactory for practically all of the bands, which lends support to the fundamentals assigned. Thus, the infrared band at 1044 cm^{-1} definitely belongs to B_2 and that at 1067 cm^{-1} to B_1, in accord with the assignments of 469, 493, and 579 as a_1, a_2, and b_2 fundamentals, respectively. In the case of a few of the combination bands the difference between calculated and observed wave numbers is greater than would off-hand be expected. However, this can readily be explained as resulting from Fermi resonance with a fundamental of the same species. Thus, the interpretations of the infrared band at 1019 cm^{-1} as $429+579=1008$ A_1, and the Raman band at 763 cm^{-1} as $285+470=755$ A_1 are satisfactory when the presence of the a_1 fundamentals at 966 and 684 cm^{-1} is considered. The rather high intensities of these combination bands, and the assumed high intensity of $238+377=575$ B_1, which is fairly close to the b_1 fundamental at 638 cm^{-1}, also are explained as arising from Fermi resonance.

In spite of the fact that the observed spectra are satisfactorily explained, some of the fundamentals are uncertain, as was pointed out in the previous section. Moreover, because of the fairly low accuracy of the Raman polarization measurements, and the fact that the contours of many of the infrared bands are not resolved, it cannot be claimed that the symmetry C_{2v} has been established for the cyclobutforene molecule. If the carbon ring should be bent so as to reduce the symmetry to C_2, there would be thirteen fundamentals of species a and eleven of species b. The polarization data do not rule out this possibility.

ACKNOWLEDGMENT

The writers gratefully acknowledge their indebtedness to Professor W. T. Miller, Department of Chemistry, Cornell University, for the gift of the sample.

Infrared and Raman Spectra of Fluorinated Ethanes. VIII. Pentafluoroethane*

J. Rud Nielsen and Howard H. Claassen,† *Department of Physics, University of Oklahoma, Norman, Oklahoma*

and

Norma B. Moran,‡ *Naval Research Laboratory, Washington, D. C.*

(Received July 2, 1954)

The infrared spectrum of gaseous CF_3CF_2H has been observed in the region from 2 to 38μ, and the spectrum of the liquid at −50°C from 2 to 22μ, with the aid of LiF, NaCl, KBr, and KRS-5 prisms. The Raman spectrum of gaseous CF_3CF_2H has been photographed with a three-prism glass spectrograph of linear dispersion 15 A/mm at 4358 A. All but one of the fundamental vibration frequencies have been assigned, and the spectra have been interpreted in detail.

INTRODUCTION

In previous papers of this series,[1–7] and in two related papers,[8,9] the vibrational spectra of twenty fluoro-, chloro-, and fluorochloroethanes having an end-group with threefold symmetry axis have been investigated. In the present paper the infrared and Raman spectra of pentafluoroethane will be reported. No previous spectral data have been published for this compound. The only remaining ethanes of this type are CF_3CH_2F, of which it has not been possible to obtain a sample, and hexachloroethane, which has been studied rather thoroughly by other investigators.

EXPERIMENTAL RESULTS

The sample of pentafluoroethane, bp −48.5°C, was kindly supplied by Minnesota Mining and Manufacturing Company. No information was available about its purity. The infrared spectrum of gaseous CF_3CF_2H at room temperature was observed in the region from 2 to 38μ, and the infrared spectrum of liquid CF_3CF_2H at −50°C from 2 to 22μ, with LiF, NaCl, KBr, and KRS-5 prisms. The Raman spectrum of the compound in the gaseous state at 5 atmospheres and 30°C was photographed with a three-prism glass spectrograph of linear dispersion 15 A/mm at 4358 A. Because of the low intensity of the Raman spectrum no polarization measurements were made.

The infrared spectra of gaseous and liquid CF_3CF_2H are shown in Figs. 1 and 2. The wave numbers of the absorption maxima are listed in the first and third columns of Table I. The observed Raman shifts are listed in the first columns of Table II. In other columns of these tables the relative intensities and appearance of the bands are given in terms of obvious abbrevations. The Kohlrausch symbols[10] for the exciting mercury lines are also given in Table II.

INTERPRETATION

The CF_3CF_2H molecule undoubtedly has the symmetry C_s, and the eighteen normal vibrations divide themselves into eleven of species a' and seven of species a''. When the following interatomic distances C−F 1.36, C−C 1.54, and C−H 1.09 A, and tetrahedral angles, are assumed, the principal moments of inertia of the molecule are found to be 236.4, 353.0, and 427.7×10^{-40} g cm^2. The axis of intermediate moment is perpendicular to the symmetry plane. From Badger and Zumwalt's curves[11] it is found that the a'' fundamentals should have type B contours with a doublet separation of 4.6 cm^{-1}, whereas the a' fundamentals should have contours that are hybrids between types A and C.

The intense Raman band at 3000 cm^{-1}, and the less accurately measured infrared band at 3008 cm^{-1}, undoubtedly represent the highest a' fundamental. It may be ascribed to C−H stretching. In the region from 800 to 1500 cm^{-1} one would expect five a' and three a'' fundamentals involving C−H bending and C−F and C−C stretching. The bands at 866 and 1308 are readily identified as a' fundamentals, and the band at 1145 cm^{-1} can with equal certainty be assigned as an a'' fundamental. The infrared contours of the strong bands at 1200 and 1358 cm^{-1} are not well resolved, although the contour of the latter resembles type *C*. However, since both of these bands are diffuse in the Raman spectrum, they are interpreted as a'' fundamentals. The very strong infrared band at 1220 cm^{-1} appears to have

* A part of this work has been supported by the U. S. Atomic Energy Commission under Contract AT-(40–1)–1074.

† Present address: Wheaton College, Wheaton, Illinois.

‡ Present address: Box 187, R.F.D. No. 1, Hope Mills, North Carolina.

[1] Nielsen, Richards, and McMurry, J. Chem. Phys. **16**, 67 (1948).

[2] Nielsen, Claassen, and Smith, J. Chem. Phys. **18**, 1471 (1950).

[3] Smith, Brown, Nielsen, Smith, and Liang, J. Chem. Phys. **20**, 473 (1952).

[4] Smith, Saunders, Nielsen, and Ferguson, J. Chem. Phys. **20**, 847 (1952).

[5] Nielsen, Liang, Smith, and Smith, J. Chem. Phys. **21**, 383 (1953).

[6] Nielsen, Liang, and Smith, J. Chem. Phys. **21**, 1060 (1953).

[7] Nielsen, Liang, Smith, and Alpert, J. Chem. Phys. **21**, 1070 (1953).

[8] Nielsen, Liang, and Daasch, J. Opt. Soc. Am. **43**, 1071 (1953).

[9] Daasch, Liang, and Nielsen, J. Chem. Phys. **22**, 1293 (1954).

[10] K. W. F. Kohlrausch, *Der Smekal-Raman-Effekt* (Julius Springer, Leipzig, 1931).

[11] R. M. Badger and L. R. Zumwalt, J. Chem. Phys. **6**, 711 (1938).

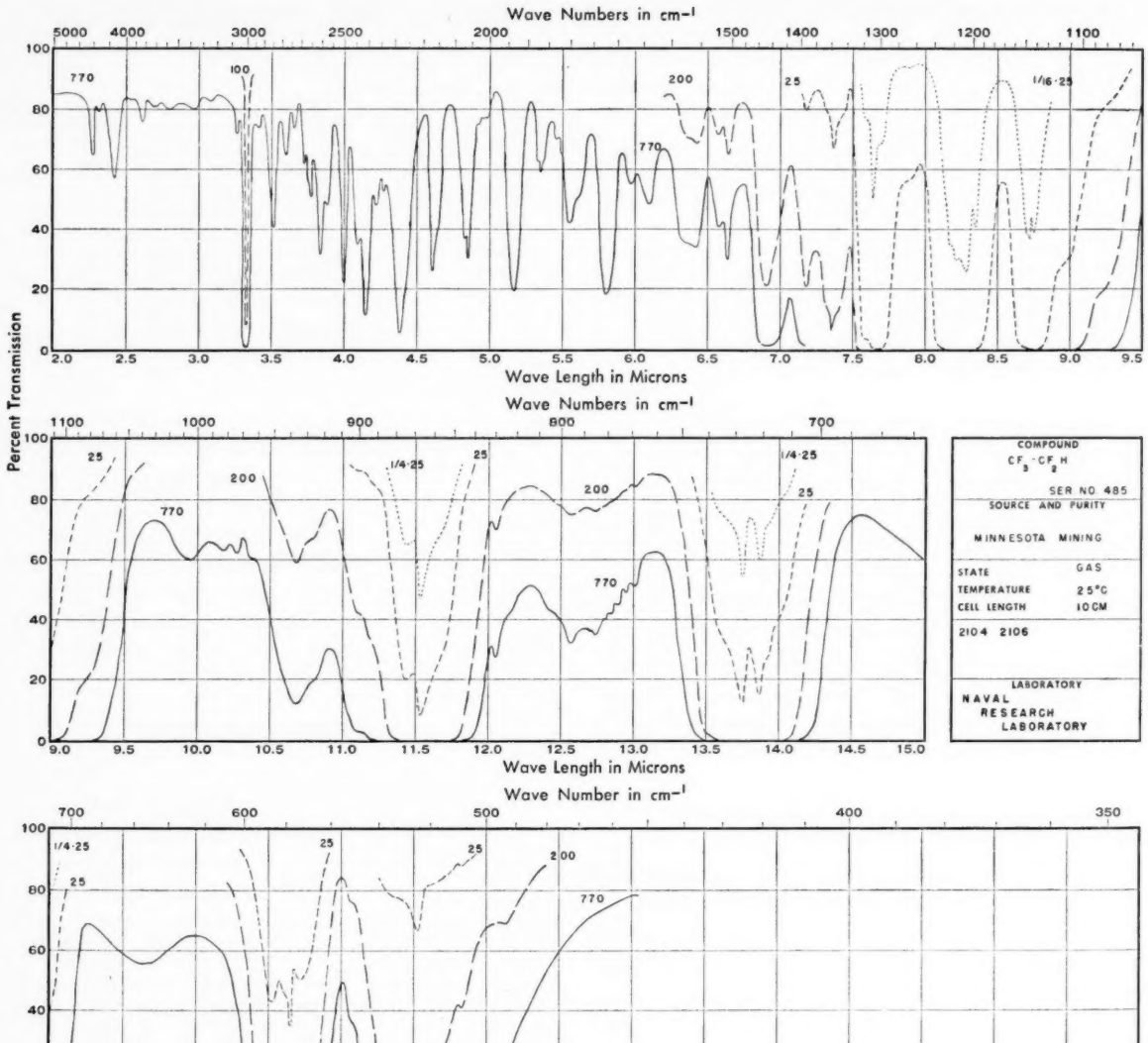

FIG. 1. Infrared absorption spectrum of pentafluoroethane gas. Not included are KRS-5 data.

a PQR structure, and the corresponding Raman band is sharp. These bands are therefore identified with an a' fundamental. The remaining two a' fundamentals in this region cannot be assigned with certainty but are assumed to be at 1111 and 1393 cm^{-1} where strong infrared bands with indefinite contours, but no Raman bands, are observed. An alternative to the latter fundamental is the slightly stronger infrared band at 1447 cm^{-1}. However, this is not as useful for interpreting the infrared spectrum and can readily be interpreted as a combination band.

At lower wave numbers there should be five a' and four a'' fundamentals, associated with deformations, rockings, and torsion. The bands at 578, 361, and 248 cm^{-1} can with considerable certainty be assigned as a' fundamentals. The intense infrared absorption maxima at 721 and 727 cm^{-1} resemble a type B band with somewhat too large QQ separation. However, the occurrence of two very sharp bands in the Raman spectrum indicates strongly that they must be interpreted as an a' fundamental in Fermi resonance with the overtone $2\times361=722$ A′. This is supported by the infrared spectrum of liquid CF_3CF_2H, which also indicates the presence of two bands. It is assumed therefore that an a' fundamental lies at about 725 cm^{-1}. The band at 525 cm^{-1}, which is strong and has fairly well resolved PQR structure in the infrared, but is not observed in the Raman spectrum, is assigned as the last a' fundamental.

The band at 414 cm^{-1} is strong in both spectra and very diffuse in the Raman spectrum. It undoubtedly represents an a'' fundamental. With somewhat less certainty the band at 270 cm^{-1}, which is weak in the

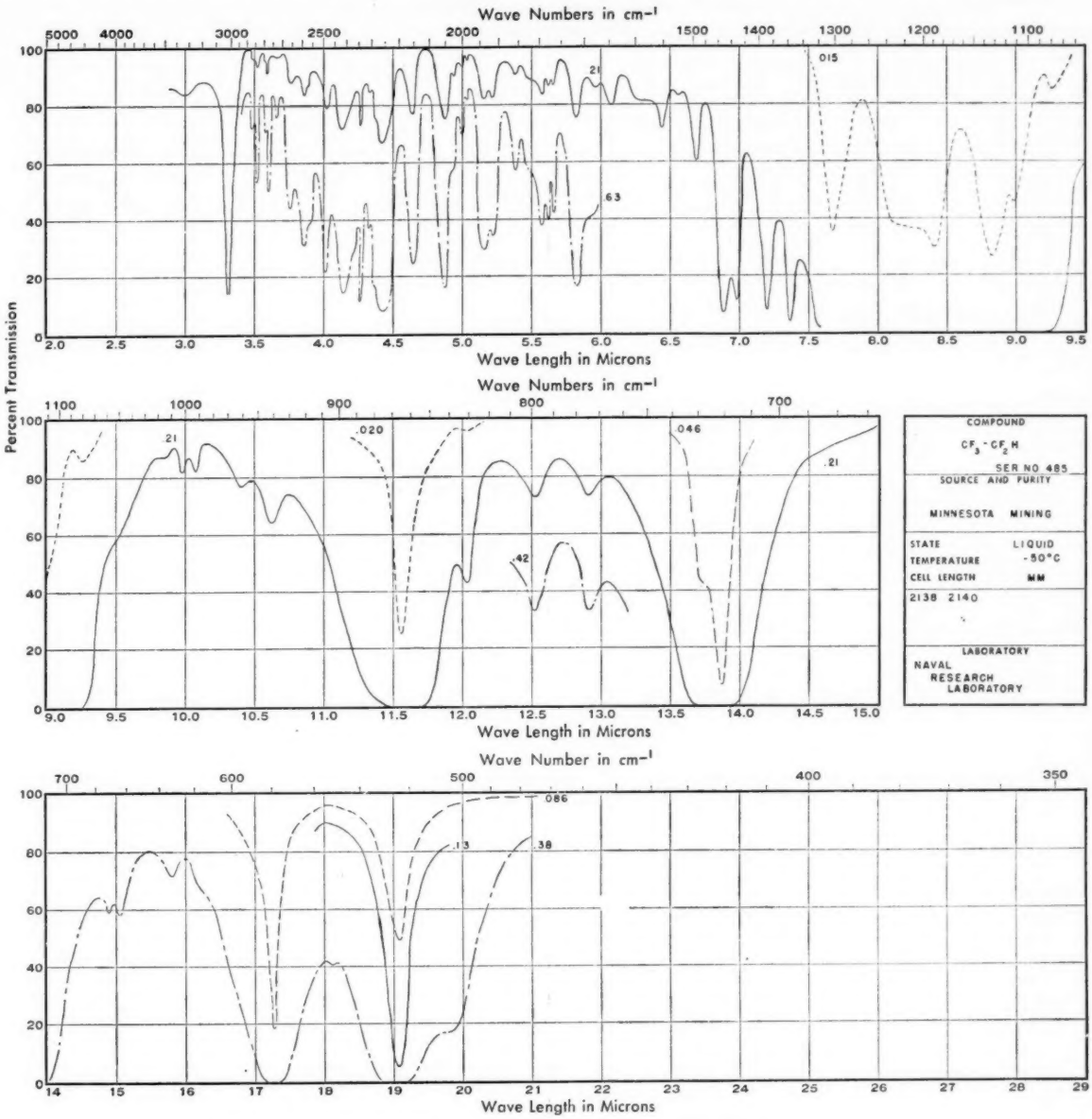

FIG. 2. Infrared absorption spectrum of liquid pentafluoroethane at −50°C.

infrared and very faint and diffuse in the Raman spectrum, is also interpreted as an a'' fundamental. There remain two fundamentals of this species. The lower of these, which can be ascribed largely to a torsional oscillation of one end of the molecule with respect to the other, undoubtedly lies outside the range of the infrared spectrometer and is masked in the Raman spectrum by the rather heavy background surrounding the exciting mercury line. Attempts to determine it from combination bands have been unsuccessful.

The higher of the two remaining a'' fundamentals, if it has been observed, must be identified either with the weak infrared band at 403 cm^{-1} or with one of the weak absorption maxima that overlap the 525 cm^{-1} a' fundamental at approximately 508 and 493 cm^{-1}. The latter band can be satisfactorily interpreted as the overtone of 248, and its wave number is not useful in interpreting the spectra. It has therefore been ruled out. The two other possibilities appear about equally probable. The assignment of 403 cm^{-1} as an a'' fundamental would explain a few weak infrared bands that cannot otherwise be interpreted satisfactorily, notably those at 1266(403+866), 926(403+525), 806(2×403), and 767 cm^{-1} (361+403). However, it does not seem reasonable that two fundamentals of the same species should lie as close together as 403 and 414 cm^{-1}. The assumption that the weak absorption maximum near 508 cm^{-1} represents the a'' fundamental in question is not quite as useful in interpreting the spectra, although it explains the weak bands at 778(270+508), 926(414+508), and

TABLE I. Infrared spectrum of pentafluoroethane.

Gas Wave number	Gas Description	Liquid (−50°C) Wave number	Liquid (−50°C) Description	Interpretation
<260[a]	s			a′ fundamental (248)
~270[a]	w			a″ fundamental
403[a]	w			
412[a]	s			a″ fundamental
493	w			2×248=496 A′
508	w	503	w	a″ fundamental
~518	s			
525	s, sh	525	s	a′ fundamental
~535	s			
~551	vw	~552	vw	2×270=540 A′
573	s			
578	s, sh	579	s, sh	a′ fundamental
~581	s			
587	s			
		608	vvw	248+361=609 A′
		633	vw	270+361=631 A″
~654	w, b	664	w	248+414=662 A″
		671	w	270+414=684 A′
~714	s			
~717	s			
721	vs, sh	720	vs, sh	2×361=722 A′
727	vs, sh	728	vs, sh	a′ fundamental
~735	s			
767	vw			2×248+270=766 A″
772	vw			248+525=773 A′
~775	vw	774	w	361+414=775 A″
778	vw			270+508=778 A′
781	w			1145−361=784 A″
784	w			
796	w	799	w	270+525=795 A″
~806	w			1220−414=806 A′
~824	w			248+578=826 A′
830	w	831	w	2×414=828 A′
~855	s			2×248+361=857 A′
867	vs, sh	864	s, sh	a′ fundamental
874	s			
~892	w			361+525=886 A′
~901	w			2×270+361=901 A′
~926	m			414+508=922 A′
936	m	941	w	361+578=939 A′
965	vw			248+2×361=970 A′
974	vw			248+725=973 A′
983	vw			414+578=992 A″
		997	vw	270+725=995 A″
1005	vw, b	1003	vw	2×248+508=1004 A″
		1013	vw	2×598=1016 A′
		1045	w, b	2×525=1050 A′
1081	m, b	1079	m	361+725=1086 A′; 508+578=1086 A″
1111	s	1110	s	a′ fundamental
1143	vs	1133	vs	a″ fundamental
1147	vs			
1198	s, sh	1188	vs	a″ fundamental
1208	s			
1218	vs	~1222	vs	a′ fundamental
~1224	s			
~1266	m			525+725=1250 A′; 414+866=1280 A″
~1299	s			
1309	vs, sh	1300	vs	a′ fundamental
~1316	s			
1359	s, sh	1355	s	a″ fundamental
1393	m, sh	1387	m	a′ fundamental
		1433	m	578+866=1444 A′
1447	m	1449	m	248+1200=1448 A″; 2×725=1450 A′
1506	w	1495	w	361+1145=1506 A″
1520	w	1524	vw	414+1111=1525 A″
1558	w	1553	w	248+1308=1556 A′; 414+1145=1559 A′; 361+1200=1561 A″
1580	w	1592	vw	361+1220=1581 A′; 270+1308=1578 A″; 725+866=1591 A′
1639	w	1645	w	525+1111=1636 A′; 248+1393=1641 A′
1675	w	1681	vw	270+1393=1673 A″; 578+1111=1689 A′
1721	w	1718	w	578+1145=1723 A″; 525+1200=1725 A″
		1772	w, sh	414+1358=1772 A′
1779	vw	1779	w, sh	578+1200=1778 A″
1802	vw	1794	w, sh	414+1393=1807 A″; 578+1220=1798 A′
1821	vw			508+1308=1816 A″
1832	vw	1828	vw	525+1308=1833 A′; 725+1111=1836 A′
1869	w, sh	1857	w	725+1145=1870 A″; 508+1358=1866 A′
1876	vw			525+1358=1883 A″; 578+1308=1886 A′
		1916	w	725+1200=1925 A″
1934	w	1934	w	578+1358=1936 A″
1992	vw	1988	vw	361+414+1220=1995 A′
2004	vw	2004	vw	866+1145=2011 A″
2016	vw			2×578+866=2022 A′
2028	vw	2028	vw	725+1308=2033 A′
2062	w, sh	2049	w	866+1200=2066 A″
2070	vw			725+1358=2083 A″; 866+1220=2086 A′
2155	w	2155	w	361+578+1220=2159 A′; 270+578+1308=2156 A″; 414+525+1220=2159 A″
2168	w, sh			866+1308=2174 A′
2257	w	2268	w, b	1111+1145=2256 A″; 866+1393=2259 A′
2283	w, sh	2291	vw	2×1145=2290 A′
		2315	vw, sh	1111+1200=2311 A″
2338	vw, sh	2347	w, sh	1145+1200=2345 A′
2364	vw, sh			1145+1220=2365 A″
2410	w, sh	2412	w	1111+1308=2419 A′; 1200+1220=2420 A″
2442	vw			2×1220=2440 A′; 1145+1308=2453 A″
2502	w, sh	2488	w, sh	1145+1358=2503 A′; 1200+1308=2508 A″; 1111+1393=2504 A′
~2574	w	~2562	w	1220+1358=2578 A″
2604	w, sh	2591	w, sh	1220+1393=2613 A′; 2×1308=2616 A′
2652	vw, sh	2660	w	1308+1358=2666 A″
2686	vw, sh			1308+1393=2701 A′
2732	vw, sh	2732	vw, sh	1358+1393=2751 A″; 866+725+1145=2736 A″
2782	vw, sh	2785	w, sh	2×1393=2786 A′
		~2801	vw	2×725+1358=2808 A″
2845	w	2849	w, sh	270+1220+1358=2848 A′
		2869	vw, sh	414+1145+1308=2867 A′; 2×866+1145=2877 A″
2933	vw			2×866+1200=2932 A″
3008	s, sh	3021	m, sh	a′ fundamental
3067	vw			725+1145+1200=3070 A′
3247	vw			248+3000=3248 A′; 270+3000=3270 A″
3367	vw	3344	vw, b	361+3000=3361 A′
3584	vw			578+3000=3578 A′
~3717	vw			725+3000=3725 A′
3831	vw			866+3000=3866 A′
4124	w			1111+3000=4111 A′; 1145+3000=4145 A″
4329	vw			1308+3000=4308 A′; 1358+3000=4358 A″
4405	w			1393+3000=4393 A′

[a] Observed with KRS-5 prism.

TABLE II. Raman spectrum of pentafluoroethane gas (5 atmos, 30°C).

Wave number	Description	Exciting Hg lines	Interpretation
248	m	*e*	*a'* fundamental
270	vw	*e*	*a''* fundamental
361.1	s, sh	±*e*	*a'* fundamental
416	m, d	*e,k*	*a''* fundamental
577.6	s, sh	*e,k*	*a'* fundamental
719.8	s, sh	*e,k*	2×361=722 A'
726.3	s, sh	*e,k*	*a'* fundamental
847	vw	*e*	270+578=848 A''
865.1	vs, sh	*e,k,i*	*a'* fundamental
890	vw	*e*	361+525=886 A'
920	vw	*e*	414+508=922 A'
1140.0	s	*e,k,i*	*a''* fundamental
~1150	w	*e*	2×578=1156 A'
1202	m, d	*e*	*a''* fundamental
1220	m, sh	*e*	*a'* fundamental
1307	m, sh	*e*	*a'* fundamental
1356	vw, d	*e*	*a''* fundamental
3000.4	vs, sh	*e,k,i,p,q*	*a'* fundamental

TABLE III. Fundamental vibration frequencies of pentafluoroethane.

Species	Infrared Gas	Infrared Liquid	Raman gas
a'	...	...	248 m
a'	...	...	361.2 s, sh
a'	525 s	525 s	...
a'	578 s	579 s	577.6 s, sh
a'	~725 vs	~725 vs	~725 s, sh
a'	867 vs	864 s	865.1 vs, sh
a'	1111 s	1110 s	...
a'	1218 vs	1222 vs	1220 m, sh
a'	1309 vs	1300 vs	1307 m, sh
a'	1393 m	1387 m	...
a'	3008 s	3021 m	3000.4 vs, sh
a''	...	...	...
a''	270 w	...	270 vw
a''	412 s	...	416 m, d
a''	508 w	503 w	...
a''	1145 vs	1133 vs	1140 s
a''	1198 s	1188 vs	1202 m, d
a''	1359 m	1355 m	1356 vw, d

1013 cm^{-1} (2×508). For the sake of definiteness in the tables, the latter assignment has been tentatively adopted.

The assigned fundamentals are listed in Table III. In terms of these fundamentals it has been possible to interpret satisfactorily all of the observed Raman bands and all but a few of the observed infrared absorption maxima. The interpretations are given in the last columns of Tables I and II.

DISCUSSION

Practically all of the infrared bands not taken as fundamentals have been interpreted as binary sum bands. Two weak bands are interpreted as binary difference bands and some ten very weak bands as ternary sum bands. Because of the large number of ternary combinations possible, not all such interpretations are listed, and most of them must be regarded as tentative.

The infrared band at 403 cm^{-1} can be interpreted in several ways in terms of the unknown torsional fundamental. However, no conclusive support could be found for any of the possibilities considered. Had 403 cm^{-1} been taken as an *a''* fundamental rather than 508 cm^{-1}, the latter could be interpreted as 248+270=518 A''.

The fundamentals assigned correlate satisfactorily with those of hexafluoroethane and CF_3CH_3.[1,2,12,13] However, since the spectra of CF_3CFH_2 are unavailable, no correlation diagram will be given.

ACKNOWLEDGMENT

The writers wish to express their indebtedness to the Minnesota Mining and Manufacturing Company for the gift of the sample.

[12] D. H. Rank and E. L. Pace, J. Chem. Phys. **15**, 39 (1947).
[13] J. Rud Nielsen and C. W. Gullikson, J. Chem. Phys. **21**, 1416 (1953).

The Kinetics of Coordinate Bond Formation. II

G. B. KISTIAKOWSKY AND R. WILLIAMS*
Gibbs Chemical Laboratory, Harvard University, Cambridge, Massachusetts
(Received August 12, 1954)

The technique of temperature pattern determination, shown previously to be suitable for the measurement of fast gaseous reactions, has been extended to reactions of boron trifluoride with ammonia, dimethylamine, *n*-butylamine, *t*-butylamine, and pyridine. The bimolecular rate constants of the first two of these show pressure dependence; those of the other three, within experimental error, do not. A comparison with the previously obtained results on methylamine and trimethylamine demonstrates that the lifetime of the "hot" quasi-molecules formed by the addition of boron trifluoride and an amine increases regularly with the number of vibrational degrees of freedom of the quasi molecule. The rates of addition are all substantially smaller than the rate of recombination of methyl radicals. They increase by about a factor of thirty from that of ammonia to those of heavier amines, being then about 1/30 of the collisional frequency. This finding is not consistent with the supposition that steric requirements alone limit the rates of addition and the existence of a small activation energy is clearly suggested, although it could not be observed experimentally. To explain the present results, the activation energy must decrease from ammonia to heavier amines. Such a decrease is found to be consistent with the presently accepted views on the electronic structure of the boron-nitrogen bond.

A NEW experimental technique for the study of fast gaseous reactions, which utilizes measurements of the temperature pattern[1,2] in the spherical "diffusion flames" of Polanyi[3] was shown to be applicable to reactions of boron trifluoride with some amines:

$$BF_3+NR_3=F_3BNR_3.$$

Quantitative results were obtained for the addition reactions of methylamine, dimethylamine, and trimethylamine.[1] The present study was undertaken to supplement the earlier results for the dimethylamine reaction and to explore the effect on the rate of the above reaction of diverse variations in the structure of the amine molecule.

EXPERIMENTAL

The general method and some of the apparatus were the same as used earlier,[2] and their description will not be given here. A modified method of admitting reagents and nitrogen carrier gas to the reactor was now employed. This consisted of four calibrated glass flow capillaries; one for each of the reactants, one for carrier gas entering the nozzle, and one for carrier gas entering the body of the reactor. Capillaries were calibrated by allowing the appropriate gas to stream through, under a known driving pressure, for a timed interval, and measuring the pressure increase in a connected flask of known volume. The dependence of flow rates on driving pressures was found to obey Poiseuille's equation quite accurately, permitting a small number of calibration points to be used for the computation of flow rates over a wide range of driving pressures. This arrangement also permitted measurements of the viscosities of some of the reactants, relative to nitrogen as a standard. These values of the viscosities were used to calculate the collision diameters of the reactant molecules which must be known to obtain rate constants by this method.

An improved thermocouple was used to measure the temperature patterns and is illustrated in Fig. 1. A flat plate of platinum 0.05 cm square and 0.003 cm thick at *A* was the hot junction. Soldered to this were 0.0018-cm diameter wires of iron, *AB*, and constantan, *AC*. *BD* was a stiff iron wire and *CD* was a fairly flexible constantan wire, having diameters considerably larger than that of the fine wires composing the hot junction. The heavier wires were soldered to copper leads at the cold junction *D*. It should be noted that the wires near the hot junction were arranged nearly tangentially to the isotherms in the reacting system. The mounting and positioning assembly were the same as used previously. The leads went through a shielded cable to the external detection equipment which consisted of a Perkin-Elmer Model-53 dc amplifier and a millivolt meter.

Temperature control was achieved by a stirred water thermostat bath.

The Reagents

Nitrogen:—Both purified nitrogen and Airco nitrogen were used as a carrier gas. They were admitted to the vacuum system by passing them through a drying column packed with "Drierite."

Dimethylamine:—The compound was prepared free of methylamine and trimethylamine by a recommended procedure[1] involving preparation and subsequent hydrolysis of the appropriate *p*-toluenesulfonamide derivative. This intermediate melted at 81.8–82.6°C. It was hydrolyzed and the resulting amine dried over sodium metal and KOH pellets.

* Shell Oil Company Predoctoral Research Assistantship 1951, Standard Oil Company of California Predoctoral Fellow 1952–1953.
[1] D. Garvin and G. B. Kistiakowsky, J. Chem. Phys. **20**, 105 (1952).
[2] Garvin, Guinn, and Kistiakowsky, Disc. Faraday Soc. (to be published).
[3] M. Polanyi, *Atomic Reactions* (Williams and Norgate, London, 1932).

n-butylamine:—Eastman Kodak *n*-butylamine was distilled from potassium hydroxide (to remove water) through a packed column at about 5 to 1 reflux ratio. A fraction boiling at 76–77°C was collected. It was dried with metallic potassium and then distilled into the vacuum system.

t-butylamine:—*t*-butylamine from Mathieson, Coleman, and Bell was distilled from KOH through a fractionating column packed with glass helices. A fraction boiling at 44–44.5°C was used; it had the reported refractive index.

Pyridine:—Mallinckrodt analytical reagent grade pyridine (bp 114–116°) was dried over sodium hydroxide and used without further purification.

Ammonia:—Mathieson anhydrous ammonia was admitted to the system through a drying column.

Boron trifluoride:—A high-pressure cylinder of BF_3 supplied by the Mathieson Company was used without further purification.

Calculations

The rate constants are obtained in the present method from the equation

$$k=\frac{c^2D_{12}}{z}, \tag{1}$$

where k is the bimolecular rate constant; z is the concentration of the atmospheric reactant; c is a parameter obtained from the shape of the experimentally determined steady state temperature pattern; D_{12} is the gas diffusion coefficient of the nozzle reactant into the gas surrounding it. The diffusion coefficient, D_{12},[2] requires a knowledge of the collision diameters of the molecules involved. These were obtained from various viscosity measurements using the equation:[4]

$$\sigma^2=\frac{0.1792(k'mT)^{\frac{1}{2}}}{\eta}, \tag{2}$$

where σ is the collision diameter; m is the mass of molecules; k' is the Boltzmann constant; T is the absolute temperature; η is the coefficient of viscosity. This equation is slightly different from that used by Garvin and Kistiakowsky.[1] Values used in this work are given in Table I along with their sources.

TABLE I. Collision diameters and viscosities at 298°K.

Substance	σ, A	η poises	Source
$(CH_3)_2NH$	6.22	···	Value reported for propane[a]
n-$C_4H_9NH_2$	7.37	0.73×10^{-4}	Calculated from reported value of η[b]
t-$C_4H_9NH_2$	7.06	0.795×10^{-4}	η measured during this work
C_5H_5N	7.35	···	[a]
NH_3	4.36	···	[a]
BF_3	4.65	1.76×10^{-4}	η measured during this work
N_2	3.57	···	From self-diffusion measurements[a]

[a] *Landolt-Börnstein Tables* (Springer Verlag, Berlin, 1951), sixth edition.
[b] A. Pochettino, Nuovo cimento 8, 33 (1914).

[4] S. Chapman and T. G. Cowling, *The Mathematical Theory of Non-Uniform Gases* (Cambridge University Press, Cambridge, England, 1939).

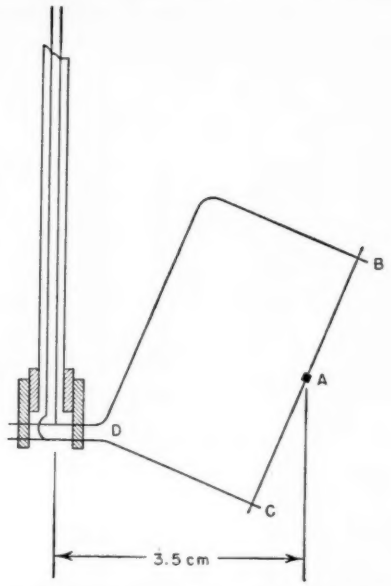

FIG. 1. Schematic drawing of the new thermocouple.

THE RESULTS

Most of the experiments were carried out near 25° with boron trifluoride acting as the nozzle reactant and the amine in the atmosphere. Some experiments were also made with the reactants interchanged and in a few experiments the reaction temperature was changed to 55°. The results are shown in Table II.

A previous attempt[1] to study the ammonia-boron trifluoride reaction was not successful because of extensive precipitation of the reaction product. The use of the dc amplifier permitted experiments to be made with smaller temperature gradients and therefore the use of more dilute reactants; this largely eliminated the condensation of the adduct on the thermocouple. The rate constants of this reaction show a strong pressure dependence, which is demonstrated in Fig. 2—a plot of the inverse of the rate constant against inverse pressure. The data are of course not accurate enough to prove that the inverse relationship is a linear one but if this is assumed, the best straight line fitting the data is shown in the plot.

The reaction of boron trifluoride with dimethylamine, which was briefly investigated before, was subjected to further experimentation because the parameters of the straight line drawn through the inverse plot of the previously obtained data seemed to be inconsistent with those of reactions with homologous amines. The present results agree, within experimental errors, with those obtained previously [after their recalculation in accord with Eq. (2)], but the straight line parameters

TABLE II. Experimental data on the reactions of several amines with BF_3.

Total flow moles/sec $\times 10^7$	x, mole fraction	z, fraction consumed	Total pressure, mm	c	$k \times 10^{-12}$ cc/mole sec	T°C
			1. BF_3+NH_3			
27.86	0.89[a]	0.004	0.167	1.0	0.072	25.4
27.86	0.89[a]	0.004	0.135	0.77	0.065	25.3
31.32	0.77[a]	0.004	0.208	1.52	0.14	25.3
30.28	0.77[a]	0.0043	0.349	2.51	0.14	25.0
30.28	0.77[a]	0.0043	0.383	2.90	0.154	24.9
25.71	0.88[a]	0.0044	0.174	1.15	0.088	24.8
27.06	0.79[a]	0.0042	0.401	3.17	0.16	21.4
24.12	0.87[a]	0.0043	0.189	1.13	0.072	21.4
11.69	0.0390[a]	0.198	1.123	2.68	0.265	24.6
11.09	0.0410[a]	0.198	0.985	2.05	0.188	24.5
8.81	0.0506[a]	0.201	1.025	1.97	0.132	22.9
8.81	0.0506[a]	0.201	1.133	2.43	0.163	22.9
			2. $BF_3+(CH_3)_2NH$			
5.33	0.199	0.06	0.108	1.26	1.07	55.5
5.33	0.199	0.06	0.108	1.56	1.59	55.5
4.44	0.248	0.05	0.120	2.27	2.18	55.5
4.62	0.247	0.05	0.114	2.05	1.98	55.5
4.94	0.188	0.05	0.114	1.80	2.07	55.5
5.94	0.084	0.20	0.301	2.66	1.58	55.5
6.15	0.084	0.21	0.301	3.53	2.74	55.5
6.48	0.062	0.28	0.312	2.6	1.85	55.5
5.72	0.117	0.22	0.074	1.00	1.93	22.0
5.99	0.118	0.21	0.102	1.34	1.79	23.1
6.43	0.120	0.19	0.105	1.67	2.62	22.1
5.73	0.117	0.22	0.134	2.52	3.72	21.8
9.14	0.095	0.17	0.135	2.51	4.55	21.7
6.43	0.120	0.19	0.163	3.4	4.49	22.3
7.43	0.121	0.19	0.178	4.24	5.86	21.7
5.91	0.118	0.21	0.194	3.83	4.14	23.0
7.78	0.082	0.15	0.372	5.0	2.71	22.4
7.34	0.061	0.22	0.314	3.82	3.05	22.6
6.98	0.060	0.26	0.247	3.44	4.11	22.1
7.25	0.105[a]	0.16	0.114	2.40	5.57	21.7
7.25	0.105[a]	0.16	0.134	2.98	6.28	21.7
16.65	0.044[a]	0.16	0.195	2.56	6.44	20.9
16.65	0.044[a]	0.16	0.238	3.21	6.75	21.0
			3. $BF_3+C_5H_5N$			
8.06	0.0583[a]	0.106	0.088	1.50	7.8	24.1
8.06	0.0583[a]	0.106	0.079	1.22	6.9	24.2
17.79	0.0236[a]	0.119	0.241	3.06	12	25.2
17.79	0.0236[a]	0.119	0.173	2.29	13	25.2
15.14	0.0244[a]	0.35	0.136	1.5	8.8	25.3
8.90	0.0416[a]	0.135	0.108	1.37	6.5	24.4
8.90	0.0416[a]	0.135	0.087	1.00	5.3	24.5
7.29	0.0631[a]	0.108	0.069	1.22	8.0	24.6
16.54	0.0278[a]	0.085	0.300	2.79	5.4	23.3
15.22	0.0243[a]	0.108	0.290	3.01	7.6	24.0
14.37	0.0258[a]	0.108	0.333	4.30	12	24.2
8.91	0.0146	0.220	0.220	2.62	9.0	23.7
8.91	0.0146	0.220	0.256	3.22	10.5	23.8
3.01	0.0415	0.240	0.117	2.60	12.0	19.1
2.93	0.0426	0.240	0.097	2.32	12.8	19.2
16.54	0.0278[a]	0.085	0.241	2.50	6.7	23.2
			4. $BF_3+n\text{-}C_4H_9NH_2$			
3.73	0.091	0.176	0.109	3.24	8.8	25.8
3.73	0.091	0.176	0.140	4.9	12.6	26.0
14.09	0.012	0.187	0.148	2.26	10.3	25.2
13.84	0.023	0.187	0.118	2.22	15.3	25.3
12.93	0.024	0.192	0.098	1.63	11.6	25.2
12.52	0.025	0.192	0.160	3.25	16.6	25.3
11.54	0.026	0.200	0.090	1.56	11.2	24.6
11.34	0.026	0.200	0.148	2.16	8.2	25.0
8.86	0.027	0.250	0.086	1.94	18.5	25.6
8.77	0.027	0.250	0.163	2.49	8.5	25.8
7.26	0.041	0.200	0.139	2.42	8.5	54.1
6.85	0.041	0.214	0.090	1.42	7.3	54.2
6.52	0.061	0.150	0.082	1.55	7.0	54.2
21.59	0.038[a]	0.134	0.203	2.80	8.6	23.6
21.59	0.039[a]	0.134	0.178	2.42	7.8	23.4
10.43	0.069[a]	0.153	0.122	2.10	6.8	23.1
			5. $BF_3+t\text{-}C_4H_9NH_2$			
9.35	0.0400[a]	0.162	0.127	1.58	6.1	23.1
6.98	0.0545[a]	0.157	0.107	1.61	6.7	22.0
6.98	0.0545[a]	0.157	0.263	4.0	6.8	22.2
6.98	0.0545[a]	0.157	0.096	1.52	7.4	22.3
17.02	0.0311[a]	0.094	0.344	3.77	6.66	24.3
16.82	0.0303[a]	0.098	0.307	3.35	6.7	24.4
12.47	0.0409[a]	0.098	0.232	2.87	6.3	24.5
7.92	0.058[a]	0.109	0.120	1.56	4.8	24.8
7.92	0.058[a]	0.109	0.194	2.73	5.7	24.9
8.72	0.052[a]	0.111	0.158	1.97	6.3	53.8
8.72	0.052[a]	0.111	0.232	2.72	5.6	53.9
8.43	0.052[a]	0.113	0.175	2.18	6.2	54.0
7.72	0.047	0.111	0.111	2.75	13.5	24.5
6.88	0.0334	0.174	0.121	2.95	18.6	25.1
6.88	0.0334	0.174	0.162	3.40	14.1	25.2
6.61	0.0333	0.182	0.166	3.83	17.1	24.1
9.13	0.0241	0.182	0.087	1.49	12.7	25.0
9.13	0.0241	0.182	0.190	3.35	13.4	25.2

[a] Runs in which the amine was the nozzle reactant.

are substantially different. We have chosen, on the accompanying Fig. 3, to plot all the available data and thus to determine the straight line parameters. This is an arbitrary procedure because it could be readily argued that the results obtained at 55° show systematic deviations from the others. However, these higher temperature rate constants are slightly lower than those at 25°, thus giving no evidence of an activation energy; therefore, it seemed preferable to include them in the averaging process. The limits of uncertainty of the resulting parameters are increased by this procedure, but the numerical values are not changed by large factors.

The other reactions investigated—with *n*-butylamine, *t*-butylamine, and with pyridine—show no pressure dependence exceeding experimental errors and therefore no inverse plots of these data are shown.

A rather puzzling situation was obtained with *t*-butylamine. While in experiments with other amines, the interchange of reactants resulted in changes of the rate constants which were well within the experimental errors; in this case a rather consistent change by nearly a factor of two was obtained, as can be seen by inspection of the data in Table II. It had been earlier suggested[1,2] that the atmospheric reactant may be depleted near the nozzle, which is not allowed for by the elementary theory used for the calculation of the rate constants. The consequence of such a depletion is an error in the calculation of the rate constant, and since a heavy amine should be more depleted than boron trifluoride,

TABLE III. Pressure dependence parameters of the reactions of several amines with borontrifluoride.

Amine	Range of total pressures investigated, mm	a	b	$P_{\frac{1}{2}}$, mm	τ, sec	No. of degrees of vibrational freedom
NH_3	0.14–1.1	37 ±30	14.7 ±4.7	0.40	2.4×10^{-7}	18
CH_3NH_2	0.1 –0.6	12.6 ±5.0	1.16 ±0.8	0.09	1×10^{-6}	27
$(CH_3)_2NH$	0.1 –0.37	1.70± 1.0	0.32 ±0.15	0.19	5×10^{-7}	36
C_5H_5N	0.07–0.33	1.07± 0.37	0.020±0.04	0.017	5×10^{-6}	39
$(CH_3)_3N$	0.04–0.40	2.68± 0.30	0.041±0.04	0.015	8×10^{-6}	45
n-$C_4H_9NH_2$	0.08–0.26	1.12± 0.47	−0.008±0.06	···	$>10^{-5}$	54
t-$C_4H_9NH_2$	0.09–0.35	1.59± 0.27	0.004±0.04	···	$>10^{-5}$	54

owing to its lower diffusion constant, the results on t-butylamine appeared thus qualitatively understood. However, the recent refined theory of the spherical diffusion flames worked out in this laboratory by Smith[7] shows that the depletion effects are negligible under the condition of the present experiments. An alternative explanation is an incorrect estimation of the collisional diameter of the amine molecule. This, however, was obtained from the relative viscosity measurements and agrees so well with the similarly determined diameters of analogous molecules that the required increase by almost 50 percent seems highly improbable. The amine used was tested for purity and found satisfactory, so that no explanation of the discrepancy can be offered, unless it be an accidental result of the random scattering of a limited number of data.

The pressure dependence parameters of all the reactions here investigated have been summarized in Table III. For the sake of completeness the previously presented data on the reactions of mono- and trimethylamine have been incorporated into this table. The parameters a and b shown in the table were derived from the equation:

$$\frac{10^{13}}{k}=a+\frac{b}{P} \qquad (3)$$

which follows if the reaction is assumed to have the Lindemann mechanism[8]:

$$A+B\rightleftarrows AB^*;\quad AB^*+M\rightarrow AB+M.$$

These parameters were obtained by the least squares method and the limits of error given are 90 percent confidence limits. The values of pressure given in the fifth column are those at which the rate constant has fallen to one half its high pressure value. The lifetimes of the quasi molecules shown in column six were calculated on the assumption that every collision results in their deactivation, the collisional diameters being estimated as those of the final adduct molecules.

The half-value pressures and the lifetimes, after allowance for large experimental uncertainties, are seen to change systematically with the total number of vibrational degrees of freedom in the adduct molecules, shown in the last column of the table.

Experimental difficulties limited the temperature interval over which measurements could be made to determine the temperature coefficients. In no case was a positive coefficient observed, as will be seen by inspection of Table II. In fact, the rate constants obtained at 55° are on the whole slightly lower than those at 25°. It has not been possible to ascertain whether this is due to accidental causes, some systematic trends due to instrumental factors, or whether it is a real effect. The large random scatter of the data permits only the conclusion that the activation energies of the reactions so studied are less than about 2 kcal.

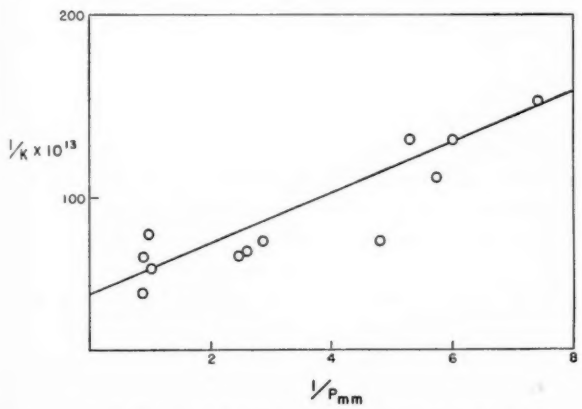

FIG. 2. Pressure dependence of the rate constants of the BF_3+NH_3 reaction.

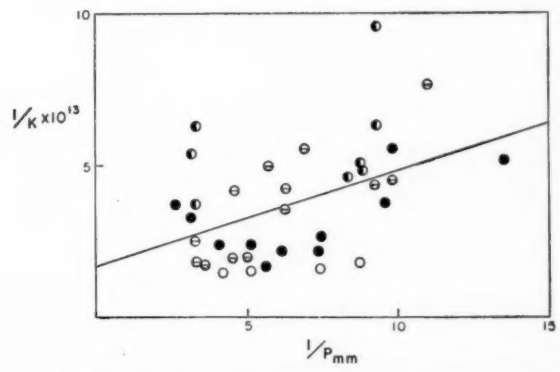

FIG. 3. Pressure dependence of the rate constants of the $BF_3+NH(CH_3)_2$ reaction. ○: z=amine; ●: $z=BF_3$; ◐: data at 55°; ⊖: data of Garvin.

[7] F. T. Smith, J. Chem. Phys. (to be published).

[8] F. A. Lindemann, Trans. Faraday Soc. **17**, 598 (1922).

TABLE IV. High pressure limiting rate constants.

Amine	k_1 cc/mole-sec	k_1/z (collision yield)
NH_3	2.7×10^{11}	0.001
CH_3-NH_2	6.7×10^{11}	0.003
$(CH_3)_2NH$	5.9×10^{12}	0.02
$(CH_3)_3N$	2.8×10^{12}	0.01
C_5H_5N	9.3×10^{12}	0.03
n-$C_4H_9-NH_2$	8.9×10^{12}	0.03
t-$C_4H_9NH_2$	6.3×10^{12}	0.02

The parameter "a" of Eq. (3) is the inverse of the rate constant for the formation of the energy rich quasimolecule F_3B-NR_3* and is also the over-all rate constant at high pressures. These constants have been assembled in Table IV, in which are also shown the ratios between these rate constants and collision frequencies of the reactants, calculated using the previously defined collision diameters. The rather surprising fact which emerges from this table is that the collision yield is smallest for ammonia and rises by about a factor of thirty for those of the heavier amines. Even for these, the association rate constants are significantly smaller than that observed for the methyl radical recombination reaction,[9] particularly if the electronic multiplicity factor in the latter is taken into consideration. Statistical calculations of the rates of these reactions have been carried out according to the Gorin-Eyring[10,11] model regardless of the implausibility of such a model for the heavier amines. It was found that the model predicts essentially the same high pressure rate constant for all these amines, the several factors entering into the theoretical equation varying in such a manner from one amine to another that the result remains substantially the same. This theoretical model, therefore, does not account for the observations. The possibility was considered then that the rotation of the components of the transition state may be restricted in some way. A model for which calculation was made assumed that free rotation about some principal axis of each reaction partner was possible only for a certain range of orientations of this axis with respect to the other reaction partner[12]—a physically rather plausible assumption. This leads, however, to the conclusion that the rate constant is reduced linearly with the allowed solid angle of orientations. Thus, to explain the observed trends it would be necessary to postulate that the rotation is more highly restricted in ammonia than in the large amines, a result which is not plausible. By elimination, therefore, one is led to the supposition that an activation energy is required for these reactions. Assuming free rotation in the transition state and unchanged vibrational frequencies, in other words a "frequency factor" which is substantially identical with the gas kinetic collision number, one finds from the data of Table IV, that the activation energies would have to decrease from about 4 kcal for ammonia to about 2.0 kcal for the heavy amines. But the assumption of a steric factor unity in the gas kinetic collision model of these reactions is highly improbable and therefore the actual activation energies must be lower, ranging perhaps from 2 kcal for ammonia to near zero for heavier amines. Thus it is not surprising that they were not observed in the present experiments.

The cause of the small activation energies in these reactions is suggested by the recent discussion of Mulliken,[13] who pointed out that the normal states of separate BF_3 and amine molecules lead to nonbonding repulsive states of the adduct molecules. He, as others before him, regards the normal state of the adduct as the consequence of a resonance between this electronic configuration and one resulting from the interaction of the ions BF_3^- and NR_3^+. The contribution of the nonbonding configuration is, of course, larger at larger distances of separation of the molecules BF_3 and NR_3, whereas at shorter distances the contribution from the bonding ionic terms predominates. Thus it is not unreasonable to suppose that at some intermediate B—N distances there exists a potential energy maximum. As substitutions are made in the ammonia molecule, two effects might be expected to decrease the resulting activation energy. The inductive effect, well-known in organic chemistry,[14] would tend to do so for all heavier amines except pyridine. An additional decrease of the net potential energy barrier will also result from the increasing London dispersion forces, which should be greater with all larger and thus more readily polarizable amines.

These two factors appear to us to be a highly plausible explanation of the observed trends in the high pressure rate constants.

Thanks are due the Mallinckrodt Chemical Company for financial support of this research and Professor William Moffitt for helpful discussions.

[9] Robert Gomer and G. B. Kistiakowsky, J. Chem. Phys. **19**, 85 (1951); G. B. Kistiakowsky and E. K. Roberts, J. Chem. Phys. **21**, 1637 (1953).

[10] E. Gorin, Acta Physicochim. U. R. S. S. **9**, 691 (1938).

[11] Glasstone, Laidler, and Eyring, *The Theory of Rate Processes* (McGraw-Hill Book Company, Inc., New York, 1941).

[12] L. Pauling and E. B. Wilson, *Introduction to Quantum Mechanics* (McGraw-Hill Book Company, Inc., New York, 1935).

[13] R. S. Mulliken, J. Am. Chem. Soc. **74**, 811 (1952).

[14] A. E. Remick, *Electronic Interpretation of Organic Chemistry* (John Wiley and Sons, Inc., New York, 1949).

A Mass Spectrometric Study of Gaseous Species in the Al-Al_2O_3 System*

RICHARD F. PORTER, PAUL SCHISSEL, AND MARK G. INGHRAM
Department of Physics, University of Chicago, Chicago, Illinois and Argonne National Laboratory, Lemont, Illinois
(Received July 7, 1954)

The vaporizing species in the Al-Al_2O_3 system are identified mass spectrometrically. Intense ion currents of Al_2O^+ formed from gaseous Al_2O are observed. At $T=1750°K$ ions formed from other gaseous oxides are at least 1000 times less intense than Al_2O^+. The appearance potential of Al_2O^+ is 7.7 ± 0.2 ev. A thermodynamic treatment of gaseous Al_2O gives for $Al_2O(g)=2Al(g)+O(g)$, $\Delta H_{298}=256\pm7$ kcal.

INTRODUCTION

IN their vapor pressure study of the aluminum-oxygen system, Brewer and Searcy[1] showed that under reducing conditions Al_2O_3 vaporizes to a different gaseous species than it does under neutral or oxidizing conditions. The volatility of Al_2O_3 in the presence of aluminum metal is over 100 times the volatility of Al_2O_3 without aluminum present. From thermodynamic arguments, Brewer and Searcy attributed this increase in volatility to the formation of gaseous Al_2O.

In the present work the vaporizing species of the Al-Al_2O_3 system, effusing from a Knudsen cell under equilibrium vapor conditions, were identified and studied directly in a mass spectrometer.

EXPERIMENTAL

Figure 1 shows the mass spectrometer mounting[2] containing the Knudsen effusion cell. The cell consisted of two crucibles, an outer tantalum crucible acting as the heating element and an inner ceramic crucible containing the Al-Al_2O_3 mixture. To prevent reaction between the two crucibles at higher temperatures, the center oxide crucible was separated from the tantalum by three small tungsten spacers. A ZrO_2 crucible proved to be a satisfactory container for the Al-Al_2O_3 mixtures in the temperature range studied. The tantalum cover on the Knudsen cell had an effusion hole one millimeter in diameter. The ratio of total vaporizing area of the Al-Al_2O_3 mixture to the effusion area was greater than 100. Unless a vaporizing species has an unusually low accommodation coefficient, the true equilibrium partial pressure of each gaseous species will exist inside the Knudsen cell. The tantalum crucible was heated by high-voltage electron bombardment from a surrounding tungsten filament. The Knudsen cell and heating filament were enclosed by tantalum radiation shielding. Temperatures were read with an optical pyrometer, sighting directly on the tantalum crucible through small holes in the radiation shields. Gases effusing out of the Knudsen cell enter directly into the ionization chamber of the ion source and are ionized. The ions are then accelerated into the magnetic field of a 60°, 12-inch, direction focusing mass spectrometer and are analyzed. Operating pressures in the ion source were less than 10^{-5} mm of Hg.

A sylphon-operated shutter between the Knudsen cell and the ion source, when open, allowed effusing gases to enter the ion source, and when closed prevented them from entering. Since backgrounds do not change by operating such a shutter, the difference in ion intensity with shutter open and shutter closed was a measure of the effect of vaporizing species only.

In a typical run, a 4 to 1 molar ratio of Al to Al_2O_3 was heated slowly to allow a gradual outgassing and was then brought to the desired operating temperature. The temperature range investigated was between 1500°K and 1800°K. A search for mass peaks corresponding to Al^+, AlO^+, Al_2O^+, $Al_2O_2^+$, and $Al_2O_3^+$ was made at different ionizing voltages and temperatures.

RESULTS

At a temperature of 1750°K intense ion peaks at masses 27 and 70 appeared with comparable intensity and were subsequently shown to be due to Al^+ and Al_2O^+, respectively. Both of these peaks were affected by operation of the shutter, showing ions were formed from gases coming out of the Knudsen cell. Under the same conditions, but at a higher sensitivity of the detector, the shutter had no detectable effect on peaks at mass 86 and 102, showing neither Al_2O_2 nor Al_2O_3 was coming out of the crucible in measurable quantities. From the detector sensitivity, we can state that, if any $Al_2O_2^+$ or $Al_2O_3^+$ ions were formed, their ion current intensities must be at least 1000 times smaller than the Al_2O^+ ion intensity. A slight shutter effect at mass 43, possibly due to AlO^+, was observed but a complicated background situation prevented a definite identification. Taking the total effect due to AlO^+, we obtain, as its upper limit, $AlO^+/Al_2O^+<1/1000$.

A weak ion peak at mass 72, due to a species coming out of the crucible, proved to be Al_2O^+ containing the O^{18} isotope. The intensity ratio of the 72 peak to the 70 peak gave the correct isotopic ratio of O^{18} to O^{16}, thus agreeing with the assignment of the mass 70 peak to Al_2O^+.

The appearance potential curves for Al_2O^+ and Al^+ are shown in Fig. 2. The observed appearance potential

* This work was supported in large part by a grant from the National Science Foundation.

[1] L. Brewer and A. W. Searcy, J. Am. Chem. Soc. **73**, 5308 (1951).

[2] W. A. Chupka and M. G. Inghram (to be published).

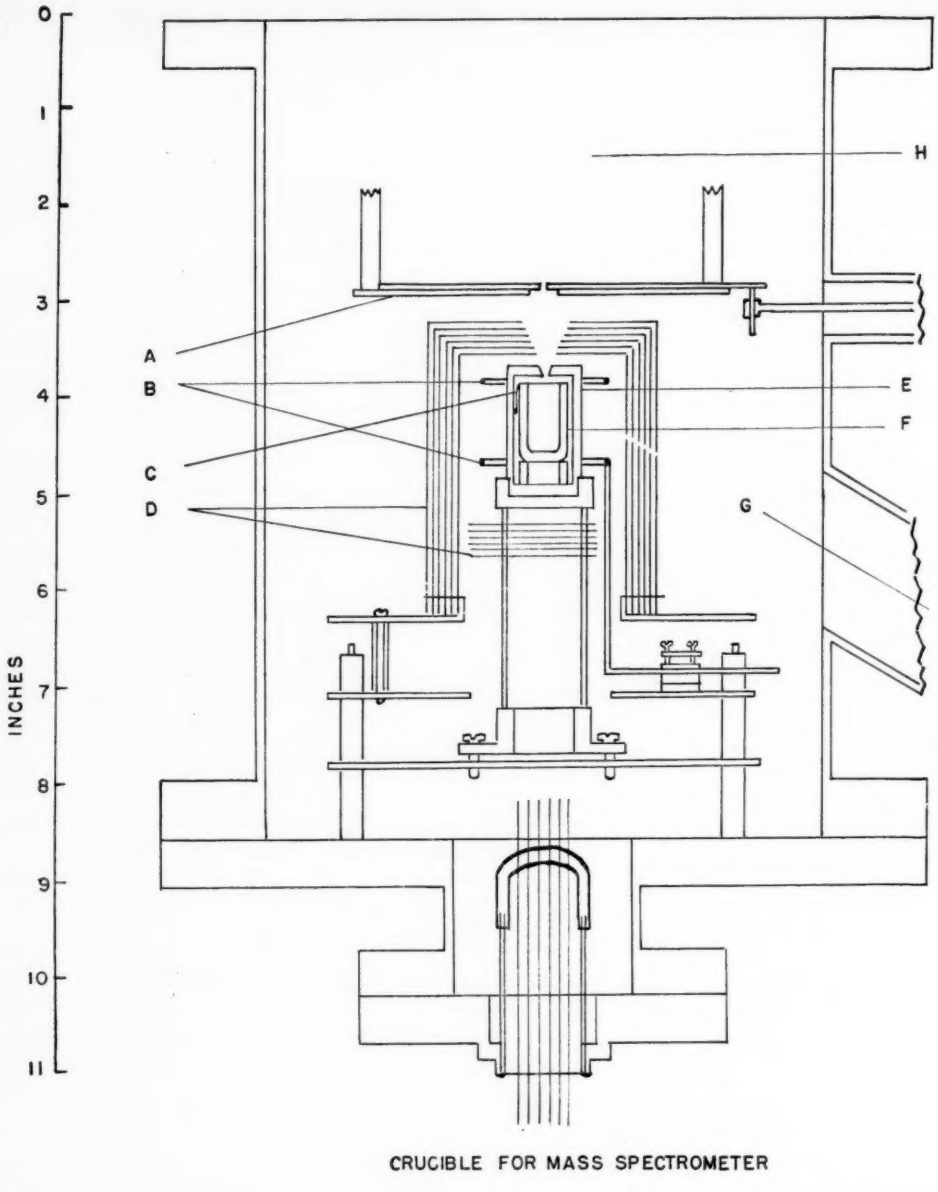

FIG. 1. The Knudsen cell assembly mounting for the mass spectrometer. (*A*) Shutter. (*B*) Filament. (*C*) Tungsten spacer. (*D*) Radiation shields. (*E*) Tantalum crucible. (*F*) ZrO_2 crucible. (*G*) Quartz window. (*H*) Position of ion source.

for Al^+ is within 0.1 ev of the ionization potential of aluminum. At low ionizing electron energies, the Al^+ is formed directly from Al gas and cannot form from dissociation of Al_2O gas. At higher voltages, however, Al^+ does form from Al_2O. Because of poorer ionizing efficiency at higher voltages, we would expect the appearance potential curve for Al^+ to have a rapid decrease in slope, as is the case for Al_2O^+. At higher voltages the Al^+ curve exhibits only a slight change in slope, and this is probably due to the formation of Al^+ from dissociation of Al_2O in addition to the Al^+ formed from ionization of Al.

The low ionization potentials required to produce sizable ion currents together with the fact that no other higher mass peaks were observed with any measurable intensity show that the Al_2O^+ ion is formed from $Al_2O(g)$ coming out of the Knudsen cell, and is not from a fragment formed by dissociation of other species in the ionization chamber.

HEAT OF FORMATION OF Al_2O GAS

For thermodynamic considerations, it will be assumed that gaseous Al_2O is in equilibrium with Al liquid and Al_2O_3. The resulting reaction is $4/3\ Al(l)+1/3\ Al_2O_3(s)=Al_2O(g)$. The heat for this reaction can be obtained by measuring the variation of Al_2O^+ ion current as a function of temperature. For temperatures above the melting point of aluminum $\Delta H=\Delta H_{932}+\Delta Cp(T-932)$ where ΔH_{932} is the heat of reaction at the melting point and ΔCp is an average difference in heat capacities between 932°K and 1800°K. An estimated heat capacity of 13 cal/deg was taken for $Al_2O(g)$. This value and the heat capacities for $Al(l)$ and $Al_2O_3(s)$, given by

Kelley,[3] give an average ΔCp of -7 cal/deg. Substituting the expression for ΔH into the van't Hoff equation and integrating gives

$$\Delta F/T=\frac{\Delta H_{932}-932\Delta Cp}{T}-\Delta Cp\ \ln T+\text{const.}$$

Setting $\Delta F/T$ equal to $-R\ \ln P_{Al_2O}$, taking the intensity of the Al_2O^+ ion current proportional to the partial pressure of $Al_2O(g)$ inside the Knudsen cell, and defining a quantity Σ, we obtain:

$$\Sigma=\log I_{Al_2O^+}+4.5\ \log T=-\frac{(6500+\Delta H_{932})}{4.575T}+\text{const},$$

where $I_{Al_2O^+}$ refers to the ion current intensity of Al_2O^+. A plot of Σ *vs* $1/T$ gives ΔH_{932}. A typical plot is shown in Fig. 3.

A similar treatment of the Al^+ peak was made. The reaction in the Knudsen cell is assumed to be $Al(l)=Al(g)$. Taking an average ΔCp of -2 cal/deg, we obtain $\Sigma=\log I_{Al^+}+2.0\ \log T=-(\Delta H_{932}-1900)/4.575T+\text{const}$, where I_{Al^+} is the ion current intensity of Al^+. A Σ plot for Al^+ is also shown in Fig. 3. Both plots were made from data taken during the same run. The ionizing electron energies for Al^+ and Al_2O^+ were 8 volts and 10 volts, respectively. These low electron energies were used so that dissociation processes would be negligible.

Slopes from three different runs on Al_2O^+ yielded an average value $\Delta H_{932}=85\pm5$ kcal for the reaction $4/3\ Al(l)+1/3\ Al_2O_3(s)=Al_2O(g)$. For $Al(l)=Al(g)$ we obtained an average value of $\Delta H_{932}=74\pm3$ kcal. Using an average ΔCp of -6 cals/deg between 298°K and 932°K, calculated from Kelley's[3] heat capacity data for $Al(s)$ and $Al_2O_3(s)$ and an estimated heat capacity of 12 cal/deg for $Al_2O(g)$, and 2.6 kcal for the heat of fusion of aluminum,[3] we obtain for the reaction

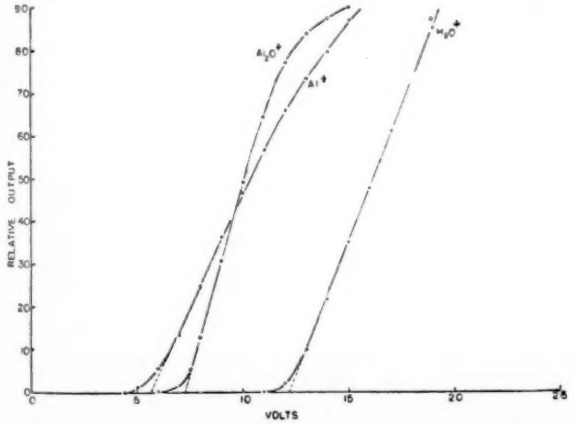

FIG. 2. The appearance of potential curves for Al_2O^+ and Al^+ which are calibrated against H_2O^+. The extrapolated curves give appearance potentials of 7.7 ± 0.2 ev for Al_2O^+ and 6.1 ± 0.2 ev for Al^+.

[3] K. K. Kelley, U. S. Bur. Mines Bull. 476 (1949).

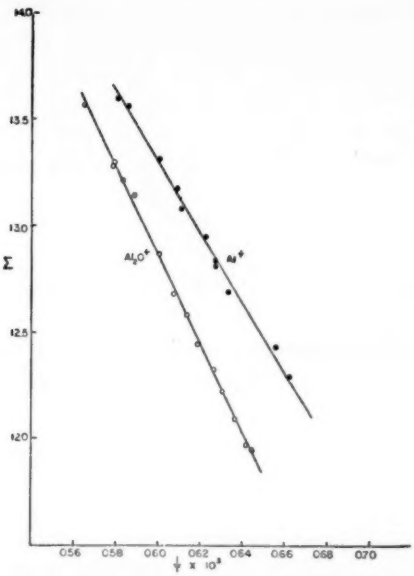

FIG. 3. The Σ plots for Al_2O^+ and Al^+. For Al_2O^+, $\Sigma=\log I_{Al_2O^+}+4.5\ \log T=-(\Delta H_{932}+6500)/4.575T+\text{const}$ and refers to the reaction $4/3\ Al(l)+1/3\ Al_2O_3(s)=Al_2O(g)$. For Al^+, $\Sigma=\log I_{Al^+}+2.0\ \log T=-(\Delta H_{932}+1900)/4.575T+\text{const}$ and refers to the reaction $Al(l)=Al(g)$.

$4/3\ Al(s)+1/3\ Al_2O_3(s)=Al_2O(g)\ \Delta H_{298}=92.5\pm5$ kcal. Combining this heat with the value of -133.4 ± 0.1 kcal for the heat of formation of $1/3\ Al_2O_3(s)$[4] yields for $2\ Al(s)+1/2\ O_2(g)=Al_2O(g)\ \Delta H_{298}=-40.9\pm5$ kcal. With the same heat of fusion of aluminum and an average ΔCp of 1.6 cal/deg between 298°K and 932°K, we obtain for $Al(s)=Al(g)\ \Delta H_{298}=77.5\pm3$ kcal. This value is to be compared with the more accurate value of 77.4 ± 1.4 kcal.[1] Using the better value for the heat of sublimation of aluminum and ΔH_{298} of 119.1 kcal for $O_2(g)=2\ O(g)$ together with the heat of formation of $Al_2O(g)$ obtained in these experiments, we now get for $Al_2O(g)=2\ Al(g)+O(g)\ \Delta H_{298}=256.3\pm7$ kcal. This is in good agreement with the value of 248 ± 7 kcal obtained by Brewer and Searcy.

In a recent high-temperature x-ray study of the Al-Al_2O_3 system, Hoch and Johnston[5] report the existence of an Al_2O solid phase in the temperature region of this investigation. Since we did not have a large excess of aluminum in our Al-Al_2O_3 mixtures, the formation of an Al_2O solid phase will remove all the liquid aluminum. The equilibria inside the Knudsen cell will actually be: $Al_2O(s)=Al_2O(g)$ and $Al_2O(s)=4/3\ Al(g)+1/3\ Al_2O_3(s)$. This will not seriously affect our final result, however, as it is reasonable to assume the heat for the reaction $4/3\ Al(l)+1/3\ Al_2O_3(s)=Al_2O(s)$ is close to zero. Hoch and Johnston have demonstrated that the Al_2O phase is unstable at low temperatures and that it becomes stable only above a temperature

[4] P. E. Snyder and H. Seltz, J. Am. Chem. Soc. **67**, 683 (1945).
[5] M. Hoch and H. L. Johnston, J. Am. Chem. Soc. **76**, 2560 (1954).

near the temperature of our experiments. Therefore, we know that the free energy of formation of Al_2O from Al and Al_2O_3 must be close to zero. Since the entropy of reaction must be small, the heat of reaction must also be close to zero. In confirmation of this, we find that the heat from the Σ plots of $Al(l)=Al(g)$ agrees with the true heat of sublimation of aluminum within experimental error. Thus we are justified in treating the data as though $Al(l)$ actually existed inside the crucible. The error in neglecting the heat of phase transition should be well within the experimental uncertainty in the heat of formation of $Al_2O(g)$.

THE JOURNAL OF CHEMICAL PHYSICS VOLUME 23, NUMBER 2 FEBRUARY, 1955

The Determination of Particle Size and Refractive Index Near the Turbidity Maximum in Monodisperse Suspensions of Spherical Particles*

WILFRIED HELLER
Chemistry Department, Wayne University, Detroit, Michigan
(Received July 7, 1954)

Theoretical values on the specific turbidity of colloidal spheres within the range of diameters of 1 to 2 microns are given. It is shown how an unambiguous particle size can be determined within this range in spite of a turbidity maximum. The latter can be determined for almost any refractive index by means of an empirical equation. An alternate turbidity maximum can be used for determining the refractive index of the light scattering material provided the diameter is known.

A PRECEDING preliminary publication[1] gave the specific turbidity, $(\tau/c)_0$, for colloidal solutions of nonabsorbing spherical particles as derived from the Mie theory. These data have now been extended to include also the lower range of microscopic diameters (up to 1.96 microns if the wavelength, *in vacuo*, $\lambda_0=5461$ a.u.) and are given in Table I for 5461 a.u.[2,3] The monotonic character of the curves observed throughout the major part of the colloidal range[1] ceases here, except for $m\leqslant 1.10$, because of the passage of the first $(\tau/c)_0(D)$ maximum. Consequently, experimental $(\tau/c)_0$ data become bivalued with regard to coordinated particle diameters, D, in microns, as illustrated in Table II for $m=1.20$ and $\lambda_0=5461$ a.u.

A suitable criterion is then necessary in order to decide whether a given $(\tau/c)_0$ is associated with the ascending or descending branch of the $(\tau/c)_0(D)$ curve. The simplest solution is a second turbidity measurement carried out at a different wavelength, say at 4358 a.u. If the alternate $(\tau/c)_0$ value is smaller, then D_0 applies whenever $D_0\gg D_2$. Any ambiguity is avoided by the compilation of a turbidity spectrum[4] which furnishes the wavelength exponent[5] as an entirely independent measure of particle size. The differential exponent[1] declines to the value of zero at the $(\tau/c)_0(\lambda)$ maximum and inverts its sign beyond it. Within a limited size range, defined by m, a closely related, but faster method suggests itself, i.e. the mere scanning of the turbidity

TABLE I.

α \ m	$(\tau/c)_0$ cm^{-1} 1.05	1.10	1.15
8	44.8018	169.033	331.500
9	50.3228	184.263	343.447
10	55.6320	197.137	346.898
11	60.7279	207.440	342.648
12	65.6199	215.249	331.531
13	70.2758	220.632	314.536
14	74.6969	223.606	292.941
15	78.8781	224.215	262.770

α \ m	$(\tau/c)_0$ cm^{-1} 1.20	1.25	1.30
8	473.482	544.076	517.976
9	456.120	471.681	404.054
10	423.747	390.457	307.033
11	380.572	312.353	228.880
12	331.282	245.654	174.339
13	280.618	193.651	148.225
14	232.722	156.163	148.461
15	190.811	132.999	168.504

* This work was carried out with the support of the Office of Naval Research.

[1] W. Heller and W. J. Pangonis, J. Chem. Phys. **22**, 948 (1954).

[2] Computation of the primary functions, from which the data given here are derived, were carried out by the Computation Laboratory of Wayne University (using the Unitized Digital Electronic Computer, UDEC). These functions, together with previous ones (reference 1) computed manually by W. J. Pangonis will appear shortly elsewhere.

[3] The meaning of symbols and the conditions under which numerical values given apply, were previously defined (reference 1), except for c which in both instances represents the concentration of light scattering material, in g per 100 g of dispersed system assuming a density of 1.0 for both. Experimental $(\tau/c)_0$ values, to agree with the theoretical ones, must be extrapolated to infinite dilution and apply to a layer of 1.0 cm.

[4] This term is proposed to supersede the term "Tyndall spectrum," previously introduced (reference 5), in those instances where the wavelength dependence of transmitted light rather than that of the laterally scattered light is meant. In spite of the intimate relation between the two wavelength functions, their differentiation in terminology is advisable in order to avoid misunderstandings.

[5] W. Heller and E. Vassy, J. Chem. Phys. **14**, 565 (1946).

spectrum in order to locate the wavelength of maximum turbidity. The scope and limits of practicality of the procedure follow from Table III which gives the theoretical diameter of the particles, D', associated with a maximum of $(\tau/c)_0(\lambda)$ at the respective wavelength, λ_0, if $m=1.20$.

Whichever of the three related methods is chosen to avoid bivalued results, it is desirable to know beforehand the location of the $(\tau/c)_0(D)$ maximum for a given m. An empirical equation can be derived which allows to pinpoint the maximum at any m, excepting $m \lesssim 1.10$, *viz.*,

$$\alpha_M=\alpha_\infty+\alpha_0 e^{-bm}. \quad (1)$$

Here α_M represents the α value at the $(\tau/c)_0(D)$ maximum, if $\lambda_0=5461$ A. The equation is tested in Table IV where the second and fourth columns give, respectively, the α value at the $(\tau/c)_0(D)$ maximum as found or interpolated from the theoretical curves ($\alpha_M{}^0$), and the particle diameter, D_M, corresponding to α_M. The values with asterisks apply to aerosols rather than liquid dispersions and were calculated from alternate light

TABLE II.

$(\tau/c)_0$:	350	370	390	410	430	450	470
D_1:	1.5198	1.465	1.409	1.348	1.288	1.208	1.080
D_2:	0.5375	0.5675	0.6092	0.6575	0.7136	0.7775	0.8845

TABLE III.

D':	0.50	0.75	1.00	1.25	1.50	1.75	2.00	3.00
λ_{0M}(a.u.):	2042	3063	4084	5105	6126	7147	8168	12252

scattering functions.[6] Their inclusion demonstrates the wide range of usefulness of Eq. (1).

The first $(\tau/c)_0(D)$ maximum is followed by a first minimum, beyond which D values derived from $(\tau/c)_0$ are triple-valued. This cannot be expected, however, for α values smaller than 20 ± 2, ($D\sim2.5$ microns) if $m=1.20$($\lambda_0=5461$ a.u.). This further complication is immaterial because particle size measurements from turbidity rapidly loose interest above $\alpha=15-20$ on account of a fast increasing insensitivity of $(\tau/c)_0$ to particle size.

[6] Light scattering functions for spherical particles, R. O. Gumprecht and C. M. Sliepcevich, University of Michigan (1951).

TABLE IV.

m:	$\alpha_M{}^0$	α_M	D_M
1.05	...		2.17_2
1.10	...		1.45_6
1.15	10.0 ± 0.5	10.0_1	1.30_6
1.20	7.55 ± 0.2	7.75	1.01_1
1.25	6.05 ± 0.05	6.12	0.798
1.30	5.00	5.00	0.652
1.35	...	4.20	0.548
1.40	4.0 ± 0.5*	3.63	0.474
1.45	...	3.23	0.421
1.50	3.25 ± 0.25*	2.94	0.384
1.55	...	2.74	0.357
1.60	2.5 ± 0.25*	2.60	0.339

The strong variation of D_M with m, at a given λ_0, implies a strong variation of λ_{0M}, the wavelength at which the $(\tau/c)_0(\lambda)$ maximum occurs, with m, at a given D. Considering for example $D=1.000$ micron, the turbidity maximum, in water at 25°C, should occur at $\lambda_0=3089$, 4125, and 5074 a.u. if $m=1.15$, 1.20, and 1.25, respectively. Locating the first $(\tau/c)_0(\lambda)$ maximum by means of turbidity spectra should therefore afford a simple and quite precise method for determining the refractive index, μ, of the light scattering material if the diameter is known from an independent method, e.g. electron microscopy. The $\lambda_{0M}(m)$ curve indicates that locating the maximum with an uncertainty of ±30 A should give μ with an uncertainty not to exceed ±1 percent.

Finally, it is noteworthy that non-monochromatized light of an incandescent source, observed through a liquid dispersion of scattering dielectric spheres, should possess nearly complementary colors above and below the $(\tau/c)_0(\lambda)$ maximum affording a rapid visual check of the minimum or maximum particle size present in a fairly monodisperse system. Considering again $m=1.20$, the transmitted light should have a purple, greenish, or bluish tinge for $D>1.0$ and <1.75 microns while it is red, orange, or yellow—depending on concentration and layer thickness—if $D<1.0$ microns. An important practical implication is that the emission of yellow radiation instead of white light, of equal total intensity, may under proper circumstances critically reduce signals of an object approaching through a turbid environment contrary to the opposite view generally held. No problem exists for D values in excess of 2.5 microns since the attenuation of visible radiation by a turbid medium is then less sensitive to wavelength.

Energy Calculations for the Linear H_3^+ Ion System*

ROLAND S. BARKER, J. CALVIN GIDDINGS, AND HENRY EYRING
Department of Chemistry, University of Utah, Salt Lake City, Utah

(Received March 4, 1954)

A study of the dependence of the energy calculations for the linear triatomic hydrogen ion system H_3, on a single polarization (electron cloud displacement) parameter g, and on two effective orbital charge parameters Z_0 and Z_m is presented. The studies, with separate screening parameters for the central and outer atomic orbitals, used normalized approximate integrals. The individual variation of Z_0, the charge associated with the outer orbitals, and of Z_m, the charge associated with the central orbital, gave little improvement of the energy calculation. From these results with approximate integrals, calculations, at this time, using the exact integrals appear unprofitable.

Only exact integrals are used in the study dealing with the off-center electron cloud parameter, g. These exact integral calculations led to an energy of -158.07 kcal/mole which is 2.74 kcal/mole better than the best previously obtained value for this linear system.

1. INTRODUCTION

THERE has recently been a revival of interest in carrying through comprehensive energy calculations for the simpler multiparticle systems of molecular quantum mechanics.[1,2] Energy evaluations for the H_3^+-linear system are here examined. Comparisons with the triangular system will be made later.[3] Methods employing exact values of the integrals that turn up from the use of various approximate treatments have received comment before.[1,4] Approximate trial functions used recently have been both expressed in terms of molecular orbital theory[5,6] and in terms of modified atom-like orbitals.[7,8] This paper belongs to the latter category.

The most complete molecular orbital formulation for this system was shown by Walsh, Moore, and Matsen[5] to be equivalent to the complete valence bond-plus-ionic-terms treatment of Hirschfelder, Eyring, and Rosen.[9] Improvements that can now be made on this latter definitive work are considered. The modifications are, first the inclusion of separate screening constants for the middle and outer nuclear orbitals and second, the use of Gurnee and Magee off-center orbitals.

First principle energy calculations for the system were made sometime ago by Coulson[10] and by Massey.[11] The Hamiltonian operator is written

$$H=-\tfrac{1}{2}\sum_{i=1}^{2}\nabla_i^2-\sum_{i=1}^{2}(r_{ai}^{-1}+r_{bi}^{-1}+r_{ci}^{-1}) +R_{ab}^{-1}+R_{bc}^{-1}+R_{ac}^{-1}+r_{12}^{-1}, \quad (1.1)$$

where the three nuclei are $\mathfrak{A}$, $\mathfrak{B}$, and $\mathfrak{C}$; the electrons 1 and 2; the fixed internuclear distances is R_{ab}, R_{bc}, and R_{ac} and the variable interelectronic distance is r_{12}. The linear symmetrical considerations used in this paper make $R_{ab}=R_{bc}=R$ and $R_{ac}=2R$.

The simple covalent bond trial function ψ_1 represents a bond between the $\mathfrak{A}$ and $\mathfrak{B}$ nuclei oscillating with one between the $\mathfrak{B}$ and $\mathfrak{C}$ nuclei. It is constructed of 1 s-like atomic orbitals; thus

$$\psi_I=\begin{pmatrix}a & b\\ \alpha & \beta\end{pmatrix}-\begin{pmatrix}a & b\\ \beta & \alpha\end{pmatrix}+\begin{pmatrix}b & c\\ \alpha & \beta\end{pmatrix}-\begin{pmatrix}b & c\\ \alpha & \beta\end{pmatrix}$$
$$=(2)^{-\frac{1}{2}}[a(1)b(2)+a(2)b(1)+b(1)c(2) +b(2)c(1)][\alpha_1\beta_2-\alpha_2\beta_1], \quad (1.2)$$

where the electron spins are α(positive) and β(negative), and the atomic orbitals are

$$a(1)=(Z_0^3/\pi)^{\frac{1}{2}}e^{-Z_0r_{a1}}, \quad b(2)=(Z_m^3/\pi)e^{-Z_mr_{b2}},$$

and so forth. The major difference in (1.2) from previous work is the inclusion in the atomic orbitals of two screening charge parameters. The results of this distinction between the screening constants Z_0 and Z_m associared with the middle and outer orbitals are given in section 2.

The H_3^+ ion employs integrals calculated by the same methods as those employed previously[8] for the H_2 molecule. However, separate integral evaluations are required because of the range of the variables. The results are not as encouraging as those for the molecule.

In the second phase of the work (reported in Sec. 3) the constituent off-center orbitals of the type first used by Gurnee and Magee[7] are employed in the trial function. Specifically, the outer orbitals associated with nuclei $\mathfrak{A}$ and $\mathfrak{C}$ are considered to center about points **A** and **C**. These orbitals are designated as $A(1)$, $A(2)$, $C(1)$, and $C(2)$. Thus, for example, the orbit of electron 1 is centered at a point displaced a distance g inward from its associated nucleus $\mathfrak{A}$ and is written

$$A(1)=(1/\pi)^{\frac{1}{2}}e^{-r_{A1}}, \quad (1.3)$$

* This work was assisted in part by a grant from the National Science Foundation.

[1] R. O. Brennan and J. F. Mulligan, J. Chem. Phys. **20**, 1635 (1952).
[2] G. E. Kimball, Ann. Rev. Phys. Chem. **2**, 181 (1951).
[3] R. S. Barker and H. Eyring (to be published).
[4] R. S. Mulliken, Chem. Revs. **41**, 201 (1947).
[5] Walsh, Moore, and Matsen, J. Chem. Phys. **18**, 1070 (1950).
[6] R. G. Pearson, J. Chem. Phys. **16**, 502 (1948).
[7] E. F. Gurnee and J. Magee, J. Chem. Phys. **18**, 142 (1950).
[8] R. S. Barker and H. Eyring, J. Chem. Phys. **22**, 1182 (1954).
[9] Hirschfelder, Eyring, and Rosen, J. Chem. Phys. **4**, 121 (1936).
[10] C. A. Coulson, Cambridge Phil. Soc. Proc. **31**, 244 (1935).
[11] H. S. W. Massey, Cambridge Phil. Soc. Proc. **27**, 541 (1931).

where r_{A1} is the variable distance of the electron 1 from the orbital center A. Orbitals associated with the nucleus ℬ are not displaced. The complete trial function used is

$$\psi = C_1\psi_1 + C_2\psi_2 + C_3\psi_3 + C_4\psi_4, \tag{1.4}$$

where the C's are variational parameters. The simplest covalent structural function ψ_I has already been defined (1.2). Slight modification of the composite orbitals are used in this second phase of this study. Thus,

$$\psi_1 = \begin{pmatrix} A & b \\ \alpha & \beta \end{pmatrix} - \begin{pmatrix} A & b \\ \beta & \alpha \end{pmatrix} + \begin{pmatrix} b & C \\ \alpha & \beta \end{pmatrix} - \begin{pmatrix} b & C \\ \beta & \alpha \end{pmatrix}$$

$$= (1/2)^{\frac{1}{2}}[A(1)b(2) + A(2)b(1) + b(1)C(2) + b(2)C(1)][\alpha(1)\beta(2) - \beta(1)\alpha(2)], \tag{1.5}$$

$$\psi_2 = \begin{pmatrix} A & C \\ \alpha & \beta \end{pmatrix} - \begin{pmatrix} A & C \\ \beta & \alpha \end{pmatrix} = (1/2)^{\frac{1}{2}}[A(1)C(2) + A(2)C(1)][\alpha(1)\beta(2) - \beta(1)\alpha(2)], \tag{1.6}$$

$$\psi_3 = \begin{pmatrix} b & b \\ \alpha & \beta \end{pmatrix} = (1/2)^{\frac{1}{2}}[b(1)b(2)][\alpha(1)\beta(2) - \beta(1)\alpha(2)], \tag{1.7}$$

$$\psi_4 = \begin{pmatrix} A & A \\ \alpha & \beta \end{pmatrix} + \begin{pmatrix} C & C \\ \beta & \alpha \end{pmatrix} = (1/2)^{\frac{1}{2}}[A(1)A(2) + C(1)C(2)][\alpha(1)\beta(2) - \beta(1)\alpha(2)]. \tag{1.8}$$

Function ψ_2 represents the covalent structure with a bond between 𝔄 and 𝔈, ψ_3 represents the ionic structure with both electrons on the central nucleus ℬ, and ψ_4 represents the ionic structure with both electrons alternately on 𝔄 and then on 𝔈. The notation $\begin{pmatrix} A & b \\ \alpha & \beta \end{pmatrix}$ is that for the usual Slater determinant,

$$\begin{pmatrix} A & b \\ \alpha & \beta \end{pmatrix} = \frac{1}{\sqrt{2}} \begin{vmatrix} A(1)\alpha(1) & b(1)\alpha(1) \\ A(2)\beta(2) & b(2)\beta(2) \end{vmatrix}. \tag{1.9}$$

Expansion of these determinant terms in the structural forms given, reduces them to the composite orbital forms following.

2. VARIATION OF THE EFFECTIVE NUCLEAR CHARGE PARAMETERS

Variational method calculations of the energy of the H_3^+ ion system were made using the Hamiltonian operator (1.1) and the trial function (1.2). For this section the energy expression may then be more simply written as

$$E \leq \frac{H_{11}}{S_{11}} = \frac{a^2b^2 + b^2ac + ab\ ab + ab\ bc}{1 + I_{ac}(2R) + 2I^2_{ab}(R)}. \tag{2.1}$$

The matrix element notation,

$$H_{11} = \int \psi_1 H \psi_1^* d\tau \quad \text{and} \quad S_{11} = \int \psi_1 \psi_1^* d\tau \text{ is used.}$$

Reduction of the H_{11} element of orbital integrals a^2b^2, b^2ac, $ab\ ab$, and $ab\ bc$ follows from consideration of the retained orbital part of the trial function (2.2) and the orbital integral symbolism given below. For example,

$$ab\ ab = \int a(1)a(2)Hb(1)b(2)d\tau_1 d\tau_2. \tag{2.2}$$

The electronic volume elements are $d\tau_1$ and $d\tau_2$. The orbital integrals and matrix elements S_{11} may be further reduced to elemental integrals by a consideration of the composite electron orbitals and of the individual terms of the Hamiltonian operator, H. Thus,

$$a^2b^2 = \frac{5}{2R} + \tfrac{1}{2}\{Z_0^2 + Z_m^2\} - \{Z_0 + Z_m\} - 2G_{a,b^2}(R,Z_m) - G_{b,a^2}(R,Z_0) - G_{c,a^2}(2R,Z_0) + L_{aa,bb}(R,Z_0,Z_m), \tag{2.3}$$

$$b^2\,ac = \left\{\frac{5}{2R} - Z_m + \tfrac{1}{2}[Z_m^2 - Z_0^2]\right\} I_{ac}(2R,Z_0) + Z_0 J_{c,ac}(2R,Z_0) - 2G_{a,b^2}(R,Z_m) I_{ac}(2R,Z_0) - 2J_{a,ac}(2R,Z_0) - K_{b,ac}(R,Z_0,Z_m) + L_{bb,ac}(R,Z_0,Z_m), \tag{2.4}$$

$$ab\ ab = \left\{\frac{5}{2R} - Z_m^2\right\} I_{ab}^2(R,Z_0,Z_m) + 2\{Z_m - 1\} J_{b,ab}(R,Z_0,Z_m) \cdot I_{ab}(R,Z_0,Z_m) - 2\{J_{a,ab}(R,Z_0,Z_m) + K_{c,ab}(R,Z_0,Z_m)\} \times I_{ab}(R,Z_0,Z_m) + L_{ab\ ab}(R,Z_0,Z_m), \tag{2.5}$$

$$ab\ bc = \left\{\frac{5}{2R} - \tfrac{1}{2}[Z_m^2 + Z_0^2]\right\} I^2_{ab}(R,Z_0,Z_m) + \{Z_m - 2\} I_{ab}(R,Z_0,Z_m) \cdot J_{b,ab}(R,Z_0,Z_m) + \{Z_0 - 2\} I_{ab}(R,Z_0,Z_m) \cdot J_{a,ab}(R,Z_0,Z_m) - 2I_{ab}(R,Z_0,Z_m) \cdot K_{a,bc}(R,Z_0,Z_m) + L_{ab,bc}(R,Z_0,Z_m). \tag{2.6}$$

The elemental integrals used above may be recognized by comparison with the five typical representative

types given below:

$$I_{ab}=\int a(i)b(i)d\tau_i$$

(an elemental overlap integral), (2.7)

$$G_{b,c^2}=\int \frac{1}{r_{ai}}[c(i)]^2 d\tau_i$$

(a nuclear attraction integral), (2.8)

$$J_{c,ac}=\int \frac{1}{r_{ci}}a(i)c(i)d\tau_i$$

(a nuclear attraction integral), (2.9)

$$K_{b,ac}=\int \frac{1}{r_{bi}}a(i)c(i)d\tau_i$$

(a nuclear attraction integral), (2.10)

$$L_{ab,ac}=\int \frac{1}{r_{12}}a(1)b(1)a(2)c(2)d\tau_1 d\tau_2$$

(electron repulsion integral). (2.11)

Kinetic energy integrals such as

$$T_{ab}=\int a(i)\left|-\tfrac{1}{2}\nabla_i^2\right|b(i)d\tau_i$$
$$=-\frac{Z_m^2}{2}I_{ab}(R,Z_0,Z_m)+Z_m\cdot J_{b,ab}(R,Z_0,Z_m) \quad (2.12)$$

may be written as illustrated in terms of the configurational and orbital constants (R, Z_0, and Z_m) and the previously listed elemental type integrals. The hydrogen-like "i" electron orbitals $a(i)$, $b(i)$, $c(i)$, and the volume elements of the ith electron $d\tau_i$ have been defined before.

Most of the specific elemental integrals used in this work are defined and have formulas given for their exact evaluation. The two-center integrals may be found in Hirschfelder and Linnett's recent paper[12] on the diatomic hydrogen molecule. Some of the three center ones are given in the cited article[9] on the neutral triatomic molecule. Tabulated values for some of these integrals are available.[13] Definitions and methods for evaluating others may be found in the work of Barker and Eyring.[8]

Energy calculations for the H_3^+ ion similar to those presented here except that $Z=Z_0=Z_m$ were made by Hirschfelder and others.[14] Their integrals with equal screening constants were evaluated for a small set of chosen R values. They obtained with the single orbital charge parameter Z a best value of -130.89 kcal/mole, considering the zero of energy as taken to be that corresponding to two separated hydrogen atoms. The corresponding values of R and Z were $R=1.546$ and $Z=1.294$. The calculations for unequal values of Z_0 and Z_m are considerably more complex. The main complications arise in the evaluation of four of the elemental integrals, specifically $K_{a,bc}$, $L_{ab,ab}$, $L_{bb,ac}$, and $L_{ab,bc}$.

The Hamiltonian operator may be written as the sum of individual terms as before (1.1). The elemental three-center nuclear attraction integral $K_{a,bc}(R,Z_0,Z_m)$ is then seen to arise from the constituent $b(i)$ and $c(i)$ orbitals of the trial function and from the operator term $1/r_{ai}$. The electron electron repulsion integrals $L_{ab,ab}(R,Z_0,Z_m)$, $L_{bb,ac}(R,Z_0,Z_m)$, and $L_{ab,bc}(R,Z_0,Z_m)$ similarly arise from the electron repulsion operator term $1/r_{12}$ and the appropriate constituent orbitals of the trial function.

Due to the difficulty in evaluating the four integrals listed, when Z_0 is not equal to Z_m, the Mulliken approximate formulas have been used together with a distance normalization method previously described.[8] The two-center resonance exchange integral $L_{ab,ab}$ could also have been approximated by methods recently described in the German literature[15] or could (with considerable more work) have been exactly evaluated.[16] Lengthy exact evaluation of the other integrals has also been considered.[17] However the Mulliken approximation for all these integrals was selected for use here through practicality and consistency considerations. Hirschfelder[9] tabulated the four integrals for $RZ=2.0$ and for $Z=Z_0=Z_m$. The normalization factors used here were obtained from these values. It is likely that these normalization factors (ratio of exact integral value to the Mulliken approximate value) do not vary greatly when R is kept fixed and Z_0 and Z_m are raised and lowered slightly from Z value previously used. More work on the magnitude of this variation however would be desirable. The normalization factors used for the four integrals approximated are given in Table I. Exact values for all the other integrals used were obtained by standard methods as stated before. The energy calculations using the outlined integral evaluation methods were carried through for several sets of the configurational and orbital parameters R, Z_0, and Z_m. The integrals involved are of such a nature as to make necessary the parameter minimizations by actual calculation of many

TABLE I. Distance normalization factors (λ) calculated for $RZ=2.0$ (e.g., $R=1.50$, $Z=1.33$).

Integral	λ
$L_{b^2,ac}$	1.1686
$L_{ab,ab}$	1.0190
$L_{ab,bc}$	0.9523
$K_{a,bc}$	0.9289

[12] J. O. Hirschfelder and J. W. Linnett, J. Chem. Phys. **18**, 130 (1950).

[13] Thorne, Barker, and Eyring, Studies in Applied Mathematics No. 10 (University of Utah), "Tables of Quantum Mechanical Integrals 1."

[14] Hirschfelder, Diamond, and Eyring, J. Chem. Phys. **5**, 695 (1937); D. Stevenson and J. O. Hirschfelder, J. Chem. Phys. **5**, 933 (1937).

[15] H. Preuss, Z. Naturforsch. **8a**, 270 (1953).

[16] K. Rudenberg, J. Chem. Phys. **19**, 1459 (1951).

[17] R. S. Barker and H. Eyring, J. Chem. Phys. **21**, 912 (1953); **22**, 114 (1954).

individual energies for individual sets of values of the parameters. Only partial minimization of the energy with respect to the three variables was achieved in this work. The internuclear distance parameter R was held fixed. The value $R=1.5$ selected for the trial calculations was near the best value found[9] when $Z_0=Z_m$. For purposes of systematization the trial calculations were made using values of Z_0 and Z_m first selected by an arbitrary weighting procedure. The value of Z_0 was weighted equal to that of Z_m and the sum fixed at 1.3, the best single parametric value found by previous workers.[9] The calculations obtained are those given in Table II. The "best" energy value ($E=129.33$ kcal/mole with $Z_0=1.28$ and $Z_m=1.32$) using the foregoing assumptions was then obtained graphically. This energy is only 0.23 kcal/mole better than the value with $Z_0=Z_m$. Of course the assumption of $R=1.5$ and the arbitrary selection of values for Z_0 and Z_m is admittedly based on guesswork. However, that such assumptions lead to nearly equal values for the Z's and to such a slight energy improvement is not encouraging. The above slight improvement achieved by the separate central and outer orbital charge parameters does not constitute a significant advance. While the tried parametric values may not be very near the "best" possible selection, and the possibility of another minima not detected may exist the results obtained did not encourage further effort with independent variation of the orbital charge parameters. The few calculations previously made for the H_3 neutral molecule[18] were different in this respect. However, the foregoing results are not incompatible. The influence on the screening constant associated with the central electronic orbital of an adjacent bare nucleus in the H_3^+ ionic structure may understandably be greatly less than that of an adjacent nucleus with an accompanying electron as in the H_3 neutral molecular structure. The obtained results were thus not entirely unexpected. While these results are not considered sufficient at this time to justify further work along this line they did demonstrate the practicality of such approximate integral calculations. At a future data a careful minimization of the energy for all three parameters R, Z_0, and Z_m using the methods developed above may be made with high-speed I.B.M. equipment. Such a procedure might lead to more promising results and could in such circumstance be easily extended to include the other covalent and ionic structural terms. Exact integral evaluations might then also be made.

TABLE II. ($R=1.5$.)

Z_0	Z_m	Energy (kcal/mole)	$-a^2\,b^2$	$-b^2\,ac$	$-ab\,ab$	$-ab\,bc$
1.30	1.30	−129.10	0.894742	0.295828	0.535549	0.503430
1.27	1.33	−129.27	0.896560	0.305022	0.539541	0.592454
1.24	1.36	−128.64	0.896313	0.314574	0.542733	0.590422
1.20	1.40	−126.08	0.892759	0.326137	0.545648	0.586400

[18] Barker, Eyring, Thorne, and Baker, **22**, 699 (1954).

3. POLARIZATION OR OFF-CENTER CLOUD DISPLACEMENT CALCULATIONS

Recognition that the factors influencing the calculations of the H_3 molecule and the H_3^+ ion may differ greatly in magnitude, was made some time ago. Hirschfelder, Eyring, and Rosen[9] commenting on the effect of inclusion of a single screening constant state, that "it is remarkable that the variation of the effective charge (Z) produces a striking change in the energy (of the H_3^+ ion) when it made so little difference in the energy of the triatomic molecule." Of course, such a statement may partially explain the disappointing results of the previous section with the use of a second orbital charge parameter. If a single such parameter suffices to give most of the improvement that can be achieved by orbital charge parameters the addition of a second such parameter may understandably lead to little improvement.

The difference in improvement of the orbital charge effect for the H_3 molecule and the H_3^+ ion described is a reversal of that associated with the polarization effect on the diatomic molecule H_2 and the diatomic ion H_2^+. The trial function composed of off-center orbitals for the H_2 molecule resulted in a significant energy improvement.[7] However when such orbitals were employed for the diatomic H_2^+ ion, rather disappointing results were obtained.[19] Inclusion of Gurnee-Magee off-center orbitals for the H_3 triatomic molecule showed but limited improvement.[20] Results from use of these orbitals in calculations with the H_3^+ ion might then be of interest. Aside from the intrinsic value of an improved exact integral energy calculation for this ion of even modest magnitude, such calculations establish the magnitude of the displacement parameter associated with this additional system.

The physical significance of the off-center orbital treatment is clear. The use of such orbitals in the original trial functions "allows the electrons to spend more time in the regions between the nuclei."[7] The off-center orbitals thus give a rather simple way of treating the electron polarization effect. Depending on the selected original fixed internuclear distance, such polarization may be visualized as an inward displacement of the outer electron cloud centers of the H_3^+ ion toward the central nucleus or as an outward displacement of the repelling similarly charged outer nuclei with positional retention of the centers of the associated electron clouds. Calculation simplification by use of integrals already evaluated resulted in selection of the latter view for the work here reported.

The optimum amount by which the two end nuclei are to be displaced from the center of their hydrogen-like atomic clouds, and the associated energy calculated

[19] Personal communication to H. Eyring from A. A. Frost.
[20] R. S. Barker (unpublished).

for this system are the objectives to be considered. The distance between the outer cloud centers and their associated nuclei is denoted by g. The internuclear distances between either of the outer nuclei and the central nucleus of this collinear system are designated as R. The centers of the electronic orbitals associated with these outer nuclei are at a distance $\mathbf{R}=(R-g)$ from the central nucleus. Quantities expressed in terms of, or directly dependent on the coordinates of the so-called off-center outer orbital clouds are represented by capitalization or boldfaced type. The Hamiltonian operator (1.1) is again used for the variational method calculations of this section.

(a) Use of a Polarization Parameter in the Simple Covalent Structural Energy Calculation

The energy for the simple covalent structure represented by ψ_1 is given in Sec. 2. This expression (2.1) is very similar to the corresponding expression (3.1) obtained using the additional off-center polarization parameter. That is

$$\mathbf{E}\leq\frac{\mathbf{H}_{11}}{\mathbf{S}_{11}}=\frac{A^2b^2+b^2\,AC+Ab\,Ab+Ab\,bC}{1+I_{AC}(2\mathbf{R})+2I_Ab^2(\mathbf{R})}. \quad (3.1)$$

The similarity of the foregoing matrix element expression to the one given before is obvious. The two treatments become distinct, however, when the orbital integrals are expressed in terms of the elemental types given before. The polarization treatment requires the explicit use of the off-center orbitals $A(i)$ and $C(i)$ as defined (1.3) in this reduction. Application of the separate operator terms of H to the modified orbital integral expressions give

$$A^2\,b^2=\left\{\frac{5}{2\mathbf{R}}+Z^2-Z\right\}-G_{a,\,A^2}(g,Z)-2G_{a,\,b^2}(R,Z)$$
$$-G_{b,\,A^2}(\mathbf{R},Z)-G_{c,\,A^2}(2\mathbf{R},Z)+L_{A^2,\,b^2}(\mathbf{R},Z). \quad (3.2)$$

$$b^2\,AC=\left\{\frac{5}{2\mathbf{R}}-Z\right\}I_{AC}(2\mathbf{R},Z)+Z\cdot J_{C,\,AC}(2\mathbf{R},Z)$$
$$-2K_{a,\,AC}(g,2\mathbf{R},Z)-K_{b,\,AC}(\mathbf{R},Z)$$
$$-2G_{a,\,b^2}(R,Z)\cdot I_{AC}(2\mathbf{R},Z)+L_{b^2,\,AC}(\mathbf{R},Z), \quad (3.3)$$

$$Ab\,Ab=\left\{\frac{5}{2\mathbf{R}}-Z^2\right\}I_{Ab}^2(\mathbf{R},Z)+2\{Z-1\}J_{b,\,Ab}(\mathbf{R},Z)$$
$$\cdot I_{Ab}(\mathbf{R},Z)-2\{K_{a,\,Ab}(g,\mathbf{R},Z)$$
$$+K_{a,\,bC}(R,\mathbf{R},Z)\}I_{Ab}(\mathbf{R},Z)+L_{Ab,\,Ab}(\mathbf{R},Z), \quad (3.4)$$

$$Ab\,bC=\left\{\frac{5}{2\mathbf{R}}-Z^2\right\}I^2{}_{Ab}(\mathbf{R},Z)+2\{Z-1\}J_{b,\,Ab}(\mathbf{R},Z)$$
$$\cdot I_{Ab}(\mathbf{R},Z)-2\{K_{a,\,Ab}(g,\mathbf{R},Z)$$
$$+K_{a,\,bC}(R,\mathbf{R},Z)\}I_{Ab}(\mathbf{R},Z)+L_{Ab,\,bC}(\mathbf{R},Z). \quad (3.5)$$

TABLE III. Interelectronic cloud distances, $\mathbf{R}=2.0$.

g	R	Energy	$-A^2b^2$	$-b^2AC$	$-Ab\,Ab$	$-Ab\,bC$
0.00	2.00	−91.92	0.991186	0.245999	0.436754	0.479703
0.05	2.05	−93.99	0.998286	0.245641	0.436508	0.479457
0.10	2.10	−94.43	1.001707	0.245065	0.435732	0.478681

Values of the orbital integrals A^2b^2, b^2AC, $Ab\,Ab$, and $Ab\,bC$ for $Z=1$, and $g=0$, 0.05, and 0.10 are given in Table III. These calculations are for the fixed interelectronic cloud distance $\mathbf{R}=(R-g)=2$. That is, the clouds are held fixed at the best previously found distance and the repelling nuclei allowed to separate. A little consideration will show this is equivalent to fixing the internuclear distance R at 2.0, 2.05, and 2.10, respectively. By considering the cloud centers thus fixed at $\mathbf{R}=2.0$ it will be noted that the values of all the difficult electron repulsion integrals are available from previous work. Graphic methods show the best energy $E=-94.47$ kcal/mole is obtained for $g=0.0885$. This is an improvement of 2.55 kcal/mole over the value previously obtained[9] without the polarization parameter g.

(b) The Covalent Structural Energy Calculation with Single Polarization and Orbital Charge Parameters

The energy calculated with a given type trial function composed of atomic orbitals may be considerably improved by the inclusion of a single effective orbital charge Z in the function. For the H_3^+ ion system here presented the orbitals then have the form $n(i)=(Z^3/\pi)^{\frac{1}{2}}\times e^{-Zr_{ni}}$. Minimization of the energy expression with respect to such an additional orbital charge parameter was first achieved by Wang[21] for the H_2 molecule. He used a differentiation procedure which requires no new integral evaluations. Modification and extension of such considerations were used by Coulson[10] and others.[14] Further extension to include the polarization parameter g is presented below.

The Hamiltonian operator (1.1), and the trial function (1.5) modified by the use of orbitals containing the charge parameter Z and by the displacement of the outer nuclei from their cloud centers, are employed. The energy expression is similar to (3.1) except for the modification of the composite orbitals to let Z be other than unity. Minimization of this energy expression with respect to the three parameters Z, R, and g may be most easily accomplished by explicitly formulating the composite orbital integrals in terms of the parameters Z, ρ ($\rho=\mathrm{Zr}$), and γ ($\gamma=\mathrm{Zg}$). For differential purposes, which are readily understood on consideration of later steps, it is best to factor out the elements of these orbital integrals that are determined only by the value of the parameters $\rho_{nm}=ZR_{nm}$ and $\gamma_{nm}=Zg_{nm}$. The structural configurational distance between the nuclei

[21] S. C. Wang, Phys. Rev. **31**, 579 (1928).

n and m is denoted by R_{nm}. Consideration of the elemental integral types that compose the orbital integrals is instructive at this point. If one makes the substitution of variables suggested, that is $\rho=RZ$ and $\gamma=gZ$, it may be seen that these two parameter (R,Z) integrals, with the exception of the overlap and kinetic energy integrals I and T, may be written as an orbital charge Z times the formerly employed one parameter (R) type. Thus,

$$G_{A,b^2}(\mathbf{R},Z)=Z\cdot G_{A,b^2}(\varrho_{ab}), \tag{3.6}$$

$$J_{A,Ab}(\mathbf{R},Z)=Z\cdot J_{A,Ab}(\varrho_{ab}), \tag{3.7}$$

$$K_{a,Ab}(g,\mathbf{R},Z)=Z\cdot K_{A,Ab}(\gamma,\varrho), \tag{3.8}$$

$$L_{Ab,Ab}(\mathbf{R},Z)=Z\cdot L_{Ab,Ab}(\varrho_{AB}). \tag{3.9}$$

The overlap integrals

$$I_{nm}(\mathbf{R},Z)=I_{nm}(\varrho). \tag{3.10}$$

Thus all terms derived from the orbital integrals that arise from parts of the Hamiltonian operator other than the kinetic energy terms have expressions unaltered except for the common factor Z and the substitutions ϱ for $\mathbf{R}$ and γ for g. Thus, for example, the term $\int A(1)b(2)|1/R|A(1)b(2)d\tau$ arising from the nuclear repulsion part of the operator in the A^2b^2 orbital integral may be written,

$$(1/R)I_{Ab^2}(\mathbf{R},Z)=Z[(1/\rho)I_{Ab^2}(\varrho)]. \tag{3.11}$$

The terms derived from the kinetic energy parts of the operator give more complicated expressions. Thus, the terms

$$\int A(1)b(2)|-\tfrac{1}{2}\nabla_i^2|b(1)C(2)d\tau \tag{3.12}$$

in the orbital integral $Ab\,bC$ give

$$\begin{aligned}&T_{Ab}(\mathbf{R},Z)\cdot I_{bC}(\mathbf{R},Z)+I_{Ab}(\mathbf{R},Z)\cdot T_{bC}(\mathbf{R},Z)\\&=\{\tfrac{1}{2}Z^2I_{Ab}(\mathbf{R},Z)-Z\cdot J_{b,bC}(\mathbf{R},Z)\}I_{bC}(\mathbf{R},Z)\\&\quad+I_{Ab}(\mathbf{R},Z)\{\tfrac{1}{2}Z^2I_{bC}(\mathbf{R},Z)-Z\cdot J_{C,bC}(\mathbf{R},Z)\}\\&=Z^2\{I_{Ab^2}(\rho)-2J_{A,Ab}(\rho)\cdot I_{Ab}(\rho)\}\\&=Z^2\{B_{Ab\,bC}(\rho)\}.\end{aligned} \tag{3.13}$$

When $Z=1$ such terms derived from the kinetic energy parts of the orbital integrals may be easily identified in the $E_{Z=1}$ formulation (3.1). By adding and subtracting Z times the terms derived from the kinetic energy expressions when $Z=1$ and $\mathbf{R}$ and g are replaced by ϱ and γ one may write the orbital integral $Ab\,bC$ as

$$(Ab\,bC)_Z=Z\{(Ab\,bC)_{Z=1}+(Z-1)B_{Ab\,bC}(\varrho)\}. \tag{3.14}$$

Similar expressions for all the orbital integrals of the energy formulation are easily obtained. Collection of terms then permits the energy equation to be expressed as

$$\begin{aligned}E_Z\leq&\frac{(\mathbf{H}_{11})_Z}{(\mathbf{S}_{11})_Z}\\&=\frac{Z\{[(A^2b^2)_{Z=1}+(Z-1)B_{A^2b^2}]+[\cdots]+[\cdots]+[\cdots]}{\mathbf{S}_{11}}\\&=\frac{Z[(\mathbf{H}_{11})_{Z=1}(Z-1)A_{11}]}{\mathbf{S}_{11}}=Z\left[\mathbf{E}_{Z=1}+(Z-1)\frac{A_{11}}{\mathbf{S}_{11}}\right],\end{aligned} \tag{3.15}$$

where

$$A_{11}=B_{A^2b^2}+B_{b^2AC}+B_{Ab\,Ab}+B_{Ab\,bC}. \tag{3.16}$$

At this point, it may also be noticed that the composite overlap orbital integrals I_{nm} and the kinetic energy integrals T_{nm} are dependent on the positions of their orbital centers and the orbital charge parameter Z but not on the actual positions of the nuclei. The B and A functions are therefore also invariant with displacement of the actual nuclei from their orbital cloud centers.

Minimization of (3.15) with respect to Z for fixed values of ϱ and γ is achieved by differentiation,

$$\frac{\partial\mathbf{E}}{\partial Z}=0=\mathbf{E}_{Z=1}+(2Z-1)\frac{A_{11}}{\mathbf{S}_{11}}. \quad \begin{pmatrix}\varrho_{nm}=\text{constant}\\ \gamma_{nm}=\text{constant}\end{pmatrix} \tag{3.17}$$

The value of Z at this minimum energy condition is then easily found to be

$$Z_{\min}=-\frac{1}{2}\mathbf{E}_{Z=1}\left(\frac{\mathbf{S}_{11}}{A_{11}}\right)+\frac{1}{2}. \quad \begin{pmatrix}\varrho_{nm}=\text{constant}\\ \gamma_{nm}=\text{constant}\end{pmatrix} \tag{3.18}$$

The energy is,

$$\mathbf{E}_{\min}=-\frac{1}{4}\frac{\mathbf{S}_{11}}{A_{11}}\left[\mathbf{E}_{Z=1}-\frac{A_{11}}{\mathbf{S}_{11}}\right]^2. \quad \begin{pmatrix}\varrho_{nm}=\text{constant}\\ \gamma_{nm}=\text{constant}\end{pmatrix} \tag{3.19}$$

For calculational purposes it is convenient to let $(R-g)Z=2.0$. A variation in g at constant Z then does not change the distance between cloud centers. Variation of Z is made with $(R-g)Z$ constant and with gZ a given fixed value γ. From Table IV below the most advantageous choice of γ is seen to be 0.10. The corresponding $Z=1.296816$. The displacement of the outer nuclei from the center of their electron clouds is then $g=\gamma/Z=0.0771$.

Graphic considerations show the best value of Z for a particular g leads to an energy minimum at $g=0.0629$

TABLE IV.

γ	Z	g	Energy
0.00	1.294037	0.000	−130.89
0.05	1.296335	0.0386	−133.80
0.10	1.296816	0.0771	−134.14

TABLE V. $(R-g)Z=2$, $\gamma=0.06$, $Z=1.31164$.

rs	S_{rs}	$-H_{rs}$	rs	S_{rs}	$-H_{rs}$
11	7.508462	9.121912	13	2.345812	3.000748
22	2.071640	1.889016	14	2.789784	3.173372
33	1.0	0.907995	23	0.687854	1.148704
44	2.071640	0.898870	24	0.757046	1.026996
12	2.789784	3.801096	34	0.687854	1.036036

and that the corresponding binding energy is 134.30 kcal/mole. This is an improvement of 3.44 kcal/mole over the $g=0$ value.

(c) Inclusion of a Polarization Parameter in the Covalent Bond Plus-Ionic-Terms Treatment

The trial function (1.4) includes consideration of one other covalent structure and two ionic ones. This introduces the structural composition parameters C_1, C_2, C_3, and C_4. Minimization of the energy with respect to these linear parameters may be obtained with the usual secular equation technique. The desired energy, E, is given by the lowest root of the fourth-order secular determinant,

$$|\mathbf{H}_{rs}-\mathbf{S}_{rs}E|=0. \tag{3.20}$$

In the above equation r and s represent, respectively, the row and column indices 1, 2, 3, and 4. The matrix components of the Hamiltonian operator and of unity are defined as $\mathbf{H}_{rs}=\int\psi_r H\psi_s d\tau$, and $\mathbf{S}_{rs}=\int\psi_r\psi_s d\tau$. The inclusion of the additional polarization parameter g requires the explicit use of off-center orbitals in expression of these matrix components in terms of orbital and elemental integrals. These reductions follow the procedures already outlined for $\mathbf{H}_{11}$ and $\mathbf{S}_{11}$. It may also be noted that Z is taken to be unity in this as well as in Sec. (3-a).

Once the energy E is known from (3.20) the C's may be found in the usual way from the normalizing condition

$$\int\psi\psi d\tau=1=C_1^2+C_2^2+C_3^2+C_4^2+2C_1C_2\cdots \tag{3.21}$$

and from the original minimizational equations which lead to the secular determinant. The energy obtained for $g=0.06$ is $\mathbf{E}=-110.73$ kcal/mole. This is 2.09 kcal/mole greater binding energy than that found when $g=0$.

(d) Inclusion of Single Polarization and Orbital Charge Parameters in the Covalent Bond Plus-Ionic-Terms Treatment

The complete trial function (1.4) may be written so the four component wave functions are normalized. Thus,

$$\psi=\frac{c_1}{(\mathbf{S}_{11})^{\frac{1}{2}}}\psi_1+\frac{c_2}{(\mathbf{S}_{22})^{\frac{1}{2}}}\psi_2+\frac{c_3}{(\mathbf{S}_{33})^{\frac{1}{2}}}\psi_3+\frac{c_4}{(\mathbf{S}_{44})^{\frac{1}{2}}}\psi_4. \tag{3.22}$$

The variational method energy formula then leads to the following expression if $Z=1$ and the total wave function ψ be normalized.

$$\mathbf{E}_{Z=1}=c_1^2(\mathbf{E}_{11})_{Z=1}+c_2^2(\mathbf{E}_{22})_{Z=1}+c_3^2(\mathbf{E}_{33})_{Z=1}+c_4^2(\mathbf{E}_{44})_{Z=1}+2c_1c_2(\mathbf{E}_{12})_{Z=1}\cdots. \tag{3.23}$$

The component energy expression definitions are apparent from the general form

$$(\mathbf{E}_{rs})_{Z=1}=\frac{(\mathbf{H}_{rs})_{Z=1}}{(\mathbf{S}_{rs})_{Z=1}}. \tag{3.24}$$

When $Z=1$ the procedure of Sec. (3-b) may be adopted and the matrix components $(\mathbf{H}_{rs})_Z$, and $(\mathbf{S}_{rs})_Z$ obtained in terms of the variables ϱ and γ. These expressions may then be factored to give the form

$$(\mathbf{H}_{rs})_Z=Z[(\mathbf{H}_{rs})_{Z=1}+(Z-1)A_{rs}]. \tag{3.25}$$

From the variational method energy formula one may then write

$$\mathbf{E}_Z=Z[\mathbf{E}_{z=1}+(Z-1)A], \tag{3.26}$$

where

$$A=c_1^2\frac{A_{11}}{\mathbf{S}_{11}}+c_2^2\frac{A_{22}}{\mathbf{S}_{22}}+\cdots+\frac{2c_1c_2}{(\mathbf{S}_{11}\mathbf{S}_{22})^{\frac{1}{2}}}A_{12}+\cdots. \tag{3.27}$$

The A_{rs}'s are compounded from the kinetic energy components of the orbital integrals as explained previously in Sec. (3-b). They are not dependent on the value of Z. The invariance of these numerical factors when the orbital cloud centers are held fixed and the actual nuclei allowed to undergo displacement has also already been dealt with. For fixed values of ϱ, γ, c_1, c_2, c_3, and c_4 the best energy and corresponding Z may be obtained from the modified Wang method already outlined. The simultaneous minimization of Z and the compositional eigenfunction parameters c_1, c_2, c_3, and c_4 may be achieved by successive approximations. The values of the compositional parameters are first taken as those obtained from the secular and normalization equations when $Z=1$. The best Z for these compositional values is then obtained, the compositional parameters redetermined and the process repeated as many times as required. In Table V are listed the matrix components of H and unity when $(R-g)Z=2$, $\gamma=0.06$, and $Z=1.31164$. The resultant binding energy calculated from the secular determinant is 158.09 kcal/mole, which is an improvement of 2.74 kcal/mole above the value calculated when $g=0$.

Vibrational Spectra, Force Constants, and Calculated Thermodynamic Properties of Methyltrifluorosilane

R. L. COLLINS* AND J. RUD NIELSEN
Department of Physics, University of Oklahoma, Norman, Oklahoma
(Received July 12, 1954)

The infrared spectrum of gaseous H_3C-SiF_3 has been obtained in the region 2.5–36μ. The Raman spectrum of the liquid phase under pressure has been photographed with a three-prism glass spectrograph of linear dispersion 15 A/mm at 4358 A, and qualitative polarization measurements have been made. The eleven active fundamental vibration frequencies have been assigned, and a tentative value has been assigned to the inactive fundamental. A normal coordinate analysis has been made, and thermodynamic properties have been calculated.

INTRODUCTION

THE microwave spectrum of methyltrifluorosilane has been studied by several investigators.[1–3] Sheridan and Gordy determined the moment of inertia I_B and gave evidence for the assumption that the H_3C-SiF_3 molecule has a staggered configuration of symmetry C_{3v}. No previous work appears to have been done on the vibrational spectra of this compound. In the present paper infrared and Raman data are presented, the fundamental vibration frequencies are assigned, force constants are determined by normal coordinate treatment, and thermodynamic properties are calculated.

EXPERIMENTAL

The sample of H_3C-SiF_3, prepared by fluorination of $H_3C-SiCl_3$, was kindly supplied by Dr. D. K. Coles of Westinghouse Research Laboratories. No information was available about its purity. The infrared spectrum of the gaseous phase was obtained with a spectrometer described previously.[4] This instrument has recently been modified by the addition of a KBr prism. An amplifier similar to that described by McAlister, Matheson, and Sweeney[5] served to amplify the output of the thermocouple sufficiently to drive a Speedomax strip chart recorder. Additional infrared data, in particular for the KRS-5 region, were kindly provided by Dr. R. E. Kagarise of the Naval Research Laboratory.

The Raman spectrum of liquid H_3C-SiF_3, contained in a sealed Raman tube at room temperature, was photographed with a 3-prism glass spectrograph of linear dispersion 15 A/mm at 4358 A. Because of the low intensity of the spectrum and a photochemical reaction resulting in the formation of a white fluorescent powder on the walls of the Pyrex Raman tube, only nine Raman bands were observed. Cooling the Raman tube to −50°C during exposure did not reduce the decomposition appreciably. Excitation with Hg 5461 A was attempted, but because of the low intensity only the strongest band was observed. Exposure of gaseous H_3C-SiF_3 in an apparatus recently described[6] yielded only the two strongest bands. Qualitative polarization data were obtained for six of the Raman bands by a single-exposure method.

RESULTS AND DISCUSSION OF RESULTS

The infrared absorption spectrum of gaseous H_3C-SiF_3 in the region from 2.5 to 15μ is shown in Fig. 1. The absorption in the KRS-5 region, as observed at the Naval Research Laboratory, is shown in Fig. 2. No bands were found in the KBr region (15–22μ). The wave numbers of the observed absorption maxima or shoulders are listed in the first column of Table I.

The agreement between the infrared data observed here and the somewhat more accurate data obtained at NRL is about as good as might be expected. However, a couple of discrepancies should be pointed out. The very weak, but sharp, absorption maxima found here at 740 and 747 cm^{-1} were not observed at NRL, but a very faint maximum was found at 734 cm^{-1}. Instead of the strong band observed here at 1148 cm^{-1}, a weak maximum at 1125 and shoulders at 1115, 1134, and 1147 cm^{-1} were observed at NRL. The extremely faint band at 954 cm^{-1} was not observed at NRL. On the other hand, several very weak bands were observed there but not here, and the contours of some bands, such as those at 1980 and 2065 cm^{-1}, were better resolved. In addition to the bands in the KRS-5 region, there are included in Table I a few bands observed only at NRL. These are marked with a superscript. The Raman data for liquid H_3C-SiF_3 are listed in Table II.

INTERPRETATION

The H_3C-SiF_3 molecule undoubtedly has the symmetry C_{3v}, and its normal vibrations hence divide

*Present address: Research and Development Department, Phillips Petroleum Company, Bartlesville, Oklahoma.

[1] J. Sheridan and W. Gordy, Phys. Rev. **77**, 719 (1950); J. Chem. Phys. **19**, 965 (1951).

[2] Minden, Mays, and Dailey, Phys. Rev. **78**, 347 (1950).

[3] D. K. Coles, private communication.

[4] Nielsen, Richards, and McMurry, J. Chem. Phys. **16**, 67 (1948).

[5] McAlister, Matheson and Sweeney, Rev. Sci. Instr. **12**, 314 (1941).

[6] H. H. Claassen and J. Rud Nielsen, J. Opt. Soc. Am. **43**, 352 (1953).

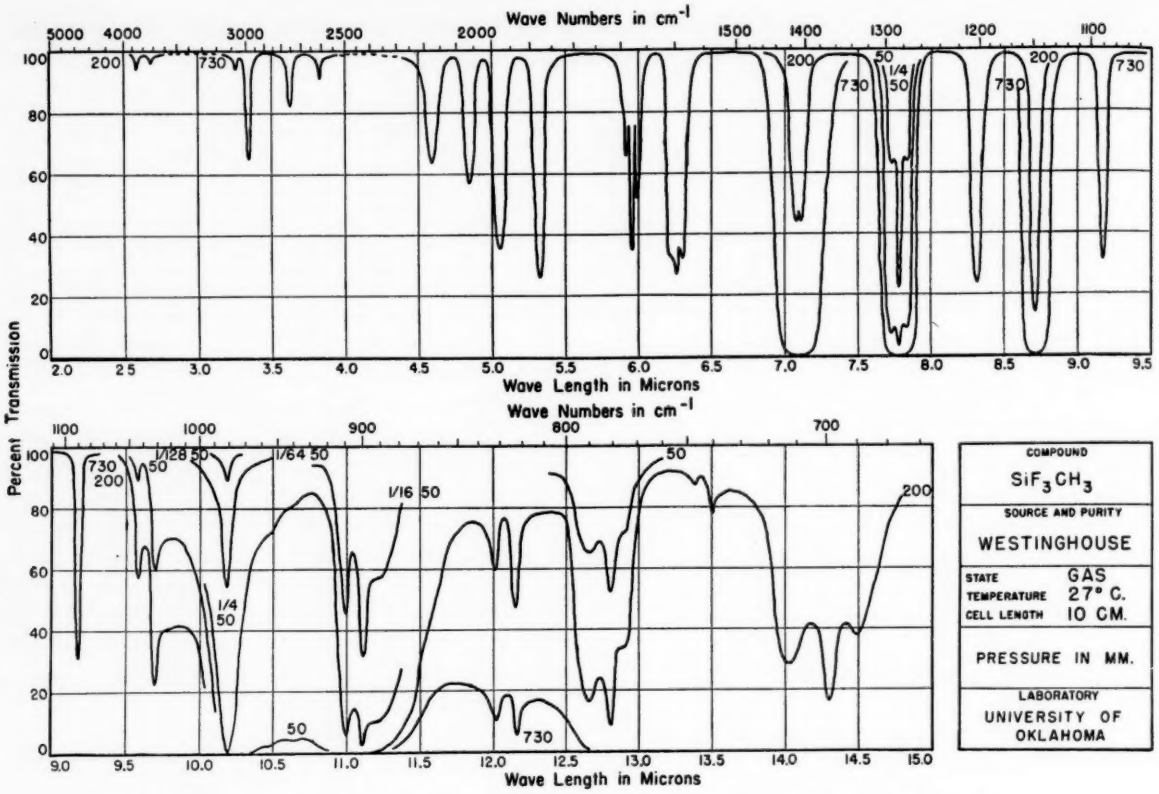

FIG. 1. Infrared absorption of gaseous methyltrifluorosilane (H_3C-SiF_3) in the region 2.5–15μ.

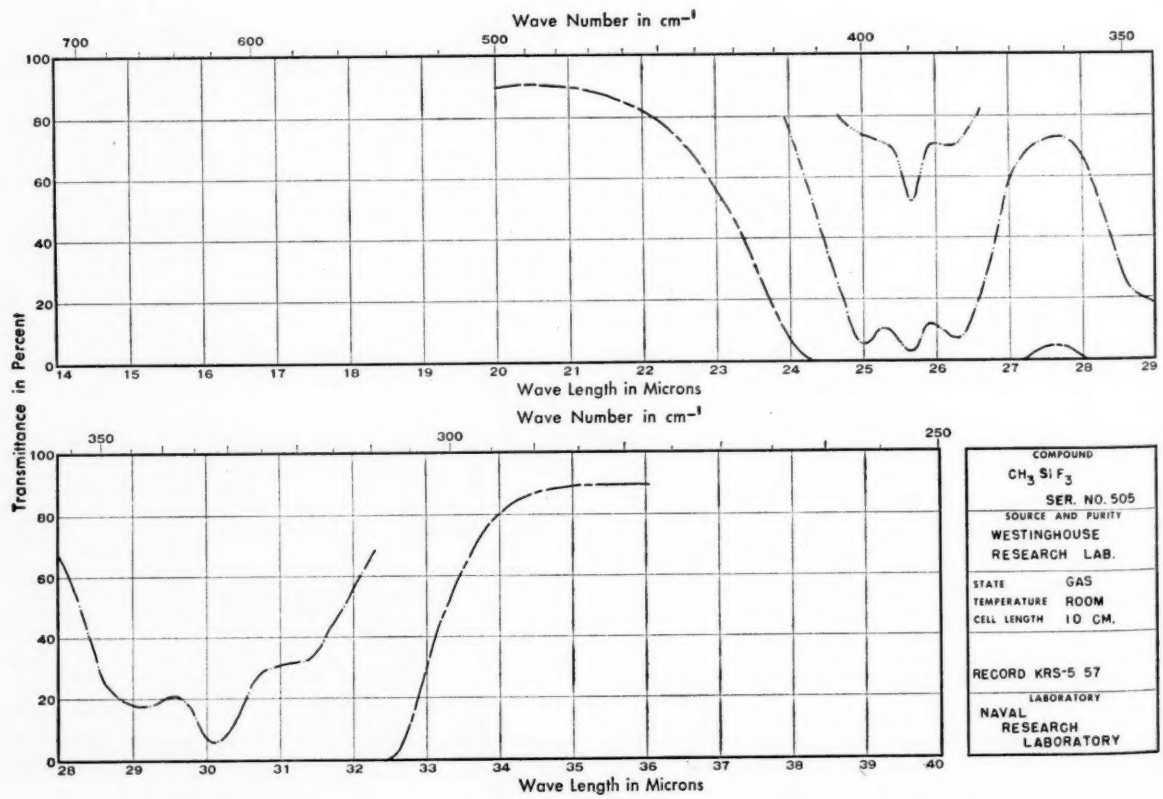

FIG. 2. Infrared absorption of gaseous methyltrifluorosilane (H_3C-SiF_3) in the region 20–36μ.

TABLE I. Infrared spectrum of gaseous SiF_3CH_3.

Wave number	Description[b]	Interpretation
320[a]	m	
332[a]	s	e fundamental
344[a]	m	
371[a]	m	
390[a]	s	a_1 fundamental
400[a]	m	
558[a]	vvw	$229+332=561$ (A_1+A_2+E)
690	w	
700	m	a_1 fundamental
713	w	
740	vvw	Impurity?
747	vvw	
775	vvw	
781	w	a_1 fundamental
790	vw	
813[a]	vvw	
823	vw	$982-156=826$ E
832	vw	
891	m	
900	vs	e fundamental
910	vs	
937	vvvw	$229+700=929$ E
954	vvvw	$1285-332=953$ E
982	vvs	e fundamental
987[a]	vs	
1020[a]	vw	
1032	w	$332+700=1032$ E
1044	vw	
1081[a]	vw	
1091	vw	$390+700=1090$ A_1
1124[a]	w	$229+900=1129$ (A_1+A_2+E)
1134[a]	w	
1148	s	$982+156=1138$ E
1203	w	$982+229=1211$ (A_1+A_2+E)
1276	m	
1285	s	a_1 fundamental
1293	m	
1405	w	$2\times700=1400$ A_1
1412	w	e fundamental
1505[a]	vvw, d	$229+1285=1514$ E
1560[a]	vvw	$2\times781=1562$ A_1
1587	vw	
1598	vw	$700+900=1600$ E
1609	vvw	
1672	vvw	
1679	vw	$982+700=1682$ E; $781+900=1681$ E
1691	vvw	
1762[a]	vvw	$781+982=1763$ E
1880	vvw	$900+982=1882$ (A_1+A_2+E)
1980	vw	$700+1285=1985$ A_1
2065	vw	$1285+781=2066$ A_1
2110[a]	vvw	$700+1412=2112$ E
2181	vw	$1285+900=2185$ E
2190[a]	vw	$781+1412=2193$ E
2615	vvw	$1412+982+229=2623$ (A_1+A_2+E)
2763	vvw	$2995-229=2766$ (A_1+A_2+E)
2822	vvvw	$2\times1412=2824$ (A_1+E)
2994	w	e fundamental
3082	vvw	$1412+700+982=3094$ (A_1+A_2+E)
3222	vvvw	$2995+229=3224$ (A_1+A_2+E)
3646	vvvw	$2927+700=3627$ A_1
3744	vvw	$2927+781=3708$ A_1
3876	vvw	$2995+900=3895$ (A_1+A_2+E)

[a] Observed only at the Naval Research Laboratory.
[b] The following abbreviations are used: vs very strong, s strong, m medium, w weak, vw very weak, etc.; d diffuse.

TABLE II. Raman spectrum of liquid SiF_3CH_3.

Wave number	Description[a]	Polarization[a]	Interpretation
229	m, d	dp	e fundamental
331	vw, d	dp	e fundamental
386.6	w	p	a_1 fundamental
700.5	vs, sh	p	a_1 fundamental
886	vvvw		e fundamental
991	vvvw		e fundamental
1412	vvw		e fundamental
2926.7	s, sh	p	a_1 fundamental
2995	w, d	dp	e fundamental

[a] The following abbreviations are used: vs very strong, s strong, m medium, w weak, vw very weak, etc.; d diffuse, sh sharp; p polarized, dp depolarized.

themselves into symmetry species in the following manner: $5a_1+a_2+6e$. The five totally-symmetric vibrations yield parallel infrared and polarized Raman bands; the six doubly degenerate vibrations give rise to perpendicular infrared and depolarized Raman bands, while the torsional a_2 vibration is inactive in both spectra.

Since the two moments of inertia of the molecule, as determined by Sheridan and Gordy,[1] are nearly equal, the parallel and perpendicular bands will have nearly the same contours, except for a possible distortion of the perpendicular bands by Coriolis coupling. Thus, the assignment of fundamentals to species a_1 and e must be based largely upon the incomplete and qualitative Raman polarization data.

The problem of assigning fundamental frequencies was attacked by considering skeletal and methyl vibrations separately. From the correlation diagrams for methylbromo- and methylchlorosilanes,[7-8] and the fundamentals of SiF_4 and $Si(CH_3)_4$,[9] the three skeletal fundamentals of species a_1 may be expected to occur near 360, 740, and in the region 800–1000 cm^{-1}, respectively, and the three skeletal e fundamentals near 260, 360, and in the region 800–1000 cm^{-1}. The methyl vibrations should consist of two C—H stretching modes (a_1 and e) near 3000 cm^{-1}, two deformation modes in the neighborhood of 1300 cm^{-1} and an e fundamental associated with rocking in the region 900–1100 cm^{-1}.

The two Raman bands at 229 and 331 cm^{-1}, which appear to be depolarized, are interpreted as e fundamentals. The bands at 390 and 700 cm^{-1} are strong in at least one of the spectra and are almost certainly polarized in the Raman spectrum. They are therefore assigned as a_1 fundamentals. The two very intense infrared bands at 900 and 982 cm^{-1}, with extremely weak and diffuse counterparts in the Raman spectrum, undoubtedly represent fundamentals. The medium infrared band at 781 cm^{-1} seems too strong to be the overtone of 390 and is therefore interpreted as a fundamental. One of the fundamentals at 781, 900, and 982 cm^{-1} must belong to a_1 and the two others to e. Since 781 has the most regular contour, and since the two

[7] H. Murata, J. Chem. Phys. **19**, 1217 (1951).
[8] Simanouchi, Tsuchiya, and Mikawa, J. Chem. Phys. **18**, 1306 (1950).
[9] K. W. F. Kohlrausch, *Ramanspektren* Eucken-Wolf, *Hand-u. Jahrb. d. chem. Phys.* Vol. 9, Part VI (Akademische Verlagsgesellschaft Becker & Erler, Leipzig, 1943).

other bands are diffuse in the Raman spectrum, it is tentatively assumed that 781 belongs to a_1 and the others to e.

The strong infrared band at 1285 cm^{-1} is assigned as an a_1 fundamental. The fact that it was not observed in the Raman spectrum lends support to the assumption that it involves symmetric CH_3 deformation. The bands at 1412 cm^{-1} are assigned as an e fundamental associated with asymmetric CH_3 deformation. The remaining two fundamentals are identified with the polarized Raman band at 2927 cm^{-1} and the depolarized Raman band and weak infrared band at 2994 cm^{-1}. The former must belong to a_1 and the latter to e.

Gordy and Sheridan[1] estimated that the inactive a_2 fundamental lies at approximately 140 cm^{-1}. In the present work a value of 156 cm^{-1} has been inferred from two infrared bands that are otherwise difficult to interpret. However, this assignment must be regarded as tentative.

In terms of these fundamentals it has been possible to interpret satisfactorily all but a couple of the observed infrared bands. These are ascribed to impurities. The somewhat high wave number of the faint E band at 937 cm^{-1} may well be caused by Fermi coupling to the e fundamental at 900 cm^{-1}. The interpretations are given in the last column of Table I.

NORMAL COORDINATE ANALYSIS

The H_3C-SiF_3 molecule was assumed to have a staggered configuration of symmetry C_{3v}, and the following generalized valence potential function was employed:

$$\begin{aligned}2V=&f_\delta\Sigma\delta_i^2+f_{\delta\delta}\Sigma\Sigma\delta_i\delta_j+f_{\delta'}\Sigma(\delta')^2+f_{\delta'\delta'}\Sigma\Sigma\delta_i'\delta_j'\\&+f_\Delta\Delta^2+2f_{\delta\Delta}\Delta\Sigma\delta_i+a^2f_\alpha\Sigma\alpha_i^2+a^2f_{\alpha\alpha}\Sigma\Sigma\alpha_i\alpha_j\\&+2af_{\Delta\alpha}\Delta\Sigma\alpha_i+b^2f_{\alpha'}\Sigma(\alpha_i')^2+b^2f_{\alpha'\alpha'}\Sigma\Sigma\alpha_i'\alpha_j'\\&+2bf_{\Delta\alpha'}\Delta\Sigma\alpha_i'+a^2f_\beta(\beta_{12}^2+\beta_{23}^2+\beta_{31}^2)\\&+a^2f_{\beta\beta}\Sigma\Sigma\beta_{ij}\beta_{kl}+2af_{\Delta\beta}\Delta(\beta_{12}+\beta_{23}+\beta_{31})\\&+2a^2f_{\alpha\beta}[\alpha_1(\beta_{12}+\beta_{31})+\alpha_2(\beta_{23}+\beta_{12})\\&+\alpha_3(\beta_{31}+\beta_{23})]+b^2f_{\beta'}[(\beta_{12}')^2+(\beta_{23}')^2+(\beta_{31}')^2]\\&+b^2f_{\beta'\beta'}\Sigma\Sigma\beta_{ij}'\beta_{kl}'+2bf_{\Delta\beta'}\Delta(\beta_{12}'+\beta_{23}'+\beta_{31}')\\&+2b^2f_{\alpha'\beta'}[\alpha_1'(\beta_{12}'+\beta_{31}')+\alpha_2'(\beta_{23}'+\beta_{12}')\\&+\alpha_3'(\beta_{31}'+\beta_{23}')].\end{aligned}$$

Here, δ_j, δ_j' and Δ are increases in the lengths of the Si—F_j and C—H_j and Si—C bonds, respectively; α_j, α_j', β_{kl} and β_{kl}' are increases in the angles C—Si—F_j, Si—C—H_j, F_k—Si—F_l, and H_k—C—H_l, respectively; a is the normal length of the Si—F bond, and b the length of the C—H bond.

Symmetry coordinates were obtained by a standard method.[10] Since they are essentially the same as those used by El-Sabban, Meister, and Cleveland[11] for H_3C-CCl_3, they will not be given here.

[10] J. Rud Nielsen and L. H. Berryman, J. Chem. Phys. **17**, 659 (1949).

[11] El-Sabban, Meister, and Cleveland, J. Chem. Phys. **19**, 855 (1951).

The G matrices for the species a_1 and e were evaluated by Wilson's method.[12] In terms of the abbreviations ρ, ξ, and η for the reciprocals of the Si—F, C—H, and Si—C bond lengths, respectively, and μ_H, μ_C, μ_{Si} and μ_F for the reciprocals of the atomic masses, the following nonvanishing matrix elements were obtained:

For species a_1

$$\begin{aligned}G_{11}&=\mu_H+(1/3)\mu_C,\\G_{13}&=-3^{-\frac{1}{2}}\mu_C,\\G_{14}&=-(4/3)\xi\mu_C,\\G_{22}&=\mu_F+(1/3)\mu_{Si},\\G_{23}&=-3^{-\frac{1}{2}}\mu_{Si},\\G_{25}&=-(4/3)\rho\mu_{Si},\\G_{33}&=\mu_{Si}+\mu_C,\\G_{34}&=3^{-\frac{1}{2}}\cdot4\xi\mu_C,\\G_{35}&=3^{-\frac{1}{2}}\cdot4\rho\mu_{Si},\\G_{44}&=2\xi^2[(8/3)\mu_C+\mu_H],\text{ and}\\G_{55}&=2\rho^2[(8/3)\mu_{Si}+\mu_F];\end{aligned}$$

For species e

$$\begin{aligned}G_{11}&=\mu_H+(4/3)\mu_C,\\G_{13}&=(4/3)2^{\frac{1}{2}}\xi\mu_C,\\G_{15}&=-2^{\frac{1}{2}}(\eta+\xi/3)\mu_C,\\G_{22}&=\mu_F+(4/3)\mu_{Si},\\G_{24}&=(4/3)2^{\frac{1}{2}}\rho\mu_{Si},\\G_{26}&=-2^{\frac{1}{2}}(\eta+\rho/3)\mu_{Si},\\G_{33}&=(\xi^2/6)(16\mu_C+15\mu_H),\\G_{35}&=-2\xi(\eta+\xi/3)\mu_C+(1/2)\xi^2\mu_H,\\G_{44}&=(\rho^2/6)(16\mu_{Si}+15\mu_F),\\G_{46}&=-2\rho(\eta+\rho/3)\mu_{Si}+(1/2)\rho^2\mu_H,\\G_{55}&=\xi^2\mu_H+(3/2)[\eta^2\mu_{Si}+(\eta+\xi/3)^2\mu_C],\text{ and}\\G_{66}&=\rho^2\mu_F+(3/2)[\eta^2\mu_C+(\eta+\rho/3)^2\mu_C].\end{aligned}$$

The G matrices are of course symmetric, *i.e.*, $G_{ji}=G_{ij}$. The matrix elements not listed, or not symmetric to any element listed, are all zero.

When the potential energy matrix is expressed in terms of the symmetry coordinates the following nonvanishing elements are found:

For species a_1

$$\begin{aligned}F_{11}&=f_{\delta'}+2f_{\delta'\delta'},\\F_{22}&=f_\delta+2f_{\delta\delta},\\F_{23}&=3^{\frac{1}{2}}f_{\delta\Delta},\\F_{33}&=f_\Delta,\\F_{34}&=(3/2)^{\frac{1}{2}}b(f_{\Delta\beta'}-f_{\Delta\alpha'}),\\F_{35}&=(3/2)^{\frac{1}{2}}a(f_{\Delta\beta}-f_{\Delta\alpha}),\\F_{44}&=(1/2)b^2(f_{\alpha'}+f_{\beta'}+2f_{\alpha'\alpha'}+2f_{\beta'\beta'}-4f_{\alpha'\beta'}),\text{ and}\\F_{55}&=(1/2)a^2(f_\alpha+f_\beta+2f_{\alpha\alpha}+2f_{\beta\beta}-4f_{\alpha\beta});\end{aligned}$$

[12] E. Bright Wilson, Jr., J. Chem. Phys. **7**, 1047 (1939); **9**, 76 (1941).

For species e

$F_{11}=f_{\delta'}-f_{\delta'\delta'}$,
$F_{22}=f_{\delta}-f_{\delta\delta}$,
$F_{33}=b^2(f_{\beta'}-f_{\beta'\beta'})$,
$F_{35}=-b^2f_{\alpha'\beta'}$,
$F_{44}=a^2(f_{\beta}-f_{\beta\beta})$,
$F_{46}=-a^2f_{\alpha\beta}$,
$F_{55}=b^2(f_{\alpha'}-f_{\alpha'\alpha'})$, and
$F_{66}=a^2(f_{\alpha}-f_{\alpha\alpha})$.

The elements not listed, and not symmetric and therefore equal to an element listed, are all equal to zero.

The two high frequencies associated with C—H stretching were split off, and the determinantal equations were expanded as described by Wilson.[12] Four force constants were transferred from the work of Voelz, Meister, and Cleveland[13] on SiF_4 and the work of El-Sabban, Meister, and Cleveland[11] on H_2C-CCl_3. Eight additional force constants were then determined by a graphical method from eight of the nine known frequencies, and the ninth frequency was calculated as a check. All nine frequencies were then calculated from the force constants to check the accuracy of the algebraic work and to provide a rough test of the assignment of fundamentals. The results are listed in Tables III and IV.

TABLE III. Force constants of SiF_3CH_3.

Force constant	Value $\times10^{-5}$ (dyne/cm)[a]	Force constant	Value $\times10^{-5}$ (dyne/cm)[a]
f_δ[b]	4.9398	f_α	0.2932
$f_{\delta\delta}$[b]	0.7410	$f_{\alpha'}$	0.3551
f_β[b]	0.4323	$f_{\alpha\alpha}$	0.1269
$f_{\beta'}$[c]	0.4395	$f_{\alpha'\alpha'}$	−0.2379
f_Δ	7.515	$f_{\beta\beta}$	0.0223
$f_{\delta\Delta}$	2.493	$f_{\beta'\beta'}$	0.0248

[a] This number of significant figures is not justified, except in that it is necessary to maintain internal consistency and reproductibility of the frequencies.
[b] Transferred without modification from SiF_4. (See reference 12.)
[c] Transferred without modification from CCl_3CH_3. (See reference 11.)

The value 7.52×10^5 dynes/cm obtained for the C—Si stretching constant f_Δ seems rather high. However, this may be explained, at least in part, by the fact that the carbon-silicon distance in H_3C-SiF_3 is only 1.88 A,[1] whereas the sum of the normal co-valent radii of carbon and silicon is 1.94 A.[14] The value of the interaction constant $f_{\delta\Delta}$ between Si—F and Si—C stretching is also larger than expected, and this may contribute to the large value of f_Δ. The six other force constants have values in the expected ranges. The vibrational spectra of D_3C-SiF_3 and Si_2F_6, and of $SiF_2(CH_3)_2$ and $SiF(CH_3)_3$, would be valuable for checking the present work.

[13] Voelz, Meister, and Cleveland, J. Chem. Phys. **19**, 1084 (1951).
[14] L. Pauling, *The Nature of the Chemical Bond* (Cornell University Press, Ithaca, 1940), p. 167.

TABLE IV. Observed and calculated fundamentals.

Observed	Species a_1 Calculated	% difference
386.6	386.8	+0.05
700.0	699.2	−0.11
781	781.6	+0.08
1285	1286.4	+0.11
Observed	**Species e Calculated**	**% difference**
229	220.4	−3.8
331	347	+4.8
900	875	−2.8
982	1004	+2.3
1412	1411	−0.1

TORSIONAL CONSTANT AND POTENTIAL BARRIER

If the value $\nu=156$ cm^{-1} is assumed for the torsional frequency, the torsional force constant $f_\varphi=4\pi^2c^2\nu^2I_r$, where c is the speed of light and I_r the reduced moment of inertia of the two end groups of the H_3C-SiF_3 molecule, is found to be 0.450×10^{-12} dyne cm rad^{-1}.

The potential barrier V_0 opposing the rotation of the methyl group relative to the SiF_3 group was estimated by means of the formula[15]

$$\nu=(\sigma_i/2\pi)(V_0/2I_r)^{\frac{1}{2}},$$

where $\sigma_i=3$ is the internal symmetry number. A value of 1440 cal mole^{-1} was obtained.

CALCULATED THERMODYNAMIC PROPERTIES

The heat capacity, the entropy, the Gibbs free energy function, and the heat content function of methyl-

TABLE V. Heat capacity, entropy, Gibbs free energy function, and the heat content function of H_3C-SiF_3 for the ideal gaseous state at 1 atmos pressure (cal deg^{-1} mole^{-1}).

T		C_p^0	S^0	$(-F^0-H_0^0)/T$	$(H^0-H_0^0)/T$
243°K	Translational	4.97	38.68	33.71	4.97
	Rotational	2.98	23.39	20.41	2.98
	Vibrational	9.70	4.07	2.09	1.98
	Torsional	1.95	2.67	1.24	1.43
	Total	19.60	68.81	57.45	11.36
298.16	Translational	4.97	39.70	34.73	4.97
	Rotational	2.98	24.00	21.02	2.98
	Vibrational	11.98	5.32	3.03	2.29
	Torsional	1.80	3.12	1.61	1.51
	Total	21.73	72.14	60.39	11.75
400	Translational	4.97	41.16	36.19	4.97
	Rotational	2.98	24.88	21.90	2.98
	Vibrational	15.65	7.50	4.91	2.59
	Torsional	1.56	3.54	2.00	1.54
	Total	25.16	77.08	65.00	12.08
600	Translational	4.97	43.17	38.20	4.97
	Rotational	2.98	26.08	23.10	2.98
	Vibrational	20.70	11.13	8.67	2.46
	Torsional	1.30	4.11	2.62	1.49
	Total	29.95	84.49	72.59	11.90

[15] S. Glasstone, *Theoretical Chemistry* (D. Van Nostrand Company, Inc., New York, 1952), p. 421.

trifluorosilane, considered as a perfect gas at 1 atmos pressure, were calculated for four different temperatures from 243°K (bp) to 600°K. The translational, rotational, vibrational, and torsional (hindered rotational) contributions are listed separately in Table V. The torsional contribution is rather uncertain, since the evidence for the torsional frequency is not very strong.

ACKNOWLEDGMENTS

The writers wish to thank Dr. D. K. Coles for the gift of the sample of methyltrifluorosilane and Dr. R. E. Kagarise for supplying valuable infrared data. One of us (J.R.N.) wishes to express his appreciation to the Research Corporation for financial assistance in the form of a Frederick G. Cottrell grant.

THE JOURNAL OF CHEMICAL PHYSICS VOLUME 23, NUMBER 2 FEBRUARY, 1955

Monte Carlo Calculation of the Average Extension of Molecular Chains

MARSHALL N. ROSENBLUTH AND ARIANNA W. ROSENBLUTH
Los Alamos Scientific Laboratory, Los Alamos, New Mexico

(Received July 15, 1954)

The behavior of chains of very many molecules is investigated by solving a restricted random walk problem on a cubic lattice in three dimensions and a square lattice in two dimensions. In the Monte Carlo calculation a large number of chains are generated at random, subject to the restrictions of no crossing or doubling back, to give the average extension of the chain $\langle R^2\rangle_{Av}$ as a function of N, the number of links in the chain. A system of weights is used in order that all possible allowed chains are counted equally. Results for the true random walk problem without weights are obtained also.

I. INTRODUCTION

AN attempt is made to simulate the behavior of chains of very many molecules by solving a restricted random walk problem[1] on a cubic lattice (or on a square lattice on two dimensions). The average squared extension of the chain as a function of the number of links is calculated. The random walk problem is set up as described below.

To the best of the authors' knowledge the first numerical calculations of chain length were made by Dr. Ei Teramoto of Kyoto University, who performed the remarkable feat of evaluating chain lengths in the two-dimensional case up to $N=20$ by a hand calculation cataloging all possible chains. After completion of the present work it was brought to the authors' attention by Dr. R. J. Rubin that machine calculations similar to ours have been performed by Wall, Hiller, and Wheeler.[2] They calculated somewhat different lattices (a cubic lattice with the bond angle restricted to 90° and a tetrahedral lattice) and used a different statistical procedure, more straightforward but probably more time consuming.

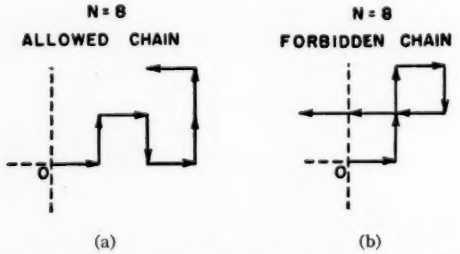

FIG. 1. Examples of an allowed chain and a forbidden chain for $N=8$ in two dimensions.

II. DESCRIPTION OF STATISTICAL PROCEDURE

For a given number of links N in the chain, any configuration consisting of N links laid out joined and in succession on a cubic lattice is considered. Regarded as a random walk problem, at any stage of m links ending at the position (x,y,z), all six of the positions $(x\pm1, y\pm1, z\pm1)$ are *a priori* equally likely at stage $m+1$. The excluded volume effect is simulated by the requirement that the chain not be allowed to cross itself or double back on itself at any stage (see Fig. 1 for an example of an allowed and a forbidden configuration in the two-dimensional case). Consequently, at any stage there are at most five possible subsequent positions. In statistical equilibrium all configurations of a given number of links satisfying the above requirements are equally probable, and are to be weighted equally in calculating $\langle R^2\rangle_{Av}$ (the average squared extension of the chain) as a function of N. $\langle R^2\rangle_{Av}$ is of importance in calculating such properties as the viscosity of the molecular chains.

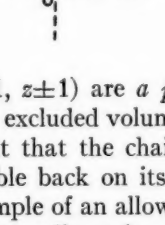

FIG. 2. A terminating chain in two dimensions. For $N>8$, if such a chain is generated, its weight is zero and a new chain is begun from the origin.

[1] W. Kuhn, Kolloid-Z. **68**, 2 (1934).
[2] Wall, Hiller, and Wheeler, J. Chem. Phys. **22**, 1036 (1954).

The mathematical random walk problem is solved by a Monte Carlo procedure carried out on the Los Alamos high speed electronic computer Maniac. In the calculation a large number of suitable configurations are successively generated at random according to the following scheme, and averages are taken over these configurations.

(1) For simplicity the first link is placed from (0,0,0) to (1,0,0).

(2) Any satisfactory set of m links reaching from the origin to position $(x,y,z)_m$ is associated with a weighting function W_m calculated at each step according to procedure (3) below. The weighting function is necessary since some configurations are generated more often than others, and a weighting function must be introduced so that all configurations are counted equally. After N links are obtained by procedure (3), with a final position $(x,y,z)_N$ and weight W_N, the value of $\langle R_N^2\rangle_{Av}=x_N^2+y_N^2+z_N^2$ is weighted with W_N in a statistical average of many such chains.

(3) At any stage of m links reaching to $(x,y,z)_m$, as was mentioned in the foregoing, the six positions $(x\pm1,\ y\pm1,\ z\pm1)$ must be considered. One of these six positions is $(x,y,z)_{m-1}$ and is ruled out immediately. Any of the other five possible positions at $m+1$ may be among the values of $(x,y,z)_i$ for $i=m-3,\ m-5,\ m-7,\ \cdots$ (geometrical considerations exclude coincidences between $m+1$ and $m,\ m-2,\ m-4,\ m-6,\ \cdots$). If comparison shows such to be the case, a modification of the weight W_m must be made to obtain W_{m+1}. There are really three possibilities:

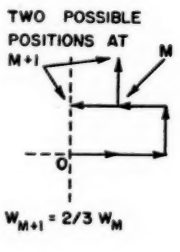

FIG. 3. An example in two dimensions of the modification of the weight in going from stage M to stage $M+1$. Only two positions at $M+1$ are possible instead of the maximum number of three.

(a) All six possible new positions are occupied (see Fig. 2 for an example in two dimensions, where only four new positions are available). The process is then terminated with a weight $W=0$, and a new chain must be generated, starting again from (0,0,0).

(b) All five positions (the position at $m-1$ being excluded) are unoccupied. Then

$$W_{m+1}=W_m(W_1=1). \tag{1}$$

One of these five positions is picked at random to give $(x,y,z)_{m+1}$. (In the actual calculation a random number which assumes one of the six values 0, 1, $\cdots$, 5 is generated, corresponding one-to-one to the six positions $(x\pm1,\ y\pm1,\ z\pm1)$. If the random number happens to correspond to $(x,y,z)_{m-1}$, a new independent random number is generated and the process repeated until one of the unoccupied positions is chosen.)

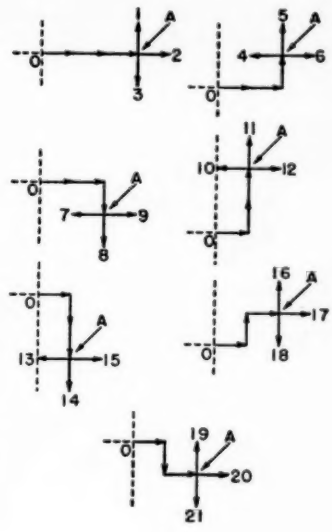

FIG. 4. All suitable configurations for $N=4$ in two dimensions [with the first link always from (0,0,0) to (1,0,0)]. In the modified random walk problem, if a configuration shown in Fig. 4(a) is generated it is given weight 1; however, if one of the configurations of Fig. 4(b) is generated it is given weight $\frac{2}{3}$.

(a)

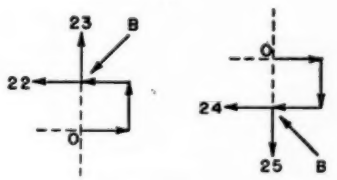

(b)

(c) Only n new positions are unoccupied, with $0<n<5$. Then

$$W_{m+1}=(n/5)W_m(W_1=1). \tag{2}$$

(In two dimensions $0<n<3$ and $W_{m+1}=(n/3)W_m$.) A random number is used to pick one of the n positions just as in (b) above (see Fig. 3).

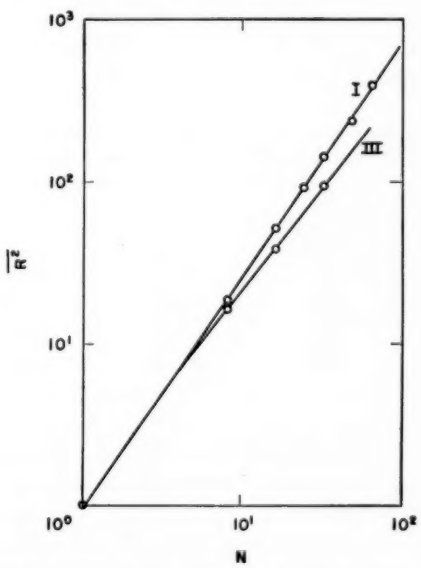

FIG. 5. Values of $\langle R^2\rangle$ *versus* N on a log-log polt for the two-dimensional case. Curve I represents $\langle R^2\rangle$ for the modified random walk problem with weights, and curve III gives values for the true random walk problem without weights.

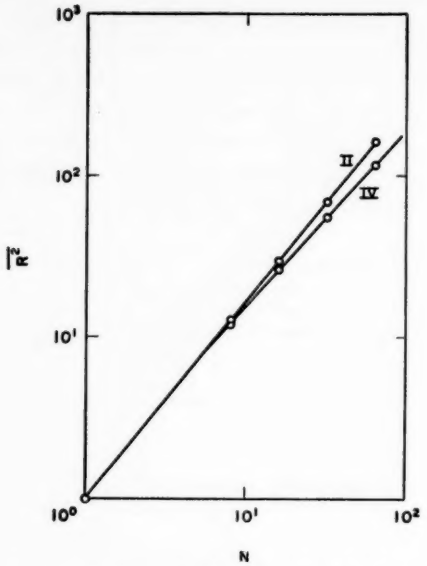

FIG. 6. Values of $\langle R^2 \rangle$ *versus* N on a log-log plot for the three-dimensional case. Curve II corresponds to averages taken with the weighting function W_N, and curve IV to direct averages without weights.

The weight W_m is calculated so that all possible allowed configurations of a given N are counted equally. Tentatively, the number of such configurations (if the chains were allowed to cross themselves but not to double back) would be $(5)^{N-1}$. This number must be multiplied by the average value of W_N, $\langle W_N \rangle_{Av}$, to obtain the true number of possible configurations of N links.

To see why Eq. (2) is correct for the weighting function, consider the simple case $N=4$ in two dimensions. All suitable configurations are shown in Figs. 4(a) and 4(b). The twenty-five possible configurations are weighted equally to give an average value of $\langle R^2 \rangle_{Av}$ of 7.04. However, any of the four configurations in Fig. 4(b) will be generated in the random walk scheme three-halves as often as any configuration of Fig. 4(a). [A point (A) is reached just as often as a point (B), but from a point (A) any of three configurations can be generated instead of only two, as from one of the points (B)]. Therefore, configurations of Fig. 4(b) have the weight $\frac{2}{3}$, as follows automatically from prescription (C), Eq. (2) above.

TABLE I. Values of $\langle R^2 \rangle_{Av}$ and $\langle W \rangle_{Av}$ as functions of N, for two-dimensional random walk problem with weights.

N	Total No. of chains	$\langle R^2 \rangle_{Av}$	$\bar{W}$
8	11 547	18.80	0.679
16	9565	51.98	0.316
24	6662	92.92	0.140
32	15 051	143.60	0.0618
48	4986	239.88	0.01065
64	5332	402.09	0.00222

TABLE II. Values of $\langle R^2 \rangle_{Av}$ and $\langle W \rangle_{Av}$ as functions of N, for three-dimensional random walk problem with weights.

N	Total No. of chains	$\langle R^2 \rangle_{Av}$	$\bar{W}$
8	11 307	12.81	0.828
16	7736	29.80	0.544
32	7369	68.35	0.214
64	4769	162.40	0.0296

III. RESULTS

The problem was calculated for two and for three dimensions, with various values of N. Results for $\langle R^2 \rangle_{Av}$ as a function of N are shown in Fig. 5, curve I, for two dimensions, and in Fig. 6, curve II, for three dimensions.

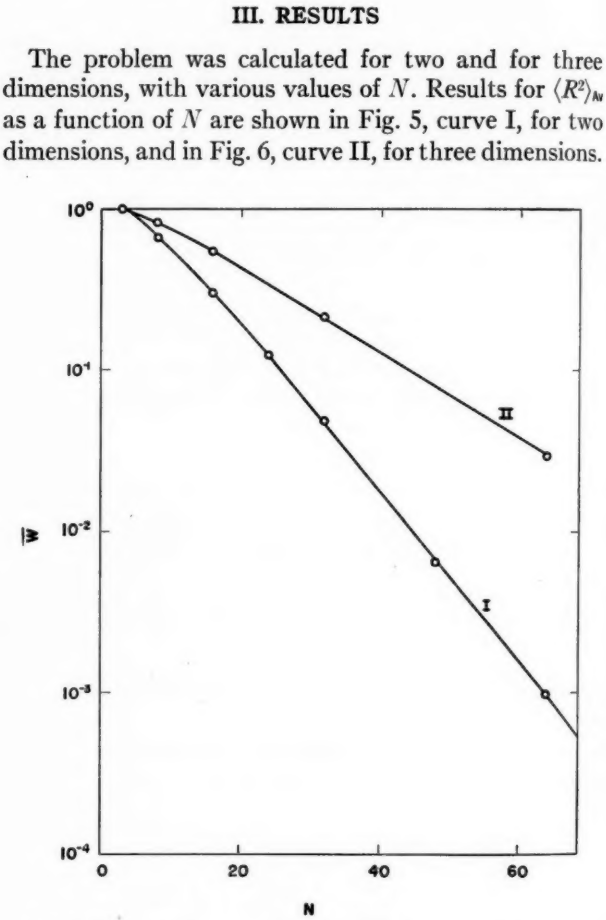

FIG. 7. Values of the average weight, $\langle W \rangle_{Av}$, *versus* N on a semi-log plot. Curve I represents the two-dimensional case, corresponding to the values of $\langle R^2 \rangle$ given in Fig. 5, curve I; curve II gives three-dimensional results corresponding to curve II of Fig. 6. Both curves, of course, correspond to the modified random walk problem with weights.

Curves for $\langle W_N \rangle_{Av}$ as a function of N are shown as curves I and II of Fig. 7. As discussed above, the average weights, when multiplied by $(5)^{N-1}$ in three dimensions or $(3)^{N-1}$ in two dimensions, give the total number of configurations of length N which exist.

Approximate fits are given by

$$\langle R_I^2 \rangle_{Av} = 0.917(N)^{1.45} \quad \text{two} \quad (3)$$

$$\langle W_I \rangle_{Av} = 2.14(0.887)^N \quad \text{dimensions} \quad (4)$$

$$\langle R_{II}^2 \rangle_{Av} = (N)^{1.22} \quad \text{three} \quad (5)$$

$$\langle W_{II} \rangle_{Av} = 1.46(0.941)^N \quad \text{dimensions.} \quad (6)$$

The numerical values (good probably to a few percent) obtained for $\langle R^2\rangle_{Av}$ and $\langle W\rangle_{Av}$ are given in Table I, (for two dimensions) and Table II (for three dimensions). The total number of chains generated for each value of N is listed also.

For mathematical interest a comparison problem was also run, the true random walk problem without crossing or doubling back, but with all generated configurations being given a weight 1. For small values of N, the presence or absence of a weight calculated according to Eq. (2) is negligible. However, for increasing N, $\langle R^2\rangle_{Av}$ drops below the values given by Eqs. (3) and (5), as shown in curves III and IV of Figs. 5 and 6. Numerical values are given in Tables III and IV. Statistics

TABLE III. Values of $\langle R^2\rangle_{Av}$ as a function of N, for two-dimensional random walk problem without weights.

N	Total No. of chains	$\langle R^2\rangle_{Av}$
8	3226	16.47
16	1379	38.39
32	1381	95.21

here are fairly poor. Fits here are

$$\langle R_{III}^2\rangle = 1.18(N)^{1.26} \text{ (two dimensions)} \quad (7)$$

$$\langle R_{IV}^2\rangle = 1.26(N)^{1.09} \text{ (three dimensions).} \quad (8)$$

The maximum values of N for which the problem can be attempted are limited not only by the number of terminating chains encountered (see Fig. 2), but in the weighted case by the increasing occurrence of very low weights and resultant large statistical fluctuations. Also, of course, the machine running time increases rapidly with N. Roughly, some twenty hours of machine-calculating time were used.

TABLE IV. Values of $\langle R^2\rangle_{Av}$ as a function of N, for three-dimensional random walk problem without weights.

N	Total No. of chains	$\langle R^2\rangle_{Av}$
8	5646	11.97
16	2576	26.18
32	1229	55.24
64	1186	116.17

IV. CONCLUSION

It is found that the restricted random walk problem on a cubic lattice for chains of length up to sixty-four links predicts an average squared extension in the three-dimensional case of

$$\langle R^2\rangle = N^{1.22}$$

and in the two-dimensional case

$$\langle R^2\rangle = 0.917(N)^{1.45}.$$

The total number of configurations of a given length is also calculated.

While these chain lengths are quite small, the above results give a remarkably good fit over the entire range. Moreover, when we consider the results of Wall, Hiller, and Wheeler,[2] it is now found that the same exponent, 1.22, applies to three different types of lattice. This is certainly suggestive of some general law. It is still an open question whether a different ratio of excluded radius to link size would affect these results. In view of the rather complete study being made by Wall, Hiller, and Wheeler the authors of the present paper do not intend to pursue this subject further.

Configuration Interaction Applied to the Hydrogen Molecule*†

EARL CALLEN
Massachusetts Institute of Technology, Cambridge, Massachusetts‡
(Received July 9, 1954)

The electronic wave function for the hydrogen molecule has been described as a sum of three configurations, each of which is expressed in terms of one-electron symmetry orbitals, which are written as variational functions of the elliptic coordinates. To a state due to Coulson, made up of orbitals which are individually even under inversion, we first added an odd-odd state, thus improving the computed binding energy from 3.535 ev to 4.125 ev. The addition of a third state, of a somewhat different character, increases the binding energy to 4.276 ev. The experimentally observed binding energy is 4.72 ev. The role of the several configurations is explained in terms of the concept of spatial correlation, following the work of Lennard-Jones and co-workers.

I. INTRODUCTION

IN molecular orbital theory it is customary to construct the molecular orbitals as linear combinations of atomic orbitals. This is a very good approximation to the orbitals for the inner electrons, whose atomic functions overlap very little. But for those outer electrons which play the key role in determining the physical behavior of the molecule the atomic functions form less satisfactory building blocks for the one-electron symmetry orbitals. In this paper we construct orbitals with the symmetry of the molecule as variational functions of the coordinates, and determine the coefficients by minimizing the energy, in a configuration interaction. The importance of the various configurations is attributed to their ability to describe the correlation in spatial position of the two electrons.[1] Throughout the calculation the internuclear distance is held fixed at the observed value, 0.7395 A.

II. THE ELECTRONIC WAVE FUNCTION

In its ground state the electronic wave function of the hydrogen molecule has the symmetry $^1\Sigma_g^+$. We restrict ourselves to a spin-free electronic Hamiltonian, containing only kinetic and electrostatic terms:

$$H=-\nabla_1^2-\nabla_2^2-\frac{2}{r_{1A}}-\frac{2}{r_{1B}}-\frac{2}{r_{2A}}-\frac{2}{r_{2B}}+\frac{2}{r_{12}}.^2$$

The $-\nabla_i^2$ operators represent the kinetic energy of the two electrons, the $-2/r_{iA}$ terms are the Coulomb energies of the two electrons, attracted to nucleus A, with similar terms for nucleus B. $2/r_{12}$ is the repulsive Coulomb energy between the electrons. For such a Hamiltonian we may factor the eigenfunction as

$$\Psi(\mathbf{x}_1,\mathbf{x}_2,s_1,s_2)=\psi(\mathbf{x}_1,\mathbf{x}_2)[\alpha(1)\beta(2)-\beta(1)\alpha(2)],$$

with $\psi(\mathbf{x}_1,\mathbf{x}_2)$ symmetric under interchange of the electronic coordinates. Though $\psi(\mathbf{x}_1,\mathbf{x}_2)$ must be even under inversion through the midpoint of the molecule, the same restriction need not be put on the one-electron functions in terms of which we expand it. As long as both one-electron functions in any configuration belong to the same eigenvalue of the inversion operator their product will be even. With ϕ taken as the angle around the molecular axis, the requirement of zero component of angular momentum along the molecular axis may be expressed analytically by employing only configurations in which the angular coordinates of the two electrons appear as $(\phi_1-\phi_2)$. The requirement of positive reflection symmetry restricts the expansion to terms in $\cos M(\phi_1-\phi_2)$. To make the wave function single-valued we allow only integral M. Let g denote an orbital which is even, and u odd under inversion through the center of symmetry, that is, when they are inverted through the midpoint of the molecular axis a g orbital goes into plus itself and u into minus itself. We may expand our two-electron function as[3]

$$\psi(\mathbf{x}_1,\mathbf{x}_2)=\sum_{ijM} a_{ijM}[g_{iM}(1)g_{jM}(2)+g_{jM}(1)g_{iM}(2)]\times\cos M(\phi_1-\phi_2)+\sum_{ijM} b_{ijM}[u_{iM}(1)u_{jM}(2)+u_{jM}(1)u_{iM}(2)]\cos M(\phi_1-\phi_2).$$

Up to this point the expansion is exact; if the g_{iM} and u_{jM} form a complete set we can expand our two-electron function in this series to any desired accuracy.

The primary approximation made in this investigation is to drop all terms with angular dependence. Furthermore, of the $M=0$ terms remaining we retain only three:

$$\psi(\mathbf{x}_1,\mathbf{x}_2)\cong ag(1)g(2)+bu(1)u(2)+c[g_k(1)g_l(2)+g_l(1)g_k(2)].$$

In addition to the three coefficients (one for normalization) a, b, and c, each of the orbitals, g, u, g_k, and g_l contains a number of internal parameters, all of which should in principle be determined by the configuration interaction. This, however, is too laborious to be

* Supported by the Office of Naval Research.
† Part of a thesis submitted in partial fulfillment of the requirements for the Ph.D. degree at the Massachusetts Institute of Technology.
‡ Present address: Philco Corporation, Philadelphia, Pennsylvania.
[1] J. E. Lennard-Jones, J. Chem. Phys. **20**, 1024 (1952).
[2] This is expressed in atomic units. The unit of length is the Bohr radius. The unit of energy is the Rydberg. See DuMond and Cohen, Revs. Modern Phys. **25**, 691 (1953).
[3] J. E. Lennard-Jones and J. A. Pople, Proc. Roy. Soc. (London) **A210**, 190 (1951).

feasible, and so the procedure actually adopted was to determine the orbitals in a stepwise fashion, first minimizing the main diagonal energy of the lowest configuration, which is the nodeless $g(1)g(2)$, then with this state fixed adding $u(1)u(2)$, and finally the third state.

The first step had already been carried through by Coulson,[4] who investigated two-term, three-term, and five-term expansions for this orbital. As the five term expansion does not gain much in accuracy to justify its additional complexity, we adopted the normalized three term expression as the lowest even orbital:

$$g_C=0.83247e^{-0.75\lambda}[1+0.21948\mu^2-0.079575\lambda].$$

Here λ and μ are the elliptic coordinates. The single configuration $g_C(1)g_C(2)$ was found by Coulson to yield a binding energy of 3.535 ev.

Were there no interelectronic interaction there would be no need for configuration interaction. A single determinant would express the effect of the Pauli exclusion on the electrons of the same spin, and the two sets of electrons of opposite spin would move completely independently of each other. The purpose of configuration interaction is to express the correlations in the positions of the electrons, due to their mutual Coulomb repulsion. The essential role of electronic correlation in the binding of molecules has been very clearly described by Lennard-Jones and co-workers in a long series of papers on this subject.[1] The type of configurations we should employ to express these correlations is dictated by the sort of correlations we may expect. As Lennard-Jones has pointed out, there are three ways the electrons can correlate in a diatomic molecule.

(1) The electrons will tend to be near different nuclei; when one is near nucleus A, the other will more probably be found near B than A. This is a left-right correlation. (2) When one electron is in close to the molecular axis, the other will tend to be further out. This Lennard-Jones calls in-out correlation. (3) The electrons will tend to be on opposite sides of an axial plane. This is an angular correlation which can be expressed only through configurations with angular dependence, those with $M\neq 0$, in our notation. We have included no such states and have thereby neglected this contribution to the energy.

Examination of the conditional probability distribution—the probability that there is an electron at $\mathbf{x}_2$ with spin s_2 given that there is an electron at position $\mathbf{x}_1$ with spin s_1—discloses the nature of the state which must be added to the even-even state to describe the left-right correlation. In our two electron problem the conditional probability distribution function is simply

$$\rho[2(1)]=\frac{\Psi^*(\mathbf{x}_1,\mathbf{x}_2,s_1,s_2)\Psi(\mathbf{x}_1,\mathbf{x}_2,s_1,s_2)}{\sum_{s_2}\int d\mathbf{x}_2\Psi^*(\mathbf{x}_1,\mathbf{x}_2,s_1,s_2)\Psi(\mathbf{x}_1,\mathbf{x}_2,s_1,s_2)}.$$

[4] C. A. Coulson, Proc. Cambridge Phil. Soc. **34**, 204 (1938).

Let us consider this function for an electronic wave function which is a linear combination of an even-even and an odd-odd state.

$$\psi(\mathbf{x}_1,\mathbf{x}_2)=ag_C(1)g_C(2)-bu(1)u(2),$$

$$\psi^*\psi=a^2g_C^2(1)g_C^2(2)-2abg_C(1)u(1)g_C(2)u(2)+b^2u^2(1)u^2(2).$$

Now suppose u to be negative in the region on the left of the plane bisecting the molecular axis and positive on the right, and let $\mathbf{x}_1'$ be such a point on the left, so that $u(\mathbf{x}_1')=-L$. Then

$$\rho[\mathbf{x}_2(\mathbf{x}_1')]=\frac{a^2g_C^2(\mathbf{x}_1')g_C^2(\mathbf{x}_2)+2abLg_C(\mathbf{x}_1')g_C(\mathbf{x}_2)u(\mathbf{x}_2)+b^2u^2(\mathbf{x}_1')u^2(\mathbf{x}_2)}{a^2g_C^2(\mathbf{x}_1')+b^2u^2(\mathbf{x}_1')}.$$

The terms in $g_C^2(\mathbf{x}_2)$ and $u^2(\mathbf{x}_2)$ are symmetric about the bisecting plane, but the term $2abg_C(\mathbf{x}_1')Lg_C(\mathbf{x}_2)u(\mathbf{x}_2)$ shows just the left-right correlation we have discussed, for if $\mathbf{x}_2$ is in the left-hand space, $u(\mathbf{x}_2)$ is negative, and $\rho[\mathbf{x}_2(\mathbf{x}_1')]$ will be decreased, whereas if $\mathbf{x}_2$ is in the right-hand space, $\rho[\mathbf{x}_2(\mathbf{x}_1')]$ is enhanced. So we learn that a configuration interaction between an even-even and an odd-odd state will produce a wave function describing the left-right spatial correlation of the electrons.

We therefore added to our even-even state a configuration of the form $u(1)u(2)$, with u an orbital expressed variationally in the elliptic coordinates as

$$u=N\mu e^{-\beta\lambda}[1+C\lambda+D\mu^2].$$

Before adding this full state, however, the screening constant β which appears in the odd orbital was first determined by employing the more tractable function

$$u'=N'\mu e^{-\beta\lambda}.$$

The secular equation was solved for a number of values of β and the choice $\beta=0.75$ gave the best result. To this approximation the wave function is

$$\psi(\mathbf{x}_1,\mathbf{x}_2)=0.993572g_C(1)g_C(2)-0.113204u'(1)u'(2)$$

with

$$u'=0.748616\mu e^{-0.75\lambda}.$$

With this wave function the computed electronic energy is -3.725728 a.u., which is a binding energy of 4.0428 ev.

The full odd orbital was now introduced with the screening constant fixed at $\beta=0.75$. Variation of the parameters now resulted in an improvement of only 0.0821 ev over the previous case. The computed binding energy was now 4.1249 ev for the wave function

$$\psi=0.9486365g_C(1)g_C(2)-0.316368u(1)u(2)$$

$$u=1.257126\mu e^{-0.75\lambda}[1-0.03\lambda+0.45\mu^2].$$

TABLE I. A number of investigations of the wave function and binding energy of the hydrogen molecule.

Authors	Binding energy	Equilibrium internuclear distance	Description	Reference
Heitler-London-Sugiura	3.14 ev	0.80 A	$a(1)b(2)+b(1)a(2)$	Z. Physik **44**, 455 (1927).
Wang (corrected by Coulson)	3.761	0.76	H.-L. z variable	Phys. Rev. **31**, 579 (1928).
Weinbaum	4.00	···	H.-L. plus ionic	J. Chem. Phys. **1**, 317 (1933).
Rosen	4.02	0.77	H.-L. z variable polarization	Phys. Rev. **38**, 2099 (1931).
Weinbaum	4.10	···	H.-L. z variable polarization ionic	J. Chem. Phys. **1**, 593 (1933).
Gurnee and Magee	4.163	0.767	H.-L. electronic functions not centered at nuclei	J. Chem. Phys. **18**, 142 (1950).
James and Coolidge	4.722	0.740	Variational. Interelectronic coordinates	J. Chem. Phys. **1**, 825 (1933).
Frost and Braunstein	4.11	0.71	Correlated MO	J. Chem. Phys. **19**, 1133 (1951).
Hirschfelder and Linnett	4.25	0.762	H.-L. x_1x_2, y_1y_2, z_1z_2, terms	J. Chem. Phys. **18**, 130 (1950).
Inui	4.038	0.76	Semilocalized orbitals	Proc. Phys.-Math. Soc. Japan **20**, 770 (1938); **23**, 992 (1941).
Mueller and Eyring	4.20	···	Semilocalized	Proc. Nat. Acad. Sci. **38**, 149 (1952).
Coulson	3.470	0.732	One config. MO=LCAO variation of z	Trans. Faraday Soc. **33**, 2, 1479 (1937).
Coulson	3.603	···	One config. self-consistent field five terms	Proc. Cambridge Phil. Soc. **34**, 204 (1938).
Callen	4.125	···	Variational MO—two config.	
Callen	4.276	···	Variational MO—three config.	
Experimental	4.72	0.7395		

To describe the in-out correlation we next added the normalized state

$$[g_k(1)g_l(2)+g_l(1)g_k(2)]$$
$$=0.191337[(P_k-\lambda_1)e^{-0.5\lambda_1}(P_l-\lambda_2)e^{-\lambda_2}$$
$$+(P_l-\lambda_1)e^{-\lambda_1}(P_k-\lambda_2)e^{-0.5\lambda_2}]$$
$$P_k=2.682874 \quad P_l=2.156431.$$

The algebraic form of the new orbitals was selected arbitrarily. Furthermore P_k and P_l were so chosen as to orthogonalize these orbitals to the nodeless Coulson orbital. Because one of these orbitals has an exponential decay constant twice that of the other, one orbital is localized in close to the molecular axis while the other is much more extended. It is this property which gives the in-out correlation. Configuration interaction between this state and the two previously detailed leads to a binding energy of 4.2756 ev (the experimental result is 4.72 ev) for the wave function

$$\psi(\mathbf{x}_1,\mathbf{x}_2)=0.9908785g_C(1)g_C(2)-0.111678u'(1)u'(2)$$
$$-0.075400[g_k(1)g_l(2)+g_l(1)g_k(2)].$$

To test the validity of our interpretation we next added, one by one, two other states composed of the same orbitals g_k and g_l. First we added $g_k(1)g_k(2)$ to our two previous states. It was found that this addition improved the energy by only a most insignificant amount. Similary, the addition of $g_l(1)g_l(2)$ proves valueless. It is only the combination in a form which effectively describes the in-out correlation which proves useful.

Lennard-Jones[5] has performed a similar dissection on the hydrogen molecule wave function of Hirschfelder and Linnett.[6] This is a function of the Heitler-London form. As it contains explicit terms linking the coordinates of the two electrons, terms of the form x_1x_2, y_1y_2, and z_1z_2, it has the interelectronic correlation built into it in a more direct manner than the wave functions presented in the present paper.

In Table I we have listed many of the investigations of the hydrogen molecule, with a brief description and reference. Where no internuclear distance is indicated, the calculation was performed at the equilibrium distance. It easily can be shown that the Heitler-London function, with variable effective nuclear charge, ionic term, and polarization term, such as was employed by Weinbaum, is very similar, both in its physical description and in its predicted binding energy, to our two configuration variational function.

III. ACKNOWLEDGMENTS

The author wishes to acknowledge his profound gratitude to Professor John C. Slater, who suggested and guided the author throughout this problem. Dr. Klaus Ruedenberg provided fundamental assistance in the evaluation of integrals. The writer is happy to express his indebtedness to his brother, Professor Herbert Callen, for many stimulating discussions.

[5] J. E. Lennard-Jones, Proc. Nat. Acad. Sci. **38**, 496 (1952).
[6] J. O. Hirschfelder and J. W. Linnett, J. Chem. Phys. **18**, 130 (1950).

Vibrational Intensities. V. BrCl and ICl*

WENDELL V. F. BROOKS† AND BRYCE CRAWFORD, JR.
School of Chemistry, University of Minnesota, Minneapolis 14, Minnesota

(Received August 2, 1954)

The intensity coefficients, A_1, of the fundamental vibrational bands of BrCl and ICl have been measured. From these, the derivatives p' have been calculated. An upper limit has been set for the overtone intensity coefficients, A_2, and the second derivatives p''. The values are: for BrCl, $A_1=105$ cm/millimole, $A_2<2.5$ cm/millimole, $p'=\pm 0.78$ debye angstrom^{-1}, $|p''|<10$ debye angstrom^{-2}; for ICl, $A_1=650$ cm/millimole, $A_2<4$ cm/millimole, $p'=\pm 2.1$ debye angstrom^{-1}, $|p''|<14$ debye angstrom^{-2}.

WE have observed the fundamental infrared band and first overtone of BrCl and the fundamental of ICl. The apparent band center of the BrCl fundamental is at 439.5 ± 0.5 cm^{-1}, in exact agreement with the frequency given by Mattraw, Pachucki, and Hawkins.[1] The BrCl overtone is at 876 ± 1 cm^{-1}, corresponding to $\omega_e=442.5$ cm^{-1} and $\omega_e x_e=1.5$ cm^{-1}. The ICl fundamental appeared at 381.5 cm^{-1} in exact agreement with the vibrational constants given by Herzberg[2] within the accuracy of the measurements.

We measured the integrated intensities of the two fundamental bands, but the BrCl overtone was accompanied by bands from the products of reaction of the halogens with the metal parts of the White cell which we were using. In shorter cells the intensities of the overtones were not sufficient for the bands to appear. However, it is possible to make an estimate of an upper limit for the overtone intensities from the spectra on which these bands did not appear. The best values of the integrated band absorption coefficients in cm/millimole (i.e., wave numbers cm^2 millimole^{-1}) are given in Table I.

Figures 1 and 2 are plots of *Bnl* against *nl* for the BrCl and ICl fundamentals. The data are given in Table II. *Bnl* is the measured band intensity at a particular concentration n and path length l. The rectangle surrounding each point represents roughly the limits of error of the measurements of *Bnl* and *nl*. The straight lines have slopes equal to the best value of A_1 as determined by least squares.

Crawford and Dinsmore[3] have given for diatomic molecules the relationships between the quantity A_1 and the dipole-moment derivative $p'=(dp/dr)_{r=r_e}$. To the degree of approximation appropriate to the data given above, their formula reduces to

$$p'=\pm 1.537\times 10^{-12}(\mu_A A_1)^{\frac{1}{2}}$$

TABLE I. Band absorption coefficients and dipole moments and derivatives of ICl and BrCl.

	BrCl	ICl
A_1(fundamental)	105 ± 14 cm/millimole	650 ± 160 cm/millimole
A_2(overtone)	<2.5 cm/millimole	<4 cm/millimole
p^0	0.57 debye [a]	0.65 debye [b]
p'	± 0.76 d/A	± 2.1 d/A
$\lvert p''\rvert$	<10 d/A^2	<14 d/A^2

[a] Smith, Tidwell, and Williams, Phys. Rev. **77**, 420 (1950).
[b] Townes, Merritt, and Wright, Phys. Rev. **73**, 1334 (1948).

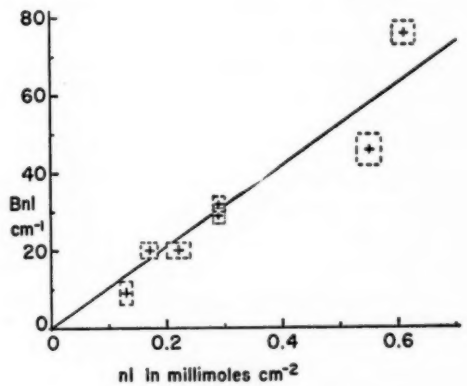

FIG. 1. Plot of *Bnl* against *nl* for BrCl.

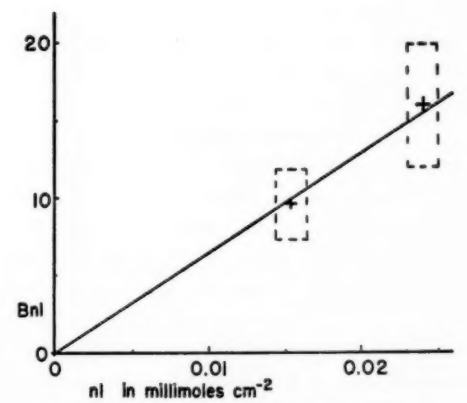

FIG. 2. Plot of *Bnl* against *nl* for ICl.

* From a thesis submitted by Wendell V. F. Brooks to the University of Minnesota in partial fulfillment of the requirements for the degree of Doctor of Philosophy. For previous papers in this series, see: I, J. Chem. Phys. **18**, 983, 1682 (1950); II, *ibid.* **20**, 977 (1952); III, *ibid.* **19**, 1554 (1951); IV, *ibid.* **22**, 179 (1954).

† Present address, Sterling Chemistry Laboratory, Yale University, New Haven, Connecticut.

[1] Mattraw, Pachucki, and Hawkins, J. Chem. Phys. **22**, 1117 (1954).

[2] G. Herzberg, *Spectra of Diatomic Molecules* (D. Van Nostrand, Company, Inc., New York, 1950), second edition.

[3] B. L. Crawford, Jr., and H. L. Dinsmore, J. Chem. Phys. **18**, 983, 1682 (1950).

TABLE II. Intensity data on the fundamental bands of BrCl and ICl.

BrCl run	$n(Cl_2)\times10^{3*}$	$n(Br_2)\times10^{3*}$	$n(BrCl)\times10^{3}$	l	nl	Bnl	B	P(atmos)
1	2.703	3.233	3.3 ±0.1	183	0.61±0.02	76±3	125	2
2	1.907	4.987	3.0 ±0.1	183	0.55±0.02	46±4	83	1.6
3	0.5081	3.705	0.91±0.07	183	0.17±0.015	20±2	118	2.5
4	0.7727	1.725	1.18±0.08	183	0.22±0.02	20±2	93	3.8
5	2.429	3.228	3.1 ±0.1	93	0.29±0.01	29±2	100	3
6	0.8309	2.435	1.35±0.10	93	0.13±0.01	9±3	71	8
7	1.975	4.779	3.1 ±0.1	93	0.29±0.01	32±2	112	6.3

ICl run	$n(ICl)\times10^{3}$	l	nl	Bnl	B	P(mm of Hg)
1	0.77±0.05	20	0.0154±0.001	9.6±2.3	620	740
2	1.20±0.05	20	0.024±0.001	16 ±4	670	720

n =concentration in millimoles cm^{-3}, l =path length in cm, Bnl is the measured band intensity in cm^{-1}, P =total pressure in the cell. n^* is the concentration before reaction.

where μ_A is the reduced mass of the molecules in atomic units. This leads to the p' values in Table I. Their formula for the intensity coefficient of the first overtone depends upon p' times the mechanical anharmonicity (the cubic coefficient in the potential-energy expression) and upon the second derivative $p''=(d^2p/dr^2)_{r=r_e}$. If the actual overtone intensities are anywhere near the upper limits, the mechanical anharmonicity term must be quite small compared to p''. Thus an upper limit may be put on p'' by assuming that the other term is zero. These limits are given in Table I.

At present, neither empirical nor quantum-mechanical information about dipole moments is sufficient to determine accurately the correct sign of p'. The larger of the two p' values (ICl) is associated with the larger moment which seems happily appropriate to the larger electronegativity difference between I and Cl and the larger polarizability of I as compared to Br.

Aroeste[4] has suggested an empirical linear relationship between p' and D/r_e^2 where D is the dissociation energy of the molecule and r_e is the equilibrium internuclear distance. The values of p' for BrCl and ICl do not fit this relationship at all. Figure 3 shows Aroeste's plot of p'/e (e=electronic charge), against D/r_e^2 for four molecules with the points for BrCl and ICl added. The D, r_e and p'/e values for BrCl and ICl are given in Table III.

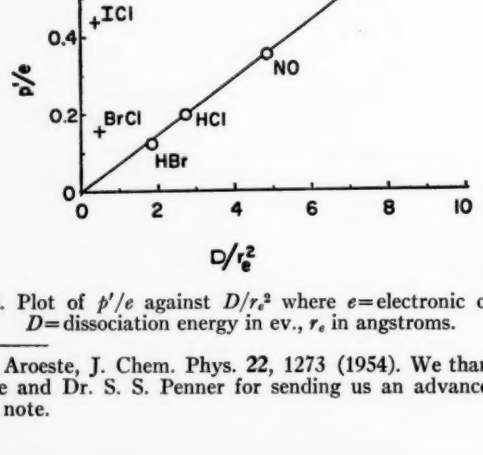

FIG. 3. Plot of p'/e against D/r_e^2 where e=electronic charge, D=dissociation energy in ev., r_e in angstroms.

[4] H. Aroeste, J. Chem. Phys. **22**, 1273 (1954). We thank Dr. Aroeste and Dr. S. S. Penner for sending us an advance copy of this note.

EXPERIMENTAL

The spectra were all recorded on a Perkin-Elmer model 12C monochromator converted to double-pass operation. The fundamental bands were investigated with a CsBr prism and the overtones with a NaCl prism; both prisms were calibrated by the method of Downie, Magoon, Purcell, and Crawford.[5] The BrCl data were taken with the gas in a White cell; nitrogen (Matheson prepurified) was added to make a total pressure between 1.6 and 8 atmospheres. As long as the total pressure of halogens remained less than about 130 mm the gases did not react with the cell walls (steel) or the aluminum coating on the mirrors. At higher halogen pressures reactions did begin, lowering the transmission of radiation as the mirrors were eroded and enriching the spectrum with a number of bands. Some of the bands were probably due to the presence of Al_2Cl_6 in the vapor phase. ICl was worse than BrCl in its tendency to react; at pressures as low as 20 mm the mirrors were attacked quite rapidly. Since the total quantity of ICl in the cell at this pressure was relatively small, the ICl soon disappeared. Therefore, the ICl spectra were taken in a 20-cm glass cell (KBr windows) pressurized to 1 atmos with N_2.

TABLE III. Molecular parameters.

	BrCl	ICl	references
D	2.26 ev	2.152 ev	a
r_e	2.138 A	2.321 A	a,b
p'/e	0.158	0.438	

[a] See reference 2.
[b] See references 2 and reference a of Table I.

[5] Downie, Magoon, Purcell, and Crawford, J. Opt. Soc. Am. **43**, 941 (1953).

The BrCl was prepared from reagent grade Br_2 (Baker) and 99-percent pure tank Cl_2 (Matheson). The Br_2 was dried by passing it over P_2O_5 three times in a vacuum line, and it was used without further purification. The Cl_2, similarly dried, was distilled once from a bulb cooled with a dry-ice butanol mixture; the middle third of the distillate was used. The vapors from the Cl_2 and Br_2 were admitted to the cell at known pressures and allowed to mix by diffusion. The concentration of BrCl can be found from the dissociation constant of BrCl[1] and the amounts of Br_2 and Cl_2 added. The ICl was a commercial product (Eastman) described by the manufacturer as "pure." It was dried over P_2O_5 and used without further purification.

Both fundamental bands are in a region of strong water bands, and despite a continuous current of dry air through the enclosed source and monochromator, the traces still showed considerable water absorption. This and the relatively weak signal at long wavelengths are the principal reasons for the large indeterminacy of the results.

ACKNOWLEDGMENT

We are indebted to the Office of Naval Research which provided financial support for this research.

THE JOURNAL OF CHEMICAL PHYSICS VOLUME 23, NUMBER 2 FEBRUARY, 1955

Some Physical Properties of Plutonium Metal

ERIC R. JETTE*
Los Alamos Scientific Laboratory, Los Alamos, New Mexico
(Received July 29, 1954)

Data on some of the physical properties of plutonium metal are given, including allotropic modifications, crystal structures, transformation temperatures, melting point, densities, expansion coefficients, electrical resistance, and magnetic susceptibility.

EARLY in 1944 it was known that a substance which was ostensibly plutonium metal could be prepared but that the densities of this material were sometimes in the range of 16 to 16.5, while in other cases they were over 18 and sometimes approached 20. Nothing could be done to resolve this question until a sufficient amount of metal could be accumulated to run certain rather routine types of experiments, such as the thermal analysis and the expansion curve. The first thermal analyses curves run on one gram samples in early June of 1944 showed thermal arrests at 130°, 222°, 324°, 480°, and 630°C. The last of these was identified as the melting point. This still left four transformation points, or a total of five allotropic modifications. This was unheard of in the field of pure metals and many conjectures were made as to what could be wrong with the material or the technique to give such a result. The cooling curve arrests gave one at 621°, again identified with the melting phenomenon, and another at 460°. The curve from there on down to the lower temperatures simply wandered and gave no definite indications of arrests, the lack of reversibility tending to support the view that something was wrong with the experiments.

A short time later enough material had accumulated to run a dilatometer curve (Fig. 1) on a specimen about 0.4 in. long. It can be seen that there are indications of phase changes at about 135°, 220°, 325° and a fourth somewhere between 465° and 510°. Instead of sharp breaks where the transformations start and end, there are generally slowing rising curves, so that an S-shaped curve represents a transformation region instead of three straight lines. The contraction between 340° and 465° is striking. The cooling curve does not retrace the heating curve. However, from about 450° to 250°C the sample expanded on cooling. The specimen ended the cycle about one percent shorter than it started. This curve showed that we had to deal with sluggish transformations in both directions and that there were some phenomena which appeared irreversible. The electrical resistance *versus* temperature was also measured and gave indications of transitions much like those in the dilatometer curve with much the same sort of sluggishness in the transformations. On cooling, the behavior was indefinite over a large part of the range below about 200°C. The lack of sharpness in all of these curves made the transition points uncertain, and we generally had to state quite large ranges in connection with our observations. These results were not very different from those reported by C. S. Smith for the end of 1945,[1] nor

* The present author is merely acting as a reporter for the work represented in this summary. Since the beginning of 1944, at least forty individuals working in this laboratory have contributed to our knowledge of plutonium metal. Individual reports on the several properties of plutonium will be written by the persons actually concerned with the work today and it is hoped that adequate acknowledgement can be made there of the efforts of the earlier workers. Some time, however, may elapse before these articles can be published and therefore this summary is being presented.

[1] C. S. Smith, Metal Progress **65**, 81–89 (1954).

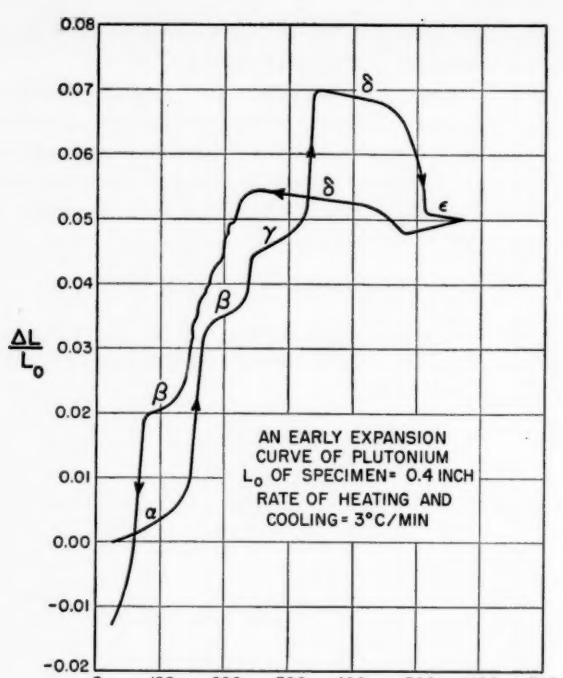

FIG. 1.

from those published by W. B. H. Lord[2] and by J. G. Ball *et al.*[3] The English investigators were troubled by the same sluggishness and hysteresis phenomena which caused us so much difficulty.

Since 1945, a number of dilatometric and resistivity measurements have been made with results not too different from the first ones. A number of other properties were measured, some of which showed the same kind of anomalies with temperature; they also appeared to vary in different specimens.

Improvement in the accuracy of the results became possible after two developments which came almost simultaneously, less than a year ago; namely, the production of higher purity metal and the development of a dilatometric technique which gave recognition to the fact that plutonium was radioactive and generated heat.

By commonly used weight-composition standards the metal used in the earlier work was really quite good. A comparison of the compositions of earlier metal with two specimens of high purity is given in Table I. The extraordinary effect of a tenth of a weight percent increase in purity on the purity in atom percent is due to the fact that practically all of the impurity elements have atomic weights less than seventy. Since plutonium has an atomic weight of 239, these low atomic weight elements have a large influence on the atomic composition.

The effect of plutonium's radioactivity is to cause its temperature to rise. This means that the inside of the piece is at a higher temperature than the outside, even when apparent equilibrium has been established with respect to a temperature bath. The effect of the temperature gradient in the specimen is to give the S-shaped transformation curves in the transformation range, such as have been observed. In dealing with relatively massive specimens, i.e., not including foils or thin wires, one can use a specimen as a self-heater and control the bath temperature and its rate of rise by the rate of rise of temperature of the specimen. In other words, the temperature bath follows the specimen rather than the usual reverse situation. We have called this method adiabatic self-heating. It is adiabatic in the sense that the specimen is in vacuo and loss or gain of heat by radiation and conduction is minimized by keeping the bath or furnace temperature only 0 to 0.5°C above the specimen temperature. It is self-heating in that the furnace contributes practically nothing to the heating of the specimen. The same technique was adapted to the thermal analysis method. It is obvious that this technique is useless in cooling curves. For dilatometric work fairly sturdy bars must be used, since the distortions produced by the density changes in the transformations, the plasticity of the metal during some of the transformations, and the softness of the higher temperature modifications, produce changes of shape which spoil the measurements.

TABLE I. Typical plutonium metal purities.

	Total plutonium	
	Weight percent	Atomic percent
Earlier material	99.87	99.01
High-purity sample No. 1	99.97	99.82
High-purity sample No. 2	99.95	99.75

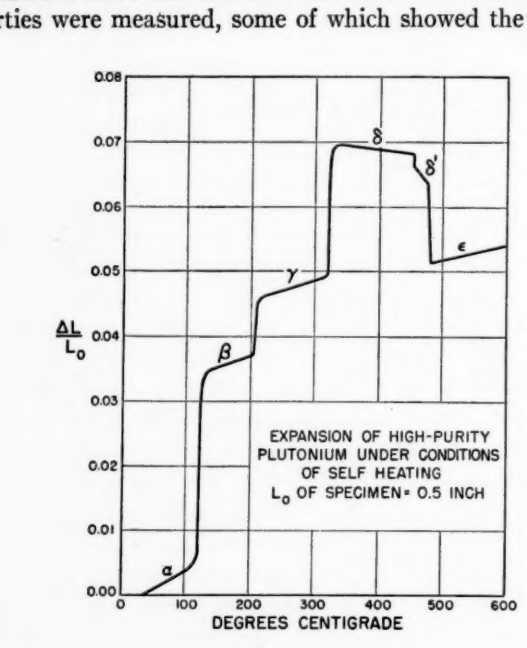

FIG. 2.

[2] W. B. H. Lord, Nature **173**, 534 (1954).
[3] J. G. Ball *et al.*, Nature **173**, 535 (1954).

The effect of the new dilatometric technique was to improve the sharpness of the curves very markedly (Fig. 2). We no longer had the long curved portion in the alpha-beta and gamma-delta transformations, and even the curve in the beta-gamma transformation was improved. In addition the vertical portions of the curve now were very nearly vertical, the slope seldom amounting to more than two to four degrees over the transformation range. Thus a large portion of the uncertainty in the transformation temperatures was eliminated and the expansion coefficients of the individual phases could be determined with a considerable degree of accuracy.

The effect of the increased purity of the metal was to reveal a new phase, delta-prime, existing between 451° and 476°C. The temperature coefficient of expansion in the delta phase region was considerably lower than it had been, but the delta-prime phase had an exceptionally high negative coefficient of expansion.

Data on the various transformations are given in Table II. The transformation temperatures by the dilatometric method are averages of seven runs. Those

TABLE II. Phase-transformation data on plutonium metal.

Transformation	Temperature °C[a] Dilatometer	Thermal analyses	ΔV[b]
$\alpha-\beta$	122±2	122	8.9%
$\beta-\gamma$	206±3	203	2.4
$\gamma-\delta$	319±5	317	6.7
$\delta-\delta'$	451±4	453	−0.4
$\delta'-\epsilon$	476±5	477	−3.0
ϵ−liq.		639.5±2	

[a] On heating only.
[b] $\Delta V=(v_2-v_1)/v_1$.

by thermal analysis are the results of only two runs but they agreed with the dilatometric results within the experimental limits stated in the second column.

The ΔV's for the alpha-beta and the beta-gamma transformations were calculated from the dilatometric curves. The other ΔV's were calculated from x-ray diffraction results extrapolated to the appropriate transition temperatures.

The delta/delta-prime region of the dilatometric curve has been from the very beginning extremely puzzling. When the delta-prime phase was still unknown, the dilatation temperature line had marked curvatures which, however, were seldom retraced in going back and forth over the total range between 320 and 475°C. Even when the delta-prime phase does not come into the picture, a large range of values of the expansion coefficient was obtained for the delta phase itself. In part the temperature coefficients seemed to be influenced by the rate of heating through the gamma-delta transformation range. If the heating was rapid, the linear expansion of the specimen in going from gamma to delta was too large, and thus on further heating within the delta range gave abnormally large

TABLE III. Phase data.[a]

Phase	Density	Linear expansion coefficient[b] $\times10^6$	Resistivity $\rho\times10^6$	$1/\rho\cdot d\rho/dt\times10^5$
α	19.737 (25°)	50.8 (25°)[c]	145 (28°)	−21
β	17.65 (150°)	38.0 (164°)[c]	110.5 (132°)	−6
γ	17.19 (210°)	34.7 (ave.)[c]	110 (230°)	−5
δ	15.92 (320°)	−10.0±0.5	103 (353°)	+7
δ'	15.99 (465°)	−120	105 (462°)	+45
ϵ	16.48 (500°)	25.7±2.0	114 (490°)	−7
Liquid	16.50 (665°) ±0.08	50[d]		

[a] Note: t = °C.
[b] $1/L\cdot\Delta L/\Delta t=\alpha$.
[c] See Table VI.
[d] Volume coefficient.

slopes. On one occasion an expansion coefficient of nearly -60×10^{-6} was observed. If, however, the specimen was carried back and forth over a temperature interval within the delta range proper, the heating and cooling curves would gradually come together and reach a value of about -10×10^{-6}/°C. The expansion coefficient given in Table III for this phase was determined by x-ray diffraction methods and can be accepted as a true value, since the specimen was held at each temperature for the length of time necessary to get the x-ray exposure in the high-temperature camera (generally several hours at each temperature). This appears to eliminate the differences observed between rising and falling temperatures.

The crystal structures have been determined for four of the six phases. The alpha and beta phases are much too complicated to solve by means of powder patterns, and thus far there has been no success in securing single crystals. However, it has been shown quite conclusively that alpha plutonium is *not* isomorphous with alpha uranium, as was once tentatively believed.[1] The crystal structures reported in Table IV were from determinations made at temperature in a high-temperature camera. It should be noted that there is direct evidence that the delta-prime phase is different from the delta phase. The 200, the 220, and 311 lines of the face-centered cubic phase split into doublets characteristic of the face-centered tetragonal cell. Perhaps the most striking feature of the crystal structure data is that the delta phase, which has the lowest density of any phase in the entire system, is the only phase with a close-packed structure. The increase in density in going from the face-centered cubic delta to the body-centered cubic epsilon is noteworthy. Inter-

TABLE IV. Crystal structure data on high-purity plutonium metal.

			Density
Gamma: face-centered orthorhombic			
At 210°C	$a_0=3.1603$A $b_0=5.7624$	$c_0=10.141$	17.19
Delta: face-centered cubic			
At 320°C	$a_0=4.6370$		15.92
Delta-prime: face-centered tetragonal			
At 465°C	$a_0=4.701$ $c_0=4.489$	$c/a=0.955$	15.99
Epsilon: body-centered cubic			
At 500°C	$a_0=3.638$		16.48

TABLE V. Inter-atomic distances in plutonium metal structures.

Phase	Structure	Coordination	Distances	Temp. °C
Gamma	Orthorhombic	10	4 Pu 3.021A	210
			2 Pu 3.160A	210
			4 Pu 3.286A	210
			Ave. 3.155A	210
Delta	Cubic F.C.	12	3.279A	320
Epsilon	Cubic B.C.	8	3.150A	500

TABLE VI. Expansion coefficients of α, β, and γ phases of plutonium metal where t = °C.

Alpha (−180° to +122°C)
$\alpha\times10^6=(48.39\pm0.01)+(0.0959\pm0.0012)t$
Beta (82 to 206°C)
$\alpha\times10^6=(26.04\pm0.01)+(0.0740\pm0.0015)t$
Gamma ($\alpha\times10^6$ in each case) (149 to 319°C)
$\alpha[100]=-19.7\pm1.7$; $\alpha[010]=39.5\pm0.9$; $\alpha[001]=84.3\pm2.3$
$\alpha_{Av}=34.7\pm3.0$

atomic distances are given in Table V. The structure of the orthorhombic gamma phase has been worked out in some detail. It fits with space group *Fddd*, which has previously not been observed for pure metals. This structure represents practically the closest packing that can be had of atoms with a coordination number of ten. It should be pointed out that in this structure there are four atoms considerably closer together than in the close-packed delta structure, and that the other atomic distances correspond quite closely to those characteristic of the delta and epsilon phases.

In Table III we give data characteristic of the individual phases. More detailed expressions for the expansion coefficients of alpha, beta and gamma are given in Table VI. The densities and expansion coefficients for the gamma, delta, delta-prime, and epsilon phases were all determined by x-ray diffraction methods. Values could be obtained at temperatures lower than the stability range in some cases because of supercooling.

The density of the alpha phase requires special comment. The production of the alpha phase makes it inevitable that the metal pass through the higher temperature phase. The transformation beta to alpha is sluggish and it is rather difficult to get complete conversion to alpha. However, x-ray diffraction will almost always show some beta phase unless special precautions are taken. Since the beta phase is of lower density than the alpha, the mixture will have a density less than the true alpha density. For example, alpha densities on as-cast material are rarely over 19.64 but usually appreciably less. By use of high pressures, perhaps accompanied by low temperatures, the transformation can be made complete or almost so, depending upon the technique used. The alpha phase density given in Table III was found on specimens pressed at 50 000 psi at 300°C and cooled under pressure to room temperature. In a few cases values close to this were obtained by cooling the metal while under pressure to the temperature of a CO_2-alcohol mixture. References 2 and 3 report alpha densities of 19.00 and 19.25, respectively, which are very low. The "true" density will probably not be known until the crystal structure has been determined.

The electrical resistivity was determined on specimens $3\frac{1}{2}$ in. in length and $\frac{1}{4}$ in. in diameter. The rate of rise of temperature was fixed at very nearly the same rate as in the self-heating dilatometer work.

It is to be specially noted that for no phase do *both* the coefficient of thermal expansion and the temperature coefficient of resistivity have the conventional sign. Thus, if the phase expands on heating, the resistance decreases.

The magnetic susceptibility has been measured on two specimens of the earlier material. Despite the fact that for metals this property is generally considered as "structure insensitive," there were differences between the samples well beyond the experimental errors of the Gouy method used. Very approximate average susceptibilities per gram atom at temperatures about the midpoints of the phase ranges are alpha, 532 (25°); beta, 553; gamma, 531; delta, 515; and epsilon, 522 $\times10^{-6}$. For the alpha phase the susceptibility is practically independent of temperature, while for each of the others it decreases with increasing temperature, particularly in the beta phase. This work is being repeated on high purity material.

ACKNOWLEDGMENT

The author wishes to thank R. B. Gibney and A. S. Coffinberry for their assistance in preparing this paper.

Absorption Spectrum of $NaNO_3$ Exposed to Ionizing Radiation

P. PRINGSHEIM
Chemistry Division, Argonne National Laboratory, Lemont, Illinois
(Received August 19, 1954)

The changes produced by ionizing radiation in the absorption spectrum of $NaNO_3$ crystals are in the main caused by two effects: the conversion of NO_3^- ions into NO_2^- ions with an absorption band, which has its peak at 345 mμ and shows a characteristic structure when observed at low temperature; and the production of color centers with a continuous absorption band with peak at 335 mμ. The formation of the color centers is assumed to be connected with the presence in the lattice of NO_2^- ions, although no precise model can be proposed for these centers. The color center band can be bleached by ultraviolet light even at −190°C; at room temperature it is partially destroyed by the ionizing radiation which is able to produce the centers, while this is not the case with respect to the NO_2^- ions. Therefore the NO_2^- band is relatively much stronger in crystals exposed to the ionizing radiation at higher temperatures, for instance in the pile, while in crystals x-rayed at −190°C the color center band prevails.

INTRODUCTION

THE absorption spectrum of $NaNO_3$ in aqueous solution shows a fairly weak band at 302 mμ and a second band of about a thousand times higher intensity with peak at 194 mμ.[1] In dilute solutions the wavelength of the peaks does not depend on the nature of the cation, but addition of cations such as Ca^{++} or Mg^{++} in high concentrations in the form of $CaCl_2$, etc., shifts the peak of the 302-mμ band appreciably towards shorter wavelengths. The absorption spectra of nitrites are similar with a first weaker band at 352 mμ and a short-wavelength band of great intensity at 210 mμ.[2]

Schaumann[3] and Rodloff[4] found that in solid crystals of $NaNO_3$, $Ba(NO_3)_2$, KNO_2, etc. the same bands appear with slight modifications (shift of peak to shorter wavelengths, band width) caused by the nature of the cations. At low temperatures (boiling oxygen and boiling hydrogen) the band at longer wavelength exhibits a structure which is only partly resolved in the nitrates, but in the nitrites shows a great number of narrow peaks. No such structure could be observed in the short-wavelength bands. By irradiation with short-wavelength ultraviolet light the normally colorless crystals of $NaNO_3$ acquire a yellow color. From these facts the two last named authors concluded that the long-wavelength bands correspond to internal electronic transitions of small probabilities in the NO_3^- and NO_2^- ions upon which vibrational frequencies also characteristic of these ions are superimposed, although the latter are influenced by the nature of the surrounding lattice. By absorption in the short-wavelength bands an electron is supposed to be ejected from the ion with subsequent formation of some kind of color center.

It was known since 1914 that when $NaNO_3$ is exposed to ultraviolet light, oxygen gas is developed.[5] The simultaneous conversion of nitrate into nitrite was proved by Narayanswamy,[6] and analogous results were obtained by irradiating barium nitrate with x-rays or γ rays.[7] Finally, it has been shown by Hennig, Lees, and Matheson[8] that KNO_3 and $NaNO_3$ after long lasting exposure in the pile acquired a yellow color and in submicroscopic pockets contained small amounts of gas, 98.5 percent of which was oxygen. About two molecules of $NaNO_2$ were found to have been formed for every molecule of O_2. By a rather qualitative evaluation of the energy absorbed the number of O_2 molecules liberated per 100 ev was calculated to be about 0.8 for KNO_3 and 0.3 for $NaNO_3$. In another series of experiments single crystals of $NaNO_3$ were irradiated with x-rays of peak voltages 49 and 25 kv, and here the quantity of O_2 recovered per 100 ev absorbed was 0.27 and 0.38 molecule, respectively. Since this was of the same order of magnitude as in the pile experiments, and since it is highly improbable that in the case of the x-ray irradiation knock-on processes contribute appreciably to the conversion, it followed that the same was probably true for the processes occurring in the crystals which had been exposed in the pile, and that also there electronic excitation and ionization play the most important part. No analysis for the quantity of NO_2 produced in the x-ray experiments was performed.

In none of the previous papers dealing with the behavior of nitrate crystals under exposure to ionizing radiation were the changes occurring in their absorption spectra discussed or even mentioned beyond the statement of the appearance of a yellow coloration.

MATERIAL AND METHODS OF INVESTIGATION

The $NaNO_3$ crystals belonged in part to a lot obtained several years ago from the Harshaw Chemical Company and used in some of the experiments by Hennig and co-workers; other samples were grown in our laboratory by the Kyropoulos method from Merck reagent grade salt. No appreciable difference was observed between

[1] G. Scheibe, Ber. deut. chem. Ges. **59**, 1321 (1926).
[2] I. Maslakowiz, Z. Physik **51**, 666 (1928).
[3] H. Schaumann, Z. Physik **76**, 106 (1932).
[4] G. Rodloff, Z. Physik **91**, 511 (1934).
[5] O. Baudrisch and E. Mayer, Z. physik. Chem. **89**, 196 (1914).
[6] L. K. Narayanswamy, Trans. Faraday Soc. **31**, 1411 (1936).
[7] A. O. Allen and J. A. Ghormley, J. Chem. Phys. **15**, 206 (1947).
[8] Hennig, Lees, and Matheson, J. Chem. Phys. **21**, 664 (1953).

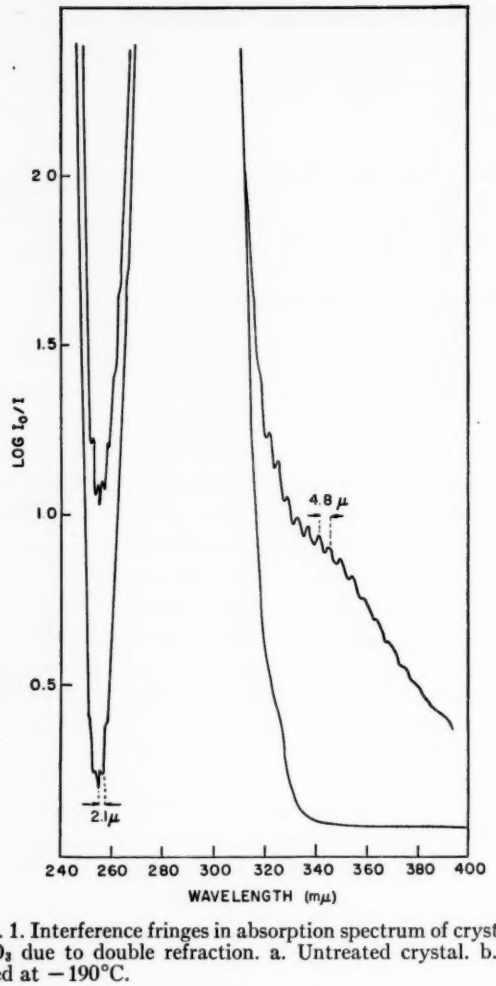

FIG. 1. Interference fringes in absorption spectrum of crystalline $NaNO_3$ due to double refraction. a. Untreated crystal. b. 1 hr x-rayed at −190°C.

the two types of crystals. Since the formation of NO_2^- was one of the interesting features, $NaNO_2$ crystals as well as $NaNO_3$ crystals containing small quantities of $NaNO_2$ as impurity were grown by the same method. Finally it seemed interesting to observe the influence of the base material upon the characteristic band of the NO_2^- ion imbedded in some foreign lattice, and therefore various alkali halides containing $NaNO_2$ in various concentrations were also investigated. In every instance plates of 0.5 to 1 mm thickness were cleaved from larger single crystals and, for irradiation and absorption studies, were inserted in a Dewar vessel of the type described previously.[9] The spectra were registered by means of a Cary spectrophotometer, in general at the temperature of liquid N_2, in one case also at the temperature of liquid He.

$NaNO_3$ crystals are strongly birefringent and also dichroic to a very appreciable degree. This must be taken into account when the absorption by single crystals of $NaNO_3$ is observed in the Cary instrument. The light emanating from the monochromator is partially linearly polarized by the reflection on the prism faces. The exit slit is protected by a crystalline quartz plate with its optical axis parallel to the plate. Therefore the polarized fraction of the transmitted light becomes elliptically polarized to various degrees depending on its wavelength, and after passing through the $NaNO_3$ crystal (oriented at random) the spectrum shows a sequence of maxima and minima with a period, in the blue green, of about 10 mμ, and at 340 mμ of about 5 mμ (see Fig. 1), which might be mistaken for a vibrational band structure.

The same kind of intensity modulation in the spectrum is obtained with much greater contrast between maxima and minima by replacing the crystal plate by a polaroid with its azimuth of greatest transmission at 45° from the vertical; at 0° and 90° the fringes disappear. The disappearance of the fringes can also be obtained in the case of the $NaNO_3$ plates by rotating the crystals around an axis perpendicular to the plate until the projection of the optical axis of the crystal upon the surface of the plate is vertical. After this had been understood, all spectra were recorded with the crystals thus oriented (compare Figs. 1 and 2).

For the investigation of the dichroism induced by

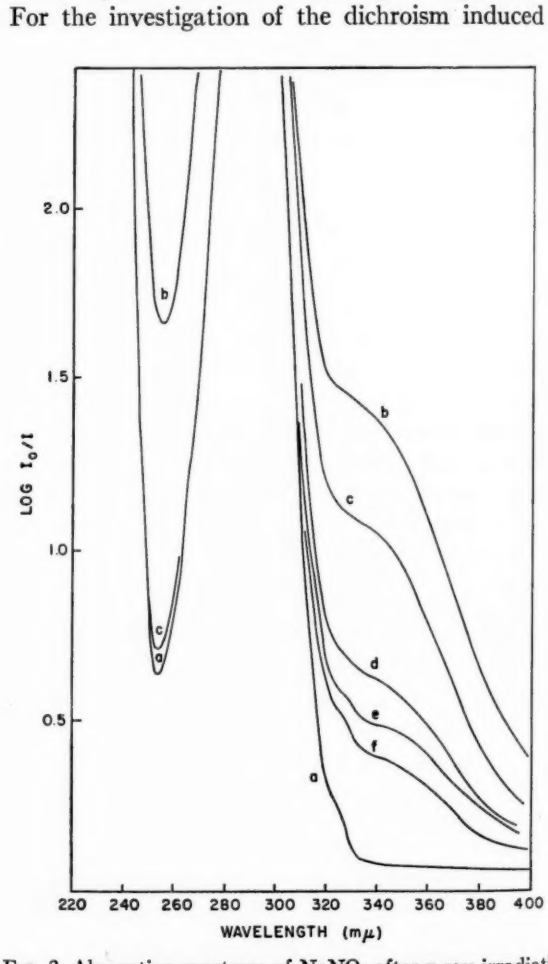

FIG. 2. Absorption spectrum of $NaNO_3$ after x-ray irradiation, measured at −190°C. a. Crystal untreated. b. 2 hr x-rays at −190°C. c. Warmed to room temperature. d. 15 minutes x-rays at room temperature. e. 15 minutes more x-rays at room temperature. f. 15 minutes more x-rays at room temperature.

[9] Casler, Pringsheim, and Yuster, J. Chem. Phys. 18, 887 (1950).

irradiation the light from a Hg AH6 lamp was focused on a pinhole in an opaque screen, and the light transmitted by the hole was focused on the crystal plate after having passed through an interference filter combined with an adequate Corning filter glass and a Wollaston prism. Only one of the polarized beams (with its electric vector vertical) was allowed to fall through the crystal on the photocathode of a photomultiplier while the other beam was screened off. The crystal was mounted so that it could be rotated around an axis vertical to its surface and parallel to the light beam, while the polarizer was left in a constant position. The two positions of the crystal for maximum and minimum transmission and the relative amounts of transmitted light in these positions for various wavelengths were determined.

The same arrangement, in general, without the pinhole screen and the polarizer was used for bleaching purposes. The much more powerful, but less monochromatic, light source was replaced only exceptionally by a double monochromator.

The following types of irradiation were used for producing changes in the optical properties of the crystals: neutron bombardment, γ rays, etc., in the CP-3′ pile of the Argonne National Laboratory; the 10^6 ev γ rays of a 400-curie Co^{60} source; x-rays from a 50-kv Machlett tube with beryllium window; ultraviolet light from a Mineralight lamp without filter ($\lambda \geq 1849$ A) and with filter ($\lambda \geq 2400$ A).

THE NO_2^- BAND AND THE COLOR CENTER BAND IN $NaNO_3$

The long-wavelength edge of the $NaNO_3$ band with peak at 292 mμ drops quite sharply between 300 and 320mμ, although the slight shoulder at the foot of the band between 320 and 330 mμ is real (Fig. 3, curve *a*). In curve *b* of the same figure the NO_2^- band caused by the addition of $NaNO_2$ in a concentration of about 0.5 percent is superimposed on the long-wavelength tail of the NO_3^- band. The structure of the NO_2^- band with seven clearly separated peaks disappears at room temperature, and then the band is very similar to the one observed in aqueous solution of $NaNO_2$. The structure is quite characteristic of the ion, and it is obtained in almost identical shape in the spectrum of NO_2^- contained as impurity in an alkali halide, with only the electronic frequency shifted by about 20 mμ toward the red (Table I).

In both instances the band, the peaks of which are only somewhat sharpened and little displaced by cooling the crystal to the temperature of liquid helium, shows much less fine structure than in pure $NaNO_2$; here each of the peaks listed in Table I is split into

TABLE I. Peaks of the NO_2^- band. Wavelengths in mμ.

In $NaNO_3$	325	(331)	(338)	343	349	355	362	370	378
In KBr	345	352		359	365	371	381	390	399

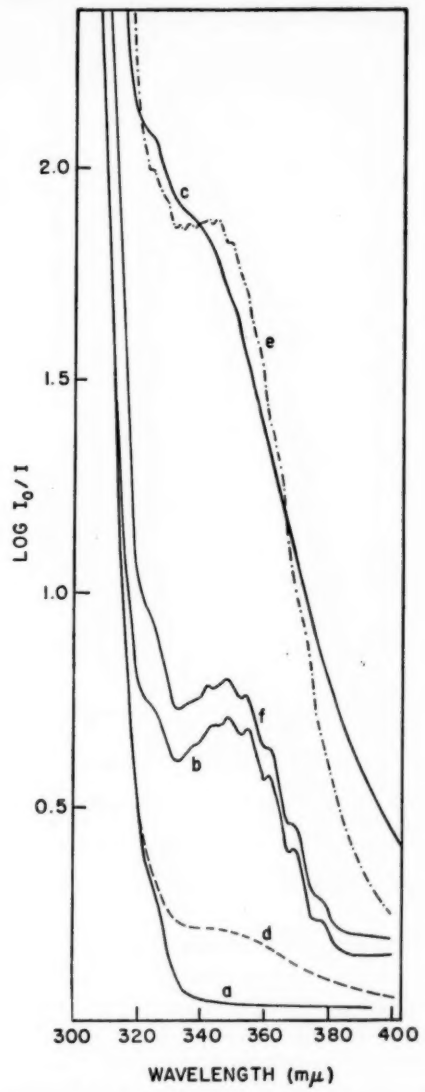

FIG. 3. Absorption of $NaNO_3$ from 300 to 400 mμ under various conditions, measured at −190°C. *a*. Untreated crystal. *b*. Untreated crystal with $NaNO_2$ added to the melt. *c*. Pure crystal 80 min x-rayed at −190°C. *d*. Same as *c*, bleached 2 hr at −190°C with full light from Hg AH6 arc. *e*. Pure crystal 800 hr under γ rays. *f*. Same as *e*, bleached 2 hr with full light from Hg AH6 arc.

several components. The center of the band at about 345 mμ, however, is nearly the same in pure $NaNO_2$ and in $NaNO_3$ containing $NaNO_2$ as an impurity.

Curve *c* of Fig. 3 shows the change occurring in the absorption spectrum of a $NaNO_3$ crystal when it has been exposed to x-rays for 80 minutes at −190°C: a new band appears, overlapping the 292 mμ band of $NaNO_3$ on one side and reaching with a flat tail beyond 500 mμ on the other side. Curve *a* in Fig. 4 was obtained by subtracting the absorption before x-ray treatment from the absorption after the exposure (curve *c* minus curve *a* in Fig. 3). It has its peak at about 335 mμ, somewhat below the peak of the $NaNO_2$ band and without its characteristic structure and represents the additional absorption produced by the x-rays. Curve *b*

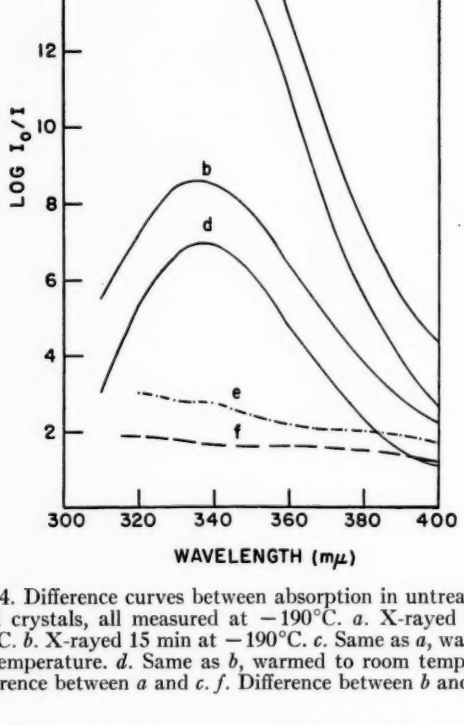

FIG. 4. Difference curves between absorption in untreated and x-rayed crystals, all measured at −190°C. *a*. X-rayed 1 hr at −190°C. *b*. X-rayed 15 min at −190°C. *c*. Same as *a*, warmed to room temperature. *d*. Same as *b*, warmed to room temperature. *e*. Difference between *a* and *c*. *f*. Difference between *b* and *d*.

of Fig. 4 shows the same absorption band obtained from a crystal which had been x-rayed only 15 minutes and which therefore, being less deeply colored, could be investigated farther towards the ultraviolet. Without suggesting any specific model for the "center" responsible for this band, it may be called the color center of $NaNO_2$. There is also, after x-ray irradiation at −190°C, a very large increase of absorption at 253 mμ in the gap between the two $NaNO_3$ bands (see, for instance, curve *b* of Fig. 2).

BLEACHING BY TEMPERATURE, ULTRAVIOLET LIGHT, OR X-RAYS

If a $NaNO_3$ crystal x-rayed at −190°, as respresented by curve *c* of Fig. 3 and the curves *a* and *b* of Fig. 4, is for a short time warmed up to room temperature and again cooled to −190°C, the intensity of the absorption between 400 and 300 mμ drops through this whole spectral range by an almost constant and not very great amount, as shown by curves *e* and *f* of Fig. 4. Simultaneously the absorption in the "gap" at 253 mμ drops almost completely to its initial value (see Fig. 2). Therefore this absorption does not belong to the color centers: on the other hand, because of its location between the adjacent strong absorption bands of $NaNO_3$, one cannot ascertain whether it is a part of the much weaker continuous absorption above 300 mμ or is due to an independent selective absorption band in the ultraviolet. Once the state charcacterized by curves *c* or *d* of Fig. 4 is reached, it is quite stable for many hours at room temperature and even at 100°C.

If in this state a crystal is exposed at −190°C to weak light of wavelengths corresponding to the color center band (340 to 365 mμ) the first phenomenon observed is not a bleaching of the band as a whole, but an increase of absorption in the region of greater wavelengths (above 350 mμ) and a corresponding decrease in the short-wavelength part of the band. Warming the crystal to room temperature and cooling it again to −190°C restores the initial energy distribution of the band; this cycle can be repeated several times.[10] The effect is saturated easily; after 2 minutes 75 percent of the change obtained in 10 minutes is produced, and longer continuation of the irradiation hardly contributes anything, except that then a general bleaching begins to become noticeable.

After 1 hour of exposure to high-intensity radiation of wavelengths between 260 and 360 mμ the color center band of an x-rayed $NaNO_3$ crystal is practically completely bleached out; only a slight shoulder remains visible on the long-wavelength tail of the $NaNO_3$ band which seems to exhibit some structure (curve *d* of Fig. 3). The bleaching efficiency of the light is as high at −190° as at +25°. No photoconductivity accompanies the bleaching process. Thus in the back reaction the electron moves through a very short distance. The same result as by ultraviolet irradiation is obtained if a $NaNO_3$ crystal after x-ray irradiation is heated for 30 minutes to 200°C.

If a $NaNO_3$ crystal is exposed to x-rays at room temperature, the growth of the color center band is

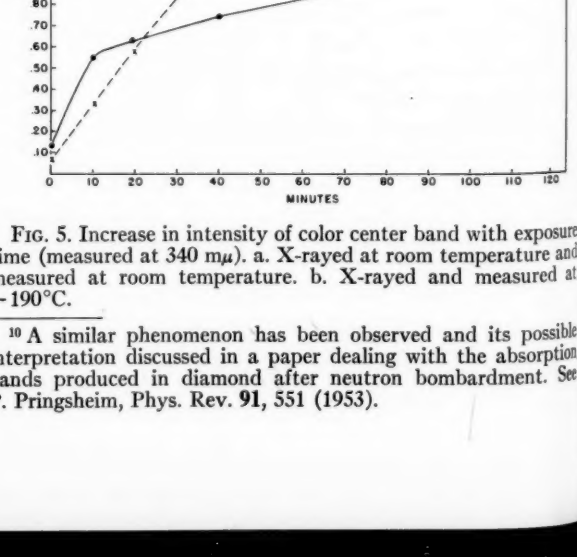

FIG. 5. Increase in intensity of color center band with exposure time (measured at 340 mμ). a. X-rayed at room temperature and measured at room temperature. b. X-rayed and measured at −190°C.

[10] A similar phenomenon has been observed and its possible interpretation discussed in a paper dealing with the absorption bands produced in diamond after neutron bombardment. See P. Pringsheim, Phys. Rev. **91**, 551 (1953).

very steep during the first few minutes and then levels off to a much lower rate of increase; this is not caused by the inhomogeneity of the x-rays and the resulting difference in depth of their penetration, since a crystal exposed to the Mev γ rays of a Co^{60} source shows in the main the same behavior. Although at $-190°$ the initial rise of the color center band is slower, the subsequent decrease in its rate is much smaller so that after longer periods of exposure crystals irradiated at $-190°$ are much more deeply colored than those irradiated at room temperature, even after the loss in absorption produced by warming the crystal to room temperature (Fig. 5). If a crystal with a strong color band produced by x-rays at $-190°$ is exposed to x-rays at room temperature, the band decreases until it has reached an equilibrium density, and then it remains nearly constant (Fig. 2).[11] Apparently x-rays at room temperature do not only create color centers but destroy them as well, when some additional energy is supplied by thermal agitation. Since no new absorption bands appear under these conditions and the contribution to the NO_2^- band remains very low, it is plausible to assume that the mechanism by which the color centers are destroyed is a back reaction with electrons ejected from the centers and returning to their normal location, or positive holes recombining with the centers, rather than the formation of some new unknown product with no visible absorption band.

While the radiation from an Hg arc of wavelengths greater than 260 mμ destroys the color centers, these are built up by radiation of wavelengths below 240 mμ. The production of color centers in $NaNO_3$ by the short-wavelength ultraviolet from a Mineralight without filter is a slow process, and not many observations were made beyond the appearance of the same absorption band which is obtained by x-ray irradiation. It could be shown, however, that when a $NaNO_3$ crystal, after strong coloration by x-rays at $-190°$, was exposed at room temperature to short wavelength ultraviolet, the intensity of the color center band did not drop to a lower level as in the case of x-ray exposure at room temperature. Thus, the ultraviolet light does not provide the energy necessary for the back reaction. Mineralight radiation passed through the filter with short wave cutoff at 240 mμ was ineffective in the production of color centers.

Curve *e* of Fig. 3 was obtained with a crystal which had been exposed for 800 hours to the Co^{60} γ rays at a distance of 3 cm from the source. The areas under this curve and under curve *c* are nearly the same. However, their shape differs appreciably in the region between 360 and 340 mμ, and this difference is greatly emphasized when the crystals are bleached by heat or ultraviolet, as shown by comparing curves *d* and *f* (Fig. 3);

[11] This behavior is very similar to that observed by Harten in the formation of *F* centers in KCl under x-ray irradiation at various temperatures. See H. U. Harten, Z. Physik **126**, 619 (1949).

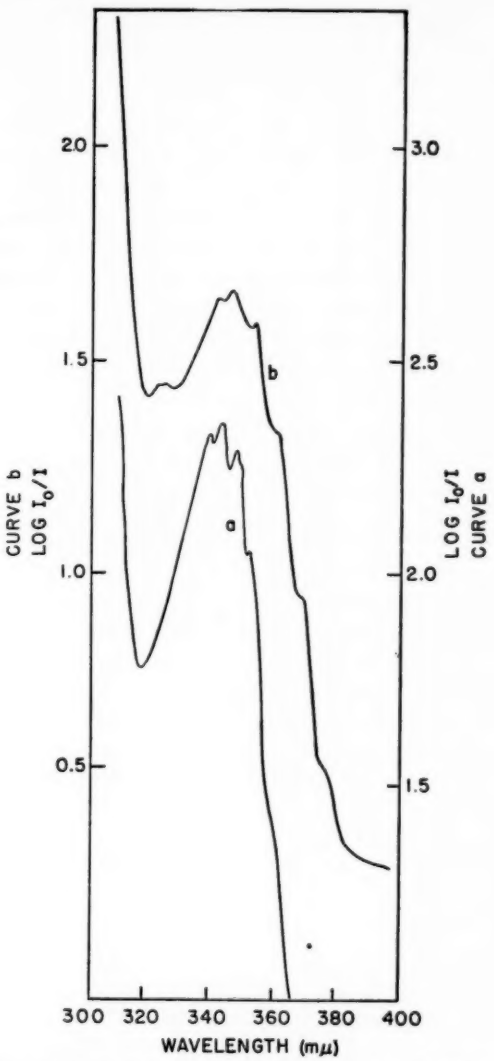

FIG. 6. Absorption of $NaNO_3$ from 300 to 400 mμ after 72 hr in the pile, measured at $-190°$C. a. No further treatment (ordinate scale on the right of figure). b. 4 hr bleached with full radiation from Hg AH6 arc (scale on left of figure).

curve *f* is almost identical with curve *b*, which is characteristic of the NO_2^- ion added as impurity to $NaNO_3$.

The crystal from which curve *a* of Fig. 6 was obtained (with the ordinate scale marked on the right side of the diagram) had undergone an exposure of 72 hours in the Argonne CP-3′ pile. By 4 hours' bleaching with the full radiation from the Hg AH6 arc curve *a* was reduced to *b* (ordinate scale on the left side). For comparison Fig. 7 shows as curve *a* again the absorption band of $NaNO_3$ with 0.5 percent of NO_2^- and under *b* the absorption of the same crystal after 1-hour x-ray irradiation at $-190°$. Curve *c* represents the difference between *b* and *a*, caused by the formation of color centers by the x-rays, and thus is analogous to curves *c* and *d* of Fig. 4. The similarity between curves *b* in Figs. 6 and 7 is striking and proves that after pile irradiation the crystal contains NO_2^- ions as well as

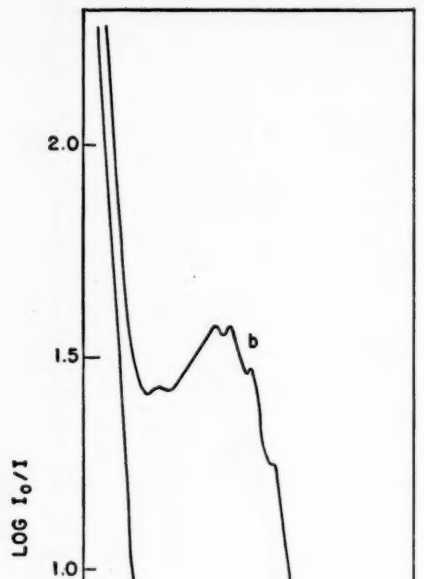

FIG. 7. Absorption of $NaNO_3$ from 300 to 400 mμ under various conditions, measured at −190°C. *a*. Untreated crystal with $NaNO_2$ added to the melt. *b*. Same 1 hr x-rayed at −190°C. *c*. Difference between curves *b* and *a*.

color centers. The crystals represented by curves *b* of the two figures differ, however, in that the crystal from the pile responds very poorly to continued exposure to bleaching light, while the other crystal can easily be bleached down again to the state of curve *a* (Fig. 7). This corresponds to a rule frequently observed in crystals containing color centers: the greater the initial density of the latter, the more difficult it is to bleach them beyond a certain limit. It seems that when a certain number of color centers has been destroyed, all *V* centers of low stability have been used up.

ANISOTROPY OF THE COLOR CENTERS

As mentioned in the introduction the well-known anisotropic character of $NaNO_3$ crystals became noticeable for the first time in this investigation by the appearance in the absorption spectrum of a structure consisting of equally spaced intensity fluctuations. This structure could not be observed in the band with peak at 392 mμ because there the absorption is too strong and its rise is too steep; and it does not show up in the region of greater wavelengths, because there the absorption is too low. However, the fringes are well developed in the "gap" at 253 mμ (Fig. 1). The fact that the fringes were quite as sharp at room temperature as at −190°C was primary evidence that they could not be interpreted as due to a vibrational band structure. This was definitively proved by the observation that the intensity of the fringes depended on the orientation of the crystal and that in a certain position of the crystal they disappeared completely.

On the other hand, when the absorption in the region between 320 and 400 mμ increased owing to the formation of color centers, the interference fringes appeared there also. This shows that the color centers must be oriented in the crystal lattice, and since they vanish at the same orientation of the crystal, at which the fringes in the "gap" disappear and since the latter correspond to normal absorbing centers of the untreated crystal it follows that the preferential orientation of both types of centers is the same.

The direct measurement of the transmission for monochromatic polarized light beams does not provide data for a quantitative determination of absorption coefficients, because refractive indices of $NaNO_3$ are not available in the spectral range below 434 mμ, and thus the losses due to reflection cannot be evaluated. Even at 434 mμ the loss by reflection on two surfaces at vertical incidence is 11.7 percent for the ordinary and 4.7 percent for the extraordinary ray. At 340 mμ, near the center of the color center band, these losses are probably a good deal larger. The absorption measurements showed that in the wavelength range of the color center band, for instance at 340 mμ, the transmission is highest when the electric vector of the incident beam and the optical axis of the crystal lie in the same plane.

If as a very rough approximation at high optical densities the reflection losses are completely neglected and relative absorption coeficients are calculated at 340 mμ for the two crystal orientations of minimum and maximum transmission, the ratio of the values

TABLE II. NO_2^- concentration in various samples. (From colorimetric analysis.)

No.	Figure	Treatment	g NO_2^-/g	Mole % NO_2^-
1	3*a*	Untreated single crystal	$0.04 \cdot 10^{-3}$	0.0075
2	...	Baker analyzed reagent	$3 \cdot 10^{-6}$	0.0005
3	3c	x-rayed 1 hr at −190°C	$0.83 \cdot 10^{-3}$	0.15
4	3d	x-rayed 1 hr at −190°C; bleached	$0.76 \cdot 10^{-3}$	0.14
5	...	x-rayed 12 hr at 25°C	$0.82 \cdot 10^{-3}$	0.15
6	3f	800 hr γ rays at 25°C	$1.52 \cdot 10^{-3}$	0.28
7	6b	72 hr in pile, bleached	$5.4 \cdot 10^{-3}$	1.0
8	3b	$NaNO_2$ added to melt	$2.75 \cdot 10^{-3}$	0.51

thus obtained is nearly constant for increasing x-ray exposure times and increasing color center density. The ratio remains the same also when subsequently the crystal is again bleached by polarized light, with the crystal oriented for maximum absorption. This last result seems to prove that the optical anisotropy is caused by a corresponding anisotropy of the individual centers and not by a difference in the number of linear oscillators oriented in two directions, for instance parallel and vertical to the optical axis.

CHEMICAL ANALYSIS

The NO_2^- concentration in some of the samples investigated in these experiments was analyzed by the colorimetric method which has been used also by Hennig and co-workers.[8] The symbols in the second column of Table II (under "Figure") refer to the curves in Figs. 3 and 6. The concentrations are listed in weight percent and in mole percent. The low but measurable content of NO_2^- in the untreated "blank crystal" may have been present in the material from which the crystal was grown, but it may be as well that in the melt some $NaNO_3$ was converted into $NaNO_2$. For comparison sample 2 is listed consisting of microcrystalline Baker "analyzed reagent" $NaNO_3$ and with a much lower NO_2^- concentration. Sample 7, a crystal exposed three days in the pile, has the highest NO_2^- content; it is of the same order of magnitude as obtained by Hennig and co-workers under similar conditions.

A comparison between curves *6b* and *7b* and between *3b* and *3f* suggests that the NO_2^- concentration in crystal No. 8 with $NaNO_2$ added to the melt and the concentrations in crystals No. 7 exposed in the pile and No. 6 exposed to γ rays should be nearly the same, while according to the colorimetric analysis the concentration in No. 7 is nearly twice as high as in No. 8 and the concentration in No. 6 only a little over half as high as in No. 8. No explanation can be given of these discrepancies. The NO_2^- concentrations in the x-rayed crystals, No. 3 to 5, are appreciably lower than in the preceding samples, but still higher, according to Table II, than should be expected from curves *c* and *d* in Fig. 3. On the other hand, as shown in this figure, the ratio of color centers to NO_2^- centers is relatively very large in the crystal x-rayed at $-190°C$; it is much lower in samples exposed to x-rays at room temperature. Even after 12 hours of x-rays at room temperature the color center band is much weaker than in the crystal x-rayed for 1 hour at $-190°$. But following Table II, the NO_2^- content of sample No. 5 is the same as that of sample No. 3, and that of sample No. 4, in which the color centers were completely bleached out, is only very little smaller. The destruction of NO_2^- ions by x-rays at room temperature either does not occur at all or at least only at a much lower rate than that of the color centers. If a crystal with $NaNO_2$ added to the melt (such as in Fig. 3b) is x-rayed at room temperature, appreciably fewer color centers are formed than at $-190°C$, but no decrease of the NO_2^- band is observed.

The fact that in the samples exposed in the pile or to Co^{60} γ rays, where collisions with high-energy particles might play a part, the ratio of NO_2^- to color center concentration is so much larger than in the samples x-rayed at $-190°C$, does not necessarily contradict the interpretation proposed by Hennig and co-workers, according to which, not knock-on processes but electronic excitation and ionization contribute most to the formation of NO_2^-. The relative low color center concentration can be due entirely to the relatively high temperature under which the processes in the pile and the γ-ray source occur and which favor the secondary destruction of color centers after their formation while the NO_2^- concentration continues to increase.

The color centers in $NaNO_3$ behave in many respects like the *F* centers in alkali halides. It seems natural also to ascribe them to electrons trapped somehow in lattice defects. The near coincidence of their band peak with that of the NO_2^- band suggests that they are connected with the presence of nitrite ions.[12] They may be, for instance, NO_2^- ions strongly perturbed by the capture of an electron in their neighborhood. It must be kept in mind that the 292-mμ band of NO_3^- is a very weak band, when its oscillator strength is taken as a measure. It is about 1000 times weaker than the short-wavelength band of the ion, and thus its oscillator strength is probably below 10^{-3}. On the other hand, the concentration of NO_2^- ions (of the order of magnitude of 10^{-3} to 10^{-2}) is exceedingly high when compared with the usual concentration of color centers. If a very small fraction of these were converted into color centers with 1000 times greater oscillator strength, the NO_2^- band would hardly lose in intensity, while a fairly strong color center band could be produced.

I want to thank Mr. E. Hutchinson for his help in preparing most of the crystal samples used in this investigation. My thanks are also due to Mrs. M. Rauh for the colorimetric analysis she made of numerous samples.

[12] Arguments in favor of this hypothesis will be discussed in a succeeding paper.

Infrared Spectrum of Solid *n*-Octane-1,1,1,8,8,8-d_6

GEORGE C. PIMENTEL AND WILLIAM A. KLEMPERER
Department of Chemistry and Chemical Engineering, University of California, Berkeley, California
(Received July 27, 1954)

The infrared spectrum of *n*-octane-1,1,1,8,8,8-d_6 has been obtained at liquid nitrogen temperature from 1500 cm^{-1} to 600 cm^{-1}. An assignment of the vibrations into methyl and methylene motions is made.

INTRODUCTION

IN the study of long normal paraffins, interpretation of the spectra has been based upon the assumption that the motions may be regarded as vibrations of the terminal methyl groups and vibrations of a chain of methylene groups.[1–3] In order to determine the degree of interaction between methyl and methylene motions and to identify the motions in a fairly long chain normal hydrocarbon the spectrum of *n*-octane-1,1,1,8,8,8-d_6 (hereafter referred to as terminal deuterooctane) was determined. Only the solid spectrum was determined because of the great spectral simplification in the solid state.[3,4] This simplification is attributed to the existence of only one rotational isomer in the solid state, presumably the planar trans configuration.

EXPERIMENTAL

The *n*-octane-1,1,1,8,8,8-d_6 was prepared by a two step reduction of suberic acid with lithium aluminum deuteride. This synthesis is discussed in detail in reference 5.

Mass spectrographic analysis indicated 90.8 percent octane-d_6, 7.7 percent d_5, and 0.5 ± 0.2 percent d_4. In view of the definitive work by Stevenson and Wagner[6] indicating the occurrence of deuterium migration before fragmentation in mass spectrographic determination, no analysis for location of the deuteriums on the carbon chain was attempted. The method of synthesis, however, should place deuteriums only on the terminal carbons.

The spectra were obtained using a Perkin-Elmer model 21 double beam spectrophotometer equipped with NaCl optics. The liquid sample was placed in a silver chloride cell[7,8] of thickness 0.30 mm. The sample was rapidly frozen and kept solid throughout the run with liquid nitrogen. Both *n*-octane and *n*-octane-1,1,1,8,8,8-d_6 were examined.

RESULTS AND DISCUSSION

The spectra are shown in Fig. 1. Because of light scattering, it was difficult to determine percent transmission; hence, the ordinate in Fig. 1 is qualitative only. The locations of absorption maxima are listed in Table I, together with those reported earlier for *n*-octane by Brown, Sheppard, and Simpson.[2]

Francis[9] has conducted systematic infrared intensity studies of two normal and ten branched paraffins. He has shown conclusively that the absorption in the 1460 cm^{-1} spectral region is caused by both methyl and methylene vibrations. In the spectrum of terminal deuterooctane, the intensity of the band at 1046 cm^{-1} establishes the correlation of this band with part of the 1460 cm^{-1} absorption of *n*-octane. That part of the 1460 cm^{-1} absorption caused by methylene motions remains unchanged in frequency, and that caused by methyl motions occurs at 1046 cm^{-1}. The 1460–1046 cm^{-1} shift is supported by similar work in terminal deuteropropane[10] where the 1460 cm^{-1} methyl motions move to 1070 cm^{-1} upon deuteration.

The characteristic motions absorbing in this region are the HCH bending motions of the methyl and methylene groups. For the methyl groups there are two infrared active bending vibrations, one (A_u), the other (B_u). For *n*-octane there are three methylene bending vibrations, all of symmetry (B_u). The fact that the motions of the same symmetry fall at the same spectral location indicates negligible interaction since interaction of vibrations of the same symmetry is accompanied by splitting. Furthermore, interaction of methyl and methylene motions would be characterized by intermediate isotopic shifts on methyl deuteration. The isotopic shifts of 1.39 and 1.00 indicate that these motions do not involve methyl-methylene interaction.

There has been controversy about the nature of the 1370 cm^{-1} band in hydrocarbons. There certainly is a methyl motion in this location which is assigned to the 1025 cm^{-1} band in terminal deuterooctane. This is the symmetric CH_3 bending motion (B_u). Calculations of Mizushima and Simanouti,[3] and Person and Pimentel[1]

[1] W. B. Person and G. C. Pimentel, J. Am. Chem. Soc. **75**, 532 (1953).
[2] (a) Brown, Sheppard, and Simpson, Discussions Faraday Soc. 261 (1950); (b) N. Sheppard and D. M. Simpson, Quart. Revs. **7**, 19 (1953). Reference to earlier work is well covered therein.
[3] S. Mizushima and T. Simanouti, J. Am. Chem. Soc. **71**, 1320 (1949).
[4] Rank, Sheppard, and Szasz, J. Chem. Phys. **17**, 83 (1949).
[5] A. Streitwieser, Jr., J. Am. Chem. Soc. (to be published).
[6] D. P. Stevenson and C. D. Wagner, J. Chem. Phys. **19**, 11 (1951).
[7] R. D. Mair and D. F. Hornig, J. Chem. Phys. **17**, 1236 (1949).
[8] D. W. E. Axford and D. H. Rank, J. Chem. Phys. **18**, 51 (1950).
[9] S. A. Francis, J. Chem. Phys. **18**, 861 (1950).
[10] H. L. McMurry and V. Thornton, J. Chem. Phys. **19**, 1014 (1951).

indicate that a methylene motion also occurs at this location. Francis,[9] however, attributed the intensity of this band entirely to methyl motion. There is much evidence that this band is caused by both methyl and methylene motions.

1. Upon deuteration of the terminal methyl groups in *n*-octane, a band is found at 1362 cm^{-1}. The possibility of a vibration in the 1460 cm^{-1} region moving to 1362 cm^{-1} seems unlikely. Such an isotopic shift (1.07) would indicate interaction of methylene and methyl motions, which, as mentioned before, is in contradiction to the implication of absence of interaction associated with the accidental degeneracy of these motions in ordinary hydrocarbons. Furthermore, it does not seem reasonable to attribute the 1362 cm^{-1} band to an impurity. The principal impurity is *n*-octane-1,1,1,8,8-d_5, and in this compound, the highest bending frequency of the terminal groups is expected below 1300 cm^{-1} (the highest frequency absorption of CHD_3 below 2000 cm^{-1} is 1299 cm^{-1}).[11] In Fig. 1(b), the pair of bands at 1277 and 1256 cm^{-1} are ascribed to this impurity. The expected amount of *n*-octane-1,1,1,8-d_4 is insufficient to account for the observed intensity of the 1362 cm^{-1} band.

2. In polythene[12] a band is found at 1375 cm^{-1}.

TABLE I. Infrared absorption bands of *n*-octane and *n*-octane-1,1,1,8,8,8-d_6.[a]

$CH_3(CH_2)_6CH_3$ Frequency cm^{-1}		$CD_3(CH_2)_6CD_3$ Frequency cm^{-1}
Brown, Sheppard, and Simpson	This research	This research
722 (s)	710 (10)	654 (10)
748 (s)	744 (7)	690 (4)
...	816 (2)	717 (8)
864 (s)	867 (6)	742 (5)
881 (s)	883 (7)	806 (7)
...	965 (1)	836 (1)
1008 (m)	1008 (3)	860 (1)
1020 (m)	1016 (5)	924 (7)
...	1040 ($\frac{1}{2}$)	967 (2)
1058 (w)	1057 ($\frac{1}{2}$)	998 (sh)
1088 (s)	1083 (7)	1025 (4)
...	1170 ($\frac{1}{2}$)	1046 (8)
1205 (w)	1205 (2)	1067 (2)
1218 (m)	1219 (3)	1113 (4)
1286 (w)	1284 (2)	1160 (3)
1303 (w)	1303 (3)	1207 ($\frac{1}{2}$)
1378 (m)	1368 (6)	1256 ($\frac{1}{2}$)
ca 1465 (s)	1460 (8)	1277 (sh)
		1287 (3)
		1304 (3)
		1362 (1)
		1467 (5)

[a] The relative intensities are given in parentheses. (sh) =shoulder.

[11] G. Herzberg, *Infrared and Raman Spectra of Polyatomic Moleclues* (D. Van Nostrand Company, Inc., New York, 1945), p. 309.

[12] Elliott, Ambrose, and Temple, J. Chem. Phys. **16**, 877 (1948); W. M. D. Bryant and R. C. Voter, J. Am. Chem. Soc. **75**, 6113 (1953).

3. In cyclopentane, cyclohexane, and decahydronaphthalene, bands occur at 1370 cm^{-1}, 1353 cm^{-1} and 1346 cm^{-1} (trans) and 1342 cm^{-1} (cis), respectively.[13]

4. In their study of 3-pentanone, Nolin, and Jones[14] found bands at 1414 cm^{-1} and 1355 cm^{-1} which remained at these frequencies in the terminal deutero compound (3-pentanone-1,1,1,5,5,5-d_6). These bands were not present in 3-pentanone-2,2,4,4-d_4. The 1355 cm^{-1} band is also assigned to methylene motions in 3-pentanone by Francis.[15] The 1414 cm^{-1} methylene motion corresponds to absorption at 1460 cm^{-1} in a normal hydrocarbon, moved in frequency presumably because of the proximity of the carbonyl group. Similarly, the 1355 cm^{-1} band might originate in the 1362 cm^{-1} region of normal hydrocarbons.

These arguments substantiate the hypothesis of a 1370 cm^{-1} methylene motion in normal hydrocarbons. The appearance of this band in polythene indicates that the motion should be assigned to a methylene wagging motion (B_u) rather than a twisting motion (A_u), since the twisting modes become inactive in the infinite chain.

The spectrum of terminal deuterooctane confirms the assignment of the 1303 cm^{-1} and 1284 cm^{-1} bands in *n*-octane to methylene motions.[2] (The low frequency side of the 1287 cm^{-1} band in terminal deuterooctane is altered in shape by the impurity *n*-octane-d_5.) The absence of deuteration shift indicates that these are pure methylene motions. This is supported by McMurry and Thornton's work on propane,[10] in which it was observed that bands are found in the spectra of both propane and propane-1,1,1,3,3,3-d_6 at 1336 cm^{-1}, but no absorption is found in this region in propane-2,2-d_2 or in propane-d_8. The pair of bands at 1219 cm^{-1} and 1205 cm^{-1} [Fig. 1(a)] are likewise assigned by

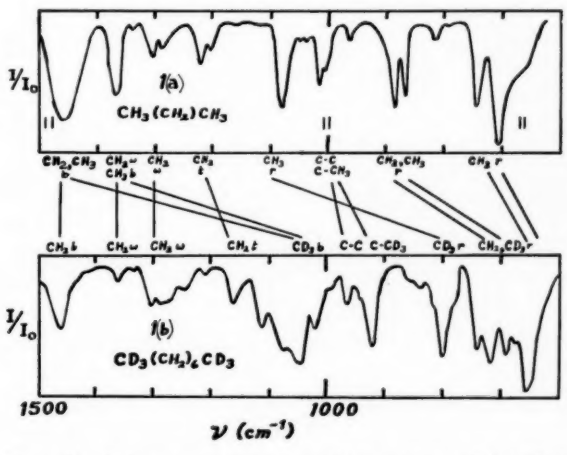

FIG. 1(a). Infrared spectrum of solid *n*-octane. 1(b). Infrared spectrum of solid *n*-octane-1,1,1,8,8,8-d_6. *b*, bend; *w*, wag; *t*, twist; *r*, rock.

[13] American Petroleum Institute Research Project 44, "Catalog of Infrared Spectrograms."

[14] B. Nolin and R. N. Jones, J. Am. Chem. Soc. **75**, 5626 (1953).

[15] S. A. Francis, J. Chem. Phys. **19**, 942 (1951).

TABLE II. Correlation of the absorption frequencies of *n*-octane and *n*-octane-1,1,1,8,8,8-d_6.

Frequency cm^{-1} CH_3-$(CH_2)_6CH_3$	Frequency cm^{-1} CD_3-$(CH_2)_6CD_3$	Frequency ratio	Probable[a] assignment	Symmetry
	1467	1.00	CH_2 HCH bend	B_u
1460	1046	1.39	CH_3 HCH bend	B_u,A_u
1368	1362	1.00	CH_2 wag	B_u
	1025	1.33	CH_3 HCH bend	B_u
1303	1304	1.00	CH_2 wag	B_u
1284	1287	1.00	CH_2 wag	B_u
1219	1160	1.05	CH_2 twist	A_u
1205	1113	1.08	CH_2 twist	A_u
1083	806	1.34	CH_3 rock	B_u
1016	924	1.10	C−C terminal stretch	B_u
1008	998	1.01	−C−C skeletal	B_u
965	967	1.00	skeletal	B_u
883	742	1.19	CH_2 and CH_3 rock	A_u
867	717	1.21		
816	*ca.*806	1.01	skeletal	B_u
744	690	1.08	CH_2 rock	A_u
710	654	1.08	CH_2 rock	A_u

[a] For the definition of wag, twist, etc., see Sheppard and Simpson, reference 2(b).

Brown, Sheppard, and Simpson[2] as methylene motions. This is consistent with the shift of frequency upon deuteration to 1160 cm^{-1} and 1113 cm^{-1}. It is interesting to note that the deuteration shift is greater than unity, indicating some methyl motion in these vibrations. Calculations[1] indicate that these bands are methylene twisting motions (A_u). Since this vibration is forbidden in the infinite chain, the intensity of the bands also suggests the participation of methyl motion since the other methylene motions of the same symmetry occur at much lower frequencies.

The strong band at 1083 cm^{-1} [Fig. 1(a)] is assigned as the in-plane methyl rocking motion (B_u). This band shifts to the strong band at 806 cm^{-1} upon deuteration. This assignment is supported by the work on methyl chloroform[16] where the band at 1087 cm^{-1} is assigned as a doubly degenerate motion.

By analogy to the 1012 cm^{-1} band of methyl chloroform the band at 1016 cm^{-1} [Fig. 1(a)] is assigned as the terminal carbon-carbon stretching motion which absorbs at 924 cm^{-1} in terminal deuterooctane. This correlation is in agreement with the expected isotope effect $(18/15)^{\frac{1}{2}}=1.10$.

Three infrared-active skeletal vibrations are expected to occur in the region 1200 to 800 cm^{-1}. A rough calculation by Brown, Sheppard, and Simpson[2] places these at 1100 cm^{-1}, 1000 cm^{-1}, and 870 cm^{-1}. These vibrations are expected to have low intensity in the infrared and no shift in frequency upon terminal deuteration. Accordingly, the relatively weak absorptions of *n*-octane at 965 cm^{-1} and 816 cm^{-1} are assigned as skeletal motions.

The pair of bands at 883 cm^{-1} and 867 cm^{-1} [Fig. 1(a)] are correlated with the pair at 742 cm^{-1} and 717 cm^{-1} [Fig. 1(b)]. The isotope ratio has the intermediate value 1.20 and indicates the assignment of these bands as mixed methyl and methylene vibrations.

The two remaining methylene rocking motions (A_u) occur at 744 cm^{-1} and 710 cm^{-1} in *n*-octane and shift to 690 cm^{-1} and 654 cm^{-1}. The intensities of the 710 cm^{-1} band in *n*-octane and the 654 cm^{-1} band in terminal deuterooctane make this correlation fairly definite.

The only impurity in the *n*-octane-1,1,1,8,8,8-d_6 present in high enough concentration to contribute to the spectrum is expected to be *n*-octane-1,1,1,8,8-d_5. The bands at 1277 cm^{-1} and 1256 cm^{-1} are attributed to the HCD bending motions and bands at 860 and 836 cm^{-1} could be caused by the in-plane CD_2H rocking mode.

The correlations discussed are summarized in Table II.

CONCLUSIONS

1. Evidence is given that the 1370 cm^{-1} band of hydrocarbons arises from methyl and methylene motions.

2. An assignment is made in which it is possible to interpret the spectrum on *n*-octane in terms of non-interacting methyl, methylene and skeletal vibrations to a large extent. The pair of bands at 883 cm^{-1} and 867 cm^{-1}, however, appear to arise from mixed methyl and methylene vibrations.

3. The assignment is consistent with the work of Person and Pimentel[1] and, in most details, with the much more detailed assignment of Brown, Sheppard, and Simpson.[2]

ACKNOWLEDGMENT

We wish to thank Dr. A. Streitwieser, Jr., for supplying the sample of terminal deuterooctane, and Dr. J. C. Guffy for determining its mass spectrum. It is a pleasure to acknowledge helpful discussions with Dr. T. Simanouti and Dr. K. S. Pitzer. This work was assisted by the American Petroleum Institute through Research Project 50.

[16] El-Sabban, Meister, and Cleveland, J. Chem. Phys. **19**, 855 (1951).

Paramagnetic Resonance Absorption in Some Cr^{+3} Complexes

L. S. SINGER
United States Naval Research Laboratory, Washington 25, D. C.
(Received August 5, 1954)

The paramagnetic resonance absorptions in several trichelate complexes of Cr^{+3} have been investigated at room temperature and at 1.2- and 3.0-cm wavelengths. From single crystal measurements on chromic acetylacetonate the orientations of the electric axes were determined and the parameters in the spin-Hamiltonian found to be $g=1.983\pm0.002$, $|D|=0.592\pm0.002$ cm^{-1}, and $|E|=0.052\pm0.002$ cm^{-1}. The asymmetric single absorption peak with $g=4$ found in several of the powders and in their liquid solutions is explained on the basis of the relatively large value of D associated with the individual trichelate molecules. The apparent inadequacy of the "ionic" model for several chromic compounds is also discussed.

I. INTRODUCTION

THE magnetic properties of most salts of the iron group elements are at present fairly well understood. Both susceptibility measurements and more recent magnetic resonance measurements[1] have shown that the crystalline field theory of Schlapp and Penney[2] and others provides a quite satisfactory explanation of the observations. However, the properties of several so-called covalent complexes cannot be explained on the basis of this rather simple ionic model. For example, an Fe^{+3} ion ($3d^5$) in an alum exhibits properties similar to a spin of 5/2, whereas in the presumably covalent hexacyanide complex, it appears more like a spin of 1/2. The first semiquantitative explanation of this type of behavior was given by Pauling,[3] using approximate atomic orbital arguments, and resulted in his well-known magnetic criterion for bond type. More detailed descriptions of the covalent case were later given by Van Vleck[4] and Howard[5] for the ferricyanide complex and by Kotani[6] for covalent complexes containing other ions of the iron group. Recently, Griffiths, Owen, and Ward[7] in a comprehensive survey of the magnetic resonance properties of the $4d$ and $5d$ transition ions, have established beyond doubt the essential correctness of these theories for covalent complexes. Some significant discrepancies which were found for the 5-electron case were explained by the very interesting work of Stevens.[8]

This paper presents the results of some magnetic resonance measurements on a series of $Cr^{+3}(3d^3)$ complexes, in particular the so-called trichelates.[9] In Sec. V, the observations are interpreted in terms of the more or less phenomenological theory of Abragam and Pryce.[10] The parameters occurring in the spin-Hamiltonian are evaluated experimentally and a detailed comparison between this theory and experiment is given. The discussion in Sec. VI attempts to deduce from these parameters and the theories mentioned above information concerning the configuration of the complex and the nature of bonding in the complex.

II. THE THREE ELECTRON CASE

According to the usual ionic model for hexacoordinated Cr^{+3} compounds, the ion in a crystal experiences a large cubic electric field caused by its surrounding octahedron of water dipoles or other ions. However, this interaction is assumed less than the mutual electrostatic repulsions of the 3 d-electrons so that the lowest Russel-Saunders term ^4F is the only energy state of the ion which needs to be considered. The cubic field splits the F state into 2 triplets and a singlet, which lies lowest. The singlet will have only 4-fold spin degeneracy which cannot be removed by either an electric field of lower symmetry or the spin-orbit coupling alone[11]; however, a small splitting of $\sim$0.1 cm^{-1} can result from a combination of the two.

The substances which can be characterized by this model should then have essentially "spin-only" susceptibilities and should possibly exhibit fine structure in their microwave magnetic resonance spectra. This has been observed to be the case in almost all chromic compounds, even though chemical evidence suggests that many of the complexes measured have considerable covalent character.

The great similarity in magnetic behavior between ionic and covalent complexes of $Cr^{+3}(3d^3)$ ion is in fact predicted by the theories mentioned above.[3,6,8] Van Vleck[4] has shown that no matter which of three methods of approximation is used, *viz.*, the strong crystalline field approach, the atomic orbital approach, or the molecular orbital approach, only the electrons in the d-orbital triplet d_{xy}, d_{xz}, d_{yz}, contribute to the magnetic properties of the covalent or penetrating octahedral complexes. Stevens,[8] without assuming any explicit

[1] B. Bleaney and K. W. H. Stevens, Repts. Progr. Phys. **16**, 108 (1953).
[2] R. Schlapp and W. G. Penney, Phys. Rev. **42**, 666 (1932).
[3] L. Pauling, J. Am. Chem. Soc. **53**, 1367 (1931).
[4] J. H. Van Vleck, J. Chem. Phys. **3**, 807 (1935).
[5] J. B. Howard, J. Chem. Phys. **3**, 813 (1935).
[6] M. Kotani, J. Phys. Soc. Japan **4**, 293 (1949).
[7] Griffiths, Owen, and Ward, Proc. Roy. Soc. (London) **219A**, 526 (1953).
[8] K. W. H. Stevens, Proc. Roy. Soc. (London) **A219**, 542 (1953).
[9] A. E. Martell and M. Calvin, *Chemistry of the Metal Chelate Compounds* (Prentice-Hall, Inc., New York, 1952).
[10] A. Abragam and M. H. L. Pryce, Proc. Roy. Soc. (London) **A205**, 135 (1951).
[11] H. A. Bethe, Ann Phys. **3**, 133 (1929).

form for the wave functions of the states in the triplet, shows that the electrostatic interaction $\Sigma_{i>j}e^2/r_{ij}$ leads to "terms" which obey rules analogous to Hund's rules for the free ion. From these considerations in the case of 3 *d*-electrons, the ground state turns out to be a spin quartet just as was obtained using the simple ionic model. It is thus evident that, to a first approximation, there should be no difference in magnetic properties between the two kinds of complexes. However, the small higher-order differences which may become apparent from accurate magnetic measurements, e.g., the deviations of the *g* factor from the free spin value, might be useful in differentiating between the two kinds of complexes. This is discussed in Sec. VI.

III. EXPERIMENTAL APPARATUS AND PROCEDURE

A. Preparation of Samples

1. The following compounds were prepared by methods given in *Inorganic Syntheses*:[12]

$K_3Cr(C_2O_4)_3 \cdot 3H_2O$, potassium trioxalatochromiate;
$[Cr(NH_2CH_2CH_2NH_2)_3]_2(SO_4)_3$, tris (ethylenediamine) chromic sulfate;
$Al(CH_3COCHCOCH_3)_3$, aluminum acetylacetonate;
$Cr(CH_3COCHCOCH_3)_3$, chromic acetylacetonate

2. The following two compounds were prepared by the method of the British Dyestuffs Corporation Ltd. and S. Coffee:[13]

$Cr(C_6H_5COCHCOCH_3)_3$, chromic benzoylacetonate;
$Cr[(CH_3)_2CHCH_2COCHCOCH_3]_3$, chromic isovalerylacetonate.

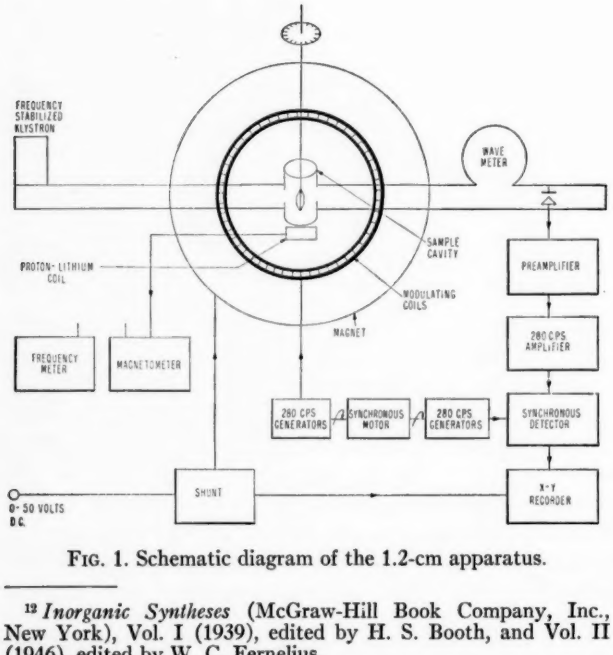

FIG. 1. Schematic diagram of the 1.2-cm apparatus.

[12] *Inorganic Syntheses* (McGraw-Hill Book Company, Inc., New York), Vol. I (1939), edited by H. S. Booth, and Vol. II (1946), edited by W. C. Fernelius.

[13] British Patent No. 289,493, British Dyestuffs Corporation Ltd. and S. Coffey.

All compounds except the last, which was a rather viscous oil, were obtained as powders.

Single crystals of both the pure chromic acetylacetonate and solid solutions containing the isomorphous aluminum compound were grown by evaporation from benzene solution at room temperature. The approximate Cr:Al ratio in the mixed crystals was obtained colorimetrically by comparison with solutions of the pure chromic acetylacetonate. The mixed crystals used

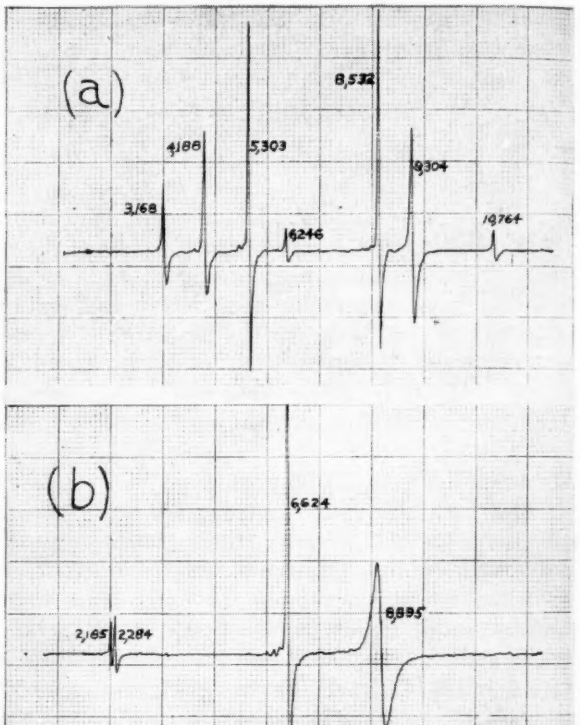

FIG. 2. Recorder charts for the resonance of a dilute single crystal of chromic acetylacetonate at two different orientations: (a) for $\eta=152°$ and (b) for $\eta=176°$. The field strengths in gauss for the points of zero slope are indicated. The microwave frequency was 23 890 mc/sec.

in the majority of the measurements had a Cr:Al ratio of 1:50.

B. Microwave Apparatus

The preliminary powder measurements were made at 3-cm wavelength using a TE_{102} rectangular resonant cavity.[14] The *723/AB* klystron was square-wave modulated at an audio-frequency and the resultant signal from a crystal diode amplified in a tuned amplifier. Measurements of amplifier output as a function of magnetic field were then made.

[14] The 3-cm measurements were carried out at the chemistry department of Cornell University. This work was supported by a du Pont Postdoctoral Fellowship in Chemistry, 1950–1951.

The remainder of the measurements were made at 1.2-cm wavelength. A block diagram of the 1.2-cm apparatus is shown in Fig. 1. A 2*K*33 klystron equipped with a Pound I. F.-type[15] frequency stabilization system held the microwave frequency constant within a few parts in 10^7. The sample cavity was cylindrical, operating in the TE_{011} mode, and was equipped with a plunger and calibrated dial for measuring angles of rotation about the cavity axis. Single crystals were mounted by means of a dab of stopcock grease on the end of a carefully machined polystyrene rod protruding from the plunger. The orienting was done under a microscope equipped with a goniometer. It is estimated that the over-all error in determining the orientation of a crystal with respect to both the static and rf magnetic field directions was $\pm 2°$.

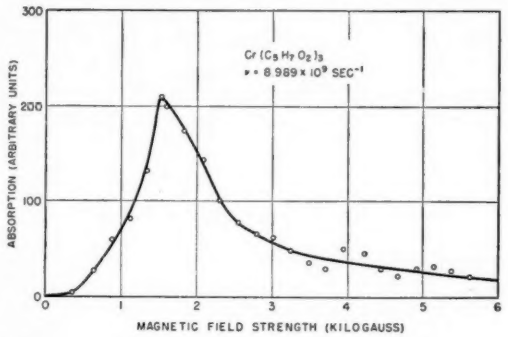

FIG. 3. Resonance absorption of chromic acetylacetonate at 3 cm.

The method of detection consisted of modulating the static magnetic field with a small 280-cycle/sec magnetic field produced by auxiliary coils and then introducing the crystal diode signal into a coherent detector after several stages of amplification. From the resonance signal obtained from 3×10^{-3} cm^3 of a 1×10^{-3} molar solution of diphenyl-picryl hydrazyl in benzene, it was estimated that $\sim10^{-11}$ mole of a free radical having a line width of 1 gauss could be detected.

Microwave frequency was measured by a wave meter calibrated by the National Bureau of Standards and magnetic field by a Laboratory for Electronics, Inc., nuclear resonance magnetometer. Magnetic fields as high as 12 000 gauss were determined within 1 gauss.

The procedure for the 1.2-cm measurements consisted of first tracing the curve of coherent detector output as a function of magnet current, on a Leeds and Northrop X−Y recorder, as the magnetic field was automatically varied from 1000 to 12 000 gauss. Since the amplitude of the magnetic field modulation was kept less than the line width of the resonances, the recorder curves were essentially plots of the slope of the resonance absorption as a function of magnet current.

The recorder charts for the resonance of a dilute single crystal of chromic acetylacetonate at two different orientations are shown in Fig. 2. The unsymmetrical appearance of the slope curves is caused by the inability of the detection system to follow the rapid slope changes produced by the relatively rapid variation of the static field. For the accurate determination of peak positions, the magnet was changed to manual operation and the microwave and nuclear resonance frequency measured at the point of zero slope corresponding to each absorption maximum.

[15] R. V. Pound, Proc. Inst. Radio Engrs. **35**, 1405 (1947).

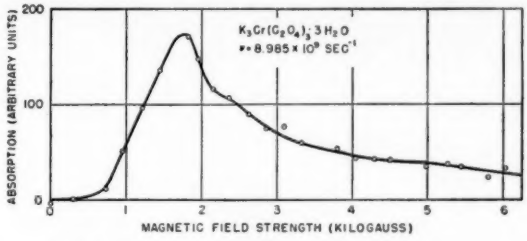

FIG. 4. Resonance absorption of potassium trioxalato chromiate at 3 cm.

IV. MAGNETIC RESONANCE MEASUREMENTS

A. Powders

The absorption curves at 3 cm for the chromic acetylacetonate, oxalate, and ethylenediamine complexes are shown in Figs. 3, 4, and 5, respectively. Note that the acetylacetonate and oxalate had very similar resonance absorptions, both being broad, asymmetric curves having an apparent g value of approximately 4. The ethylenediamine absorption had a strong maximum at a magnetic field corresponding closely to a g of 2. The same compounds at 1.2 cm had roughly the same type resonance curves; however, the apparent g factors of the acetylacetonate and oxalate were 3.6 and 3.1, respectively. The ethylenediamine complex at 1.2 cm showed a strong absorption corresponding to a g of 2 and two weak, almost unresolved side peaks on either side of the main peak. The resonances for the benzoylacetonate and isovalerylacetonate were indistinguishable from that of the acetylacetonate.

B. Single Crystals

In order to investigate in more detail the seemingly strange resonance properties of these chromic complexes,

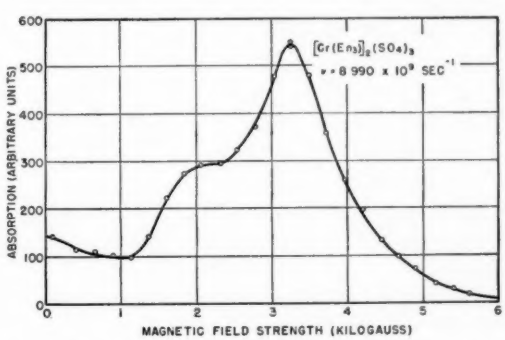

FIG. 5. Resonance absorption of tris (ethylenediamine) chromic sulfate at 3 cm.

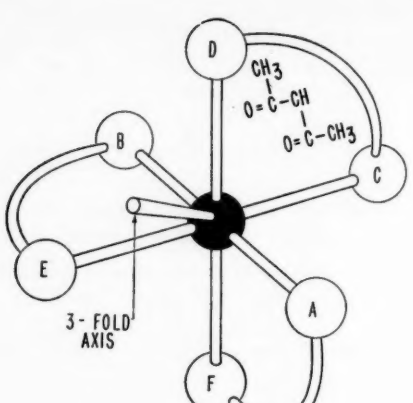

FIG. 6. Model of a chromium trichelate molecule.

single crystals of both the pure acetylacetonate and solid solutions containing the isomorphous aluminum acetylacetonate were grown and their resonances measured.

(1) *Crystal Structure*

The crystal structure of the acetylacetonates has been investigated by Astbury[16] and by Morgan and Drew.[17] Although it was not possible to determine the atom positions in these monoclinic crystals, both the aluminum and chromium acetylacetonates were found to have four molecules per unit cell and to have the space-group symmetry C_{2h}^5. The most frequently occurring faces of the crystals are the (100), (001), and (110), the β angle, which is the angle between the a and c axes, being very close to 99° in both compounds.

Each "molecule" consists of a trivalent metal ion surrounded by three acetylactonate groups in a manner probably similar to the model shown in Fig. 6. The black circle represents the metal ion and the white circles oxygen atoms. The model illustrates the main structural difference between these so-called chelate complexes and the ordinary hexacoordinated complexes like the hydrates, *viz.*, each chelate group occupies 2 coordinating positions. The molecule has the point-group symmetry D_3 consisting of one 3-fold rotation axis and three 2-fold axes. Neither a plane of symmetry nor a center of inversion is present. The 3-fold axis, which looks like a 3-bladed propeller axis, is indicated in the figure.

It was not possible by means of x-ray measurements to determine the orientation of these molecules within a unit cell; however, Astbury suggests that the line DF in Fig. 6 probably lies along the c axis of the crystal while the b axis contains one of the shorter edges BC or CA. The resonance measurements indicate that CA is approximately parallel with the b axis but that DF makes an angle of about 22° with the c axis. The details of this determination of the molecular orientations in the crystal are discussed in Sec. IV. B. 3.

(2) *Choice of Crystal Orientations*

The relatively low symmetry of the trichelate molecules has no effect on the choice of those crystal orientations which will yield easily interpretable resonance spectra. Since the space group symmetry of the crystal demands that the four molecules in a unit cell must be two pairs of enantiomorphs, one pair differing from the other by a rotation about the b axis by π, the parity arguments in Sec. V. A reduce the orientation problems of the acetylacetonates to those of the apparently simpler Tutton salts.[18]

The principal magnetic directions of the crystals are denoted as follows. K_1 and K_2 lie in the ac plane, K_1 bisecting the angle between the two electric axes, and K_2 perpendicular to the plane of the two electric axes. K_3 lies along the b axis of the crystal. Figure 7 shows the orientations of these various axes for a crystal oriented such that the static magnetic field H was perpendicular to the b axis of the crystal.

(3) *Orientation of Electric Axes*

The resonance was first measured in a single crystal of the undiluted chromic acetylacetonate with its b axis perpendicular to the static magnetic field and parallel to the high-frequency magnetic field as shown in Fig. 7. Since the absorption lines were several hundred gauss wide, much of the fine structure was unresolved. However, the results indicated the presence of two stationary points 90° apart in the variation of peak positions with angle of rotation about the b axis. These two points presumably corresponded to the orientations for which the principal axes K_1 and K_2 became parallel to the static field.

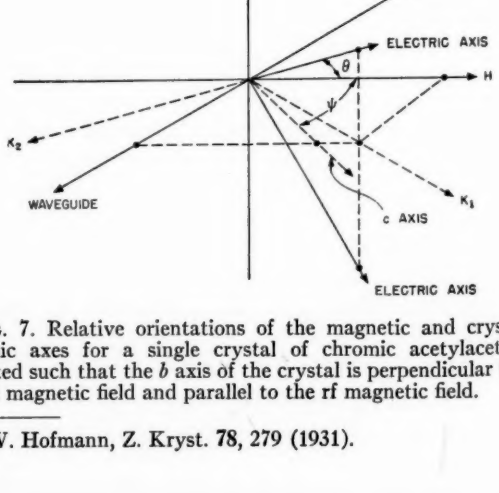

FIG. 7. Relative orientations of the magnetic and crystallographic axes for a single crystal of chromic acetylacetonate oriented such that the b axis of the crystal is perpendicular to the static magnetic field and parallel to the rf magnetic field.

[16] W. T. Astbury, Proc. Roy. Soc. (London) **112A**, 448 (1926).
[17] G. T. Morgan and H. D. K. Drew, J. Chem. Soc. **119**, 1059 (1921).
[18] W. Hofmann, Z. Kryst. **78**, 279 (1931).

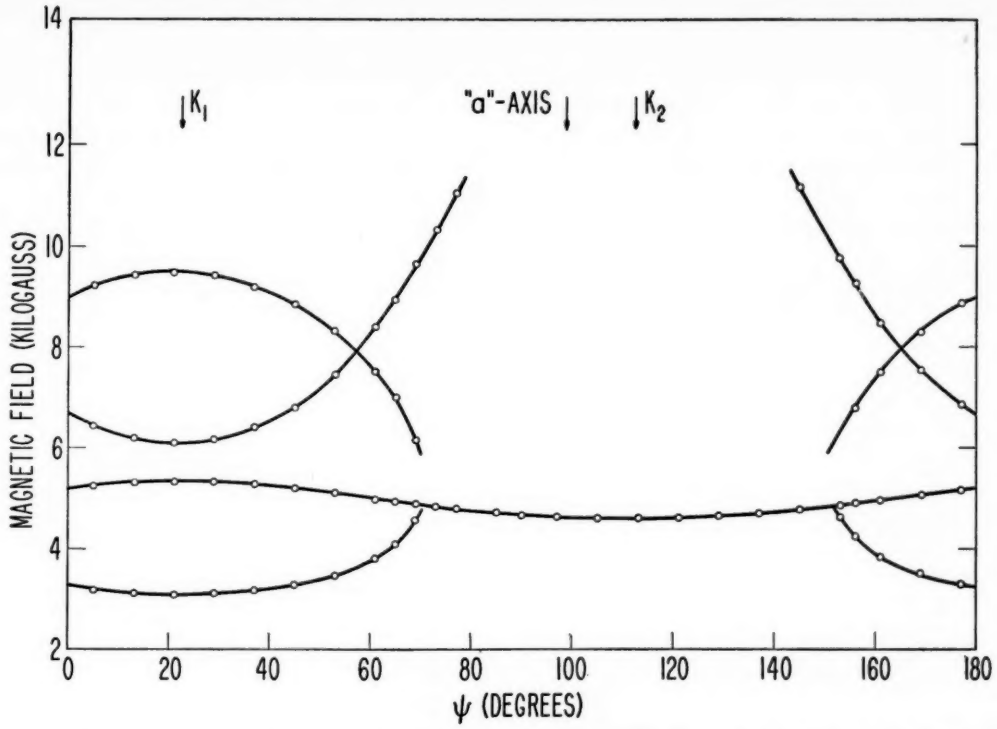

FIG. 8. Peak positions as a function of the angle of rotation about the b axis. ψ is the angle between the c axis and the static magnetic field as is shown in Fig. 7.

Another crystal having a Cr:Al atom ratio of 1:50 was measured at the same orientations as the above-mentioned undiluted crystal. The absorption lines in this case were about 20 gauss wide. A careful mounting of the crystal yielded resonance spectra in which the absorption lines for the two inequivalent Cr^{+3} ions were essentially superimposed. At a few critical rotation angles, however, certain peaks were still not superimposed but were separated by less than 150 gauss. Since in many cases the sensitivity of the resonance spectra to crystal alignment was such that a 1° change in angle of rotation of the crystal produced a 200 gauss shift in peak position, it was estimated that in this case the alignment of the crystal was accurate to within 1°.

These rapid changes of peak position with angle are probably responsible for the broadening of certain absorption lines at various critical orientations. One possible explanation for the broadening is that the crystals might have considerable mosaic structure due to their rather rapid growth. Differences in orientation of the mosaic blocks of a quarter of a degree would produce the observed broadening. The broad line in Fig. 2(b) is the $(-1/2 \rightarrow -3/2)$ transition for the orientation $\eta = 176°$ (see Fig. 11).

The results for the above dilute crystal are shown in Fig. 8, which is a plot of the peak positions as a function of ψ, the angle between the c axis and the static field. In the few cases where the peaks for a given transition were not superimposed because of the slight inaccuracy of alignment, the arithmetic mean of the field strengths at the two maxima was plotted. The assignment of K_1 and K_2 to the observed stationary points follows from the theoretical considerations in Section V, B. The observed angle between K_1 and the c axis was $22.5° \pm 1°$ and between K_1 and the a axis $(\beta - 22.5) = 76.5°$. The difference in angle between the two stationary points K_1 and K_2 was 90°.

In order to find the angle between electric axes, the crystal was remounted so that the K_2 axis determined above was perpendicular to the static field and parallel to the rf magnetic field. A complicated fine structure was observed with as many as 8 peaks occurring at certain orientations. Some of the results for the $(1/2 \rightarrow -1/2)$ transitions are shown in Fig. 9. The peak positions are plotted as a function of the angle of rotation about K_2, where η is the angle between the b axis (K_3) and the static magnetic field. The two curves are associated with the two inequivalent magnetic ions and are seen to be reflected into each other through K_1. The assignment of the "z axis" or electric axis to the angles corresponding to the minima of the curves is unambiguous when other transitions not shown in Fig. 9 are considered. If the assumption of a single electric axis for each molecule is valid, the angle between the electric axes is immediately determined by inspection of the figure. The acute angle between the electric axes and the b axis was thus found to be $31° \pm 1°$, the angle between the electric axes and K_1 being the complement 59°.

If the preferred electric direction in the trichelate

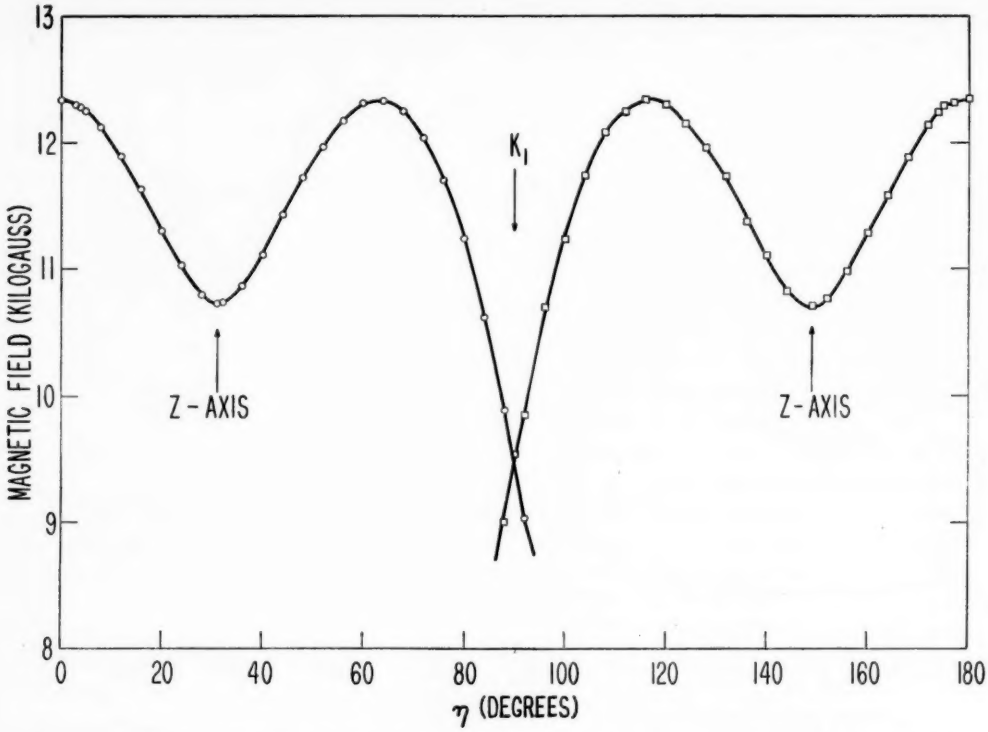

FIG. 9. Peak positions for some of the $1/2 \rightarrow -1/2$ transitions as a function of the angle of rotation about the K_2 axis. η is the angle between the b axis and the static magnetic field. The magnetic field H was in the plane of the two electric axes for all angles η.

molecule can be associated with the threefold or "propeller" axis, the above data suggest certain possible orientations for the molecules in a unit cell. Astbury[16] has proposed two possible orientations for the trichelate molecules in the crystal based on the size of the molecules and the size of the unit cell. Referring to the model in Fig. 6, one of the possibilities he suggests is that *CA* and *BE* lie along the *b* axis and *DF* is parallel to the *c* axis of the crystal. This assumption implies that the angle between the "propeller" axis and the *b* axis is $\cos^{-1}(2/3)^{1/2}=35.3°$ which is comparable with the value 30° determined from the resonance measurements. However, if this were the correct orientation, the angle between the projection of the "propeller" axis in the ac plane and the *c* axis (angle between K_1 and the *c* axis) would be 0°, whereas the resonance measurements yield 22.5° for this angle. The resonance data thus suggest that the molecules are rotated slightly about the *b* axis so that *DF* is not parallel with the *c* axis but makes an angle of about 22° with it. Such an orientation would not be inconsistent with the relative dimensions of the molecules and the unit cell.

C. Liquid Solutions

Resonance measurements were made at *K* band on a concentrated benzene solution of the acetylacetonate, and concentrated aqueous solutions of potassium trioxalato chromiate and potassium chrome alum. The resonances obtained for solutions of the acetylacetonate and oxalate complexes were indistinguishable from those found for the powders. On the other hand, the resonance curves for chrome alum powder and its aqueous solution were quite different as is shown in Fig. 10. These curves were both obtained using the same magnetic field modulation amplitude, and the same gain and time constant for the lock-in amplifier. The data indicate that the fine structure observed in the powdered alum is not present in solution.

V. THE EXPERIMENTS AND THE CRYSTALLINE FIELD THEORY

In this section the experimental results for the single crystals and powders are interpreted on the basis of the usual crystalline field model.

A. The Trichelate Complex

If one assumes that the model in Fig. 6 is good representation of the trichelate complex and in addition assumes a reasonable point charge distribution in the chelate rings, the electrical potential at the central chromic ion can be calculated in the form of a Taylor's expansion at the center. Since in the acetylacetonate, for example, the oxygen atoms which surround the chromium will have considerable net negative charge, a charge distribution consisting of a charge $-e$ at each of the 6 oxygen atoms and a charge $+e$ at the center of each chelate ring should be a reasonable first approximation to the real situation. The result of such a calcu-

lation carried out to include second-power terms is a potential having axial symmetry about the threefold molecular axis. The negative charges at the corners of a regular octahedron can be considered to give rise to the fourth-power terms having cubic symmetry.

Since neither the trichelate molecule nor the assumed point charge distribution possesses a center of inversion, the Hamiltonian for the chromic ion must contain terms of odd powers in the coordinates. However, it can be shown rigorously that the eigenvalues of any Hamiltonian are invariant under an inversion of the coordinates.[19] By similar arguments, the intensities of the magnetic dipole transitions observed in resonance experiments are also independent of an inversion of the coordinates. Hence two trichelate molecules which differ only by an inversion will have identical magnetic resonance spectra.

B. The Spin-Hamiltonian

If the model for the trichelate molecule is correct, the usual spin-Hamiltonian (1) should apply,

$$\mathcal{H}=g\beta\mathbf{H}\cdot\mathbf{S}+D[S_z^2-(1/3)S(S+1)], \qquad (1)$$

where the first term is the Zeeman energy and the second the interaction energy of the chromium with a crystalline field of axial symmetry. Since the experiments indicate the two terms to be of comparable magnitude, it is necessary to diagonalize both terms simultaneously. Since this has already been done for the chrome alums[20,21] and the vanadium Tutton salt,[22] the details of the calculation will be omitted here. The secular equation for this case is

$$\epsilon^4-(\epsilon^2/2)(1+20x^2)+4x^2(1-3\cos^2\theta)\epsilon +(1/16+9x^4+x^2/2-3x^2\cos^2\theta)=0, \qquad (2)$$

where $x=g\beta H/4D$, $\epsilon=\lambda/2D$, θ is the angle between the cylindrical axis and the magnetic field, and λ is the eigenvalue of the energy. When $\theta=0$, Eq. (2) can be easily solved and the eigenvalues are

$$\begin{aligned}\lambda_1&=(3/2)g\beta H+D,\\ \lambda_2&=(1/2)g\beta H-D,\\ \lambda_3&=(-1/2)g\beta H-D,\\ \lambda_4&=(-3/2)g\beta H+D.\end{aligned} \qquad (3)$$

For either of the orientations denoted "z axis" in Fig. 9, half of the molecules have their electric or z axis parallel to the magnetic field so that the two parameters g and D in (3) can be evaluated from any two different observed transitions. For the case $\theta=0$, two strong absorption peaks occurred at 8607 and 4157 gauss and can be shown to correspond to the transitions $\lambda_2\rightarrow\lambda_3$ and $\lambda_4\rightarrow\lambda_3$, respectively. From the measured microwave frequency of 23 890 mc/sec and the field strengths for these transitions, the values $g=1.983\pm0.002$ and $|D|=0.592\pm0.002$ cm^{-1} were obtained. The errors, which are presumably due to inaccuracies in crystal alignment, are estimated from the difference in the parameter values obtained at the two different "z axis" orientations shown in Fig. 9. The peak positions for two other transitions whose intensities become vanishingly small at zero angle were estimated by interpolation and found to be consistent with these parameters. Using the parameters g and D, the peak positions which had been calculated previously[22] for many other values of θ were plotted *vs* the angle η, assuming the experimentally determined angles between electric axes. The calculated curves, the solid one for one kind of chromic ion and the dashed one for its inequivalent neighbor, are shown in Fig. 11. The circles and squares were determined experimentally. The various transitions are labeled with the "high-field" quantum numbers. This notation is unambiguous for all angles except $\theta=0$ since none of the 4 energy levels cross. For $\theta=0$, some accidental degeneracy occurs in the range of magnetic fields of interest, so that a slight ambiguity of identification will exist. For this reason different indices were used for the eigenvalues (Eqs. (3)).

The absorptions corresponding to the transition $(-1/2\rightarrow-3/2)$ were strong at all orientations, while the absorptions corresponding to other transitions varied widely in intensity for different orientations. A detailed comparison of the experimental and theo-

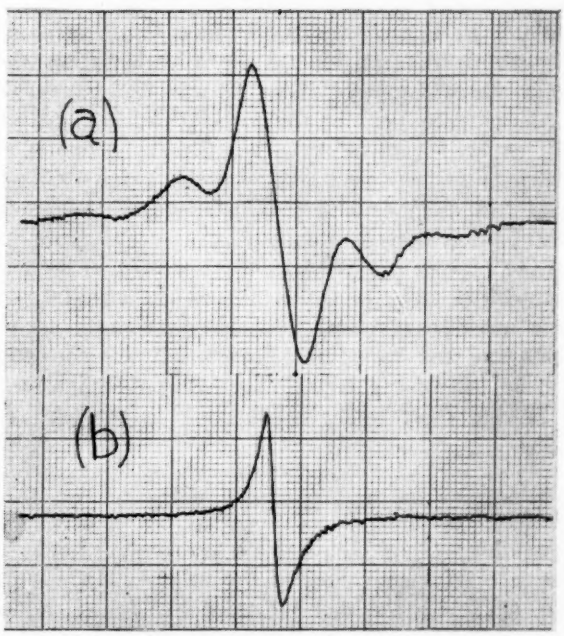

FIG. 10. Resonance absorption of potassium chrome alum; (a) power; (b) aqueous solution.

[19] The proof of this statement follows directly from the fact that the Hamiltonian can always be written as a sum of two terms, one of odd inversion character and the other of even inversion character. The same is true for the eigenfunctions.

[20] P. R. Weiss, Phys. Rev. **73**, 470 (1948).

[21] C. Kittel and J. M. Luttinger, Phys. Rev. **73**, 162 (1948).

[22] C. A. Hutchison, Jr., and L. S. Singer, Phys. Rev. **89**, 256 (1953).

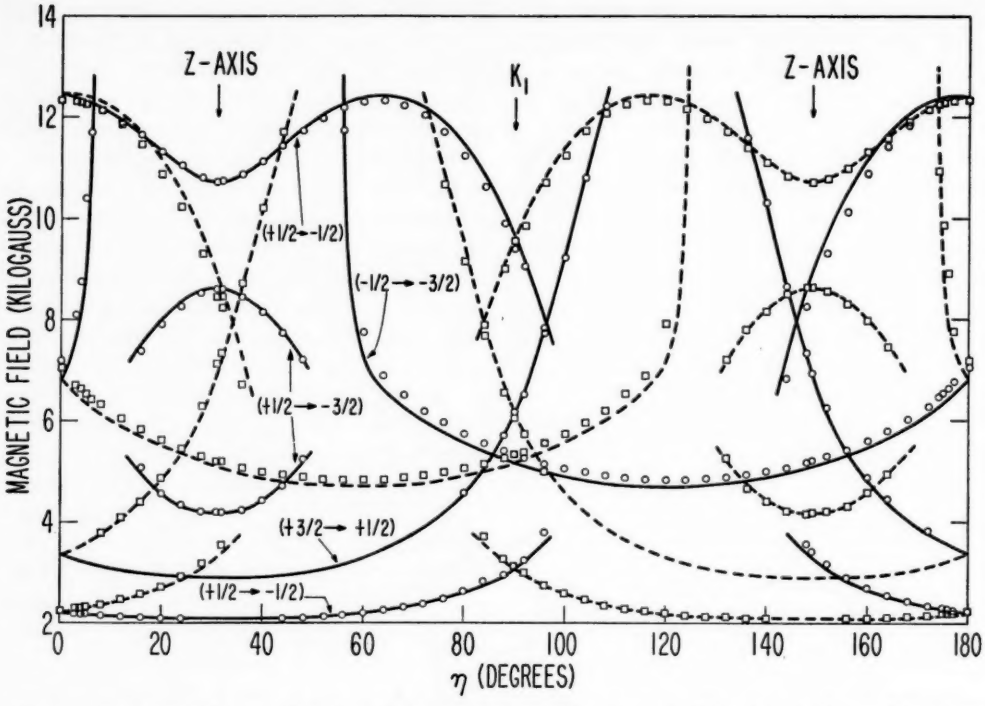

Fig. 11. Peak positions as a function of the angle of rotation about the K_2 axis. η is the angle between the b axis and the static magnetic field. The solid and dashed curves are calculated, the squares and circles the experimental points.

retical intensities was not made; however, the observed intensities appear to be in good general agreement with those calculated previously.[22]

The deviations of the experimental points from the calculated curves in Fig. 11 are small but well outside experimental error. In addition, the field strength for the $(-1/2\rightarrow-3/2)$ transition at the K_2 orientation ($\theta=90°$) in Fig. 7 was 4589 gauss, while the field strength for this transition at the 90° orientation when the crystal was rotated about K_2 was 4829 gauss. The calculated peak position for both 90° orientations was 4697 gauss. It can be seen that the deviations of the experimental peak positions from this value are about equal and of opposite sign. This suggests two possibilities. Either there is rhombicity in the crystalline field but the g factor is still essentially isotropic, or both the rhombicity of the crystal field and the anisotropy of the g factor are involved. Since the data on the chrome alums and the vanadium Tutton salt are consistent with an isotropic g factor,[1] the first possibility seems to be the most likely explanation of the observed deviations.

C. The Rhombic Field

Assuming the g factor to be isotropic, we now investigate the eigenvalues of the original Hamiltonian [Eq. (1)] with the rhombic term $E(S_x^2-S_y^2)$ added. Since the model in Fig. 6 yields no information about the directions of rhombic distortion of the molecules in the crystal, it is simply assumed that the rhombic z axis is in the same direction as the z axis of quantization in Eq. (1).

The eigenvalues of the Hamiltonian, including the rhombic term, for the case $\theta=0$ are

$$\lambda=-G/2\pm[(G-D)^2+3E^2]^{1/2},$$
$$\lambda=G/2\pm[(G+D)^2+3E^2]^{1/2}, \quad (4)$$

where $G=g\beta H$. Since no linear terms in E appear in these expressions, the only information about E which can be obtained from the $\theta=0$ orientation is that it is 0.05 cm^{-1} or less. This is because the correction to the axial case is of order E^2 which, if E is 0.05 cm^{-1} is about the same as the experimental error involved in determining D.

For the evaluation of E, it was thus necessary to consider angles other than $\theta=0$. This was most conveniently done by carrying out a first-order perturbation calculation using the wave functions which diagonalize the Hamiltonian [Eq. (1)] as the zeroth-order functions. These wave functions which had been

TABLE I.

Orientation	Transition	H_{obs} (gauss)	Rot. axis	θ	$H_{ax}-H_{obs}$ (gauss)	$Corr_{Rhom.}$ (gauss)
1	$-1/2\rightarrow-3/2$	4589	K_3	90°	+110	+110
2	$-1/2\rightarrow-3/2$	5212	K_3	65°	−210	−210
3	$-1/2\rightarrow-3/2$	4892	K_2	90°	−130	−110
4	$-1/2\rightarrow-3/2$	5456	K_2	54.9°	−128	−130
5	$1/2\rightarrow-1/2$	2925	K_2	54.9°	−99	−60

determined previously are[21,22]

$$\Psi_m = N_m^{-1}(\Phi_{3/2} + a_m\Phi_{1/2} + b_m\Phi_{-1/2} + c_m\Phi_{-3/2}),$$

where

$$N_m = (1 + |a_m|^2 + |b_m|^2 + |c_m|^2)^{1/2},$$

$$a_m = -\frac{(1/2 + 3x\cos\theta - \epsilon_m)e^{i\varphi}}{(3)^{1/2}x\sin\theta},$$

$$b_m = -\left[(3/4)^{1/2}e^{2i\varphi} + \frac{(-1/2 + x\cos\theta - \epsilon_m)e^{i\varphi}}{2x\sin\theta}a_m\right],$$

$$c_m = -\frac{(3)^{1/2}x\sin\theta e^{i\varphi}b_m}{(1/2 - 3x\cos\theta - \epsilon_m)}, \tag{5}$$

and φ is the angle between the projection of the static field in the xy plane and the x axis. The diagonal elements of the rhombic perturbation $R = E(S_x^2 - S_y^2)$ are then given by

$$R_{mm} = 3^{1/2}N_m^{-2}E(b_m + a_m^*c_m + b_m^* + c_m^*a_m). \tag{6}$$

The corrections R_{mm} to the eigenvalues ϵ_m of the axial field case were calculated for five different crystal orientations in terms of the angle φ and the parameter E using values of ϵ_m obtained graphically.

The values $|E| = 0.052\ \text{cm}^{-1}$ and $|\cos 2\gamma| = 0.156$ were obtained from the data for two orientations. γ is the angle between the x axis and K_2, both x and y having been assumed to lie in the K_1K_2 or ac plane. The predicted rhombic corrections for three other orientations are compared with the observed deviations from the axial case in Table I. The first two corrections in the last column were used for the computation of E and γ.

The observed and calculated deviations from the axial case for the last three orientations are seen to be in approximate agreement. Part of the remaining discrepancies may be due to the assumption that the rhombic z axis and the cylindrical axis are parallel. If this were exactly true, then the observed deviations for the two different $\theta = 90°$ orientations shown in the table should be exactly equal and opposite in sign, as was only approximately the case.

C. Powders

We now wish to see if the line shape and apparent g factor of 4 for the powdered chromic acetylacetonate are consistent with the angular dependence of the single crystal resonance. The required averaging process would be prohibitively difficult for the situation as it stands; however, several simplifying assumptions can be made. Since for the 3-cm measurements the zero field axial splitting $2D$ is considerably larger than the microwave quantum $h\nu$, one can make the approximation that $x = g\beta H/4D \ll 1$. Making this assumption, the secular equation (2) can be solved assuming ϵ is a power series of the form $a + bx + cx^2 + \cdots$. The eigenvalues including terms in x^2 are then

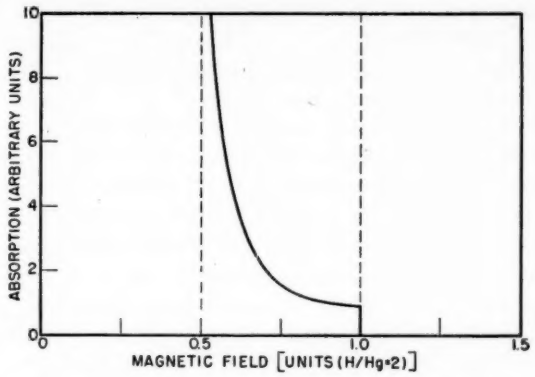

FIG. 12. Theoretical resonance absorption curve for a powdered chromic salt, assuming the axial field splitting of the ground state $\gg h\nu$.

$$\epsilon_{\pm 3/2} = 1/2 \pm 3x|\cos\theta| + 3x^2\sin^2\theta,$$
$$\epsilon_{\pm 1/2} = -1/2 \pm x(4 - 3\cos^2\theta)^{1/2} - 3x^2\sin^2\theta, \tag{7}$$

where the ϵ's are indexed now by the "low-field" quantum numbers. The assumption $x \ll 1$ also implies that the transitions $(3/2 \rightarrow -3/2)$ will be forbidden so that we will consider only the transitions $(1/2 \rightarrow -1/2)$. It can be seen from Eq. (7) that the field strength H_0 for a $(1/2 \rightarrow -1/2)$ transition is given by

$$H_0 = (h\nu/g\beta)(4 - 3\cos^2\theta)^{-1/2} \tag{8}$$

and is thus independent of D to the approximation used. It will also be assumed that the absorption intensity $I(H_0)$ is independent of θ. This is not strictly true but both experiment and theory show this to be approximately the case. The shape of the absorption curve for a powder can then be written

$$I(H) \propto \int_0^{\pi} f(H - H_0)\sin\theta d\theta, \tag{9}$$

where $f(H - H_0)$ is the distribution function for the absorption by a single crystallite. Assuming the absorption lines to have zero width, f can be replaced by a δ function so that

$$I(H) \propto \left|\sin\theta\frac{d\theta}{dH_0}\right|_{H_0 = H} \propto \left|\frac{d(\cos\theta)}{dH_0}\right|_{H_0 = H}. \tag{10}$$

Expressing $\cos\theta$ in terms of H_0 from Eq. (8), the powder absorption becomes

$$I(H) \propto 4[4H^2 - (h\nu/g\beta)^2]^{-1/2} - (1/H^2)[4H^2 - (h\nu/g\beta)^2]^{1/2}. \tag{11}$$

The asymmetric curve in Fig. 12 is a plot of this function. Both the asymmetry of the absorption and the apparent g factor of 4 indicated by the experimental powder absorption in Fig. 3 are thus explained on the basis of the single crystal results and the axial field model with large zero-field splitting.

As a result of the $\sin\theta$ dependence in Eq. (9), the crystal orientations near $\theta=\pi/2$ are the most heavily weighted in the averaging process. In fact, to the approximations made, an apparent $g=4$ is just the value of $h\nu/\beta H_0$ for the single crystal orientation corresponding to $\theta=\pi/2$. For the cases where the large D approximation becomes poorer we might still expect the peak position for the powder to correspond closely to the peak position for the $\theta=90°$ single crystal orientation. This appeared to be roughly the case for the acetylacetonate, where $2D$ was only slightly larger than $h\nu$ at 1.2 cm. From this relation, the splitting $2D$ for the chromic oxalate was estimated from its powder resonance at 1.2 cm to be about 0.9 cm^{-1}. Since the ethylenediamine complex at 3 cm showed considerable zero-field absorption, the splitting $2D$ for this substance was estimated to be about 0.3 cm^{-1}. The rhombic contributions to the splittings were neglected in making these estimates.

VI. DISCUSSION

The g factor 1.983 obtained for the chromic acetylacetonate is intermediate between 1.976 obtained for the $Cr(H_2O)_6$ complex in an alum[1] and 1.992 obtained for the $Cr(CN)_6$ complex.[1] As Bleaney and Stevens have pointed out,[1] if the free ion spin-orbit coupling constant $\lambda=87$ cm^{-1} is used, the over-all cubic field splitting Δ of the orbital levels is shown by the relation $g=2-72\lambda/5\Delta$ to be $>50\,000$ cm^{-1} for all three compounds. Not only is this value almost twice as large as that estimated by Van Vleck,[23] but it is much larger than the observed Russel-Saunders term separations of the free Cr^{+3} ion.[24] The ground term ^4F lies only 14 000 cm^{-1} below the next higher term ^4P; in fact all the higher terms belonging to the $3d^3$ configuration lie within 36 000 cm^{-1} of the ground term ^4F. It would therefore seem that the ionic model of Schlapp and Penney, which assumes the term separation to be greater than the cubic-field splitting Δ, should not be applicable. This apparent discrepancy suggests that the "strong-field" case, in which the electric field interaction is larger than the electrostatic repulsions between the electrons, should apply. The covalent model, which can be considered to be formally equivalent to the strong field case,[8] seems to be the most likely possibility for Cr^{+3} compounds in view of considerable chemical evidence. For example, a slow rate of exchange of complexes with their components in solution, and a slow rate of racemization of optically active complexes are considered to be evidence for greater covalent character of the bonds between the metal ion and its ligands.[25] However, as Taube[26] has pointed out, the bond character is probably only one of several important factors determining the slow rates in the case of Cr^{+3} complexes.

The value of D, the parameter which describes the magnitude of a crystalline field of axial symmetry, appears to be much larger in the trichelates than in any of the other chromic compounds which have been reported. Since the atom positions in these molecules are not known, any attempt to explain the large D would be largely speculative. The charge distribution assumed for the model in Fig. 6 may be satisfactory in so far as symmetry considerations are concerned; however, it seems rather unlikely that the distant positive charges at the centers of the chelate rings could produce a very large axial field at the chromium. Possibly the dipole moments associated with the carbonyl groups are the important factors in producing the large field in the oxalate and acetylacetonates. The rhombic distortion, which is also inconsistent with the simple model, is seen from the value of E to be quite small.

From the observations on liquid solutions of these complexes, it is evident that in the trichelates, the electric fields which give rise to the fine structure are not dependent upon crystal symmetry, but are properties of the isolated individual molecules. This is in contrast to the alums in which the preferred direction associated with each chromium ion in the crystal is destroyed upon solution of the salt in water.

[23] J. H. Van Vleck, J. Chem. Phys. **7**, 61 (1939).
[24] *Atomic Energy Levels*, Vol. II, Circular No. 467 of the National Bureau of Standards (1952).
[25] A. E. Martell and M. Calvin, reference 9, p. 225.
[26] H. Taube, Chem. Revs. **50**, 69 (1952).

Pressure Broadening of Linear Molecules. II. Theory*

WILLIAM V. SMITH, H. A. LACKNER, AND A. B. VOLKOV
Department of Physics, University of Delaware, Newark, Delaware
(Received August 2, 1954)

The large collision diameters for the self pressure broadening of OCS and BrCN can be explained in terms of P. W. Anderson's general theory as due to the first order dipole-dipole interaction. The temperature dependence of the pressure broadening requires the introduction of other interactions. It is possible to obtain both the magnitude and temperature dependence of the pressure broadening by considering both the first order dipole-dipole and quadrupole-dipole interactions.

INTRODUCTION

A GENERAL theory of pressure broadening in the microwave region has been developed by P. W. Anderson.[1] By making the approximation that only quasi-resonant "collisions" are important in the self-broadening process, Anderson was able to obtain good agreement, considering only dipole-dipole interactions, with the self-broadening data of the inversion spectrum of ammonia. The term quasi-resonance is used to indicate that Anderson made the approximation of assuming that the energy difference of the two inversion states of ammonia is negligible. In treating the rotational transitions of the radiating and colliding molecule, Anderson considered only true resonant collisions. However, this approximation of pure rotational resonance collisions and dipole-dipole interactions does not give satisfactory agreement with the self-broadening data of linear molecules, specifically with those of OCS and BrCN.

An adequate theory of the pressure broadening of linear molecules in the microwave region must be able to account for the observed large collision diameters which are several fold larger than the values calculated on the basis of pure resonance collisions. The observed collision diameters are about 9 A for the $J=1$ to $J=2$ OCS transition and 20 A for the $J=2$ to $J=3$ BrCN transition.[2] Furthermore, it would be desirable for the theory to be capable of explaining (a) the temperature dependence of the collision diameters, $T^{-0.2}$ for OCS[3] and $T^{-0.5}$ for BrCN,[4] and (b) the dependence of the collision diameters on the rotational state J of the radiating molecule, the collision diameter increasing with increasing J.[5]

The results of this paper indicate that the general theory of Anderson is adequate to account for the self-broadening of linear molecules provided the approximation of pure resonance collisions is abandoned, and all contributing collisions are included. Although the effect of individual nonresonant collisions is comparatively small, the much larger population (Boltzmann distribution) of the contributing molecules results in these nonresonant collisions being responsible for the major portion of the collision cross section.

It is found that first order dipole-dipole interactions alone are sufficient to give the required magnitude of the collision diameters of OCS and BrCN and a good portion of the observed temperature and J dependence. The correct temperature dependence and magnitude of the pressure broadening can be obtained for BrCN by a slightly modified calculation which includes both the first order dipole-dipole interactions and the dipole-quadrupole interaction. The temperature dependence can be used to determine the value of the molecular quadrupole moment. In the case of BrCN the quadrupole moment obtained in this manner is $Q/e=5.7\times10^{-16}$ cm^2. This is compatible with the value of $Q/e=2.4\times10^{-16}$ cm^2 obtained for ClCN by Smith and Howard.[6] However, this agreement may be fortuitous since the latter value was obtained by neglecting the dipole-dipole contribution and by using an overly simple averaging procedure.

RESUMÉ OF ANDERSON'S THEORY

The observed line breadth $2\Delta\nu$ is related to the effective collision cross section σ of the molecules by the kinetic theory relation[1]

$$2\pi\Delta\nu=n\bar{v}\sigma, \tag{1}$$

where $\bar{v}$ is the mean relative velocity of the colliding molecules and n is the number of particles per unit volume. Anderson has obtained this effective cross section in terms of a unitary time transformation operator, the "collision" operator, which is determined by the molecular motions and the molecular interaction.

The total effective cross section is given by the average of the partial cross sections

$$\sigma=\sum_{J_2}\rho_{J_2}\sigma_{J_2}, \tag{2}$$

where ρ_{J_2} is the Boltzmann distribution function for the colliding molecule (the radiating molecule will be

* This work was supported by the U. S. Air Force, through the Office of Scientific Research of the Air Research and Development Command.

[1] P. W. Anderson, Phys. Rev. **76**, 647 (1949).
[2] Gordy, Smith, and Trambarulo, *Microwave Spectroscopy* (John Wiley and Sons, Inc., New York, 1953).
[3] Feeny, Lackner, Moser, and Smith, J. Chem. Phys. **22**, 79 (1954).
[4] Trambarulo, Lackner, Moser, and Feeny, Phys. Rev. **95**, 622(A) (1954).
[5] C. M. Johnson and D. M. Slager, Phys. Rev. **87**, 677 (1952).
[6] W. V. Smith and R. Howard, Phys. Rev. **79**, 132 (1950).

labeled (1) while the colliding molecule will be labeled (2)). The partial cross section σ_{J_2} is the effective partial cross section for collisions of the radiating molecule with a molecule in the state J_2. This partial cross section for the case of interest is given by the expression[1]

$$\sigma_{J_2}=\int d\sigma\left[\frac{Tr(T^{i,J_2}(d\sigma)^{(-1)}\mu_z{}^{if}T^{f,J_2}(d\sigma)\mu_z{}^{fi}}{Tr(\mu_z{}^{if}\mu_z{}^{fi})(2J_2+1)}-1\right]. \quad (3)$$

$\mu_z{}^{if}$ is the "Teilmatrix" between the initial state i and final state f for the radiating molecule of the z component of the molecular dipole moment, and $T^{f,J_2}(d\sigma)$ is the "Teilmatrix" of a unitary transformation matrix closely related to the time or collision matrix $T(t)$. $T(t)$ satisfies the differential equation

$$i\hbar\dot{T}(t)=H_1'(t)T(t); \quad T(-\infty)=1, \quad (4)$$

where $H_1'(t)$ is related to the molecular interaction Hamiltonian $H_1(t)$ by the expression

$$\langle m|H_1'(t)|n\rangle=\langle m|H_1(t)|n\rangle\exp[(E_m-E_n)t/i\hbar]. \quad (5)$$

An approximate solution can be obtained for $T(t)$ if the molecular interaction is assumed to be small, i.e., weak collisions, and noncommuting portions of the collision Hamiltonian $H_1'(t)$ can be ignored. With these restrictions $T(t)$ can be written as

$$T=T_0+T_1+\cdots$$
$$T_0=1, \quad T_1=-iP, \quad T_2=P^2/2, \quad (6)$$

where

$$P=\frac{1}{\hbar}\int_{-\infty}^{\infty}H_1'(t)dt. \quad (7)$$

The partial cross section Eq. (3) can be evaluated in a system where the impact parameter **b** is the axis of quantization and we obtain[1] for Eq. (3)

$$\sigma_{J_2}=\int_0^{\infty}2\pi bdbS(b,J_2), \quad (8)$$

where $S(b,J_2)$ is a complicated relation depending on the matrix elements of the dipole moment operator and the collision matrix Eq. (4). $S(b,J_2)$ may be considered to represent the probability of a complete interruption of the radiation of a molecule (with initial state i and final state f) by collision with a molecule in state J_2. $S(b,J_2)$ has a maximum value of $S(b,J_2)=1$ which represents a collision process strong enough to either interrupt the radiation completely or to introduce an arbitrarily large phase change in the radiation. Either of these changes of the radiation lead to the usual Lorentz, Van Vleck, and Weisskopf broadening. $S(b,J_2)$ can be expanded in terms of the operator P Eq. (7) and it is found that the first term to give a contribution to the pressure broadening is one of the two possible second order terms[1] (called by Anderson (S_2) outer)

$$S_2(b,J_2)=\frac{1}{2}\left[\sum_{m,M}\frac{\langle i,m,J_2,M|P^2|i,m,J_2,M\rangle}{(2J_i+1)(2J_2+1)}+\sum_{m,M}\frac{\langle f,m,J_2,M|P^2|f,m,J_2,M\rangle}{(2J_f+1)(2J_2+1)}\right], \quad (9)$$

where again i and f refer to the initial and final states of the radiating molecule, m is the magnetic quantum number of the radiating molecule, J_2 is the rotational state of the colliding molecule, and M is the magnetic quantum number of the colliding molecule.

A typical matrix element necessary to evaluate Eq. (9) is given by [using Eq. (5) and Eq. (7)]

$$\langle\alpha|P|\beta\rangle=\langle i,m,J_2,M|P|i',m',J_2',M'\rangle=\frac{1}{\hbar}\int_{-\infty}^{\infty}\exp(i\omega_{\alpha\beta}t)\langle\alpha|H_1(t)|\beta\rangle dt, \quad (10)$$

where

$$\omega_{\alpha\beta}=\frac{E(\alpha)-E(\beta)}{\hbar}=\frac{E(i)+E(J_2)-E(i')-E(J_2')}{\hbar}.$$

$H_1(t)$ is the molecular interaction term and $E(i)$ is the energy of the radiating molecule in the initial state, etc.

In evaluating $S_2(b,J_2)$ Anderson assumed for rotational transitions that only those $\langle\alpha|P|\beta\rangle$ where $\omega_{\alpha\beta}=0$ made any significant contribution. This is the case of a resonant collision in that for dipole-dipole interactions $\omega_{\alpha\beta}=0$ implies that the molecules have interchanged their rotational state values, i.e., $J_2=J_i\pm1$, $J_2'=J_i$, and $J_i'=J_i\pm1$.

In the following work all terms of the type $\langle\alpha|P|\beta\rangle$ will be included in the calculation of $S_2(b,J_2)$ taking into account the nonzero values of $\omega_{\alpha\beta}$. The values of $S_2(b,J_2)$ for a constant (and not too small) value of b will decrease with increasing J_2 until finally the contribution of $\rho_{J_2}\sigma_{J_2}$ to the total cross section σ becomes negligible and no higher values of J_2 need be considered.

APPLICATION—DIPOLE-DIPOLE INTERACTION

The interaction Hamiltonian of primary interest in the collison of two polar molecules is the usual dipole-dipole interaction

$$H_{DD}(t)=\left[\boldsymbol{\mu}_1\cdot\boldsymbol{\mu}_2-\frac{3(\boldsymbol{\mu}_1\cdot\mathbf{r})(\boldsymbol{\mu}_2\cdot\mathbf{r})}{r^2}\right]r^{-3}. \quad (11)$$

$\boldsymbol{\mu}_1$ and $\boldsymbol{\mu}_2$ are the dipole moments of the radiating and colliding molecules respectively, and $\mathbf{r}$ is the distance between them.

In the coordinate system where the impact parameter **b** is the polar axis of the spherical coordinates of each molecule, and where $\psi=\tan^{-1}[vt/b]$ is the angle which

$\mathbf{r}$ makes with $\mathbf{b}$, $H_{DD}(t)$ is given by

$$H_{DD}(t)=\frac{\mu^2}{r^3}[\cos\theta_1\cos\theta_2(1-3\cos^2\psi)$$
$$+\sin\theta_1\sin\theta_2\cos\phi_1\cos\phi_2(1-3\sin^2\psi)$$
$$+\sin\theta_1\sin\theta_2\sin\phi_1\sin\phi_2-3\sin\psi\cos\psi$$
$$\times(\cos\theta_1\sin\theta_2\cos\phi_2+\sin\theta_1\cos\theta_2\cos\phi_1)]. \quad (12)$$

The angles θ_1, ϕ_1 and θ_2, ϕ_2 are the polar angles of the two molecules, μ is the magnitude of the dipole moment of the molecules, and

$$r^2=b^2+v^2t^2; \quad \cos\psi=b/r; \quad \sin\psi=vt/r. \quad (13)$$

Only straight paths of the colliding particles need be considered in the approximations being used since the microwave collision diameters are much larger than the kinetic theory values which would result in curved paths. Since, in general, $\omega_{\alpha\beta}\neq 0$ the interaction Eq. (12) is more complicated than that used by Anderson in that the terms which are odd in the time t no longer vanish.

The general matrix element of P may now be written as

$$\langle\alpha|P|\beta\rangle=\langle\alpha|A(\omega_{\alpha\beta})\cos\theta_1\cos\theta_2$$
$$+B(\omega_{\alpha\beta})\sin\theta_1\sin\theta_2\cos\phi_1\cos\phi_2$$
$$+C(\omega_{\alpha\beta})\sin\theta_1\sin\theta_2\sin\phi_1\sin\phi_2+D(\omega_{\alpha\beta})$$
$$\times[\cos\theta_1\sin\theta_2\cos\phi_2+\sin\theta_1\cos\theta_2\cos\phi_1]|\beta>, \quad (14)$$

where

$$A(\omega_{\alpha\beta})=\frac{\mu^2}{\hbar}\int_{-\infty}^{\infty}\frac{(1-3\cos^2\psi)}{r^3}\exp(i\omega_{\alpha\beta}t)dt, \quad (15a)$$

$$B(\omega_{\alpha\beta})=\frac{\mu^2}{\hbar}\int_{-\infty}^{\infty}\frac{(1-3\sin^2\psi)}{r^3}\exp(i\omega_{\alpha\beta}t)dt, \quad (15b)$$

$$C(\omega_{\alpha\beta})=\frac{\mu^2}{\hbar}\int_{-\infty}^{\infty}\frac{\exp(i\omega_{\alpha\beta}t)}{r^3}dt, \quad (15c)$$

$$D(\omega_{\alpha\beta})=\frac{-\mu^2}{\hbar}\int_{-\infty}^{\infty}\frac{\sin\psi\cos\psi}{r^3}\exp(i\omega_{\alpha\beta}t)dt. \quad (15d)$$

These integrals can be evaluated by contour integration and are reducible to Hankel functions of the first kind of the zero and first order with complex argument. Thus as an example Eq. (15c) becomes,[7] defining $x=vt/b$, $k=b\omega_{\alpha\beta}/v$ and using Eq. (13),

$$C(\omega_{\alpha\beta})=\frac{\mu^2}{\hbar}\int_{-\infty}^{\infty}\frac{\exp(i\omega_{\alpha\beta}t)dt}{(b^2+v^2t^2)}$$
$$=\frac{\mu^2}{\hbar b^2v}\int_{-\infty}^{\infty}\frac{e^{ikx}}{(1+x^2)}dx=\frac{-\pi\mu^2}{\hbar}\frac{k}{b^2v}H_1^{(1)}(ik). \quad (16)$$

[7] G. N. Watson, *A Treatise on the Theory of Bessel Funtions* (Cambridge University Press, 1944), second edition, p. 172.

With the evaluation of the integrals Eq. (15) it is comparatively simple to calculate the remainder of the matrix element Eq. (14) between the appropriate rotational states of the two molecules. The appropriate matrix elements are given in Anderson's paper, where for the case of linear molecules the quantum number K equals zero.

The approximations made in order to obtain $S_2(b,J_2)$ Eq. (9) are only valid in the perturbation limit, i.e., in the limit where P is small and $S_2(b,J_2)\ll 1$. Since the interaction Hamiltonian Eq. (11) varies as the inverse third power of the distance between the two molecules, the calculation of Eq. (9) is valid only for relatively large impact parameters b. However, the calculation Eq. (8) of the partial cross section σ_{J_2} requires the integration of $bS_2(b,J_2)$ over all values of b. It is therefore necessary to interpolate between the value $S_2(b,J_2)=1$ for small impact parameters (strong collisions) and the calculated value of $S_2(b,J_2)$ which is valid for large impact parameters (weak collisions). The interpolation used in most of the calculations in this paper is the same as the No. 2 approximation of Anderson. In this case $S_2(b,J_2)$ is calculated from Eq. (9) for all values of b such that $S_2(b,J_2)\leqslant 1$. A critical impact parameter b_1 is obtained from the calculated value $S_2(b_1,J_2)=1$. For all values of $b\leqslant b_1$ the value of $S_2(b,J_2)=1$ is assumed, i.e., b_1 is defined as the limit of strong collisions. This approximation was found by Anderson to be the most satisfactory of the three interpolations he used.

The critical impact parameter b_1 and $S_2(b,J_2)$ for all values of $b\geqslant b_1$ must be determined as functions of J_2. This is done by performing detailed calculations for enough values to determine $S_2(b,J_2)$ as a function of b for several given values of J_2. A characteristic plot of $S_2(b,J_2)$ for the $J_1=1-2$ transition in OCS at a temperature of 195°K is given in Fig. 1 for several values of J_2. In obtaining this plot, the interpolation discussed in the previous paragraph was used. Figure 1 is then used to determine the critical impact parameter b_1 as a function of J_2 by graphical means.

An analytical approximation to $S_2(b,J_2)$ is found which gives a good fit for all the calculated values. This analytical approximation requires one additional parameter which is a function of J_2 and is also determined graphically from the calculated values of $S_2(b,J_2)$. The partial cross sections are then given by

$$\sigma_{J_2}=\pi b_1^2=2\pi\int_{b_1}^{\infty}bS_2^*(b,J_2)db, \quad (17)$$

where

$$S_2^*(b,J_2)=\exp[-A(b-b_1)] \quad b\geqslant b_1. \quad (18)$$

Equation (18) is the analytic approximation to $S_2(b,J_2)$ in the region $b\geqslant b_1$. A and b_1 are the two parameters, functions of J_2, which must be determined by graphical means from the calculated values of $S_2(b,J_2)$. The partial cross sections, calculated on this basis, for

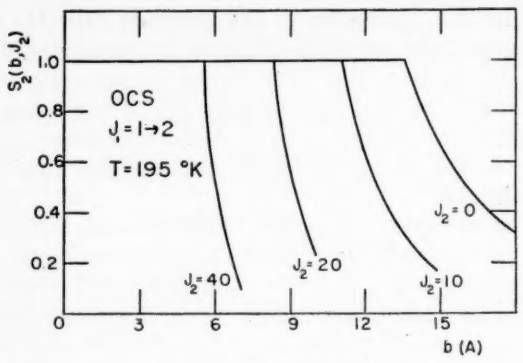

FIG. 1. A plot of the values of $S_2(b,J_2)$ as a function of the impact parameter b as calculated from Eq. (9) in the text. Anderson's second interpolation proceedure is used.

OCS are plotted in Fig. 2. The plot includes the partial cross sections for the $J_1=1$ to $J_1=2$ transition plotted for the two temperatures 195°K and 476°K.

These partial cross sections are used to calculate the total cross section Eq. (2). Figure 3 is a plot of $\rho_{J_2}\sigma_{J_2}$ as a function of J_2 for the two cases considered in Fig. 2. The area under each of these curves gives the respective cross section σ for the pressure broadening.

CONCLUSIONS CONSIDERING ONLY FIRST-ORDER DIPOLE-DIPOLE INTERACTIONS

Magnitude of Collision Diameters

The collision diameters are calculated for the two extreme temperatures of the experimental regions of interest. Table I gives the experimental and theoretical collision diameters for the $J_1=1-2$ and $J_1=5-6$ transitions in OCS. The experimental collision diameter for the $J_1=5-6$ OCS transition has been corrected for the nonlinear absorption of power with the length of the cell.[5,8] This correction is necessary because of the strong absorption of the $J_1=5-6$ transition. Only the room temperature experimental collision diameter has been quoted since there is some question as to the correct temperature dependence of the $J_1=5-6$ transition data. The corresponding theoretical value is determined by interpolation between the two calculated values at the temperature extremes. The interpolation is based on an assumed T^{-n} temperature dependence of the collision diameter d.

The agreement in magnitude of the experimental and theoretical values of d is well within the combined experimental and theoretical errors. Generally the theoretical values of d are too small for the low temperature extreme and too large for the high temperature extreme when compared to the experimental values. The primary uncertainty in the theoretical calculation is in determining the correct interpolation for $S_2(b,J_2)$ between the weak collision and strong collision limits of b. It is not actually possible to determine the strong collision limit b_1, but it is reasonable to believe that $S_2(b,J_2)$ would approach its limiting value more smoothly than in the interpolation procedure used in this paper. Any reasonable modification to this end would tend to make the calculated collision diameters smaller. However, a very extreme modification of this type, in which $S_2(b,J_2)$ approached its limiting value at $b_1=0$, only lowered the calculated collision diameters by 20 to 30 percent. This interpolation procedure leads to the same general shape as Anderson's No. 3 approximation, but represents a much greater deviation away from the undoubtedly more correct approximation No. 2.

Table II gives the corresponding results for the $J_1=2-3$ and $J_1=8-9$ transitions of BrCN. As yet no experimental results are available for the $J_1=8-9$ transition. The calculations are included in this case in order to obtain more information concerning the J_1 dependence of the collision diameters. This J_1 dependence is discussed in more detail in a later section. The general features of the calculated values are similar to the OCS values. Again there is good agreement with respect to magnitude and again the low temperature theoretical value is too small while the high temperature magnitude is too large.

The J_1 Dependence of the Collision Diameters

In Table I and Table II, it is seen that the collision diameter increases as the J_1 of the radiating molecule increases for most temperatures. The experimental increase of the OCS collision diameter, Table I, with respect to J_1 at 300°K is confirmed theoretically within

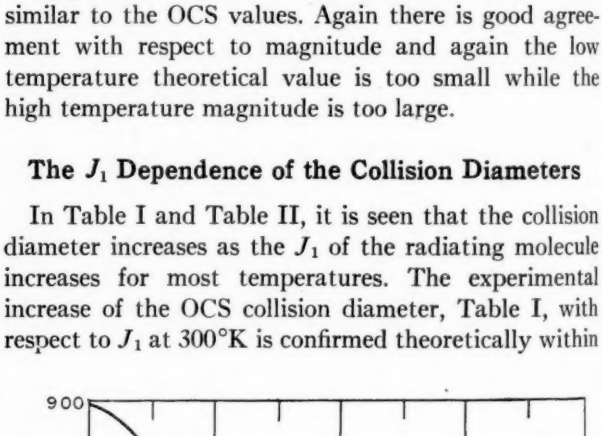

FIG. 2. The partial cross sections σ_{J_2} for the OCS $J_1=1-2$ transition at the two temperatures 195°K and 476°K.

[8] Raydeen Howard, Ph.D. thesis, Duke University (1950). Johnson and Slager's data have been corrected for nonlinearity resulting from the strong absorption at high J_1 according to the relation (Raydeen Howard thesis) $\Delta\nu=\delta\nu\sqrt{3}[1-(\alpha_0 l/4)]$. When the peak fractional absorption $\alpha_0 l$ exceends 30 percent, as it does for $J_1=7-8$ and, possibly, the dry ice run of $J_1=5-6$, the data are considered unreliable.

the experimental and theoretical uncertainties. However, the increase is rather small at best in the case of OCS, and is somewhat obscured because of the rather complicated nature of the dependence when the J_1 values are not too different. The calculated values for BrCN in Table II show a fairly strong J_1 dependence.

The simpler aspects of the J_1 dependence of the collision diameters can be understood by the study of Fig. 4. In this figure the partial cross sections σ_{J_2} are given for BrCN for the two transitions $J_1=2-3$ and $J_1=8-9$. In both cases, the partial cross sections are calculated for the temperature $T=228°$K. The resonant nature of the partial cross sections is clearly shown in Fig. 4. The maximum partial cross sections occur in the region $J_2=0$ to $J_2=4$ for the $J_1=2-3$ transition and in the region $J_2=7$ to $J_2=10$ for the $J_1=8-9$ transition. As can be seen by comparing Fig. 2 and Fig. 4, the resonant partial cross section peaks are considerably sharper for the case of BrCN than for the case of OCS. This is one reason for the greater J_1 dependence of the BrCN collision diameter.

The Boltzmann distribution has its maximum value in the region $J_2=24$ for the case of BrCN at a temperature of 228°K. The shifting of the resonant peak of the partial cross sections in the direction of this maximum results in a larger total cross section, i.e. a larger collision diameter. Thus the collision diameters, d, can be expected to have the following qualitative dependence on the J_1 of the radiating molecule: d increases as J_1 increases until the maximum value of the Boltzmann distribution is reached at which point d will begin to decrease as J_1 continues to increase.

Because of the very complicated nature of the quantity $S_2(b,J_2)$, it is not feasible to give a more detailed description of the J_1 variation of the collision diameters at this time. However, in the microwave range of experimental interest it is probable that the collision diameters will always increase with increasing J_1 except possibly at higher temperatures and low J_1 (as indicated by the results for OCS at 476°K). The exception in the case of OCS is probably to some extent fortuitous and results from the comparatively large breadth of the resonant peaks (Fig. 4). In the infrared region, with HCN, it is possible to observe the ultimate decrease in σ at high J_1.[1]

TABLE I. The experimental and theoretical collision diameters for the self pressure broadening of OCS.

Temp. (°K)	$J_1=1-2$ Transition collision diameter d (A) Reference 3 Experimental d	Theoretical d	$J_1=5-6$ Transition collision diameter d (A) Reference 5 Experimental d	Theoretical d
195.0	10.2	10.0	...	10.8
300.0	9.3	9.5[a]	10.0	9.9[a]
373.0	8.8	...	...	...
476.0	8.6	9.0	...	8.9

[a] Interpolated value assuming the temperature dependence $d\sim 1/T^n$.

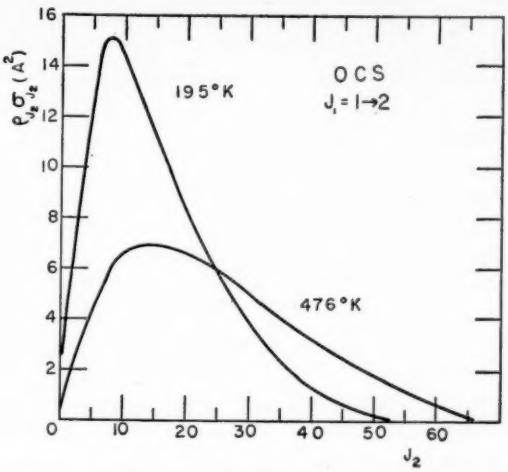

FIG. 3. The Boltzmann distribution weighted partial cross sections $\rho_{J_2}\sigma_{J_2}$ for the OCS $J_1=1-2$ transition at the two temperatures 195°K and 476°K.

Temperature Dependence of the Collision Diameters

The results of Table I and Table II show that about half of the observed temperature dependence is obtained theoretically. In both cases, the temperature dependence is in the correct direction.

In general the temperature dependence of the collision diameters is extremely complex since it depends on at least three separate factors: (a) the temperature dependence of the Boltzmann distribution, (b) the temperature dependence of the partial cross sections, and (c) the J_1 values of the radiating molecule.

The maximum of the Boltzmann distribution shifts with respect to J_2 directly with the temperature, i.e an increase of temperature leads to the maximum number of colliding particles occurring in a higher J_2 state. Thus, if all other factors remained constant, the collision diameter would decrease as the temperature is increased, provided the maximum of the partial cross section curve is at a J_2 value lower than or equal to the Boltzmann maximum. Conversely, if the maximum of the partial cross-section curve is above the Boltzmann maximum, then the collision diameter would increase with increasing temperature.

In the microwave region the J_1 of the radiating molecule is invariably below the Boltzmann maximum. This accounts for the observed decrease of the collision diameters with an increase of temperature. The temperature dependence of the Boltzmann distribution is sufficient to give the observed temperature dependence of BrCN, provided other factors remain constant.

However, it is now necessary to consider the temperature dependence of the partial cross sections as indicated in Fig. 2. This temperature variation is characteristic and leads to a theoretical temperature variation, when combined with the Boltzmann distribution temperature dependence, which is too small. This disagreement between the theoretical and experimental temperature

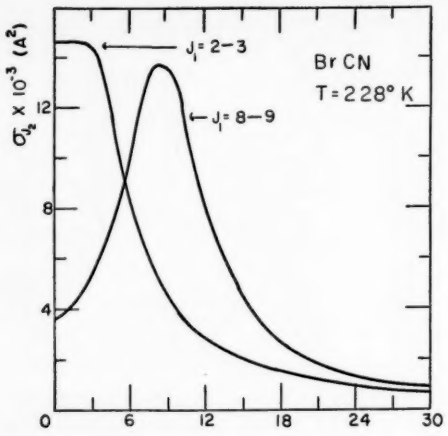

FIG. 4. The partial cross sections σJ_2 for the BrCN $J_1=2=3$ and $J_1=8-9$ transitions at a temperature of 228°K.

variations suggests that interactions, other than first order dipole-dipole interactions, must also be considered in a completely satisfactory theory of the pressure broadening of linear molecules. The contribution due to quadrupole-dipole interactions is discussed in the next section.

As shown in Fig. 2 the low-temperature partial cross sections are always larger in the region of resonance while the high-temperature partial cross sections are always larger in the limit far from resonance. The cross-over point for the partial cross-section curves with respect to the Boltzmann distribution maximum will determine the contribution of the partial cross-section temperature dependence to the over-all temperature dependence of the collision diameters. In the case of OCS (generally where the J_1 of the radiating molecule is small compared to the Boltzmann distribution maximum), the cross-over of the partial cross section occurs at a point which results in a reduction of the over-all temperature dependence of the collision diameters.

Finally, it is of interest to consider qualitatively the effect on the temperature dependence of the value J_1 of the radiating molecule. This temperature dependence is closely related to the temperature dependence effect of the Boltzmann distribution. It can be shown that the effect of the Boltzmann distribution temperature dependence is sensitive to the shape of the partial cross-section curve. As can be seen in Fig. 4, the shape of the partial cross curve is quite sensitive to the value of J_1. Specifically, it can be shown that the higher J_1 partial cross section resonant curves lead to a greater temperature dependence of the collision diameters in the microwave region. A comparison of the theoretical temperature variations for different J_1 given in Table I and Table II substantiates these qualitative results. However, as yet the experimental data needed to test the increase of the temperature dependence of the collision diameters with increasing J_1 are not available.

QUADRUPOLE-DIPOLE INTERACTION

As mentioned in the previous section, the lack of agreement between the experimental temperature and the theoretical temperature dependence of the collision diameters indicates that molecular interactions, other than the first order dipole-dipole interaction, contribute to the pressure broadening. The lack of agreement is primarily due to the temperature dependence of the partial cross sections of the dipole-dipole interaction in the region of high J_2 away from resonance (see Fig. 2). Thus, any interaction which would eliminate (or reverse) the temperature dependence of the partial cross sections in the region of comparatively high J_2 would lead to better agreement with the data.

Additional interactions will increase the magnitude of the theoretical collision diameters. However, this increase is not too serious since the collision cross sections are not simply additive but must be determined from the condition $S_2(b_1,J_2)=1$. In any event, the approximation used to interpolate the values of $S_2(b,J_2)$ undoubtedly overestimates the collision diameter.

TABLE II. The experimental and theoretical collision diameters for the self pressure broadening of BrCN.

	$J_1=2-3$ Transition collision diameter d (A) Reference 4		$J_1=8-9$ Transition collision diameter d (A)	
Temp. (°K)	Experimental d	Theoretical d	Experimental d	Theoretical d
228	24.9	22.0	...	29.2
247	24.0	...	...	...
296	22.0	...	...	...
338	19.8	...	...	...
373	19.0	19.3	...	24.2

An entirely reasonable interaction to consider in the case of linear molecules is the quadrupole-dipole interaction. Smith and Howard have explained the foreign broadening of the ammonia inversion spectra by linear molecules by means of a quadrupole-dipole interaction. Their analysis is especially meaningful for symmetric linear molecules such as CO_2 and CS_2 which have no static dipole moments, i.e., there is no dipole-dipole interaction. The quadrupole moments of these molecules as calculated from the pressure broadening are very nearly the same ($Q/e=0.65\times10^{-16}$ cm^2 and $Q/e=0.64\times10^{-16}$ cm^2 respectively). The value of the quadrupole moment of the "composite" molecule OCS, neglecting the possibility of a dipole-dipole interaction, was found to be $Q/e=0.61\times10^{-16}$ cm^2. The agreement in magnitude of the quadrupole moments of these similar molecules appears quite reasonable. The neglect of the dipole-dipole interaction in the case of the OCS foreign broadening of ammonia may not be too serious when determining the order of magnitude of the quadrupole moment. However, an appropriate matrix calculation rather than the averaging procedure

used by Smith and Howard would probably tend to increase the above values of Q significantly.†

The quadrupole-dipole interaction is given by[6,9]

$$H_{QD}=-\frac{3}{4}\frac{\mu_1 Q}{r^4}[\cos\theta_1(1-3\cos^2\theta_2) +2\cos\theta_2\sin\theta_2\cos(\phi_1-\phi_2)], \quad (19)$$

where the angles are taken with respect to the **r** axis. This expression can be transformed to a coordinate system based on the impact parameter **b** where terms which are odd in time, t, can be neglected on the basis of subsequent assumptions.

$$H_{QD}=-\frac{3}{4}\frac{\mu_1 Q}{r^4}\cos\psi[(1-3\cos^2\theta_2)\cos\theta_1 +2\cos\theta_2\sin\theta_2\sin\theta_1\cos(\phi_1-\phi_2) +5\sin^2\psi\{\cos\theta_1(\cos^2\theta_2-\sin^2\theta_2\cos^2\phi_2) -2\cos\theta_2\sin\theta_2\sin\theta_1\cos\phi_1\cos\phi_2\}]. \quad (20)$$

The quantities in Eq. (20) are the same as those defined for Eq. (12). We are primarily interested in determining the contribution of Eq. (20) in the region of large J_2. In evaluating the matrix element $\langle\alpha|P|\beta\rangle$ Eq. (10) in this region, it can be shown that either $\omega_{\alpha\beta}\gg 0$ or $\omega_{\alpha\beta}\approx 0$. The only significant contribution to the collision cross section occurs when $\omega_{\alpha\beta}\approx 0$, and the assumption made is that $\omega_{\alpha\beta}=0$ for the transitions of interest. In this case the matrix element $\langle\alpha|P|\beta\rangle$ must be of the form $\langle J_1,J_2|P|J_1\pm 1,\ J_2\rangle$. This assumes that J_1 is sufficiently small to make the energy difference between the J_1 and $J_1\pm 1$ states negligible. The expectation value in J_2 is allowed by the selection rules of the quadrupole operator. It is this property of the dipole-quadrupole operator which makes this operator so important since its contribution to the partial cross sections will not decrease with increasing J_2. The value of $S_2(b,J_2)$ in the limit of high J_2 is found by integrating with respect to time and then taking a simple average over the angles of the radiating molecule (this is valid assuming that J_1 and $J_1\pm 1$ are effectively degenerate) and explicitly evaluating the matrix elements for the colliding molecules. In the limit $J_2\to\infty$, it is found that

$$S_2(b,J_2)=\frac{11}{180}\left(\frac{\mu_1 Q}{\hbar b^3\bar{v}}\right)^2. \quad (21)$$

The partial cross section resulting from this value of $S_2(b,J_2)$, which is independent of J_2, is

$$\sigma_{QD}=\tfrac{3}{2}\pi\left(\frac{11}{180}\right)^{\frac{1}{3}}\left(\frac{\mu_1 Q}{\hbar\bar{v}}\right)^{\frac{2}{3}}=1.86\left(\frac{\mu_1 Q}{\hbar\bar{v}}\right)^{\frac{2}{3}}. \quad (22)$$

† The matrix calculation for the NH_3 foreign gas problem will differ slightly from the present treatment since NH_3 is a symmetric top molecule with inversion.

[9] Hirschfelder, Curtiss, and Bird, *Molecular Theory* (John Wiley and Sons, Inc., New York, 1954), p. 27. See p. 840 for a discussion of units.

A more detailed calculation of the effect of the quadrupole-dipole interaction would lead to some modification of the partial cross sections in the region of smaller J_2. The problem becomes very complicated in the region of competition between the dipole-dipole and quadrupole-dipole interactions and, therefore, was not considered in detail. It is interesting to note that Eq. (22) reverses the temperature dependence of the partial cross sections in the region of high J_2 as compared to the dipole-dipole interaction. The assumption was made that Eq. (22) gives the correct partial cross section in the whole region where $\sigma_{QD}\gtrsim\sigma_{J_2}$, where σ_{J_2} is the partial cross section due to the dipole-dipole interaction (see Fig. 5).

The quadrupole moment, Q, of the two linear molecules OCS and BrCN are determined from the temperature dependence of the pressure broadening in the following manner. For an arbitrary Q the collision cross section is determined by the expression

$$\sigma=\alpha(Q)\left[\sum_{J_2=0}^{N}\rho_{J_2}\sigma_{J_2}+\sigma_{QD}\sum_{J_2=N}^{\infty}\rho_{J_2}\right], \quad (23)$$

where $\alpha(Q)$ is the factor necessary to give the correct high temperature (low collision diameter) collision cross section for a given Q. This factor takes into account the overestimate of the partial cross sections because of the particular interpolation used for $S_2(b,J_2)$. In this connection, it is interesting to note that all the high temperature theoretical collision diameters are larger than the corresponding experimental collision diameters even without considering the quadrupole-dipole contributions (see Table I and Table II). After having determined $\alpha(Q)$, the value of Q which gives

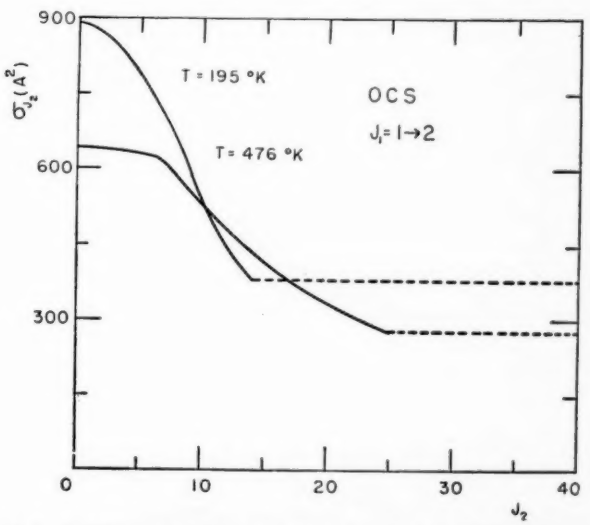

FIG. 5. The partial cross sections σ_{J_2} for the OCS $J_1=1-2$ transition including both the dipole-dipole and quadrupole-dipole interactions at the temperatures of 195°K and 476°K. The solid line represents the dipole-dipole contribution while the broken lines represent the quadrupole-dipole contribution assuming a quadrupole moment of $Q/e=3.43\times 10^{-16}$ cm².

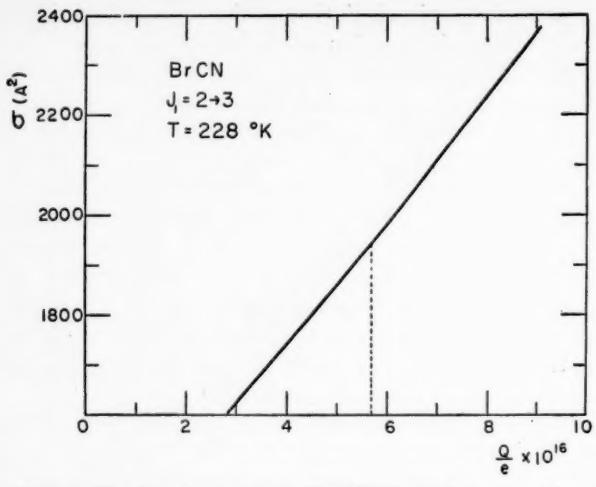

FIG. 6. The low temperature $T=228°K$ total cross section σ for the BrCN $J_1=2-3$ transition as a function of Q/e. The broken line indicates the observed cross section.

the correct cross section σ for the low temperature determines the desired quadrupole moment.

For BrCN the determination of Q in this manner is unambiguous and $Q/e=5.7\times10^{-16}$ cm^2 with a corresponding $\alpha=0.6$. A plot of σ at a temperature of 228°K as a function of Q/e is given in Fig. 6. The high temperature cross section is 1950 A^2.

For OCS the determination of Q is ambiguous with no value of Q giving the correct σ from Eq. (23) for both temperatures. However, a large range of Q gives almost the correct answer reflecting the fact that the quadrupole-dipole interaction *alone* is capable of giving nearly the correct temperature dependence of the pressure broadening of OCS.

The contrast between the results for BrCN and OCS indicates that the comparatively large dipole moment of BrCN makes the dipole-dipole interaction largely responsible for the observed pressure broadening. On the other hand for OCS the results of the temperature dependence calculations indicate that the quadrupole-dipole interaction is most important, quite possibly masking the dipole-dipole interaction completely. However, the results of these calculations do indicate that Q may be considerably larger than determined by Smith and Howard. Thus, if the only interaction considered is the quadrupole-dipole interaction, the value of Q obtained from the self-broadening data of OCS is $Q/e=2.4\times10^{-16}$ cm^2 ($\alpha(Q)=1$) which is about a factor four greater than obtained by Smith and Howard.

However, it must be emphasized that the determination of Q by means of the temperature dependence of the pressure broadening represents a maximum value for Q. Thus still other interactions are probably operative in both the region of high J_2 and low J_2. These interactions, either higher order interactions or higher multipole interactions, would further complicate the general problem, but qualitatively it can be seen that to obtain a comparable partial cross section for high J_2 a smaller Q would be required. This fact taken in conjunction with the underestimate of Smith and Howard probably makes the two theoretical determinations of the quadrupole moments compatible.

CONCLUSIONS

The magnitude of the self-pressure broadening of the linear molecules, OCS and BrCN, can be explained in terms of the first order dipole-dipole interaction by means of Anderson's general theory. The temperature dependence of the pressure broadening cannot be satisfactorily accounted for on the basis of the first order dipole-dipole interaction. In the case of BrCN it is possible to obtain the correct temperature dependence of the pressure broadening by including the quadrupole-dipole interaction while assigning a quadrupole moment $Q/e=5.7\times10^{-16}$ cm^2. However, in the case of OCS the ambiguity of the results indicates that there is effective competition between the two interactions and that very possibly the predominant effect is the result of the quadrupole-dipole interaction.‡

In any event it seems clear that the pressure broadening can serve as a very useful tool in the investigation of intermolecular forces. It is hoped that other investigations will allow a further separation of the effects of the dipole-dipole and quadrupole-dipole interactions.

The authors would like to acknowledge helpful discussions with Dr. R. F. Jackson in the course of this work.

‡ *Note added in proof.*—This conclusion applies only to low J transitions. The experimental observation of a marked increase in the cross section at high J (reference 5, also R. S. Anderson, private communication) indicates that for high J transitions the predominant interaction is the dipole-dipole interaction.

Letters to the Editor

THIS section will accept reports of new work, provided these are terse and contain few figures, and especially few half-tone cuts. The Editorial Board will not hold itself responsible for opinions expressed by the correspondents. Contributions to this section should not exceed 600 words in length and must reach the office of the Editor not later than the 15th of the second month preceding that of the issue in which the Letter is to appear. No proof will be sent to the authors. A publication charge of $10.00 per Letter is made which, when honored, will entitle the Institution to 100 free reprints.

Infrared Investigation of the Benzene-Chlorine Molecular Complex

J. COLLIN AND L. D'OR
Institut de Chimie Générale, Université de Liège (Belgium)
(Received December 3, 1954)

THE charge-transfer theory of molecular complexes, and in particular, of the complexes between benzene and halogens, as proposed by R. S. Mulliken,[1] gives an excellent interpretation of their properties.

In particular, the appearance of a specific absorption of the complex in the near ultraviolet region, its intensity, the relation between its position in the wavelength scale, and the ionization potential of the electron donor (here the benzene),[2] as well as the polar character of this complex formed by the association of nonpolar molecules,[3] are easily explained on the basis of this theory.

Neither experimental facts, nor theoretical considerations now available are sufficient to decide with certainty what is the actual geometric organization of the complex. In the case of benzene and halogens, several arrangements may be considered.

The existence of an electric moment in the complex is compatible as well with those models where the halogen molecule is parallel to the benzene-molecule plane as with those models where the axis is perpendicular to the plane. (These two types of organization seem to be the more probable.)

However, in given relative positions of benzene and halogen molecules, the charge transfer should let appear an electric moment in the halogen molecule, while in other positions, the charge repartition in the halogen molecule would remain symmetrical with respect to the symmetry plane perpendicular to the nuclear axis. In the first case, and only in that one case, could the halogen molecule absorb infrared radiations.

It is thus not excluded that an infrared absorption band would appear for the complex, which is not found for pure benzene or for the halogen itself.

As the dative function weight in the wave function of the complex is small, the frequency corresponding to the maximum of that band must be very near the fundamental vibration frequency of the halogen molecule; on another side, the electron being transferred to a anti-bonding orbital of this molecule, the stretching strength between the two halogen atoms must be reduced in the complex, that is the frequency must be lowered with respect to that of the normal molecule.

We have studied the infrared absorption of the benzene-halogen complexes.

With our equipment, we could not reach the region of the fundamental frequency of iodine. We therefore studied only the bromine and chlorine cases. The case of bromine itself is not very favorable because of the water vapor absorption in the region of 320 cm^{-1}.

On the contrary, for chlorine, we could make evident an indisputable absorption characteristic of the benzene-chlorine complex, of which the maximum is found at 526 cm^{-1} while the fundamental frequency of chlorine is found at 557 cm^{-1}. (See Fig. 1.)

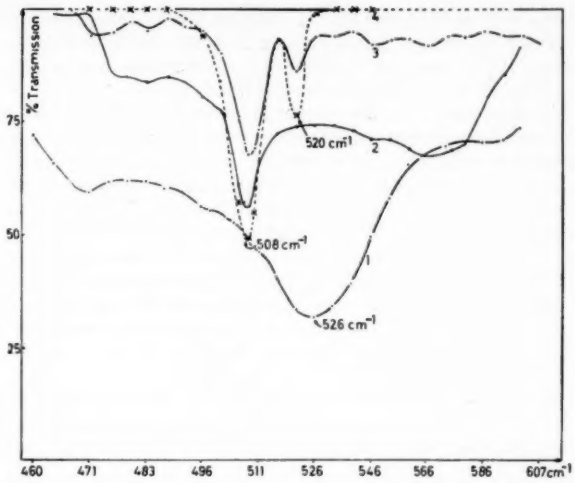

FIG. 1. Infrared absorption. Curve 1°: Freshly prepared solution of Cl_2 in benzene. Curve 2°: Same sample as 1°, but after outgassing of Cl_2 by pumping. Curve 3°: Solid residue of evaporation of sample 2°. Curve 4°: Pure γ-hexachlorocyclohexane crystals.

The enthalpy of formation of the benzene-chlorine complex is not known; it is probably of the same order of magnitude as that of the benzene-iodine complex, that is, about one kilocalorie.[4] The experimental lowering of frequency is well of the order of magnitude one would expect on the basis of such an association energy.

Thus it seems that the absorption at 526 cm^{-1} is characteristic for the chlorine molecule when engaged in the complex.

The existence of a disymmetrical polarization of Cl_2, responsible for this absorption, leads to the conclusion that the chlorine-molecule axis in the complex, is not parallel to the benzene plane and must be oriented in a nonsymmetrical way with respect to that plane.

The broadness of the 526 cm^{-1} absorption band could be the consequence of thermal motion bearing on the distance between the two constituants or on their relative orientation.

We express our thanks to Dr. P. Tarte for his assistance in the experimental part of this work.

[1] R. S. Mulliken, J. Am. Chem. Soc. **72**, 600 (1950); **74**, 811 (1952); J. Phys. Chem. **56**, 801 (1952); J. chim. phys. **51**, 341 (1954).
[2] McConnell, Ham, and Platt, J. Chem. Phys. **21**, 66 (1953); J. Collin, Bull. soc. roy. sci. Liège (November, 1954).
[3] F. Fairbrother, Nature **160**, 87 (1947).
[4] Hartley and Skinner, Trans. Faraday Soc. **46**, 621 (1950).

Molecular Compounds and Their Spectra. V. Orientation in Molecular Complexes

R. S. MULLIKEN
University of Chicago, Chicago 37, Illinois
(Received December 28, 1954)

THE discovery of a strong infrared band at 526 cm^{-1} in solutions of Cl_2 in Bz (benzene)[1] is of great interest: (1) it furnishes new evidence for the reality of benzene-halogen complexes and for the charge-transfer theory of their structure; (2) it gives evidence about their geometry.

The reality of the loose iodine complexes of Bz and its methyl derivatives has been questioned[2] because of the smallness of the observed changes in the infrared spectrum of the aromatic component. However, one would scarcely have expected large effects in the latter if, as has been supposed,[3] its donor action is spread over the six tightly bound ring carbon atoms. A much larger effect was to be expected on the binding in the halogen component, whose acceptor action should be localized in the already rather loose bond between the two halogen atoms. The reduction of the

Cl—Cl frequency in the $Bz \cdot Cl_2$ complex, from 557 cm^{-1} for free Cl_2 down to 526 cm^{-1}, harmonizes with the theory for a loose charge-transfer complex in which the accepted electron goes into an antibonding MO (molecular orbital) of the acceptor.[3]

The fact that the Cl_2 frequency is strongly infrared-active agrees with the charge-transfer theory (and seems not reasonably explainable otherwise) provided the Cl_2 molecule is unsymmetrically oriented. An unsymmetrical orientation, while incompatible with the symmetrical "resting" model R (halogen axis parallel to Bz plane with Cl_2 center on Bz sixfold axis) earlier[3] considered probable, is not unreasonable. In view of the new evidence, an "oblique" model O,[3] or perhaps an unsymmetrical R model, now seems likely. For example, one Cl atom might be above one C—C bond, the other above the middle of the ring, or, possibly, outside the ring. The axial model A (Cl_2 axis coincident with Bz sixfold axis) remains very improbable.

The present occasion seems suitable for detailing some considerations mentioned[4] but not stressed earlier. In a charge-transfer complex between an electron donor D and acceptor A, with

$$\psi \approx a\psi(D,A)+\Sigma_i\, b_i\psi_i(D^+-A^-)+\cdots,$$

there should in general be *many* dative (D^+-A^-) terms, but it is plausible that usually the lowest energy dative term may be predominant. In this event, a simple "orientation principle" follows.[5] However, the simplification is justified only if the matrix element for resonance between the no-bond (D,A) and dative structures falls sharply for the more highly excited dative structures. Although there seems to be empirical evidence and perhaps some theoretical basis for such a simplification, it is reasonable to expect exceptions, partial or complete.

To illustrate, let us consider the ether-halogen complexes. Here[3] (assuming still that only the maximum electron affinity of the acceptor is involved) the halogen molecule axis should stand

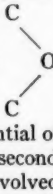

perpendicular to the O plane if only the minimum (first lone pair) ionization potential of the O atom mattered. It should lie *in* the plane if only the second lone pair mattered, and *oblique* to the plane if both are involved. An example of the latter case apparently occurs in the dioxane-bromine *solid* complex,[6] where each Br-Br is reported to lie collinearly between O atoms of two adjacent dioxane molecules. The partial donor activation of the second lone pair is evidently favored here by the cooperation of *two* O atoms as donors toward each Br_2. As expected, the Br-Br distance is found slightly greater than in free Br_2.

The unsymmetrical location of the Cl_2 in $Bz \cdot Cl_2$ similarly may be attributed to partial charge transfer from more than one MO of Bz and/or into more than one MO of Cl_2^-. Further work on related complexes should be extremely interesting.

[1] J. Collin and L. D'Or, J. Chem. Phys. **23**, 397 (1955).
[2] Ham, Rees, and Walsh, J. Chem. Phys. **20**, 1336 (1952). See also Glusker, Thompson, and Mulliken, J. Chem. Phys. **21**, 1407 (1953), and Haller, Jura, and Pimentel, J. Chem. Phys. **22**, 720 (1954).
[3] R. S. Mulliken, J. Am. Chem. Soc. **74**, 811 (1952).
[4] Reference 3, footnotes 11 and 34.
[5] Compare reference 3 and R. S. Mulliken, J. chim. phys. **51**, 341 (1954).
[6] O. Hassel and J. Hvoslef, Acta Chem. Scand. **8**, 873 (1954).

Erratum: A Quantum-Mechanical Equation of Reaction Rates

[J. Chem. Phys. **22**, 1790 (1954)]

IWAO YASUMORI AND KENJI FUEKI
Laboratory of Physical Chemistry, Tokyo Institute of Technology, Ookayama, Meguro-ku, Tokyo, Japan

THE following corrections should be made: The first term in Eq. (1) should be $-(\hbar^2/2\mu)(\partial^2/\partial r^2)$; the Eckart potential should be $E_c/\cosh^2(\pi r/l)$ and $E_c<2h\nu_0$ in the footnote 5.

On the Dependence of the Constants in the Curie-Weiss Law on Exchange

C. M. HERZFELD
U. S. Naval Research Laboratory, Washington, D. C.
(Received December 16, 1954)

THE temperature dependence of the magnetic susceptibility of many paramagnetic compounds may be represented[1] by

$$\chi = C/T^+$$

over a considerable temperature range, where C and Δ are constants and T is the temperature. Several effects contribute to Δ, notably the perturbation of the paramagnetic ions by crystal electric fields,[2] and (if Δ is positive) antiferromagnetic exchange.[3] The theories for antiferromagnetic exchange assume generally that C is independent of exchange, provided T is larger than the antiferromagnetic transition temperature.

In order to investigate the dependence of Δ on the concentration of paramagnetic ions several authors have studied the magnetic susceptibility of paramagnetic compounds having large Δ, in solid solution with isomorphous diamagnetic compounds over a wide range of temperatures. These studies have given an indication of the dependence of exchange between ions on their distance.

It is instructive to analyze these results to see if C is affected by exchange, i.e. whether it depends on the concentration of paramagnetic ions. For this purpose we have assembled published data for the compounds listed in Table I. These data were converted to

TABLE I. Compounds for which dependence of C on exchange was studied.

Compound	C_e	Δ_e	Electron configuration	Diluent	Reference
MnF_2	4.47	97	$3d^5$	ZnF_2	a
UO_2	1.21	208	?	ThO_2	b
UO_2	1.28	233	?	ThO_2	c
UF_4	1.36	102	?	ThF_4	d
PuF_4	0.77	125	$5f^4$	ThF_4	e

[a] Corliss, Delabarre, and Elliott, J. Chem. Phys. **18**, 1256 (1950).
[b] E. Slowinski and N. Elliott, Acta Cryst. **5**, 768 (1952).
[c] J. K. Dawson and M. W. Lister, J. Chem. Soc. 5041 (1952).
[d] J. K. Dawson, J. Chem. Soc. 1185 (1952).
[e] J. K. Dawson, J. Chem. Soc. 1882 (1952).

C as function of concentration and to Δ as function of concentration, and plotted in Fig. 1 as C/C_e *versus* Δ/Δ_e, where C_e and Δ_e are the values of C and Δ for the pure paramagnetic compound. This representation makes it possible to compare the effect for systems whose C and Δ vary widely from one another.

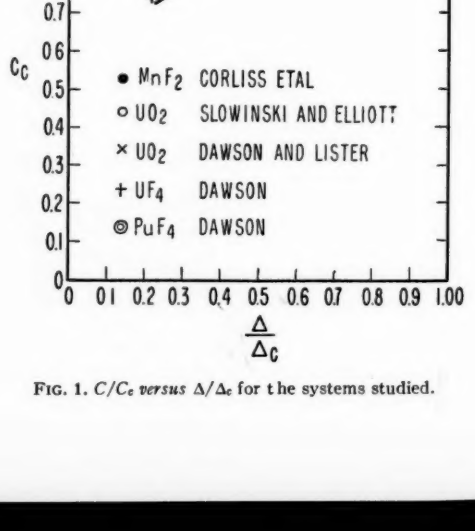

FIG. 1. C/C_e *versus* Δ/Δ_e for the systems studied.

The variation of C with Δ gives a more direct indication of the effect of exchange on C than the variation of C with concentration, since the former is less affected by inhomogeneities in the solid solution than the latter. This assertion is supported by the fact that the points in plots of C *versus* Δ scatter much less than the points in plots of C *versus* concentration.

Several published results have been excluded from our comparison because their points of C/C_c *versus* Δ/Δ_c scatter excessively.

The comparison of five studies on four systems does not justify the drawing of detailed conclusions. The following does, however, appear: (1) It is in general not correct to assume that C does not depend on exchange. (2) It seems that C is nearly independent of exchange when the orbital angular momentum of the paramagnetic ion is only slightly quenched (as in Pu^{+4}) or when it is nearly zero for the free ion (as in Mn^{++}).

[1] J. H. Van Vleck, *Electric and Magnetic Susceptibilities* (Oxford University Press, New York, 1932).
[2] W. G. Penney and R. Schlapp, Phys. Rev. **41**, 194 (1932) and R. Schlapp and W. G. Penney, Phys. Rev. **42**, 666 (1932).
[3] J. H. Van Vleck, J. Chem. Phys. **9**, 85 (1941); P. W. Anderson, Phys. Rev. **79**, 705 (1950); and J. S. Smart, Phys. Rev. **86**, 968 (1952).

to below unity, but it seems that any analysis of the optical problem involved must include in addition to reabsorption corrections, corrections for fluorescence resulting from the internal absorption of primary fluorescence. Because absorption and fluorescence bands do not overlap significantly in rigid glass solutions at 77°K, our experiments were free of this complication. One of us is presently engaged in the effort to estimate the magnitudes of these secondary effects for systems in which they can be expected. The quantum values of Umberger and La Mer,[5] and of Forster and Livingston,[6] do not require a correction for the refraction effect.

We acknowledge also Dr. W. Metcalf's recognition of the error in our article although one of us had become aware of it before his communication arrived.

* Now at Department of Chemistry, Oklahoma Agricultural and Mechanical College, Stillwater, Oklahoma.
[1] E. J. Bowen and A. H. Williams, Trans. Faraday Soc. **35**, 765 (1939).
[2] S. I. Vavilov, Z. Physik **22**, 266 (1924).
[3] H. Hellstrom, Arkiv Kemi, Mineral. Geol. **12A**, 17 (1937).
[4] I. C. Ghosh and S. B. Sen-Gupta, Z. physik. Chem. **B41**, 117 (1938).
[5] J. Umberger and V. K. La Mer, J. Am. Chem. Soc. **67**, 1099 (1945).
[6] L. S. Forster and R. Livingston, J. Chem. Phys. **20**, 1315 (1952).

Errata: Absolute Quantum Efficiencies of Luminescence of Organic Molecules in Solid Solution

[J. Chem. Phys. **20**, 829 (1952)]

EARL H. GILMORE,* GEORGE E. GIBSON, AND DONALD S. MCCLURE
Department of Chemistry and Chemical Engineering, University of California, Berkeley, California

THE correction for the ratio of the apparent solid angle to the actual solid angle due to the passage of the luminescence emission from a denser to a rarer optical medium was incorrectly calculated in the above-named article. This correction factor was given for a 45° angle of observation of the specimens as $(2n^2-1)^{-\frac{1}{2}}$ in which n is the refractive index in the denser medium referred to air as unity, which is the rarer medium.

A reconsideration of the geometry of the situation shows that this correction factor for an arbitrary value of the angle of observation, ϕ, from the normal should be $I(\phi,\nu)=I_\nu n^{-1}\cos\phi\,(n^2-\sin^2\phi)^{-\frac{1}{2}}$ which gives $n^{-1}\,(2n^2-1)^{-\frac{1}{2}}$ for $\phi=\pi/4$.

Such a correction will have the effect of increasing the quantum yields of the various luminescences listed in Table II, page 835 by the following factors: benzophenone, 1.43; acetophenone, 1.44; acetone, 1.43; benzene phosphorescence, 1.44-fluorescence, 1.47; fluorobenzene, 1.47; chlorobenzene, 1.43; bromobenzene, 1.42; naphthalene phosphorescence, 1.42-fluorescence, 1.45; triphenylene phosphorescence, 1.42-fluorescence, 1.44. The error has an insignificant effect on the quantities listed in Table III. The corrected lifetime in Table IV should read as follows:

Compound	Corrected lifetime sec
Benzophenone	0.008
Acetophenone	0.013
Acetone	0.014
Benzene	21.0
Chlorobenzene	0.007
Naphthalene	11.0
Triphenylene	29.0

It is to be noted that, with this correction, our quantum yield values for the fluorescence of both benzene and naphthlene are considerably greater than those obtained by Bowen and Williams for liquid solutions.[1]

Several workers who measured fluorescence yield values for solutions of sodium fluorescein have not included this correction.[2-4] For observations along the direction normal to the fluorescing surface this correction requires that their quantum yield values be multiplied by n^2 (about 1.75 for water). Their quantum yield values would thereby be raised considerably above unity. It is not clear just what compensating error may have reduced their values

Absorption Spectra of Lanthanide and Actinide Ions

CHR. KLIXBÜLL JØRGENSEN
Chemistry Department A, Technical University of Denmark, Copenhagen, Denmark
(Received August 16, 1954)

THE narrow absorption bands of lanthanide and actinide ions are due to transitions between states which are equivalent to the states of the free ion in vacuo. In the case of two effective f-electrons as exemplified by trivalent praseodymium[1] and thulium[2] it has been possible to identify the transitions and assign quantum numbers to the excited states, while the ground state is invariable. Recently, Satten[3] interpreted the neodymium spectrum and applied Condon and Shortley's theory[4] to this f^3 system. The ratio between the parameters of electrostatic interaction F_6/F_2 is erroneously given[3] to be <0.00306, while the condition really is <0.0306. If F_6 is given not negligible values, the weak bands of Nd^{+++} seem better in accordance with theory, while the strong bands still are identified as the quartet-transitions. If $F_6=0.02F_2$ and $F_4=0.2F_2$, it is nearly certain that the weak band groups at 6250, 4710, and 4620 A correspond to transitions to ^2H, ^2G, and ^2K, respectively. The single band at 4275 A is presumably due to $^2P_{\frac{1}{2}}$.

In the actinides, Gruen[5] has extrapolated the Condon-Shortley parameters for NpO_2^+ and PuO_2^{++} from the f^2 system Th^{++}, known from atomic spectroscopy.[6,7] It can be questioned if the electrostatic interaction is proportional to the atomic number minus a large shielding constant (34 in the lanthanides[3] and 58 in the actinide ions[5]). Thus,[1] F_2 is 232 cm^{-1} in Pr^{+++}, but only 93 cm^{-1} in La^+. The isoelectronic species Np^{+++} and Pu^{+4} have absorption bands[8] which are nearly biuniquely corresponding, with the wave numbers 19 percent higher in Pu^{+4} than in Np^{+3}. The strong-shielding theory would give only three percent difference, while of course the increased Lande factor ζ is also important for the evolution of intermediate coupling. The electrostatic interaction seems nevertheless to be roughly proportional to $z+1$, where z is the external charge of the ion. This can be connected with the behaviour of the outer electrons, i.e., the ionic radius, which is strongly dependent of z.

The absorption spectra of the actinide ions can also be used for estimate of the energy difference between $5f$- and $6d$-electrons. Transitions $f^n\rightarrow f^{n-1}d$ are not forbidden as free dipole radiation and have correspondingly high intensity as found in the ultraviolet bands of Ce^{+++}. These bands must of course not be confused with the molecular spectra, due to internal electron transfer, found e.g. in the chlorocomplexes of U^{+4}, Pu^{+4}, Fe^{+3}, Cu^{+2}, Ir^{+4}

with decreasing wave number by increasing ease of the redox process to the next lower oxidation state. The actinide hypothesis of Seaborg[8] seems to be strongly supported by the absence of such strong bands in uranium (IV) aquo ions over 2400 A. Papers on the spectra of U^{+3}, U^{+4} and other actinide ions will be published elsewhere. The strong deviations from Russell-Saunders coupling intermix in some cases the quantum states with same J completely. This may explain anomalous intensity relations, as found in Am^{+++}. The interaction between different electron configuration causes slight deviations from the Condon-Shortley theory.

[1] F. H. Spedding, Phys. Rev. **58**, 255 (1940).
[2] H. Bethe and F. H. Spedding, Phys. Rev. **52**, 454 (1937).
[3] R. A. Satten, J. Chem. Phys. **21**, 637 (1953).
[4] E. U. Condon and G. H. Shortley, *The Theory of Atomic Spectra* (Cambridge University Press, Cambridge, England, 1953).
[5] D. M. Gruen, J. Chem. Phys. **20**, 1818 (1952).
[6] P. F. A. Klinkenberg, Physica **16**, 618 (1950).
[7] G. Racah, Physica **16**, 651 (1950).
[8] Seaborg, Katz, and Manning, *The Transuranium Elements*, Natl. Nuclear Energy Series, Vol. 14 B, (1947).

Reply to Jørgensen's Letter, Absorption Spectra of Lanthanite and Actinide Ions

ROBERT A. SATTEN
University of California, Los Angeles, California
(Received October 13, 1954)

JØRGENSEN is correct in pointing out in the accompanying letter[1] that the radial integrals F_6 and F_2 satisfy $F_6/F_2<0.0306$ instead of <0.00306 as reported.[2] However, the ratio *was* correctly calculated and reported in the form $F_6/F_2<225/7361.64$, the error being made in the placement of the decimal point upon division. Furthermore, no conclusion of the paper is affected. The only use made of this inequality was, along with the one for F_4/F_2, to show that the *set* of F_k's used by Lange[3] for the Pr^{+++} spectrum must be incorrect. This conclusion is still true since Lange's assignments lead to a value of 0.606 for the ratio F_4/F_2, which is about three times too large. This ratio is the one to which the energy calculations are the most sensitive.

The values of the F_k ratios which I used for the calculations of the doublet levels were chosen to agree with the assignments of Condon and Shortley[4] for the $4f^2$ configuration of the La II spectrum. These ratios were also used by Spedding[5] for the Pr^{+++} spectrum. Although it was realized and stated at the time that the F_4/F_2 ratio of Condon and Shortley was too large, it was regarded as too uncertain a procedure at this stage to modify it or to attempt to adjust the F_k integrals to agree with doublet assignments to the Nd^{+++} spectrum, for this adjustment can be made in more than one way within the limits of accuracy imposed by the use of a Russell-Saunders model for the Nd ion. One can expect the Russell-Saunders model to be only a rough approximation because of the relatively strong spin-orbit interaction as well as because of the effect of the strong crystalline electric field on those $4f^3$ free ion states which are very close together. The influence of the latter in a particular case is discussed in the next to last paragraph of this letter.

To attempt to adjust F_k values or ratios on the basis of an empirical fit to the doublet states of the Nd^{+++} spectrum when the quantum number assignments are largely uncertain is thus not easy to do correctly. The quartet states, however, satisfy relations which are independent of the F_k values so that in these assignments, or at least in some of them, one can hope to be correct. It is for this reason that no doublet assignments were made except in one case ($^2D_{\frac{1}{2}}$) where an observed level occured in the midst of a wide region in which no quartet levels were predicted. Even this doublet assignment is questionable.

One can definitely say, however, that the F_4/F_2 ratio will *not* equal its limiting value as assumed by Jørgensen, since this equality would imply that the square of the radial part of the $4f$ one-electron wave function is a delta function, which of course is very far from the case. The greater the spread of the $4f$ radial wave function for a given position of its maximum value (roughly) the smaller the F_k/F_k, $(k'>k)$ ratios will be. Furthermore, it is impossible, as Jørgensen does, to choose the limiting value of F_4/F_2 without at the same time choosing the limiting value of F_6/F_2. Thus while Jørgensen may turn out to be correct or partially correct in interpreting the 6250, 4710, and 4620 A groups as ^2H, ^2G, and ^2K, there seems to be at present no compelling reason to single out these particular interpretations.

The case of the 4275 A group involving only a single upper level is probably an example of a $^2P_{\frac{1}{2}}$ level, as Jørgensen says, strongly perturbed by some other state.[2] The perturbation is most likely to be the result of the interaction with another of the $4f^3$ states of the free ion which is very close to the $^2P_{\frac{1}{2}}$ level. This perturbation is a result of the mixing of states due to the strong crystalline electric field. The evidence in part for this explanation is that the 4275 A group has a higher energy than can result from any assignment of the F_k or ζ integrals even in intermediate coupling as the spin-orbit interaction would not be nearly large enough even if in the right direction and configuration interaction would most likely push the level to even lower energies. In agreement with the latter we note that the sharp absorption line at 4273 A is so sharp even at room temperatures that it is very unlikely that much contribution to the wave function of its upper level comes from outer electronic configurations. If this argument is a valid one, the transition is probably largely magnetic dipole and the perturbing state is $^2G_{9/2}$.

I should also like to point out that in reference 2 there is an obvious misprint in Table I. The expression for ^2L should begin with $3F_0$ and not $3F_2$. The F_2 term is absent.

[1] C. K. Jørgensen, J. Chem. Phys., **23**, 399 (1955).
[2] R. A. Satten, J. Chem. Phys. **21**, 637 (1953).
[3] H. Lange, Ann. Physik **31**, 609 (1938).
[4] E. U. Condon and G. H. Shortley, *The Theory of Atomic Spectra* (Cambridge University Press, Cambridge, England).
[5] F. Spedding, Phys. Rev. **58**, 255 (1940).

Excitation of Molecules in the Beta Decay of a Constituent Atom*

H. M. SCHWARTZ
Department of Physics, University of Arkansas, Fayetteville, Arkansas
(Received November 1, 1954)

ATOMIC excitation in beta decay has been studied theoretically.[1] This report summarizes initial results for the corresponding molecular problem.[2]

By sudden perturbation theory, the probability, P_{AB}, for a molecular transition $A\rightarrow B$ to accompany a radioactive process within the molecule, is

$$\left|\int \psi_B^{(2)*} \exp(i\mathbf{q}\cdot\mathbf{x}_1/\hbar)\psi_A^{(1)} d\tau\right|^2, \tag{1}$$

where $\mathbf{x}_1$=position vector of decaying nucleus and $\mathbf{q}$=its recoil momentum. With the Born-Oppenheimer approximation for the ψ and a Franck-Condon type of evaluation, this is

$$\begin{aligned} &P_{AB}=P_{\alpha\beta}P_{ab}, \quad P_{\alpha\beta}=\left|\int \varphi_\beta^{(2)*}(\xi;\bar{x})\varphi_\alpha^{(1)}(\xi;\bar{x})d\xi\right|^2, \\ &P_{ab}\equiv P_{ab}(\alpha,\beta;\mathbf{q})=\left|\int \chi_{b,\beta}^{(2)*}(x)\exp(i\mathbf{q}\cdot\mathbf{x}_1/\hbar)\chi_{a,\alpha}^{(1)}(x)dx\right|^2, \end{aligned} \tag{2}$$

where ξ, x symbolize the set of electronic and nuclear coordinates respectively. The completeness theorem for the χ yields $\Sigma_b P_{ab}=1$ with the consequent obvious interpretation of the $P_{\alpha\beta}$ and P_{ab} as absolute and relative probabilities respectively.

For polyatomic molecules the P_{ab} can be evaluated readily in the approximation of separated vibrational motion under Hooke's law forces, when the normal coordinates are known.[3] Comparison of Eq. (2) and the vibrational equation solution,[3] shows that P_{ab} is a product involving for each degree of freedom an integral of the same type as occurs in the diatomic case, discussed below.

When P_{ab} are required to a better approximation and with inclusion of the effect of rotational motion, introduction of relative coordinates $\mathbf{r}_j=\mathbf{x}_j-\mathbf{x}_1$ ($j=2, \cdots, N=$number of nuclei) and elimination of the motion of center of mass, can serve as a suitable starting point. With this transformation, one finds for P_{ab} an expression similar to Eq. (2) with the χ representing solutions of the corresponding wave equations involving only the $\mathbf{r}_j$ and with the exponential factor replaced by

$$\exp(-i\mathbf{q}/\hbar m\cdot\sum_{j=2}^{N} m_j\mathbf{r}_j);\ m=m_1+\cdots+m_n,$$

$$m_i=\text{mass of } i\text{th nucleus.} \quad (3)$$

For diatomic molecules (a, b representing v_i, k_i, M_i ($i=1, 2$) respectively), using relative coordinates, Eqs. (2) and (3) show that one must have $M_1=M_2$ and that

$$P_{ab}(\alpha,\beta;\mathbf{q})=\left|\int_0^\pi d\theta\,\sin\theta\Theta k_2 M_1(\theta)\Theta k_1 M_1(\theta) J_{v_1k_1,v_2k_2}(\theta;\mathbf{q})\right|^2$$

$$J_{v_1k_1;\,v_2k_2}(\theta;\mathbf{q})=\int_0^\infty dr R_{v_2k_2}^{(2)}(r)\exp(-ikr\cos\theta)R_{v_1k_1}(r), \quad (4)$$

$$k=\frac{qm_2}{\hbar m}.$$

The J can be readily evaluated in the Hooke's law potential approximation, by the method of Hermite polynomial generating function.[4]

The estimate of the electronic transition probabilities $P_{\alpha\beta}$ involves essentially the difficulties encountered in the corresponding spectroscopic questions.[5] A beginning can be made by considering the two extremes: (1) the lightest molecules for which relatively accurate wave functions are known, and (2) heavy molecules for which a perturbation method can be used.

The most accurate wave functions (1) are those of James and Coolidge[6] for H_2, and that of Toh[7] for the ground state of HHe^+ at the equilibrium value of r, $\bar{r}=1.346a_0$. By following the method of integration outlined in reference 6, the value 0.93 was found for $P_{\alpha\beta}(\bar{r})$, α, β referring to the ground states.[8]

For molecules (2), since the change of potential resulting from the change of nuclear charge is small relative to the total potential, one obtains by standard perturbation procedure the following first order approximations

$$\int\varphi_\beta^{(2)*}\varphi_\alpha^{(1)}d\xi=\frac{\mp e^2}{W_\beta^{(1)}-W_\alpha^{(1)}}\int\varphi_\beta^{(1)*}\sum_k\frac{1}{|\xi_k-\mathbf{x}_1|}\varphi_\alpha^{(1)}d\xi$$

$$(W_\beta^{(1)}\neq W_\alpha^{(1)})$$

and the same relation with $W_\beta^{(1)}$ replaced by $W_\alpha^{(2)}$ when $\beta=\alpha$, the W referring to the relevant electronic energies. With this formula one can compute $P_{\alpha\beta}$ to practically the same approximation with which the $\varphi_\alpha^{(1)}$ and W_α are known, it being assumed that the φ derive from a variation method. It can be seen also that in many cases particularly simple calculations would be involved when using the molecular orbital method.

The assistance of Veronica C. Fink with the numerical work involved in computing the electronic transition probability for HH^3 is gratefully acknowledged.

* This work is supported in part by the U. S. Atomic Energy Commission.

[1] E. L. Feinberg, J. Phys. (USSR) **4**, 423 (1941); A. Migdal, J. Phys. (USSR) **4**, 449 (1941); H. M. Schwartz, J. Chem. Phys. **21**, 45 (1953); H. Primakoff and F. T. Porter, Phys. Rev. **89**, 930 (1953); and J. S. Levinger, Phys. Rev. **90**, 11 (1953).

[2] This is of particular interest in some hot atom investigations. See for instance, R. R. Edwards and T. H. Davies, Nucleonics, **2**, No. 6, 44 (1948). Also, J. E. Willard, Ann. Rev. Nuclear Sci. **3**, 193 (1953).

[3] See for instance, Pauling and Wilson, *Introduction to Quantum Mechanics* (McGraw-Hill Book Company, Inc., New York, 1935), p. 288f.

[4] Reference 3, p. 80. Results of such calculations will be published at a later date.

[5] See, for instance, R. S. Mulliken and C. A. Rieke, Repts. Progr. Phys. **8**, 231 (1941).

[6] H. M. James and A. S. Coolidge, J. Chem. Phys. **1**, 825 (1933).

[7] S. Toh, Proc. Phys. Math. Soc. Japan **22**, 119 (1940).

[8] M. Cantwell at Washington University, employing less accurate wave functions, has obtained the value 0.7. He has also computed a few of the lowest level P_{ab} for HH^3. (Private communication from Professor H. Primakoff.)

Detonation Waves and the Principle of Minimum Entropy Production

GEORGE H. DUFFEY
Department of Chemistry, South Dakota State College, College Station, South Dakota
(Received December 1, 1954)

RECENTLY the thermodynamics of steady state irreversible processes has been developed.[1–4] Fundamental to this theory is the principle of minimum entropy production. This principle may be stated as follows. When constraints prevent a system from reaching equilibrium, a steady state will be set up in which the rate of entropy production is a minimum consistent with the constraints. This principle can be applied to detonation waves.

Consider a detonation wave in which the steady state has been set up. Choose a coordinate system fixed with respect to the wave. Then one can set up three conservation equations based on the fact that there is no accumulation of mass, momentum, or energy between the shock front and the end of the reaction zone.[5] These equations and the physico-chemical properties of the explosive and its reaction products make up the constraints.

These constraints are not sufficient for calculating the detonation velocity; one additional condition is needed. This is supplied by the principle of minimum entropy production. Following Scorah,[6] one can show that application of this principle leads to the Chapman-Jouguet condition

$$D=W+C. \quad (1)$$

Here W and C are evaluated at the Chapman-Jouguet point (the end of the effective reaction zone). The symbol D is the detonation velocity, W is the particle velocity in a coordinate system fixed in the unreacted explosive, and C is the velocity of sound.

There are two parts in the demonstration. First, one shows that Eq. (1) follows if one assumes that the entropy change per gram of explosive reacting is a minimum. Then, one shows that this condition corresponds to the minimum detonation velocity consistent with the constraints.

Now, alternate derivations of the Chapman-Jouguet principle have been given.[5] These alternate derivations evidently support the principle of minimum entropy production.

[1] I. Prigogine, *Etude Thermodynamique des Phénomènes irréversibles* (Editions Desoer, Liège, 1947).
[2] S. R. de Groot, *Thermodynamics of Irreversible Processes* (Interscience Publishers, Inc., New York, New York, 1951).
[3] K. G. Denbigh, *The Thermodynamics of the Steady State* (Methuen and Company, Ltd., London, 1951).
[4] M. J. Klein and P. H. E. Meijer, Phys. Rev. **96**, 250 (1954).
[5] Eyring, Powell, Duffey, and Parlin, Chem. Revs. **45**, 69 (1949).
[6] R. L. Scorah, J. Chem. Phys. **3**, 425 (1935).

Errata: Free-Electron Network Model for Conjugated Systems. V. Energies and Electron Distributions in the Fe Mo Model and in the LCAO Mo Model

[J. Chem. Phys. **22**, 1878 (1954)]

KLAUS RUEDENBERG
Laboratory of Molecular Structure and Spectra, Department of Physics, The University of Chicago, Chicago 37, Illinois

PAGE 1888, second line before Eq. (4.39):

"when" should read "then."

Page 1893, Footnote 13 should read:

"It should be noted that it is *inadequate* to base the discussion on the finite difference approximation. . . ."

Page 1893, second last line of the page should read:

". . . any conclusion concerning the FE model based on this approximation. . . ."

Exciton Multiplicities

R. E. MERRIFIELD
Chemical Department, Experimental Station, E. I. du Pont de Nemours and Company, Inc., Wilmington 98, Delaware
(Received November 17, 1954)

IT is the purpose of this note to point out some effects of electronic spin on properties of the exciton. The importance of considering spin in this connection has recently been emphasized by Slater,[1] but this feature has been generally neglected in previous treatments.[2,3]

Consider a lattice of N equivalent molecules or ions each in its ground state having two electrons in its highest filled orbital, u_i. [The subscript denotes the unit cell in which the orbital is located. It is assumed that u_i is nondegenerate and that $(u_i|u_j)=\delta_{ij}$.] Then, if only these $2N$ electrons are considered, the determinantal wave function for the ground state of the crystal may be written,

$$\varphi^0=\sigma \text{ Det.}|u_1\alpha(1)\cdots u_n\alpha(2n-1)u_n\beta(2n)\cdots u_N\beta(2N)|, \quad (1)$$

where $\sigma=[(2N)!]^{-\frac{1}{2}}$ and α and β denote positive and negative spin, respectively. Excitation of an electron in the nth unit cell to the orbital u_n' may result in any of the four following wave functions:

$$\begin{aligned}
\varphi_n'(\alpha,\beta)&=\sigma \text{ Det.}|u_1\alpha(1)\cdots u_n'\alpha(2n-1)u_n\beta(2n)\cdots u_N\beta(2N)|\\
\varphi_n'(\beta,\alpha)&=\sigma \text{ Det.}|u_1\alpha(1)\cdots u_n'\beta(2n-1)u_n\alpha(2n)\cdots u_N\beta(2N)|\\
\varphi_n'(\alpha,\alpha)&=\sigma \text{ Det.}|u_1\alpha(1)\cdots u_n'\alpha(2n-1)u_n\alpha(2n)\cdots u_N\beta(2N)|\\
\varphi_n'(\beta,\beta)&=\sigma \text{ Det.}|u_1\alpha(1)\cdots u_n'\beta(2n-1)u_n\beta(2n)\cdots u_N\beta(2N)|.
\end{aligned} \quad (2)$$

In the usual manner functions corresponding to definite multiplicities can be constructed from this set. These are:

$$\text{Singlet:}\quad {}^1\varphi_n'=2^{-\frac{1}{2}}[\varphi_n'(\alpha,\beta)-\varphi_n'(\beta,\alpha)] \quad (3)$$

$$\begin{aligned}
\text{Triplet:}\quad {}^3\varphi_n'&=\varphi_n'(\alpha,\alpha), && M_s=+1\\
&=2^{-\frac{1}{2}}[\varphi_n'(\alpha,\beta)+\varphi_n'(\beta,\alpha)], && M_s=0\\
&=\varphi_n'(\beta,\beta), && M_s=-1.
\end{aligned} \quad (4)$$

Resolution of the degeneracy between states of the same multiplicity but with the excitation localized in different unit cells leads to the usual exciton states,[2]

$${}^M\psi_{\mathbf{k}}=N^{-\frac{1}{2}}\sum_n \exp(i\mathbf{k}\cdot\mathbf{R}_n){}^M\varphi_n', \quad (5)$$

where $\mathbf{R}_n$ is the position of the nth unit cell, M is the multiplicity, and the values of $\mathbf{k}$ range over the points of a single Brillouin zone. The exciton energy is then given in terms of the matrix components of the crystal Hamiltonian, $\mathcal{H}$, between the functions (3) or (4) by the expression,

$${}^ME(\mathbf{k})=({}^M\varphi_n'|\mathcal{H}|{}^M\varphi_n')+\sum_m{}' \exp i\mathbf{k}\cdot(\mathbf{R}_m-\mathbf{R}_n)({}^M\varphi_n'|\mathcal{H}|{}^M\varphi_m'), \quad (6)$$

where Σ' indicates that the term $m=n$ is excluded from the summation. Evaluation of the nondiagonal matrix components appearing in equation (6) gives

$$({}^1\varphi_n'|\mathcal{H}|{}^1\varphi_m')=2\int u_n'^*(1)u_m^*(2)\frac{e^2}{r_{12}}u_n(1)u_m'(2)d\tau \quad (\text{"coulomb"}), \quad (7)$$

$$-\int u_r'^*(1)u_m^*(2)\frac{e^2}{r_{12}}u_m'(1)u_n(2)d\tau \quad (\text{"exchange"}),$$

$$({}^3\varphi_n'|\mathcal{H}|{}^3\varphi_m')=-\int u_n'^*(1)u_m^*(2)\frac{e^2}{r_{12}}u_m'(1)u_n(2)d\tau. \quad (8)$$

The "exchange" integral appearing in Eqs. (7) and (8) depends on the overlap of orbitals centered in different unit cells, and will be very small even for nearest neighbors in most molecular and ionic crystals. However, Heller and Marcus[3] have pointed out that the "coulomb" integral, which appears only in the singlet matrix elements, can have appreciable magnitude under the same conditions as a result of electromagnetic interaction of the virtual dipoles of the transition. Thus, the singlet nondiagonal matrix elements will be at least an order of magnitude greater than the triplet elements which implies that such exciton properties as band width and velocity of propagation will be much greater in the singlet state of the exciton than in the triplet state.

[1] J. C. Slater, Tech. Report No. 6 (M.I.T. Solid State and Molecular Theory Group, April 15, 1954), pp. 3–21.
[2] J. Frenkel, Phys. Rev. **37**, 17 (1931); **37**, 1276 (1931); R. Peierls, Ann. Phys. **13**, 905 (1932).
[3] W. R. Heller and A. Marcus, Phys. Rev. **84**, 809 (1951).

Effect of Turbulence on Incipient Flame Propagation

H. L. OLSEN AND E. L. GAYHART
Applied Physics Laboratory, The Johns Hopkins University, Silver Spring, Maryland*
(Received October 25, 1954)

TURBULENT flame research underway at this Laboratory has produced results of interest to workers in the field of combustion. The experimental techniques have been adapted from those used in laminar flame studies previously reported.[1,2] The accompanying photographs illustrate the phenomena observed. In the lower portion of Fig. 1 there are presented schlieren photographs of two series of spark-ignited flame kernels propagat-

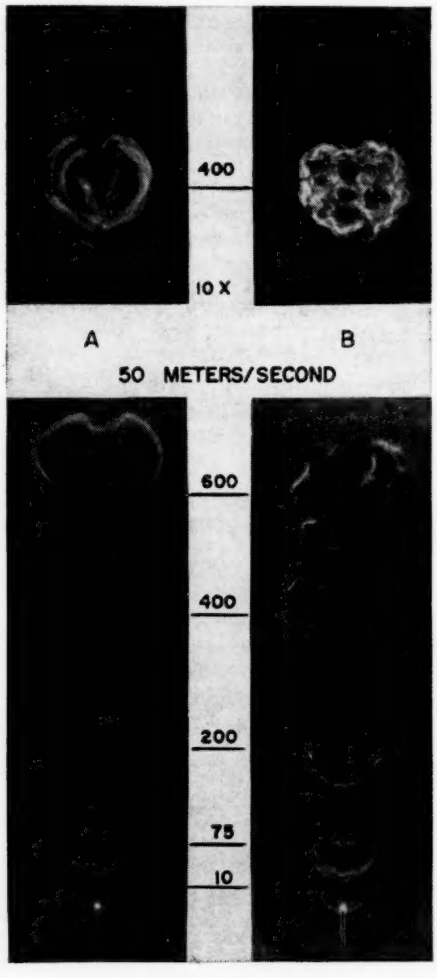

FIG. 1. Effect of isotropic turbulence on free flames. Delay timer in microseconds. Left-hand photographs laminar. Right-hand photographs turbulent.

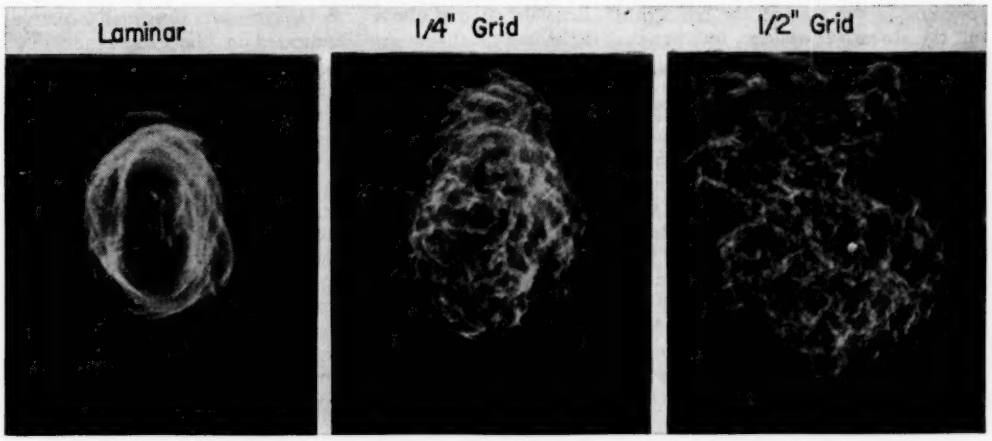

FIG. 2. Effect of grid size on apparent flame propagation rate. Jet velocity 50 m/sec. Delay from ignition 1000 microseconds.

ing in a free combustible gas jet. In each of these series the flame kernels are recorded as multiple exposures on the same film in order to present the sequence as a unit. The delay time from ignition associated with each flame kernel is indicated in microseconds. In the left-hand picture the jet is laminar, whereas, the right-hand jet possesses an isotropic turbulent flow field produced by a precision ten-mesh screen. The obvious toroidal geometry of the kernels produced by the ignition spark has been discussed elsewhere.[1] The effect of the turbulence in distorting the flame fronts is apparent. When several exposures of independent flames at the same delay time are superposed, the result is as shown in the upper photographs of Fig. 1. This procedure averages the flame travel and configuration, thus allowing a comparison of the rate of flame propagation in laminar and in isotropic turbulent flow fields. The comparison shows that this isotropic turbulence produces no apparent increase in the flame propagation rate. Such observation is contrary to the generally accepted idea that flame propagation rate is appreciably increased by turbulence.

That turbulence will increase the apparent flame propagation rate under other conditions is shown by Fig. 2. The increase in rate is associated with (1) an increase in size of the turbulence-inducing grid, and (2) a difference in position of the flame with respect to the grid. For these flames, the grid was nearer to the ignition spark. The ignition was therefore in a region having greater velocity gradients than those which occur in the isotropic turbulence. However, further experimentation has shown that velocity gradients, of appreciably greater magnitude than those involved here, actually quench the flame rather than enhance its propagation rate thus indicating the existence of an optimum gradient for maximum flame spreading.

Even with the larger grid, when the ignition is in the isotropic field, there is no appreciable effect on the apparent flame propagation rate within the time observable in these experiments. It is expected that flames propagating within an isotropic flow field for which the velocity gradients are as great as those encountered in Fig. 2 would show the same apparent increase in flame propagation rate. It is also possible that if flame kernels produced in such isotropic fields as used in Fig. 1 could be observed at considerably later times, an increase in flame propagation rate might be found. Experiments are in progress to test these possibilities.

We wish to acknowledge with thanks the assistance of Professor S. Corrsin, JHU, in defining the experimental conditions necessary to produce isotropic turbulence in our jets and the helpful comments and discussion of Dr. W. G. Berl, Dr. A. A. Westenberg, and Dr. P. Rosen of this laboratory.

*Operating under contract with Bureau of Ordnance, Department of Navy.

[1] Olsen, Gayhart, and Edmonson, J. Appl. Phys. **23**, 1157 (1952).
[2] Olsen, Gayhart, and Edmonson, "Propagation of incipient spark-ignited flames in hydrogen-air and propane-air mixtures," Fourth Symposium International on Combustion 144 (1952).

Thermal Stability of *Ortho*-, *Para*-, and *Meta*-Xylyl Radicals and the Formation of Quinodimethanes*

J. B. FARMER,† D. G. H. MARSDEN,† AND F. P. LOSSING
Division of Pure Chemistry, National Research Council, Ottawa, Canada
(Received December 8, 1954)

IN the course of preparing the *ortho*-, *para*-, and *meta*-xylyl free radicals for ionization potential measurements, some information on their relative stabilities has been obtained. The radicals were formed by pyrolysis of xylyl iodides in a quartz capillary furnace leading to the ionization chamber of a mass spectrometer.[1] At 825°C the xylyl iodides were almost completely decomposed into the corresponding free radicals and iodine atoms, as indicated by the ratios of the peaks at mass 105 (xylyl ion) and mass 232 (xylyl iodide ion) using 50 V electrons.[2] In the case of the *ortho*- and *para*-xylyl radicals the mass 105 peak decreased rapidly with a further increase of temperature above 825°C and was replaced by a peak at mass 104. At 1000°C almost all the *ortho*- and *para*-xylyl radicals were decomposed to form the substance of mass 104.

With *meta*-xylyl radicals the situation was quite different, the radical peak decreasing only slightly from 825°C to 1050°C, and the mass 104 peak becoming appreciable only above 1050°C. No significant amounts of the corrresponding xylenes were formed. Although at the low pressure (10^{-3} mm) in the furnace the reactions must be mainly on the wall, it may still be concluded that the thermal stability of the *meta*-xylyl radical is much greater than that of the *ortho*- and *para*-forms.

Szwarc reported[3,4] that the pyrolysis of *para*-xylene differed from that of *meta*-xylene in that in the former a high polymer was found in the cold trap instead of the expected dimer. This polymer was shown to arise from *para*-quinodimethane, 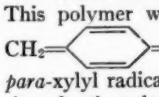 , itself formed by the disproportionation of *para*-xylyl radicals. No polymer was reported in the decomposition of *ortho*-xylene, although a structure for *ortho*-quinodimethane

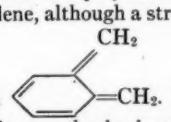

can be written . The absence of polymer might be accounted for on the basis of steric hindrance in the polymerization of this substance. A corresponding structure cannot be written for *meta*-quinodimethane without invoking excited states such as

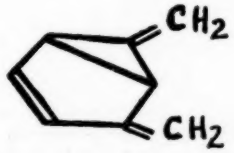

It is reasonable to assume that the increase in the mass 104 peak can be attributed to the formation of a quinodimethane. The low

pressure in the reactor, the temperature dependence, and above all the absence of xylenes, indicate that the quinodimethanes are here formed as products of the thermal decomposition of *ortho*- and *para*-xylyl radicals and not as products of disproportionation as under the conditions prevailing in Szwarc's work. The relative stabilities of the radicals would indicate a considerable reduction the CH_2—H bond dissociation energy in the *ortho*- and *para*-xylyl radicals as compared with that in the *meta*-xylyl radical. This would be the case if the resonance stabilization of *ortho*- and *para*-quinodimethanes were considerably greater than that of the *meta*-quinodimethane. That this is probably so is indicated by the fact that a structure for *meta*-quinodimethane cannot be written without recourse to excited forms.

Calculations of the resonance stabilization energy, although dependent on whether the valence-bond or molecular orbital methods are used[5,6] suggest that the *ortho*- and *para*-quinodimethane structures are stabilized (as compared to the di-radical forms) to a considerably greater extent than is the hypothetical *meta*-quinodimethane. This is in accord with the observed difference in the stability of the radicals as indicated by the behavior of the mass 104 and 105 peaks.

The substance of mass 104 produced from the *meta*-xylyl radical at $T>1050°C$ may result from isomerization of the *meta*-xylyl radical to the *para*- or *ortho*-form, followed by decomposition to *para*- or *ortho*-quinodimethane.

A fuller account of this work will be given in a forthcoming paper on the ionization potentials of the xylyl radicals.

* National Research Council Contribution No. 3469.
† National Research Council Postdoctorate Research Fellow.
[1] J. A. Hipple and D. P. Stevenson, Phys. Rev. **63**, 121 (1943).
[2] F. P. Lossing and A. W. Tickner, J. Chem. Phys. **20**, 907 (1952).
[3] M. Szwarc, J. Chem. Phys. **16**, 128 (1948).
[4] M. Szwarc, Disc. Faraday Soc. **2**, 46 (1947).
[5] F. Seel, Z. physik. Chem. **51**, 229 (1942).
[6] Namiot, Diatkina, and Syrkin, Compt. rend. Acad. Sci. URSS **48**, 267 (1945).

On the Theory of Photographic Process

K. P. Sinha and A. B. Biswas
National Chemical Laboratory of India, Poona-8, India
(Received June 28, 1954)

SEVERAL theories, based more or less on the model of the theory of Gurney and Mott, have been proposed to explain the latent image formation in photographic process.[1] Mitchell's results support the view that, in nonsensitized emulsions, the trapping centers are structural imperfections, such as dislocations and grain boundaries.[2] Artificial sensitization, particularly by sulfur, is of much interest and importance. Stasiw and Teltow[3] and Mitchell[4] postulated the presence of divalent sulfur (S^{--}) anions in the matrix of the emulsion grain, which introduce negative ion vacancies. But the recent trend of views is to regard the role of Schottky defect as unimportant in this mechanism because of its very low concentration at room temperature.

We suggest the existence of a lattice structure, in sulfur sensitized silver halide emulsions, of a kind which leads to a more rational view of the latent image formation mechanism. Thus, during the process of digestion in emulsion making, we picture AgBr and Ag_2S as reacting to form a complex $(Ag_3S)^+Br^-$, whereby the electronic structure of sulfur changes from

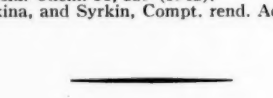

in Ag_2S to

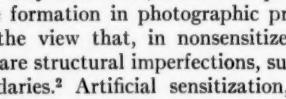

in the complex. That such a complex is indeed formed seems to be indicated by the ionic conductivities of mixtures of AgBr and Ag_2S in water.[5]

The lattice structure of the complex in the dry emulsion, is assumed to be of the $BaTiO_3$ type, as in the perovskite lattice, with Br at the corners, Ag at the face centers, and S in the body center of the cubic lattice. The AgBr lattice, with or without interstitial silver ions, cannot effectively trap electrons at room temperature because of its high dielectric constant. Simpson[6] also suggested on theoretical grounds, that the electron is not bound tightly to an interstitial ion, which thus becomes unimportant for photographic darkening since the electron would wander around until it finds a more stable trap. But the new lattice sites in our postulated structure should be able to act as effective trapping centers because of the lower dielectric constant and the highly localized positively charged center. The force field of this impurity lattice may extend to quite a few lattice positions as in the case of an impurity ion in semiconductors. The strain produced thereby in the neighboring host lattice may cause dislocations and strains producing trapping centers and also resulting in an environment of more mobile ions such as occur in the surface of a crystal. A photoelectron, trapped in such a center, will cause neighboring silver ions to migrate towards the center where on neutralization the latent image is formed.

A further discussion will be published elsewhere.

[1] Fundamental mechanism of photographic sensitivity. (a) Bristol conference (1950); (b) Paris conference (1951); and (c) F. Seitz, Revs. Modern Phys. **23**, 328 (1951).
[2] Hedges and Mitchell, Phil. Mag. (7) **44**, 223, 357 (1953).
[3] O. Stasiw and J. Teltow, Ann. Physik. **40**, 181 (1940).
[4] J. W. Mitchell, Phil. Mag. **40**, 249, 669 (1949).
[5] K. P. Sinha and A. B. Biswas (to be published).
[6] J. H. Simpson, Proc. Roy. Soc. (London) **A197**, 269 (1949).

Symmetry of the Local Crystalline Field about Rare Earth Ions in Octahydrated Sulfate Crystals

R. A. Satten and D. J. Young
University of California, Los Angeles, California
(Received December 3, 1954)

IT was assumed by Penney and Schlapp[1] in their paramagnetic susceptibility calculations that the crystals of rare earth octahydrated sulfates have a cubic local symmetry about the rare earth ion. Spedding, Hamlin, and Nutting[2] reported that their spectroscopic data indicated that the local field is cubic as they found that the $^4I_{9/2}$ ionic ground state in neodymium sulfate is split into only three levels (0, 77, 260 cm^{-1}) by the crystalline electric field instead of five levels as would be the case for lower symmetry fields. Jackson[3] and Krishnan and Mukherji[4] have shown by their paramagnetic susceptibility experiments that neodymium sulfate is magnetically quite anisotropic thus calling for a noncubic local field. Specific heat measurements,[5] being insensitive to higher levels, essentially confirm the 77 cm^{-1} level, but require this level to have a statistical weight twice that of the lowest level, thereby indicating a cubic field. Penney and Kynch[6] surveyed the situation in 1939 and concluded that it was impossible to reconcile the then current interpretations of the absorption spectrum and specific heat data with the magnetic properties.

We have photographed and analyzed the absorption spectrum of $Nd_2(SO_4)_3 \cdot 8H_2O$ crystals, and we find that the $^4I_{9/2}$ ground state of the free ion splits into *five* levels in the crystal at 0, 76, 226, 263, 301 cm^{-1} (good to about ± 1 cm^{-1}). Our analysis was facilitated by concentrating first on the 4300 and 8600 A groups which we know from examining the bromate[7] and other salts involve transitions to only one and two upper levels respectively. The ground splitting thus obtained was then used successfully to obtain the level schemes for more complicated groups of lines, and complete agreement was obtained. The results also check with the observation of the spectrum at liquid helium temperature

wherein only the lowest of the ground levels contributes to the absorption pattern.

Penney and Schlapp showed that a cubic field would result in the upper two of the three cubic levels being each 4-fold degenerate and the lowest one 2-fold. A slight departure from cubic symmetry would then split each of the upper two cubic levels into two close, doubly degenerate levels, each pair being symmetrically located about the original cubic positions. From the separations reported here, it can be seen that the departure from cubic symmetry is not slight.

The local symmetry about the rare earth ion must in fact be one of the six groups C_s, C_2, C_{2h}, C_{2v}, D_2, D_{2h} as the following argument shows. The spectrum of neodymium sulfate shows hardly any dependence on the direction of polarization of the light[8,9] whereas that of praeseodymium sulfate shows a strong dependence.[9] Now the corresponding crystallographic "double" group to each of these six groups as well as to C_1 and C_i has either one two-dimensional or two degenerate one-dimensional irreducible representations, and this is true of no other crystallographic double group. Thus every level of an ion (Nd^{+++}) with an odd number of electrons in such a field would combine with every other level for all polarization directions and for all types of transitions, electric dipole, and quadrupole as well as magnetic dipole. However, for an even number of electrons (Pr^{+++}), the six mentioned "single" groups have more than one irreducible representation (without essential degeneracies) so that there will be selection rules. (Although C_i also has two irreducible representations, the transitions we would observe would connect states of the same parity so that there would be no observed dependence of these lines on the polarization for this case.)

[1] W. G. Penney and R. Schlapp, Phys. Rev. **41**, 194 (1932).
[2] Spedding, Hamlin, and Nutting, J. Chem. Phys. **5**, 191 (1937).
[3] L. C. Jackson, Proc. Roy. Soc. (London) **170A**, 266 (1939).
[4] K. S. Krishnan and A. Mukherji, Trans. Roy. Soc. (London) **A237**, 135 (1938).
[5] Ahlberg, Blanchard, and Lundberg, J. Chem. Phys. **5**, 552 (1937).
[6] W. G. Penney and G. J. Kynch, Proc. Roy. Soc. (London) **170A**, 112 (1939).
[7] R. A. Satten, J. Chem. Phys. **21**, 637 (1953).
[8] R. W. Krueger, thesis, University of California at Los Angeles (1942).
[9] K. S. Krishnan and D. C. Chakrabarty, J. Chem. Phys. **6**, 224 (1938).

Self-Diffusion in Sodium Near the Melting Point*

ROBERT E. MEYER AND NORMAN H. NACHTRIEB
Institute for the Study of Metals, The University of Chicago, Chicago 37, Illinois
(Received December 3, 1954)

SELF-DIFFUSION coefficients for solid sodium in the temperature range 0° to 94.5°C have been reported in this journal.[1] These measurements have now been extended to include the melting point region. Drickamer and Eckert[2] reported that in both polycrystalline and single crystal indium the rate of self-diffusion begins to rise abruptly about one-half degree below the melting point and increases continuously with temperature into the liquid phase. To determine whether a similar "pre-melting" phenomenon occurs in sodium, we have measured the rate of self-diffusion in both states at temperatures to within 0.10°C of the melting point.

Spectrographic examination of the once-distilled metal revealed 0.05 percent potassium, 0.001 percent silicon, and less than 0.001 percent of iron, magnesium, and copper. Its melting point was determined to be 97.91±0.06°C by means of a cooling curve taken in vacuum with a chromel-alumel thermocouple calibrated at the steam point and several other standard thermometric points. The technique used for measurements in the solid has been described.[1] Cylinders of radioactive and ordinary sodium of very coarse grain size (~2 mm diam) were pressure-welded together at liquid nitrogen temperatures and diffusion was allowed to proceed in an oil thermostat which was controlled to ±0.015°C. The composite cylinder was then sectioned in a microtome and the diffusion coefficient calculated in the usual manner. The results of four runs are given in Table I, together with values of D calculated for 94.4° and the melting point from the empirical equation resulting from the earlier study.[1] The newer values are slightly higher, but the agreement is to within the limits of error.

TABLE I. Self-diffusion coefficients in sodium about the melting point.

T (°C)	D_{obs} (cm² sec⁻¹)	D_{calc} (cm² sec⁻¹)[a]
94.4	$1.59\times10^{-7}\pm0.09$	1.46×10^{-7}
97.65	$1.78\times10^{-7}\pm0.54$	
97.73	$1.78\times10^{-7}\pm0.23$	
97.83	$2.16\times10^{-7}\pm0.20$	
97.91 (M.P.)		1.63×10^{-7}
98.0	4.19×10^{-5}	
98.0	4.35×10^{-5}	
98.0	4.14×10^{-5}	
98.6	3.87×10^{-5}	

[a] Calculated from $D=0.242\exp(-10\,450/RT)$. See reference 1.

Diffusion coefficients for the liquid were measured from 98.0° to 226° by the capillary reservoir technique first mentioned by Anderson and Saddington.[3] The results of these runs may be represented by the equation: $D=1.10\times10^{-3}\exp(-2450/RT)$. The values found just above the melting point are given in the lower part of Table I, and deviate only slightly from the value of 4.06×10^{-7} cm² sec⁻¹ calculated for 98.0° by means of this equation. It appears that the transition from the rate of solid state self-diffusion to the rate of liquid state self-diffusion is as discontinuous in sodium as the melting process, itself. A more complete report of self-diffusion in liquid sodium will be submitted later.

* This research was supported in part by contract with the United States Air Force, the sponsoring agency being the Aeronautical Research Laboratory of the Wright Air Development Center, Air Research and Development Command.
[1] Nachtrieb, Catalano, and Weil, J. Chem. Phys. **20**, 1185 (1952).
[2] R. E. Eckert and H. G. Drickamer, J. Chem. Phys. **20**, 13 (1952).
[3] J. S. Anderson and K. Saddington, J. Chem. Soc. (London) **S381** (1949)

Microwave Dispersion of Monosubstituted Benzenes; Evidence for Molecular Resonance Absorption

J. PH. POLEY
Physical Laboratory of the National Defense Research Council, Waalsdorp, the Hague, The Netherlands
(Received November 29, 1954)

SYSTEMATIC investigation of the microwave dispersion of mono-substituted benzenes has revealed discrepancies of sometimes substantial magnitude between the values of the dielectric constant ϵ_∞ constituting the lower limit to the microwave dispersion-region, and the values of the refractive index n^2 in the longwave infrared.

TABLE I.

Substance	Temp. °C	μ^2	n^2	ϵ_∞	$\Delta\epsilon_2$	$\Delta\epsilon_2/\mu^2$
C_6H_5F	21	2.5	2.15	2.30[a]	0.15[a]	0.06[a]
C_6H_5Cl	22	2.9	2.33	2.58	0.25	0.09
C_6H_5Br	22	3.0	2.43	2.64	0.21	0.07
C_6H_5I	21	2.8	2.63	2.83	0.20	0.07
$C_6H_5NO_2$	20	17.6	2.43[a]	4.08	1.65	0.09
C_6H_5CN	21	19.3	2.34	3.82	1.48	0.08

[a] Preliminary value.

Numerical data are given in Table I. The values given for n^2 are determined, either from measurements in the extreme infrared,[1] or by use of the value of n_D^2. The value of n^2 following from this last procedure will be in error for not much more than 1 percent.

The molecules of the liquids investigated can be approximated fairly well by ellipsoids, with a dipole moment which is bound to the longest axis, involving thus a single relaxation time. According to the formal theory of the relaxation, only one dispersion region would be expected for these molecules. Our data, however, show the presence of a second dispersion-region at millimeter wavelengths; actually absorption data corresponding to this new dispersion have been obtained in our measurements at a wavelength of 0.8 cm for nitrobenzene, benzonitrile, and iodobenzene.

The explanation of these discrepancies and this second dispersion-region might be given in terms of the mechanism of molecular rotational oscillation around an equilibrium position. As Pauling[2] has indicated, for polar molecules under influence of directing forces of increasing strength, the possibility exists of a gradual transition from free molecular rotation (in gases) to molecular oscillation around an equilibrium position (in solids). The liquid mono-substituted benzenes might represent condensed phases with intermediate stages of order, as a certain regular arrangement due to steric effects will exist in these substances. For such an intermediate case two absorption regions might be found, the first one corresponding to hindered "orientation" of the molecules (orientation-absorption); the second one due to oscillation of the molecules (resonance absorption). As van Vleck[3] and Fröhlich[4] have shown, the contribution $\Delta\epsilon_2=\epsilon_\infty-n^2$ to the total dielectric constant of a dispersion due to resonance-absorption would be proportional to $N\mu^2/I\nu_0^2$, when dipolar interaction is neglected. (I=moment of inertia, ν_0=resonance frequency of molecular oscillation, N=number of molecules per unit volume.) Now the values of $I\nu_0^2$ and N vary only slightly for the substances investigated, and the variation in the correction for dipolar interaction is only small. When, therefore, the theory of molecular resonance would be applicable to these substances, the value of $\Delta\epsilon_2/\mu^2$ would have to be about constant. The actual constancy of this quantity, given in the last column of the table, is remarkably good, in view of the wide range of μ values. These data represent the evidence for the dipolar origin of the second dispersion region, and support strongly the assumption that this dispersion region is due to molecular resonance.

The corresponding theoretical account for liquids, together with further experimental details will be given in a forthcoming publication.[5]

[1] C. H. Cartwright and J. Errera, Proc. Roy. Soc. (London) **154A**, 138 (1936).
[2] L. Pauling, Phys. Rev. **36**, 430 (1930).
[3] J. H. van Vleck, *Electric and Magnetic Susceptibilities* (Oxford University Press, London, 1932), Chap. III.
[4] H. Fröhlich, *Theory of Dielectrics* (Oxford University Press, London, 1949), Secs. 13 and 17.
[5] J. Ph. Poley, Appl. Sci. Research (to be published).

Crystal Structure of Aluminum Nitride*

G. A. Jeffrey and G. S. Parry†
The University of Pittsburgh, Pittsburgh 13, Pennsylvania
(Received December 6, 1954)

A REEXAMINATION of the crystal structure of AlN, originally determined by Ott,[1] shows that it departs from the ideal wurtzite structure in two respects,

(1) The axial ratio c/a is found to be 1.600 instead of 1.633.

(2) The u parameter, which determines the Al—N separation along the trigonal axis, is 0.385 instead of 0.375 (3/8).

In the ideal wurtzite structure, each atom forms four equal bonds tetrahedrally disposed to atoms of the opposite type. It is therefore possible to regard the crystal structure as built up of a series of interpenetrating regular tetrahedra at the corners of which are atoms of one type only. The height of each tetrahedron is $c/2$ while the length of one side of the base is a, so that the ratio of height to base length of the tetrahedron completely determines the axial ratio c/a, which for a regular tetrahedron is 1.633. The departure of the observed axial ratio from its ideal value is a common feature of wurtzite type binary compounds, and was noted by Ott when he established the structural type of AlN. It shows that there is a compression of the tetrahedra along the c axis which must lead to some distortion of the Al—N bonds from a regular tetrahedral arrangement. Whether this is a distortion in bond length, bond angle, or both cannot be determined from the numerical value of the axial ratio alone, but it must always be such as to preserve trigonal symmetry in the c direction.

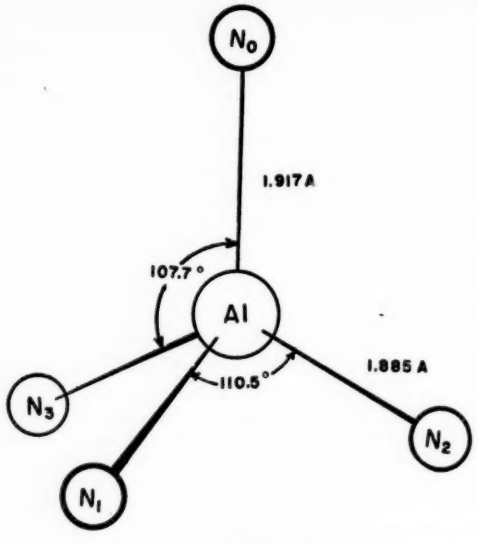

FIG. 1.

The increased value of the u parameter implies that the center of electron density of any one atom is not coincident with the centroid of the tetrahedron formed by its nearest neighbors, but that the atom is displaced along the c axis towards the base of the tetrahedron by about 0.05A. If there is any polar character associated with the AlN linkage, it follows that this displacement will give rise to a permanent dipole moment in the direction of the c axis of the crystal. Other wurtzite structures are now being re-examined, for it is possible that the energetically significant difference between the wurtzite and zinc blende structures lies not in the arrangement of the second nearest neighbors, but in the fact that these displacements are compatible with the symmetry of the former and not the latter.

The distribution of the bond lengths and valence angles in AlN is shown in Fig. 1. The compression of the tetrahedron alone would make $AlN_0<AlN_{1,2,3}$; the change in the u-parameter appears to overcompensate for this, for Δu is twice the shift required to bring the bond lengths back to equality.

The experimental measurement of the spacings and structure amplitudes for the 26 hkl reflections within the range of CuKα radiation was made on a G. E. XRD-3 spectrometer using the powder slab reflection technique. The theoretical structure amplitudes were calculated for the value $u=0.375$ using the Hoerni and Ibers atomic scattering factors[2] for neutral nitrogen and the Viervoll and Ogrim factors[3] for neutral aluminum. This gave a disagreement index of the observed and calculated structure amplitudes of $R=0.058$. Subsequent refinement of the u parameter by the method of difference syntheses, and the introduction of small isotropic temperature factors (B_{Al} 0.26, B_N 0.79, A^{-2}) for the N and Al atoms reduced this value to 0.026. There is evidence that the thermal parameters are anisotropic, with the greater value in the direction of the hexagonal axis. Further experimental measurements are in progress to determine the quantitative extent of this and the possible influence of nonstoichiometry.

* This work was supported by contract with the Office of Ordinance Research.
† Scaife Foundation Fellow.
[1] Ott, Z. Physik **22**, 201 (1924).
[2] Hoerni and Ibers, Acta Cryst. (to be published).
[3] Viervoll and Ogrim, Acta Cryst. **2**, 277 (1949).

Nuclear Quadrupole Resonances of As^{75}

R. G. BARNES,* *Physics Department, University of Delaware, Newark, Delaware*

AND

P. J. BRAY,† *Physics Department, Rensselaer Polytechnic Institute, Troy, New York*

(Received November 22, 1954)

THE As^{75} nuclear quadrupole resonance was first detected and measured in arsenic trioxide.[1] The present letter reports As^{75} resonances in some trihalides and in the triphenyl, and the Br^{81} resonance frequencies for $AsBr_3$. Observed frequencies and signal-to-noise ratios are listed in Table I. Coupling constants are

TABLE I.

Compound	(As^{75}) Mcps	Temp.	S/N	$\alpha°C^{-1}$
$AsCl_3$	78.950±0.030[a]	77°K	5–6	
$AsBr_3$	61.180±0.010	77°K	12	$<10^{-6}$
	61.184±0.002	23°C	5–7	
AsI_3	116.860±0.020	77°K	3	0.25×10^{-4}
	116.193±0.020	28°C	2	
$As(C_6H_5)_3$	98.900±0.010	77°K	3	0.80×10^{-4}[b]
	98.500±0.010	77°K	5	
	97.320±0.010[c]	19.5°C	2–3	
	96.788±0.010[c]	19.5°C	2–3	
	(Br^{81}) Mcps			
$AsBr_3$[d]	173.143±0.015	77°K	10	0.89×10^{-4}
	172.728±0.015	77°K	10	0.95×10^{-4}
	171.480±0.015	77°K	10	0.86×10^{-4}
	169.705±0.015	25°C	7	
	169.036±0.015	25°C	7	
	168.240±0.015	25°C	7	

[a] Attempts to detect this resonance at 193°K have been unsuccessful so that its temperature dependence cannot be given at this time.
[b] Calculated from the average frequency at each temperature.
[c] Two other resonances with frequencies 97.140±0.030 and 96.945±0.030 Mcps may lie between these listed values. Overlapping of superregenerative response patterns obscures the exact situation.
[d] The Br^{79} frequencies have also been measured and are found to check the known ratio of the coupling constants for Br^{81} and Br^{79}.

not given since the asymmetry parameter ϵ in the expression[2] $h\nu=|eQq|(1+\epsilon^2/3)^{\frac{1}{2}}$ for spin $\frac{3}{2}$ nuclei can be evaluated only by Zeeman splitting experiments.

Assuming the resonance frequency to be a linear function of temperature over the range investigated, the temperature coefficients, $\alpha=(1/\nu)d\nu/dT$, have been calculated from the room temperature and liquid nitrogen temperature data and are listed in Table I. The temperature dependences of the arsenic resonances in the normally solid tribromide and triiodide are unusually small. Arsenic triiodide has a layer structure[3] with each arsenic atom linked to six iodine atoms. There is a considerable degree of symmetry about the arsenic atom which may cause the asymmetry parameter to be small. If torsional oscillations of the type treated by Bayer[4] are either limited to small amplitude by multiple linking throughout the plane or confined to take place about the symmetry axis through the arsenic nucleus and perpendicular to the layers, the axial field gradient would be relatively unaffected by the averaging process. These conditions of small ϵ and limited torsional oscillations would lead to an unusually small temperature dependence of the frequency.

Little is known about the structure of other arsenic trihalides. If they form molecules with the arsenic nucleus at the apex of a triangular pyramid, one might expect torsional oscillations about the molecular symmetry axis. Again, the axial electric field gradient would be relatively unaffected by the averaging process, and one would expect the coupling constant eQq to show very little temperature dependence. On the other hand, the field gradient components normal to the symmetry axis would be strongly averaged and the asymmetry parameter ϵ should decrease with increasing temperature. In this case, one might expect a normal temperature dependence of the As^{75} resonance. Since the observed dependence in $AsBr_3$ is very small, probably ϵ is small or the compound does not contain distinct pyramidal molecules.

A check on the ϵ and eQq temperature dependences of these compounds is not possible with the present data. However, such a check is possible in the similar compound $SbCl_3$. A room temperature measurement of the entire $Sb^{121,123}$ spectrum has been made. At 23°C: $(eQq)_{121}=376.970\pm0.10$ Mcps; $(eQq)_{123}=479.714\pm0.14$ Mcps; $\epsilon_{121}{}^2=0.02672$; $\epsilon_{123}{}^2=0.02668$. Comparing these values with data[5] for 83°K shows that the temperature dependence of the coupling constants is $\alpha(eQq)=0.86\times10^{-4}$ °C^{-1}, whereas the temperature dependence of the asymmetry parameter is $\alpha(\epsilon)=6.0\times10^{-4}$ °C^{-1}. The latter quantity is therefore more strongly averaged by the torsional oscillations. That the coupling constants show fairly normal temperature dependence may be a consequence of the crystal structure of $SbCl_3$. The halogen spectrum in this compound shows doublets,[5] indicating two nonequivalent lattice sites for Cl atoms, whereas in $AsBr_3$ the Br spectrum consists of triplets. In AsI_3 the I^{127} spectrum is a single line below 90°C and a triplet above this temperature.[6] The low-frequency I^{127} line in this compound has a very small temperature coefficient.[6] A small temperature coefficient has also been found[7] for the chlorine resonances in $AsCl_3$ over the temperature range from 4°K to 77°K.

Various superregenerative spectrometers were employed in obtaining the data. Sweep frequency modulation was used and the resonances were displayed visually on a cathode-ray oscilloscope. The authors wish to thank F. O. Wooten for assisting with some of the measurements.

* Research supported by the Office of Ordnance Research and the Research Corporation.
† Research supported by a grant from the National Science Foundation and a grant-in-aid from the Rensselaer Polytechnic Institute Research Grants Committee.

[1] H. Krüger and U. Meyer-Berkhout, Z. Physik **132**, 221 (1952).
[2] H. Krüger, Z. Physik **130**, 371 (1951).
[3] D. Heyworth, Phys. Rev. **38**, 351 (1931).
[4] H. Bayer, Z. Physik **130**, 227 (1951).
[5] H. G. Dehmelt and H. Krüger, Z. Physik **130**, 385 (1951).
[6] Kojima, Tsukada, Ogawa, and Shimauchi, J. Chem. Phys. **21**, 2237 (1953).
[7] R. Livingston, J. Phys. Chem. **57**, 496 (1953).

Electrophoretic "Line Spectra"*

ALEXANDER KOLIN
University of Chicago, Chicago, Illinois

(Received December 16, 1954)

IN a previous communication[1] it was shown that proteins can be separated in a solution of varying pH by a current flowing in the direction of increasing pH. By combining the pH gradient with a conductivity gradient, the method is made effective for nonampholytes as well. Ions having no isoelectric points in the given pH range can thus also be concentrated in form of thin lamina and be separated.

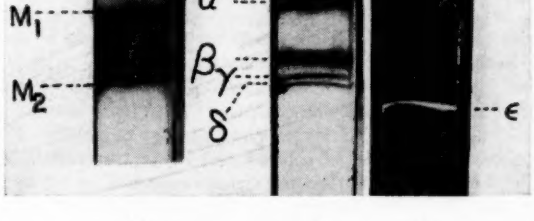

FIG. 1. (a) M layer (containing the dyes shown separated in Fig. 2) with boundary marks M_1 and M_2. These marks indicate in all photographs the boundaries of the original M layer. (b) Electrophoretic line spectrum of a protein mixture. α: Cytochrome C, β: hemoglobin, γ: catalase, δ: azo coupled collagen. (c) ϵ: colorless protein impurity. The separation was accomplished in 6 minutes.

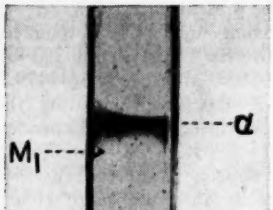

FIG. 2. Separation of a mixture of dyes (time, 10 minutes). α: basic fuchsin, β: chrome hematoxylin, γ: brom thymol blue, δ: brom phenol blue. [The original M layer is shown in Fig. 1(a).]

The electrophoresis cell is the same as shown in Fig. 1 of the previous communication. The lower portion of the U-tube contains the acid buffer saturated with sucrose. The arms A and L contain the basic buffer and the arms R and B contain the acid buffer free of sucrose. The layer M contains the mixture to be analyzed in a glycerol solution (25 percent by volume). The acid and the basic buffers are obtained by mixing two stock solutions in desired proportions. The stock solutions are: Solution B (pH 9.6): 19.43 gm of sodium acetate ($+3\ H_2O$) and 29.43 gm of sodium barbital per liter of solution. Solution A (pH 2.6) is obtained from solution B by adding to 1 liter of B 3 liters of 0.1 N H Cl and 600 ml of water. In the experiments described below the volume ratio of solution A to solution B is 8/1 for the acid buffer and 2/1 for the basic buffer. A current of 13 mA passes through the cell at 110 volts.

A conductivity gradient is combined with the pH gradient by making the conductivity of the M layer small as compared to the conductivity of the buffers. The low conductivity of the M layer has the following effect: The potential gradient in the M layer is much larger than in the buffer solutions. Consequently, the ions move very fast in M, and slow down greatly as they enter the buffer solutions. Thus, ions which form a wide belt in the poorly conducting M layer are contracted into a narrow "line" when they pass the boundary between M and the buffer. The ratio of the width W of an ion belt in two media of conductivities σ_1 and σ_2 is $W_1/W_2=\sigma_2/\sigma_1$. When the layer M contains a mixture of ions which do not encounter their isoelectric pH before reaching the boundary of M, they form roughly a thin common layer (which appears as a line in side view) at the boundary of M. Because of differences in mobilities, the different ions eventually separate forming distinct layers beyond the boundaries of M. Protein ions, however, may not reach the boundaries of M, being concentrated in thin isoelectric layers inside the M region. The "lines" of non-ampholytes are not nearly as sharp and stable as those of ampholytes. The fact that the protein ions migrate in the direction of diminishing speed (i.e. toward the isoelectric point) has a focusing effect upon the "lines" which remain sharp. The stability of the "isoelectric protein lines" is due to the fact that a protein molecule when removed from the "line" by some disturbance, such as convection, will acquire a charge of such a sign as to be moved back to the isoelectric line by the electric field.

The following figures show electrophoretic "line spectra". Figure 1 shows simultaneous separation of 5 proteins in a mixture. Figure 1(a) shows an M layer before passage of current. Figure 1(b) shows four "lines" of colored proteins in transmitted light. In Fig. 1(c) a fifth colorless protein is made visible by Tyndall effect with dark field illumination. Figure 2 illustrates, for comparison, the separation pattern of a mixture of nonproteins.

The author wishes to thank the Abbott Laboratories Fund for a generous research grant and Dr. N. Nicolaides for the colored proteins.

* This work has been supported by the Office of Naval Research.

[1] A. Kolin, J. Chem. Phys. 22, 1628–29 (1954).

Pure Rotation Lines of OH*

R. P. MADDEN AND W. S. BENEDICT
Laboratory of Astrophysics and Physical Meteorology, The Johns Hopkins University, Baltimore, Maryland
(Received December 15, 1954)

THE pure rotation lines $K''=13-18$ of the OH radical, which lie between 15–20.4μ, have been observed in the emission spectrum of the oxy-acetylene flame. In previous studies[1,2] with prism spectrometers the resolution was insufficient to distinguish the OH lines from the pure rotation lines of H_2O which are also strong in this region. By using a grating spectrometer of large light-gathering power, the fine structure of the OH lines is excellently resolved, permitting positive identification. From the relative intensity of OH and H_2O lines in controlled flames it may be possible to determine the dipole moment of OH.

The spectrometer is of the Ebert type,[3] $f/8$ with a 30 in. mirror. It has a 12 in.$\times$8 in. 1200 lines/in. grating and a Golay-cell detector. A plexiglass chopper and two reflections off MgO eliminate unwanted signal. The image of a 1 in. segment of the outer cone of an oxy-acetylene flame was admitted through curved slits. Good signal-to-noise response was obtained with slits 1 mm wide, corresponding to a spectral band 0.3 cm^{-1} wide at 19μ. In absorption, resolution of $\sim$0.15 cm^{-1} can be achieved, limited principally by the optical quality of the grating.

The emission spectrum was scanned between 490–660 cm^{-1}. At some frequencies the emission is eliminated or reduced by the absorption lines of H_2O and CO_2 in the optical path. All possible OH lines from K'' 13–18 appear at the frequencies calculated from the known energy levels,[4] to within $\pm$0.2 cm^{-1}. This is within the accuracy limitation of wavelength calibration imposed by the present grating drive. In addition, some OH lines from the $V=1$ level also may appear, with intensity about $\frac{1}{6}$ as great, as well as numerous emission lines of H_2O. Most of the H_2O emission lines may be classified as transitions between high energy levels in the (000) and (010) vibration states, as derived from absorption measurements at high temperature[5,6] and emission measurements at shorter wavelengths.[7]

The OH lines fall in groups of 4, due to Λ and spin doubling. The groups $K''=13$, near 498 cm^{-1}, and $K''=14$, near 531 cm^{-1}, are particularly free from distortion by H_2O absorption or emission. Figure 1 shows the $K''=14$ group, together with the H_2O

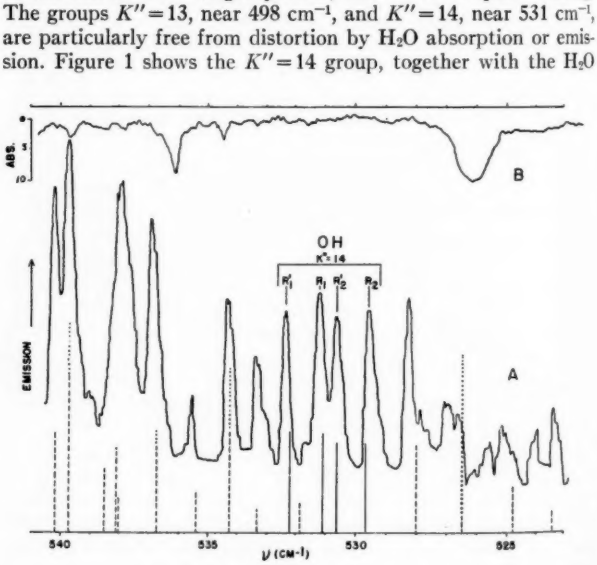

FIG. 1. OH and H_2O spectra between 523–540 cm^{-1}. Curve A: Emission of oxy-acetylene flame. Curve B: Globar source, showing H_2O lines in atmospheric path. The vertical lines above the frequency scale correspond to analyzed lines, with height proportional to calculated intensity: solid lines, OH; dashed lines, H_2O; portions of lines reduced by absorption are dotted.

emission and the background absorption, from 523–540 cm^{-1}. The calculated positions of the OH lines are indicated by solid lines; of identified H_2O lines by dashed lines, dotted when they originate

from lower energy levels, and hence reduced by room-temperature absorption.

The heights of the identifying lines in Fig. 1 are proportional to the calculated intensity. The intensity of a pure rotation line depends on the rotational transition moment and initial energy level, which is known for both OH and H_2O; in addition, it depends on the number of molecules in the emitting path, the temperature of these molecules, and the dipole moment. Fortuitously, the excitation energy of several H_2O lines is close to that of the adjacent OH lines, so that their relative intensity is not very temperature-sensitive. The relative OH:H_2O concentration is uncertain, and the dipole moment of OH is unknown. If the OH/H_2O concentration ratio were known, the OH dipole moment could be determined from the relative intensity. From a number of H_2O lines, we derive μ_{OH} (Debyes) $=0.51\times(N_{H_2O}/N_{OH})^{\frac{1}{2}}$, with an uncertainty of ± 10 percent. The calculated intensities in Fig. 1 correspond to $N_{H_2O}/N_{OH}=9$, and $T=2877°K$. These are reasonable estimates for flames of this type,[8] and lead to $\mu_{OH}=1.54$ Debyes. By making studies of the relative OH—H_2O intensities from selected portions of controlled flames, it may be possible to obtain detailed information concerning the OH/H_2O concentration ratio, and a more reliable value of the OH moment.

* This work was supported in part by contract with the Office of Naval Research and in part by contract with Air Force Cambridge Research Center.

[1] E. K. Plyler and C. J. Humphreys, J. Research Natl. Bur. Standards 40, 449 (1948).
[2] S. Silverman and R. C. Herman, J. Opt. Soc. Am. **39**, 216 (1949).
[3] W. G. Fastie, J. Opt. Soc. Am. **42**, 641, 647 (1952).
[4] G. H. Dieke and H. M. Crosswhite, Bumblebee Report No. 87 (The Johns Hopkins University, Baltimore, Maryland, 1948).
[5] Benedict, Claassen, and Shaw, J. Research Natl. Bur. Standards 49, 91 (1952).
[6] Taylor, Benedict, and Strong, J. Chem. Phys. **20**, 1884 (1952).
[7] Benedict, Bass, and Plyler, J. Research Natl. Bur. Standards **52**, 161 (1954); and unpublished data.
[8] *Cf., Energy Transfer in Hot Gases* (National Bureau of Standards, Washington, D. C., 1954), Circular No. 523.

A Note on the Preparation of Solid Ozone and Atomic Oxygen

H. P. Broida and J. R. Pellam
National Bureau of Standards, Washington 25, D. C.
(Received November 3, 1954)

A RECENT note[1] points out that the literature contains only two research accounts of solid ozone. During some preliminary experiments, designed to determine the possibility of obtaining free radicals at very low temperatures,[2] two novel methods of preparing solid ozone were found. In both methods gaseous products of a high-frequency electrodeless discharge through oxygen are condensed on a pyrex surface at 4.2°K. If the vessel is clean and dry, ozone is deposited directly on the surface. If some water vapor is first admitted to the vessel, an active material is deposited, which upon heating forms solid ozone. It is suggested that the active material contains free oxygen atoms.

Oxygen gas at low pressure (0.1 to 3 mm Hg) flows through a discharge region maintained by a microwave (2450 mc/sec) voltage. The products from the discharge, containing a large concentration of oxygen atoms[3,4] are condensed on cold walls surrounded by liquid helium. The vessel immersed in liquid helium is a trap freezing out all gases except helium, and effectively acts as a high-speed vacuum pump. To prevent solidification of discharge products above 4.2°K, the flow is carried to the cold walls within a passageway (2 cm i.d.) kept at nearly room temperature by warm helium gas. The distance from the discharge region to the cold walls is 50 cms.

The apparatus is cleaned with a 10 percent solution of HF, rinsed several times with distilled water, and thoroughly dried. Within 15 to 30 seconds after the flow of oxygen through the discharge has been started, a violet coloration is observed on the walls of the vessel immersed in liquid helium. In 5 minutes a $\frac{1}{2}$ mm thick film of the colored material can be deposited. After several minutes the film begins to crack and to "peel" off the surface in sections as large as 1 by 5 cm; these fall into the bottom of the vessel. The violet solid melts at a temperature above the melting point of oxygen (54°K) and forms a deep blue-violet liquid which vaporizes at some temperature above the boiling point of nitrogen (77°K) but below 273°K. The vapor has the pungent odor of ozone and quickly decomposes rubber. The color, odor, melting point, boiling point, and oxidizing action strongly indicate that the solid contains a large concentration of ozone. No crystals were observed, the deposit always appearing as an "amorphous" solid.

If a small amount of water vapor is admitted to the apparatus before the oxygen flow is started, the material deposited at 4.2°K has completely different characteristics than those described above. A colorless, "amorphous" solid somewhat like a thin clear ice covers the inside of the vessel; small cracks develop after several minutes. In addition to the clear solid, a small ring of blue-violet solid deposits near the inlet to the cold chamber. With transmitted light, this ring of material is brown rather than clear or blue-violet.

When the temperature is raised to a point above 4.2°K but less than 54°K, the transparent material disappears and a white cloud is seen in the volume. Within a few seconds the entire inner surface is coated with a purple solid, but the color density continues to increase for about 30 seconds. The material appears violet when observed with transmitted light. It liquefies above 54°K and vaporizes considerably above 77°K. In this case, as before, it seems that a solid with a large concentration of ozone has been prepared.

There is some evidence that the active oxygen material can be formed on surfaces other than pyrex coated with water. In one experiment the products from an oxygen discharge were condensed on a thick solid layer from a discharge through nitrogen. A light blue film was observed to become a much deeper violet upon warming.

One explanation of the deposit (which upon heating produces ozone) is that a solid containing free oxygen atoms has been deposited from the products of the discharge through oxygen. Such an explanation is consistent with the atomic concentration in the gas phase of similar discharges[3] and with the formation of ozone. In addition, the work of Rice and co-workers[5] on the condensation of radicals at liquid nitrogen temperatures lends plausibility to this hypothesis.

[1] Brown, Berger, and Hersh, J. Chem. Phys. **22**, 1150 (1954).
[2] H. P. Broida and J. R. Pellam, Phys. Rev. **95**, 845 (1954).
[3] L. C. Copeland, Phys. Rev. **36**, 122 (1930).
[4] R. E. Ferguson and H. P. Broida, Fifth Combustion Symposium (to be published).
[5] F. Rice and M. Freamo, J. Am. Chem. Soc. **73**, 5529 (1951); **75**, 548 (1953).

Mechanism of Detonation

Melvin A. Cook
Explosives Research Group, University of Utah, Salt Lake City, Utah
(Received November 12, 1954)

CONSERVATION of mass and momentum require that conditions in the detonation reaction zone follow the "Rayleigh line" constant $(D/v_0)^2=(p-p_0)(v_0-v)$. For steady-state reaction zones, therefore,

$$v=v_0-P(v_0-v_1)\pi_1+\pi_0(v_0-v_1) \tag{1}$$

(definitions tabulated below). Assuming thermal equilibrium, one may introduce conservation of energy for gaseous explosives through M in the equation of state $P=Mv_1/v$, where

$$M=n\bar{C}v_1(Q+\varphi P^2+\bar{C}_vT_0)/\bar{C}_vn_1H.$$

Whence,

$$P=(\gamma+1)/2\pm[(\gamma+1)^2/4-M\gamma]^{\frac{1}{2}}. \tag{2}$$

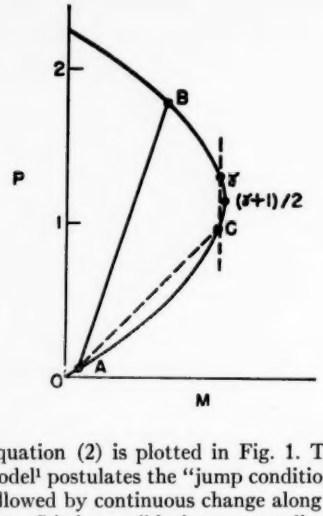

FIG. 1. Plot of Eq. (2).

Equation (2) is plotted in Fig. 1. The Zeldovich-von Neumann model[1] postulates the "jump condition" A to B at the shock front followed by continuous change along BCA to C. Continuity from A to C is impossible for reasons discussed by Zeldovich and von Neumann. The "jump condition" A to B also seems very improbable! It requires (for continuity) $M_s=(\gamma+1)^2/4\gamma$, $(dM/dN)_s=0$, and $1\leq M\leq 1.02$ for $1\leq P\leq\gamma$. But this effectively fixes the $P(x)$ curve which is therefore not determined by shock wave phenomena at all, but by reaction rate.

Using Eq. (2), the identity $dP/dN=(dP/dx)(dx/dt)(dt/dN)$ and appropriate thermo-hydrodynamic relations (for θ and θ')

$$\frac{dP}{dx}=\delta\theta T e^{-\Delta H^{\ddagger}/RT}F(N,Z)/[\gamma+1-2P(1+\gamma\theta')](\gamma+1-P). \quad (3)$$

In the $P\geq 1$ model T/T_1 increases with N from about $\frac{1}{2}$ to 1 while the denominator increases (mostly near $N=1$) from about -1 to values near zero. F in the usual case (branching chain mechanisms) also increases with N, e.g., in H_2-O_2 systems $F\approx(N+C)(1-N)^{\frac{1}{2}}e^{-A/T}$, $(C\ll 1)$. Even for $F=C\ (1-N)$, Eq. (2) increases (exponentially) with N over most of the reaction zone. Consequently the $P(x)$ curve exhibits in general a broad flat of $P\sim P_f$, and falls (suddenly) to unity at or near the $C-J$ plane. In fact the dP/dx *vs* x curve and, in cases such as H_2-O_2, even the $P(x)$ curve becomes discontinuous at the $C-J$ plane in the Zeldovich-von Neumann model. Such $P(x)$ curves are physically unacceptable.

It is believed that a way out of the dilemma that neither point A nor point B applies at the front of the reaction zone may be found by reference to some recent experimental results from this laboratory, which together with the observation that the reaction zone has high electrical (and presumably therefore thermal) conductivity, seem to show that some enthalpy of external origin may be carried along in the reaction zone. Thus a "jump" A to B in which B now lies between A and C is indicated. However, for B appreciably below C the reaction zone would not be steady. Hence, the "jump" appears to be directly from A to C (dotted line A to C Fig. 1). The above experimental and theoretical results will be the bases of a detailed article dealing with the mechanism of detonation.

Symbols and Definitions.—

v—specific volume
p—pressure
P—reduced pressure p/p_1
T—temperature
n—moles per unit mass
M—nT/n_1T_1
t—time
$\Delta H^{\ddagger}$—heat of activation
δ, C, A—positive constants
x—distance measured from wave front in reduced units $(x_1=1)$
D—detonation velocity
N—fraction of reaction
Q—heat of explosion
C_v—constant volume heat capacity
$\bar{C}_v$—average heat capacity (T_0 to T)
C_p—constant pressure heat capacity
γ—C_p/C_v
R—gas constant
$\pi_1=p_1/(p_1-p_0)$
$\pi_0=p_0/(p_1-p_0)$.

Subscript 0 applies to (initial) conditions at point A; subscript 1 applies to conditions at point C; subscript s applies to conditions at $P=(\gamma+1)/2$; subscript f applies to conditions at point B; no subscript applies to other conditions on "Rayleigh line."

$F(N,z)$—"Order of reaction" functions; Z—chain branching factors.
$Q=Q(N)\doteq Q_1(1+B\log P)N$; $\varphi=\frac{1}{2}(p_1+p_0)(v_0-v_1)$
$\theta(N)\doteq M(n_1-n_0)+\bar{C}_{v1}nQ_1(1+B\log P)/\bar{C}_vn_1H$; $B=0.0$ to 0.1
$\theta'(N)\doteq(BN/P+2P\varphi n\bar{C}_{v1}/n_1\bar{C}_vH)$; $H=Q_1+\varphi+\bar{C}_{v1}T_0$

[1] Y. B. Zeldovich, J. Exptl. Theoret. Phys. (U.S.S.R.) **10**, 542 (1940); J. von Neumann, OSRD 549 (1942); W. Döring, Ann. Physik **43**, 421 (1943).

Studies on Solid State Reactions with Radiotracers

R. LINDNER
Institute for Silicate Research, Chalmers University of Technology, Gibraltargatan 5 j, Gothenburg, Sweden
(Received November 19, 1954)

A RESEARCH program, dealing with the mechanism of reactions in the solid state and sponsored by the Swedish Council for Technical Research, has been carried out at this institute during the last seven years.

Some of the results have been published since 1949, mostly in the Swedish papers: Acta Chemica Scandinavica and K. Vetenskapsakademiens (Stockholm) Arkiv för Kemi. A short survey of the present state of the work is given:

(1) Self-diffusion has been measured with radioactive tracers in the following systems (preliminary values in brackets).

TABLE I.

Diffusion system	D_0 (cm² sec⁻¹)	Q (kcal/mole⁻¹)
Oxides		
Ca in CaO	0.4	81
Zn in ZnO (pure)	1.3	74
Zn in ZnO (on metal)	about 10^{-16} cm²/sec at 400°C	
Pb in α-PbO	10^5	66
Pb in PbO (on metal)	practically identical with pure PbO	
Fe in Fe_2O_3	$4\cdot10^5$	112
Silicates (and Titanates)		
Pb in $PbSiO_3$	$8.5\cdot10^1$	59.5
Pb in Pb_2SiO_4	8.2	47
Ca in α-$CaSiO_3$	$7\cdot10^4$	112
(Ca in β-$CaSiO_3$	0.2	78)
(Ca in $Ca_3Si_2O_7$	10^{-2}	73)
Ca in α-Ca_2SiO_4	$2\cdot10^{-2}$	55
Ca in α′-Ca_2SiO_4	$3.6\cdot10^{-2}$	65
(Ba in $BaSi_2O_5$	$5\cdot10^2$	80)
Ba in $BaTiO_3$	0.8	89
Ferrites		
Ca in $CaFe_2O_4$	$3\cdot10^1$	86
Fe in $CaFe_2O_4$	0.4	72
Zn in $ZnFe_2O_4$	$8.8\cdot10^2$	86
Fe in $ZnFe_2O_4$	$8.5\cdot10^2$	82
Other Compounds		
Ag in α-Ag_2SO_4	2.4	26.7
Ag in β-Ag_2SO_4	$6.7\cdot10^{-5}$	13.4

Most of the measurements have been done with sintered pellets. Diffusion of radioactive material can be traced within the crystallites and also in the interstices between the single grains by exact analysis of the concentration gradient and by radioautographic control.

(2) Transfer numbers in solid oxides and silicates have been measured by application of a 1000 volts dc field to a system of sintered pellets, and values ranging from $10^{-3}-10^{-2}$ have been found, e.g., for the transfer number of calcium in calcium oxide (at *ca* 900−1300°C).

(3) The first stage in reactions between powders (mixtures compressed in order to obtain good contact between the reactants) has been studied with radiotracers. The so-called phase-boundary reaction stage was investigated in the case of the reactions of radioactive oxides of lead and calcium with silica. A linear reaction rate is observed up to yields equivalent to layer thicknesses of about 100 lattice constants, which indicates a highly accelerated diffusion during the first stage of reaction.

(4) The diffusion stage of solid state reactions as high temperature metal oxidation, formation of silicates and spinels has been investigated and compared with reaction rates calculated on basis of the mobilities determined by the self-diffusion measurements.

The well known theory by C. Wagner, which assumes a predominant cation diffusion in the case of metal oxidation and a diffusion of both cations in opposite direction within the silicate and spinel reaction layer, has been tested. Sufficient accordance between the two series of experiments to support the Wagner hypothesis could be obtained in the case of zinc oxidation and the formation of zinc-iron spinel; no agreement could be found in the case of lead oxidation and the formation of silicates as no sufficient mobility of lead and silicon ions respectively could be detected. In the latter cases a mobility of oxygen ions within the reaction layer must be considered. Experiments to elucidate this are under work.

The detailed description of all experiments mentioned will be published in Transactions of Chalmers University, Gothenburg (Sweden).

Theoretical Study of the Ozone Molecule

INGA FISCHER-HJALMARS
Institute of Theoretical Physics, University of Stockholm, Stockholm, Sweden

(Received December 10, 1954)

RECENTLY[1,2] it has been finally proved that the three oxygen atoms of the ozone molecule form an isosceles triangle, the shortest O−O distance being 1.278±0.003 A and the apex angle 116°49′±30′. Thus, the steric structure of ozone is very similar to those of NO_2, SO_2, ClO_2, and other dioxides. A comparison between SO_2 and O_3 shows that the dipole moment and the double bond character are considerably smaller in O_3 than in SO_2. Accordingly, it has been suggested[3] that O_3 is best described as a hybrid between two structures of type I and two of type II:

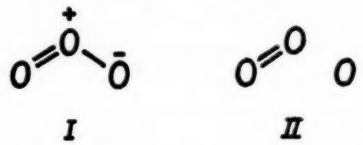

I II

The present study consists of a theoretical investigation of O_3 according to the molecular orbital (MO) method in the LCAO approximation. As O_3 does not show any paramagnetism originating from the electronic structure,[2,4] there are only closed shells in the ground state of the molecule. However, this fact does not fix the electronic configuration. To discuss the different possibilities we must consider the point group C_{2v}, where the different irreducible representations are denoted[5]: a_1, a_2, b_1, and b_2. When only 2*s* and 2*p* AO:*s* are considered, the maximum number of ozone MO:*s* belonging to these representations are given by:

$$(a_1)^{10}(b_1)^8(a_2)^2(b_2)^4.$$

Then, the most probable, orthogonal electronic configurations are as follows:

$$\Psi_1: \quad (a_1)^8(b_1)^4(a_2)^2(b_2)^4, \quad A_1,$$
$$\Psi_2: \quad (a_1)^8(b_1)^6(b_2)^4, \quad A_1,$$
$$\Psi_3: \quad (a_1)^6(b_1)^6(a_2)^2(b_2)^4, \quad A_1,$$
$$\Psi_4: \quad (a_1)^8(b_1)^6(a_2)^2(b_2)^2, \quad A_1.$$

When only 2*p* AO:*s* are taken into account, each configuration should be diminished by $(a_1)^4(b_1)^2$.

Self-consistent field computations have been carried out for each of the four configurations, both in the 2*p* approximation (only 2*p* AO:*s*) and in the 2*s*, 2*p* approximation (2*s* and 2*p* AO:*s*). In the 2*p* approximation the configurational interaction has also been studied. As for the choice of AO:*s* it seems to be of some value to compare results obtainable from simple, analytical AO:*s* of the Slater type and from the best AO:*s* of the Hartree-Fock type.[6] Such a comparison has been carried out in the 2*p* approximation and will soon be completed in the 2*s*, 2*p* approximation.

It has been found that Ψ_4 corresponds to the lowest energy level in all the different approximations, although the other levels are so close that the configurational interaction is not negligible. In the configuration Ψ_4 the main part of the bonds originates from the b_2 MO:*s*, that is, the 2*p* orbitals perpendicular to the plane of the molecule. The order of the bond between the apex O atom and one of the others is only slightly more than that of a single bond, and the atoms at the base of the triangle repel each other. The computed values of dissociation energy and dipole moment are rather different in the different approximations. The results of the 2*p* approximation are listed in Table I. As could be expected, the results from different choice of AO:*s* are similar for such properties as most stable configuration but different for properties such as dissociation energy and dipole moment depending on differences between almost equal numbers. The preliminary results of the 2*s*, 2*p* approximation seems to agree somewhat better with experiments than the 2*p* approximation, e.g. with respect to the sign of the dipole moment.

TABLE I. Computational results in the 2*p* approximation.

	Energy a.u.	Dissociation energy a.u.	Dipole moment Debye
Slater AO:*s*			
Ψ_1	−22.25	0.52	+0.05
Ψ_2	−22.13	0.40	−0.24
Ψ_3	−22.11	0.38	−0.11
Ψ_4	−22.28	0.55	−1.15
Hartree AO:*s*			
Ψ_1	−21.66	1.12	−0.59
Ψ_2	−21.52	0.97	+0.24
Ψ_3	−21.51	0.96	−0.39
Ψ_4	−21.82	1.27	−1.84
Experimental		0.228	+0.53

Full details of the present study will be published in Arkiv för Fysik.

[1] R. H. Hughes, Phys. Rev. **85**, 717 (1952); J. Chem. Phys. **21**, 959 (1953).
[2] Trambarulo, Ghosh, Burrus, Jr., and Gordy, J. Chem. Phys. **21**, 851 (1953).
[3] Phillips, Hunter, and Sutton, J. Chem. Soc. (London), 146 (1945).
[4] P. Lainé, Ann. phys. **3**, 461 (1935).
[5] See, e.g., G. Herzberg, *Infrared and Raman Spectra of Polyatomic Molecules* (New York, 1945), p. 106.
[6] Hartree, Hartree, and Swirles, Philos. Trans. **A238**, 229 (1938).

Intermolecular Force Field of Linear Molecules with Quadrupole Moments

A. D. BUCKINGHAM
Department of Theoretical Chemistry, University of Cambridge, England
(Received November 29, 1954)

POPLE[1] showed that the second virial coefficient of an assembly of axially symmetric molecules, the interaction energy u_{12} of any two of them, distant r apart, being

$$u_{12}=4\epsilon\left\{\left(\frac{r_0}{r}\right)^{12}-\left(\frac{r_0}{r}\right)^{6}\right\}+\text{quadrupole}-\text{quadrupole energy}, \quad (1)$$

where ϵ and r_0 are parameters having the dimensions of energy, and length is given by

$$B(T)=\frac{2\pi N r_0^3}{3}\left\{F(y)-\frac{7}{320}\left(\frac{\Theta^2}{\epsilon r_0^5}\right)^2 H_{10}(y)+\cdots\right\}, \quad (2)$$

where

$$y=2\left(\frac{\epsilon}{kT}\right)^{\frac{1}{2}}, \quad F(y)=-\frac{y^3}{4}\sum_{p=0}^{\infty}\Gamma\left(\frac{2p-1}{4}\right)\frac{y^p}{p!},$$
$$H_n(y)=y^{(27-n)/6}\sum_{p=0}^{\infty}\Gamma\left(\frac{6p+n-3}{12}\right)\frac{y^p}{p!}. \quad (3)$$

The quadrupole moment Θ is defined by $\Theta=\Sigma_i e_i(z_i^2-x_i^2)$ where z_i is measured along the axis, and x_i perpendicular to it. Subsequent terms in the expansion, which include both odd and even powers of $\Theta^2/\epsilon r_0^5$, are alternatively positive and negative, so make only a small contribution to $B(T)$ (see Buckingham and Pople[2]). Pople determined ϵ, r_0, and Θ by obtaining the best fit of the second virial data, and then compared the calculated heat of sublimation at absolute zero with the observed value. However, since the virial data can be fitted nearly as well by considerably different values of the parameters, a preferable procedure is to use a successive approximation method to determine $\Theta^2/\epsilon r_0^5$ so that the heat of sublimation is given precisely and to employ the second virial data to yield ϵ and r_0.

TABLE I. Calculated and experimental data for N_2 and CO_2.

Substance	E (cal/mole)	ϵ/k (°K)	r_0 (A)	$\Theta\times10^{26}$ (esu) calc	$\Theta\times10^{26}$ (esu) from microwave data	a_0 (A) calc	a_0 (A) exptl
N_2	1800[a]	94	3.78	1.20	1.5[c]	4.09	4.00
CO_2	6530[b]	182.4	3.94	5.29	3.1[c]	4.07	3.92

[a] See reference 3.
[b] W. F. Giauque and C. J. Egan, J. Chem. Phys. **5**, 45 (1937).
[c] Hirschfelder, Curtiss, and Bird, *Molecular Theory of Gases and Liquids* (John Wiley and Sons, Inc., New York, 1954), p. 1028.

The heat of sublimation H, of a face centred cubic lattice of molecules interacting according to (1), at absolute zero, is related to the Debye temperature θ by (see Pople[1] and Lupton[3]).

$$H+\frac{9}{8}Nk\theta=E=2N\epsilon\left\{12.1318\left(\frac{r_0}{a}\right)^{12}-14.4539\left(\frac{r_0}{a}\right)^{6}-5.3533\frac{\Theta^2}{\epsilon r_0^5}\left(\frac{r_0}{a}\right)^{5}\right\}, \quad (4)$$

and E must be minimized with respect to a, yielding a_0, where a is the distance between nearest neighbors. The inclusion of quadrupole-induced dipole interactions would not affect E, owing to the symmetry of the lattice.

Lupton[2] performed somewhat similar calculations on N_2 and CO, but he employed ϵ and r_0 values computed from the second virial data using a Lennard-Jones potential only, and then adjusted the quadrupole moment to fit the observed E. A more consistent procedure is the one outlined above, and this was applied to N_2 and CO_2. The data and results are shown in Tables I and II.

TABLE II. Calculated and experimental second virial coefficients for N_2 and CO_2.

N_2 T (°C)	$B(T)_{exptl}$[a] (cm³/mole)	$B(T)_{calc}$ (cm³/mole)	CO_2 T (°C)	$B(T)_{exptl}$[b] (cm³/mole)	$B(T)_{calc}$ (cm³/mole)
0	−10.4	−10.2	0	−156.4	−147.3
25	−4.8	−4.5	50	−101.7	−102.3
50	−0.3	0.2	100	−71.9	−73.1
75	3.2	4.1	150	−51.6	−52.7
100	6.6	7.6	200	−34.3	−37.6
125	9.6	10.2	300	−13.3	−17.2
150	12.5	12.6	400	−2.0	−4.0
			500	6.0	5.1
			600	12.0	11.8

[a] Michels, Wouters, and de Boer, Physica **1**, 587 (1934).
[b] K. E. MacCormack and W. G. Schneider, J. Chem. Phys. **18**, 1269 (1950).

The author is indebted to Dr. J. A. Pople for some valuable suggestions, and to the Royal Dutch/Shell Group for the award of a Postgraduate Scholarship.

[1] J. A. Pople, Proc. Roy. Soc. (London) **A221**, 508 (1954).
[2] A. D. Buckingham and J. A. Pople, Trans. Faraday Soc. (to be published).
[3] J. M. Lupton, Thesis (University of Amsterdam, 1954).

Applications of the Alternant Molecular Orbital Method to Six- and Four-Electron Systems

HIROYUKI YOSHIZUMI AND TAKASHI ITOH
Department of Physics, University of Tokyo, Tokyo, Japan
(Received December 6, 1954)

IN many molecules and crystals the electronic wave function of the ground state is to the first approximation given by a single determinant constructed from molecular orbitals (or Bloch orbitals); each doubly occupied by electrons of opposite spins. The greatest shortcoming of such a determinantal wave function is found in its incapability of taking into account the correlation between the motions of electrons. It contains, however, some correlation between electrons of parallel spin introduced by the Pauli exclusion principle, but none for the antiparallel spin.

To remedy this defect one must carry out the extensive C.I. (configuration interaction) calculation. But the complete C.I. calculation becomes practically impossible for large systems.

Recently Löwdin proposed a new attack for the treatment of antiparallel spin using the alternant molecular orbital.[1,2] His method seems to present a powerful method by which the major part of the effect of C.I. can be taken into account. In this letter the applications of the method to benzene (six π electron system) and to acetylene (four π electron system) are reported.

(1) Benzene. The alternant MO are defined by

$$\left.\begin{aligned}\phi_{I1}&=\cos\theta\phi_l+\sin\theta\phi_{l+3},\\ \phi_{I11}&=\cos\theta\phi_l-\sin\theta\phi_{l+3},\end{aligned}\right\},$$

where

$$\phi_l(r)=(6\sigma_l)^{-\frac{1}{2}}\sum_{k=1}^{6}\exp\left(\frac{2\pi ikl}{6}\right)\cdot U_k(r).$$

The I-type orbitals have large amplitudes on the alternant atoms (say 1,3,5), while the II-type orbitals on the other atoms (2,4,6). Using these orbitals, we construct the ground state wave function $(^1A_{1g})$,

$$\Psi_i(\theta)=N_i\sum_P(-1)^P P\phi_{0I}(1)\phi_{1I}(2)\phi_{-1I}(3)\phi_{0II}(4)\phi_{1II}(5)\phi_{-1II}(6)\cdot\chi_i,$$

where χ_i represents a singlet spin function. By adjusting θ to the optimum value, maximum depression of total energy is obtained, and this value is to be compared with the result of the C.I.

There are five singlets for six electron system,[3] and two of them are shown in Fig. 1.

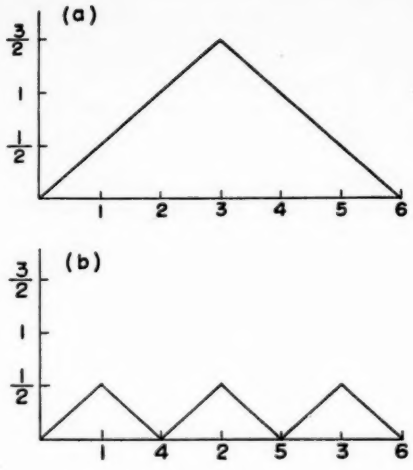

FIG. 1. Two types of spin coupling.

$$\chi_a=\alpha_1\alpha_2\alpha_3\beta_4\beta_5\beta_6$$
$$-\tfrac{1}{3}(\beta_1\alpha_2\alpha_3+\alpha_1\beta_2\alpha_3+\alpha_1\alpha_2\beta_3)(\alpha_4\beta_5\beta_6+\beta_4\alpha_5\beta_6+\beta_4\beta_5\alpha_6)$$
$$+\tfrac{1}{3}(\alpha_1\beta_2\beta_3+\beta_1\alpha_2\beta_3+\beta_1\beta_2\alpha_3)(\beta_4\alpha_5\alpha_6+\alpha_4\beta_5\alpha_6+\alpha_4\alpha_5\beta_6)$$
$$-\beta_1\beta_2\beta_3\alpha_4\alpha_5\alpha_6,$$

$$\chi_b=(\alpha_1\beta_4-\beta_1\alpha_4)(\alpha_2\beta_5-\beta_2\alpha_5)(\alpha_3\beta_6-\beta_3\alpha_6).$$

Now, the type (a) coupling of Fig. 1 is expected to give a satiss factory result. When the type (a) coupling is adopted, the spin- of electrons in the same type (I or II) orbitals are added to the resultants $\frac{3}{2}$, and then the two resultants are added to singlet. Then $\Psi_a(\theta)$ contains the correlation effect of antiparallel spins through the alternant character of I- and II-type orbitals and that of parallel spins through the Pauli principle. The results of the calculation are shown in Fig. 2, which shows clearly the superiority of coupling (a). The energy depression for curve (a) is 2.35 ev, which is 85 percent of the value obtained by the C.I. of nine $^1A_{1g}$ functions.[4]

(2) Acetylene. The same method is applied for acetylene as for benzene. The energy depression is about 70 percent of the complete C.I. calculation carried out by Nakamura *et al.*[5] Generally speaking the curves for this case show the similar tendency as in benzene case.

The full paper for benzene will be published shortly in the *Journal of the Physical Society of Japan*, and the detailed results for acetylene including the applications for the excited states will be reported elsewhere.

The authors express their sincere thanks to Professor M. Kotani for his kind guidance and to Professor P. O. Löwdin for his valuable communications.

[1] P. O. Löwdin, "Symposium on molecular physics," Nikko, Japan (1953).
[2] P. O. Löwdin, "Quarterly progress report," Solid-State and Molecular Theory Group, M.I.T., July 15, 1954, p. 22.
[3] G. W. Pratt, Jr., Phys. Rev. **92**, 278 (1953).
[4] Parr, Craig, and Ross, J. Chem. Phys. **18**, 1561 (1950).
[5] Nakamura, Ohno, Kotani, and Hijikata, Progr. Theoret. Phys. **8**, 387 (1952).

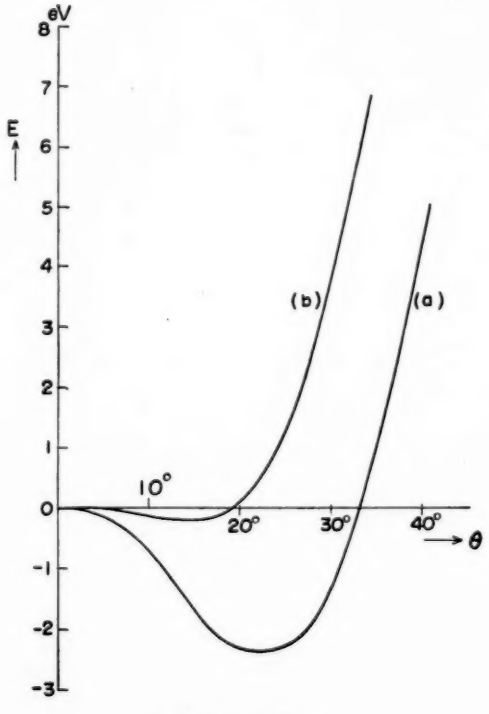

FIG. 2. Energy curves.

Pure Rotational Absorption Spectrum of Hydrogen

J. A. A. KETELAAR, J. P. COLPA, AND F. N. HOOGE
Laboratory for General and Inorganic Chemistry of the University of Amsterdam, Amsterdam, The Netherlands
(Received December 8, 1954)

IN the course of our investigations[1] on the infrared absorption spectra of gases and gas mixtures we observed that compressed hydrogen contrary to, e.g., nitrogen did show a remarkable absorption at wavelengths in the 8μ to 15μ region.

The observed extinction curves for hydrogen at pressures up to 114 atmospheres with an optical pathlength of 100 cm are reproduced in Fig. 1.

The extinction is very nearly proportional to the square of the pressure ($\simeq$density). The observed spectrum has to be ascribed to the pressure induced pure rotation spectrum of hydrogen. The shoulders are due respectively to the transitions $J=2\rightarrow J=4$ and $J=3\rightarrow J=5$; calculated at 813.9 cm^{-1} and 1034.1 cm^{-1} according to Herzberg[2] with the formula

$$F_{v=0}(J)=59.300J(J+1)-0.04581J^2(J+1)^2$$
$$+0.0000518J^3(J+1)^3.$$

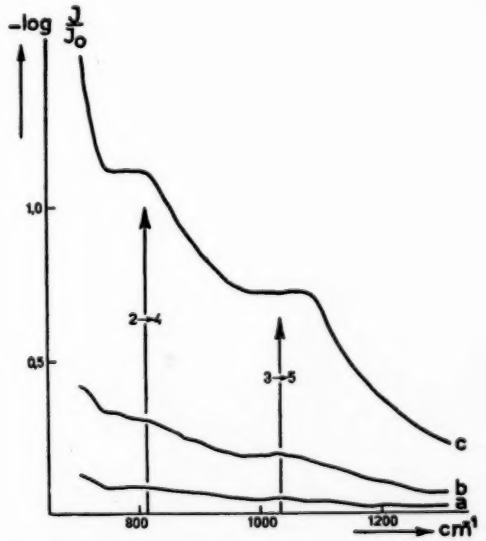

FIG. 1. Minus $\log I/I_0$ *versus* wave number for pure hydrogen, where *a* is 28.5 atmos, *b* is 57 atmos, and *c* is 114 atmos. The arrows indicate the calculated wave numbers of the transitions $J=2\rightarrow J=4$ and $J=3\rightarrow J=5$.

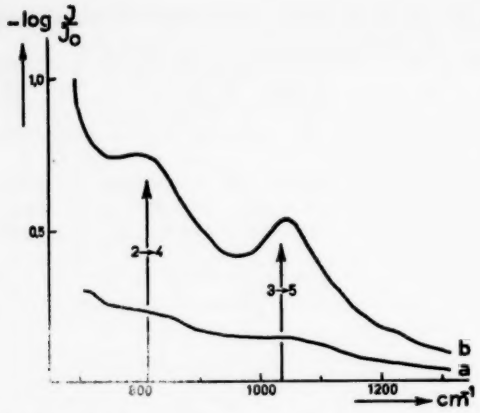

FIG. 2. Minus $\log I/I_0$ *versus* wave number, where *a* is H_2 50 atmos and *b* is H_2 50 atmos and N_2 added to a total pressure of 100 atmos. In measuring I_0 the cell was filled with N_2 100 atmos. The arrows indicate the calculated wave numbers for the transitions $J=2\rightarrow J=4$ and $J=3\rightarrow J=5$.

We propose to study the spectrum also in the KBr region, where the very strong $J=1\rightarrow J=3$ transition must be expected at 587 cm^{-1}.

In mixtures of hydrogen with nitrogen (Fig. 2) and also with carbondioxide the rotation spectrum is observed too, and the maxima are even more pronounced there than in the case of pure hydrogen.

These absorption spectra have to be ascribed to the collision complex. Apparently the collisions of H_2 with N_2 are more effective in producing induction than the H_2-H_2 collisions. With CO_2 an even stronger effect than for N_2 is observed.

This work is part of the research program of the "Stichting voor Fundamenteel Onderzoek der Materie" (Foundation for Fundamental Research of Matter F.O.M.) and was made possible by financial support from the "Nederlandse Organisatie voor Zuiver Wetenschappelijk Onderzoek" (Netherlands Organization for Pure Research Z.W.O.).

[1] J. Fahrenfort and J. A. A. Ketelaar, J. Chem. Phys. **22**, 1631 (1954); Fahrenfort, de Kluiver, and Babeliowsky, de phys. radium **15**, 617 (1954).
[2] G. Herzberg, *Molecular Spectra and Molecular Structure I, Spectra of Diatomic Molecules* (New York, 1950), second edition, pp. 109 and 532.